Advances in Geographical and Environmental Sciences

R. B. Singh
Manish Kumar
Dinesh Kumar Tripathi *Editors*

Remote Sensing and Geographic Information Systems for Policy Decision Support

Springer

Advances in Geographical and Environmental Sciences

Advances in Geographical and Environmental Sciences synthesizes series diagnostigation and prognostication of earth environment, incorporating challenging interactive areas within ecological envelope of geosphere, biosphere, hydrosphere, atmosphere and cryosphere. It deals with land use land cover change (LUCC), urbanization, energy flux, land-ocean fluxes, climate, food security, ecohydrology, biodiversity, natural hazards and disasters, human health and their mutual interaction and feedback mechanism in order to contribute towards sustainable future. The geosciences methods range from traditional field techniques and conventional data collection, use of remote sensing and geographical information system, computer aided technique to advance geostatistical and dynamic modeling.

The series integrate past, present and future of geospheric attributes incorporating biophysical and human dimensions in spatio-temporal perspectives. The geosciences, encompassing land-ocean-atmosphere interaction is considered as a vital component in the context of environmental issues, especially in observation and prediction of air and water pollution, global warming and urban heat islands. It is important to communicate the advances in geosciences to increase resilience of society through capacity building for mitigating the impact of natural hazards and disasters. Sustainability of human society depends strongly on the earth environment, and thus the development of geosciences is critical for a better understanding of our living environment, and its sustainable development.

Geoscience also has the responsibility to not confine itself to addressing current problems but it is also developing a framework to address future issues. In order to build a 'Future Earth Model' for understanding and predicting the functioning of the whole climatic system, collaboration of experts in the traditional earth disciplines as well as in ecology, information technology, instrumentation and complex system is essential, through initiatives from human geoscientists. Thus human geosceince is emerging as key policy science for contributing towards sustainability/survivality science together with future earth initiative.

Advances in Geographical and Environmental Sciences series publishes books that contain novel approaches in tackling issues of human geoscience in its broadest sense — books in the series should focus on true progress in a particular area or region. The series includes monographs and edited volumes without any limitations in the page numbers.

More information about this series at https://link.springer.com/bookseries/13113

R. B. Singh · Manish Kumar ·
Dinesh Kumar Tripathi
Editors

Remote Sensing and Geographic Information Systems for Policy Decision Support

Springer

Editors
R. B. Singh
Department of Geography
University of Delhi
New Delhi, India

Manish Kumar
Department of Geography
Central University of Haryana
Mahendragarh, Haryana, India

Dinesh Kumar Tripathi
Rana Pratap Post Graduate College
Sultanpur, Uttar Pradesh, India

ISSN 2198-3542 ISSN 2198-3550 (electronic)
Advances in Geographical and Environmental Sciences
ISBN 978-981-16-7730-4 ISBN 978-981-16-7731-1 (eBook)
https://doi.org/10.1007/978-981-16-7731-1

This Springer imprint is published by the registered company Springer Nature Singapore Pte Ltd.
The registered company address is: 152 Beach Road, #21-01/04 Gateway East, Singapore 189721, Singapore

Preface

The assurance of geo-ecological sustainability is the greatest global challenge of this era. This issue seeks to address not only global geo-environmental issues such as natural resource depletion, deforestation, global warming, and ozone layer depletion, but also local issues related to socio-economic system maintenance. Sustainability process includes several dynamic, complex, and interwoven ecological, socio-economic and cultural facets. The researchers, planners, and decision-makers analyse a large volume of real-world data obtained from various sources for required judgement, determination, and a sequence of actions for sustainable development. In this way, the need of such an information system has been felt for a long time in the research and development arena that can support decision-making activities effectively through the proper management of both the spatial and non-spatial information in computer environment.

Modern geospatial technologies of remote sensing (application of sensors in capturing geospatial data) and geographic information system (geospatial data capturing, storing, manipulating, processing, and publishing system) have emerged as powerful tools for researchers and decision-makers. Remote sensing and geographic information system-based policy decision support not only helps them to solve spatially related environmental and socio-economic issues; they also provide an important tool for integrating spatial and non-spatial datasets with analytical and spatial models and knowledge domains. Recent developments in modern remote sensing and geographic information system technologies, along with advanced computing techniques, have improved policy formulation efficiency and capabilities.

The book expands the scientific knowledge base in various physical and socio-economic issues among scholars, planners, and decision-makers for policy development and research regarding sustainable development. Furthermore, the book discusses case studies providing new insights as to how remote sensing and geographic information system-based decision support systems contribute to understanding physical and socio-economic processes and developing pragmatic policy for sustainable development. This book demonstrates the importance of modern spatial decision support tools of remote sensing and geographic information system

for a better understanding of sustainable development processes and policy development issues, enhancing the scientific knowledge base on various physical and socio-economic issues. This book covers cross-cutting issues, attracting trans-disciplinary researchers, city planners, and decision-makers. It may contribute in developing appropriate policy decision support systems for sustainable development.

The book covers both physical and human dimensions and includes remote sensing and geographic information system-based studies and researches on various issues such as estimation of land surface temperature, landslide susceptibility mapping, evaluation of river basin hydrological processes, site suitability analysis for water conservation, monsoon impacted magnetic and geomorphological changes, vulnerability assessment of avalanches, assessment of soil risk by RUSLE model, socio-economic livelihood vulnerability to mountain hazards, land surface temperature and ground water temperature responses to land use/land cover dynamics, land use/land cover change detection and its effect on land surface temperature, spatio-temporal changes in metropolitan cities, assessment of particulate pollutants, assessment of tiger tourism, inventory and phenological assessment of apple orchards, sustainable forest management, flood mitigation, crime hotspots and vulnerable areas detection, land use/land cover change and landscape fragmentation, urban sprawl, geospatial database for village resources, effect of urban expansion on groundwater crisis, spatial modelling for municipal solid waste management. Readers will find this book to be an invaluable resource for enhancing scientific knowledge base and policy development related to sustainable planning and management.

This book incorporates twenty five chapters contributed by scholars, scientists, planners, administrators who belong to various universities and institutions of India as well as from other countries of world such as National Institute of Technology Raipur, Chhattisgarh; Chhattisgarh Council of Science and Technology, Raipur, Chhattisgarh; Nazrul Balika Vidyalaya, Guna, west Bengal Shivaji University Kolhapur, Maharashtra; Banasthali Vidyapith, Rajasthan Regional Remote Sensing Centre, Jodhpur; Indian Institute of Geomagnetism, Mumbai; GSS College, Belgaum; S.N. Arts, D.J.M. Commerce and B.N.S. Science College, Sangamner HPT Arts, RYK Science College,Nashik Savitribai Phule Pune University, Pune; Universal Geotechnical, Nashik Aryabhatta Geo-informatics and Space Application Centre, Shimla, Himachal Pradesh; G. B. Pant National Institute of Himalayan Environment, Itanagar, Arunachal Pradesh; Central University of Jharkhand Ranchi, Jharkhand; Ministry of Chemicals and Fertilizers, Government of India, New Delhi; University of Delhi, Himalayan Forest Research Institute, Shimla, Himachal Pradesh; Central University of Haryana, Haryana; G. B. Pant National Institute of Himalayan Environment Kosi-Katarmal, Almora G. B. Pant National Institute of Himalayan Environment, Himachal Regional Centre, Mohal-Kullu National Remote Sensing Centre, Hyderabad; Indian Institute of Remote Sensing, Dehradun; Andhra University, Visakhapatnam; Haryana Space Applications Centre, Hisar; Jawarharlal Nehru University Indira Gandhi Conservation and Monitoring Centre WWF-India, New Delhi; Mohanlal Sukhadia University, Udaipur; Soban Singh Jeena University, Almora Kumaun University, Nanital, Uttarakhand; Regional Remote Sensing Centre, Bengaluru; Maharaja Institute of Technology, Mysuru; University of Mysore,

Mysuru; Sam Higginbottom University of Agriculture, Technology and Sciences, Prayagraj, U. P; R. M. S. Mahavidyalaya, Bankura University, West Bengal; Indian Institute of Technology, Jammu; Vidyasagar University, Midnapore, West Bengal; Ethiopian Civil Service University, Addis Ababa, Ethiopia; Rana Pratap Post Graduate College, Sultanpur Suresh Gyan Vihar University, Jaipur; Indian Institute of Technology, BHU, Varanasi; K. M. C. Language University,Lucknow Earthresearch Company, Cluj-Napoca Romania Central University of South Bihar,Gaya Government First Grade Women's College Koppal, Karnataka. This book would undoubtedly be beneficial to policymakers, scholars, academicians, and everyone else who is concerned, directly or indirectly, with the use of remote sensing and geographic information systems in sustainable development and policymaking.

New Delhi, India — R. B. Singh
Mahendragarh, India — Manish Kumar
Sultanpur, India — Dinesh Kumar Tripathi

Contents

About the Editors

R. B. Singh was secretary general and treasurer of the International Geographical Union (IGU); chair of the Research Council for Scientific and Industrial Research (CSIR)–Central Food Technological Research Institute of the Government of India; and a member of the International Council for Science (ICSU) and the scientific committee of Urban Health and Well–Being. He has served as professor and head of geography at the Delhi School of Economics, University of Delhi. Earlier, he was the vice president of the IGU during the period of 2012–2018. He was awarded the prestigious Japan Society for the Promotion of Scientific Research Fellowship and has presented papers and chaired sessions in more than 40 countries. He has published 13 books, 34 edited research volumes, and more than 230 research papers. He has supervised 33 Ph.D. and 81 M.Phil. students. In 1988 the United Nations Educational, Scientific and Cultural Organization/the International Social Science Council awarded him research and study grants in social and human sciences. Recently, the Government of India—National Institution for Transforming India (NITI) Aayog (policy think-tank) invited him to join the prestigious committee Vision India 2035.

Manish Kumar is currently working as an assistant professor in the Department of Geography, School of Basic Sciences, Central University of Haryana, Mahendergarh. Earlier, from January 2016 to February 2020, he worked as an assistant professor in the Department of Geography, Kalindi College, University of Delhi. Prior to that, from January 2009 to December 2014, Dr. Kumar worked as a lecturer in the M.Sc. Remote Sensing and GIS Course of Kumaun University, Nainital. He has also worked as a research associate in the United Nations Development Programme (UNDP) project on "rurbanization". In addition, he has been a visiting faculty member at the School of Planning and Architecture (SPA), Delhi. Dr. Kumar holds a Ph.D. degree from Kumaun University and a postgraduate diploma in remote sensing and GIS from the Indian Institute of Remote Sensing (IIRS) of the Indian Space Research Organisation (ISRO), Dehradun. He has published more than 25 research papers in various national and international Science Citation Index and Scopus-indexed journals. His special area of research interest includes the application of remote sensing and GIS in urban and regional planning, land use and land cover dynamics, and urban climate change, among others.

Dinesh Kumar Tripathi is a Principal of Rana Pratap Post Graduate College Sultanpur, Uttar Pradesh (affiliated with Dr. Rammanohar Lohia Avadh University, Ayodhya, Uttar Pradesh). He has been engaged in teaching and research for the past 26 years. Earlier, he worked as an associate professor in the Department of Geography, Kamla Nehru Institute of Physical & Social Sciences, Sultanpur Uttar Pratdesh (India). Dr. Tripathi's academic interests include remote sensing, GIS, and natural resource management. He is a keen researcher and has published 37 research papers in various professional research journals of high repute and presented research papers at a number of national and international conferences and seminars. He has supervised five Ph.D scholars Dr. Tripathi completed the Indian Council of Social Science Research (ICSSR) research project on management of degraded land using satellite remote sensing and GIS, a case study of Gauriganj block, Amethi-UP, in 2012. Dr.Tripathi is also engaged in the research project on remote sensing and GIS based modelling of land degradation for agricultural sustainability in Sultanpur District, Uttar Pradesh sanctioned by department of higher education , Uttar Pradesh government from 2020.

Chapter 1
Estimated Error Analysis in Downscaled Land Surface Temperature

Subhanil Guha, Himanshu Govil, Anindita Dey, and Neetu Gill

Abstract The present study analyzes the estimated root mean square error (RMSE) in the various remote sensing indices based downscaled land surface temperature (LST) of Raipur City, India using four Landsat 8 OLI and TIRS data acquired on 5 June, 25 September, 12 November, and 30 December of 2014. Downscaled LST was determined by the thermal sharpening (TsHARP) method using four spectral indices (normalized difference built-up index (NDBI), normalized difference vegetation index (NDVI), normalized difference water index (NDWI), and normalized multi-band drought index (NMDI)). The results show that the NDBI-based downscaled LST achieves the lowest RMSE, irrespective of all the multi-date imageries. The post-monsoon image reflects the best result followed by the monsoon image.

Keywords Downscaling · Landsat · Land surface temperature · NDVI

1.1 Introduction

Thermal infrared (TIR) band of remotely sensed data is invariably used in determining land surface temperature (LST) which is considered as an important biophysical factor to balance the energy level in landscape and ecological system (Wan and Li 1997, 2008; Anderson et al. 2008; Li et al. 2013; Duan et al. 2014; Guha and Govil 2020). LST is used in a large scale to determine the effects on various types of landscape systems (Voogt and Oke 2003; Jeganathan et al. 2011; Zhan et al. 2013; Guha et al. 2019, 2020a, b), to assess the urban heat island effect (Sobrino et al. 2004; Zakšek and Oštir 2012; Guha et al. 2017, 2018), to examine the fluctuation in

S. Guha (✉) · H. Govil
Department of Applied Geology, National Institute of Technology Raipur, Raipur, Chhattisgarh, India

A. Dey
Department of Geography, Nazrul Balika Vidyalaya, Guma, West Bengal, India

N. Gill
Chhattisgarh Council of Science and Technology, Raipur, Chhattisgarh, India

R. B. Singh et al. (eds.), *Remote Sensing and Geographic Information Systems for Policy Decision Support*, Advances in Geographical and Environmental Sciences,
https://doi.org/10.1007/978-981-16-7731-1_1

diurnal temperature (Weng et al. 2004; Dennison et al. 2006; Agam et al. 2007a, b; Stathopoulou and Cartalis 2009) to measure the surface long wave radiation (Nichol 2009; Yang et al. 2011), to investigate different types of evapotranspiration (Nishii et al. 1996; Gualtieri and Chettri 2000; Sandholt et al. 2002; Pardo-Iguzquiza et al. 2011), and to compute the surface albedo (Mpelasoka et al. 2001).

Downscaling method is considered as an effective method to obtain high-resolution LST at small time interval (Moran 1990; Kustas et al. 2003; Essa et al. 2012; Weng and Fu 2014; Duan and Li 2016).

Different types of sharpening techniques were generated to obtain fine-resolution LST from a coarse-resolution TIR band (Wan and Dozier 1996; Pardo-Igúzquiza and Atkinson 2006; Yang and Yao 2009; Chen et al. 2010; Zhan et al. 2013; Chen et al. 2014; Zhang 2015). Among these algorithms, the DisTrad algorithm is the most popular (Kustas 2003) algorithm. TsHARP algorithm was developed by a modification of the DisTrad algorithm (Agam 2007b) in which the LST-NDVI relationship was the main principle. The accuracy level of these different techniques was evaluated in the various types of land surface compositions, including agricultural land (Jeganathan et al. 2011) or heterogeneous built-up area (Essa et al. 2012). The limitation of this TsHARP algorithm is that the LST-NDVI relationship is quite variable. Thus, the NDVI is not very much suitable for the LST sharpening process conducted in a mixed urban land surface (Nichol 2009; Stathopoulou and Cartalis 2009; Dominguez et al. 2011; Essa et al. 2012; Zakšek and Oštir 2012; Govil et al. 2019, 2020). Different types of land surfaces can generate a unique emission rate. Emissivity (Nichol 2009; Stathopoulou and Cartalis 2009) was used as one of the most important environmental parameters for highly heterogeneous urban land surfaces. Dominguez et al. (2011) proposed a new high-resolution urban thermal sharpener (HUTS) algorithm for LST sharpening in an urban land by integrating surface albedo and NDVI. Impervious surface percentage (Essa et al. 2012, 2013) and pure pixel index (Yang 2010) were applied as the basic factors in the mixed urban land surface. Impervious surface performs well as a LST sharpening parameter compared to NDVI in the diversified urban land surface by comparing 15 different parameters (Essa et al. 2012). Although different types of LST sharpening processes were suggested, they also have some limitations in the available remotely sensed data and land surface features. Moreover, the selection of suitable environmental factors for LST sharpening in mixed urban land surface is still very challenging.

Mukherjee et al. (2015) examined the seasonal fluctuation in the sharpened LST in DisTrad, TsHARP, and local model using Landsat TM 5 data in a heterogeneous agricultural land in India. Bonafoni et al. (2016) derived sharpened LST using Landsat TM data in Florence, Italy and proposed a traditional LST sharpening method. Another research work based on the vegetation and built-up indices was adopted for the LST sharpening technique using Landsat TM and MODIS data conducted in Milan city, Italy (Bonafoni 2016). The scale effect was investigated in the LST sharpening method in the Beijing city and Zhangye oasis, China (Zhou et al. 2016).

In the present study, four remote sensing indices (NDBI, NDVI, NDWI, and NMDI) were examined as the basis of TsHARP downscaling technique applied on an urban landscape. The main objective of the research was to determine the best index for LST sharpening method in a heterogeneous urban land with respect to multi-date satellite imageries.

1.2 Study Area and Data

Raipur, the Capital city and the largest city of Chhattisgarh State of Central India has been selected as the study area for the entire research work. Raipur is considered one of the fastest-growing smart cities in India in terms of the urban area and urban population. The total study area extends from 21°11′22″N to 21°20′02″N and from 81°32′20″E to 81°41′50″E with an average elevation of 219–322 m (Fig. 1.1). The Mahanadi River flows to the east of the city of Raipur, and the southern side has dense forests. The Maikal Hills rise on the north-west of Raipur; on the north, the land rises and merges with the Chota Nagpur Plateau, which extends north-east across

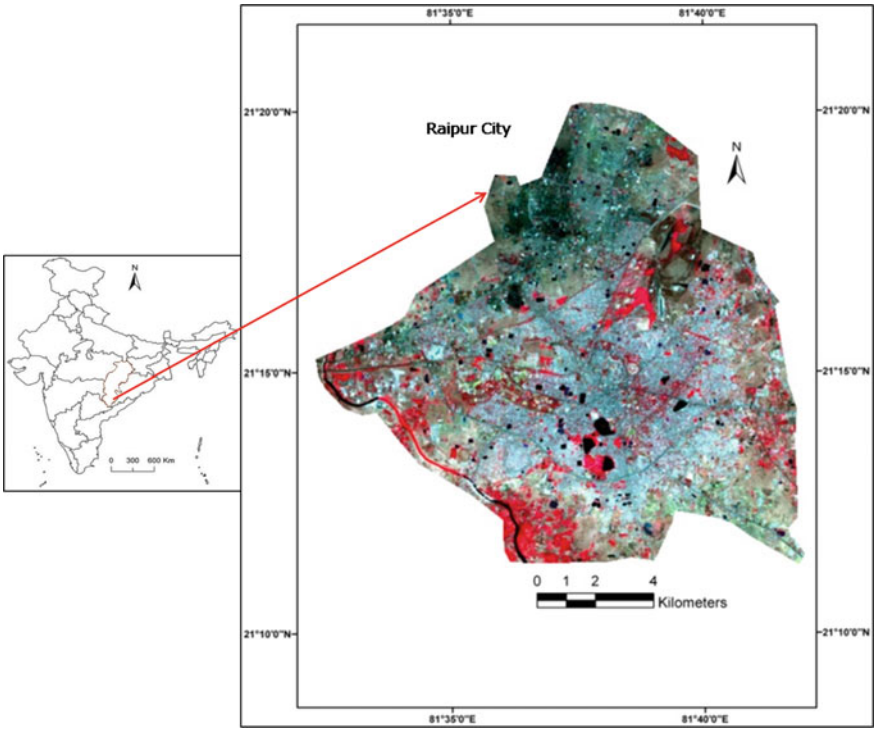

Fig. 1.1 Location of Raipur city

Table 1.1 Landsat data used in the study

Date of acquisition	Time	Path/Row	Sun elevation (°)	Sun Azimuth (°)	Cloud cover (%)	Earth-sun distance (astronomical unit)
5 Jun 2014	14:25:45	142/044	68.3821	83.3098	0.02	1.0146
25 Sep 2014	14:26:11	142/044	59.2100	134.1804	0.81	1.0030
12 Nov 2014	14:26:21	142/044	46.2266	152.4664	7.59	0.9899
30 Dec 2014	14:26:09	142/044	39.3441	150.8364	0.41	0.9834

Jharkhand state. The area is under a tropical wet and dry climate with four typical seasons (pre-monsoon, monsoon, post-monsoon, and winter). Pre-monsoon season extends from March to May. At that time hot and dry and dust storms occur frequently. June to September (rainy months) is significantly considered under the monsoon season. October and November months are often considered as the post-monsoon season, characterized by low pollution, moderate temperature, and moderate moisture content in plants and air, and a high percentage of green plants. December to February months (winter season) experience a cool and dry climate. The study area is also characterized by tropical mixed deciduous vegetation and mixed red soil.

Four Landsat 8 data sets acquired on 5 June, 25 September, 12 November, and 30 December of 2014 were selected for the current study (Table 1.1). Landsat 8 data of 30 m spatial resolution in visible and near-infrared (VNIR) bands (band 2, 3, 4, and 5) and shortwave infrared (SWIR) bands (band 6 and 7) with 100 m spatial resolution of thermal infrared (TIR) band (band10) were used for analyzing the spectral indices based downscaling technique.

1.3 Methodology

1.3.1 Resampling the TIR Band

At first, TIR band 10 (100 m resolution) of Landsat 8 TIRS data was resampled into 30 m by raster data aggregation method to coincide with Landsat 8 (Operational land imager) OLI data (30 m resolution). A further aggregation method is used to aggregate this 30 m resampled data into 960 m. This 960 m aggregated data was used in the relationship model, whereas the 30 m reference data was used in LST sharpening. The reference LST of 30 m pixel size was used in the validation of the sharpened LST 30 m pixel size. Subsequently, NDBI, NDWI, NDVI, and NMDI (each of 30 m pixel size) were estimated from the Landsat 8 OLI data of 30 m pixel size. Finally, the downscaled LST of 30 m pixel size was generated by using different remote sensing indices and compared the accuracy level by simple root mean square error (RMSE) method.

1.3.2 LST Retrieved from Landsat 8 TIRS data

Brightness temperature calculation and the emissivity correction are the main parts of LST determination by using Landsat 8 TIRS data. An atmospheric correction method was applied to obtain at-surface reflectance (Chavez 1996). The conversion formula (Zhou et al. 2016) from the at-sensor spectral radiance L to the at-sensor brightness temperature T_B is shown by Eq. 1.1.

$$T_B = \frac{K_2}{\ln(\frac{K_1}{L_\lambda} + 1)} \tag{1.1}$$

where, T_B is the brightness temperature in Kelvin (K), L_λ is the calibration constants, K_2 and K_1 are the spectral radiance (Wm^{-2} sr^{-1} mm^{-1}) [For Landsat 8 TIRS data, K_1 is 774.89 Wm^{-2} sr^{-1} mm^{-1}, K_2 is 1321.08], λ is the effective wavelength (11.335 μm for band 10 in Landsat 8 TIRS data).

LST is retrieved by Eq. 1.2:

$$\text{LST} = \frac{T_B}{1 + \left(\frac{\lambda \sigma T_B}{hc}\right) * \ln \varepsilon} \tag{1.2}$$

σ is Boltzmann constant (1.38×10^{-23} J/K), h is Plank's constant (626×106^{-34} Js), c is the velocity of light at a vacuum (2.998×10^{-8} m/s), ε is emissivity. Based on earlier studies, ε is determined as follows: if NDVI is $\geq$0.157 and $\leq$0.727, ε for that pixel is calculated by Eq. 1.3 (Van et al. 1993):

$$\varepsilon = 1.0094 + 0.047 \ln(\text{NDVI}) \tag{1.3}$$

NDVI $\geq$ 0.727 shows the green vegetation area and a constant value of 0.99 is assumed (Sobrino et al. 2004) and ε is set to 0.995 for water bodies and 0.92 for the other types of land surface features.

1.3.3 LST Sharpening Method Based on the Regression of LST and Remote Sensing Indices

LST is retrieved by using the TIR bands with coarse pixel size. The regression model between LST and remote sensing indices was widely established to obtain fine-resolution LST. If the relationship between LST and the indices does not vary at various resolutions, a fine-resolution LST can be determined by these indices using such relationships. Table 1.2 shows the used remote sensing indices to estimate the sharpened LST.

Table 1.2 Remote sensing indices used for LST downscaling

Indices	Description	Formula	References
NDVI	Normalized difference vegetation index	$\frac{NIR-Red}{NIR+Red}$	Tucker (1979)
NDWI	Normalized difference water index	$\frac{Green-NIR}{Green+NIR}$	McFeeters (1996)
NDBI	Normalized difference built-up index	$\frac{SWIR1-NIR}{SWIR1+NIR}$	Zha et al. (2003)
NMDI	Normalized multi-band drought index	$\frac{NIR-(SWIR1+SWIR2)}{NIR+(SWIR1+SWIR2)}$	Yuan (2007)

The original TsHARP algorithm was based on the LST-NDVI relationship. After the aggregation of NDVI into coarse-resolution (960 m) the coefficientsa_0, a_1 change with the moving window size. The same equation was applied to NDBI, NDWI, and NMDI. The fine-resolution (30 m) LST, ($\mathrm{LST}_{\mathrm{fine}}$) could be determined by Eq. 1.4:

$$\mathrm{LST}_{\mathrm{fine}} = a_0 + a_1 \cdot \mathrm{NDVI}_{\mathrm{fine}} \tag{1.4}$$

Therefore, from the coarse-resolution (960 m) LST, the sharpened LST with coarse-resolution ($\mathrm{LST}_{\mathrm{coarse}}$) could be determined by Eq. 1.5:

$$\mathrm{LST}_{\mathrm{coarse}} = a_0 + a_1 \cdot \mathrm{NDVI}_{\mathrm{coarse}} + \Delta T_{\mathrm{coarse}} \tag{1.5}$$

Then, a residual of LST ($\Delta T_{\mathrm{coarse}}$) is computed as the difference between the retrieved LST ($\mathrm{LST}_{\mathrm{coarse}}$) and the reference LST ($\mathrm{LST}_{\mathrm{ref}}$) by Eq. 1.6 (Kustas et al. 2003):

$$\Delta T_{\mathrm{coarse}} = \mathrm{LST}_{\mathrm{ref}} - \mathrm{LST}_{\mathrm{coarse}} \tag{1.6}$$

The residual $\Delta T_{\mathrm{coarse}}$ is introduced in the algorithm to take into account part of LST spatial variability that depends on the environmental factors other than the applied predictors, such as soil moisture, emissivity, or other remote sensing indices. Finally, downscaled fine-resolution (30 m) LST ($\mathrm{LST}_{\mathrm{down}}$) is estimated by Eq. 1.7:

$$\mathrm{LST}_{\mathrm{down}} = a_0 + a_1 \cdot \mathrm{NDVI}_{\mathrm{fine}} + \Delta T_{\mathrm{coarse}} \tag{1.7}$$

Where, the coarse-resolution regression coefficients are applied to fine-resolution remote sensing indices, adding the residual error of the corresponding coarse-resolution reference image to decrease the estimated error.

The NDVI-LST relationship is changeable with the changes in the land surface materials and seasons. Thus, different land surface indices can be examined along with NDVI to obtain higher accuracy level in the sharpened LST. The multiple least-squares linear regression method was applied as LST sharpening technique in some recent studies (Bonafoni 2016; Bonafoni et al. 2016). A number of land surface indices were also investigated separately to obtain a better sharpening (Essa et al. 2012). The present research work investigates the accuracy of NDVI, NDBI, NDWI, and NMDI individually in four different seasons.

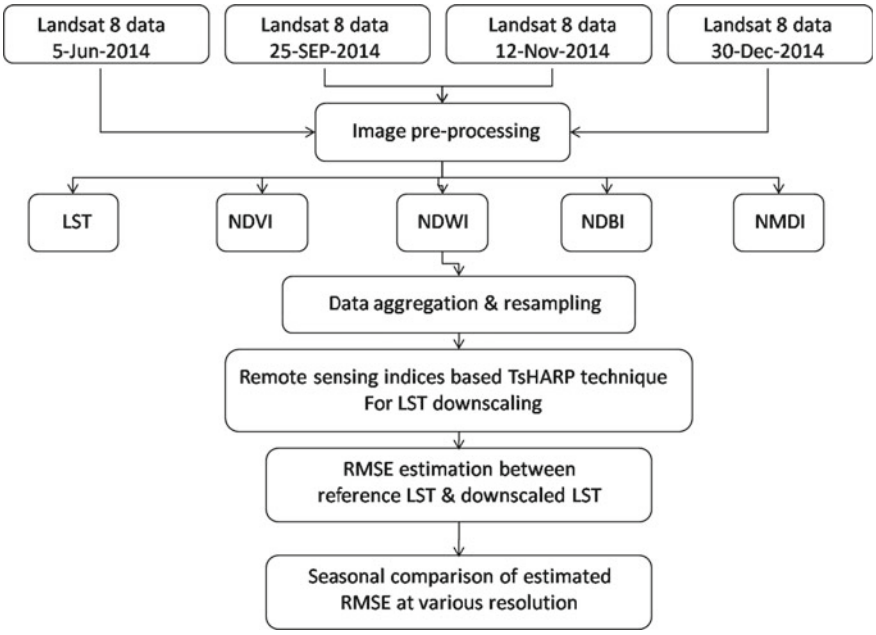

Fig. 1.2 Flowchart of methodology for the present study

1.3.4 Accuracy Assessment and Validation

The LST of 100 m coarse-resolution is aggregated to 960, 480, 240, and 120 m resolutions and these new aggregated data are known as reference data (LST_{ref}). The aggregated 960 m resolution LST was sharpened (LST_{down}) to 30 m resolution. RMSE statistics were applied to estimate the error in the sharpened LST with respect to the reference LST. RMSE was determined by Eq (1.8).

$$\mathrm{RMSE} = \sqrt{\left[\sum_{i=1}^{n} (\mathrm{LST}_{\mathrm{down}} - \mathrm{LST}_{\mathrm{ref}})^2\right]} \tag{1.8}$$

A flowchart of the methodology for the entire study is presented in Fig. 1.2.

1.4 Results and Discussion

Table 1.3 presents the variation of RMSE generated in the downscaled LST of four different images using NDBI, NDVI, NDWI, and NMDI-based TsHARP method. Percentage of RMSE in the Downscaled LST is increased with the decrease of resolution. This is a very common fact for the downscaled LST by using any remote

Table 1.3 Mean RMSE for downscaled LST for multi-date imageries

Remote sensing indices based downscaled LST	At 30 m resolution	At 120 m resolution	At 240 m resolution	At 480 m resolution
05-June-2014				
NDBI-based downscaled LST	1.09	0.96	0.91	0.87
NDVI-based downscaled LST	1.22	1.17	1.13	1.06
NDWI-based downscaled LST	1.24	1.20	1.15	1.07
NMDI-based downscaled LST	1.09	1.03	0.10	0.96
25-September-2014				
NDBI-based downscaled LST	1.11	0.81	0.70	0.61
NDVI-based downscaled LST	1.21	0.97	0.86	0.75
NDWI-based downscaled LST	1.26	1.08	0.98	0.86
NMDI-based downscaled LST	1.18	0.92	0.82	0.76
12-November-2014				
NDBI-based downscaled LST	0.91	0.72	0.65	0.60
NDVI-based downscaled LST	0.75	0.66	0.60	0.55
NDWI-based downscaled LST	0.74	0.66	0.60	0.54
NMDI-based downscaled LST	0.81	0.79	0.78	0.76
30-December-2014				
NDBI-based downscaled LST	0.80	0.71	0.65	0.59
NDVI-based downscaled LST	0.86	0.84	0.79	0.72
NDWI-based downscaled LST	0.86	0.84	0.80	0.72
NMDI-based downscaled LST	0.81	0.79	0.76	0.70

sensing indices. The lowest RMSE is found in NDBI-based downscaled LST, irrespective of any season. In this heterogeneous study area, built-up area is the most influential land feature regulating LST. The original TsHARP method was based on the correlation between LST and NDVI and it is regarded as one of the most popular methods for determining downscaled LST in forest areas or agricultural land (Agam et al. 2007; Jeganathan et al. 2011). Here, NDVI, NDWI, NDBI, and NMDI are used as the successful determining factors for generating downscaled LST. Accuracy level of the four used remote sensing indices is also estimated by using RMSE statistics. The best result (the lowest RMSE) is found in the post-monsoon season; irrespective of any remote sensing indices based downscaled LST. NMDI and NDBI-based sharpened LST shows a lower RMSE value for pre-monsoon, monsoon, and winter seasons; whereas NDVI and NDWI-based downscaled LST provides a lower RMSE value for the post-monsoon season. Figures 1.3, 1.4, 1.5, and 1.6 represent the values of RMSE for the NDVI, NDWI, NDBI, and NMDI-based sharpened LST. Generally, it is observed that the extremely high or low LST regions generate the high values of RMSE. The northwest and the southeast parts of the study area reflect the high RMSE values due to the heterogeneous nature of the land surface.

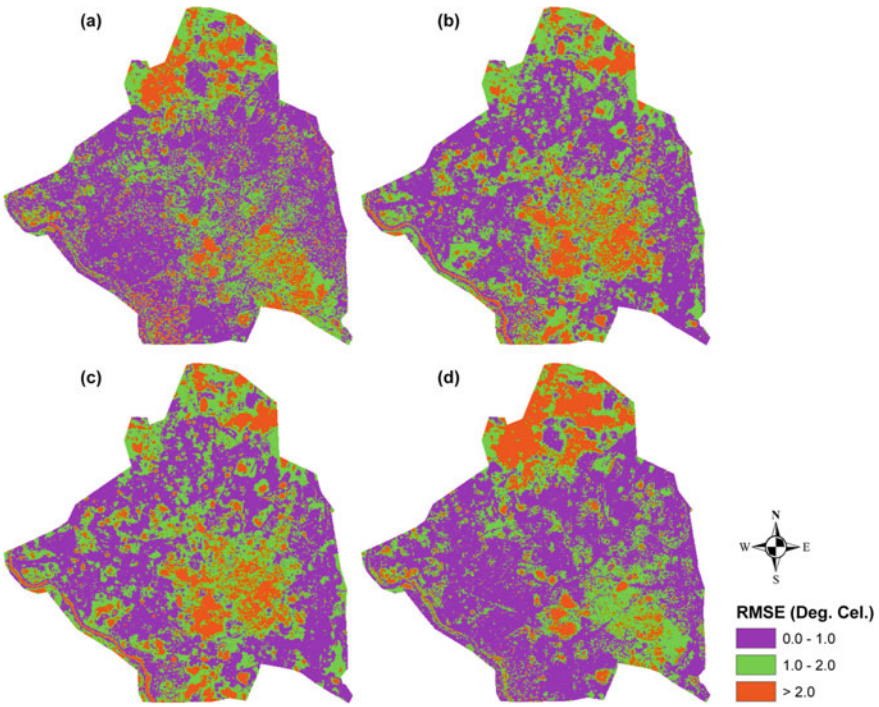

Fig. 1.3 RMSE at 30 m resolution for JUN-05-2014: **a** NDBI-based downscaled LST **b** NDVI-based downscaled LST **c** NDWI-based downscaled LST **d** NMDI-based downscaled LST

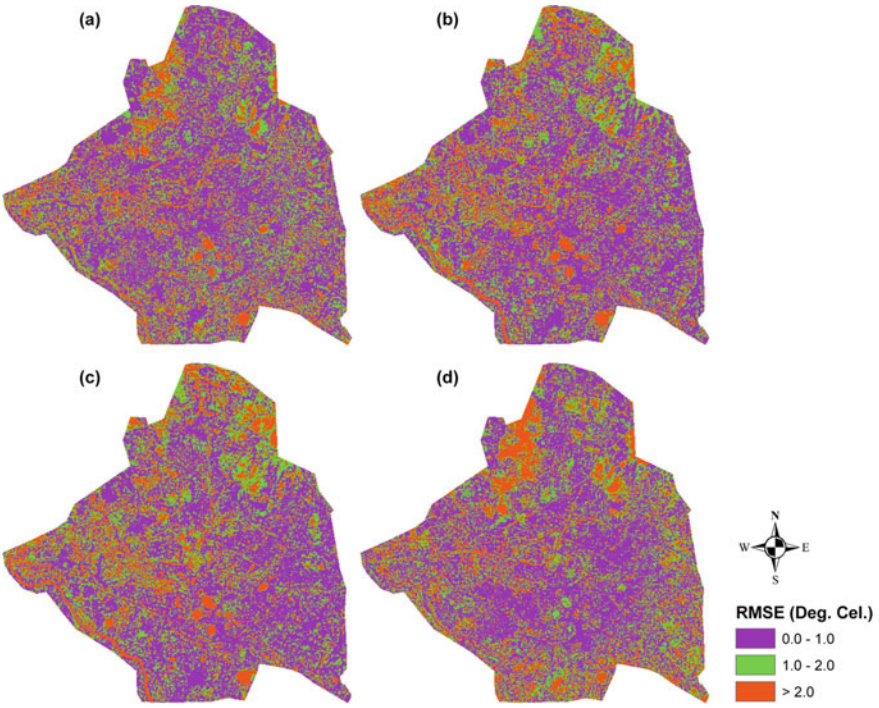

Fig. 1.4 RMSE at 30 m resolution for SEP-25-2014: **a** NDBI-based downscaled LST **b** NDVI-based downscaled LST **c** NDWI-based downscaled LST NMDI-based downscaled LST

Table 1.4 shows the values (in %) of RMSE for the different indices based sharpened LST at 30 m pixel size for the four multi-date imageries. In pre-monsoon image (5-JUN-2014), NDBI-based sharpening technique provides the best output (86.31% pixels are below 2 °C RMSE in downscaled LST), followed by NMDI-based technique (85.83% pixels < 2°C RMSE), NDWI-based technique (83.10% pixels < 2°C RMSE), and NDVI-based technique (82.46% pixels < 2°C RMSE). In monsoon image (25-SEP-2014), NDBI-based sharpening technique provides the lowest RMSE (84.61% pixels < 2°C RMSE), followed by NDVI-based technique (83.75% pixels < 2°C RMSE), NDWI-based technique (82.42% pixels < 2°C RMSE), and NMDI-based technique (82.21% pixels < 2°C RMSE). In the post-monsoon image (12-NOV-2014), NDVI-based sharpening technique provides the lowest RMSE (95.58% pixels < 2°C RMSE), followed by NDWI-based technique (95.53% pixels < 2°C RMSE), NDBI-based technique (95.08% pixels < 2°C RMSE), and NMDI-based technique (92.03% pixels < 2°C RMSE). In winter image (30-DEC-2014), NDBI-based sharpening technique provides the lowest RMSE (94.56% pixels < 2°C RMSE), followed by NMDI-based technique (94.42% pixels < 2°C RMSE), NDVI-based technique (94.36% pixels < 2°C RMSE), and NDWI-based technique (92.80% pixels < 2°C RMSE). Overall it is seen that the best result in

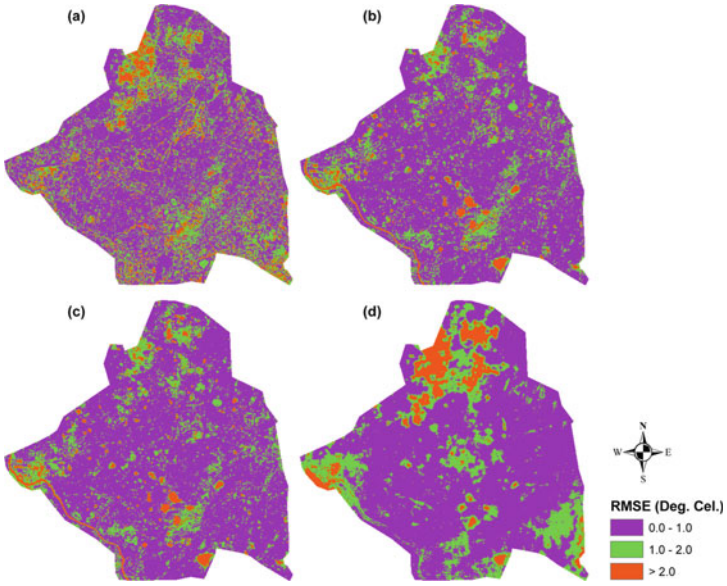

Fig. 1.5 RMSE at 30 m resolution for NOV-12-2014: **a** NDBI-based downscaled LST **b** NDVI-based downscaled LST **c** NDWI-based downscaled LST **d** NMDI-based downscaled LST

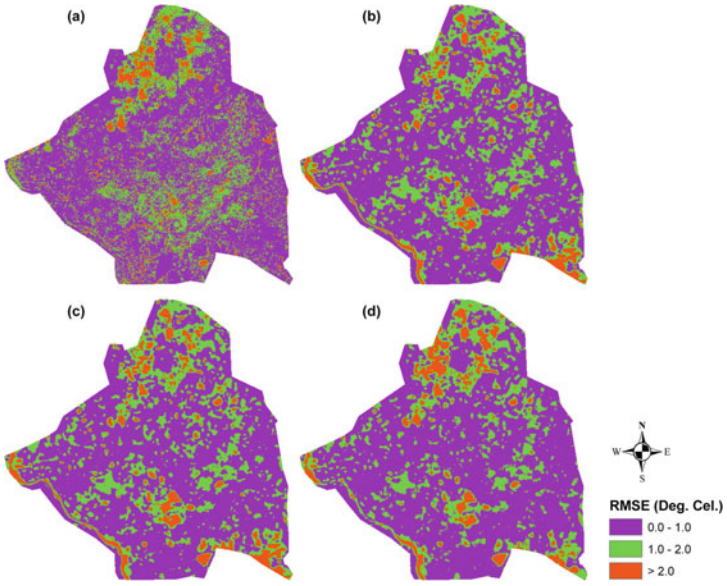

Fig. 1.6 RMSE at 30 m resolution for DEC-30-2014: **a** NDBI-based downscaled LST **b** NDVI-based downscaled LST **c** NDWI-based downscaled LST **d** NMDI-based downscaled LST

Table 1.4 Percentage of RMSE in downscaled LST (°C) at 30 m resolution

RMSE in LST (°C)	0.0–1.0	1.0–2.0	>2.0
5-JUN-2014			
NDBI-based downscaled LST	53.13%	33.18%	13.69%
NDVI-based downscaled LST	47.13%	35.33%	15.89%
NDWI-based downscaled LST	46.04%	37.06%	15.89%
NMDI-based downscaled LST	55.26%	30.47%	14.27%
25-SEP-2014			
NDBI-based downscaled LST	54.09%	30.52%	15.39%
NDVI-based downscaled LST	53.75%	30.00%	17.25%
NDWI-based downscaled LST	52.75%	29.67%	17.60%
NMDI-based downscaled LST	52.09%	30.21%	17.70%
12-NOV-2014			
NDBI-based downscaled LST	67.59%	27.49%	4.92%
NDVI-based downscaled LST	75.10%	20.48%	4.42%
NDWI-based downscaled LST	76.85%	18.68%	4.47%
NMDI-based downscaled LST	71.29%	21.44%	7.27%
30-DEC-2014			
NDBI-based downscaled LST	65.69%	27.88%	6.44%
NDVI-based downscaled LST	66.63%	26.77%	6.64%
NDWI-based downscaled LST	66.95%	25.85%	7.20%
NMDI-based downscaled LST	70.13%	23.29%	6.58%

remote sensing indices based TsHARP technique is found in the post-monsoon image due to high vegetation coverage and moisture content.

In the present study, four remote sensing indices (i.e., NDBI, NDVI, NDWI, and NMDI) based sharpened LST were analyzed. Results show that the lower RMSE was generated in the coarser resolution. The NDBI-based TsHARP model outperformed (RMSE ~0.87 °C in pre-monsoon image, RMSE ~0.61 °C in monsoon image, RMSE ~0.59 °C in post-monsoon image, and RMSE ~0.59 °C in winter image) any other indices-based TsHARP model at 480 m downscaled LST. At 30 m resolution, NDVI-based (RMSE ~ 0.75 °C) and NDWI-based (RMSE ~ 0.74 °C) downscaled LST achieve a higher accuracy than other indices based downscaled LST. Here, TsHARP algorithm was assessed with various indices and in various multi-date imageries and has achieved a good accuracy. At 30 m resolution downscaled LST, NDBI-based TsHARP model achieves an excellent accuracy level (>84% pixels have less than 2 °C RMSE, irrespective of all imageries).

1.5 Conclusion

The present research work focuses to evaluate the error produced in the downscaled LST estimated by the different remote sensing indices based TsHARP downscaling method at 30, 120, 240, and 480 m pixel size for four multi-date imageries selected from four different seasons in Raipur City of India. The original TsHARP downscaling technique was based on the relationship between NDVI and LST. Apart from NDVI, there are three more remote sensing indices (NDBI, NDWI, and NMDI) were separately applied in the present study to examine their effectiveness in estimating the RMSE for the downscaled LST. The results were examined at various levels of spatial resolutions (30, 120, 240, and 480 m). At 30 m spatial resolution, NDBI-based TsHARP technique generates the lowest RMSE. This result did not vary in different seasons. A decreasing trend of the RMSE is noticed with the increase of the resolution level. The post-monsoon season reveals the best result (lowest RMSE in downscaled LST) followed by the winter season.

Acknowledgment The authors' thanks to United States Geological Survey.

References

Agma N, Kurtas WP, Anderson MC, Li FQ, Colaizzi PD (2007) Utility of thermal sharpening over Texas high plains irrigated agricultural fields. J Geophys Res 112:D19110. https://doi.org/10.1029/2007JD008407

Agam N, Kustas WP, Anderson MC, Li FQ, Neale CMU (2007) A vegetation index based technique for spatial sharpening of thermal imagery. Remote Sens Environ 107:545–558

Anderson MC, Norman JM, Kustas WP, Houborg R, Starks PJ, Agam N (2008) A thermal-based remote sensing technique for routine mapping of land-surface carbon, water and energy fluxes from field to regional scales. Remote Sens Environ 112(12):4227–4241

Bonafoni S, Anniballe R, Gioli B, Toscano P (2016) Downscaling Landsat land surface temperature over the urban area of Florence. European J Remote Sens 49(1):553–569. https://doi.org/10.5721/EuJRS20164929

Bonafoni S (2016) Downscaling of Landsat and MODIS land surface temperature over the heterogeneous urban area of Milan. IEEE J Appl Earth Obs Remote Sens 9(5):2019–2027

Chen L, Yan GJ, Ren HZ, Li AH (2010) A modified vegetation index based algorithm for thermal imagery sharpening. In: Proceedings of IEEE international geoscience and remote sensing symposium, IGARSS '10. https://doi.org/10.1109/IGARSS.2010.5651428

Chen Y, Zhan W, Quan J, Zhou J, Zhu X, Sun H (2014) Disaggregation of remotely sensed land surface temperature: a generalized paradigm. IEEE Trans Geosci Remote Sens 52(9):5952–5965

Dennison PE, Charoensiri K, Roberts DA, Peterson SH, Green RO (2006) Wildfire temperature and land cover modeling using hyperspectral data. Remote Sens Environ 100(2):212–222

Dominguez A, Kleissl J, Luvall JC, Rickman DL (2011) High-resolution urban thermal sharpener (HUTS). Remote Sens Environ 115(7):1772–1780

Duan SB, Li ZL (2016) Spatial downscaling of MODIS land surface temperatures using geographically weighted regression: case study in northern China. IEEE Trans Geosci Remote Sens 54(11):6458–6469

Duan SB, Li ZL, Tang BH, Wu H, Tang R (2014) Generation of a time-consistent land surface temperature product from MODIS data. Remote Sens Environ 150:339–349

Essa W, van der Kwast J, Verbeiren B, Batelaan O (2013) Downscaling of thermal images over urban areas using the land surface temperature–impervious percentage relationship. Int J Appl Earth Obs Geoinf 23:95–108

Essa W, Verbeiren B, van der Kwast J, van de Voorde T, Batelaan O (2012) Evaluation of the DisTrad thermal sharpening methodology for urban areas. Int J Appl Earth Obs Geoinf 19:163–172

Gualtieri JA, Chettri S (2000) Support Vector Machines for classification of hyperspectral data. In: Proceedings of the 2000 international geoscience and remote sensing symposium (IGARSS 2000), Honolulu, HI, USA, 24–28 July 2000. IEEE, Honolulu, HI, USA, pp 813–815

Govil H, Guha S, Dey A, Gill N (2019) Seasonal evaluation of downscaled land surface temperature: a case study in a humid tropical city. Heliyon 5(6):e01923. https://doi.org/10.1016/j.heliyon.2019.e01923

Govil H, Guha S, Diwan P, Gill N, Dey A (2020) Analyzing Linear Relationships of LST with NDVI and MNDISI Using Various Resolution Levels of Landsat 8 OLI and TIRS Data. In: Sharma N, Chakrabarti A, Balas V (eds) Data management, analytics and innovation. Advances in intelligent systems and computing, vol 1042. Springer, Singapore, pp 171–184. https://doi.org/10.1007/978-981-32-9949-8_13

Guha S, Govil H (2020) An assessment on the relationship between land surface temperature and normalized difference vegetation index. Environ Dev Sustain. https://doi.org/10.1007/s10668-020-00657-6

Guha S, Govil H, Dey A, Gill N (2018) Analytical study of land surface temperature with NDVI and NDBI using Landsat 8 OLI and TIRS data in Florence and Naples city, Italy. Eur J Remote Sens 51(1):667–678. https://doi.org/10.1080/22797254.2018.1474494

Guha S, Govil H, Mukherjee S (2017) Dynamic analysis and ecological evaluation of urban heat islands in Raipur city, India. J Appl Remote Sens 11(3):036020. https://doi.org/10.1117/1.JRS.11.036020

Guha S, Govil H, Diwan P (2019) Analytical study of seasonal variability in land surface temperature with normalized difference vegetation index, normalized difference water index, normalized difference built-up index, and normalized multiband drought index. J Appl Remote Sens 13(2):024518. https://doi.org/10.1117/1.JRS.13.024518

Guha S, Govil H, Dey A, Gill N (2020) A case study on the relationship between land surface temperature and land surface indices in Raipur City. Geogr Tidsskr, India. https://doi.org/10.1080/00167223.2020.1752272

Guha S, Govil H, Gill N, Dey A (2020) Analytical study on the relationship between land surface temperature and land use/land cover indices. Ann GIS. https://doi.org/10.1080/19475683.2020.1754291

Jeganathan C, Hamm NAS, Mukherjee S, Atkinson PM, Raju PLN, Dadhwal VK (2011) Evaluating a thermal image sharpening model over a mixed agricultural landscape in India. Int J Appl Earth Obs Geoinf 13(2):178–191

Kustas WP, Norman JM, Anderson MC French AN (2003) Estimating subpixel surface temperatures and energy fluxes from the vegetation index–radiometric temperature relationship. Remote Sens Environ 85(4):429–440

Li ZL, Tang BH, Hua Wu, Ren H, Yan G, Wan Z, Trigo IF, Sobrino JA (2013) Satellite-derived land surface temperature: current status and perspectives. Remote Sens Environ 131:14–37

McFeeters SK (1996) The use of the Normalized Difference Water Index (NDWI) in the delineation of open water features. Int J Remote Sens 17(7):1425–1432. https://doi.org/10.1080/01431169608948714

Moran MS (1990) A window-based technique for combining Landsat Thematic Mapper thermal data with higher-resolution multispectral data over agricultural lands. Photogramm Eng Remote Sens 56(3):337–342

Mpelasoka FS, Mullan AB, Heerdegen RG (2001) New Zealand climate change information derived by multivariate statistical and artificial neural networks approaches. Int J Climatol 21:1415–1433

Mukherjee S, Joshi PK, Garg RD (2015) Evaluation of LST downscaling algorithms on seasonal thermal data in humid subtropical regions of India. Int J Remote Sens 36(10):2503–2523
Nichol J (2009) An emissivity modulation method for spatial enhancement of thermal satellite images in urban heat island analysis. Photogramm Eng Remote Sens 75(5):547–556
Nishii R, Kusanobu S, Tanaka S (1996) Enhancement of low spatial resolution image based on high resolution bands. IEEE Trans Geosci Remote Sens 34(5):1151–1158
Pardo-Igúzquiza E, Chica-Olmo M, Atkinson PM (2006) Downscaling cokriging for image sharpening. Remote Sens Environ 102:86–98
Pardo-Igúzquiza E, Rodríguez-Galiano VF, Chica-Olmo M, Atkinson PM (2011) Image fusion by spatially adaptive filtering using downscaling cokriging. ISPRS J Photogram Remote Sens 66(3):337–346
Sandholt I, Rasmussena K, Andersen J (2002) A simple interpretation of the surface temperature/vegetation index space for assessment of surface moisture status. Remote Sens Environ 79:213–224
Sobrino JA, Jiménez-Muñoz JC, Paolini L (2004) Land surface temperature retrieval from Landsat TM 5. Remote Sens Environ 90(4):434–440
Stathopoulou M, Cartalis C (2009) Downscaling AVHRR land surface temperatures for improved surface urban heat island intensity estimation. Remote Sens Environ 112:2592–2605
Tucker CJ (1979) Red and photographic infrared linear combinations for monitoring vegetation. Remote Sens Environ 8(2):127–150
Van D, Griend AA Owe M (1993) On the relationship between thermal emissivity and the normalized difference vegetation index for natural surfaces. Int J Remote Sens 14:1119–1131
Voogt JA, Oke TR (2003) Thermal remote sensing of urban climates. Remote Sens Environ 86(3):370–384
Wan Z, Dozier J (1996) Generalized split-window algorithm for retrieving land-surface temperature from space. IEEE Trans Geosci Remote Sens 34:892–905
Wan Z, Li ZL (1997) A physics-based algorithm for retrieving land-surface emissivity and temperature from EOS/MODIS data. IEEE Trans Geosci Remote Sens 35(4):980–996
Wan Z, Li ZL (2008) Radiance-based validation of the V5 MODIS land surface temperature product. Int J Remote Sens 29(17/18):5373–5395
Weng Q, Fu P (2014) Modeling diurnal land temperature cycles over Los Angeles using downscaled GOES imagery. ISPRS J Photogramm Remote Sens 97:78–88
Weng QH, Lu DS, Schubring J (2004) Estimation of land surface temperature vegetation abundance relationship for urban heat island studies. Remote Sens Environ 89:467–483
Yang Y, Yao L (2009) The influence of urban design factors on urban heat environment in urban residential area with remote sensing. In: Proceedings of the sixth international symposium on multispectral image processing and pattern recognition, Yichang, China, 30 October–1 November 2009; International Society for Optics and Photonics. Bellingham, WA, USA, pp 74984K
Yang GJ, Pu RL, Zhao CJ, Huang WJ, Wang JH (2011) Estimation of subpixel land surface temperature using an endmember index based technique: a case examination on ASTER and MODIS temperature products over a heterogeneous area. Remote Sens Environ 115(5):1202–1219
Yang G, Pu R, Huang W, Wang J, Zhao C (2010) A novel method to estimate subpixel temperature by fusing solar-reflective and thermal-infrared remote-sensing data with an artificial neural network. IEEE Trans Geosci Remote Sens 48(4):2170–2178
Yuan F, Bauer ME (2007) Comparison of impervious surface area and normalized ifference vegetation index as indicators of surface urban heat island effects in Landsat imagery. Remote Sens Environ 106:375–386
Zakšek K, Oštir K (2012) Downscaling land surface temperature for urban heat island diurnal cycle analysis. Remote Sens Environ 117:114–124
Zhang Y (2015) Land surface temperature inversion and downscaling research for Landsat 8. Master Thesis, Hohai University, Nanjing, China

Zhan W, Chen Y, Zhou J, Wang J, Liu W, Voogt J, Zhu X, Quan J, Li J (2013) Disaggregation of remotely sensed land surface temperature: literature survey, taxonomy, issues, and caveats. Remote Sens Environ 131:119–139

Zha Y, Gao J, Ni S (2003) Use of normalized difference built-up index inautomatically mapping urban areas from TM imagery. Int J Remote Sens 24(3):583–594

Zhou J, Liu S, Li M, Zhan W, Xu Z, Xu T (2016) Quantification of the scale effect in downscaling remotely sensed land surface temperature. Remote Sens 8:975. https://doi.org/10.3390/rs8120975

Chapter 2
Frequency Ratio Approach for Landslide Susceptibility Mapping of Phonda Ghat of Maharashtra

Abhijit S. Patil, S. S. Panhalkar, and Sambhaji D. Shinde

Abstract The Western Ghats of Maharashtra frequently suffer from landslides caused by various geo-environmental factors. The prime aim of this study is to produce a suitable landslide susceptibility map of the Phonda Ghat region of Western Ghats of Maharashtra. The present study reveals the application of the Frequency Ratio (FR) model using GIS techniques to assess the influence of geo-environmental factors on the occurrence and distribution of landslides. The FR model is derived from the landslide inventory and geo-environmental factors viz, Slope angle, Slope curvature, Aspect, Relief, Drainage, Land Use/Land Cover, Lineament, Geology, NDVI, Geomorphology, Rainfall, and Soil depth. The main focus of this investigation is to categorize the land surface of the study area on the basis of the degree of potential landslide susceptibility. The model is validated by performing the AUC curve method. The result shows the landslide susceptibility map, which demarcated more than 13% of the land area of the study region, is highly potential to the landslide.

Keywords Frequency ration (FR) · Phonda ghat · GIS · Landslide susceptibility

2.1 Introduction

Landslides are natural hazards that are caused by several geophysical & anthropogenic factors. These landslides are dangerous, occur suddenly, and cause significant damages (Guzzetti et al. 1999). Generally, landslides occur in mountainous and rugged terrain all over the world. The Himalayas and Western Ghats of India characterize highly undulating and mountainous terrain. The Western Ghats contain a significant highland range running parallel to the western coast of India. Several studies on landslide mapping have shown that the Western Ghats region of India is highly vulnerable to landslide hazards (Ramchandra et al. 2010; Patil et al. 2019). Remote Sensing (RS) and Geographical Information Systems (GIS) play a crucial role as they are used as the leading tools for detection, classification, analysis, and

A. S. Patil · S. S. Panhalkar (✉) · S. D. Shinde
Department of Geography, Shivaji University Kolhapur, Kolhapur, Maharashtra, India

R. B. Singh et al. (eds.), *Remote Sensing and Geographic Information Systems for Policy Decision Support*, Advances in Geographical and Environmental Sciences,
https://doi.org/10.1007/978-981-16-7731-1_2

mapping of landslides. Recently, landslide hazard mapping is quite possible due to easy access and a fine resolution of remote sensing data and thematic layers using Geographical Information Systems (Gupta et al. 1990; Scaioni 2013; Qiao et al. 2013). The study of landslide hazard mapping based on Remote Sensing and GIS techniques is carried out by a number of authors (Mantovani et al. 1996; Gupta et al. 1999; Saha et al. 2002; Lee et al. 2007). In recent times, a number of methods and techniques of GIS and RS for landslide mapping have been proposed and applied (Wang et al. 2005; Pardeshi et al. 2013; Balasubramani K et al. 2013; Merrett et al. 2013; Patil et al. 2020).

The advances in GIS and Multi-Criteria Decision Analysis (MCDA) have changed the perspective of the landslide study. The integration of GIS and MCDA creates new tools that help for the management of data and spatial analysis (Guzzetti et al. 1999; Kayastha et al. 2013). Bayes Ahmed (2014) has used three different methods of Geographical Information System based on Multi-Criteria Decision Analysis methods. Artificial Hierarchy Process (AHP), Weighted Linear Combination (WLC), and Ordered Weighted Average (OWA) were applied scientifically to assess the landslide susceptible areas in Chittagong Metropolitan Area, Bangladesh. van Wstern et al. (2011) have given an overview of a recent research project between GSI, the National Remote Sensing Centre (NRSC), and ITC (the Netherland) on how the existing technique for landslide inventory, susceptibility, and hazard assessment for India could be improved, and how these could be used for quantitative risk assessment. Westen et al. (1999) have made a comparative study of landslide hazard maps of the Alpago region in Italy to get a better insight into decision rules in their direct mapping approach and to improve GIS-based indirect mapping techniques. The present study has been carried out to demarcate the landslide susceptibility zone of the PhondaGhat region of Maharashtra using Remote Sensing and GIS techniques.

Over the last few years, landslide susceptibility assessment is considered as a significant and beneficial approach to predict the probability of spatial distribution of landslide occurrence under certain geo-environmental circumstances. Thus, it is valuable to do a landslide susceptibility assessment for landslide disaster risk reduction (Srivastava et al. 2010; Mahalingam et al. 2016; Persichillo et al. 2016).In the past years, many models have been applied for landslide susceptibility assessment, and these models can be mainly divided into qualitative models and quantitative models (Devkota et al. 2013; Wu et al. 2016). The frequency ratio (FR) is a quantitative model that can be easily applied and provides high accuracy for landslide susceptibility assessment (Lee and Talib 2005; Lee and Pradhan 2006; Yilmaz 2009).

2.2 Study Area

The entire study area is located towards the extreme southern part of the Maharashtra state of India. It lies between 16°17′35″N to 16°26′41″N latitude and 73°46′52″E to 73°56′ 37″E longitude thereby covering a total geographical area of approximately 291 km^2 (Fig. 2.1). It is extended in part of Kolhapur and Ratnagiri districts. The average height of the study area is about 525 m. The maximum height is 945 m, which is observed towards the ridgeline area of a western ghat in the study area. The lowest point is the extreme west part, where the height is 105 m above sea level. The parts of the Radhanagari reservoir, Kurli dam, Kalammawadi, and other small dams, have occupied 24.5 km^2 of the study region.

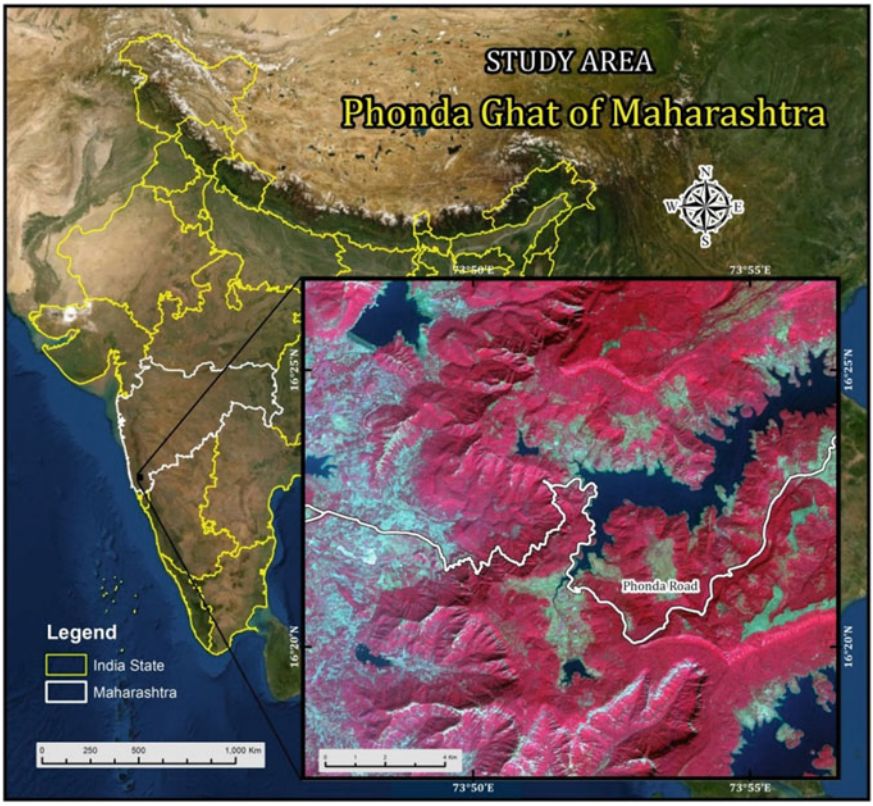

Fig. 2.1 Geographical location of study area

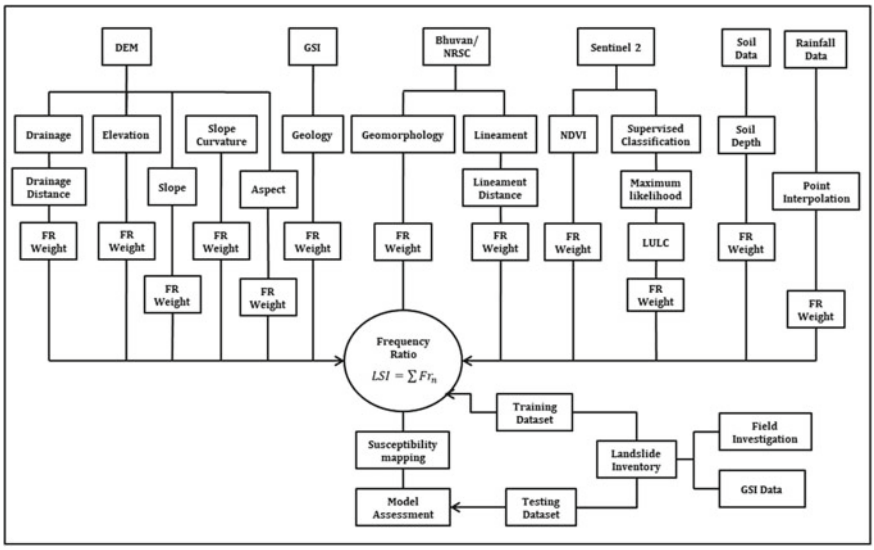

Fig. 2.2 Research methodology

2.3 Research Methodology

The processes of Landslide Susceptibility Assessment (LSA) include data sources preparation, landslide-related environmental factors analysis, and calculation of landslide susceptibility indexes (LSI). A precise and effective prediction of landslide susceptibility index is essential for producing the landslide susceptibility map (LSM).

The main object of this study is to prepare LSM using the Frequency Ratio model for the PhondaGhat region.

In the beginning, the landslide inventory and other data are obtained from different data sources and landslide-associated 12 geo-environmental factors are studied. Further, the FR values of these geo-environmental factors are calculated. Then third, the FR model is used to calculate the LSI based on landslide inventories, selected environmental factors, and field investigation data. Meanwhile, the LSM of the PhondaGhat area is produced in ArcGIS and QGIS software. Finally, to assess the reliability and efficiency of the method, the Area Under Curve (AUC) is calculated using a cumulative percentage of testing landslide inventory and susceptible zone. Figure 2.2 is providing a brief and systematic flow of entire research work.

2.3.1 *Frequency Ratio Method*

The FR method is used to study the relationships between past landslide sites and subclasses of each potentially influential factor (Lee and Min 2001; Lee and Pradhan 2006).In this investigation, all the influential factors are classified into their respective classes and the frequency ratio (Eq. 2.1.1) is calculated based on each class, i. Further, the normalized frequency ratio (Eq. 2.1.2) is computed for all classes in the same factor. The summation of the normalized frequency ratio of each influential factor results in the landslide susceptibility index (Eq. 2.1.3) (Pradhan and Lee 2010; Wang et al. 2016).

Fr_i (Frequency Ratio of class *i*):

$$\mathrm{Fr}_i = \frac{\left(\frac{\mathrm{NL}_i}{\mathrm{NL}_t}\right)}{\left(\frac{\mathrm{NC}_i}{\mathrm{NC}_t}\right)} \tag{2.1.1}$$

Fr_n (Normalized Frequency Ratio):

$$\mathrm{Fr}_n = \frac{\mathrm{Fr}_i}{\sum \mathrm{class}i\mathrm{Fr}\ ,} \tag{2.1.2}$$

LSI (Landslide Susceptibility Index):

$$\mathrm{LSI} = \sum \mathrm{Fr}_n \tag{2.1.3}$$

where

NL_i = number of landslides in class *i*.

NL_t = total number of landslide.

NC_i = number of cell points of class *i*.

NC_t = total number of cell points.

2.4 Result and Discussion

2.4.1 *Landslide Inventory*

The initial step to produce the landslide susceptibility map is the production of updated landslide inventory maps (Varnes 1984; Choi and Min 2004). The Geological Survey of India, field investigation, and local land resource departments have

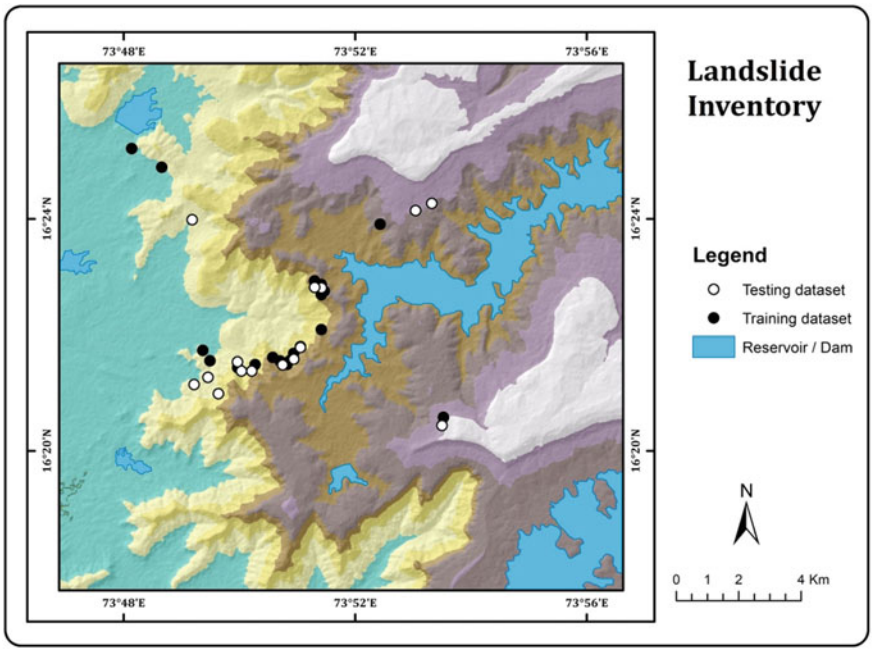

Fig. 2.3 Landslide inventory

identified 34 landslide point locations in the study area (Fig. 2.3). In which, 20 landslides are used as a training dataset for FR model while 14 are utilized for the model testing or assessment. The landslide inventory of the study area shows that most of the landslides have occurred along the road.

2.4.2 Influential Geo-environmental Factors of Landslide

2.4.2.1 Geology

Geology or rock type is an important factor in controlling slope stability. It controls the nature of the weathering and erosion of the region (Citrabhuwana et al. 2016). The Western Ghats is the vital orographic feature of Peninsular India, which denotes the long-lived uplift history. It is rugged, faulted, and eroded edge of the Deccan Plateau (Envi. & Forest Gov of India 2013). The spatial distribution of different rock types of the study area with geological formation is shown in Fig. 2.4. It has been observed that nine geological features existed in the study area viz. Deccan trap, Essentially Aa simple flow, Granite, Laterite, Mainly Aasimple flow, Megacryst flow, Quartz chlorite amphibole schist, Quartzite (Sedimentary) and Shale.

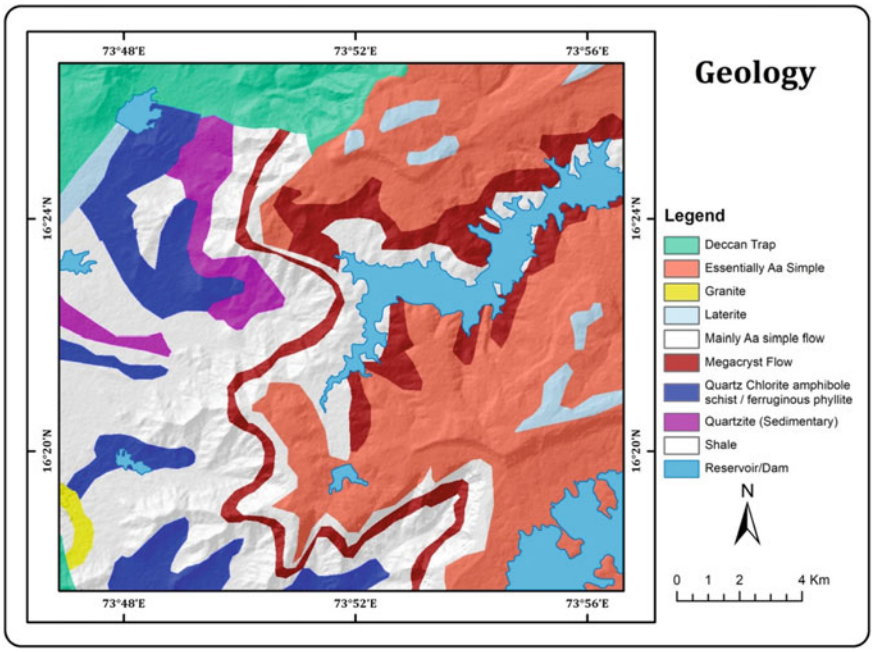

Fig. 2.4 Geology

2.4.2.2 Geomorphology

Geomorphology is science that studies the origin, evolution, and development of topographic features and how those topographies associate to form landscapes (Stetler 2014). The South Indian tectonic shield landscape is believed to have formed through a slow geomorphic process (Radhakrishna 1993). The spatial distribution of different landforms of the study area (Geomorphic Units) is shown in Fig. 2.5. It is being observed that six geomorphic landforms existed in the study area viz. Anthropogenic Origin-Anthropogenic Terrain, Denudational Origin-Mod Dissected Upper Plateau, Denudational Origin-Pediment-PediPlain Complex, Structural Origin-Low Dissected Lower Plateau, Structural Origin-Moderately Dissected Lower Plateau and Waterbody.

2.4.2.3 Drainage

In Peninsular India, Western Ghats is the major water divider for the east and west-flowing rivers. The rivers originate in the Western Ghats, flow down the steep scarp on the west and meet to the Arabian Sea, or they flow east, on the gently sloping plateaus and drain into the Bay of Bengal. The study area includes large numbers of small gullies, small streams, and tributaries (Fig. 2.6). The landslide analysis has

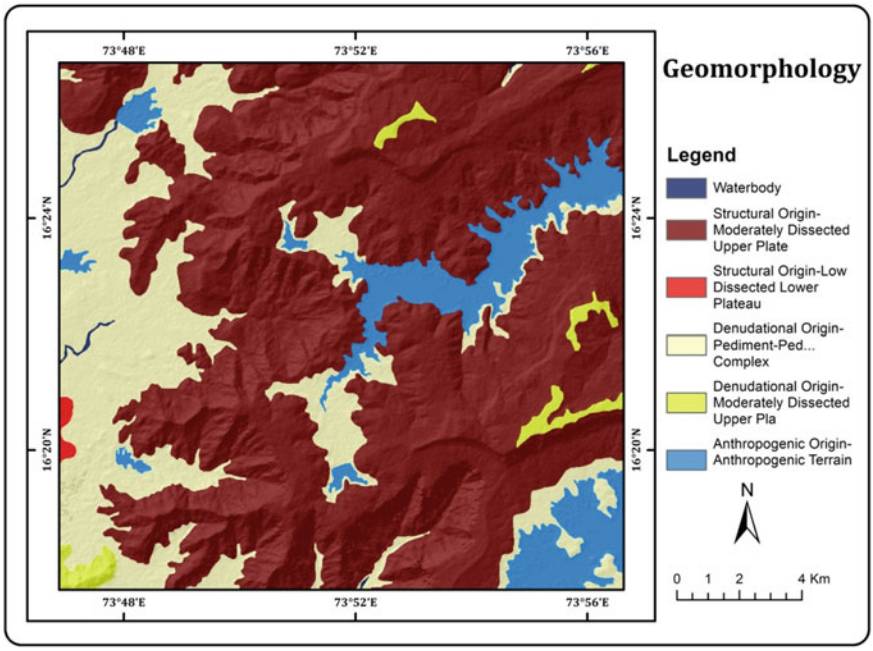

Fig. 2.5 Geomorphology

been done by using drainage distance. The drainage distance has been categorized into five categories in the study area viz. less than 200, 500, 1000, 2000 m, and more than 10000 m.

2.4.2.4 Relief

The relief of the Western Ghats of Maharashtra has two major parts that are Konkan and Ghat (Desh) region. Both regions reveal greater differences in elevation. The relief differs remarkably from place to place and the wide relief changes are seen in the west–east direction of Western Ghats with local variations (Deshpande 1971). The part of Konkan of the study area shows the greatest changes in elevation, whereas the plateau (Ghati) part is quite a monotonous feature with the least elevation change (Fig. 2.7). The relief is categorized into seven categories in the study area viz. less than 110 m, 111–241 m, 242–416 m, 417–565 m, 566–664 m, 665–785 m, and 786–948 m. The maximum height is 948 m, which is observed along the ridgeline of the Western Ghats in the study area. The lowest point is towards the extreme west part, where the height is 105 m above sea level. Comparatively, the western part of the study area has a lower elevation, whereas the eastern part of the study area is covered by higher elevation.

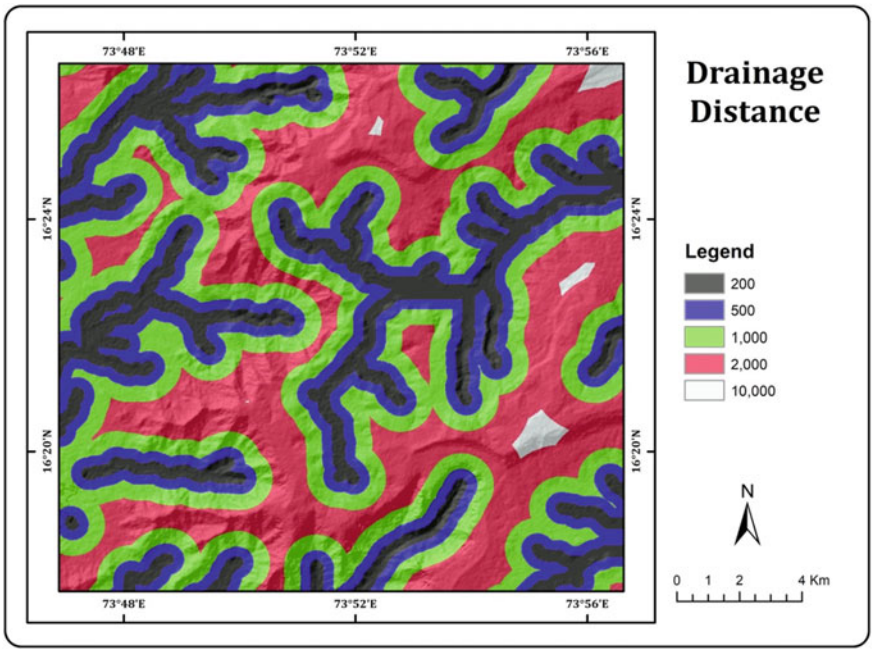

Fig. 2.6 Drainage distance

2.4.2.5 Slope

The geometry of slope is an important factor that affects slope stability (Chaulya et al. 2016). The degree or angle of slope very much governs the movement and extent of the landslide (Donnarumma et al. 2013; Chen et al. 2016). The slope map of the study area is prepared by using ALOS Pulsar DEM, which has 12.5 m spatial resolution. The slope of the entire study area has been divided into five categories, from 0 to 78 degrees range (Fig. 2.8). The ridgeline of the mountain range of Western Ghats is located at the center of the study area, which shows a greater degree of slope.

2.4.2.6 Land Use/Land Cover

Land Use and Land Cover (LU/LC) replicates the physical and socio-economical characteristics of land or surface of the earth (Mohammed et al. 2014). According to Rajan K.S and Shibasaki R (2001), Land Use and Land Cover is a significant component in understanding the interactions of human activities with the environment. The LU/LC map of the study area is prepared with a depiction of LU/LC unit viz. Barren Rocky, Deciduous Forest, Evergreen / Semi-evergreen, Fallow, Plantation, River, Rural, Scrub Forest, and Water Bodies/Reservoir (Fig. 2.9).

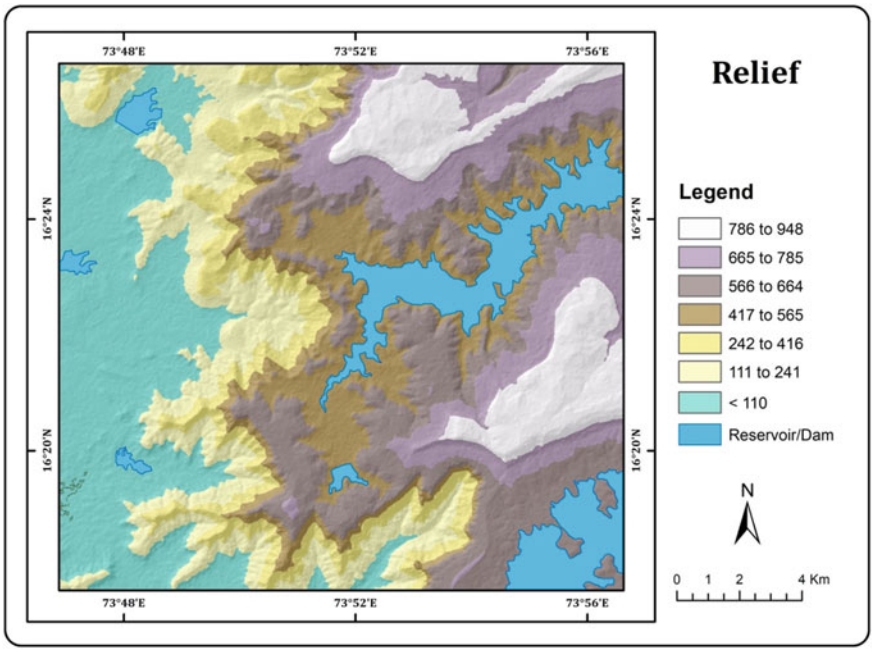

Fig. 2.7 Relief

2.4.2.7 Lineament

The lineaments are significant lines of the landscape caused by joints and faults, revealing the hidden architecture of the rock basement (Hobbs 1904). The structural geology of the area has a significant influence on the occurrence of landslides (Anbalagan and Singh 1996; Atkinson et al. 1998). Occurrences of landslides are mostly acknowledged in the areas of linear patterns or lineaments (Nagarajan et al. 1998a, 1998b). The lineaments are detected and mapped in the study area by using remote sensing data and GIS techniques. The Lineament Distance has been used as a landslide influencing factor, which is categorized into seven categories viz. 500, 1000, 3000 and 5000 m. While analyzing the lineament map, it is observed that about 39 lineaments have been passing through the area under investigation (Fig. 2.10).

2.4.2.8 Rainfall

Rainfall is recognized as a main triggering factor to create slope instability and further causing the occurrence of a landslide (Chen et al. 2003; Seul Bi Kim et al. 2015; OgbonnayaIgwe 2015; Aristizábal et al. 2017). In the study area, the western slopes of the mountains experience heavy rainfall (during the southwest monsoon from June to September), while the eastern slopes have moderate rainfall. The great

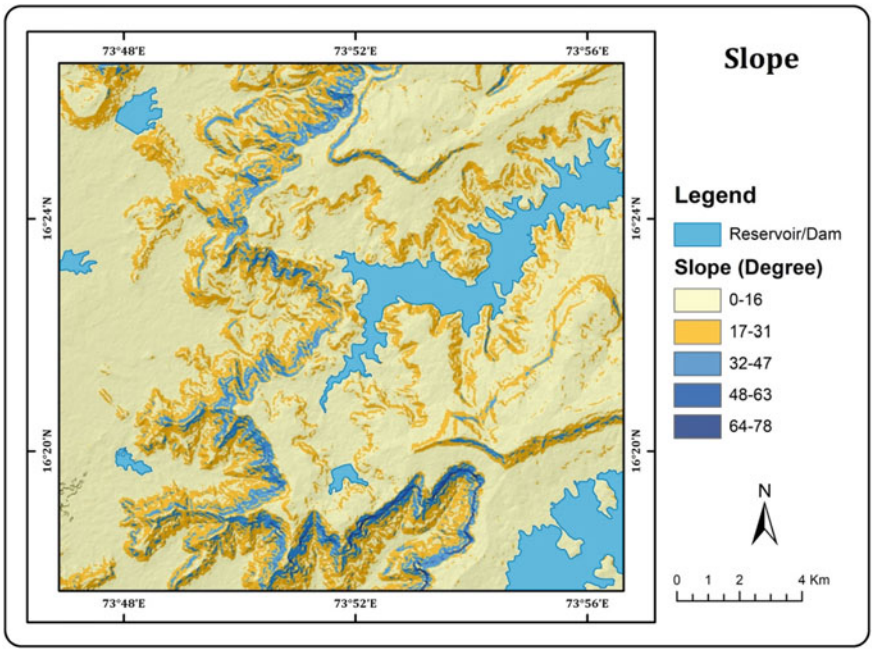

Fig. 2.8 Slope

variation of rainfall patterns in the Western Ghats also produces a great variety of vegetation types (Envi. & Forest Gov of India 2013). The distribution of rainfall in the study area is divided into four categories viz. 3001–3200 mm, 3201–3400 mm, 3401–3600 mm, and 3601–3800 mm. The annual average rainfall in this part is 3400 mm. The isohyet of rainfall of the study area reveals that the rainfall increases from east to west (Fig. 2.11).

2.4.2.9 NDVI

The dense vegetation cover reduces the impact of weathering and erosion, which increases slope stability, whereas the lands without vegetation cover are usually enhancing weathering and erosion of the slope. Thus it is responsible for slope failure (Normaniza et al. 2011; Normaniza et al. 2018). The wide variation of rainfall patterns in the Western Ghats also produces a great variety of vegetation types (Envi. & Forest Gov of India 2013). Ultimately, Normalized Difference Vegetation Index (NDVI) is an essential parameter to detect the concentration of vegetation for landslide studies. In the present research, the NDVI map is prepared by using Sentinel 2 satellite images (Fig. 2.12).

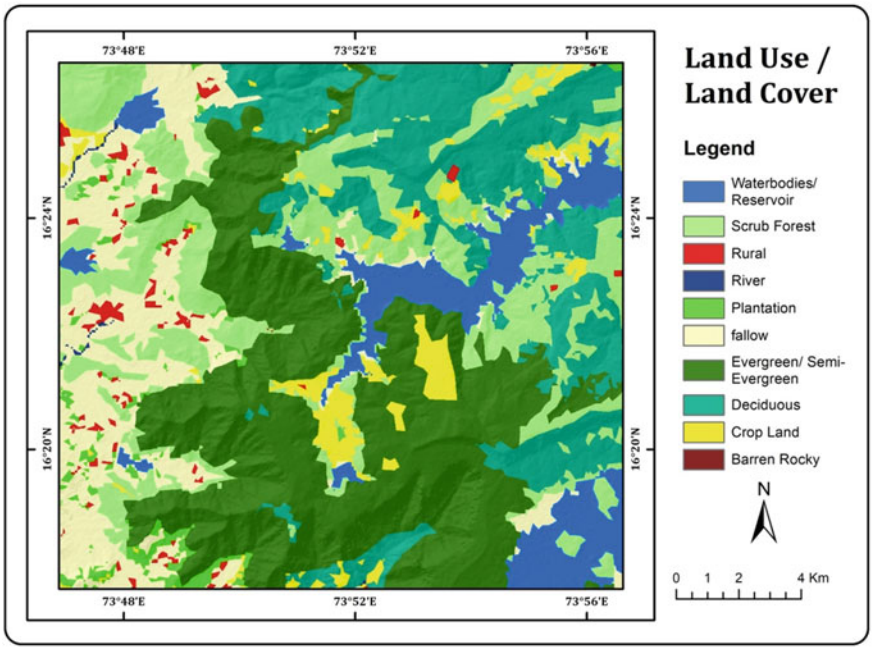

Fig. 2.9 Land use/land cover

Aspect

Aspect is one of the important topographic factors which affects a landslide (Hossein et al. 2014). The orientation of slope affects the distribution of sunlight, wind, and rainfall, thus indirectly affect to landslide occurrence (Clerici et al. 2006). The aspect map of the study area (Fig. 2.13) was produced by using the aspect tool of ArcGIS Software. The aspect of the study area is categorized into flat, north, northeast, east, southeast, south, southwest, west, and northwest facing classes from 0 to 360°.

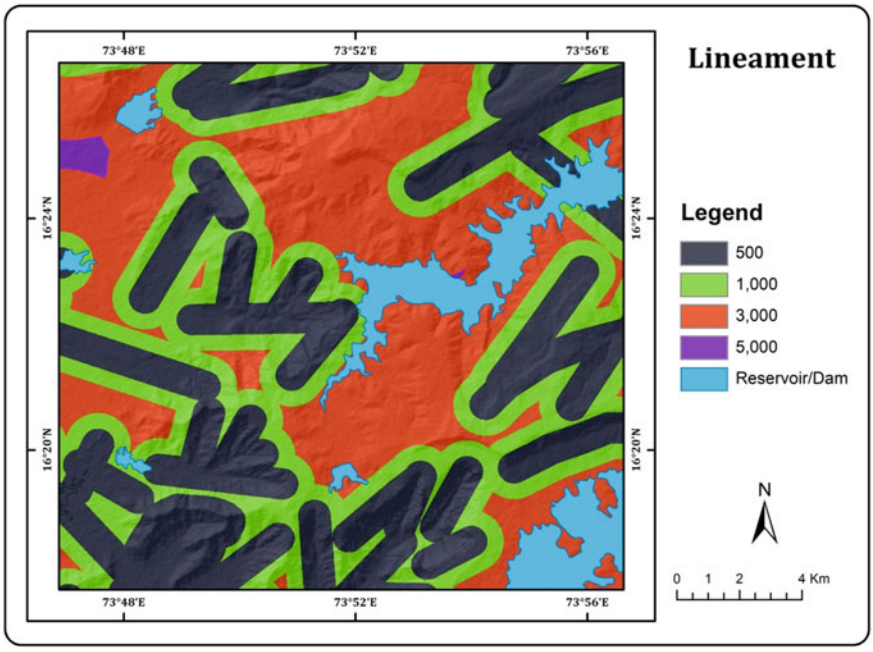

Fig. 2.10 Lineament

Curvature

Profile and plan curvatures of the slope are used for landslide investigation (Ayalew and Yamagishi 2004). Both profile and plan curvatures of a slope affect the landslide susceptibility (Carson and Kirkby 1972). The plan curvature of the slope is calculated using ALOS Pulsar DEM for the landslide susceptibility of the study area. The curvature map is classified into seven categories, from −33.91 to 33.27 value (Fig. 2.14).

Soil Depth

Soil depth is a crucial influential factor in slope stability and hillslope hydrology (Tromp-van Meerveld and McDonnell 2006). Soil depth factor is prepared by using a district resource map of the Geological Survey of India. The spatial distribution of soil depth of the study area is shown in Fig. 2.15. There are three classes of soli depth viz. Deep (>50 cm), Shallow (25–50 cm) and Very shallow (10–25 cm).

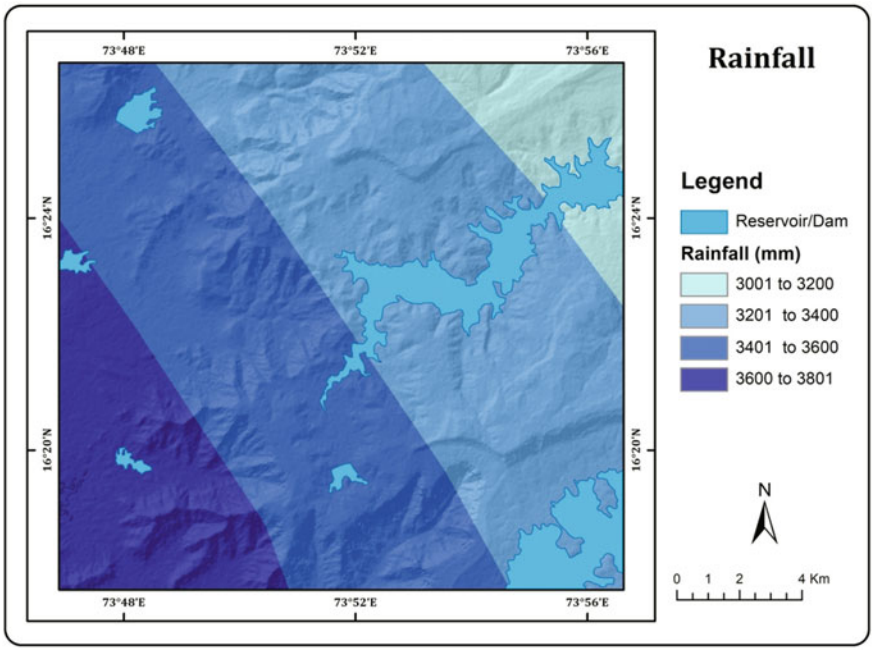

Fig. 2.11 Rainfall

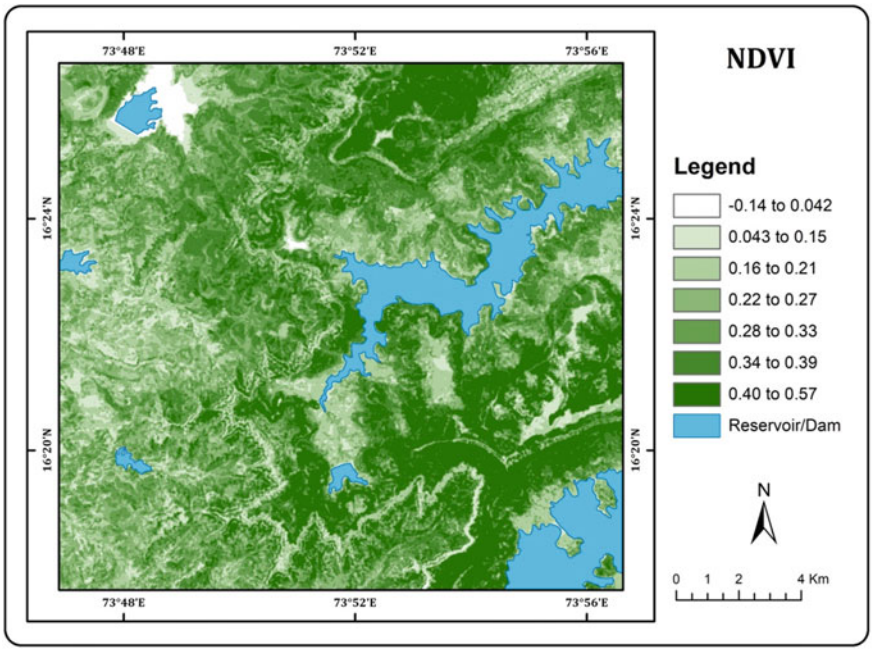

Fig. 2.12 Normalized difference vegetation index

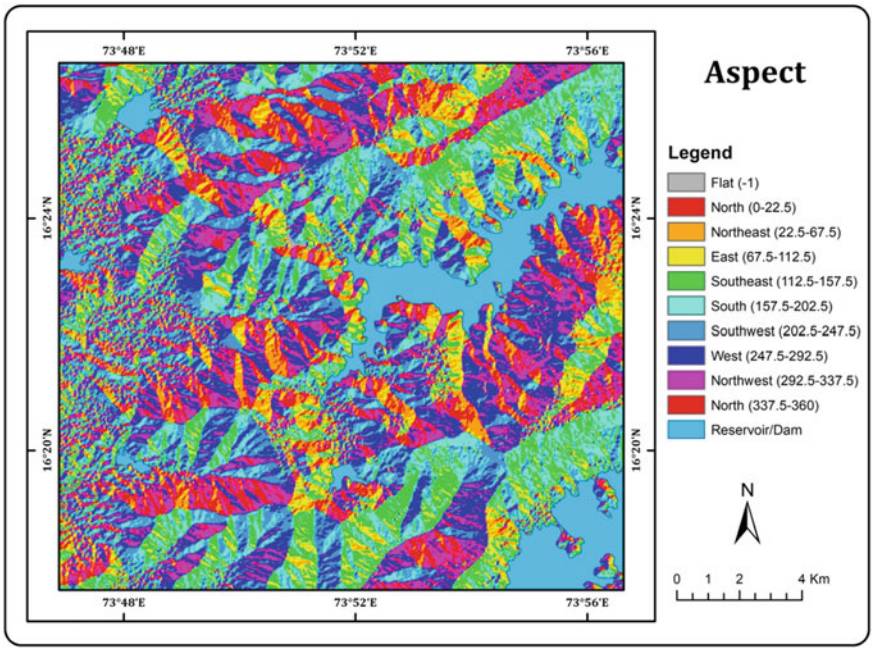

Fig. 2.13 Aspect

2.4.3 LSA by Frequency Ratio

For the present landslide investigation, the frequency ratio is calculated, which reveals the spatial relationships among the landslides inventory and influential factors (Table 2.1). The LSI values of PhondaGhat area range from 1.11 to 11.98. A higher LSI suggests a higher vulnerability to landslide occurrence. This study implements the equal interval method to classify the calculated LSI values into five categories: very high (1.39%), high (12.18%), moderate (35.49%), low (42.79%), and very low landslide susceptibility (8.16%) for easy and visual interpretation (Table 2.2). The susceptibility map (Fig. 2.16) demonstrates that about 13% of the land area of the study

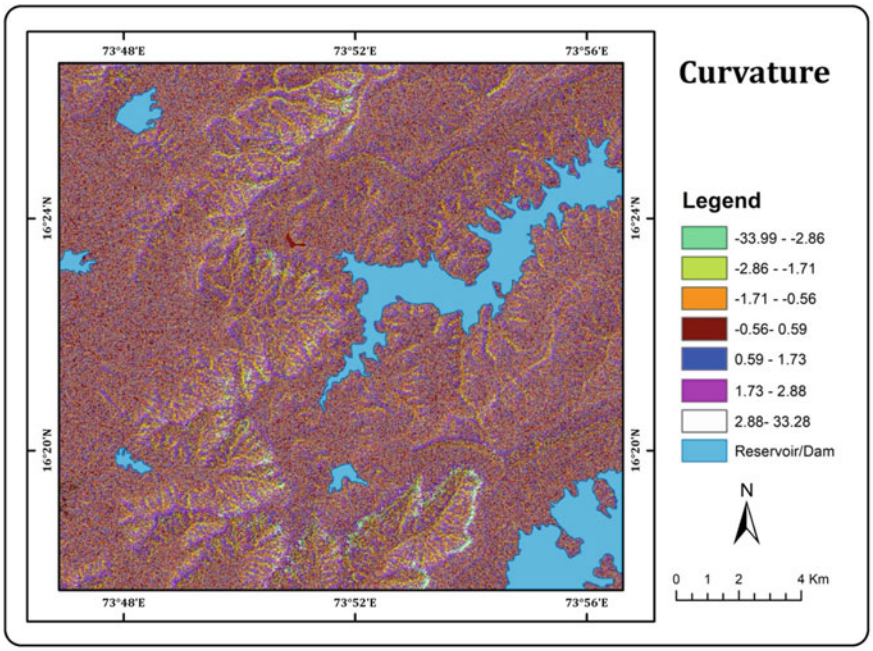

Fig. 2.14 Slope curvature

region is shown in the very high and high zone of landslide susceptibility. Hereafter, it is observed that most of the landslide-prone areas are found along State Highway No. 179.

2.4.4 Validation of the Frequency Ratio Model

In this study, a frequency ratio approach for estimating the susceptible areas of landslide using a GIS is applied and tested. Field investigation-based landslide inventory (Testing data) is used for the model validation. Area Under Curvature (AUC) is calculated from the cumulative percentage of susceptible zones of LSI in the study area and the cumulative percentage of landslide occurrences in the classes as per Table 2.3. As per the result, the AUC value of 0.823 is obtained for the frequency ratio. It shows the accuracy of the model (Fig. 2.17). The intensive field investigation is carried out in the study area for validation of the result (Fig. 2.18).

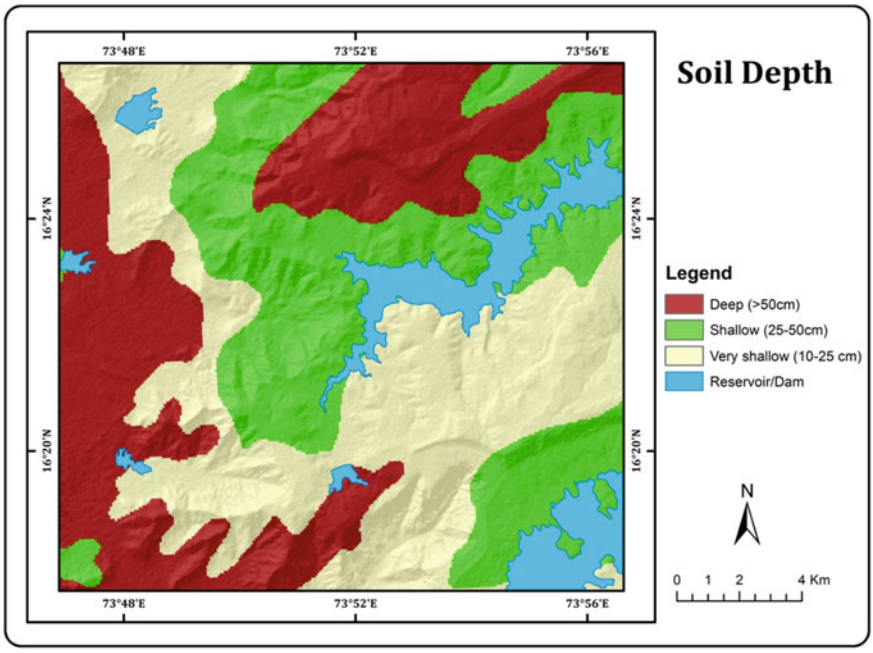

Fig. 2.15 Soil depth

2.5 Conclusion

The present study illustrates that the landslide susceptibility mapping of Phonda Ghats of Maharashtra. The Frequency Ratio model is applied and tested using Remote Sensing and GIS techniques. The susceptibility map shows that more than 13% of the land area of the study region is highly susceptible to the occurrence of the landslide. Hence, the major portion along PhondaGhatroad (SH-179) is represented as highly vulnerable to the landslide. Therefore, this road is dangerous for unplanned anthropogenic activities. The study reveals that the frequency ratio is an effective method for landslide susceptibility mapping of hilly and rugged mountainous areas. The performance of the Frequency Ratio model is validated by cumulative frequency diagram, which shows that the model has an accuracy of 82% based on field investigation. The landslide susceptibility map will be useful for planners and engineers in choosing locations for the prevention and mitigation of existing and future landslides.

Table 2.1 Result of FR model for each factor

Factors	Class	No. of landslide	Landslide (%)	No of pixel in domain	Area (%)	Frequency ratio	Normalization
Drainage	200	1	5	206,334	16	0.31	0.15
	500	1	5	276,820	21	0.23	0.11
	1000	5	25	407,165	31	0.79	0.37
	2000	13	65	391,131	30	2.15	1
	10,000	0	0	12,415	1	0	0
Geology	Deccan Trap	0	0	93,356	7	0	0
	Laterite	0	0	36,313	3	0	0
	Megacryst Flow	4	20	138,942	11	1.86	0.87
	Mainly a simple flow	13	65	393,404	30	2.14	1.00
	Essentially a simple flow	1	5	438,908	34	0.15	0.07
	Quartzite (Sedimentary)	0	0	43,645	3	0.00	0
	Shale	0	0	29,181	2	0.00	0
	Quartz Chlorite amphibole schist/ferruginous phyllite	2	10	113,504	9	1.14	0.53
	Granite	0	0	6,612	1	0	0
Geomorphology	Structural origin-moderately dissected upper plateau	19	95	874,983	68	1.40	1
	Denudational origin-moderately dissected upper plateau	0	0	21,125	2	0.00	0

(continued)

Table 2.1 (continued)

Factors	Class	No. of landslide	Landslide (%)	No of pixel in domain	Area (%)	Frequency ratio	Normalization
	Denudational origin-pediment-pediplain complex	1	5	282,778	22	0.23	0.16
	Anthropogenic origin-anthropogenic terrain	0	0	109,740	8	0	0
	Waterbody	0	0	2,301	0	0	0
	Structural origin-low dissected lower plateau	0	0	2,938	0	0	0
Lineament	500	7	35	459,827	36	0.98	0.73
	1000	7	35	337,709	26	1.34	1.00
	3000	6	30	484,439	37	0.80	0.60
	5000	0	0	11,890	1	0	0
LULC	Rural	0	0	14,785	1	0	0
	Crop land	0	0	57,245	4	0	0
	Plantation	0	0	22,153	2	0	0
	Fallow	2	10	173,499	13	0.75	0.32
	Evergreen/Semi-evergreen	15	75	414,769	32	2.34	1
	Deciduous	1	5	248,214	19	0.26	0.11
	Scrub forest	2	10	251,671	19	0.51	0.22
	Barren rocky	0	0	97	0	0	0
	River	0	0	1,525	0	0	0
	Waterbodies/Reservoir	0	0	109,907	8	0	0

(continued)

Table 2.1 (continued)

Factors	Class	No. of landslide	Landslide (%)	No of pixel in domain	Area (%)	Frequency ratio	Normalization
NDVI	– 0.14 to 0.042	0	0	67,698	5	0	0
	0.043–0.15	0	0	94,464	7	0	0
	0.16–0.21	4	20	179,804	14	1.44	0.94
	0.22–0.27	4	20	229,535	18	1.13	0.73
	0.28–0.33	6	30	252,323	20	1.54	1
	0.34–0.39	5	25	244,662	19	1.32	0.86
	0.40–0.57	1	5	225,379	17	0.29	0.19
Rainfall	3201–3400	4	20	540,558	42	0.48	0.21
	3600–3801	0	0	200,848	16	0	0
	3401–3600	16	80	451,239	35	2.29	1
	3001–3200	0	0	101,220	8	0	0
Elevation	<110	2	10	267,210	21	0.48	0.10
	111–241	2	10	165,391	13	0.78	0.15
	242–416	9	45	114,646	9	5.08	1
	417–565	5	25	254,266	20	1.27	0.25
	566–664	1	5	259,186	20	0.25	0.05
	665–785	1	5	194,923	15	0.33	0.07
	786–948	0	0	38,243	3	0	0
Slope	0–16	4	20	919,223	71.04	0.28	0.10
	17–31	13	65	297,697	23.01	2.83	1
	32–47	3	15	70,323	5.44	2.76	0.98

(continued)

Table 2.1 (continued)

Factors	Class	No. of landslide	Landslide (%)	No of pixel in domain	Area (%)	Frequency ratio	Normalization
	48–63	0	0	5,671	0.44	0	0
	64–78	0	0	951	0.07	0	0
Slope curvature	−33.91999817 to − 2.855695834	0	0	8,517	0.7	0	0
	−2.855695833 to − 1.707654161	3	15	62,724	4.8	3.09	0.42
	−1.70765416 to − 0.559612488	4	20	399,969	30.9	0.65	0.09
	− 0.559612488 to 0.588429185	3	15	354,344	27.4	0.55	0.07
	0.588429185–1.736470858	8	40	397,075	30.7	1.30	0.18
	1.736470859–2.884512532	1	5	62,530	4.8	1.03	0.14
	2.884512533–33.27999878	1	5	8,706	0.7	7.43	1.00
Soil	Deep & moderately deep (depth > 50 cm)	0	0	375,944	29.06	0	0
	Shallow (25–50 cm)	15	75	453,928	35.08	2.14	1
	Very shallow (10–25 cm)	5	25	463,993	35.86	0.70	0.33
Aspect	0.5162–45.45	3	15	129,954	10.0	1.49	0.63
	45.46–90.39	2	10	103,952	8.0	1.24	0.53
	90.4–135.3	1	5	147,952	11.4	0.44	0.19

(continued)

Table 2.1 (continued)

Factors	Class	No. of landslide	Landslide (%)	No of pixel in domain	Area (%)	Frequency ratio	Normalization
	135.4–180.3	0	0	199,217	15.4	0	0
	180.4–225.2	3	15	179,886	13.9	1.08	0.46
	225.3–270.1	3	15	172,906	13.4	1.12	0.48
	270.2–315.1	2	10	195,522	15.1	0.66	0.28
	315.2–360	6	30	164,476	12.7	2.36	1.00

Table 2.2 Landslide susceptibility zones

Sr. No	Susceptibility zone	No. of pixels within zone	Area of zone (%)
1	Very low	105,581	8.16
2	Low	553,620	42.79
3	Moderate	459,176	35.49
4	High	157,545	12.18
5	Very high	17,943	1.39

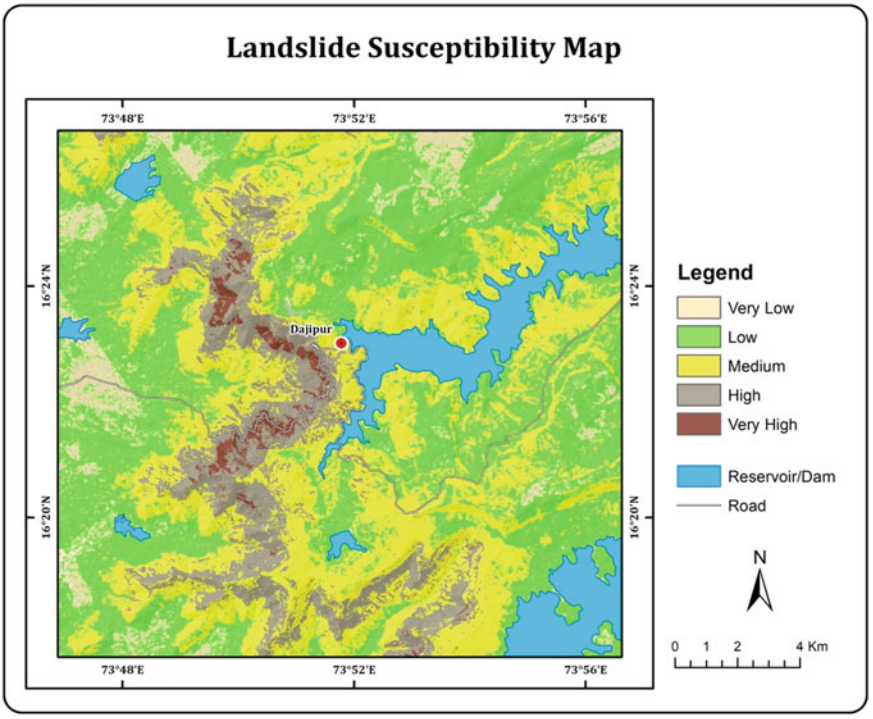

Fig. 2.16 Landslide susceptibility map using FR

Table 2.3 Distribution of susceptible classes and landslide occurrence

Susceptibility zone	No. of testing landslide	Percentage of testing landslide	Area percentage
Very low	0	0	8.16
Low	1	6.67	42.79
Medium	4	26.67	35.49
High	6	40	12.18
Very high	4	26.67	1.39

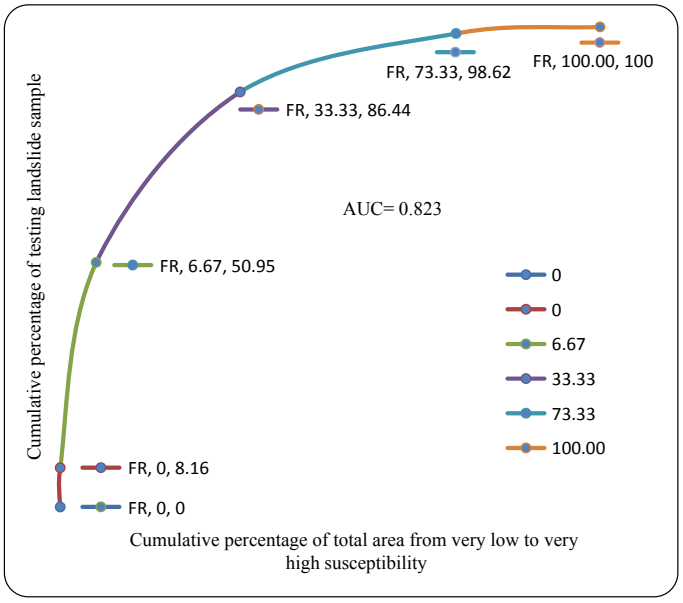

Fig. 2.17 Cumulative frequency diagram showing landslide susceptibility classification in the cumulative percentage of landslide occurrence

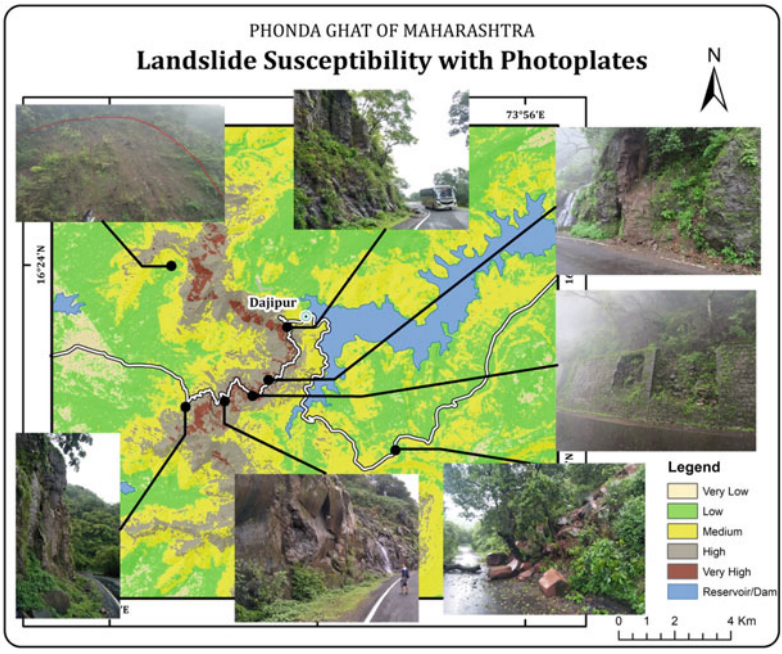

Fig. 2.18 Photo-plates of field investigation

References

Ahmed B (2014) Landslide Susceptibility mapping using multi-criteria evaluation techniques in Chittagong Metropolitan Area Bangladesh. Landslides 12:1077–1095. https://doi.org/10.1007/s10346-014-0521-x

Anbalagan R, Singh B (1996) Landslide hazard and risk assessment mapping of mountainous terrains- a case study from Kumaun Himalaya, India. EngGeol 43:237–246. https://doi.org/10.1016/S0013-7952(96)00033-6

Aristizábal E, Martínez-Carvajal H, García-Aristizábal E (2017) Modelling shallow landslides triggered by rainfall in tropical and mountainous basins. In: Mikoš M, Casagli N, Yin Y, Sassa K (eds) Advancing culture of living with landslides. WLF 2017. Springer, Cham. https://doi.org/10.1007/978-3-319-53485-5_23

Atkinson PM, Massari R (1998) Generalised linear modelling of susceptibility to landsliding in the Central Apennines. Italy. Comput Geosci 24(4):373–385. https://doi.org/10.1016/S0098-3004(97)00117-9

Ayalew L, Yamagishi H (2004) Slope failures in the Blue Nile basin, as seen from landscape evolution perspective. Geomorphology 57:95–116. https://doi.org/10.1016/S0169-555X(03)00085-0

Balasubramani K, Kumaraswamy K (2013) Application of geospatial technology and Information value technique in landslide hazard zonation mapping: a case study of Giri valley Himachal Pradesh. Disaster Adv 6(1):38–47

Bello MN, Abbas II and Akpu B (2014) Analysis of land use-land cover changes in Zuru and its environment of Kebbi state, Nigeria using remote sensing and geographic information system technology. J Geogr Earth Sci 2:113–126

Carson MA, Kirkby MJ (1972) Hillslope form and process. Cambridge University Press, London, p 475

Chaulya, S. K., & Prasad, G. M. (2016) Slope Failure Mechanism and Monitoring Techniques. Sensing and Monitoring Technologies for Mines and Hazardous Areas, 1–86. https://doi.org/10.1016/B978-0-12-803194-0.00001-5

Chen H, Lee CF (2003) A dynamic model for rainfall-induced landslides on natural slopes. Geomorphology 51(4):269–288. https://doi.org/10.1016/S0169-555X(02)00224-6

Chen XL, Liu C-G, Chang Z-F, Zhou Q (2016) The relationship between the slope angle and the landslide size derived from limit equilibrium simulations. Geomorphology 253:547–550. https://doi.org/10.1016/j.geomorph.2015.01.036

Citrabhuwana BN, Kusumayudha SB, Purwanto (2016) Geology and slope stability analysis using markland method on road segment of Piyungan–Patuk, Sleman and Gunungkidul regencies, Yogyakarta special region Indonesia. Int J Econ Environ Geol 7(1):42–52

Clerici A, Perego S, Tellini C, Vescovi P (2006) A GIS-based automated procedure for landslide susceptibility mapping by the Conditional Analysis method: the Baganza valley case study (Italian Northern Apennines). Environ Geol 50:941–961. https://doi.org/10.1007/s00254-006-0264-7

Deshpande CD (1971) Geography of Maharashtra, National book trust, India A-5 Green Park, New Delhi-16

Donnarumma A, Revellino P, Grelle G, Guadagno FM (2013) Slope angle as indicator parameter of landslide susceptibility in a geologically complex area. Landslide Sci Pract, 425–433. https://doi.org/10.1007/978-3-642-31325-7_56

Gupta RP, Saha AK, Arora MK and Kumar A (1999) Landslide hazard zonation in a part of the Bhagirathi valley, Garhwal Himalayas, using integrated remote sensing—GIS. Himal Geol 20:71–85

Gupta R, Joshi B (1990) Landslide hazard zoning using the gis approach—a case study from the Ramganga catchment, Himalayas. Eng Geol 28:119–131. https://doi.org/10.1016/0013-7952(90)90037-2

Guzzetti F, Carrara A, Cardinali M, Reichenbach P (1999) Landslide hazard evaluation: a review of current techniques and their application in a multi-scale study. Central Italy, Geomorphology 31:181–216

Hobbs WH (1904) Lineaments of the Atlantic border region. Geol Soc Am Bull 15:483–506

Igwe O (2015) The study of the factors controlling rainfall-induced landslides at a failure-prone catchment area in Enugu, Southeastern Nigeria using remote sensing data. Landslides 12:1023–1033. https://doi.org/10.1007/s10346-015-0627-9

Kayastha P, Dhital MR and De Smedt F (2013) Application of the analytical hierarchy process (AHP) for landslide susceptibility mapping: a case study from the Tinau watershed, West Nepal. Comput Geosci 52:398–408. https://doi.org/10.1016/j.cageo.2012.11.003

Kim SB, Na JH and Seo YS (2015) Prediction of rainfall-induced slope failure using Hotelling's T-Square statistic. J Eng Geol 25(3):331. https://doi.org/10.9720/kseg.2015.3.331

Lee S, Min K (2001) Statistical analysis of landslide susceptibility at Yongin, Korea. Environ Geol 40:1095–1113

Lee S and Pradhan B (2006) Probabilistic landslide hazards and risk mapping on Penang Island, Malaysia. J Earth Syst Sci 115(6):661–672. https://doi.org/10.1007/s12040-006-0004-0

Lee S, Choi J and Min K (2004) Probabilistic landslide hazard mapping using GIS and remote sensing data at Boun, Korea. Int J Remote Sens 25(11):2037–2052. https://doi.org/10.1080/01431160310001618734

Lee S, Oh H, Park NW (2007) Extraction of landslide-related factors from ASTER imagery and its application to landslide susceptibility mapping using GIS. IEEE international geoscience and remote sensing symposium, Barcelona, Spain

Lee S, Talib JA (2005) Probabilistic landslide susceptibility and factor effect analysis. Environ Geol 47:982–990. https://doi.org/10.1007/s00254-005-1228-z

Mahalingam R, Olsen MJ, O'Banion MS (2016) Evaluation of landslide susceptibility mapping techniques using lidar-derived conditioning factors (Oregon case study). Geomat Nat Hazards Risk. 7(6):1–24. https://doi.org/10.1080/19475705.2016.1172520

Mantovani F, Soeters R, Van Westen CJ (1996) Remote sensing techniques for landslide studies and hazard zonation in Europe. Geomorphology 15(3–4):213–225. https://doi.org/10.1016/0169-555X(95)00071-C

Masoumi H, Jamali AA, Khabazi M (2014) Investigation of role of slope, aspect and geological formations of landslide occurrence using statistical methods and GIS in some watersheds in ChaharMahal and Bakhtiari province. J Appl Environ Biol Sci 4(9):121–129

Merrett HC, Chen WW (2013) Applications of geographical information systems and remote sensing in natural disaster hazard assessment and mitigation in Taiwan. Geomat Nat Haz Risk 4(2):145–163. https://doi.org/10.1080/19475705.2012.686064

Ministry of Environment and Forests Government of India (2013) Report of the high level working group on Western Ghats, vol 1. http://www.uttarakannada.nic.in/docs/Publication/HLWGWESTERNGHATSVOLUME1.pdf

Nagarajan R, Mukherjee A, Roy A, Khire MV (1998a) Temporal remote sensing data and GIS application in landslide hazard zonation of part of Western Ghat, India. Int J Remote Sens 19:573–585

Nagarajan R, Mukherjee A, Roy A and Khire MV (1998b) Technical note temporal remote sensing data and GIS application in landslide hazard zonation of part of Western ghat, India. Int J Remote Sens 19(4):573–585

Normaniza O, Barakbah SS (2011) The effect of plant succession on slope stability. Ecol Eng 37:139–147. https://doi.org/10.1016/j.ecoleng.2010.08.002

Normaniza O, Aimee H, Ismail 0y, Tan G Y A and Rozainah M Z (2018) Promoter effect of microbes in slope eco-engineering: effects on plant growth, soil quality and erosion rate at different vegetation densities. Appl Ecol Environ Res 16(3):2219–2232. https://doi.org/10.15666/aeer/1603_22192232

Pardeshi SD, Autade SE, Pardeshi SS (2013) Landslide hazard assessment: recent trends and techniques. Springerplus 2013(2):523. https://doi.org/10.1186/2193-1801-2-523

Patil AS, Bhadra BK, Panhalkar SS, Patil PT (2020) Landslide susceptibility mapping using landslide numerical risk factor model and landslide inventory prepared through OBIA in Chenab Valley, Jammu and Kashmir (India). J Indian Soc Remote Sens 48:431–449. https://doi.org/10.1007/s12524-019-01092-5

Patil AS, Panhalkar S (2019) Analytical hierarchy process for landslide hazard zonation of South-Western ghats of Maharashtra, India. Disaster Adv 12:26–39.

Persichillo MG, Bordoni M, Meisina C, Bartelletti C, Barsanti M, Giannecchini R, Avanzi GDA, Galanti Y, Cevasco A, Brandolini P (2016) Shallow landslides susceptibility assessment in different environments. Geom Nat Hazards Risk 8(2):748–771. https://doi.org/10.1080/19475705.2016.1265011

Pradhan B, Lee S (2010) Landslide susceptibility assessment and factor effect analysis: backpropagation artificial neural networks and their comparison with frequency ratio and bivariate logistic regression modelling. Environ Modell Softw 25(6):747–759. https://doi.org/10.1016/j.envsoft.2009.10.016

Qiao G et al (2013) Landslide investigation with remote sensing and sensor network: from susceptibility mapping and scaled-down simulation towards in situ sensor network design. Remote Sens 5:4319–4346. https://doi.org/10.3390/rs5094319

Radhakrishna BP (1993) Neogene uplift and geomorphic rejuvenation of the Indian Peninsula. Curr Sci 64(11&12):787–793

Rajan K and Shibasaki R (2001) A GIS-based integrated land use/cover change model to study agricultural and urban land-use changes. In: Proceedings of 22nd Asian conference on remote sensing. https://crisp.nus.edu.sg/~acrs2001/pdf/250Rajan.pdf

Ramachandra TV, Kumar U, Aithal B (2010) Landslide Susceptible Locations in Western Ghats: Prediction through OpenModeller

Saha AK, Gupta RP, Arora MK (2002) GIS-based landslide hazard zonation in the Bhagirathi (Ganga) Valley. Himalayas. Int J Remote Sens 23(2):357–369. https://doi.org/10.1080/01431160010014260

Scaioni M (2013) Remote sensing for landslide investigations: From research into practice. Remote Sens 5:5488–5492. https://doi.org/10.3390/rs5115488

Srivastava V, Srivastava HB, Lakhera RC (2010) Fuzzy gamma based geomatic modelling for landslide hazard susceptibility in a part of tons river valley, northwest Himalaya. India. Geom Nat Hazards Risk. 1(3):225–242. https://doi.org/10.1080/19475705.2010.490103

Stetler LD (2014) Geomorphology. Ref Modul Earth Syst Environ Sci. https://doi.org/10.1016/B978-0-12-409548-9.09078-3

Tromp-van Meerveld, H.J., McDonnell, J.J (2006) Threshold relations in subsurface stormflow: 2. The fill and spill hypothesis. Water Resour Res, W02411. https://doi.org/10.1029/2004WR003800

Varnes DJ (1984) Landslide hazard zonation: a review of principles and practices commission on landslides of the IAEG. UNESCO, Paris

van Wstern CJ, Ghosh S, Jaiswal P, Martha TR and Kuriakose SL (2011): From landslide inventories to landslide risk assessment; an attempt to support methodological development in India, the second world landslide forum. Rome, pp 3–7

Wang Q, Li W, Yan S, Wu Y, Pei Y (2016) GIS based frequency ratio and index of entropy models to landslide susceptibility mapping (Daguan, China). Environ Earth Sci 75(9):1–16. https://doi.org/10.1007/s12665-016-5580-y

Wang HB, Sassa K (2005) Comparative evaluation of landslide susceptibility in Minamata area, Japan. Environ Geol 47:956–966. https://doi.org/10.1007/s00254-005-1225-2

Westen et al., 1999.Van Westen CJ, Seijmonsbergen AC, Mantovani F (1999) Comparing landslide hazard maps. Nat Hazards 20:137–158

Yilmaz I (2009) Landslide susceptibility mapping using frequency ratio, logistic regression, artificial neural networks and their comparison: a case study from Kat landslides (Tokat–Turkey). Comput Geosci 35:1125–1138. https://doi.org/10.1016/j.cageo.2008.08.007

Chapter 3
Evaluation of the Hydrological Process Prevalent in Ghaggar River Basin Using Interferometrically Derived Sentinel-1 DEM

Nitin Chauhan, Vipin Kumar, and Rakesh Paliwal

Abstract The deleterious effects of anthropogenic activities on the environment can be traced back to the era when man came into existence on this earth. The environment is being severely degraded due to over exploitation of the existing natural resources in order to meet the never-ending demand of human beings for food, fuel, and fiber. Globally, an estimated 1,965 million hectares of land is subjected to one or other kind of degradation out of which soil erosion by water and wind accounts for 1,904 million hectares. According to the report's areas such as Shivalik Hills, North-Western Himalayan regions, Western Ghats, and parts of Peninsular India are most severely affected by soil erosion, i.e., about 20 Mg/ha/year (Singh et al. 1992). The present research focuses on the flimsiest ecosystem in India, i.e., lower Shivaliks because of highly erodible soils which are lost at an alarming rate of 25–225 tones/hectare/year. Various techniques have evolved over a period of time to evaluate soil erosion and to develop a watershed management protocol out of which morphometric analysis has given promising results in synergy with advanced techniques such as Geographical Information System and Remote Sensing. This study emphasizes the geospatial evaluation of hydrological processes using interferometrically derived DEM from Sentinel—1 Satellite for the Ghaggar river basin. The watershed delineation and stream extraction from the DEM is done using ARCSWAT which works as an extension with ArcGIS software as well as through hydrology extension of ArcGIS. The morphometric analysis is being carried out for 33 fourth-order drainage basins of Ghaggar river up to its confluence with Medkhali River.

Keywords Morphometry · Ghaggar basin · Sentinel-1 · Interferometry

N. Chauhan (✉)
Haryana Space Applications Centre, CCS HAU Campus, Hisar 125004, India

V. Kumar
Faculty of Earth Sciences, Banasthali Vidyapith, Tonk, Rajasthan, India

R. Paliwal
Regional Remote Sensing Centre–West, NRSC, ISRO, Jodhpur, India

R. B. Singh et al. (eds.), *Remote Sensing and Geographic Information Systems for Policy Decision Support*, Advances in Geographical and Environmental Sciences,
https://doi.org/10.1007/978-981-16-7731-1_3

3.1 Introduction

Morphometry is defined as the mathematical analysis of the Earth's surface, and the shape and dimension of its landform (Clarke 1996). R.E. Horton, America's most renowned hydrologist made an attempt to pronounce the erosional morphology in a quantitative way based on morphometric techniques even when the landform development by erosional and gradational process persisted principally qualitative (Horton 1945). The erosional drainage basin is considered a basic unit of study in the science of geomorphometry (Chorley et al. 1957). It acts as an ideal unit for sustainable management of natural resources such as water and land which supports in averting natural disasters arising otherwise. Morphometric analysis is a vital characteristic for watershed characterization which involves the computation of quantitative traits of the landscape such as linear, relief, and aerial aspects from the stream networks and elevation information within the watershed. Morphometric analysis is an imperative tool that provides a holistic insight into the watershed's hydrological behavior by describing its soil physiological properties, landform formation processes, and its erosional characteristics (Strahler 1964). The drainage morphometric studies have acted as a prerequisite criterion for runoff modeling, site suitability of recharge sites, groundwater prospect zonation, and many other geotechnical investigations. But the conventional methods of morphometric characterization were very expensive, time and labor-intensive for large watersheds. Recently, with the advent of remote sensing technologies data with synoptic coverage and improvised spatial accuracies now available making it easier to perform drainage morphometric analysis of inaccessible areas. Similarly, advancements in computational power of the systems and Geographic Information System (GIS) have enabled the morphometric parameters extraction and evaluation in a more precise and easy manner. In order to explore holistic stream properties through analysis of varied drainage attributes, in-depth morphometric analysis is being carried out for 33 fourth-order drainage basins of Ghaggar river up to its confluence with Medkhali River and also an attempt has been made in order to identify the geomorphic development stages with the help of linear, areal and relief aspect evaluation.

3.2 Study Area

The present study focuses on the flimsiest ecosystem in India, i.e., lower Shivaliks because of highly erodible soils which are lost at an alarming rate of 25–225 tones/hectare/year (Singh and Khera 2009). The Shivaliks are composed of sandstones and conglomerates having characteristic fluvial deposits, making them geologically weak structures and simultaneously prone to erosion. Large-scale deforestation, road construction, mining, and faulty agriculture practices have resulted in the desertification of land in the Shivalik hills. The studies of (Patnaik 1981) revealed that degraded land has increased in the Shivaliks from 194 km^2 in 1852, 2000 km^2 in

1939 to 20,000 km^2 in 1981. The Ghaggar river is one of the major ephemeral streams which drains the Shivaliks and Himalayas. The Ghaggar river basin extends over an area of about 42,200 km^2 extending over parts of states such as Haryana, Himachal Pradesh, Rajasthan, Punjab, and Union Territory of Chandigarh. The Ghaggar basin is a part of Indo-Gangetic basin. The river originates from Dagshai village near Shimla in Himachal Pradesh from the foothills of Shivaliks. Its main tributaries are Markanda, Saraswati, Tangri, and Chotang River. The overall length of Ghaggar river is about 291 ^{km} and it terminates in Hanumangarh of Bikaner district. The Ghaggar is a non-perennial river, which carries its optimum flow throughout the year in the upstream part only. Therefore, for the current research upper part of the Ghaggar river basin up to confluence of Medkhali River is taken. The study area extends from 76°51′45.06″ and 30°36′46.50″ to 77°12′45.30″ and 30°54′27.18″ and covers an area of 559.14 km^2 (Fig. 3.1).

3.3 Methodology and Data Used

The European Commission in association with European Space Agency (ESA) is evolving a new series of Satellite constellations named Sentinel. One of the satellites designed by ESA with all-weather and day and night capability is Sentinel 1A & B. It is a C band spaceborne SAR that collects the images with 250 km of swath in Interferometric Wide Swath (IW) mode. The spatial resolution of the images is 5 m in range direction and 20 m in Azimuth direction. The Sentinel 1 Satellite provides dual polarization data, i.e., VV and VH. One scene each from Sentinel 1 A and Sentinel 1 B of date 19 September 2016 were used for generating the DEM. The preprocessing of the pair of single look complex products acquired in IW mode was performed in SNAP software version 6.0. The data acquired is in form of sub-swath and is formed on bursts that are demarcated by zones of no data value. The first step of the preprocessing Sentinel data is co-registering the two images to create a stack utilizing the Precise Orbit Ephemerides (POE) orbit files. In this one image is master and slave and pixel values of the slave images are moved to align with the master dataset to attain a sub-pixel accuracy so as to ensure the same range and azimuth is contributed by each ground object. The next step is the generation of the interferogram by multiplying the complex conjugate of master image with slave. The images are then seamlessly merged into one file by the process of TOPS Deburst and Tops Merge. The SAR images are associated with speckle noise which is nothing but the collective response of many small reflectors within a particular pixel. The SNAP software comes with many inbuilt speckle filtering algorithms and Goldstein Phase Filtering (Goldstein et al. 1988) was used to reduce the speckle while maintaining the radiometric information. The resultant phase generated as a result of filtering was unwrapped using SNAPHU (Chen and Zebker 2000). The unwrapped phase was imported using the NEST software and DEM was prepared from it. The DEM generated from Sentinel -1 is having a spatial resolution of 13.96 m against the most popularly used SRTM data with 30 m resolution which generates optimum

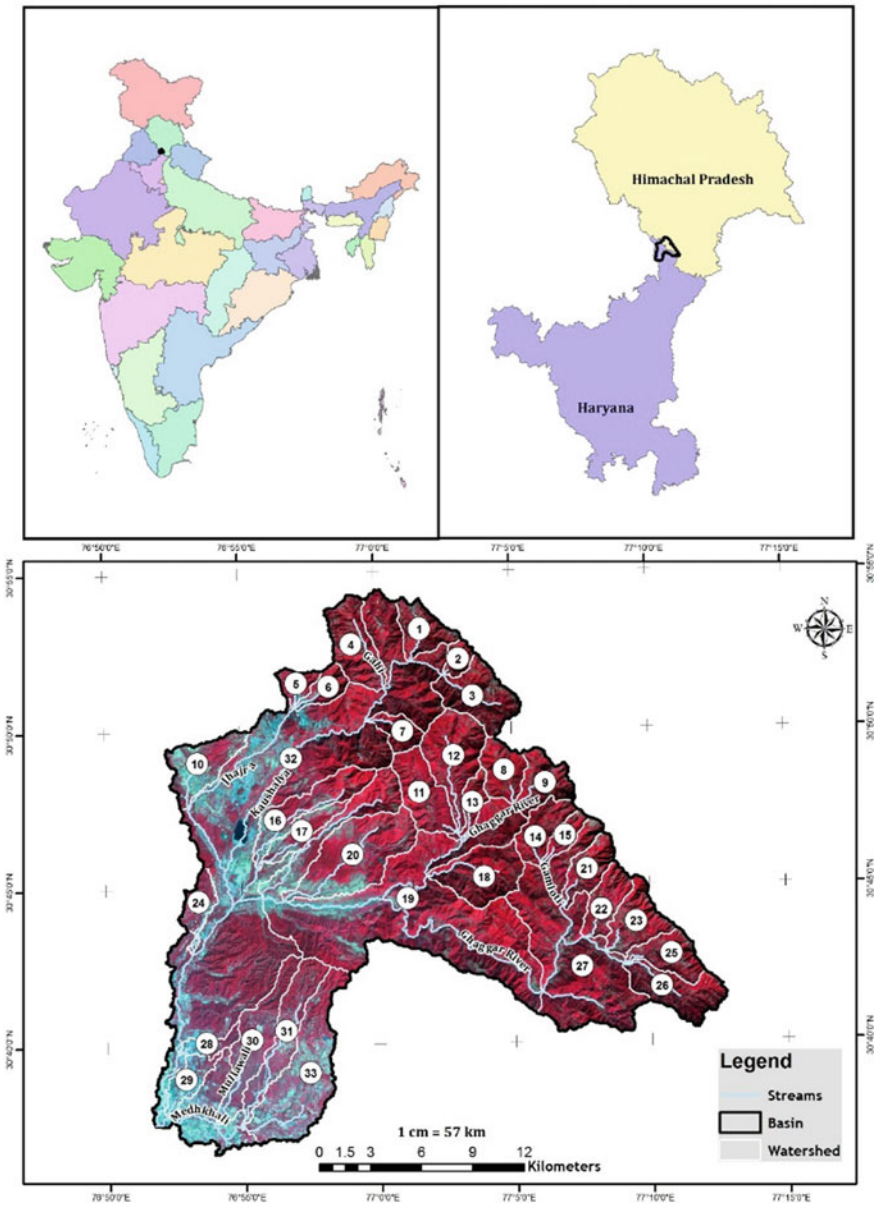

Fig. 3.1 Location map of the study area

results for morphometric analysis. The watershed delineation and stream extraction from the DEM is done using ARCSWAT which works as an extension with ArcGIS software (version 10.2.2) as well as through hydrology extension of ArcGIS. The list of morphometric parameters calculated for this study are given in Table 3.1.

3.4 Results and Discussion

3.4.1 Linear Aspects

Linear aspects of the basin deal with the detailed aspects of the stream network morphometry which act as a means of water and sediment transport through a single outlet point. The first stage of basin analysis is stream ordering.

3.4.1.1 Stream Order (SO_u)

The technique of designating a numeric order to links in a stream network is known as stream ordering. This order facilitates the identification and categorization of stream types based on their tributaries number. Strahler, Quantitative Analysis of Watershed Geomorphology (1957) designated the smallest fingertip tributaries as Order 1; When two first-order streams join an Order 2 stream is created; When two of Order 2 join a channel segment of Order 3 is formed and so on. Similar work on stream ordering has been done by (Horton 1945) and (Shreve 1967). In the current study, Sentinel 1 data is used for automatic delineation of the streams from the interferometrically generated DEM. The data is of 2016 so changes in river morphology as per the recent topographical changes are easily identified. The delineated streams are categorized according to (Strahler 1957) as given in Fig. 3.2 and Table 3.2.

3.4.1.2 Stream Number (SN_u)

The total stream segments number in a particular order is known as stream number. It is being observed that as the stream order increases there is a gradual decrease in stream number (N_u). This is in accordance with the Horton's Law of drainage composition (Horton 1945) which states that the "stream number falling in each order follows an inverse geometric progression with order number". The total stream numbers in the Ghaggar basin up to its confluence with Madhekali is 6943 (Table 3.2).

The study divulges that the development of 1st order streams is maximum in the Structural Hills Highly Dissected region of lower Shivalik and minimum in the alluvial plains. Similarly, second, third, and fourth order are also more prominent

Table 3.1 Methods used to calculate the Morphometric Parameter along with their formulae

Sr. No.	Parameter	Formula	References
1	Stream order	SO_u = Hierarchical rank	Strahler (1957)
2	Stream number	$SN_u = SN_1 + SN_2 + \ldots SN_n$	Horton (1945)
3	Stream length	$SL_u = SL_1 + SL_2 \ldots\ldots SL_n$	Strahler (1964)
4	Mean stream length	$MSL_u = \frac{\sum_{i=1}^{N} SO_u}{SN_u}$	Strahler (1964)
5	Mean stream length ratio	$MSLR_u = \frac{MSL_u}{MSL_u - 1}$	Horton (1945)
6	Bifurcation ratio	$R_b = \frac{SN_u}{SN_u + 1}$	Strahler (1964)
7	Valley length	VL	Mueller (1968)
8	Channel length	CL	Mueller (1968)
9	Air distance	AD	Mueller (1968)
10	Coefficient of topographical sinuosity (Ts) or Valley index (VI)	$Ts or VI = \frac{VL}{AD}$	Mueller (1968)
11	River sinuosity coefficient (Ks) or Channel index (CI)	$Ks or CI = \frac{CL}{AD}$	Mueller (1968)
12	Hydraulic sinuosity index (HSI)	$HSI = \frac{CI - VI}{CI - 1}$	Mueller (1968)
13	Topographic sinuosity index (TSI)	$TSI = \frac{VI - 1}{CI - 1}$	Mueller (1968)
14	Coefficient of hydraulic sinuosity (Hs)	$Hs = \frac{CL}{VL}$	Mueller (1968)
15	Rho coefficient	$\rho = \frac{MSLR_u}{Rb}$	Horton (1945)
16	Basin area (A)	ArcGIS/DEM	Schumm (1956)
17	Perimeter (P)	ArcGIS/DEM	
18	Basin length (Lb)	$L_b = 1.312A^{0.568}$	Schumm (1956), Gardiner (1975), Nookaratnam et al. (2005)
19	Lemniscate's value	$L_k = \frac{L_b^2 \pi}{4A}$	Chorley et al. (1957)
20	Form factor	$F_f = \frac{A}{L_b^2}$	Horton (1932)
21	Elongation ratio	$R_e = \frac{1}{L_b} \times \sqrt{\frac{4A}{\pi}}$	Schumm (1956)
22	Ellipticity index	$I_e = \frac{\pi VL^2}{4A}$	Stoddart (1965)

(continued)

Table 3.1 (continued)

Sr. No.	Parameter	Formula	References
23	Circularity ratio	$R_c = \frac{4\pi A}{P^2}$	Miller (1953)
24	Drainage density	$D_d = \frac{\sum SL_u}{A}$	Horton (1932)
25	Drainage texture	$D_t = \frac{1}{(t+P)/2}$ $t = \frac{(t_1+t_2)/2}{\sqrt{2}}$ $P = \frac{P_1+P_2+P_3+P_4}{4}$ Where t1 & t2 = number of intersections between the drainage network and grid diagonal P1 to P4 = number of intersections between the drainage network and grid edges	Horton (1932), Singh (1976)
26	Stream frequency	$S_f = \frac{\sum_{i=1}^{K} SN_u}{A}$	Horton (1945)
27	Drainage intensity	$D_i = \frac{S_f}{D_d}$	Faniran (1968)
28	Infiltration number	$I_f = D_d \times S_f$	Faniran (1968)
29	Relative relief	$R_r = Max.Elevation - Min.Elevation$	Smith (1935)
30	Relative relief ratio	$R_{hp} = 100 \times \frac{R_r}{Perimeter of the basin}$	Melton (1958)
31	Dissection index	$D_i = \frac{R_r}{R_a}$	Nir (1957)
32	Ruggedness number	$R_n = R_r \times D_d$	Strahler (1964)
33	Slope	ArcGIS/DEM	
34	Aspect	ArcGIS/DEM	
35	Hypsometric analysis		Strahler (1952), Pike and Wilson (1971)

in the Structural Hills Highly Dissected region whereas fifth-, sixth-, and seventh-order streams availability is more in Piedmont Alluvium and Valley fills. Figure 3.3 displays the relation of stream order to stream number in different sub-basins.

3.4.1.3 Stream Length (SL_u)

The stream length is the total length of individual stream segments of a particular order. The stream length acts as an important parameter for the calculation of drainage density. The stream segment lengths have been measured in kilometers and represented in Table 3.3 for different orders of all the basins. The total length

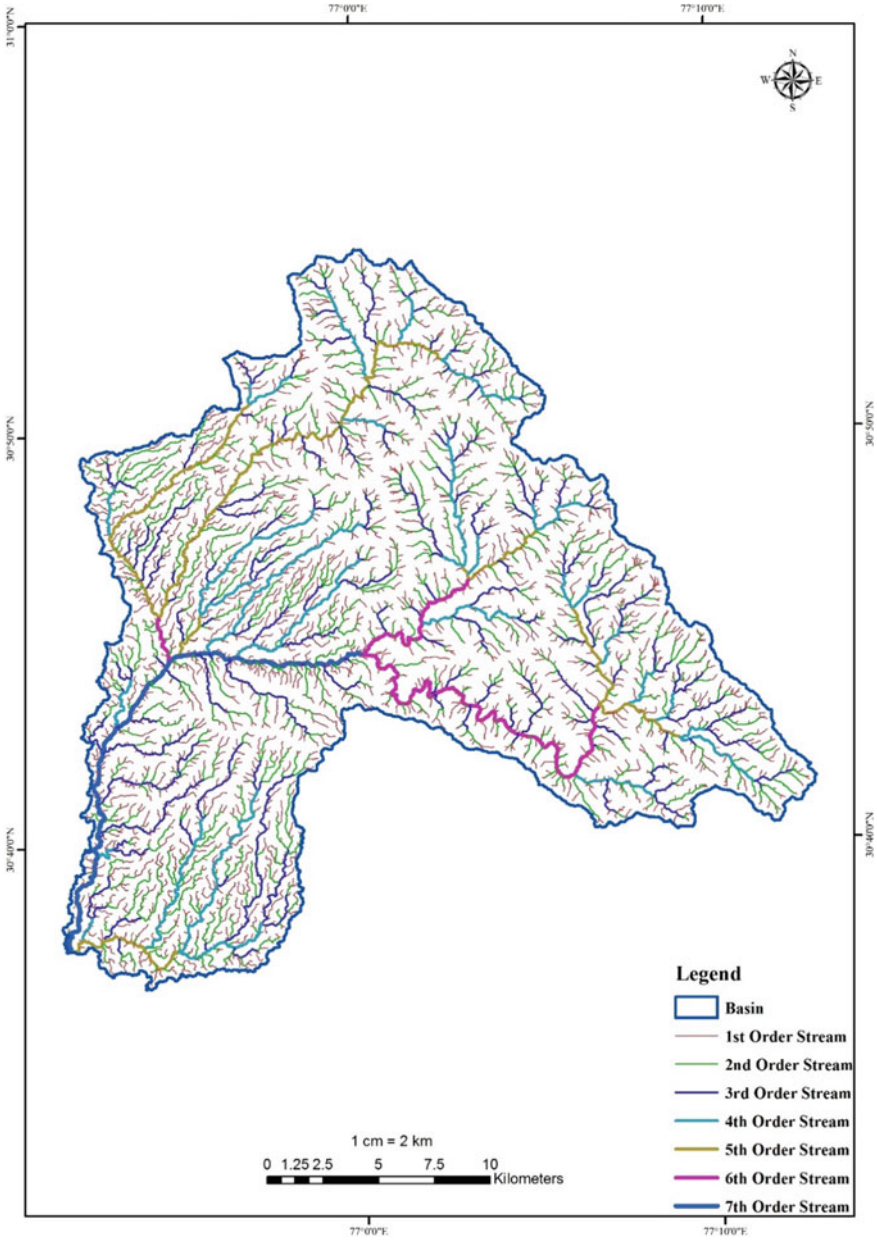

Fig. 3.2 Stream order in Ghaggar river basin as extracted from Sentinel 1 DEM

Table 3.2 Stream order in Ghaggar river basin

Sub-basin	Stream order							
	1	2	3	4	5	6	7	Total number of streams within a sub-basin
1	50	10	3	1				64
2	19	4	2	1				26
3	83	19	5	1				108
4	74	20	4	1				99
5	21	6	2	1				30
6	25	5	2	2	1			35
7	32	7	2	1				42
8	49	13	3	1				66
9	58	17	4	2	1			82
10	59	12	2	1				74
11	63	16	2	1				82
12	101	21	6	1				129
13	21	5	2	3	1			32
14	45	9	3	2	1			60
15	18	5	2	1				26
16	66	11	4	1				82
17	32	8	3	1				44
18	72	17	4	1				94
19	569	130	22	3	2	2	1	729
20	139	24	6	1				170
21	52	11	3	1				67
22	46	11	2	1				60
23	63	12	3	1	1			80
24	27	7	3	1				38
25	45	11	2	1				59
26	71	16	3	1	1			92
27	270	59	14	4	2	1		350
28	21	5	2	1				29
29	34	6	2	1				43
30	86	18	4	1				109
31	78	15	3	1				97
32	934	186	33	13	4	1	1	1172
33	153	33	5	1				192
Total number of streams within the watershed								4462

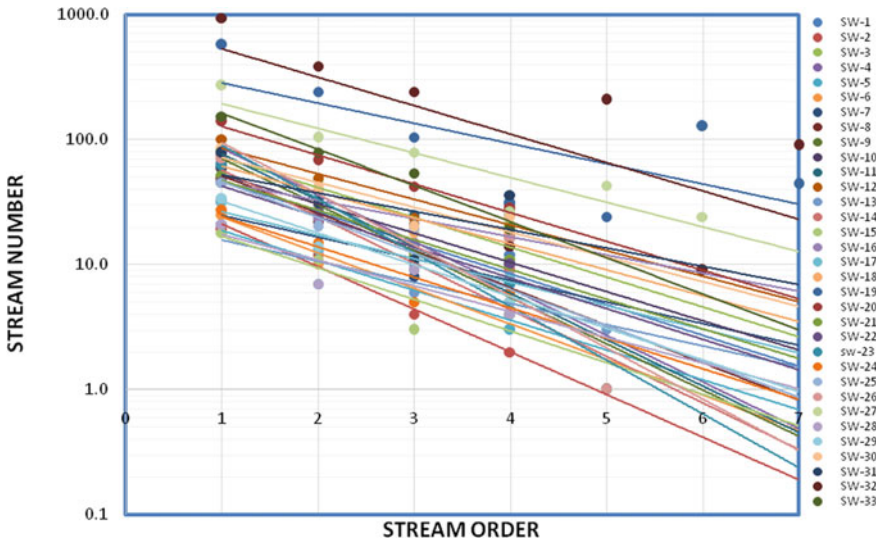

Fig. 3.3 Relation of stream order to stream number in different sub-basins of Ghaggar river basin

of various orders has no significant deductions since they may not be compared. Strahler (1964) has explained the **Mean Stream Length (MSL_u)** as a dimensional property that unveils the distinguishing size of drainage network components and its contributing sub-basin surfaces. The order-wise mean stream lengths of all the sub-basin are given in Table 3.4.

3.4.1.4 Mean Stream Length Ratio ($MSLR_u$)

The stream length ratio is the ratio of the mean stream length of a particular order (MSLu) to the mean stream length of the next lower order (MSL_{u-1}). It is similarly calculated for each subsequent pair of the orders. The mean stream length ranges from 0.033 to 22.493. According to Horton's Law of stream length (Horton 1945), the mean stream length of the successive orders of a basin closely approximates a direct geometric series with an increase in streams length with an increase in order. The $MSLR_u$ in the study area divulges that there is a variation in $MSLR_u$ in each sub-basin given in Table 3.5. The variation in stream length ratio is accredited to dissimilarity in topographic slope indicating the youth stage of geomorphic development in the streams of the study area (Vittala et al. 2004). The stream length ratio displaying an increasing trend from smaller order to higher order indicates their matured geomorphological development stage as against the sub-basins displaying abrupt changes between the orders indicating the late youth stage of geomorphological development.

Table 3.3 Stream length in Ghaggar river basin

Sub-basin	Stream order							
	1	2	3	4	5	6	7	Total length
1	10.89	5.43	1.37	2.50				20.19
2	4.48	2.84	0.87	0.59				8.78
3	16.67	11.75	2.70	4.67				35.79
4	15.25	9.94	4.00	4.94	0.02			34.16
5	4.68	1.85	2.21	1.02				9.76
6	6.71	2.16	1.12	2.43	0.01			12.43
7	6.89	1.87	1.65	2.33				12.74
8	9.88	5.19	4.51	1.28				20.85
9	12.27	4.54	2.86	3.18	0.01			22.85
10	18.20	15.52	2.71	2.53				38.96
11	14.16	11.99	5.36	1.12				32.62
12	19.10	11.99	5.83	6.70				43.62
13	4.72	1.21	2.62	2.06	0.47			11.09
14	12.01	7.12	2.63	1.82	0.01			23.59
15	3.01	4.43	1.48	1.34				10.27
16	17.48	9.49	4.24	8.54				39.74
17	10.35	6.48	4.77	3.33				24.93
18	15.52	8.85	7.19	5.63				37.19
19	147.30	65.06	29.25	11.08	4.45	26.21	8.48	291.82
20	42.82	23.39	11.29	8.86				86.35
21	13.01	4.83	3.51	2.24				23.59
22	10.39	7.60	2.65	2.33				22.96
23	13.49	8.62	6.53	1.99	0.01			30.64
24	6.95	6.90	2.32	3.12				19.29
25	11.88	7.07	5.19	1.53				25.66
26	13.41	12.14	2.78	4.56	0.01			32.91
27	65.09	26.67	21.41	4.27	10.34	3.83		131.60
28	5.93	2.65	3.18	1.45				13.21
29	10.66	4.45	4.02	1.18				20.31
30	23.66	18.99	6.45	8.25				57.35
31	24.16	13.53	2.82	10.27				50.78
32	244.70	121.96	69.49	0.15	48.90	2.36	19.17	506.71
33	44.28	29.63	20.24	5.24				99.40

Table 3.4 Mean stream length in Ghaggar river basin

Sub-basin	Stream order						
	1	2	3	4	5	6	7
1	0.21	0.18	0.17	0.21			
2	0.24	0.24	0.22	0.30			
3	0.20	0.25	0.23	0.22			
4	0.21	0.33	0.33	0.17	0.02		
5	0.22	0.27	0.22	0.34			
6	0.27	0.22	0.22	0.27	0.01		
7	0.22	0.14	0.21	0.23			
8	0.20	0.24	0.22	0.26			
9	0.21	0.18	0.20	0.19	0.01		
10	0.31	0.49	0.25	0.18			
11	0.23	0.36	0.22	0.28			
12	0.19	0.25	0.25	0.25			
13	0.23	0.17	0.44	0.30	0.16		
14	0.27	0.31	0.22	0.20	0.01		
15	0.17	0.40	0.50	0.34			
16	0.27	0.41	0.28	0.34			
17	0.32	0.50	0.43	0.42			
18	0.22	0.27	0.40	0.31			
19	0.26	0.27	0.28	0.36	0.19	0.21	0.19
20	0.31	0.34	0.27	0.32			
21	0.25	0.18	0.29	0.20			
22	0.23	0.29	0.29	0.23			
23	0.21	0.25	0.33	0.28	0.01		
24	0.26	0.46	0.46	0.52			
25	0.26	0.35	0.27	0.31			
26	0.19	0.30	0.21	0.29	0.01		
27	0.24	0.26	0.27	0.16	0.24	0.16	
28	0.28	0.38	0.35	0.36			
29	0.31	0.32	0.31	0.24			
30	0.28	0.46	0.32	0.34			
31	0.31	0.44	0.26	0.29			
32	0.26	0.32	0.29	0.01	0.24	0.26	0.21
33	0.29	0.38	0.38	0.28			

Table 3.5 Stream length ratio in Ghaggar river basin

Sub-basin	Stream length ratio					
	2/1	3/2	4/3	5/4	6/5	7/6
1	0.85	0.94	1.22			
2	1	0.92	1.36			
3	1.25	0.9	0.99			
4	1.61	1.01	0.49	0.1		
5	1.19	0.84	1.54			
6	0.81	1.04	1.21	0.03		
7	0.67	1.43	1.13			
8	1.17	0.91	1.19			
9	0.86	1.12	0.92	0.04		
10	1.57	0.51	0.73			
11	1.62	0.59	1.3			
12	1.29	1.04	0.98			
13	0.77	2.52	0.68	0.54		
14	1.16	0.71	0.92	0.05		
15	2.41	1.23	0.68			
16	1.56	0.68	1.21			
17	1.54	0.87	0.96			
18	1.24	1.49	0.78			
19	1.04	1.04	1.27	0.52	1.11	0.93
20	1.12	0.78	1.18			
21	0.72	1.64	0.7			
22	1.29	1.01	0.79			
23	1.18	1.29	0.87	0.04		
24	1.79	1.01	1.12			
25	1.34	0.77	1.12			
26	1.61	0.71	1.33	0.04		
27	1.07	1.05	0.61	1.47	0.66	
28	1.34	0.94	1.03			
29	1.01	0.97	0.76			
30	1.68	0.7	1.07			
31	1.41	0.59	1.11			
32	1.2	0.92	0.04	22.49	1.11	0.81
33	1.3	1	0.74			

3.4.1.5 Bifurcation Ratio (Rb)

Horton (1945) defined bifurcation ratio as the ratio of number streams of a particular order to that of the next higher order. The bifurcation ratio is usually constant for all orders of stream in a given basin or sub-basin but there is the chance of the presence of lithological and geological developmental irregularities causing its deviation (Strahler 1964). Horton (1945) explained the results of the bifurcation values and stated that the value ranges from 2 for flat or rolling basins and may go up to 3–4 for highly dissected or mountainous river basins. Strahler (1964) concluded from his study that the bifurcation ratios values between 3 to 5 for the watersheds indicates that the geological development of the basin is ineffective in altering the drainage patterns. He further indicated that basins with higher R_b values produce a low but extended peak flow whereas basins with lower R_b will produce a sharp peak flow. The Mean Bifurcation ratio for the 33 sub-basins is given in Table 3.6.

3.4.1.6 Sinuosity Indices

Rivers are of enormous significance in the landscape evolution and many studies have revealed a number of quantitative Sinuosity Indices characterizing the river channel configuration. Mueller (1968) identified two of such indices hydraulic sinuosity index and topographic index. The calculation of these sinuosity coefficients requires Channel Length (CL), Valley Length (VL), and Air Distance (AD) of the stream channel are required. Channel Length (CL) is measured along the river course. Valley Length (VL) is the length of a line between the base of the valley walls. Valley length and channel length wherever the valley and water course are near to each other whereas it will be less than channel length in case of floodplains. Air distance is the shortest aerial distance between the source and mouth of the river stream or two extreme points of individual sub-basin. Coefficient of Topographical Sinuosity (Ts) or Valley Index (VI) is the ratio of Valley Length (VL) to the Air Distance (AD) (Mueller 1968). Topographical sinuosity is indicative of present relief formation due to interaction of geological and geomorphological factors. Mueller (1968) gave Hydraulic Sinuosity Index (HSI) which is a percentage equivalent of how much a stream departs from a straight-line course within the valley owing to hydraulic sinuosity. Mueller (1968) gave Topographic Sinuosity Index (TSI) which is a percentage equivalent of how much a stream departs from a straight-line course within the valley owing to topographic interferences. Coefficient of hydraulic sinuosity (Hs) is given by ratio of Channel Length (CL) to the Valley length (VL). The values of Hs are generally higher than unity except where Valley length is equal to the channel length. Topographical sinuosity is explicitly associated with regions that are in an early stage of geomorphological evolution, whereas hydraulic sinuosity arises typically in flatlands or in regions matured relief evolution. The Sinuosity Indices for the 33 sub-basins are given in Table 3.6.

Table 3.6 Bifurcation ratio, sinuosity indices and Rho coefficient in Ghaggar river basin

Sub-basin	Mean bifurcation ratio	Valley length	Channel length	Air distance	Topographical sinuosity coefficient (Ts)-Valley index	Hydraulic sinuosity coefficient (Hs)	River sinuosity coefficient (Ks) - Channel index	Hydraulic sinuosity index	Topographic sinuosity index	Rho
1	2.04	4.02	4.28	3.47	1.16	1.07	1.23	32.00	68.00	0.49
2	2.19	2.23	2.37	1.98	1.13	1.06	1.20	36.56	63.44	0.50
3	2.09	5.34	5.75	4.82	1.11	1.08	1.19	43.59	56.41	0.50
4	8.84	6.16	6.65	5.44	1.13	1.08	1.22	40.79	59.21	0.09
5	2.34	2.53	2.72	2.30	1.10	1.08	1.18	45.45	54.55	0.51
6	3.51	3.72	4.00	3.53	1.06	1.08	1.13	58.99	41.01	0.22
7	1.63	3.60	3.86	2.96	1.22	1.07	1.31	28.96	71.04	0.66
8	2.49	4.13	4.29	3.94	1.05	1.04	1.09	46.89	53.11	0.44
9	5.48	4.38	4.79	3.41	1.29	1.09	1.41	29.55	70.45	0.13
10	1.85	6.67	7.22	5.46	1.22	1.08	1.32	31.19	68.81	0.51
11	3.16	6.13	6.49	5.57	1.10	1.06	1.17	39.09	60.91	0.37
12	1.68	7.61	8.30	6.60	1.15	1.09	1.26	40.62	59.38	0.66
13	1.84	4.34	4.87	4.07	1.07	1.12	1.20	66.64	33.36	0.61
14	3.55	4.79	5.14	3.89	1.23	1.07	1.32	28.15	71.86	0.20
15	2.02	3.97	4.34	3.66	1.08	1.09	1.19	54.48	45.52	0.71
16	1.67	9.83	10.64	8.73	1.13	1.08	1.22	42.31	57.69	0.69
17	1.67	7.38	8.08	6.55	1.13	1.09	1.23	45.55	54.46	0.67
18	1.67	6.61	7.35	5.41	1.22	1.11	1.36	38.08	61.92	0.70

(continued)

Table 3.6 (continued)

Sub-basin	Mean bifurcation ratio	Valley length	Channel length	Air distance	Topographical sinuosity coefficient (Ts)-Valley index	Hydraulic sinuosity coefficient (Hs)	River sinuosity coefficient (Ks) - Channel index	Hydraulic sinuosity index	Topographic sinuosity index	Rho
19	2.07	24.51	27.15	17.35	1.41	1.11	1.57	26.97	73.04	0.48
20	1.72	10.77	11.81	8.86	1.22	1.10	1.33	35.34	64.66	0.60
21	1.76	5.15	5.57	4.62	1.12	1.08	1.21	43.86	56.14	0.58
22	1.85	5.01	5.37	4.55	1.10	1.07	1.18	43.25	56.76	0.56
23	3.35	5.10	5.44	4.43	1.15	1.07	1.23	33.72	66.28	0.25
24	1.88	5.43	6.59	4.94	1.10	1.21	1.33	70.54	29.46	0.70
25	2.37	5.36	5.84	4.48	1.20	1.09	1.30	35.14	64.86	0.45
26	5.42	6.92	7.36	6.04	1.14	1.06	1.22	33.69	66.32	0.17
27	1.87	12.48	13.48	10.14	1.23	1.08	1.33	29.91	70.09	0.52
28	2.01	4.80	5.78	3.86	1.24	1.20	1.50	51.06	48.95	0.55
29	2.04	5.54	6.34	4.83	1.15	1.14	1.31	52.45	47.55	0.45
30	1.66	12.05	13.86	10.75	1.12	1.15	1.29	58.29	41.71	0.69
31	1.88	12.09	13.39	10.62	1.14	1.11	1.26	46.97	53.03	0.55
32	7.42	40.62	44.94	33.95	1.20	1.11	1.32	39.32	60.68	0.60
33	2.08	13.07	15.07	10.92	1.20	1.15	1.38	48.08	51.92	0.49

3.4.1.7 Rho Coefficient (ρ)

This Rho Coefficient (ρ) was defined by (Horton 1945) as the ratio of stream length ratio (MSLRu) and the bifurcation ratio (Rb). The Rho Coefficient is dependent on hydrologic, geologic, and physiographic factors which ultimately determine the relation of drainage composition and physiographic development of a sub-basin. Rho values of the Ghaggar sub-basin are given in Table 3.6. Rho Coefficient values of sub-basin number 1,2,3,4,5,6,8,9,10,11,14,19,23,25,26,29,33 are low ranging from 0.0908 to 0.5077 indicative of low water storage during flood periods and has high erosion effect while sub-basin number 7,12,13,15,16,17,18,20,21,22,24,27,28,30,31,32 have higher value ranging from 0.5188 to 0.7128 indicative of higher hydrologic storage during floods and thus reduces erosion effects at peak discharges.

3.4.2 Areal Aspects

The two-dimensional properties of the basin are defined by the areal aspects. The basin area contributing water at an outlet point can be delineated for individual streams. The outline of a watershed can be delineated from the stream having its union with higher-order stream network along the ridgeline to move upslope of the source and finally returning to the junction. This watershed boundary separates the area feeding the water toward its stream from the areas which drain in streams falling in another watershed boundary. The configuration of a basin plays a vital role in understanding the hydrological nature of the basin. The basin area and perimeter control the spatial distribution of a number of morphometric parameters such as drainage frequency, drainage density, Lemniscate's value, Form Factor, Elongation Ratio, Circularity Ratio, etc. which will be discussed in the following section.

3.4.2.1 Basin Area (*A*)

The basin area is the total area that is being drained by a stream or its system so the water falling at its farthest point on ridge is collected and discharged at a single outlet also known as pour point. The total area of Ghaggar river basin up to its confluence of Madhekali river is 559.14 km^2 and the individual area of all the 33 fourth-order streams is given in Table 3.7. It has been evident from several studies that alluvial region basins are large when compared to other geomorphological zones. Generally, the basin area and the basin length both follow a positive relation and are proportional to each other.

Table 3.7 Sub-basin-wise areal aspects in Ghaggar river basin

Sub-basin	Area (Km^2)	Perimeter (Km)	Valley length	Basin length	Lemniscate's value	Form factor	Elongation ratio	Ellipticity index	Circularity ratio
1	7.24	17.23	4.02	4.04	1.77	0.44	0.75	1.75	0.31
2	2.75	9.44	2.23	2.33	1.55	0.51	0.80	1.42	0.39
3	12.37	22.16	5.34	5.48	1.90	0.41	0.73	1.81	0.32
4	11.60	20.60	6.16	5.28	1.89	0.42	0.73	2.57	0.34
5	3.30	11.05	2.53	2.58	1.59	0.49	0.79	1.52	0.34
6	4.13	13.00	3.72	2.94	1.64	0.48	0.78	2.63	0.31
7	4.41	13.14	3.60	3.05	1.65	0.48	0.78	2.30	0.32
8	7.43	15.37	4.13	4.10	1.78	0.44	0.75	1.80	0.40
9	8.27	19.49	4.38	4.36	1.80	0.44	0.75	1.83	0.27
10	10.51	23.39	6.67	4.99	1.86	0.42	0.73	3.33	0.24
11	11.08	19.99	6.13	5.14	1.88	0.42	0.73	2.66	0.35
12	15.02	24.72	7.61	6.11	1.95	0.40	0.72	3.03	0.31
13	3.87	15.65	4.34	2.83	1.63	0.48	0.78	3.82	0.20
14	7.40	16.87	4.79	4.09	1.78	0.44	0.75	2.43	0.33
15	3.46	12.70	3.97	2.65	1.60	0.49	0.79	3.59	0.27
16	11.88	30.93	9.83	5.35	1.89	0.42	0.73	6.39	0.16
17	6.04	21.80	7.38	3.64	1.73	0.46	0.76	7.09	0.16
18	13.40	21.33	6.61	5.73	1.92	0.41	0.72	2.56	0.37
19	91.26	121.47	24.51	17.04	2.50	0.31	0.63	5.17	0.08
20	22.77	32.85	10.77	7.74	2.07	0.38	0.70	4.00	0.27
21	6.88	17.37	5.15	3.93	1.76	0.45	0.75	3.03	0.29

(continued)

Table 3.7 (continued)

Sub-basin	Area (Km^2)	Perimeter (Km)	Valley length	Basin length	Lemniscate's value	Form factor	Elongation ratio	Ellipticity index	Circularity ratio
22	7.32	17.37	5.01	4.06	1.77	0.44	0.75	2.70	0.31
23	9.61	20.77	5.10	4.74	1.84	0.43	0.74	2.13	0.28
24	5.18	19.04	5.43	3.34	1.69	0.46	0.77	4.47	0.18
25	7.95	18.32	5.36	4.26	1.79	0.44	0.75	2.84	0.30
26	11.64	24.30	6.92	5.29	1.89	0.42	0.73	3.23	0.25
27	44.89	61.64	12.48	11.39	2.27	0.35	0.66	2.72	0.15
28	3.22	15.98	4.80	2.55	1.59	0.50	0.79	5.61	0.16
29	5.28	19.88	5.54	3.38	1.70	0.46	0.77	4.57	0.17
30	14.56	36.75	12.05	6.01	1.95	0.40	0.72	7.83	0.14
31	13.27	35.75	12.09	5.70	1.92	0.41	0.72	8.65	0.13
32	145.29	197.92	40.62	22.19	2.66	0.30	0.61	8.92	0.05
33	25.86	41.68	13.07	8.32	2.10	0.37	0.69	5.19	0.19

3.4.2.2 Basin Perimeter (P)

The outer boundary of the basin enclosing its area is known as its perimeter. It is measured along the watershed divide line separating it from other sub-basins and is a vital indicator reflecting the size and shape of the basin. The basin perimeter is positively correlated to basin area and channel length. The individual perimeter of all the 33 fourth-order streams is given in Table 3.7.

3.4.2.3 Basin Length (Lb)

Schumm (1956) while explaining the relief ratio described basin length as the longest dimensional part of basin which is parallel to primary stream channel line. According to (Gardiner 1975) basin length is measured from the basin's mouth up to a point to its perimeter which is equidistant from the basin's mouth in any direction around the perimeter. Although to explain it in a more quantitative manner (Nookaratnam et al. 2005) gave the equation as given in

Sr. No	Parameter	Formula	References
36	Stream order	SOu = Hierarchical rank	Strahler (1957)
37	Stream number	$SN_u = SN_1 + SN_2 + \ldots SN_n$	Horton (1945)
38	Stream length	$SL_u = SL_1 + SL_2 \ldots\ldots SL_n$	Strahler (1964)
39	Mean stream length	$MSL_u = \frac{\sum_{i=1}^{N} SO_u}{SN_u}$	Strahler (1964)
40	Mean stream length ratio	$MSLR_u = \frac{MSL_u}{MSL_u - 1}$	Horton (1945)
41	Bifurcation ratio	$R_b = \frac{SN_u}{SN_u + 1}$	Strahler (1964)
42	Valley length	VL	Mueller (1968)
43	Channel length	CL	Mueller (1968)
44	Air distance	AD	Mueller (1968)
45	Coefficient of topographical sinuosity (Ts) or valley index (VI)	$TsorVI = \frac{VL}{AD}$	Mueller (1968)

to calculate the basin length. The basin lengths for all the 33 sub-basins are given in Table 3.7.

3.4.2.4 Lemniscate's Value (L_k)

Chorley et al. (1957) derived the Lemniscate's value since the conventional circularity ratio used in sedimentary petrology provides very little insight into the actual shape of the drainage basin. The Lemniscate's values are given in Table 3.7 for Ghaggar basin. The L_k values drastically control the shape of the drainage basin. The L_k values

are one for circular basins and as its value increases, the shape of the drainage basins becomes more and more elongated.

3.4.2.5 Form Factor (Ff)

Horton (1932) defined the Form Factor as the ratio of the area to the length of the drainage basin. The basin length is to be measured from a point on the watershed perimeter opposite the mouth of the mainstream. The length of the drainage basins having a side outlet may have less length as compared to the width. Form Factor is an indicative morphometric parameter of the flood-regime of the stream in case of long and elongated drainage basins but the same is not the case with drainage basins of irregular shapes. The value of F_f varies from 0 for highly elongated basins to unity, i.e., 1 for perfectly circular shaped basins. The sub-basins of Ghaggar river basins evidently show that they have slightly elongated basin shape having low Form Factor with a flatter peak of flow for a longer duration which results in groundwater percolation. The Form Factor (F_f) values of sub-basins of Ghaggar river basin are shown in Table 3.7.

3.4.2.6 Elongation Ratio (Re)

Schumm (1956) defined Elongation Ratio as the ratio of diameter of a circle having the same area as that of the basin to the maximum basin length. It acts as an imperative index for basin shape analysis. The areas having higher Elongation Ratio values possess high infiltration capacity and low surface runoff. An elongated basin is less effectual in runoff discharge as compared to a circular basin (Singh and Singh, Morphometric analysis of Kanhar river 1997). According to (Strahler 1964) following inferences about the shape of a basin were deduced from the Elongation Ratios: circular (>0.9), oval (0.8–0.9), less elongated (0.7–0.8), elongated (0.5–0.7) and more elongated (<0.5). The Re values of sub-basins of Ghaggar basins range from 0.613 to 0.803 and are tabulated in Table 3.7. The Re values of Ghaggar sub-basins reveal that majority of the them are elongated in shape and are associated with strong relief and steep slope.

3.4.2.7 Ellipticity Index (Le)

The ellipticity index similarly to Form Factor and Elongation Ratio provides a comparable relationship between morphometry and hydrology (Stoddart 1965). Lower ellipticity values indicate a quick runoff draining basin because of which the stream channels might swell or overflow resulting in downstream flooding in case of heavy rainfall. The values of the ellipticity index are given in Table 3.7.

3.4.2.8 Circularity Ratio (R_c)

Circulatory ratio was defined by (Miller 1953) as the ratio of basin area of the area of a circle having an equal perimeter as that of the basin. Circularity ratio defines the circularity of the basin and is a dimensionless entity. R_c values of the Ghaggar river sub-basin ranges from 0.046 to 0.3953. The lowest value of R_c (0.3953) lies in Sub-Basin 8 attributes to the high to moderate relief and structurally controlled drainage system. The values of the circularity ratio are given in Table 3.7.

3.4.3 Drainage Characteristics

Drainage density, drainage texture, stream frequency, Infiltration number, and drainage intensity are the vital elements reflecting the areal and relief characteristics of a basin as a whole. These elements supplemented the prediction of overland flow, runoff estimation, sediment yield of a river, etc. the analysis of these elements supports the spatio-temporal distribution of drainage basin processes.

3.4.3.1 Drainage Density (D_d)

Horton (1932) defined drainage density as the ratio of stream length to that of drainage area. Drainage density act as a permeability indicator of the drainage basin surface. High drainage densities are pertinent to the regions having impervious subsurface with weak structure whereas low densities are associated with highly resistant subsurface covered by vegetation and having low relief. But there are limitations associated with Horton's methods that first it indicates a single value for drainage density and secondly it doesn't take into consideration the study of frequency analysis and spatial variations of drainage density within a physiographic region. Gardiner (1971) suggested the use of grid square method of equal sizes to minimize the scale distortion. This methodology is the most widely accepted providing a faster and easier method for the drainage density analysis by dividing the complete basin into a number of grids of 1 Km^2 and then measuring the stream links, junctions intersecting with the boundary of grid square and grid square diagonal. The drainage density spatial distribution within the Ghaggar basin is depicted in Fig. 3.4. The sub-basins-wise values of the drainage density of Ghaggar basin are given in Table 3.8.

3.4.3.2 Drainage Texture (D_t)

Horton (1945) defined drainage texture on the basis of stream frequency, i.e., number of streams per unit of basin area. Drainage texture is defined as the cumulative length of permanent and temporary streams per unit of area. Singh (1976) defined the drainage texture on the basis of relative spacing of the streams per unit length in a square grid. In

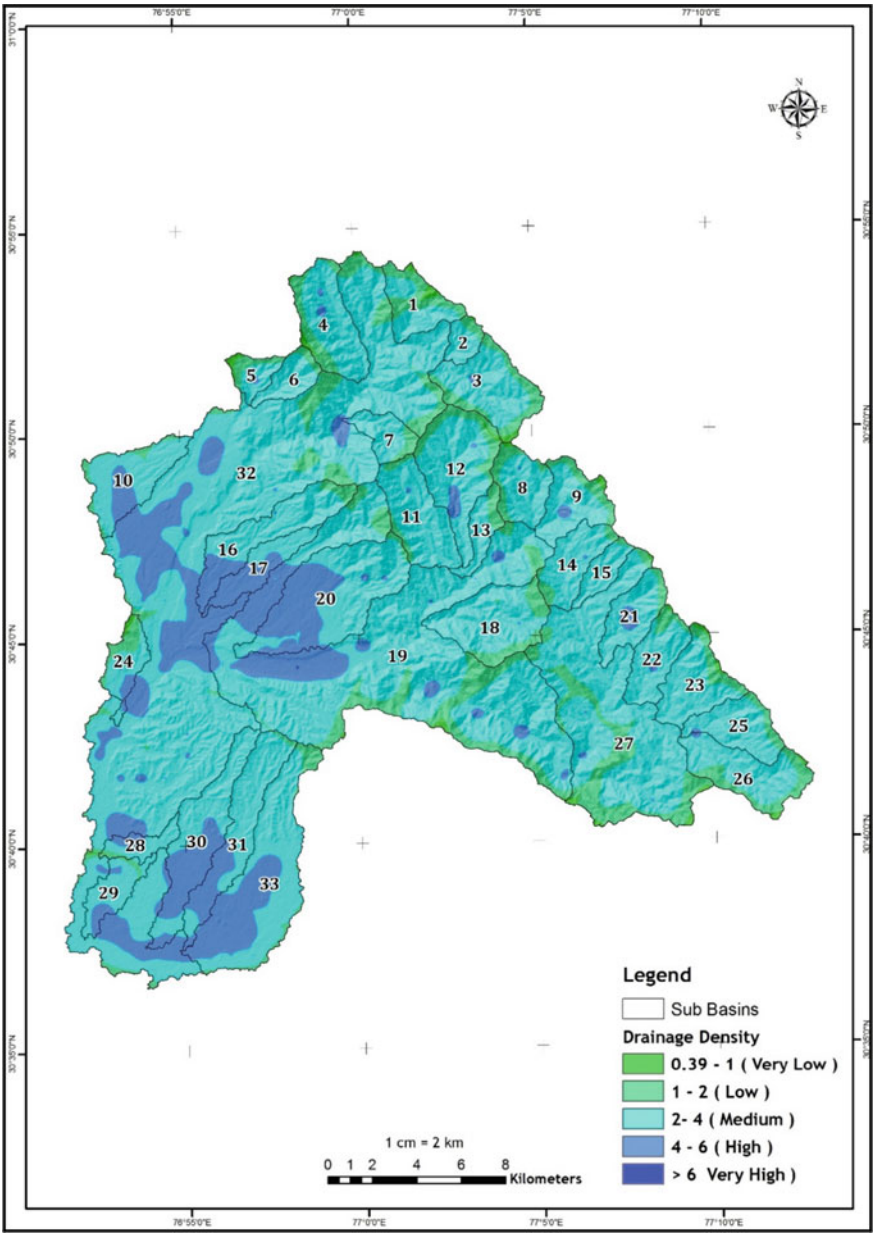

Fig. 3.4 Spatial distribution of drainage density in Ghaggar basin

Table 3.8 Sub-basins wise drainage characteristics values of the Ghaggar basin

Sub-basin	Drainage characteristics (Mean values)				
	Drainage density	Drainage texture	Stream frequency	Drainage intensity	Infiltration number
1	2.10	1.16	15.24	6.16	37.48
2	2.58	0.72	12.60	5.17	38.97
3	2.48	0.73	15.19	5.79	39.71
4	2.61	0.78	14.60	5.80	47.47
5	2.33	1.20	11.67	5.88	50.72
6	2.71	0.74	12.86	5.45	42.47
7	2.66	0.68	16.64	5.89	52.31
8	2.41	0.67	15.04	6.19	39.42
9	2.64	0.82	15.90	5.91	52.41
10	3.13	0.68	13.70	4.11	61.73
11	2.75	0.61	15.14	5.50	45.98
12	2.80	0.63	16.54	5.63	51.12
13	2.56	0.56	14.34	5.87	36.66
14	2.84	0.63	15.46	5.14	51.03
15	2.86	0.70	14.33	4.97	46.25
16	3.24	0.54	14.39	4.66	52.24
17	4.02	0.41	13.99	3.93	63.88
18	2.52	0.61	13.63	5.57	38.74
19	2.96	0.63	15.27	5.27	55.95
20	3.74	0.43	16.82	4.73	66.15
21	3.08	0.60	17.18	5.55	63.29
22	2.77	0.61	15.58	5.68	51.14
23	2.85	0.68	16.09	5.68	53.97
24	2.60	1.08	12.38	4.30	54.85
25	2.98	0.65	13.44	4.73	48.05
26	2.49	0.71	13.19	5.35	46.82
27	2.57	0.65	14.19	5.45	50.24
28	3.44	0.48	15.14	4.13	64.53
29	3.44	0.57	15.78	4.26	56.57
30	3.78	0.45	15.91	4.26	62.88
31	3.57	0.44	16.02	4.51	59.87
32	3.25	0.58	15.62	4.97	60.44
33	3.46	0.65	14.29	4.24	61.42

the current work, his method of counting the streams crossing the perimeter (4 edges) of the square grid and two of its diagonals is used. The drainage texture spatial distribution within the Ghaggar basin is depicted in Fig. 3.5. The sub-basins-wise values of the drainage density of Ghaggar basin are given in Table 3.8.

3.4.3.3 Stream Frequency (S_f)

Horton (1945) defined the computation of stream frequency as the total number of streams per unit area. Stream frequency shows a positive correlation with the drainage density. He also used it as an index of drainage texture but the concept lasted not long. But it signifies a single value of stream frequency and hence is practically not useful. Therefore, a most widely accepted methodology of providing a faster and easier method for the stream frequency analysis is adopted by dividing the complete basin into a number of grids of 1 km^2 and then counting the stream orders within the grid square. The sub-basins wise values of the drainage density of Ghaggar basin are given in Table 3.8.

3.4.3.4 Drainage Intensity (D_i)

Drainage intensity was defined by (Faniran 1968) as the ratio of the stream frequency (S_f) to the drainage density (D_d). But it signifies a single value of drainage intensity and hence is practically not useful. Therefore, a most widely accepted methodology of providing a faster and easier method for the drainage intensity analysis is adopted by dividing the complete basin into a number of grids of 1 Km^2 and then using it to calculate the drainage density and stream frequency to further calculate the drainage intensity. The entire region was divided into 646 grids of one square km. Figure 3.6 portrays the drainage intensity spatial distribution within the Ghaggar basin. The study area has low to moderate drainage intensity implying that drainage density and stream frequency have marginally low effects (if any) on the extent to which the surface has been depressed by denudational agent. The sub-basins-wise values of drainage intensity of the Ghaggar basin are given in Table 3.8.

3.4.3.5 Infiltration Number (I_n)

Faniran (1968) defined the Infiltration number of a drainage basin as the product of drainage density (D_d) and stream frequency (S_f) of a basin. But it signifies a single value of Infiltration Number and hence is practically not useful. Therefore, a most widely accepted methodology of providing a faster and easier method for the Infiltration Number analysis is adopted by dividing the complete basin into a number of grids of 1 Km^2 and then using it to calculate the drainage density and stream frequency based upon which Infiltration Number is calculated. The Infiltration Number spatial distribution within the Ghaggar basin is depicted in Fig. 3.7. The sub-

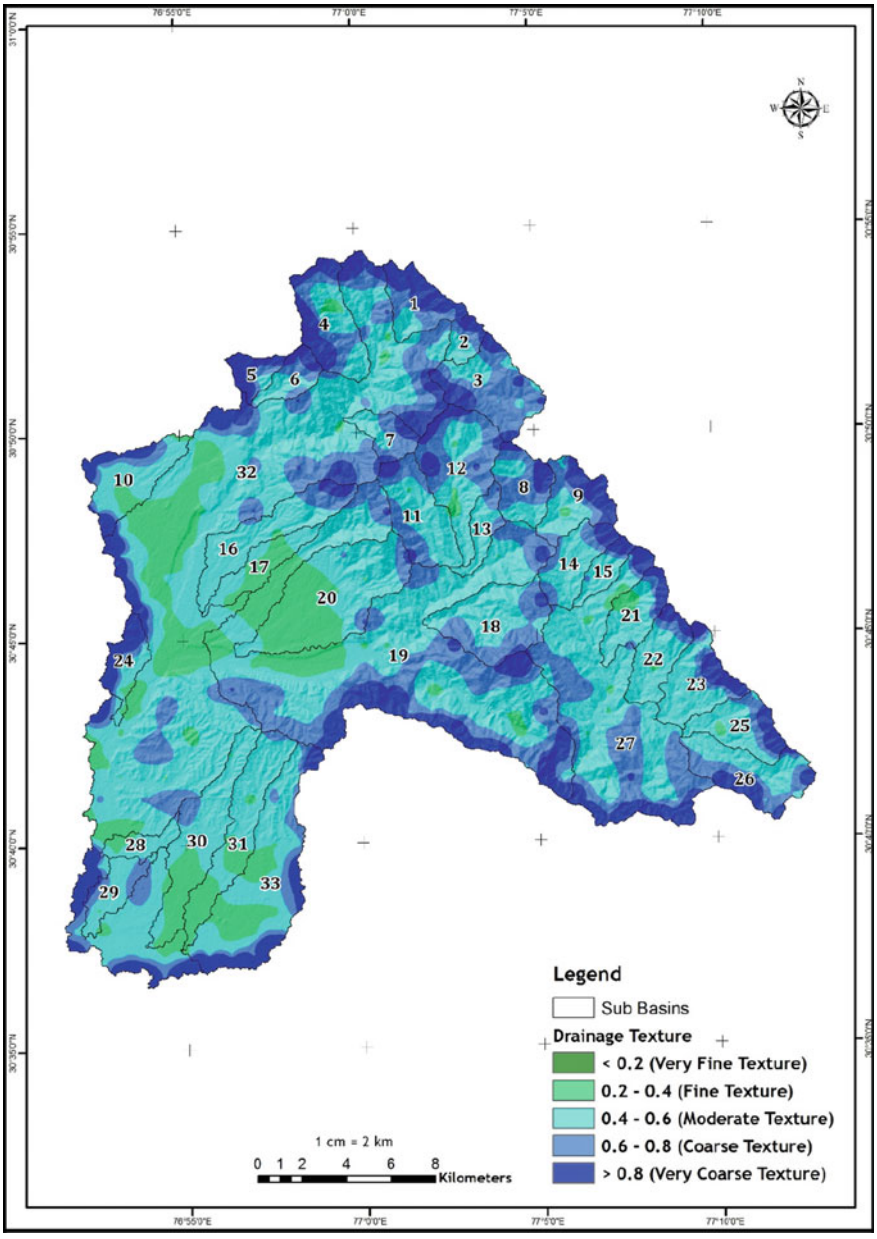

Fig. 3.5 Spatial distribution of drainage texture in Ghaggar basin

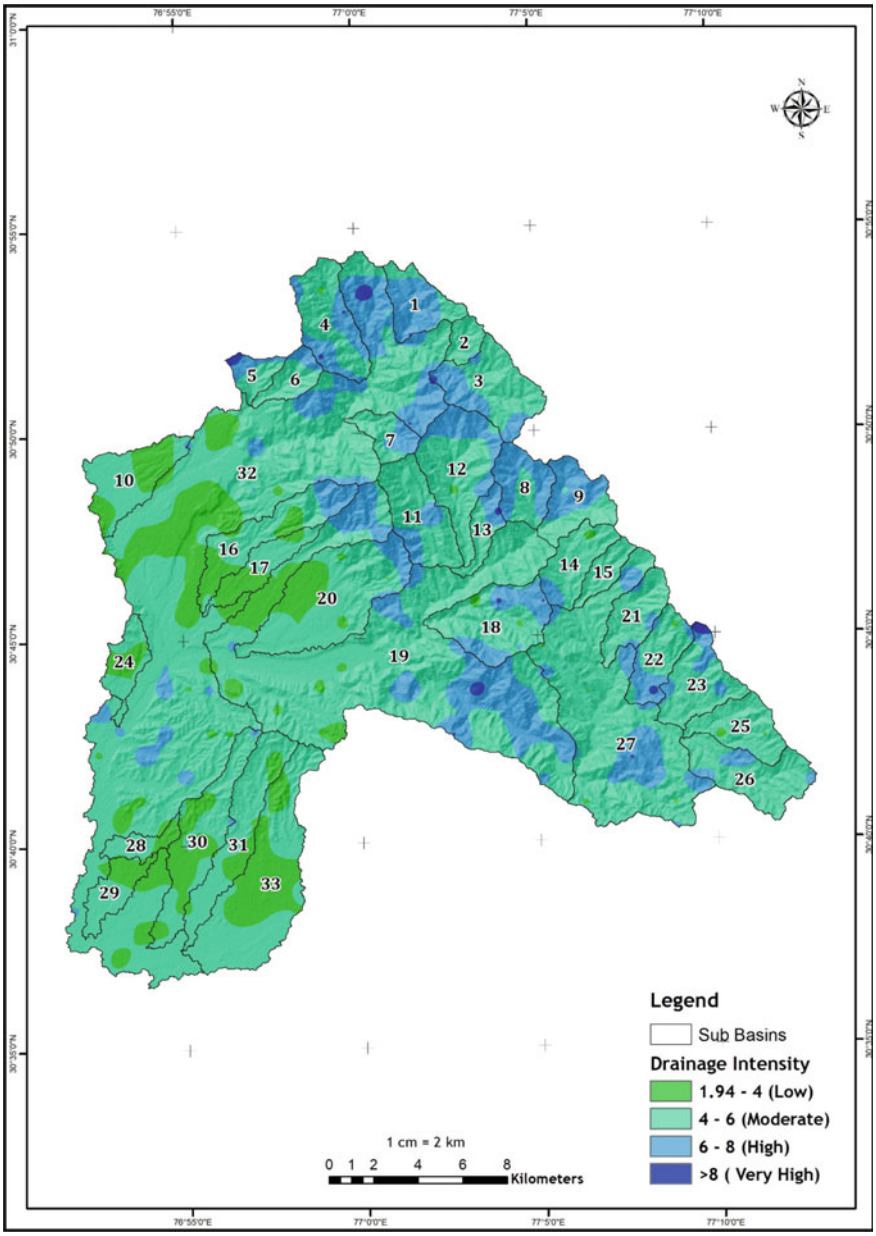

Fig. 3.6 Spatial distribution of drainage intensity in Ghaggar basin

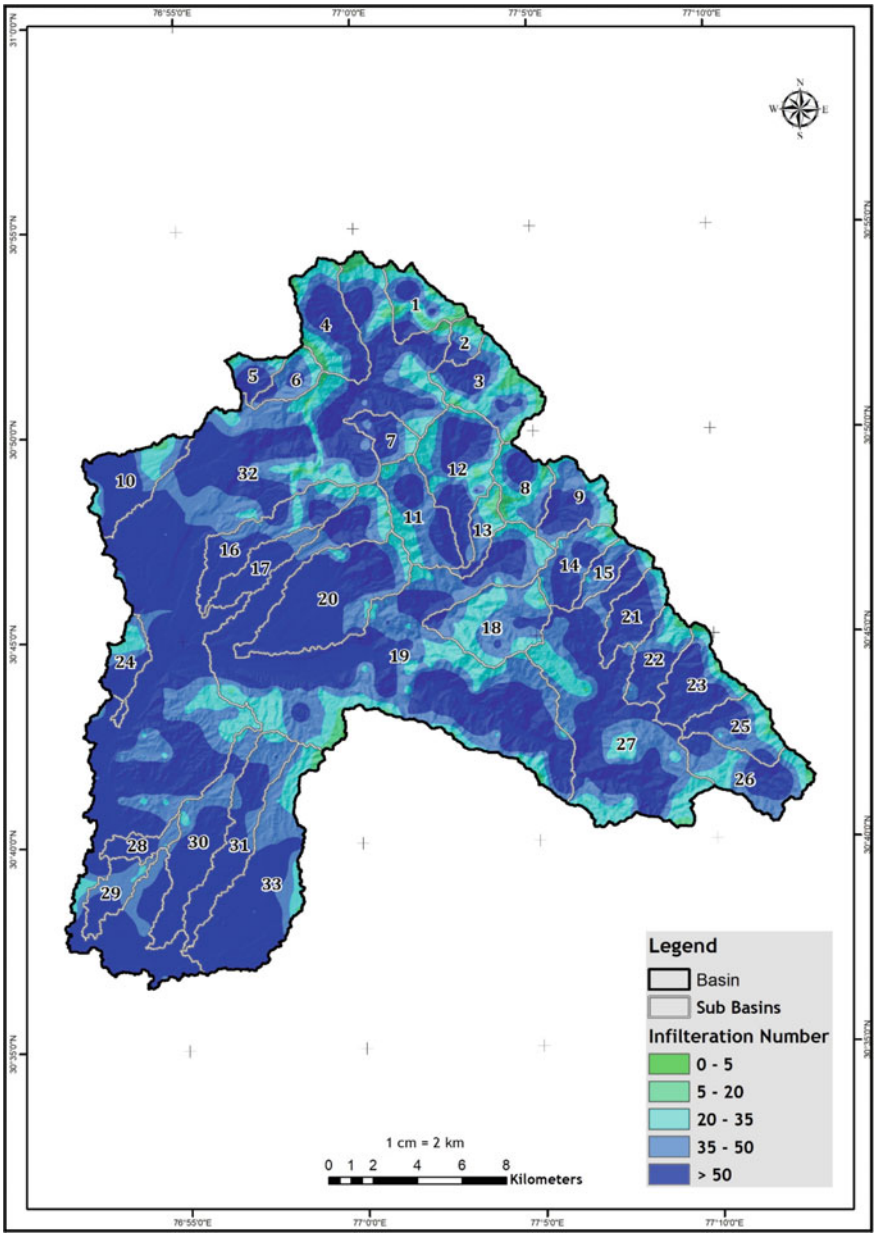

Fig. 3.7 Spatial distribution of infiltration number in Ghaggar basin

basins-wise values of the drainage density of Ghaggar basin are given in Table 3.8. The Infiltration Number within the Ghaggar basin ranges from 0.707 to 205 and about 46 percentage of this is above 50 and this value indicates low infiltration and medium to high runoff, the lithology of basin is hard and impermeable. The higher values of Infiltration Number contribute to lower infiltration rates and result in the higher runoff.

3.4.4 Relief Characteristics

The relief characteristics of a basin are a representation of the areal, volume, and altitudinal aspects of the basin landscape. The relief characteristics of morphometric analysis include absolute relief, aspect, dissection index, relative relief ratio, relative relief, Ruggedness Number, and slope.

3.4.4.1 Absolute Relief (Ra)

Absolute relief defines the maximum elevation of a basin area. This parameter helps in determining the rate of erosion with respect to the current summit or hilltops of a basin since these hilltops or summits act as the last remnant of the endangered relief. The absolute relief of Ghaggar basin ranges from 260 to 1858 m and the mean height of the basin stands at 910.2 m. The sub-basins wise values of absolute relief of the Ghaggar basin are given in Table 3.9. The absolute relief of the Ghaggar basin has been grouped into five classes, i.e., low (<300 m) occupying 5.81%, moderately low (300–600 m) occupying 28.74%, moderate (600–900 m) occupying 12.97%, moderately high (900–1200 m) occupying 23.00% and high (>1200 m) occupying 29.48% of area respectively. The absolute relief spatial distribution within the Ghaggar basin is shown in Fig. 3.8.

3.4.4.2 Relative Relief (R_r)

Relative relief plays a vital role in the calculation average slope, dissection determination, and in assessing the terrain development stages. Smith (1935) coined the term relative relief in order to highest and lowest altitude points of a particular area. The sub-basins-wise values of relative relief of the Ghaggar basin are given in Table 3.9. The relative relief of the Ghaggar basin has been grouped into six classes, i.e., low (<70 m) occupying 22.31%, moderately low (70–140 m) occupying 14.57%, moderate (140–220 m) occupying 12.20%, moderately high (220–320 m) occupying 19.59%, high (320–420 m) occupying 20.78%, and very high (> 420 m) occupying 10.55%, of area respectively. The absolute relief spatial distribution within the Ghaggar basin is shown in Fig. 3.9.

Table 3.9 Sub-basins wise relief characteristics values of the Ghaggar basin

Sub-basin	Relief characteristics (Mean values)					
	Absolute relief	Relative relief	Relative relief ratio	Dissection index	Ruggedness number	Slope
1	1803.12	838.01	4.86	0.47	1.76	44.05
2	1803.71	728.70	7.72	0.40	1.88	46.34
3	1743.79	668.79	3.02	0.38	1.66	39.40
4	1869.24	1007.27	4.89	0.54	2.63	47.79
5	1467.04	757.43	6.85	0.52	1.77	40.32
6	1691.08	982.09	7.55	0.58	2.66	54.91
7	1572.49	825.86	6.29	0.53	2.20	47.45
8	1499.51	696.31	4.53	0.46	1.68	43.77
9	1724.91	921.71	4.73	0.53	2.44	44.58
10	595.74	159.12	0.68	0.27	0.50	7.91
11	1612.31	962.44	4.82	0.60	2.65	45.12
12	1568.10	918.23	3.71	0.59	2.57	43.94
13	1382.21	745.25	4.76	0.54	1.91	41.48
14	1757.03	865.36	5.13	0.49	2.46	36.28
15	1749.25	857.58	6.76	0.49	2.45	37.91
16	1522.85	1127.72	3.65	0.74	3.65	28.49
17	1026.53	631.41	2.90	0.62	2.54	9.93
18	1447.10	882.60	4.14	0.61	2.22	45.73
19	1610.25	1250.60	1.03	0.78	3.70	35.79
20	1318.35	937.23	2.85	0.71	3.50	21.50
21	1850.07	1030.22	5.93	0.56	3.17	41.32
22	1840.28	1048.79	6.04	0.57	2.90	38.03
23	1804.79	983.59	4.74	0.55	2.80	40.92
24	501.00	189.50	1.00	0.38	0.49	11.65
25	1624.53	776.53	4.24	0.48	2.32	38.51
26	1560.62	712.62	2.93	0.46	1.77	38.05
27	1782.66	1073.64	1.74	0.60	2.76	37.65
28	393.22	127.64	0.80	0.33	0.44	7.33
29	315.72	65.86	0.33	0.21	0.23	5.11
30	692.80	433.93	1.18	0.63	1.64	11.70
31	727.48	460.46	1.29	0.63	1.64	13.59
32	1721.41	1471.75	0.74	0.86	4.78	22.54
33	740.73	473.72	1.14	0.64	1.64	8.83

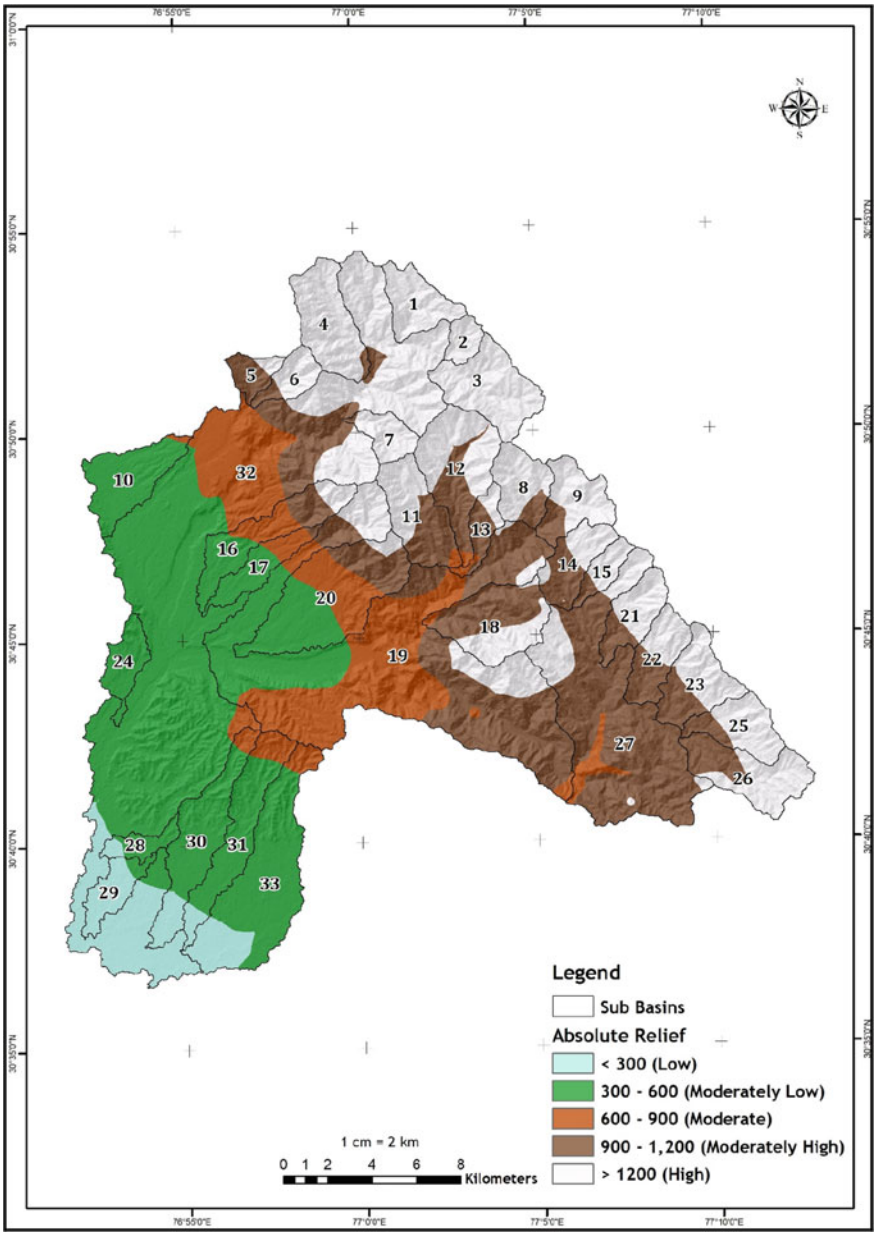

Fig. 3.8 Spatial distribution of absolute relief in Ghaggar basin

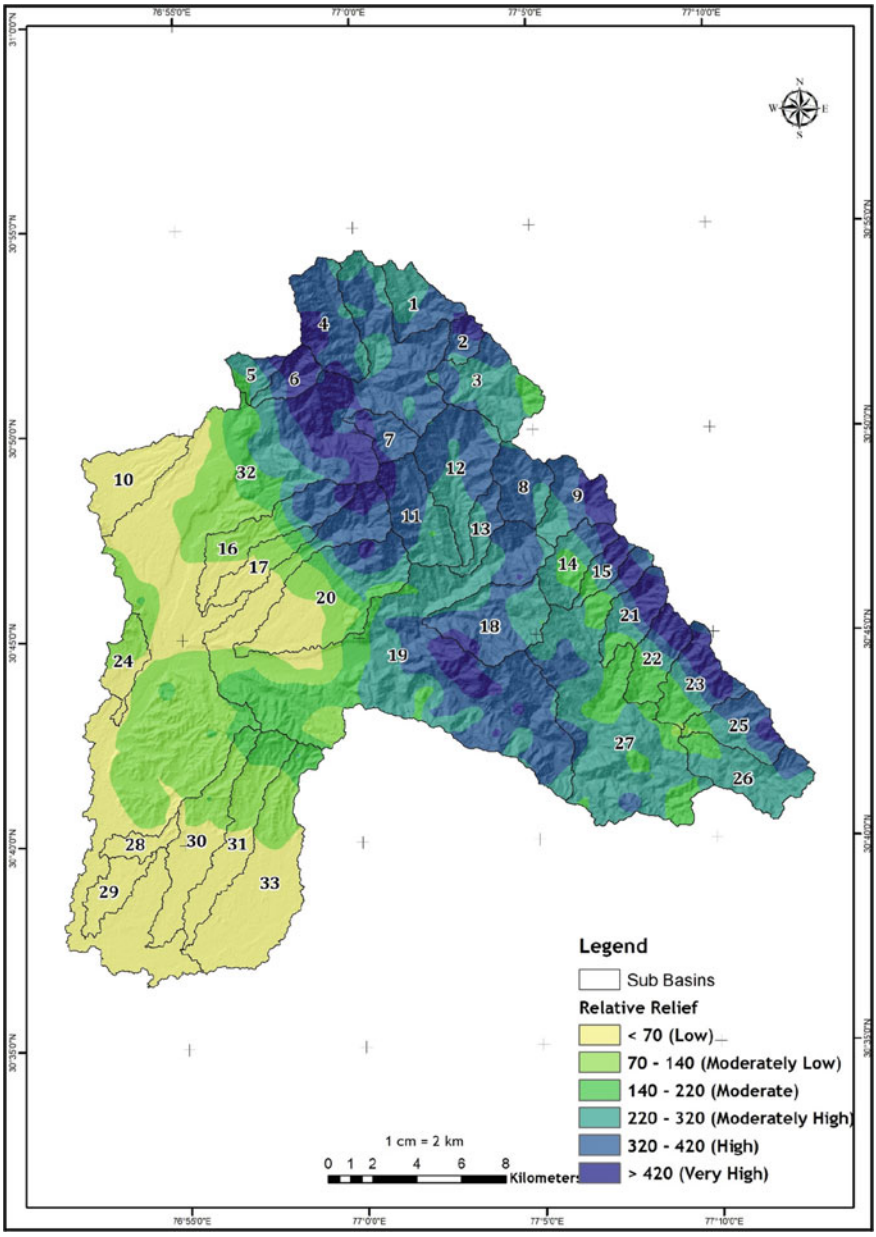

Fig. 3.9 Spatial distribution of relative relief in Ghaggar basin

3.4.4.3 Relative Relief Ratio (R_{hp})

Relative relief ratio (Melton 1958) is the ratio of the difference between maximum altitude and minimum altitude for a given area denoted by R_r, and the perimeter (P) of the area. Relative relief ratio acts as an indicator of relative velocity of the perpendicular tectonic movements. The sub-basins-wise relative relief ratio values of the Ghaggar basin are given in Table 3.9. The lower values of the relative relief ratio pertain to the less resistive rocks.

3.4.4.4 Dissection Index (Di)

Dissection index is expressed as the ratio of relative relief to absolute relief of an area (Nir 1957). It acts as a vital parameter for developing an understanding of the degree of dissection (high, moderate, or low) and evolution of the stages of landform (young, mature, and old) development in any given physiographic region. Dissection index also offers valuable insight into the slope nature (steep, moderate, or gentle). The values of dissection range from 0 (implying a theoretical value as there is no region in nature which is passive to erosion) to 1. However, the ratio can be more than 1 only in case of incomparable cases of cliff. The sub-basins-wise dissection index values of the Ghaggar basin are given in Table 3.9. The dissection index spatial distribution within the Ghaggar basin is shown in Fig. 3.10.

3.4.4.5 Ruggedness Number (R_n)

The structural complexity of the terrain is measured by Ruggedness Number. It is a dimensionless property which is a product of R_r and drainage density of a given basin area having the same units. If the drainage density D_d is increased keeping the R_r constant there is an increase in slope steepness whereas if the R_r is increased keeping D_d constant it is also accompanied by slope steepness. In case the values of R_r and D_d are both high then slopes will be steep as well as long (Strahler 1964). The sub-basins-wise Ruggedness Number values of the Ghaggar basin are given in Table 3.9. The Ruggedness Number spatial distribution within the Ghaggar basin is shown in Fig. 3.11. Patton and Baker (1976) discussed that the areas having higher ruggedness numbers accompanied with fine drainage texture, and minimalistic length of overland flow on steep slopes have the expectancy of potential flash flooding. These morphometric parameters combination may lead to higher flood peaks for an are having low Ruggedness Number even for equivalent of rainfall events.

3.4.4.6 Slope (S)

The angular inclination of topography formed between top of the hills and valley bottoms is known as slope. It may also be defined as the maximum rate of change in

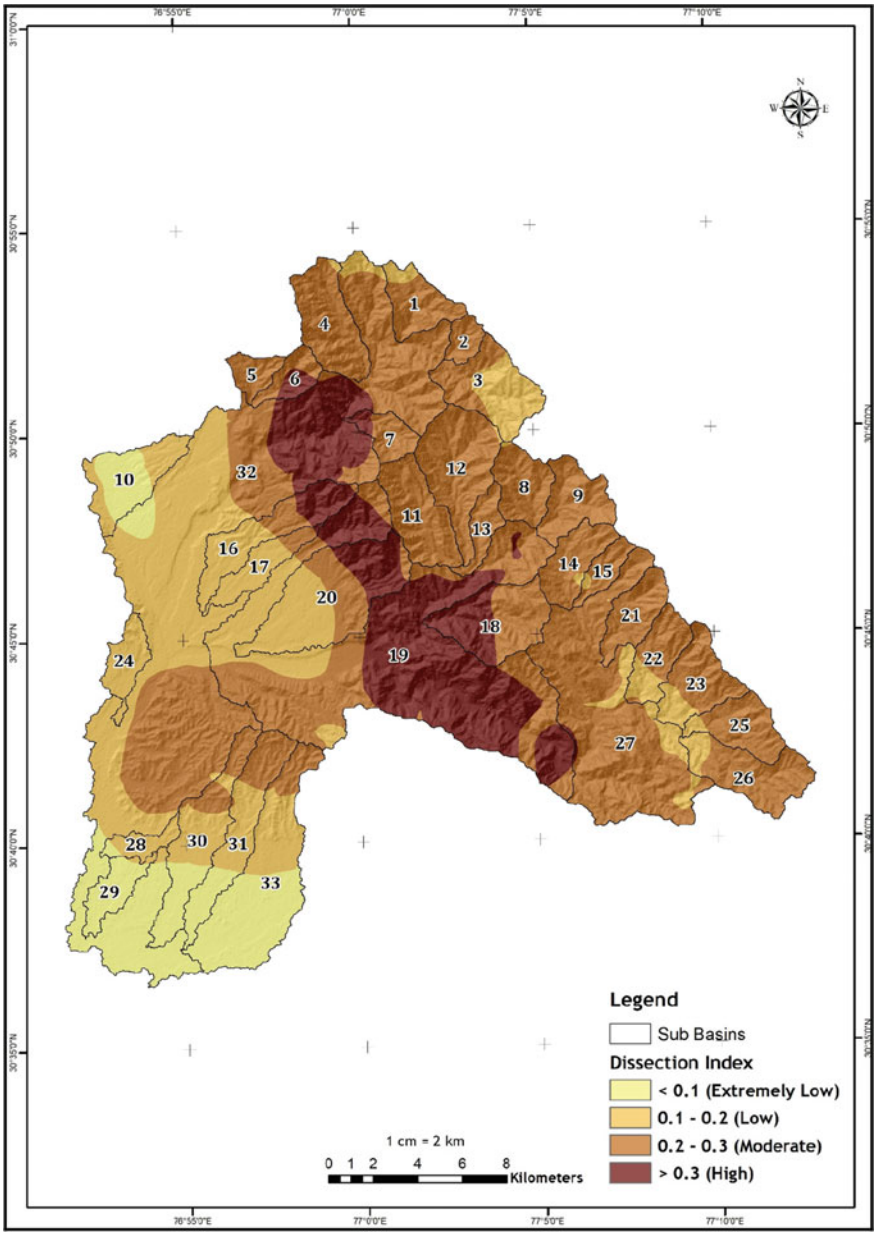

Fig. 3.10 Spatial distribution of dissection index in Ghaggar basin

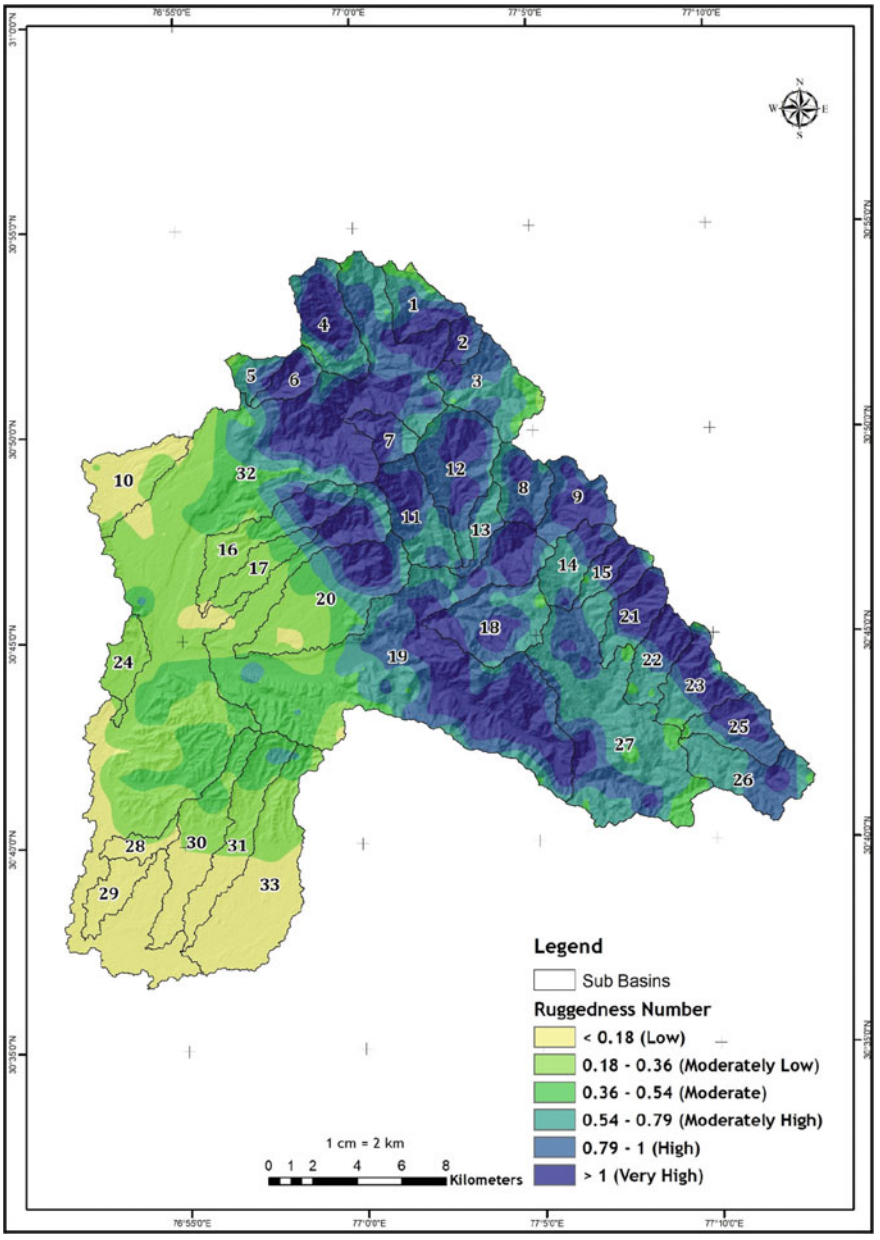

Fig. 3.11 Spatial distribution of ruggedness number in Ghaggar basin

elevation values for each cell to its neighboring cells. The slope plays a vital role in geomorphic studies as it acts act a controlling factor for natural and anthropogenic activities such as soil, agriculture, communication, transport, and settlements. The steepness of a drainage basin slope is an indicator of erosion intensity operable in the basin. The slope map of Ghaggar basin is prepared using Sentinel 1 DEM in ArcGIS. The slope angles of Ghaggar basin have been grouped into five categories (1) level (0–2°), gentle (2–5°), moderate (5–10°), high (10–15°) and very high (>15°). The sub-basins-wise slope values of the Ghaggar basin are given in Table 3.9. The slope spatial distribution within the Ghaggar basin is shown in Fig. 3.12.

3.4.4.7 Aspect (AS)

Aspect as calculated from the ArcGIS software shows the relative position of slopes with respect to sun angle direction. It can be also described as the downward slope direction of the extreme change in value from each cell to its neighbors. The values in the output raster indicate the compass direction which the surface faces at that particular cell value location. The aspect is clockwise in degrees from 0 (due north) to 360 (again due north). Flat areas are given a value of −1. The aspect spatial distribution within the Ghaggar basin is shown in Fig. 3.13.

3.4.5 Hypsometric Analysis

Strahler (1952) defined the hypsometric analysis as the relationship between horizontal cross-sectional drainage basin area to its elevation for small basin. It is being used extensively in identifying the stages of evolution of the erosional landforms. Hypsometric curves and integrals are important watershed conditions indicator. The interpretation of the hypsometric curves and integrals is based upon the degree of basin dissection and relative age of landform. The shape of the curve is convex-up with high integrals for youth stage; disequilibrium stage for undissected landscape; smooth S-shaped curve signifies mature landscapes in mature stage and finally concave up curves having lower integrals curve values represent old and deeply dissected landscapes (Strahler 1952). The difference in the shape of the curve implies the relationship between erosion and tectonic forces balance prevailing within the basin. The hypsometric curve for the current study is expressed as the ratio of relative height to the relative area in respect to the total height and total area of a drainage basin. The hypsometric curve of the entire Ghaggar basin represents a typical S-shaped curve indicating the mature development of the basin as given in Fig. 3.14. The sub-watershed of Ghaggar basin have varied shaped hypsometric curves from convex, concave to S-shaped characterizing their development from youth to mature stage. The difference in the shape of the curve owes to the lithological characteristics, bedrock incision, sediment removal, and downward movement of eroded materials prominent within the individual watersheds.

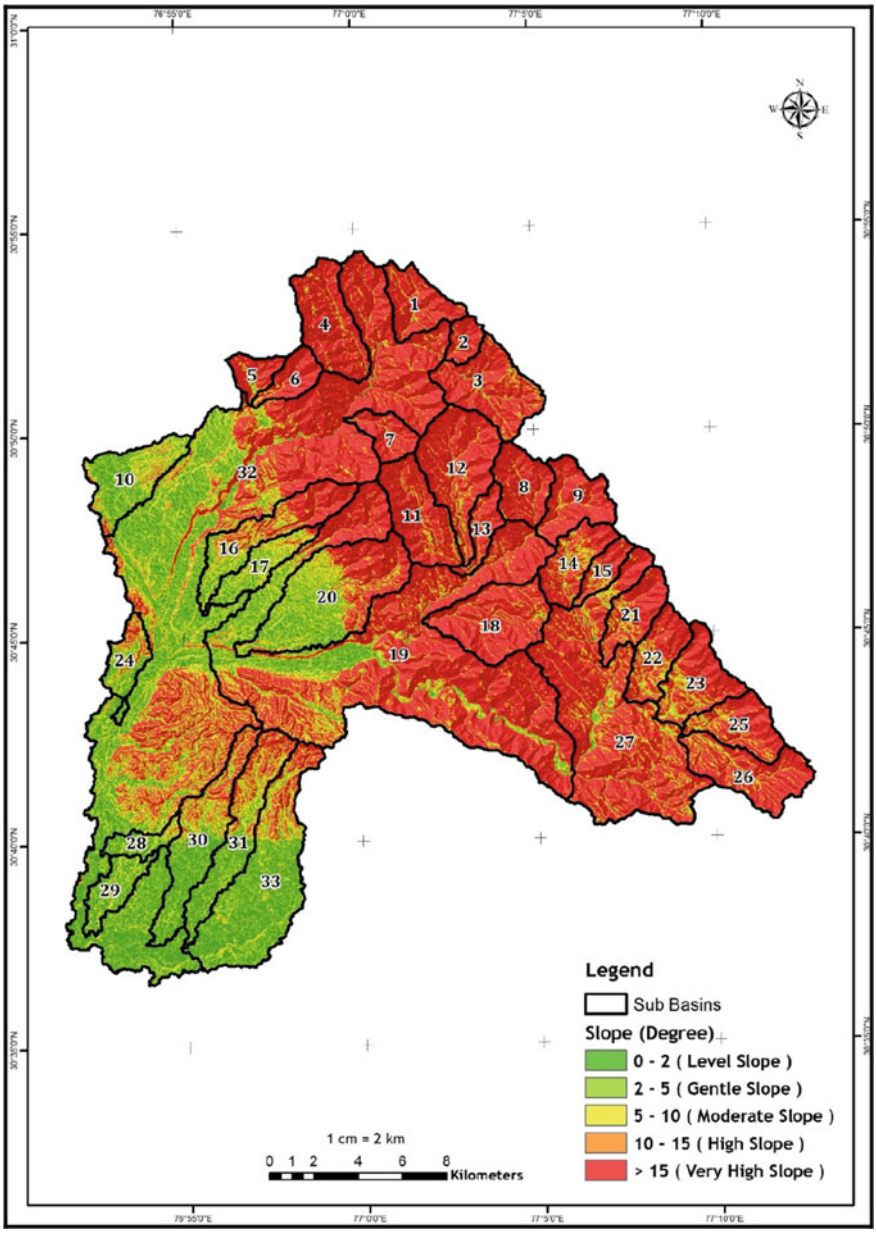

Fig. 3.12 Spatial distribution of slope in Ghaggar basin

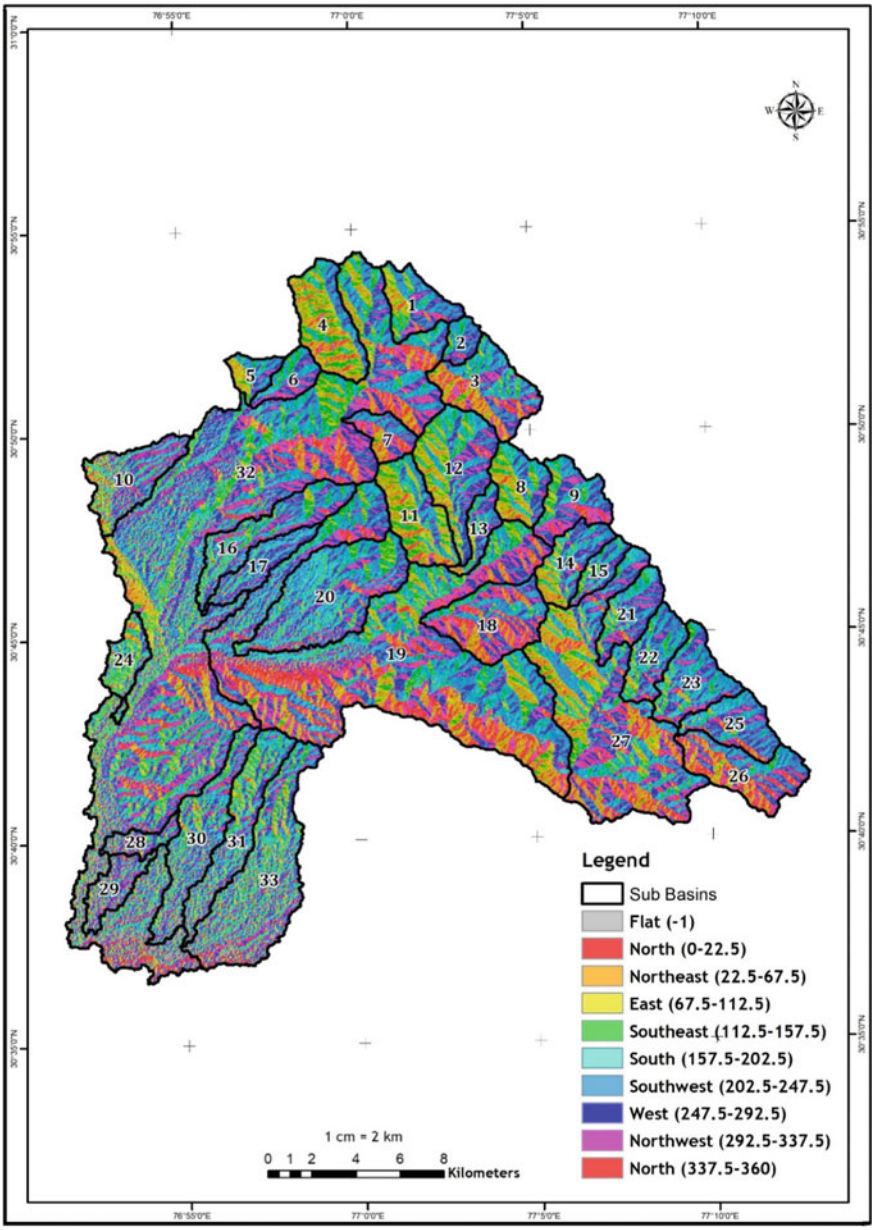

Fig. 3.13 Spatial distribution of aspect in Ghaggar basin

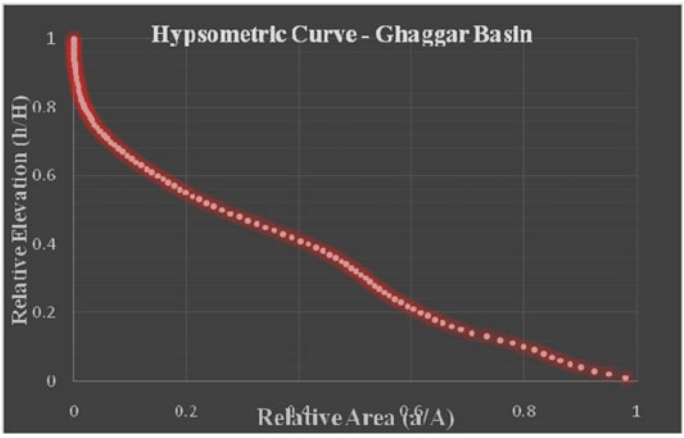

Fig. 3.14 Hypsometric curve of the Ghaggar basin

3.4.5.1 Hypsometric Integral

Pike and Wilson (1971) expressed the hypsometric integral based upon the mean, maximum and minimum elevation prevalent in the sub-watershed. Strahler (1952) classified the hypsometric integrals values base upon three threshold limits representing the characteristic phases of geomorphic cycle.

$HI \geq 0.60$: in equilibrium or young stage.

$0.35 \leq HI \leq 0.60$: the equilibrium or mature stage and

$HI \leq 0.35$: the monadnock or old stage.

In the equilibrium or young stage of early development, the transformation of the slopes is rapid owing to the expansion and branching of the drainage system. An equilibrium stage signifies the mature stage wherein the steady-state has been attained resulting due to diminishing of the relief. The monadnock phase signifies the old stage which is in the transitory phase since the removal of the monadnock results in refurbishment of the curve toward the equilibrium stage. The hypsometric integral value of the Ghaggar basin is calculated to be 0.33, which reveals that 33 percent of the rock masses still exist in basin. The calculated hypsometric integral values for all the sub-watersheds of the Ghaggar basin range from 0.15 to 0.58 as shown in Table 3.10. The spatial distribution of hypsometric integral (HI) values obtained for thirty-three sub-watersheds are shown in Fig. 3.15.

Table 3.10 Hypsometric integral values of sub-watershed within Ghaggar basin

Sub-watersheds	Elevation			Integral	Geological stage
	Minimum	Maximum	Mean		
1	965.11	1803.12	1343.35	0.45	Maturity stage
2	1075.01	1803.71	1413.10	0.46	Maturity stage
3	1075.01	1743.79	1366.69	0.44	Maturity stage
4	861.96	1869.24	1377.71	0.51	Maturity stage
5	709.61	1467.04	934.67	0.30	Old stage
6	708.99	1691.08	1182.91	0.48	Maturity stage
7	746.63	1572.49	1230.83	0.59	Maturity stage
8	803.20	1499.51	1120.64	0.46	Maturity stage
9	803.20	1724.91	1176.78	0.41	Maturity stage
10	436.62	595.74	492.70	0.35	Maturity stage
11	649.87	1612.31	1039.78	0.41	Maturity stage
12	649.87	1568.10	1092.19	0.48	Maturity stage
13	636.96	1382.21	943.48	0.41	Maturity stage
14	891.67	1757.03	1144.84	0.29	Old stage
15	891.67	1749.25	1218.53	0.38	Maturity stage
16	395.13	1522.84	701.32	0.27	Old stage
17	395.13	1026.53	530.77	0.21	Old stage
18	564.50	1447.10	1004.45	0.50	Maturity stage
19	359.65	1610.25	732.69	0.30	Old stage
20	381.13	1318.35	631.36	0.27	Old stage
21	819.85	1850.07	1209.62	0.38	Maturity stage
22	791.49	1840.28	1132.43	0.33	Old stage
23	821.21	1804.79	1166.50	0.35	Maturity stage
24	311.51	501.00	388.26	0.41	Maturity stage
25	848.00	1624.53	1169.82	0.41	Maturity stage
26	848.00	1560.62	1125.09	0.39	Maturity stage
27	709.01	1782.66	980.55	0.25	Old stage
28	265.58	393.22	303.30	0.30	Old stage
29	249.86	315.72	271.47	0.33	Old stage
30	258.87	692.80	362.54	0.24	Old stage
31	267.02	727.48	398.33	0.29	Old stage
32	249.66	1721.41	611.89	0.25	Old stage
33	267.02	740.73	340.39	0.15	Old stage
Ghaggar basin	249.66	1869.24	787.91	0.33	Old stage

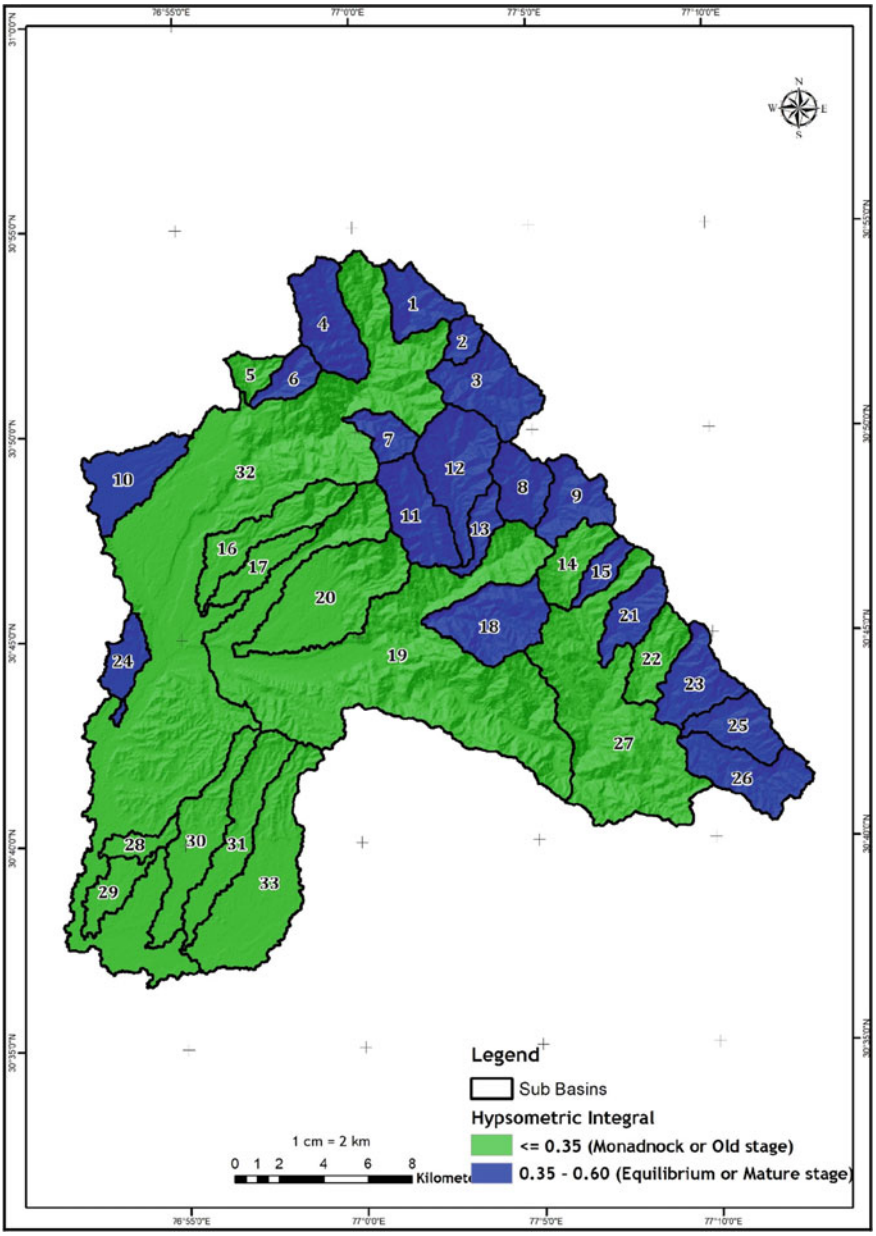

Fig. 3.15 Hypsometric integral map of the Ghaggar basin

3.5 Conclusion

This current study has helped in deciphering the geomorphological and hydrological processes prevalent in the 33 watersheds of the Ghaggar river basin up to its confluence with Madhekali river. This morphometric analysis coupled with landuse/Landcover, climate, soil data can provide vital results on prioritizing the watersheds based upon their erosion extent. This data can further supplement the site suitability analysis of water harvesting structures to recharge the groundwater level.

References

Chen CW, Zebker HA (2000) Network approaches to two-dimensional phase unwrapping: intractability and two new algorithms. J Opt Soc Am 17:401–414

Chorley RJ, Malm DE, Pogorzelski HA (1957) A new standard for estimating drainage basin shape. Am J Sci 255:138–141

Clarke JJ (1996) Morphometry from Maps. Essays in Geomorphology. Elsevier Publishing Company, New York, pp 235–274

Faniran A (1968) The index of drainage intensity—a provisional new drainage factor. Aust J Scienec 31:328–330

Gardiner V (1971) A drinage density map of Dartmoor. Trans Devon Assoc 103:167–180

Gardiner V (1975) Drainage basin morphometry. Br Geomorphol Res Group.

Goldstein RM, Zebker HA, Werner CL (1988) Satellite radar interferometry' Two-dimensional phase unwrapping. Radio Sci 23(4):713–720

Horton RE (1932) Drainage basin characteristics. Trans Am Geophys Union 13(1):350–361

Horton RE (1945) Erosional development of streams and their drainage basins; hydrophysical approach to quantitative morphology. Geol Soc Am Bull 56(3):275–370

Melton MA (1958) Correlation structure of morphometric properties of drainage systems and their controlling agents. J Geol 66(4):442–460

Miller VC (1953) Quantitative geomorphic study of drainage basin characteristics in the Clinch Mountain area, Virginia and Tennessee. Columbia University, Department of Geology, Columbia

Mueller JE (1968) An introduction to the hydraulic and topographic sinuosity indexes. Ann Assoc Am Geogr 58(2):371–385

Nir D (1957) The ratio of relative and absolute altitudes of Mt. Carmel: a contribution to the problem of relief analysis and relief classification. Geogr Rev. 47(4):564–569.

Nookaratnam K, Srivastava YK, Rao VV, Amminedu E, Murthy KR (2005) Check dam positioning by prioritization of micro-watersheds using SYI model and morphometric analysis—remote sensing and GIS perspective. J Indian Soc Remote Sens 33(1):2–38

Patnaik N (1981) Role of soil conservation and deforestation for flood moderation. In: Proceedings of conference on flood disasters. New Delhi, India.

Patton PC, Baker VR (1976) Morphometry and floods in small drainage basin subject to diverse hydrogeomorphic controls. Water Resour Res 12(5):941–952

Pike RJ, Wilson S (1971) Elevation-relief ratio, hypsometric integral, and geomorphic area-altitude analysis. GSA Bull 82(4):1079–1084

Schumm SA (1956) Evolution of drainage systems and slopes in Badlands at Perth Amboy, New Jersey. Bull Geol Soc Am 67:597–646

Shreve RL (1967) Infinite topologically random channel networks. J Geol 75(2):178–186

Singh G, Babu R, Narain P, Bhushan LS, Abrol IP (1992) Soil erosion rates in India. J Soil Water Conserv 47(1):97–99

Singh MJ, Khera KL (2009) Physical indicators of soil quality in relation to soil erodibility under different Landuses. Arid Land Res Manag 23(2):152–167
Singh S (1976) On the quantitative parameters for the computation of drainage density, texture and frequency: a case study of a part of the Ranchi Plateau. National Geographer 10(1):21–31
Singh S, Singh MC (1997) Morphometric analysis of Kanhar river. Natl Geogr J India 43(1):31–43
Smith GH (1935) The relative relief of Ohio. Geogr Rev 25:247–248
Stoddart DR (1965) The shape of atolls. Mar Geol 3(5):369–383
Strahler AN (1952) Hypsometric (area-altitude) analysis of erosional topography. Geol Soc Am Bull 63(11):1117–1142
Strahler AN (1957) Quantitative analysis of watershed geomorphology. Trans Am Geophys Union 38(6):913–920
Strahler AN (1964) Quantitative geomorphology of drainage basins. In: Chow VT (ed) Handbook of applied hyrology. McGraw Hill Book Company, New York, pp 4–11
Vittala SS, Govindaiah S, Gowda HH (2004) Morphometric analysis of sub- watershed in the Pavagada area of Tumkur District, South India using remote sensing and GIS techniques. J Indian Soc Remote Sens 32(4):351–362

Chapter 4
Site Suitability Analysis for Identifying Water Conservation Structures Using Geoinformatics of Eastern Part of Satara District of Maharashtra, India

P. T. Waghmare and S. S. Panhalkar

Abstract Identification of a suitable site for water harvesting structure is significant for drought mitigation and management. Water conservation needs an in-depth study of rainfall-runoff features and a thorough assessment of surface topographical conditions. In this study, the researcher has identified appropriate site for water harvesting structures in the eastern part of Satara district of Maharashtra. The present investigation uses physical components as well as social components. Remote sensing data and toposheets and integrated weighted overlay methods are used to identification of proper suitable sites for water harvesting system. The minimum value was assigned to the factor that is least suitable for the water harvesting system and the maximum value was given to the factor that is highly favorable for the water harvesting structure. The influence factor values of thematic layers were summed up and the total score was calculated. Finally, the calculated score was classified into four classes. The investigation brings out that 31.15% area is highly suitable for establishing water harvesting structures. Moderately suitable area is about 45.65, whereas less suitable area is 20% for water conservation structures. The present study will be helpful to reduce the risk of future drought conditions.

Keywords Runoff · Weighted overlay analysis · SCS-CN method · GIS · Remote sensing

4.1 Introduction

Water is an essential component for fulfilling the basic needs of biotic and abiotic components. Water scarcity has increased due to quickly rising population, industry, economy, and climate change; managing water resources has always been a difficult task during the drought years in past decades (Hirsch 1981; Frick et al. 1990; Randall et al. 1990; Johnson and Kohne 1995; Smithers 1997). Due to over-exploitation and inadequate natural recharge, groundwater table in the study area is going

P. T. Waghmare (✉) · S. S. Panhalkar
Department of Geography, Shivaji University Kolhapur, Kolhapur, Maharashtra, India

R. B. Singh et al. (eds.), *Remote Sensing and Geographic Information Systems for Policy Decision Support*, Advances in Geographical and Environmental Sciences,
https://doi.org/10.1007/978-981-16-7731-1_4

down steadily, causing frequent drought conditions in the study area. This problem of abstraction and imbalance in resources can be solved by enhancing artificial recherché system thoroughly by adopting scientific methods.

Surface, sub-surface, river basin, pits, ponds, unsaturated porous and permeable zones, and fracture planes play a very important role in groundwater recharge. The hydrogeology of unsaturated zones, especially the fractures and fault zones, lineaments, etc., helps in the transporting and storing of recharged water. Therefore geology, geomorphology, and land use land cover are significant for selecting sites for groundwater recharge. Water conservation measures depend on various factors such as geographical, environmental, technical, and socio-economic.

As evidence that the use of remote sensing and GIS technology has become widely accepted as a drought prevention technique in many parts of the world. GIS facilitates integrated watershed management, a multi-disciplinary rational approach to make optimal use of existing natural resources in the watershed to enable sustainable development. The fundamental aim of site suitability assessment for watershed management is to save water for watershed use, reduce sediment, flood prohibition, and enhance groundwater level tables for agriculture and land use (Rao and Raghavendra 2009). Long-term policy is needed to overcome the challenges posed by frequent droughts and mitigate the consequences, and therefore to develop effective strategies for drought mitigation and management.

4.2 Study Area

The present study is focused on the drought-prone area of the eastern Satara district of Maharashtra (Fig. 4.1). The entire study area is located in the southwestern part of Maharashtra. It lies between 17°22′57″ to 18°6′03″ North latitude and 74°09′38″ to 74°55′32″ East longitude. The total geographical area of approximately 3894 km^2 and comprises Man, Khatav, and Phaltan tehsil of Satara district. The average height of the study area is about 713 m. The maximum height is 1004 m which is observed toward the western part of the study area. The lowest elevation is observed toward the extreme east part where the height is 423 m. The study area annually receives average rainfall between 700 and 1100 mm.

4.3 Research Methodology

The drainage network is obtained from the SOI topographic map on a 1:50,000 scale. The stream ordering has been measured by using the Strahler method. In the present study, remote sensing data have been downloaded from the Bhuvan Data Archive with the DEM from Cartosat—1 satellite. The slope map has been generated using DEM in the study area. The LULC map has been prepared by using LISS-III of Resourcesat—I satellite data. The daily precipitation data has been obtained from

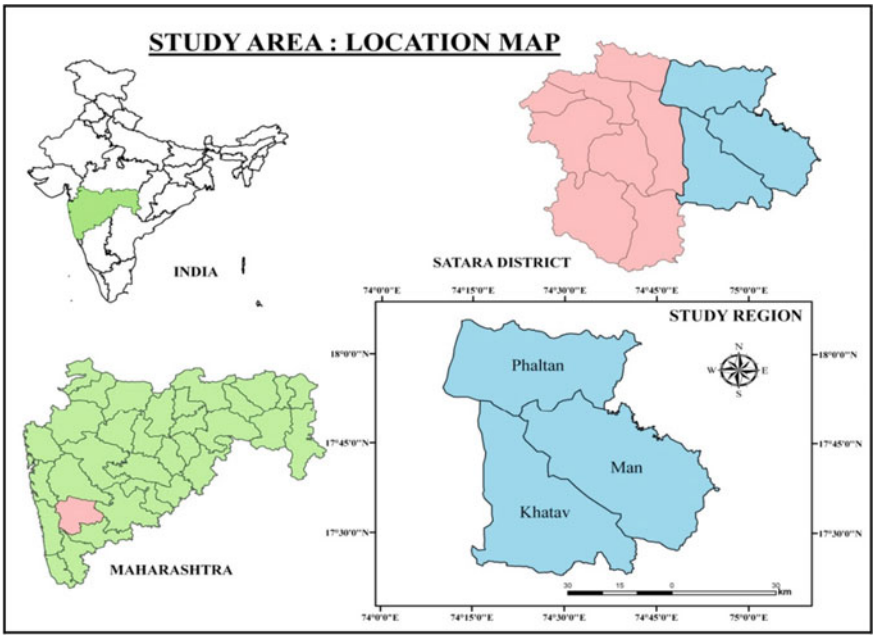

Fig. 4.1 Geographical location of the study area

the Meteorological Department of India (IMD), Pune. Geological Survey of India, Pune (GSI) has provided data for preparation of Geology and Geomorphology maps. Soil map is prepared from the data published by the National Bureau of Soil Survey (NBSS). Bhuvan thematic services are utilized for extracting lineaments features by using ArcGIS software. In deciding the site suitability of the study area, SCS Curve Number Method is used. The SCS method is one of the most popular and extensively used techniques for estimating surface runoff from small catchment areas. The SCS method considers the relationship between LULC and hydrologic soil groups, which together form the curve number (Ramakrishnan et al. 2009). LULC data represent how much area is occupied by physical and socio-economical components. NRCS classified hydrological soil group into four groups which are A, B, C, and D on the basis of characteristics of soil infiltration. The curve number indicates the proportion of surface runoff. The variation in curve number is between 0 to100 where higher curve numbers indicate greater proportion of surface runoff. The systemic flow of research methods is described in fig. 4.2.

The SCS-CN technique equation can be indicated as below:

$$P = \mathrm{Ia} + F + Q \tag{4.1}$$

$$Q/P - \mathrm{Ia} = F/S \tag{4.2}$$

$$\mathrm{Ia} = \lambda S \tag{4.3}$$

here,

P is the total rainfall (mm).

Ia is the preliminary abstraction (mm).

F is the cumulative infiltration (mm).

Q is the runoff (mm).

S is the potential maximum retention (mm).

λ is the initial abstraction coefficient (0.3).

The SCS-CN equation is obtained from a combination of the first two equations given below.

$$Q = (P - \mathrm{Ia})2/(P - \mathrm{Ia} + S) \tag{4.4}$$

In practice, S is generated from the mapping equation indicated in terms of curve number (CN):

$$\mathrm{S} = (25400/\mathrm{CN}) - 254 \tag{4.5}$$

4.4 Result and Discussion

4.4.1 Physical Environment

4.4.1.1 Climate

Climate is the most important factor in regulating the physical environment. The temperature of the study area varies from January to December. Generally, November to February is cool, and March to May are the hottest months in the study area. In the summer month, the temperature range is between 26 and 38 °C. The highest temperature is mostly recorded in April and May months. Normally in the monsoon season, the normal temperature varies between 25 and 28 °C. A seasonal variation in temperature is high in the study area. The study area annually receives average rainfall between 700 and 1100 mm (Fig. 4.3).

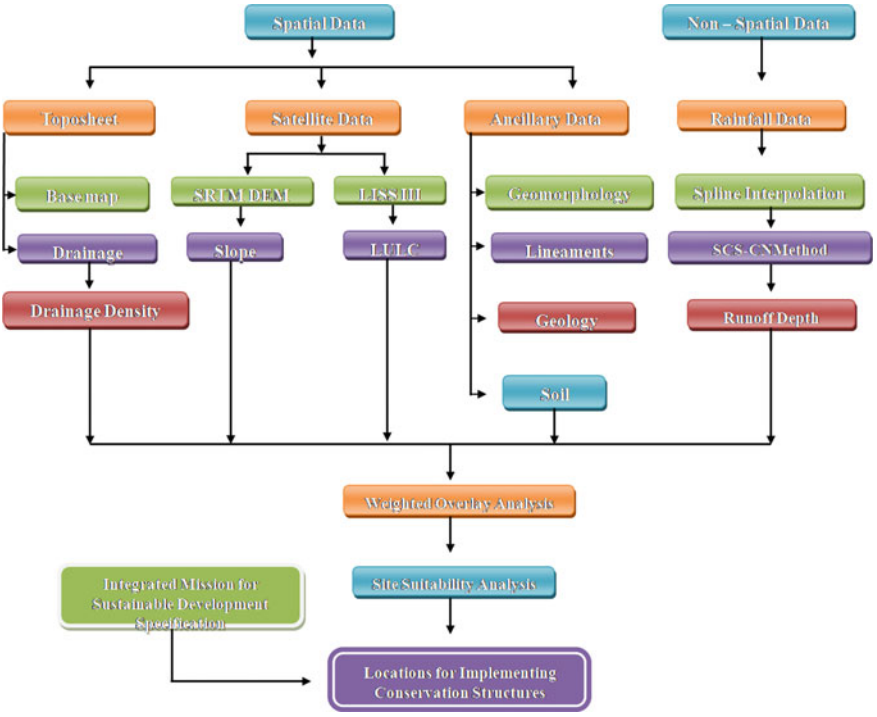

Fig. 4.2 Research methodology for water conservation structure

4.4.1.2 Drainage

In the study area, the Sahyadri hill range and its subdivision divided the drainage network into three areas; the Nira in the northern zone, the Manganga in the eastern zone, and Yerala in the western zone. The pattern of drainage in the study area is semi-dendritic. High drainage density is observed in western and northern parts of the study area (Fig. 4.4), whereas the central part of the study area falls under the lowest drainage density. The study area has the highest 7th stream order.

4.4.1.3 Geology

The study area is entirely occupied by Deccan trap lava flows with aa, pahoehone, and flows showing mixed characteristics. The lava pile is classified into two formations viz. Diveghat formation, and Purandargarh formation. The oldest Diveghat formation comprises 15 flows showing predominantly mixed characters of aa and pahoehone lava types. The formation has been exposed along the valley of Man. It also occurs around Mhasvad, and Phaltan. The flows of this formation are almost aphyric in nature. Purandargarh formation comprises of eight basaltic flows that are mostly aa

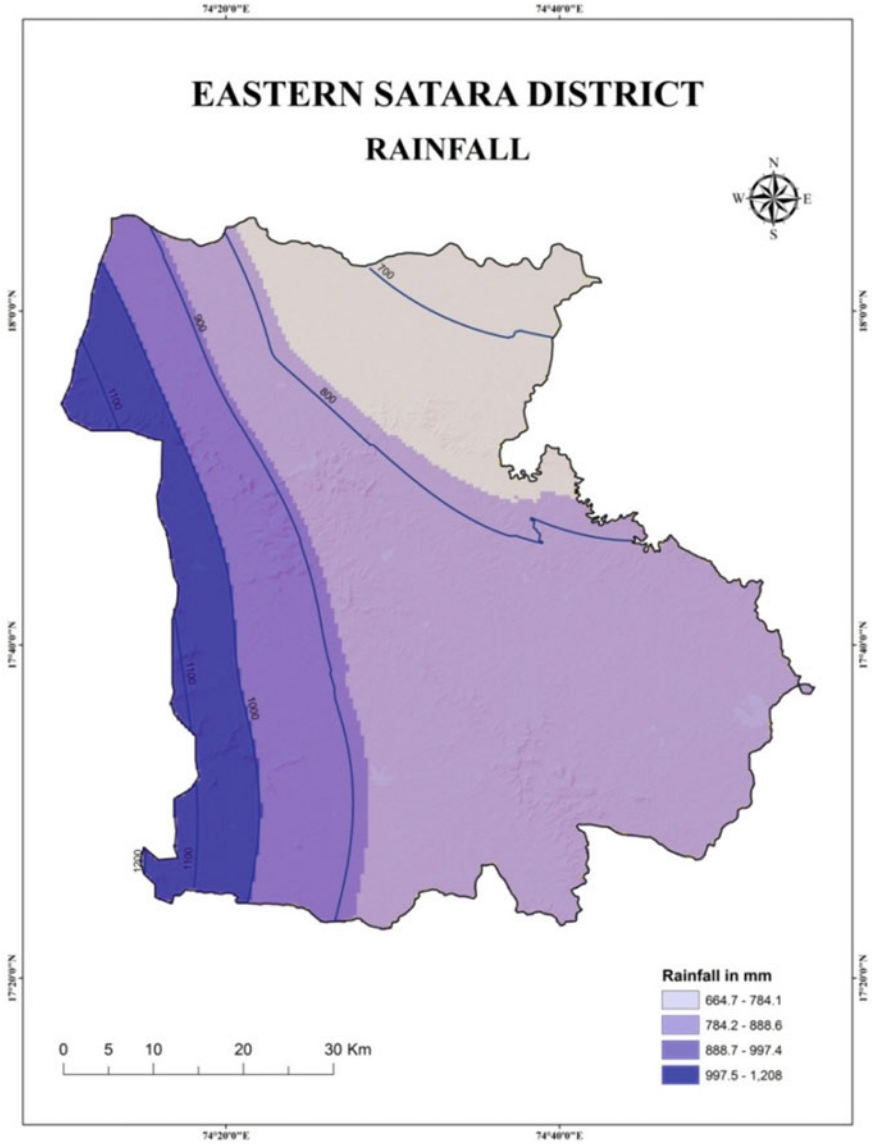

Fig. 4.3 Rainfall distribution (1979–2014)

flows. A few pahoehone flows are also seen. This formation is extensively exposed around Vaduj, and northwest and west of Dahiwadi. A megacryst flow (M4), showing large plagioclase laths of 1–2 cm. in a fine-grained groundmass, occurs at the top of Purandargarh formation. This flow has a maximum thickness of 30 m and is noticed throughout the area shown in Fig. 4.5.

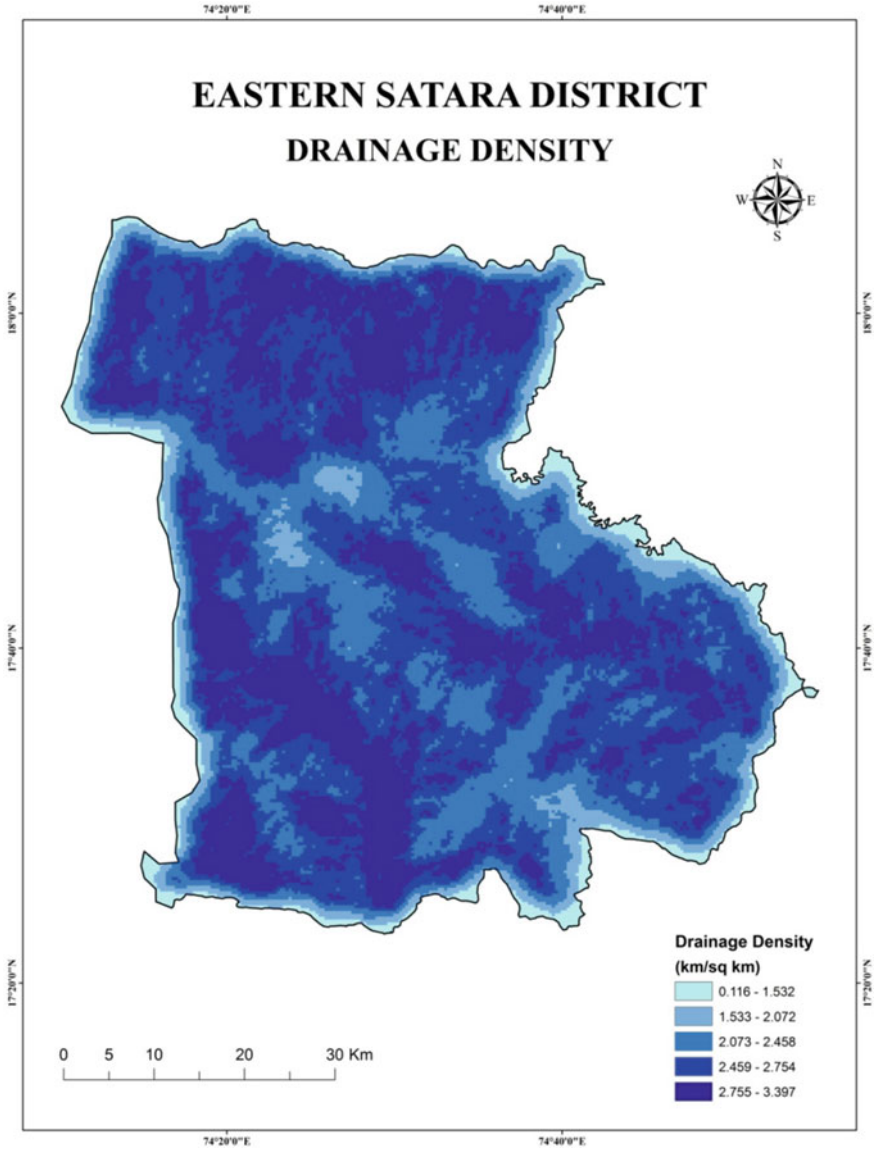

Fig. 4.4 Drainage density

4.4.1.4 Geomorphology

Geomorphologically, the study area forms part of the Deccan Plateau. The weathering extent and soil thickness criterion broadly divide this area into six units viz. Plateau Un-dissected (PLU) with less than 1 m weathering, Plateau Slightly Dissected (PLS)

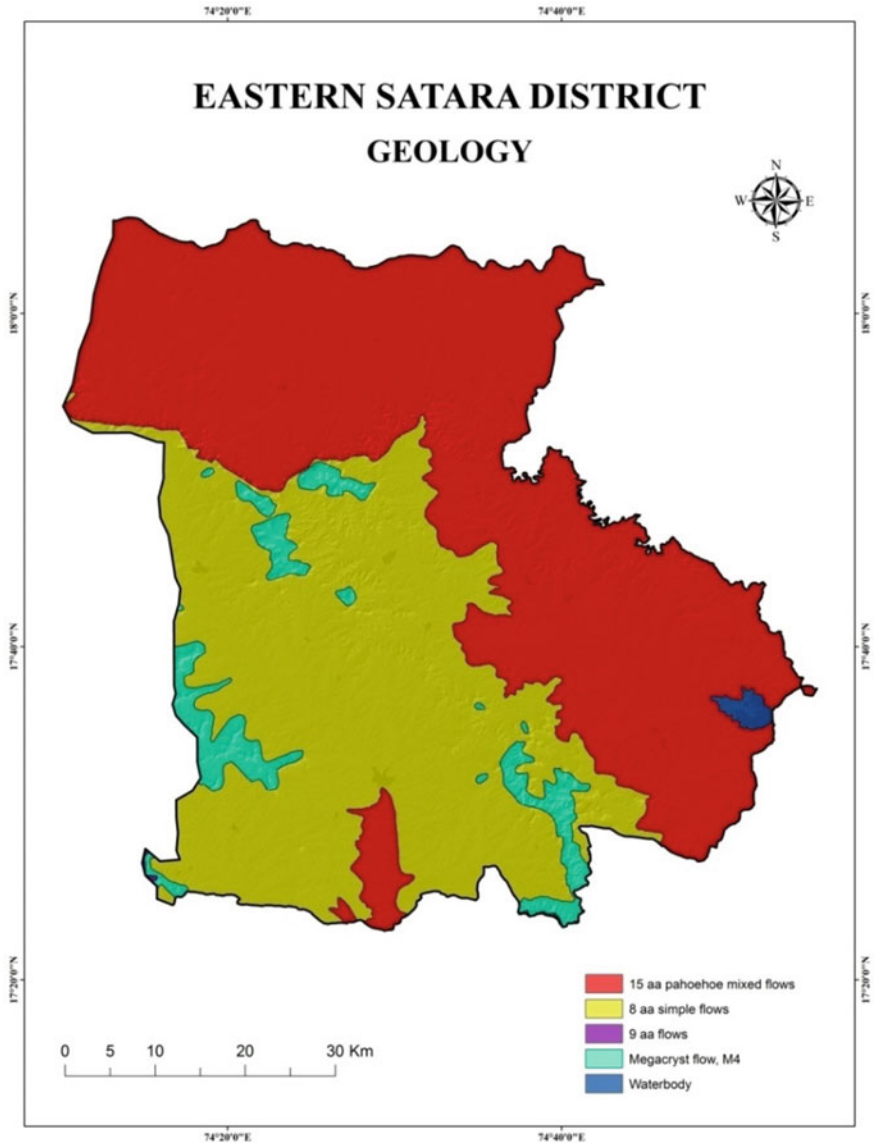

Fig. 4.5 Geology

with less than 1 m weathering, Plateau Moderately Dissected (PLM), Plateau Highly Dissected (PLH), Plateau Weathered (PLW) with 2–3 m weathering, and isolated Mesas as evident from. Entire Man tehsil is occupied by denudational slop on Deccan traps, whereas northwest part consists of middle-level plateau on the Deccan trap. The older flood plain is prominently observed on the northern side of the study

area. In the study area, maximum part is covered by denudational slop on Deccan traps. The southern part of the study area is covered by older flood plain and some patches of the western area occupied by denudational hills and valleys on Deccan traps (Fig. 4.6).

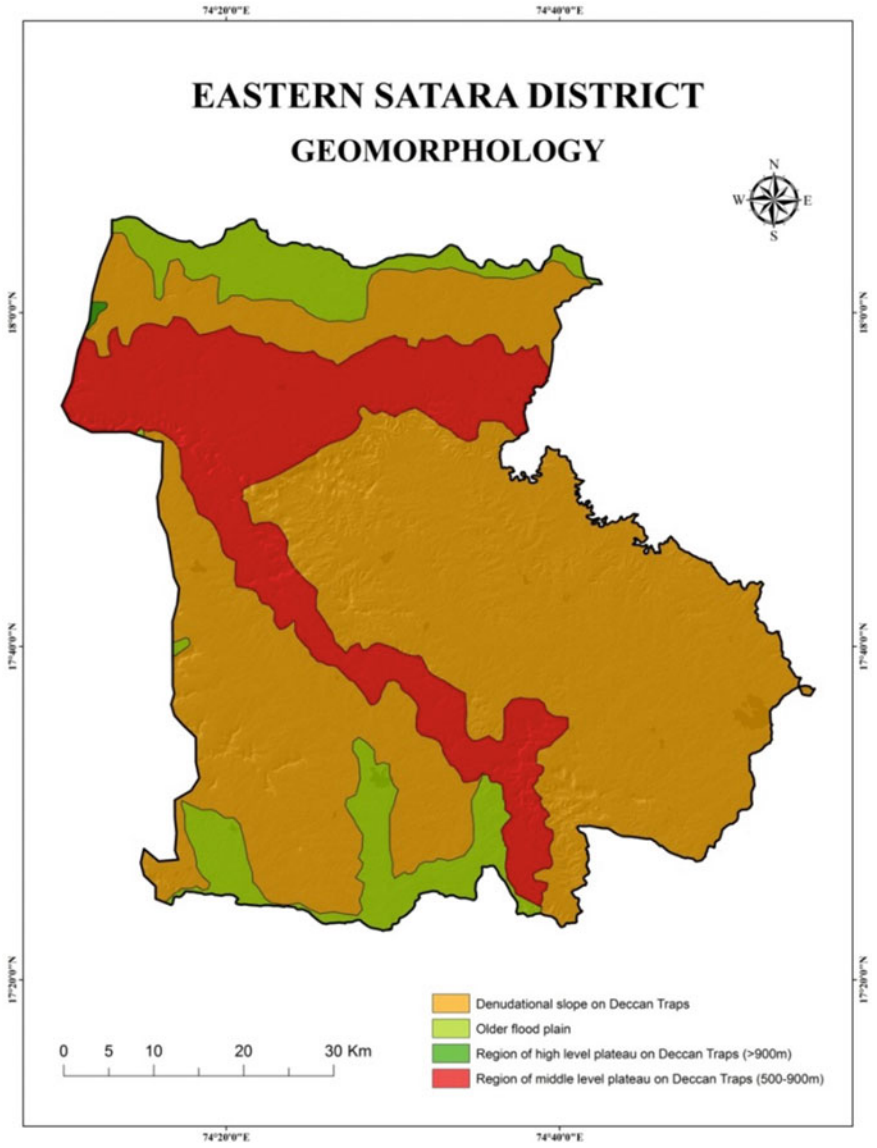

Fig. 4.6 Geomorphology

4.4.1.5 Lineaments

A lineament plays a crucial role in transporting and storing water to uplifting groundwater levels. In the study area, geomorphic lineaments and structural lineaments are observed. The western part of the study area is noticed geomorphic lineaments, whereas the structural lineament is observed in the entire study area (Fig. 4.7).

4.4.1.6 Soil

The clay, sand, sandy clay loam, sandy loam, and loamy sand types of soil are observed in the study area. The central part of the study area noticed the thickness of the soil is deep whereas the northern part of the study area observed shallow soil. Sandy clay loam is found along the banks of the river and along the channel. The sandy loam mostly occurs over the hilly area in the central part of the study area (Fig. 4.8).

4.4.1.7 Slope

The range of slope varies from 0 to 60 degrees. The slope map is composed of CartoDEM (30 m) which was collected from Bhuvan. In the study, area slope is classified into five categories which are level slope, gentle slope, moderate slope, steep slope, and very steep slope. The level slope category maximum area has covers 2018.7 sq. km or 51.81%. This category is the largest coverage, in terms of expansion. This category covers large areas of the northern part of the study area. The gentle slope has an area of 1267.4 sq. km or 32.52% of the study area. It is the second-largest category, in terms of areal coverage. Near about 361.69 sq. km or 9.28% of the study area has been covered by the moderate slope category (Fig. 4.9).

4.4.2 Social Environment

The cropland covered the largest area in the field of the study. These classes cover approximately 2160 sq. km of the study area. Near about 22.59% of the study area is under fallow land. It is the second-largest category, in terms of areal coverage. Near about 15.98% of the study area is covered by scrubland. About 1.37% study area is occupied by scrub forest, 0.25% of land is under deciduous forest, and 0.002% area is under semi-evergreen forest (Table 4.1).

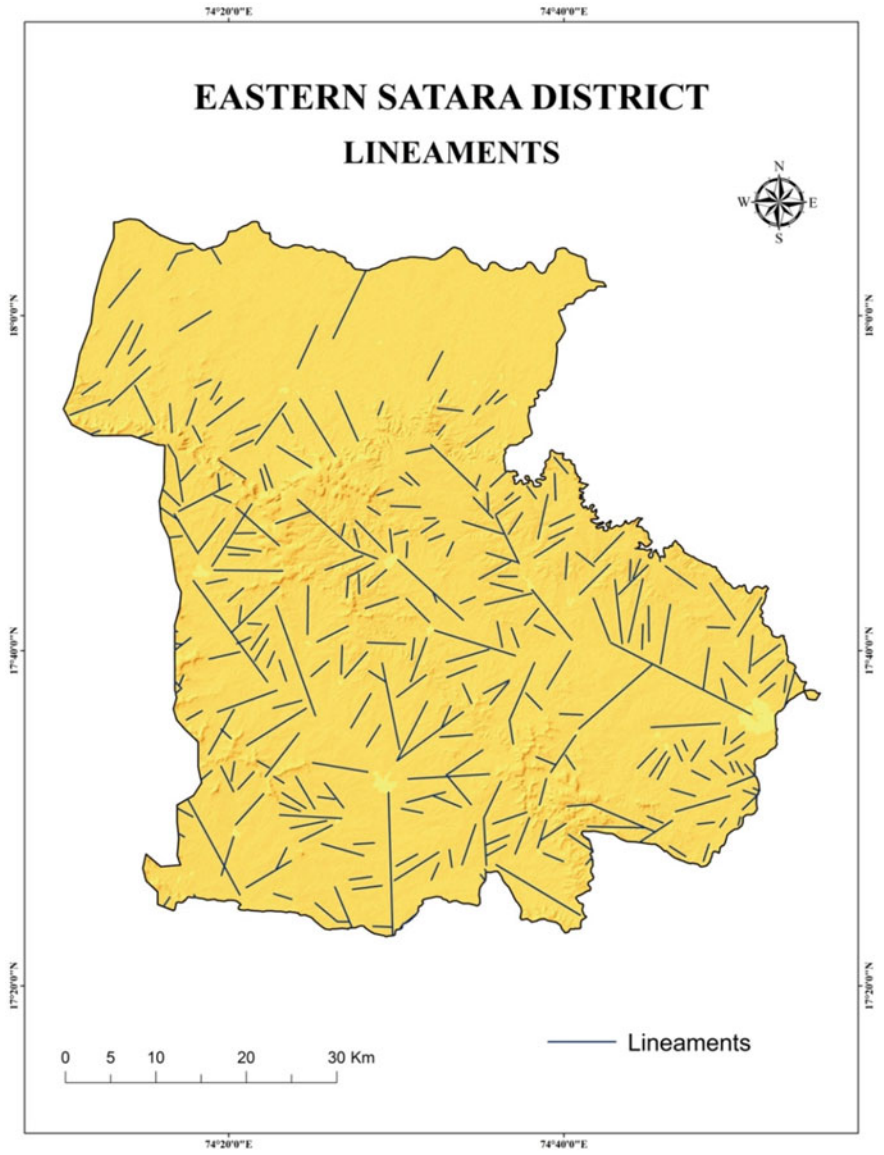

Fig. 4.7 Lineament

4.4.3 Rainfall-Runoff Estimation

Runoff refers to the downward flow of rainwater to a channelized stream, once they reach the ground as rainfall. There are many influencing factors depending on complex conditions, such as the amount of rainfall, intensity of rainfall, types of

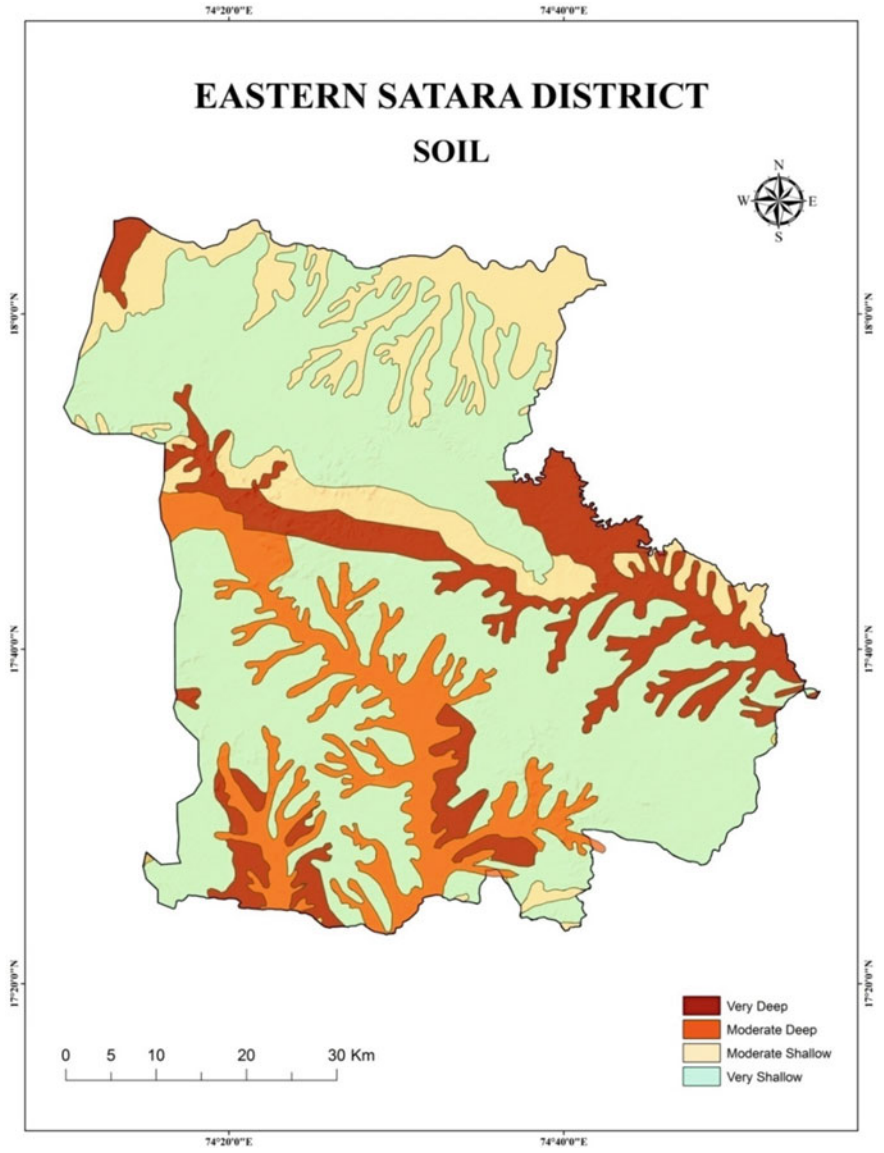

Fig. 4.8 Soil

soil, slope of the earth surface, and configuration of catchment basin (Jain and Singh 2003). It is also affected by geological composition, forest, wind, and some other factors.

Rainfall-runoff modeling is used for many reasons. It helps to well understand runoff hydrological events and how it affects the hydrological cycle. Furthermore,

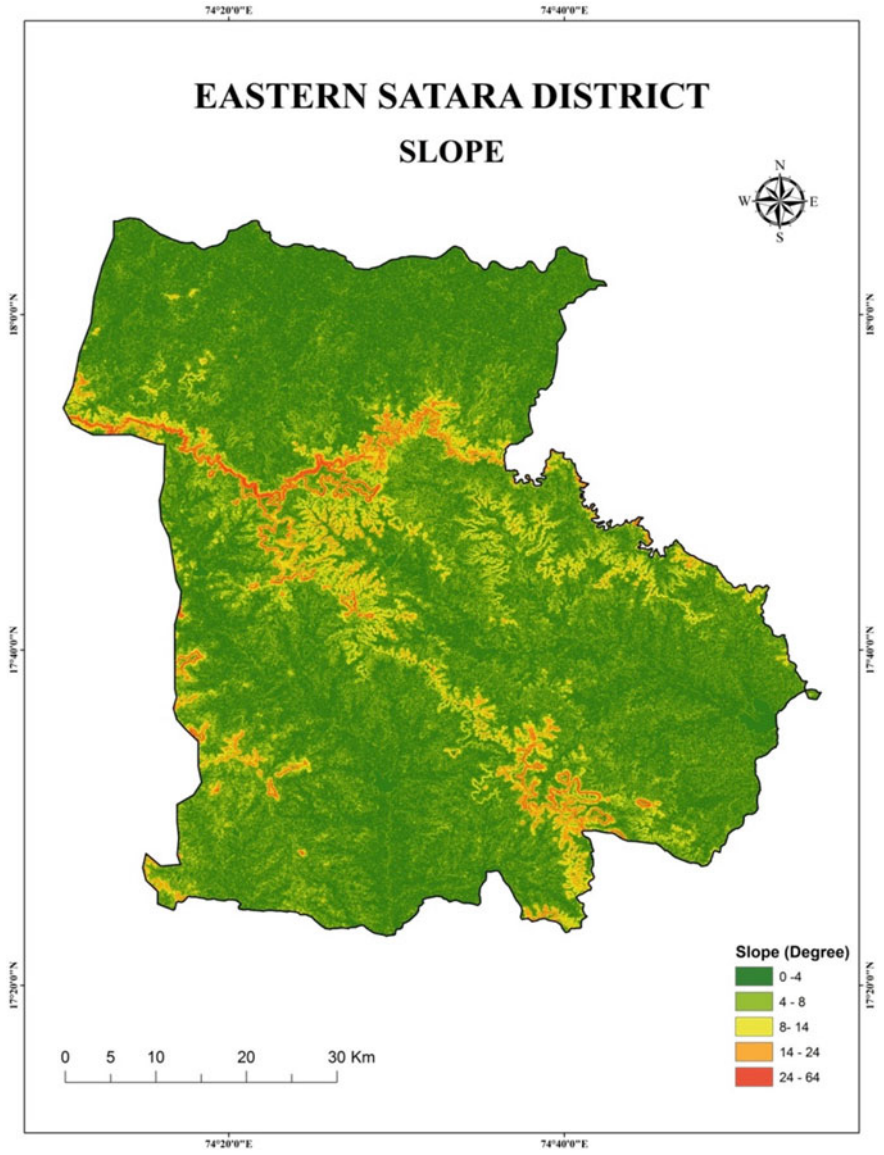

Fig. 4.9 Slope

it also helps to understand how much quality and quantity of water resources are available in a particular field. To design reservoirs or to establish medium to large water conservation structures, relatively simple rainfall-runoff models can be used (Rao et al. 2001).

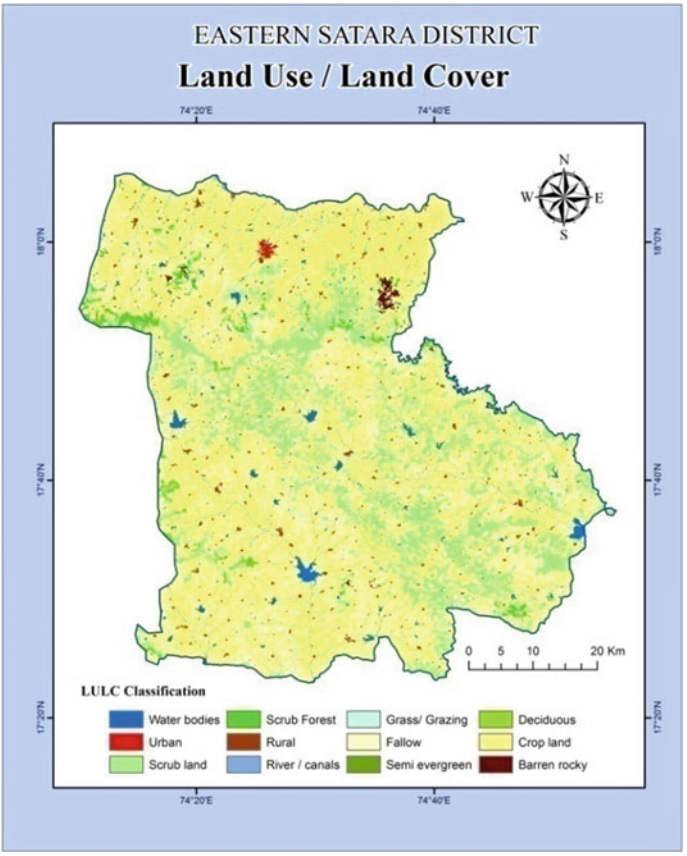

Fig. 4.10 LULC

Table 4.1 Classification of land use and land cover

Sr. no.	Categories	Area (sq. km)	Area (%)
1	Urban	6.05	0.15
2	Rural	37.94	0.97
3	Crop land	2159.41	55.42
4	Fallow land	880.11	22.59
5	Semi-evergreen	0.09	0.002
6	Deciduous	9.78	0.25
7	Scrub forest	53.54	1.37
8	Grass/Grazing	1.20	0.030
9	Scrub land	622.64	15.98
10	Barren rocky	10.12	0.25
11	River/Stream/Canals	65.98	1.69
12	Water bodies	49.14	1.26

4.4.3.1 Rainfall

The study area has 16 rainfall gauging stations. The annual rainfall data from 1979 to 2014 was collected from IMD, Pune. Western parts of the study area receives 1150 mm rainfall, and the eastern part of the study area receives 800 mm rainfall.

4.4.3.2 Rainfall-*R*unoff Modeling

Rainfall-runoff calculations are essential for identifying an appropriate location for impounding harvesting structures. A quantitative measurement report in hydrology, published by Perrault (1974), compares the measured annual precipitation (Pa) and estimated annual streamflow (Qa) of the Seine River in Paris. Various hydrologic models are put to use in order to estimate the amount of direct precipitation runoff from the watershed area (Jonathan 2003). The direct runoff estimation can be calculated using the soil conservation service (SCS) model; this method is most popular for the estimation of direct runoff.

4.4.3.3 Hydrological Soil Groups

The soil is classified on the basis of the following criteria (USDA 2007).

While assigning hydrologic soil groups following aspects are considered: percolation of water at the time of high wetness in the year, soil not exposed to frozen conditions, high swelling of expansive clays, and the slope of the soil surface.

The USDA categorized hydrologic soil in four groups as follows:

Group A The soil in this group has low runoff potential when thoroughly wet. Water freely runs through the soil. The clay content of this group is 10% whereas the sand or gravel and have a sand or sand texture percentage is 90. Even soil with loamy nature and silt loam texture may be in this group when it has low density or contains more than 35% of the rock fragments.

Group B In this group, when soil is thoroughly wet then the soil has moderate low runoff potential. This loamy sand structured group has typically 10–20% clay and the sand content 50–90%. The soil having low density or containing more than 35% rock fragment is included in this group.

Group C In this group, when soil is thoroughly wet then the soil has moderate low runoff potential. Water percolation in this soil is somewhat restricted. The group C soils generally have between 20 and 40% clay and 50% sand with loam, silt loam, sandy clay loam, and clay loam texture. The soils having clay or sandy clay texture are placed in this group if they are well aggregated, low density, or contain more than 35% rock fragments.

Group D The soils in this group has a high potential for a runoff when thoroughly wet. The group D Soils have very low penetration rates when thoroughly wet. Water

transmitted through the soil is restricted. This soil group peculiarly has more than 40% clay, less than 50% sand with clayey textures.

Table 4.2 shows soil groups based on soil composition. The curve number represents the runoff properties for specific soil and LULC. The SCS runoff equation is used for the curve value as an input parameter. On the basis of the pixel value of LULC and soil map, the curve numbers are evaluated which were reclassified into hydrologic soil groups. Thus, the curve numbers were created using the LULC and Hydrological Soil Group (HSG) classification system. The area that has greater runoff potential and less infiltration is derived from a higher value of curve number.

Infiltration rate depends on the nature of the soil which affects the relation between rainfall and runoff (Arun 2003). According to the United States Department of Agriculture (USDA), soil is classified into four groups on the basis of infiltration rate, soil texture, and soil composition. Table 4.3 indicates runoff curve numbers in combinations of LULC and hydrological soil groups based on the USDA classification system.

Table 4.2 Group of soil corresponding specification of runoff and soil texture (*Source* USDA (1986)

Group of soil	Specification of runoff	Specification of soil texture
A	Runoff potential is low because of high infiltration rates	Sand, loamy sand, and sandy loam
B	Runoff potential is moderate because of Moderate infiltration rates	Silty loam and loam
C	High/moderately runoff potential because of slow infiltration rates	Sandy clay loam
D	High runoff potential with very low infiltration	Clay loam, silty clay loam, sandy clay, silty clay and clay

Table 4.3 Runoff curve numbers

LULC	Hydrological soil group			
Classes	A	B	C	D
Built-up area	48	66	78	83
Agriculture	67	78	85	89
Plantation	65	73	79	81
Fallow land	76	85	90	93
Deciduous forest	68	79	86	89
Evergreen forest	48	67	77	83
Scrub forest	48	67	77	83
Wastelands	64	75	83	85
Waterbody	90	94	98	100

4.4.3.4 Rainfall-Runoff Depth

SCS-CN method has been used for calculating rainfall-runoff depth. In ArcGIS 10.5, LULC and Hydrological Soil Group curve numbers with average yearly rainfall were calculated with the help raster calculator. The western part of the study area observed high runoff potential (undulating hills and moderately sloppy terrain). The eastern part of the study area found moderate runoff potential (Fig. 4.11).

Site suitability analysis is a type of analysis used in GIS technique to determine the paramount site for water conservation structure (Patel et al., 2012). In suitability analysis potential sites such as location of check dams and rainwater harvesting structures are used. Weighted overlay site selection method based on raster dataset is one of the popular and most used techniques for site suitability analysis. In weighted overlay analysis technique permit users to allocate a relative weight to each layer and rank raster cells. This results in a suitability surface that ranks potential sites from 1 to 9. Sites with value 1 represent the site that is least suitable and those sites with value 9 are most suitable.

4.4.4 Weighted Index Model

In this study, a weighted index model was used for data integration. All the maps assembled for the study area are reclassified with reference to the site suitability for water conservations structures. In this study, assess the area of a high potential zone for water resource management. This is done by keeping in mind that all the parameters are interdependent on each other with respect to the study area (Prasad et al. 2014).

4.4.5 Site Suitability Analysis

Water resource harvesting models are based on the gradient of area, runoff, geology, geomorphology, soil types, drainage density, LULC, and lineaments for identification of suitable sites (Prasad et al. 2014). Using ArcGIS- 10.5 software, each layer was prepared in the vector format. The rasterization of every layer was performed by using conversion tools in the ArcToolbox Window. So, the first step is rasterization for converting different vector datasets into raster dataset format. After that, the entire raster layer was reclassified using the scale values of each unit. All the layers were ranked based on their influence following Lynn (2009). Weightage overlay analysis was used for the site suitability of water conservation structures in the study area. Weightages from 1 to 9 were determined based on the influencing factors. Low values 1 represent low or inappropriate sites, while high values 9 represent highly suitable sites over the study area (Table 4.4). Further that, using the Spatial Analyst Tool, the weighted overlay function was processed and the suitability zones were identified

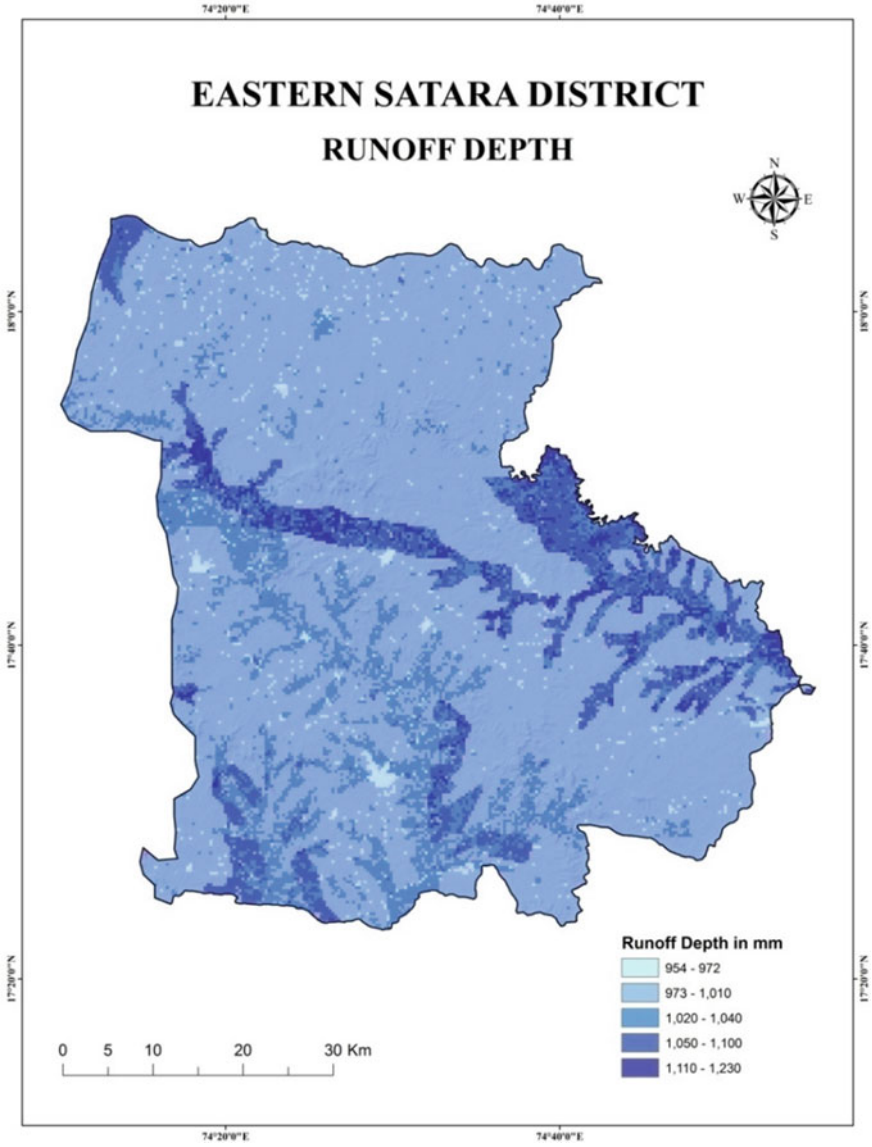

Fig. 4.11 Runoff depth

(Fig. 4.12). The resulted values range from 2 to 9. These are classified into highly suitable (7–9), moderately suitable (5–7), less suitable (3–5), and not suitable (2–3) classes.

Table 4.4 Weight determination of different layers

Factor	% of influence	Feature classes	Weightage
Slope (in degree)	10	<4 (gentle slope)	5
		4–8 (Moderately Slope)	9
		8–16 (Strongly Slope)	7
		16–24 (moderately steep slope)	3
		>24 (Very steep slope)	1
Runoff (in mm)	15	950–1000	1
		1000–1050	3
		1050–1100	5
		1100–1150	7
		>1150	9
Geomorphology	15	Region of middle-level plateau on Deccan traps (500–900 m)	7
		Region of high-level plateau on Deccan traps (>900 m)	3
		Denudational slop on Deccan traps	5
		Older flood plain	9
Geology	15	15 aa, pahoehone mixed flows	9
		8 aa simple flows	7
		9 aa flows (350–400 m)	3
		Megacryst flow, M4 (30 m)	5
		Waterbody	1
Drainage density (in sq. km)	10	<1.5	1
		1.5–2	3
		2–2.5	5
		2.5–3	7
		>3	9
LULC	10	Urban	1
		Rural	1
		Crop land	3
		Fallow land	7
		Semi-evergreen forest	3
		Deciduous forest	5
		Scrub forest	9
		Grass land	3
		Scrub land	5
		Barren rocky	5

(continued)

Table 4.4 (continued)

Factor	% of influence	Feature classes	Weightage
		Water bodies	1
		River	1
Soil	10	Moderate deep	3
		Moderate shallow	7
		Very deep	1
		Very shallow	9
Lineaments	15	Lineament buffer <500 m	9
		Lineament buffer 500–1000 m	5
		Lineament buffer 1000–2000 m	3
		Lineament buffer >2000 m	1

4.4.5.1 Highly Suitable Areas

The site is considered to be the most suitable site for the construction of soil and water conservation structures. The northern part of the study area, especially, in an area where there is a gentle slope, is suitable for soil and water conservation. Near about 31.15% area is under highly suitable for implementing water conservation structures.

4.4.5.2 Moderately Suitable Areas

The central and western part of the study area where there is a moderate drainage density, moderate to high runoff rate, gentle to moderate slope these sites are useful for soil and water conservation structure. The majority of the study area is moderately suitable for soil and water conservation. About 45.64% of the study area is moderately suitable for applying water conservation structures.

4.4.5.3 Less Suitable Areas

It is considered to be less suitable for the construction of soil and water conservation structures. Conservation structures constructed in such areas will not be beneficial. Due to topographical adverse conditions, upper part of the study area is less suitable for soil and water conservation. As a consequence, 20% of the study area is less suitable for implementing water storage structures.

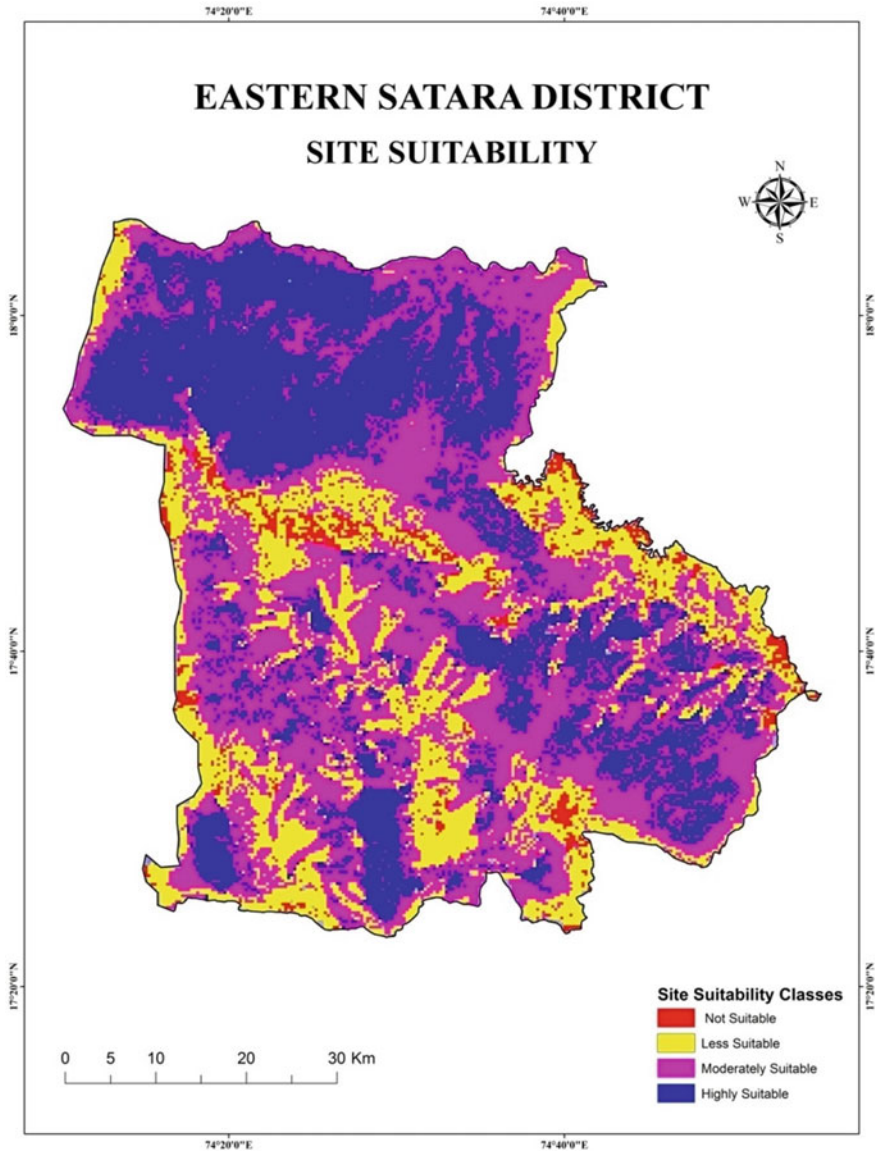

Fig. 4.12 Site suitability

4.4.5.4 Not Suitable Areas

The site is considered to be inadequate for construction water conservation structures. The construction and cost of any water conservation structure in this area are not effective (Chopra et al. 2005). Ridge line and hilly area of the study region are not suitable for implementing water conservation structure.

4.5 Conclusions

Site suitability is identified for the structure of water conservation based on rainfall characteristics and rainfall-runoff processes. Rainfall-runoff method of the study area uses soil conservation service-curve number (SCS-CN) method. The basis of estimating runoff gives better results if remote sensing and GIS technique is used. These methods are very effective in getting input parameters and spatial analysis. The average yearly precipitation from 1979 to 2014 is used to estimate the runoff depth in coordination with SCS-CN method in this study. The analysis shows that yearly runoff is important when it comes to deciding a potential water conservation structure.

The eastern part of Satara district is drought-prone region, therefore water resources need to be properly conserved. Hence, site suitability analysis is identified on basis of physical components as well as social components. The weightage overlay analysis was used to demarcate potential zones for building up conservation structures because the method gives relative importance to the influencing parameters. Site suitability of the study area will be useful for constructing conservation structures such as check dams, stop dams, percolation tanks, and farm ponds and helpful for drought mitigation and management purpose.

References

Arun WD (2003) Runoff estimation for Darewadi Watershed using RS and GIS. International Journal of Recent Technology and Engineering 1(6), pp 46–49

Chopra R, Dhiman R, Sharma PK (2005) Morphometric analysis of sub watersheds in Gurdaspur-District.Punjab using remote sensing and GIS Technique. J Indian Soc Remote Sens 33(4):531–539

Frick DM, Bode D, Salas JD (1990) Effect of drought on urban water supplies. I: drought analysis. J Hydrol Eng 116:733–753

Hirsch RM (1981) Stochastic hydrologic model for drought management. J Water Resour Plann Manage 107(2):303–313

Jain S, Singh V (2003) Water Resources Planning and Management. Dev Water Sci 51:68–76

Johnson WK, Kohne RW (1995) Susceptibility of reservoirs to drought using Palmer index. J Water Resour Plann Manage 119(3):367–387

Jonathan DJ (2003) Spatially distributed watershed mapping and modeling: GIS- based storm runoff response and hydrograph analysis: Part 2. J Spat Hydrol 3(2, 1–26

Lynn EJ (2009) Geographic information systems in water resources engineering, New York, pp 94–102

Patel DP, Mrugen BD, Naresh N, Prashant KS (2012) Water harvesting structure positioning by using geo-visualization concept and prioritization of mini-watersheds through morphometric analysis in the lower Tapi Basin. J Indian Soc Remote Sens 40(2):299–312

Prasad CP, Parul B, Sarvesh P (2014) Site suitability analysis of water harvesting structures using remote sensing and GIS—a case study of Pisangan Watershed, Ajmer District, Rajasthan. Int Arch Photogramm, Remote Sens Spat Inf Sci, 1471–1482. https://doi.org/10.5194/acp-8-591-2008.

Perrault P (1974) The Man And His Contribution To Modern Hydrology. J Am Water Resour Assoc. https://doi.org/10.1111/j.1752-1688.1974.tb05623.x.

Ramakrishnan D, Bandyopadhyay A, Kusuma KN (2009) SCS-CN and GIS- based approach for identifying potential water harvesting sites in the Kali watershed, Mahi river basin. India. Journal of Earth System Science 118(4):355–368

Randall D, Houck MH, Wright JR (1990) Drought management of existing water supply system. J Water Resour Plann Manage 116(1):1–20

Rao K, Raghavendra (2009) Soil erosion inventory and micro watershed modeling using digital technologies a case study of Mula basin Maharashtra, Thesis

Rao DKHV, Hari Prasad V, Roy PS (2001) A suitable site: Geographic Information Systems and remote sensing technology, making water everybody's business (Ed. Agarval et al). Centre for Science and Environment, New Delhi. https://eng.warwick.ac.uk/ircsa/12th.html. 243–245

Smithers HA (1997) Operational water management in northwest England in the light of the 1995/96 drought. In: Proceedings of the European water resources association conference (EWRA), Copenhagen, Denmark. Rotterdam, Bulkema, pp 455–462

USDA (1986) Natural Resources Conservation Service, Urban Hydrology for Small Watersheds, Technical Release 55, Washington, DC. pp 2–11

Chapter 5
Monsoon Impacted Magnetic and Geomorphological Changes Along the Redi Beach, Sindhudurg District, West Coast of Maharashtra, India

Praveen Gawali, B. V. Lakshmi, Pramod Hanamgond, Sainath Aher, Pragati Deshmukh, Milind Herlekar, Satish Sangode, and Prafull Kamble

Abstract The Redi beach of Sindhudurg district, West Coast of India was studied for its morphological and magnetic mineralogical changes brought by the changes in precipitation. Annual and seasonal data was collected to decipher the erosive/accretion pattern of the beach sediments. The microtexture on the surface of sand grains was used to understand the wave energy conditions along this beach through Scanning Electron Microscopy (SEM). The quantum of magnetic minerals was found to be quite high in 2003 at stations 1, 2, 3, and 6 post-monsoon; and at stations 4 and 5 pre-monsoon. On the other hand, in 2004, the average concentration of magnetic minerals was more at station 1 pre-monsoon; at stations 2, 3, and 5 post-monsoon; and at stations 4 and 6 during monsoon season. The overall concentration

P. Gawali · B. V. Lakshmi
Indian Institute of Geomagnetism, Navi Mumbai 410218, India
e-mail: pravin.g@iigm.res.in

B. V. Lakshmi
e-mail: lakshmi.bv@iigm.res.in

P. Hanamgond
Department of Geology, GSS College, Belgaum 590 006, India

S. Aher (✉)
Department of Geography, S.N. Arts, D.J.M. Commerce and B.N.S. Science College, Sangamner 422605, India

P. Deshmukh
Department of Geography, HPT Arts, RYK Science College, Nashik 422005, India

M. Herlekar · S. Sangode · P. Kamble
Department of Geology, Savitribai Phule Pune University, Pune 411007, India
e-mail: milindk@unipune.ac.in

S. Sangode
e-mail: sangode@unipune.ernet.in

S. Aher
Universal Geotechnical, Nashik 411007, India

R. B. Singh et al. (eds.), *Remote Sensing and Geographic Information Systems for Policy Decision Support*, Advances in Geographical and Environmental Sciences,
https://doi.org/10.1007/978-981-16-7731-1_5

of magnetic minerals decreased in 2004 compared to 2003, reflecting the influence of monsoon on the erosive/accretion pattern on this beach, apart from beach morphology, winds, tides, and longshore currents. This will help better strategize management plans for beach wellbeing in many parts of the world.

Keywords Beach · SEM · Magnetic and geomorphological changes · Monsoon

5.1 Introduction

The world is experiencing climate change and its deleterious effects are now evident globally (Barnosky et al. 2011; Kantamaneni et al. 2017; Aher et al. 2019) in the form of extreme climate events, which are seen to have socioeconomic ramifications (INCCA 2010). Industrialization is considered to exacerbate the deleterious impact of climate change (Chigbo et al. 2016; Deshmukh et al. 2017). Understandably, the UN is persuading industrial giants to minimize emissions that lead to climate variability (Brauch 2012), with little success. Earth has a long geological history of a plethora of climatic and environmental changes (Wadia 1976; Gawali et al. 2017). The tropical and subtropical climate of the Indian subcontinent is seasonal in its nature, whose precipitation is dominantly controlled by the gigantic Himalayas and also by variegated geomorphology of the subcontinent (Wadia 1976; Sen 2002). These changes affect the sediments, especially the magnetic minerals, hence their interrelationship with climate-change-induced monsoonal fluctuations and geomorphological dynamics need to be assessed carefully.

The compositional investigations regarding rock, sediment, and soil properties through magnetic measurements are gaining prominence (Thompson and Oldfield 1986; Walden et al. 1999). This technique has been used on sediments from different depositional environments (Oldfield et al. 1979; Arkell et al. 1982; Schmidt et al. 1999; Wheeler et al. 1999; Oldfield and Yu 1994; Clifton et al. 1997, 1999; Chan et al. 1998; Petrovsky et al. 1998; Xie et al. 1999, 2000; Booth et al. 2005, 2008) are some of the studies that have explored the relationship between mineral magnetic measurements and chemical/physical properties of sediments. The mineral magnetic investigations have been found to be suitable for delineating the provenance of sediments (Oldfield and Yu 1994; Gawali et al. 2010). Lepland and Stevens (1996) found sediment transport pathways. This technique is also an effective proxy for radioactivity, geochemical, and particle size (Oldfield et al. 1993; Hutchinson and Prandle 1994; Clifton et al. 1997, 1999; Xie et al. 1999, 2000; Zhang et al. 2001). The coastal stretch containing beach sands, coastal foreland, swash zone, tidal flats, and estuaries have been studied successfully through the environmental magnetic method to understand sediment provenance, their pathways of transportation, particulate pollution, distribution of heavy minerals, sediment dynamics, and heavy metal pollution using magnetic inclusions and magnetic fingerprinting (Oldfield et al.1985; Lees and Pethick 1995; Zhang et al. 2001; Bandaru et al. 2016; Maher et al. 2008; Maher

et al. 2009; Maher and Hatfield 2009; Maher and Kinnersley 2010, Cioppa et al. 2010, Hatfield et al. 2010, Hansard et al. 2011; Gallaway et al. 2012).

Rainfall, being an important climate parameter, affects water availability on a temporal and spatial scale (De et al. 2000; Barbara et al. 2016; Aher et al. 2017). The centennial-scale Indian Himalayan rainfall trend (Basistha et al. 2009) suggests a sudden decrease. Kumar and Jain (2011), found 15 basins, out of 22, had a decreasing trend in yearly rainfall and precipitational days. The precipitational decrease is seen all over Asia in studies by Sinha Ray and Srivastava (1999), Shrestha et al. (2000), Mirza (2002), Lal (2003), Min et al. (2003), Goswami et al. (2006), and Dash et al. (2007). Studies by Cayan and Peterson (1989) and Lins and Slack (1999) found long-term natural and anthropogenic activity influenced climate variability, which suggests South Asia can be vulnerable to climatic changes. The monsoonal change has a significant hydrological and ecological impact, apart from socioeconomic distress (Sawant et al. 2015), since it creates water paucity. Rainfall variability due to climate change combined with an inability to optimally manage the water resources can lead to food and water insecurity.

How the magnetic minerals are enriched within the beach sands, the pathways that they take is yet not well understood because of which it becomes difficult to hazard forewarning about its distribution dynamics and extant hydrodynamics This chapter presents magnetic susceptibility, SEM, and time-lapsed geomorphological changes along Redi beach of Sindhudurg district, Maharashtra to assess the impact of monsoonal variation on the deposition/erosion of the beach. Satellite imageries obtained from web-based Google earth software have also been harnessed to physically examine the changes, if any, which have occurred along the shoreline. The regional studies on monsoonal changes have been attempted by many. However, understanding trends that are region-specific and local is also very important, since these may not be in consonance with the overall regional trend. Such studies that have a limited geographical sweep are few and far between. The present attempt is to look more closely at this microcosm.

Based on the origin, microtextures are defined as mechanical, mechanical-chemical, and chemical. Microfeatures such as straight or arcuate steps, v-shaped fractures, and conchoidal fractures are attributed to the mechanical origin, whereas particles that adhere to the grain, pitting caused by aeolian activity are inferred to have formed by mechanical-chemical action. Precipitation structures, silica globules, and dissolution structures are attributed to chemical origin. Based on the type of microtextures present, it is proposed to (1) identify and define the microtextures present on detrital sand surfaces of Redi beach grains, (2) their origin, and (3) interpret the depositional environment.

5.2 Study Area

The Redi beach is situated at the southernmost coastal end of the Sindhudurg district, within the Konkan coast of Maharashtra state (Fig. 5.1). This beach experiences semi-diurnal tides and is microtidal in nature. Overall, the Konkan Coast has geomorphological features that are quite unique (Chandramohan et al. 1992). During the Miocene-Pliocene period, the coastal stretch of Konkan was tectonically active, and since then the dominance of exogenetic processes has been established (Tandale 1993). The rainfall (Fig. 5.2) ranges between 300 and 470 cm/year, though it is not evenly spread over the Sindhudurg district. The precipitation is moderate toward sea and Redi beach and rises considerably high over the Sahyadri Mountains toward the east. Beyond this mountain range the precipitation is seen to be comparatively low (Fig. 5.2). The wave height around the Redi beach is seen to reach up to 1.0 m, having a wave period of 5 to 6 s on average. The waves near Redi have multiple breakers and are predominantly of plunging type.

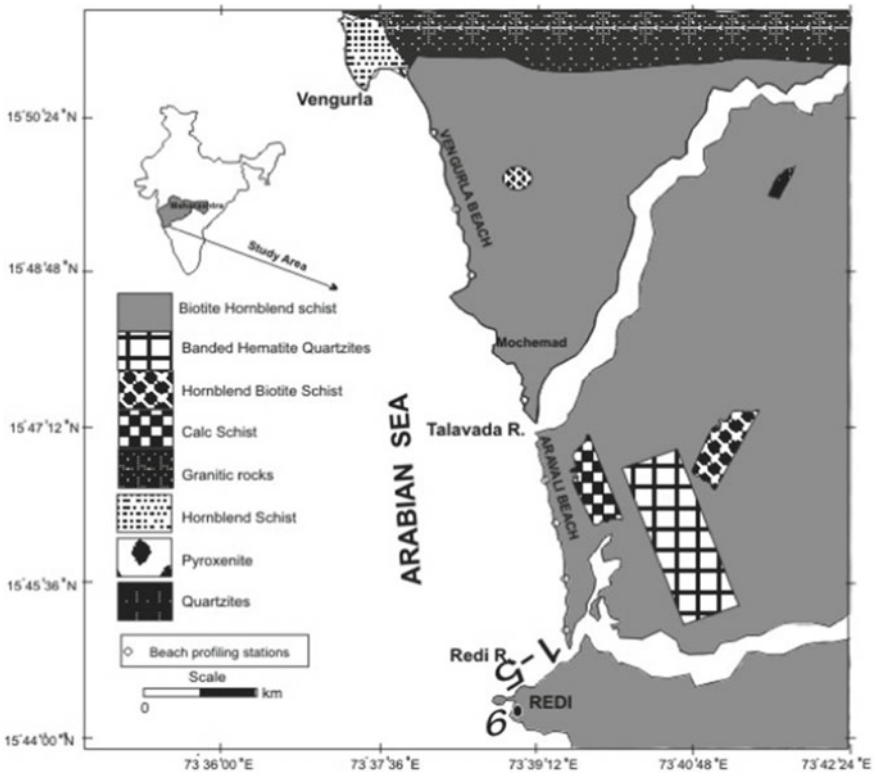

Fig. 5.1 Sample collected locations (marked in numbers from 1 to 6) and general geology encountered in the area around the Redi beach

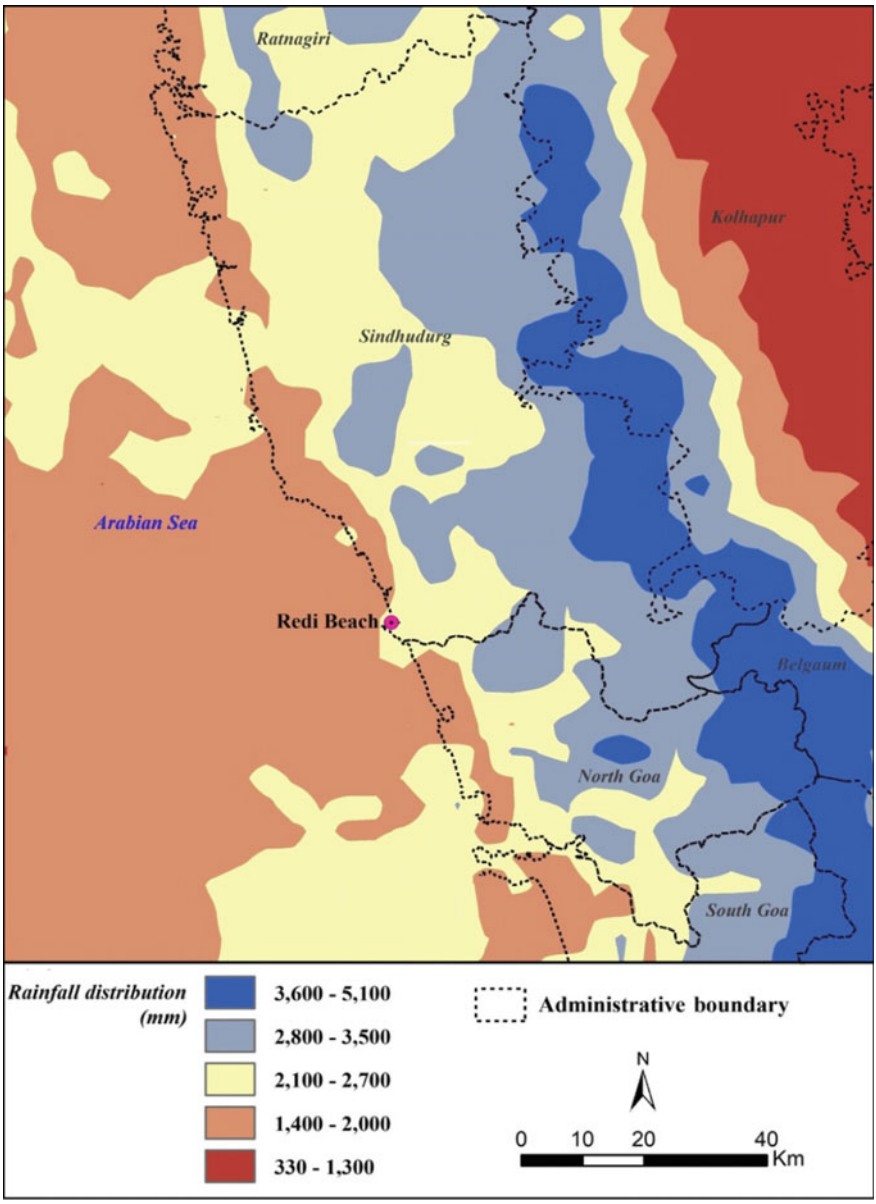

Fig. 5.2 Rainfall distribution around the Redi beach

Banded hematite quartzite, different forms of schist and granitic rocks form the geological constituents of the Sindhudurg district (Fig. 5.1; Deendar 2003). It also consists of Kaladgi formation and Deccan Traps. The area close to Redi beach has moderate to bold relief with hills and deep valleys to its east. The coastline on its western side trends in an NNW–SSE direction. The Sindhudurg coastline is rocky to the north, but not in the south. Rivers like Karli, Talvada, and Redi are seen to join the Arabian Sea at Devbag, Mochemad, and Shiroda, respectively. These rivers are seen to flow in a general north–south trend, and are seen to abruptly change their course in east–west direction, which means they are effectively controlled by the tectonics of the area (Deendar 2000). The deformations and rock alterations are attributed to faulting in this area which has facilitated iron ore formation. The iron ore deposits and reserves to the tune of 48 metric tons (Hiremath 2003) formed near Redi have initiated mining in this area.

5.3 Materials and Methods

Surface sediments (upper 3–4 cm) were collected seasonally from the Redi beach in May 2003 and May 2004 (pre-monsoon), July 2003 and July 2004 (during monsoon), and November 2003 and November 2004 (post-monsoon) at 6 stations along Redi beach (Fig. 5.1). The samples were collected with respect to a reference point from land (0 m) and then collected every 10 m from the land reference point, 10, 20 m toward the sea. Polythene bag was used in the field to collect the samples, which were dried in an oven at 40 °C. The dried-out samples were then weighed to be packed in 8 cm^3 plastic bottles. They were tightly packed before using them for measurements in the environmental magnetism laboratory. MFK1-FA Kappa Bridge of AGICO was used to measure low-frequency mass-specific magnetic susceptibility (χ_{lf}). The laboratory procedures were followed as prescribed by Walden et al. (1999). The detrital grains collected at this beach in different seasons were examined using TESCANs scanning electron microscope (SEM). This technique was used to understand and define the surface morphology of the grains. These sets of two measurements (magnetic and SEM) were carried at the Indian Institute of Geomagnetism (IIG), Navi Mumbai, India.

The http://www.geog.ucsb.edu/~bodo/TRMM/ portal was used to download Tropical Rainfall Measuring Mission (TRMM) satellite-derived data to know the precipitational distribution around Redi beach (Fig. 5.2). Bookhagen (2016) processed TRMM data, wherein high- and medium-resolution precipitation data from tropical regions are freely disseminated (Hunink et al. 2014; Shinde et al. 2020). Similarly, satellite images were downloaded from web-based Google Earth software to understand the time-lapsed geomorphological changes around Redi beach.

5.4 Results and Discussion

5.4.1 Concentration-Dependent Parameter: Magnetic Susceptibility (Year 2003)

Station 1: Very low magnetic susceptibility (χ_{LF}) is inferred in all three seasons, where the variability is more pronounced in post-monsoon values (Fig. 5.3). Magnetic susceptibility is quite low during monsoon, intermediate pre-monsoon; and is maximum at this station post-monsoon.

Station 2: A reversal can be seen for this station, wherein 0 m samples pre-monsoon magnetic susceptibility is 35.41, for the same sample it doubles (64.17) during monsoon season and reduces to 52.30 post-monsoon (Fig. 5.3). During monsoon magnetic susceptibility at sampling locations from 10 to 70 m, is quite low and does not vary too much (1.28–3.69). An increase is seen post-monsoon at 10 and 20 m sampling location and is maximum (52.30) at 0 m. The concentration of magnetic minerals is more near water and seen to drastically decrease as one moves toward land.

Station 3: Here, magnetic susceptibility continues to be on the rise. Pre-monsoon magnetic susceptibility (Fig. 5.3) is maximum (38.73) at 0 m and quite decreased (18.78 and 15.74) at 10 and 20 m, respectively. A sudden fall is seen to occur at 30 m (3.36) and 40 m (2.91). But, in monsoon, when compared to pre-monsoon, magnetic susceptibility is more (57.01) at 0 m and (24.67) at 10 m. It is considerably low at 20 m (7.09), marginally more at 40 m (3.19), and considerably low at 50 m (2.30). Post-monsoon magnetic susceptibility is quite variable: (63.59) at 0 m, (1.25) at 10 m, and (11.72) at 20 m. The concentration of magnetic minerals is more near to the sea, which is seen to decrease toward land.

Station 4: The magnetic susceptibility at this station is quite high (Fig. 5.4), especially at 10 m (43.89) pre-monsoon. But compared to other stations the magnetic susceptibility is seen to decrease here considerably during monsoon (24.69 and 10.40) at 10 m and 20 m, respectively. Post-monsoon, it came down at 10 m (1.09) and 20 m (1.80), enhancing a little at 30 m (9.10). Concentration of magnetic minerals is more near to water than on land.

Station 5: Pre-monsoon magnetic susceptibility values are high at 10 and 20 m sampling locations (44.37 and 39.1, respectively; Fig. 5.4) and gradually come down to 6.25 at 50 m. However, in monsoon, at all sampling locations, a sharp drop in magnetic susceptibility is seen. Post-monsoon magnetic susceptibility seems to have increased at sampling locations between 10 and 30 m, at around 15.

Station 6: This station is distinguished by high magnetic susceptibility values (Fig. 5.4) from 0 to 20 m (also 30 m post-monsoon) in all three seasons. These values are seen to range from 10 to 25, though the remaining sampling locations display low magnetic susceptibility.

From the foregoing, it can be concluded that magnetic mineral concentration is quite high at Redi beach except station 1. Most of the magnetic mineral concentration is confined to the sampling locations near the sea and is seen to decrease substantially

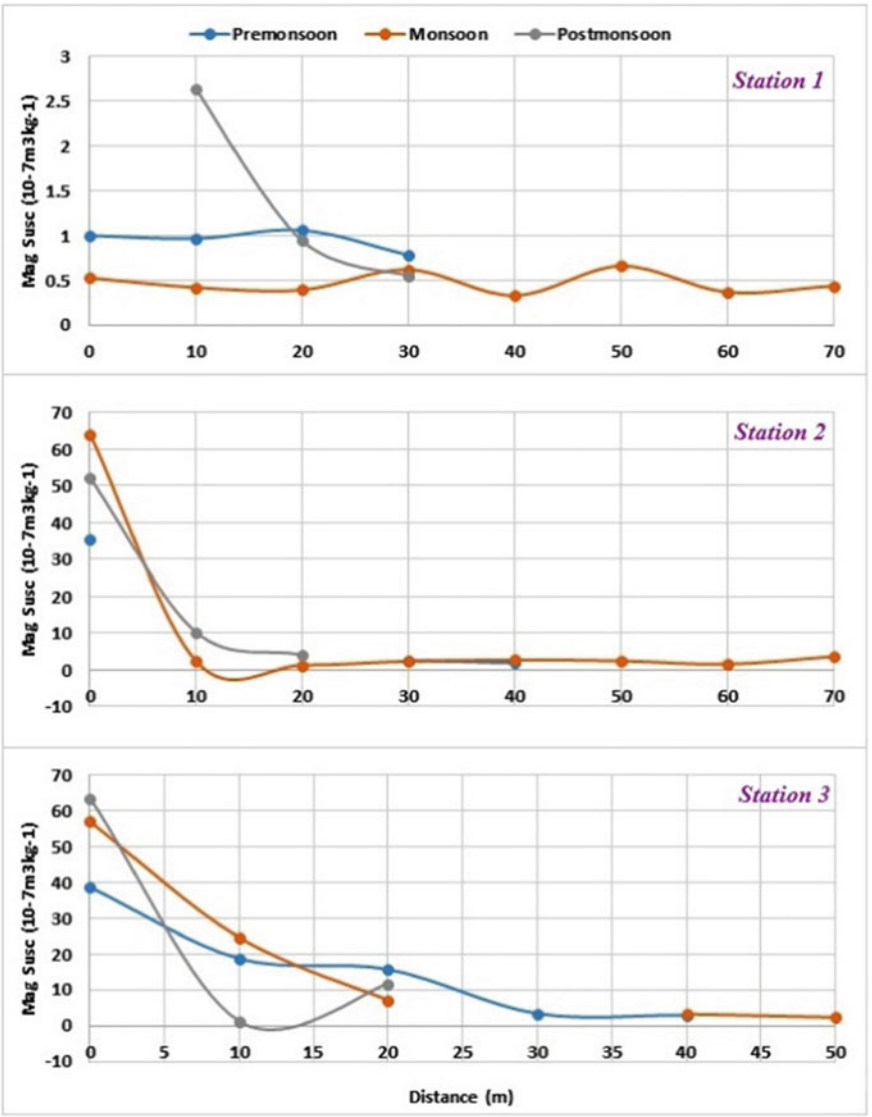

Fig. 5.3 Magnetic susceptibility variation in 2003 at station 1, 2 and 3 of Redi beach

as one move toward land. At station 1 there are scarce magnetic minerals in all three seasons and their spread is almost uniform throughout the station. High magnetic mineral concentration is seen at station 2 near to sea at 0 m sampling location in all the three seasons, though it is the maximum during monsoon, followed by post-monsoon and pre-monsoon. However, the drastic fall witnessed at 10 m sampling location is seen to continue all the way through to 70 m sampling location. Station 3

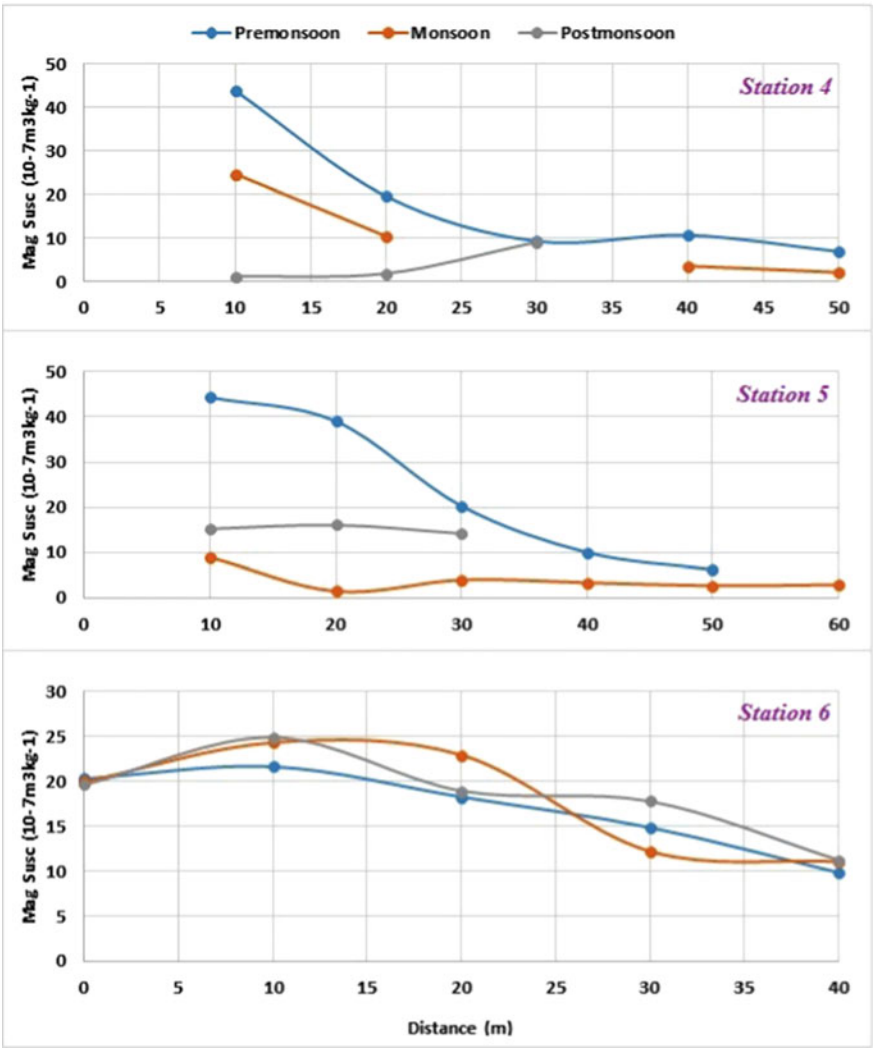

Fig. 5.4 Magnetic susceptibility variation in 2003 at stations 4, 5, and 6 of Redi beach

also contains high mineral concentration at 0 m sampling location, which is seen to have tapered considerably till 20 m sampling location. The concentration of magnetic minerals is seen to decrease drastically at station 3 from the sea to land. Station 4 has an overall high concentration of minerals even near to the land, though it is quite high at locations near to the sea. It shows high magnetic susceptibility pre-monsoon. Station 5 also contains more magnetic concentration pre-monsoon and low during monsoon. The intermediate values are present post-monsoon. Here too, the magnetic minerals are more near the sea than land. The last station, station 6, has the maximum

content of magnetic minerals throughout its sampling locations from sea to land. It shows low amplitude fluctuations from one sampling location to another, though the range in magnetic susceptibility values is quite modest. The primary mode of transport pre-monsoon and post-monsoon could be winds and longshore currents. During monsoon, the local precipitation may be playing a dominant role in bringing the detrital material to the beach. The concentration of magnetic minerals is quite high at stations 1, 2, 3, and 6 post-monsoon; and at stations 4 and 5 pre-monsoon. In general, the average magnetic mineral concentration is more pre-monsoon, followed by post-monsoon, and then monsoon.

5.4.2 Concentration-Dependent Parameter: Magnetic Susceptibility (Year 2004)

Station 1: The pre-monsoon magnetic susceptibility is high at 20 m and 10 m (8.6 and 6.6, respectively) and is seen to drastically lower down at 30 m and the other remaining sampling locations (Fig. 5.5). Severe to mild amplitude changes in magnetic susceptibility are seen in monsoon where magnetic susceptibility is seen to range from 0.32 to 2.8. Seasonal changes are prominent and magnetic susceptibility is seen to be more pre-monsoon than in monsoon and post-monsoon.

Station 2: The concentration of magnetic minerals is considerable at 0 m sampling location (Fig. 5.5) signified by magnetic susceptibility value (36), which is seen to reduce drastically at 10 m and the remaining sampling locations pre-monsoon. The range of magnetic susceptibility in monsoon is seen to be from 1.2 to 12 and is highest at 60–70 m sampling location. Mid-amplitude variations are observed from one sampling location to another. Post-monsoon, magnetic susceptibility is more at all the sampling locations, especially 10 and 20 m locations.

Higher concentrations of magnetic minerals are seen to be present at the sampling locations near the water body, which is seen to have diluted in the mid-sampling locations. The 60–70 m sampling location has more magnetic minerals during monsoon than the sampling locations closer to sea.

Station 3: Pre-monsoon, magnetic susceptibility is high (46) at 0 m sampling location which is seen to reduce drastically in the rest of the sampling locations (Fig. 5.5). Magnetic susceptibility is seen to rise at 0–80 m during monsoon, compared to pre-monsoon, magnetic susceptibility is highest post-monsoon at all the sampling locations, except 0 m.

Station 4: Pre-monsoon magnetic susceptibility is quite high at 0 m, which is seen to reduce drastically at the remaining sampling locations (Fig. 5.5). During monsoon, 20 m sampling location has the highest magnetic susceptibility (68), which is seen to

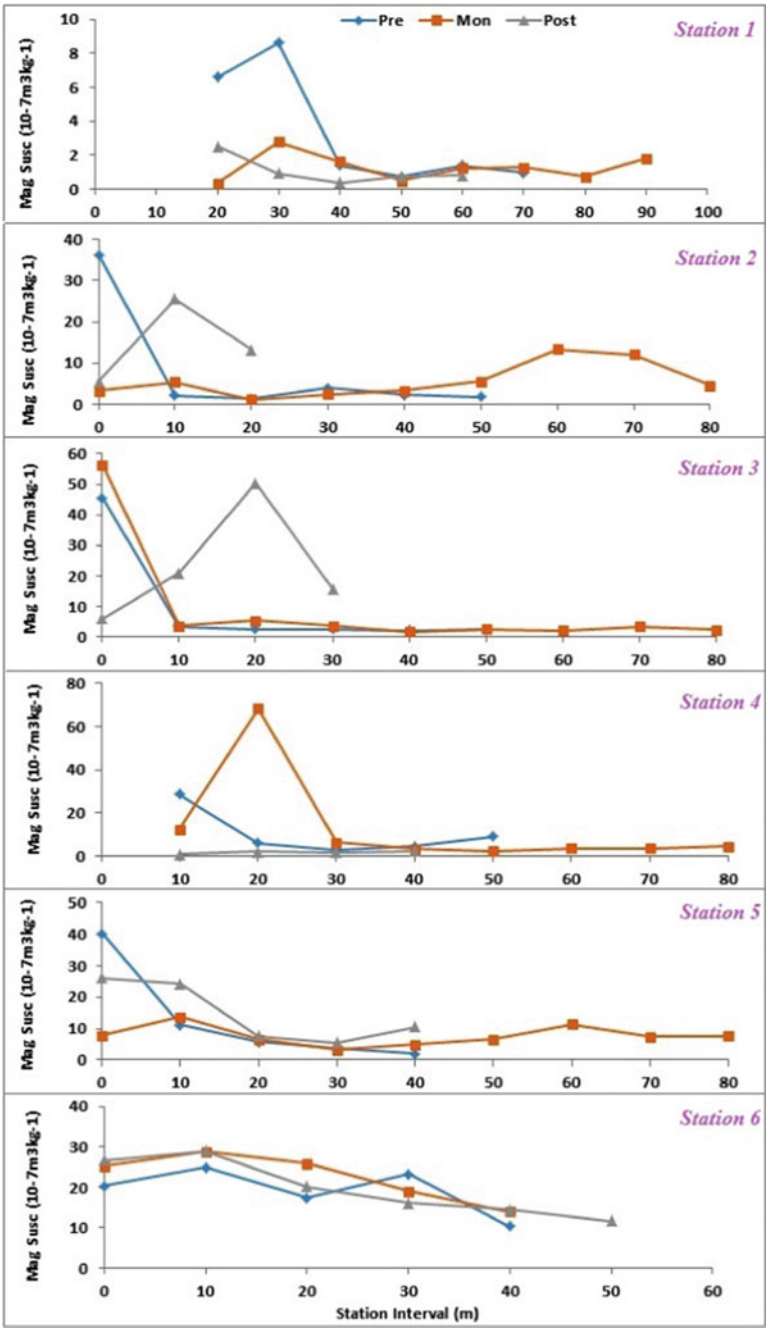

Fig. 5.5 Magnetic susceptibility variation in 2004 at station 1, 2, 3, 4, 5 and 6 of Redi beach

reduce considerably in its nearby sampling locations. Post-monsoon, the concentration of magnetic minerals is considerably reduced along with the remaining sampling locations of this station.

Station 5: At 10 m sampling location (Fig. 5.5) magnetic susceptibility is the highest pre-monsoon (40), which is seen to reduce gradually from 10 to 40 m sampling location. During monsoon, the concentration of magnetic minerals is more at the ends of sampling locations 20 m (14), 10 m (8), and 60–90 m, and comparatively less at the sampling locations at the center of the beach. Post-monsoon, magnetic susceptibility is more at sampling locations 0 m and 10 m, and comparatively low at the remaining sampling locations.

Station 6: High amplitude magnetic susceptibility variations are seen pre-monsoon (Fig. 5.5) ranging from 17 to 25. High magnetic susceptibility is seen to be present during monsoon at almost all the sampling locations where the range of these values is from 14 to 29. The same trend is also found post-monsoon where magnetic susceptibility is seen to range from 14 to 29. The magnetic mineral concentration is more toward the sea than land.

In the year 2004, at Redi beach, most of the magnetic mineral concentration is confined to the sampling locations near to the sea and is seen to decrease substantially as one moves toward land. At station 1 seasonal changes are prominent and magnetic susceptibility is seen to be more pre-monsoon than in monsoon and post-monsoon. At station 2 high concentrations of magnetic minerals are seen to be present at the sampling locations near to the water body, which is diluted in the mid-sampling locations. The 60–70 m sampling location has more magnetic minerals during monsoon than the sampling locations closer to sea. The concentration of magnetic minerals is maximum post-monsoon at station 3 compared to the other two seasons. At station 4, pre-monsoon magnetic susceptibility is quite high near the sea and decreases considerably toward land. Post-monsoon, it has a very low concentration of magnetic minerals. Overall, the concentration of magnetic minerals is more at stations 5 and 6, apart from the few pockets of high magnetic susceptibility in the other Redi beach stations. The primary mode of transport pre-monsoon and post-monsoon could be winds and longshore currents. During monsoon, the local precipitation may be playing a dominant role in bringing the detrital material to the beach. On average the concentration of magnetic minerals in 2004 is more at station 1 pre-monsoon; at stations 2, 3, and 5 post-monsoon; and at stations 4 and 6 during monsoon season. In general, the concentration of magnetic minerals is more post-monsoon, followed by pre-monsoon and then monsoon. It will be quite interesting to see how the concentration of magnetic minerals has changed from season to season and from 2003 to 2004 that can be calculated from Table 5.1.

The average seasonal magnetic susceptibility values for the years 2003 and 2004 are given in Table 5.1. It reveals the average concentration of magnetic minerals, in 2003, is more post-monsoon at stations 1–3 and 6; and at stations 4 and 5. However, the overall concentration of magnetic minerals at Redi beach, in general, is marginally more pre-monsoon, followed by post-monsoon and then monsoon. The concentration of magnetic minerals is quite low during monsoon compared to the other two seasons.

Table 5.1 Season-wise concentration of average magnetic minerals in 2003 and 2004

Station	Pre-monsoon		Monsoon		Post-monsoon	
	2003	2004	2003	2004	2003	2004
1	0.95	3.23	0.47	1.28	1.38	1.07
2	13	8.01	10	5.68	22	14.76
3	16	9.80	19	9.04	26	23.26
4	18.05	10.10	10.17	13.00	4.00	1.67
5	24.00	12.54	3.91	7.73	15.16	14.75
6	16.99	19.30	18.11	22.64	18.50	19.73
Average	15	10.50	10.28	9.90	14.51	12.54

There is a dramatic change in the pattern of deposition at Redi beach in the year 2004 (Table 5.1). The average concentration of magnetic minerals is more at station 1 during pre-monsoon; at stations 4 and 6 during monsoon; and at stations 2 and 3 during post-monsoon. The overall concentration of these minerals is marginally more post-monsoon, followed by pre-monsoon and then monsoon. However, there is not much of a difference in the quantum of magnetic minerals during monsoon and pre-monsoon. Table 5.1 also reveals there is a loss of sediments in the year 2004 compared to 2003 in all the three seasons. Thus, from the foregoing, it can be surmised that the detrital processes operating in the Redi region are most closely associated with the monsoonal precipitation which was more vigorous during monsoon and subdued in pre- and post-monsoon seasons in 2003 and 2004. In fact, the comparative magnetic minerals present along this beach suggest precipitation was more in 2003 than 2004. The quantified loss of magnetic minerals seen in Table 5.1 can stand testimony to this supposition. Data presented by Kothavale and Rajeevan (2017) reveal the same thing which can be verified from Table 5.2. Except for the month of August, the Konkan region, of which Sindhudurga district is an integral part, the remaining months, received more rainfall in 2003 than in 2004. This is also reflected in the presence/absence of magnetic minerals. The longshore currents and wind action is seen to be more prominent during the non-monsoon seasons.

Table 5.2 Monthly rainfall data for the Konkan region denoted in 10th of mm (From Kothavale and Rajeevan 2017)

	Jan	Feb	Mar	Apr	May	Jun	Jul	Aug	Sep	Oct	Nov	Dec
2003	8	4	0	0	0	7994	9656	4127	2659	173	47	0
2004	0	0	0	0	1189	6873	8552	7603	2277	324	110	0

5.4.3 Scanning Electron Microscopy (SEM)

Deciphering the rock and mineral history becomes easy when microtextures on detrital sand grains are identified through SEM. This technique has now become an important tool to understand sediment provenance and transport mechanisms (Mahaney et al. 2004; Alekseeva and Hounslow 2004; Madhavaraju et al. 2004; Kenig 2006; Kasper-Zubillaga and Faustinos-Morales 2007). The morphology of microtextures is to a large extent dependent on the source and the transport pathways undertaken by the detrital grains. This helps understand whether it is the fluvial, marine, aeolian, or glacial mechanism that has impacted their transportation. The erosive and weathering regimes of different hues imprint diverse signatures of surface of grains, helping to identify the medium of their transport (Newsome and Ladd 1999; Chakroun et al. 2009).

SEM unveils microstructures that could be in the form of tiny mineral collages, intertwines, or intergrowths. It can also identify whole or partial grain microtextures. With the help of this technique dissolution characteristics and/or precipitates-coatings of various thicknesses and compositions residing on the grain surfaces or within the pits can also be identified. The angularity microtexture is important in understanding the quantum of wear and tear the grain has undergone. This physical comminution reflects the stress and strain and the energy regime through which the detrital grain traversed. There is also a form of microtexture that manifests through fractures, abrasion marks, and sharp edges that lacerate the upper portions of the detrital grain and are of mechanical origin. The percussion marks result from grain collisions that usually are v-shaped. The adhering particles are generally attached to quartz grain surface, and/or within grooves. Microtextures associated with the chemical activity are seen to be in the form of dissolution objects, which blunt the sharp edges and obliterate the fresh surfaces. They also lead to secondary growths within the grooves or depressions.

Figure 5.6(A) shows a subrounded grain, collected at station 1, 20 m distance, exhibiting pits and depressions. It also reveals a hint of weak planes and striations. Adherents and/or overgrowth are also notably visible on the surface of this grain. The morphology of the grain suggests long-distance travel. Figure 5.6(B), reveals angular grain collected at station 1, 20 m distance exhibiting conchoidal to subconchoidal fracturing with pits and depressions spread all over its surface. Striations are also visible on this grain. Another grain collected at station 1, 20 m distance (Fig. 5.6(C)) is angular with weathering pits and depressions and a few adhering particles nestled within the depressions of its surface. Figure 5.6(D) reveals angular grain, collected at station 1, 20 m distance, which seems to be highly weathered, exhibiting pits and depressions. The depressions are seen to be filled with overgrowths.

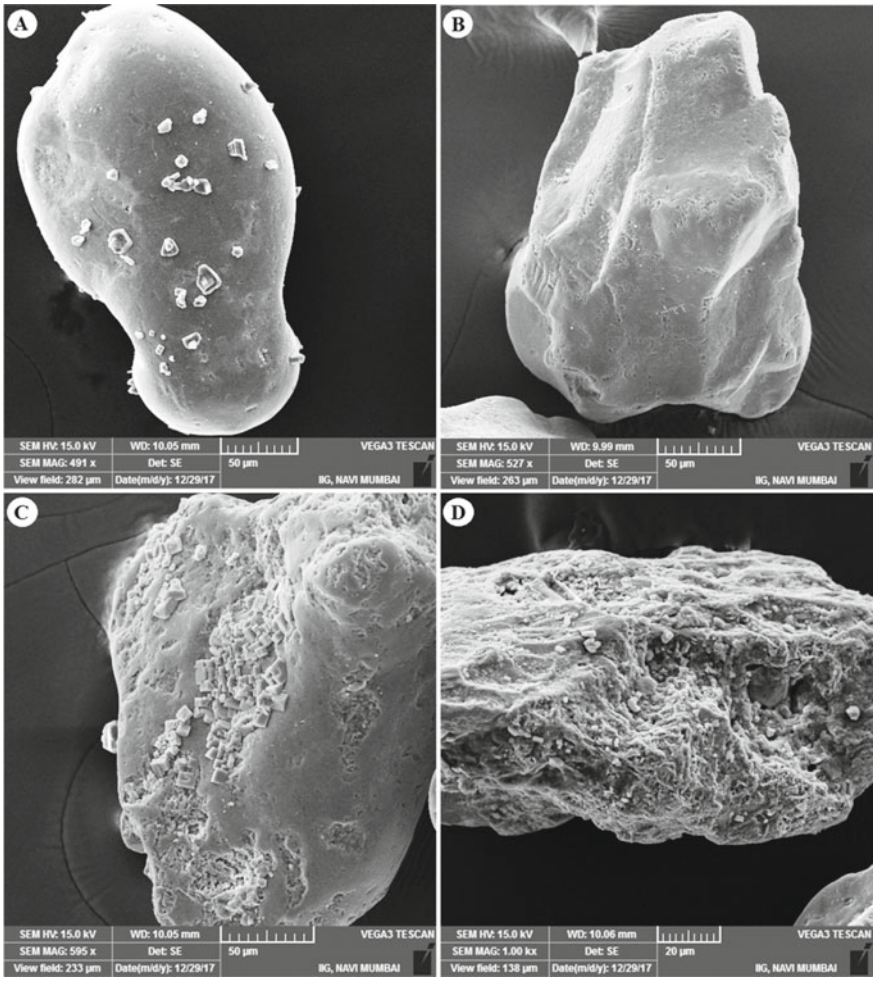

Fig. 5.6 SEM-based morphology of grains collected pre-monsoon at station 1, 20 m distance

5.4.4 Morphological Studies around Redi Beach

Redi beach is a long linear one that is breached by a river at its southern end. This beach is quite wide along its northern side and quite constricted at the southern side. The time elapsed images were utilized to demarcate the changing boundaries of the beach with the base year as 2006 (Fig. 5.7). The image reveals the Redi River is debouching its contents in the Arabian Sea. The first image taken in 2006 reveals the vibrant nature of the river and the many small sandy islands developed near the meeting point to the sea. The beach is punctuated by the flow entering the sea. The broad river stream witnessed in 2006 is seen to have shrunk quite appreciably in

Fig. 5.7 Changes in Redi beach morphology from 2006 to 2018

2012. Some of the sandy islands also are absent in 2012. The Redi beach seems to have grown into the river in 2012 (Fig. 5.7). The sandy islands so conspicuous in 2006 are seen to be in decline in the 2012 image and are completely absent in 2016. In fact, the opening of the beach from where the Redi River makes its entry into the sea is gouging out the sand from the beach. It is seen to make a broader opening in 2016. The beach that was wider in 2016 seems to have shrunk considerably in 2018. The plumes of sand entering the sea are seen to be prominent as well in 2018 (Fig. 5.7).

Thus, to summarize, high susceptibility values at Redi beach are inferred to have been controlled by magnetite and titanomagnetite like ferrimagnetic minerals. There is also a distinct possibility of the presence of antiferromagnetic minerals like hematite at stations where magnetic susceptibility (χ_{LF}) is found to be low. The presence of distinct geology in the form of Archaean, Proterozoic, and basaltic formations force us to infer this possibility. The magnetic susceptibility signal also points toward this possibility. From the foregoing, it can be seen that beach sediments

show a seaward coarsening trend, which is particularly evident in low water levels and breaker samples. The study also suggests a seaward coarsening trend in samples in low water level and breaker samples. It must be remembered that maximum turbulence is expected near backwash or breaker zone owing to the formation of high-energy domain brought about by wave energy (Bascom 1951; King 1972). Kurian et al. (2000) contend placer formations emanate from hydrodynamic processes; and also, by the movement of sediments brought about by alongshore and cross-shore currents (Chandrasekar et al. 2003). The Konkan coast has copious placers of heavy minerals like ilmenite and magnetite. Some of the index heavy minerals like zircon, tourmaline, kyan ite, and staurolite coming from granitic and metamorphic rocks are also found along the coast, though the quantum of these minerals varies from bay to bay (Siddiquie and Rajamanickam 1979; Siddiquie et al. 1982; Wagle et al. 1989; and Gujar et al. 2000). Black sand on the surface and beach scarp was noted during the present study across the Redi beach.Li et al. (2002) have linked the morphology and shore stability to sediment migratory processes operative in the swash zone. Chandrasekar et al. (2005) consider heavy mineral concentration does not reveal just the provenance but their accumulation on the beach is a function of shoreline geometry and seasonally changing wave climate of the region. The sediment provenance and current dynamics involved in transporting the sediments are shown to influence grain morphology and mineral composition (Chavadi and Hegde 1989). The sediment size decreases progressively in the direction it is transported (Pettijohn 1975); the sediment gets better sorted, finer, and positively skewed (McLaren and Bowles 1985), whereas feldspar like light minerals are progressively impoverished in the direction they are transported (Russel and Tylor 1937; Plumley 1948). Rill structures are produced by groundwater percolation (Hanamgond 1990), leaving behind coarser, rolling coarser, or both, including the pebbles, by taking away finer particles when the inflow is much stronger. Hegde et al. (2006) have found heavy mineral concentration is related to the erosional profile. They have inferred strong wave winnowing leads to concentration of heavies and this action is predominant compared to alongshore current transfer.

Silica deposition and solution pits are seen on Redi beach detrital grains and their presence can be attributed to chemical processes operative in tropical or in areas where silica saturation goes on in intertidal areas of a beach (Le-Ribault 1975; Higgs 1979; Moral-Cardona et al. 1997). The detrital grains exhibit chemically induced microtextures. The presence of overgrowths or precipitation entities suggests these features represent the final event in the life of these deposited detrital grains. Pye and Mazzullo (1994) and Kasper-Zubillaga et al. (2005) have also associated silica precipitation with high rainfall and humidity, apart from intertidal silica saturation zones. It has also been unraveled that silica flower, globules, and pellicles on quartz grains are formed by post-depositional diagenetic activity on lacerated surfaces (Madhavaraju et al. 2004). In the samples studied, detrital grains exhibit rounded to subrounded morphology having bulbous corners. This is inferred to be the result of fluvial transport. Therefore, the data generated suggest that all forms of scratches are an outcome of fluvial processes combined with the energy associated with high to mid-energy beach domain.

The crystalline rocks are seen to possess arcuate steps and conchoidal fractures on the grains related to mechanical processes feature formed in a littoral environment subject to wave action and high energy (Madhavaraju et al. 2004; Kenig 2006). In the Konkan tract of Sindhudurg district, the Precambrian are the oldest rocks exposed, in addition to Deccan Trap formations. Hence, the presence of these features etched on Redi sands indicates their derivation from the crystalline rocks that were deposited in coastal environment experiencing high-energy condition. The straight scratches are related to riverine high-energy regime involved in transportation, and/or littoral environments (Alekseeva and Hounslow 2004). Some of the grains reveal diverse surface textures and grain morphology. This is indicative of multicyclic processes having different histories of sources, provenance, and transportation.

The magnetic mineral concentration is high and evenly spread at all the sampling locations along Redi beach, probably because sediments are disseminated by the processes of alongshore currents and waves. Furthermore, sediments are coarser at the backshore (berm) compared to upper foreshore possibly due to fine material removal farther landward by winnowing action of the wind. The heavy minerals are found to drift toward either ends based on density, shape, and size in response to turbulence brought about by high-energy dynamics (May 1973). Thus, the differences observed at Redi beach in the concentration of magnetic minerals are due to the impact of wave energy and shoreline morphology. In 2003 and 2004, during monsoon, local precipitation was found to be a dominant eroding/depositing agency; whereas pre- and post-monsoon season, winds and longshore currents were the dominant eroding/depositing agency in both years. In 2003 the magnetic susceptibility signal is mostly imparted by fine particle magnetic grains; whereas in 2004 it is mostly imparted by very coarse to coarse magnetic grain size particles in all three seasons. Some samples analyzed for magnetic grain size revealed SP and 0.02–0.04 μm range ferrimagnetic grains are absent in these beach sands during 2004. Magnetite and haematite are the main magnetic minerals. Wear and tear during transport in high and intermediate energy conditions of sand grains was deciphered in both years.

Redi beach is characterized by a very significant feature that sets it apart. Iron ore deposits contained within banded hematite quartzite and hematite are found near the Redi beach. The ore is also transported from here to other parts of India because of which this ore is seen dumped near the beach. This ore, stacked around, spills while transporting it through the jetty built at the confluence of Redi River and sea. The iron ore found around Redi is related to banded ferruginous quartzites and Precambrian ferruginous phyllites. Haematite is predominantly present in this iron ore, apart from magnetite, goethite, and limonite in small amounts, which can be seen as lensoid bodies and reefs. The Redi headland, in the north, is lacerated by River Redi and Terekhol River in the south. This geomorphology may preclude redistribution of magnetic minerals at its ends.

Hanamgond (2007) carried geomorphological studies along Sindhudurg coast, which revealed the beaches are accreting post-monsoon and eroding pre-monsoon. But, during monsoon, the beaches reveal cyclic and episodic morphological processes. Erosion and deposition of sediments are ascribed to tide and wave action, as also the longshore currents. The Redi beach follows the general prograding trend

pre-monsoon and post-monsoon. Erosion was found to be prominent during June and July 2003 in consonance with processes observed along India's West Coast. However, Hanamgond (2007) unraveled northerly currents in fair-weather season and southerly in monsoon. This trend, however, is absent at Redi beach, possibly because of its orientation and shelteredness.

Beach sands undergo sorting that is proportionate to the energy levels exposed. High wave energy environments are therefore expected to have coarser sediments. The presence of fine-grained, as well as better sorted sands made up of quartz-rich entities, can be inferred to have come from selective processes defined by longshore transport and the presence of favorable wind patterns. The variation seen at Redi beach in cross-shore variation in grain size, like mean size and sorting indicates coarsening seaward trend. This is mainly due to the influence of Redi River and oceanic waves giving rise to the mixing of river and wave currents producing a higher energy regime. The sediments coming toward Redi beach are the result of traction currents as well as are carried in graded suspension reflecting relict type sediments. Redi beach has an appreciable concentration of gravels and pebbles that are quite well rounded and present all year round lending support to the reworking of sediments. The role of longshore currents in the mixing and homogenization of sands is not significant.

5.5 Conclusions

The magnetic susceptibility results from the Redi beach sands collected in the years 2003 and 2004, seasonally have thrown up interesting results. Magnetic minerals are more close to the sea than land. The synthesis of two years' data can lead us to a comprehensive understanding of the processes' operative along with one of the most important beaches of the Sindhudurg district. There is a decrease in the volume of the magnetic minerals in 2004 compared to the levels of 2003. This beach has experienced a comparatively more influx of material containing magnetic minerals pre-monsoon in 2003 and post-monsoon in 2004. In fact, in both the years during monsoon, the sediments carrying magnetic minerals were quite low compared to the other two seasons. The percentage change in the sediment influx with respect to 2004 has been −64%, −33% and 100%, respectively pre-monsoon, in monsoon, and post-monsoon. The drop was comparatively higher post-monsoon, quite low in monsoon and intermediate pre-monsoon. This change can be attributed to subdued precipitation in 2004 compared to the previous year. Thus, the impact of monsoonal precipitation can be conspicuous on the beach sediments and can be evident in even small scale timeframe. Thus, monsoonal changes are potent to initiate changes even within a very short timeframe. This has been brought out adequately by the magnetic studies, SEM, and time-lapsed images of the Redi beach. The beach from its initial configuration in 2006 prograded in 2012, and then receded considerably in 2016, from then on it seems to be prograding again in 2018. Thus, the prograding and retrograding of

beaches are cyclic and seasonal. Wear and tear during transport in high and intermediate energy conditions of sand grains was deciphered through SEM. Pre- and post-monsoon winds and longshore currents are the dominant eroding/depositing agency. Some encrustation and secondary chemical growth were also identified. This will help better management of beaches to shield them from natural and anthropogenic onslaughts.

Acknowledgements PBG and BVL thank the Director, IIG, for giving the permission to publish this paper. It is with great grief that we have to announce the sad demise of Praveen Gawali sir during the publication of this manuscript. He was the main contributor and inspiration behind the present work.

References

Aher SP, Shinde SD, Guha S, Majumder M (2017) Identification of drought in Dhalai river watershed using MCDM and ANN models. J Earth Syst Sci 126(21):1–14

Aher SP, Shinde SD, Gawali PB, Deshmukh PP, Venkata LB (2019) Spatio-temporal analysis and estimation of rainfall variability in and around upper Godavari River basin, India. Arab J Geosci 12: 682

Alekseeva VA, Hounslow MW (2004) Clastic sediment source characterization using discrete and included magnetic particles—their relationship to conventional petrographic methods in early Pleistocene fluvial-glacial sediments, Upper Don River Basin (Russia). Phys Chem Earth 29:961–971

Arkell B, Leeks G, Newson M, Oldfield F (1982) Trapping and tracing: some recent observations of supply and transport of coarse sediment from upland Wales. Spec Publ Intl Assoc Sedi. 6:117–129

Bandaru VL, Gawali PB, Hanamgond PT, Deenadalayan K (2016) Heavy metal monitoring of beach sands through environmental magnetism technique: a case study from Vengurla and Aravali beaches of Sindhudurg district, Maharashtra, India. Environ Earth Sci 75:678

Barbara T, Aher SP, Gawali PB, Laxmi BV (2016) Seismic hazard analysis along Koyna dam area, Western Maharashtra, India: a contribution of remote sensing and GIS. Geosciences 6:1–20

Barnosky et al (2011) Has the Earth's sixth mass extinction already arrived? Nature 471:51–57

Bascom WN (1951) The relationship between sand size and beach face slope. Trans Am Geophy Uni 32:866–874

Basistha A, Arya DS, Goel NK (2009) Analysis of historical changes in the Indian Himalayas. Int J Climatol 29:555–572

Bookhagen B (2016) High resolution spatiotemporal distribution of rainfall seasonality and extreme events based on a 12-year TRMM time series 2

Booth CA, Fullen MA, Walden J, Worsley T, Marcinkonis S, Coker AO (2008) Problems and potential of mineral magnetic measurements as a soil particle size proxy. J Env Engg Land Mgmt 16(3):151–158

Booth CA, Walden J, Neal A, Smith JP (2005) Use of mineral magnetic concentration data as a particle size proxy: a case study using marine, estuarine and fluvial sediments in the Carmarthen Bay area, South Wales, UK. Sci Tot Environ 347:241–253

Brauch HG (2012) Climate paradox of the G-8: legal obligations, policy declarations and implementation gap. Revista Brasileira De Política Int 55:30–52

Cayan DR, Peterson DH (1989) The influence of north Pacific atmospheric circulation on stream flows in the west. Geophys Monogram Ser 55:375–397

Chakroun A, Miskovsky JC, Zaghbib-Turki D (2009) Quartz grain surface features in environmental determination of aeolian Quaternary deposits in northeastern Tunisia. Mineral Mag 73(4):607–614

Chan LS, Yeung CH, Yim WWS, Or OL (1998) Correlation between magnetic susceptibility and distribution of heavy metals in contaminated sea-floor sediments of Hong Kong Harbour. Env Geol 36:77–86

Chandramohan P, Anand NM, Nayak BU (1992) Surfzone dynamics of the Konkan Coast, India. In: Desai BN (eds) Oceanography of the Indian Ocean. New Delhi, India: Oxford and IBH 751–759

Chandrasekar N, Cherian A, Paul DK, Rajamanickam GV, Loveson VJ (2005) Geospatial application in the study of beach placer along the coast of Gulf of Mannar, India. Geocarta Int 20(2):69–74

Chandrasekar N, Cherian A, Rajamanickam M, Rajamanickam GV (2003) Formation of heavy minerals in the beaches between Kallar and Vembar. J Curr Sci 3(1):207–212

Chavadi VC, Hegde VS (1989) A note on the textural variation of beach sediments in the vicinity of Gangavali river mouth near Ankola, west coast of India. Mahasagar 22(2):89–97

ChigboAMe CCN, Chekwubechukwu N (2016) Industrialization and its Backlash: focus on climate change and its consequences. J Environ Sci and Techno 9:301–316

Cioppa MT, Porter NJ, Trenhaile AS, Igbokwe B, Vickers J (2010) Beach sediment magnetism and sources: Lake Erie, Ontario, Canada. J Great Lake Res 36(4):674–685

Clifton J, McDonald P, Plater A, Oldfield F (1999) Derivation of a grainsize proxy to aid the modelling and prediction of radionuclide activity in saltmarshes and mud flats of the Eastern Irish Sea. Estuar Coast Shelf Sci 48:511–518

Clifton J, McDonald P, Plater A, Oldfield F (1997) Relationships between radionuclide content and textural properties in Irish Sea intertidal sediments. Water Air Soil Pollut 99:209–216

Dash SK, Jenamani RK, Kalsi SR, Panda SK (2007) Some evidence of climate change in twentieth-century India. Clim Change 85:299–321

De LM, Raventós J, González-Hidalgo JC, Sánchez JR, Cortina J (2000) Spatial analysis of rainfall trends in the region of Valencia (east Spain). Int J Climatol 20(12):1451–1469

Deendar DI (2000) Structural controls in the formation of iron ore deposits and laterite in Vengurla area, workshop: 'sustainable resource management in mining: with special reference to coastal regions of Karnataka and Maharashtra. Mining Engineers Association of India, Belgaum chapter 8–10

Deendar DI (2003) Structural controls in the formation of iron ore deposits and laterite in Vengurla area, In: Sustainable resource management in mining with special reference to coastal regions of Karnataka and Maharashtra. Mining Engineers Association of India, Belgaum Chapter Workshop 8–10

Deshmukh KK, Aher SP, Gawali PB, Deshmukh PP (2017) Groundwater quality in Deccan upland region of Chandanapuri valley, Sangamner, Maharashtra, India. Sustain Water Resour Manag 4:687–697

Gallaway E, Trenhaile AS, Cioppa MT, Hatfield RG (2012) Magnetic mineral transportand sorting in swash-zone: Northern Lake Erie, Canada. Sedimentol 59(6):1718–1734

Gawali PB, Basavaiah N, Hanamgond PT (2010) Mineral magnetic properties of sediments of beaches, Redi-Vengurla Coast, Central West Coast of India: a seasonal characterization and provenance study. J Coast Res 263:569–579

Gawali PB, Aher SP, Lakshmi BV, Gaikwad RD, Dcendayalan K, Hanamgond PT, Mahesh Babu JLV, Arote SA, Bairage SI (2017) Identification of landslide susceptible villages around Kalsubai region, Western Ghats of Maharashtra using geospatial techniques. J Geo Soc India 90:301–311.

Goswami BN, Venugopal V, Sengupta D, Madhusoodanam S, Xavier PK (2006) Increasing trends of extreme rain events over Indiaina warming environment. Science 314:1442–1445

Gujar AR, Rajamanickam GV, Wagle BG (2000) Shoreline configurations control on the concentration of nearshore heavy minerals: a case study from Konkan, Maharashtra, central west coast of India. Proc Intl quat Seminar on INQUA shoreline Indian Ocean sub-commission 140–147

Hanamgond PT (2007) Morphodynamics of the beaches between Redi and Vengurla, Maharashtra, West Coast of India. Department of Science and Technology, Government of India (ESS/23/VES/138/2001), pp 292

Hanamgond PT (1990) Ripple structure and Rill structure, Mudga beach, west coast, India. Shore Beach 58(3):30

Hansard R, Maher BA, Kinnersley R (2011) Biomagnetic monitoring of industry-derived particulate pollution. Environ Pollut 159:1673–168

Hatfield RG, Cioppa MT, Trenhaile AS (2010) Sediment sorting and beach erosion along a coastal foreland: magnetic measurements in Point Pelee National park, Ontario, Canada. Sed Geol 231:63–73

Hegde VS, Shalini G, Kanchanagouri DG (2006) Provenance of heavy minerals with special reference to ilmenite of the Honnavar beach, central west coast of India. Cur Sci 91(5):644–648

Higgs R (1979) Quartz grain surface features of Mesozoic- Cenozoic sands from the Labrador and Western Greenland continental margins. J Sediment Petrol 49:599–610

Hiremath DA (2003) Iron ore deposits of Sindhudurg district Maharashtra state and their export potentiality. In: Sustainable resource management in mining with special reference to Coastal Regions of Karnataka and Maharashtra. Mining Engineers Association of India, Belgaum Chapter Workshop 21–25

Hunink JE, Immerzeel WW, Droogers P (2014) A high-resolution precipitation 2-step mapping procedure (HiP2P): development and application to a tropical mountainous area. Remote Sens Environ 140:179–188

Hutchinson SM, Prandle D (1994) Siltation in the saltmarsh of the Dee Estuary derived from 137Cs analysis of shallow cores. Estuar Coast Shelf Sci 38:471–478

Indian Network on Climate Change Assessment (INCCA) (2010) Climate change and India: A 4X4 assessment (A sectoral and regional analysis for 2030s). INCCA report #2. Delhi: Ministry of Environment and Forests

Kantamaneni K, Du X, Aher S, Singh RM (2017) Building blocks: a quantitative approach for evaluating coastal vulnerability. Water 9(12):1–15

Kasper-Zubillaga JJ, Dickinson WW, Carranza-Edwards A, Hornelas-Orozco Y (2005) Petrography of quartz grains in beach and dune sands of Northland, North Island, New Zealand. NZ J Geol Geophys 48:649–660.

Kasper Zubillaga JJ, Faustinos-Morales R (2007) Scanning electron microscopy analysis of quartz grains in desert and coastal dune sands (Altar Desert, NW Mexico). Ciencias Marinas 33(1):11–22

Kenig K (2006) Surface microtextures of quartz grains from Vistulian loesses from selected profiles of Poland and some other countries. Quat Int 152–153:118–135

King CAM (1972) Beaches and Coasts. Edward Arnold, London

Kothawale DR, Rajeevan M (2017) Monthly, Seasonal and annual rainfall time series for All-India, homogeneous regions and meteorological subdivisions: 1871–2016. Contribution from IITM Research Report No. RR-138 ESSO/IITM/STCVP/SR/02(2017)/189. Accessed 25 July 2019

Kumar V, Jain SK (2011) Trends in rainfall amount and number of rainy day sin river basins of India (1951–2004). Hydrol Res 42:4

Kurian NP, Prakash TN, Jose F, Black KP (2000) Hydrodynamic processes and heavy mineral deposits of southwest coast of India. J Coast Res Spec Issue 34:154–163

Lal M (2003) Global climate change: India's monsoon and its variability. J Env Stud Policy 6:1–34

Lees JA, Pethick JS (1995) Problems associated with quantitative magnetic sourcing of sediments of the Scarborough to Mablethorpe coast, Northeast England, U.K. Earth Surf Procand Land 20:795–806

Lapland A, Stevens RL (1996) Mineral magnetic and textual interpretations of sedimentation in the Skagerrak, eastern North Sea. Mar Geol 135:51–64

Le-Ribault L (1975) L'exoscopie, methode et applications. Notes et Memoires Compagnie Francaise des petroles 12:231

Li L, Barry DA, Pattiaratchi CB, Masselink G (2002) Beach win: modeling groundwater effects on swash sediment transport and beach profile changes. Environ Model Softw 17:313–320

Lins HF, Slack JR (1999) Stream flow trends in the United States. Geophys Res Lett 26(2):227–230
Madhavaraju J, Ramasamy S, Mohan SP, Hussain SM, Gladwin GAN, Stephen PV (2004) Petrography and surface textures on quartz grains of Nimar Sandstone, Bagh Beds, Madhya Pradesh—implications for provenance and depositional environment. J Geol Soc India 64:747–762
Mahaney WC, Dirszowsky RW, Milner MW, Menzies J, Stewart A, Kalm V, Bezada M (2004) Quartz microtextures and microstructures owing to deformation of glacio lacustrine sediments in the northern Venezuelan Andes. J Quat Sci 19:23–33
Maher BA, Hatfield RG (2009) Fingerprinting upland sediment sources: particle size-specific magnetic linkages between soils, lake- and suspended sediments. Earth Surf Proc Land 34:1359–1373
Maher BA, Kinnersley R (2010) Rates of particulate pollution deposition onto leaf surfaces: temporal and inter-species analyses. Environ Pollut 10. https://doi.org/10.1016/j.envpol.2009.12.029
Maher BA, Pates JM, Barker PA (2008) Sediment dynamics in an upland temperate catchment: changing sediment sources, rates and deposition. J Paleolimnol 40:1143–1158
Maher BA, Watkins SJ, Brunskill G, Alexander J, Fieldings CR (2009) Sediment provenance in a tropical fluvial and marine context by magnetic fingerprinting of transportable sand fractions. Sedimentol 5:841–861
May JM (1973) Selective transport of heavy minerals by shoaling waves. Sedimentol 20:203–211
McLaren P, Bowles D (1985) The effects of sediment transport on grain size distributions. J Sed Petro 55(4):0457–0470
Min SK, Kwon WT, Parkand EH, Choi Y (2003) Spatial and temporal comparisons of droughts over Korea with East Asia. Int J Climatol 23:223–233
Mirza MQ (2002) Global warming and changes in the probability of occurrence of floods in Bangladesh and implications. Glob Environ Chang 12:127–138
Moral-Cardona JP, Gutiérrez-Mas JM, Sánchez-Bellón A, LópezAquayo F, Caballero MA (1997) Provenance of multicycle quartz arenites of Pliocene age at Arcos, Southwestern Spain. Sed Geol 112:251–261.
Newsome D, Ladd P (1999) The use of quartz grain microtextures in the study of the origin of sand terrains in Western Australia. CATENA 35:1–17
Oldfield F, Maher BA, Donoghue J, Pierce J (1985) Particle size related, mineral magnetic source sediment linkages in the Rhode River catchment, Maryland, USA. J Geo Soc (Lond) 142:1035–1046
Oldfield F, Richardson N, Appleby PG, Yu L (1993) 241Am and 137Cs activity in fine grained salt marsh sediments from parts of the NE Irish Sea shoreline. J Environ Radioact 19:1–24
Oldfield F, Rummery TA, Thompson R, Walling DE (1979) Identification of suspended sediment sources by means of magnetic measurements: some preliminary results. Water Resour Res 15:211–218
Oldfield F, Yu L (1994) The influence of particle size variations on the magnetic properties of sediments from the north-eastern Irish Sea. Sedimentol 41:1093–1108
Petrovsky E, Kapicka A, Zapletal K, Sebestova E, Spanila T, Dekkers MJ (1998) Correlation between magnetic parameters and chemical composition of lake sediments from Northern Bohemia—preliminary Study. Phys Chem Earth 23:1123–1126
Pettijohn FJ (1975) Sedimentary rocks, vol 3. Harper and Row, New York.
Plumley WJ (1948) Black hills terrace gravels: A study in sediment transport. J Geol 56:527–577
Pye K, Mazzullo J (1994) Effects of tropical weathering on quartz shape: an example from northeastern Australia. J Sediment Res 64(3a):500–507
Russel RD, Tylor RE (1937) Roundness and shape of Mississipi river sands. J Sed Petro 45:225–276
Sawant S, Balasubramani K, Kumaraswamy K (2015) Spatio-temporal analysis of rainfall distribution and variability in the twentieth century, over the Cauvery Basin, South India. Environmental management of river basin ecosystems, pp 21–41
Schmidt AM, Von Dobeneck T, Bleil U (1999) Magnetic characterization of Holocene sedimentation in the South Atlantic. Palaeoceanography 14:465–481

Sen PK (2002) An introduction to the geomorphology of India. Allied publishers PVT LTD, New Delhi

Shinde S, Aher S, Pawar A, Kantamaneni K (2020) Spatio-temporal Variability of Discharge Over the Past 40 Yearsin Krishna and Koyna Rivers, India. Iran J Sci Technol, Trans Civ Eng. 10.1007/s40996-020-00375-z

Shrestha AB, Wake CP, Dibb JE, Mayewski PA (2000) Precipitation fluctuations in the Nepal Himalaya and its vicinity and relationship with some large scale climatological parameters. Int J Climatol 20:317–327

Siddiquie HN, Rajamanickam GV (1979) Surficial mineral deposits of continental shelf of India. Proc BRGM 7:233–258

Siddiquie HN, Rajamanickam GV, Gujar AR, Ramana MV (1982) Geological and geophysical exploration for offshore ilmenite placers off Konkan coast, Maharashtra, India. Proc OTS 749–762

Sinha Ray KC, Srivastava AK (1999) Is there any change in extreme events like droughts and heavy rainfall? INTROPMET-97, 2–5 December 1997, IIT New Delhi

Tandale TD (1993) Coastal environ of Maharashtra: evolution and human activities aided with satellite remote sensing. Photonirvachak 21(2):59–65

Thompson R, Oldfield F (1986) Environmental magnetism. Unwin and Allen, London

Wadia DN (1976) Geology of India, Tata McGraw Hill, New Delhi

Wagle BG, Gujar AR, Mislankar PG (1989) Impact of coastal features on beach placers: a study using remote sensing data. Proc OTC Houston, Texas 229–233

Walden J, Oldfield F, Smith J (eds) (1999) Environmental magnetism: a practical guide, quaternary research association. Technical guide, London, p 6

Wheeler AJ, Oldfield F, Orford JD (1999) Sedimentology and postdepositional controls on magnetic signals from saltmarshes on the north-west coast of Ireland. Sedimentol 46:545–558

Xie S, Dearing JA, Bloemandal J (2000) The organic matter content of street dust in Liverpool, UK and its association with dust magnetic properties. Atmos Environ 34:269–225

Xie S, Dearing JA, Bloemandal J, Boyle JF (1999) Association between the organic matter content and magnetic properties in street dust, Liverpool, UK. Sci Total Environ 241:205–214

Zhang W, Yu L, Hutchinson SM (2001) Diagenesis of magnetic minerals in the intertidal sediments of the Yangtze Estuary, China, and its environmental significance. Sci Total Environ 266:160–175

Chapter 6
Vulnerability Assessment of Avalanches in Upper Satluj Basin, District Kinnaur, Himachal Pradesh, India: A Geographic Information System (GIS)-Based Approach

Amit Jamwal and Kesar Chand

Abstract The satellite images interpretation and its analysis through the geographic information system (GIS) is one of the technical and scientific methods to analyze the avalanches. The selected parameters such as slope, slope aspect, slope profile, relative relief and land use, land cover and their subclasses are major base triggering factors for the impacts and its vulnerability analysis. All base factors indicate the threat of avalanches and its vulnerabilities depend on the impact value of the parameters classes. The overlay analysis reveals that the about 6% region of basin has very high vulnerability of avalanches. Out of which 0.9% area has high vulnerability and the remaining portion 99.1% of basin area has low vulnerability and not recorded incidences of avalanches. The average vulnerability (0.41) and impact score (0.54) indicates low vulnerability of avalanches.

Keywords Geographic information system (GIS) · Avalanches · Vulnerability

6.1 Introduction

The down slope movement of snow masses under the impact of gravity and consist of rocks, soil, debris, uproot tree and rocks is known as avalanches (Colbeck et al. 1990). The avalanches occurrences are triggered by some factors such as high relative relief, a high degree of slope, slope aspect, slope profile, the volume of snow and land use and land cover (Fohn 1993). The high relative relief (>3000 m) and a high degree of slope (>30°–40°) provides acceleration to avalanches. Sometime avalanches are generated due to the high intensity of earthquakes (Dunning et al. 2007). The avalanches are

A. Jamwal (✉)
Aryabhatta Geo-Informatics & Space Application Centre (AGiSAC), 34, SDA Complex, Kasumpti, Shimla 171009, Himachal Pradesh, India

K. Chand
North East Regional Centre, G.B. Pant National Institute of Himalayan Environment (NIHE), Itanagar 791113, Arunachal Pradesh, India

R. B. Singh et al. (eds.), *Remote Sensing and Geographic Information Systems for Policy Decision Support*, Advances in Geographical and Environmental Sciences,
https://doi.org/10.1007/978-981-16-7731-1_6

also generated due the excessive snowfall in a short period. Even human induced avalanches are also generated because of blasting activities (Bocchiola et al. 2008). In Kinnaur district the blasting activities are common due to hydro power construction (Lata et al. 2017). If we see the frequency and magnitude of snow avalanches it shows that Himachal Pradesh are less disastrous and effected very limited spatial extent. The incidences of avalanches are most prevalent in the districts of Lahul and Spiti, Kinnaur, Kullu and Chamba, before the 1971 the information regarding the incidences of avalanches are very limited (Chandel 2015). The Lahul and Spiti district is the most vulnerable district which has highest number of avalanches and Kinnaur (36.59%) is the second leading district. In district Kinnaur about 15 people were died because of avalanches (GHP 2006). Snow avalanches are a disastrous type of hazard in mountainous terrain. The potential vulnerability of avalanches and their assessment can be done during the time of planning of new settlements. It could be helpful to mitigate the potential damage of avalanches. Vulnerability and the degree of loss to a given element or set of elements within the area affected by avalanche(s); it is expressed on a scale of 0 (no loss) to 1 (total loss); for property, the loss could be the value of the property, probability of particular life loss (the element at risk) of given the person(s) affected by the avalanche (IUGS 1997; IPCC 2012).

6.2 Study Area

The River Sutlej Basin in Himachal Pradesh forms a part of the Northwestern Himalaya which is topographically fragile and ecologically delicate. The Sutlej catchment in Himachal Pradesh extends approximately 30° 50′ N to 32° 50′ N latitudes and 76° 50′ E to 79° 09′ E longitudes, occupying an area from the Shiwalik to Greater Himalayan region (Fig. 6.1). The Sutlej basin rises from beyond the Indian borders in the Southern slope of the Kailash mountain near the Mansarovar lake of the Rakastal lake. Being the largest river of Himachal Pradesh, it enters into Himachal Pradesh from Shipki La Pass at an altitude 6608 m and flow in the south-westerly direction through Kinnaur, Shimla, Solan, Mandi, Kullu, and Bilaspur districts. In Himachal Pradesh, the Sutlej Basin covers an area of about 21,457 km^2. Geologically and geomorphologically, the basin is considered to be the youngest mountain chain in the world and is still in the building process. The relative relief of the basin varies from 452 to 6735 m as ml. The study area of the upper Sutlej basin in district Kinnaur extended from approximately 31° 19′ 4″ N to 32° 05′ 59″ N latitudes and 77° 82′ 01″ E to 78° 83′ 05″ E longitudes, climate of whole of the Satluj valley is generally temperate. But due to a large variation in the altitude (455–6735 m), there is also a wide range of climatic variations (Sharma et al. 2008). Climate varies from the sub-tropical, sub-mountainous at the bottom of the Sutlej valley to the alpine in the upper reaches, parts of which remain perpetually under snow. In this region, the temperature generally starts rising from the beginning of March till June, which is the hottest month of the year. The mean minimum and maximum temperatures were observed to be around 15.6 °C and 24 °C respectively. The month of January

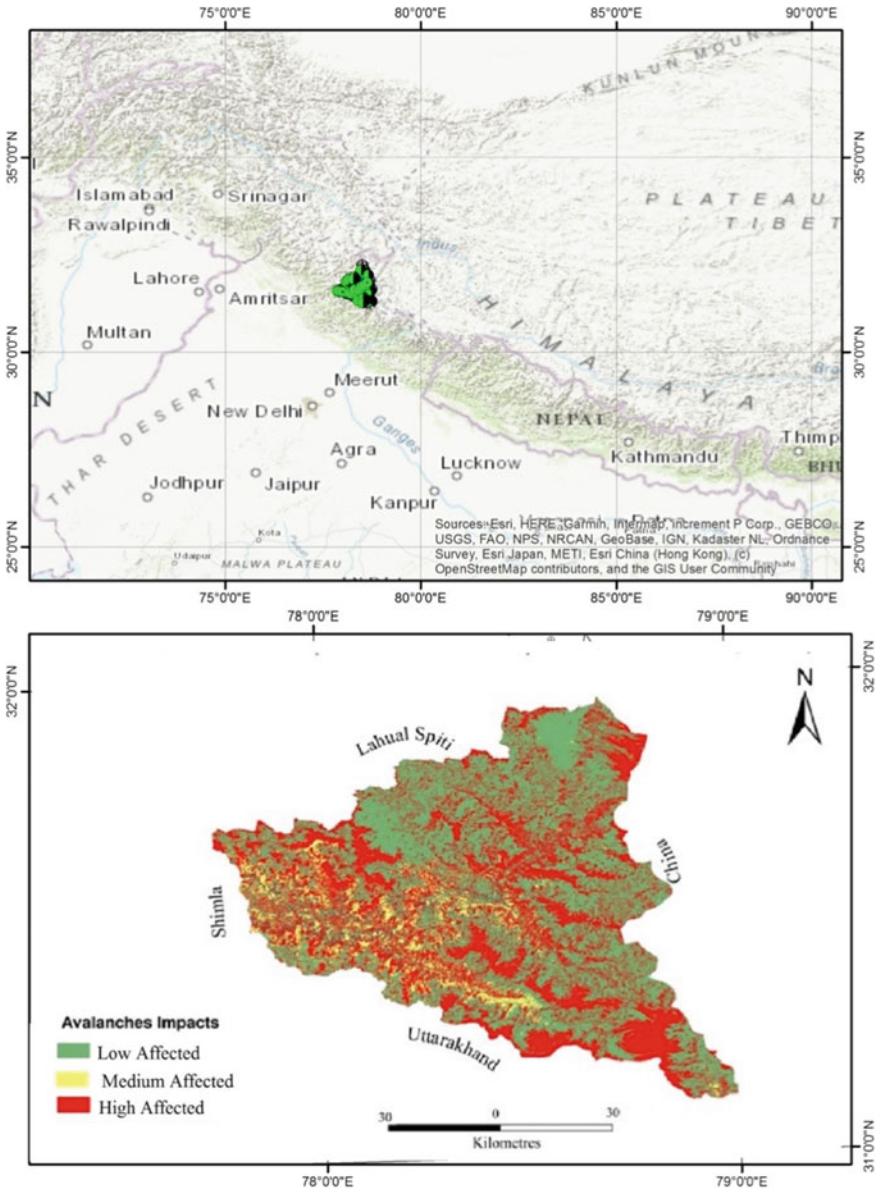

Fig. 6.1 Study area

is the coldest month with the mean maximum and minimum temperatures of around 8.9 °C and 1.7 °C respectively. During winters, under the influence of the western disturbances, the temperature falls considerably and it may go even below 0°. The climate of the Sutlej valley shows a gradual alteration from the heavy monsoon of the outer Himalayas to the arid Tibetan type with a winter snowfall practically there is no summer rains. The total annual rainfall is observed to be 766 mm in Kinnaur. The abundance rainfall is received between the month of January and March all over the year.

6.3 Methodology

Avalanches monitoring and observation are based on field survey and satellite images interpretation. The field survey has done along the river Satluj and points (Location coordinates) are taken (GPS) of near to the actual incidences sites. A total of 25 points are taken in surrounding villages of sites. These points are taken and export in the kml format and visually interpreted. The avalanches are identified and area is calculated through the kml files as in polygon format. Then polygon kml files are exported in arc GIS for calculation of area. The Land use land cover (LULC) map is prepared on the basis of digital glove image (DGI) at the resolution of 5 m. The Slope and relative relief maps are prepared on the basis of Digital Elevation Model (DEM) at 30 m resolution (USGS 2004). Local survey is conducted in the study region to understand the geophysical setting of the region. Relative relief, land use lands cover (LULC) are measured and using surface analysis tool in Arc GIS 10.3 (Moges and Bhole 2015).

Some important or selected parameter is exported in GIS environment and the incidences locations are overlaid and then the degraded and vulnerable area is identified. Then identified area is cross checked and validated with field survey (Stoffel et al. 1998). The highest affected area is scored with the highest number from the total number of subclasses. The values are normalized from 0 to 1 to check the impacts on parameter classes. The formula is used to normalized as PN (parameters normalized) = Ps (Parameters Score)/Np(Total number of parameters). The degraded areas are identified on every selected parameter. The weighted score is based on parameter classification (Fig. 6.2).

6.4 Result and Discussion (Parameters–Based Analysis)

6.4.1 Relative Relief

High relative relief had high vulnerability as a hazard point of view, high soil erosion, high surface runoff (Clung and Schaefer 1993). DEM (Digital Elevation Model) is

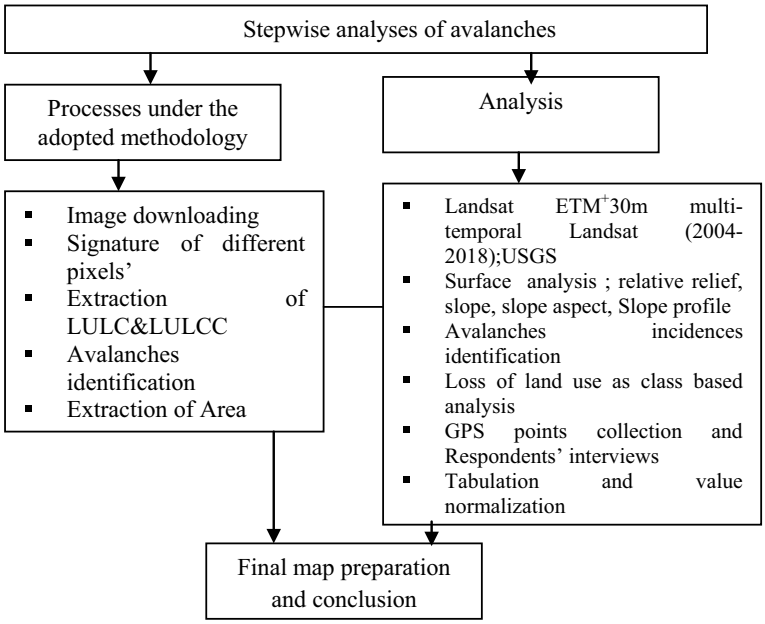

Fig. 6.2 Stepwise analyses of avalanches

used widely for landscape analysis not only in geo-morphometric, but also in other geosciences-based studies, such as geomorphology, hydrology, meteorology, soil sciences and vegetation studies. The relative relief of the basin has a high value of 1244–6755 m. The dissection index value 0.64–0.87 has high risk as an avalanches point of view. In the basin, the area falls under the altitudes 3000–6755 m is falls under the high risk (Singh 2004). The unstable layers of snow easily moved downward on high relative relief (>3000 m). More the 50% area of the upper basin is fallen under the snow-covered and avalanches risk. If we see the history of incidences impacts about 129 people died from 1970 to 2015. The relative relief area of 1244–3000 m is less affected by incidences and impact and risk point of view scored as 1 and relative area 3000–6755 m area are scored as 0.5 (Table 6.1).

6.4.2 Slope

The slope is one of the trigging factors which accelerates or slows the incidences of avalanches. The high degree of slope greater than the >35° has high vulnerability and risk of snow avalanches (Jurg and Martina 2001). The study region of the different slopes is classified as gentle slope 8%, moderate slope 13%, moderately steep slope 17%, steep slope 18% and very steep slope 30%. The highest affected area (1.5 km^2) of the basin is recorded under the high vertical slope (45°–90°) which is scored

Table 6.1 Parameters-based analysis, identification and status of avalanches

Parameters	Classification	Affected area in terms of land degradation Identification and	Weight score (Score/Total No. of Parameters = P_s/N_p)	Vulnerability	Avalanches incidences impacts
1. Slope $P_{1=}\ P_s/N_p$	Gentle slope	0	0	0	Snow avalanches region, where slope greater than $>35^0$ more vulnerable to landscape loss. In this region the avalanches incidences are very high
	Moderate slope (5°–10°)	0.31	0.8	0	
	Moderate Steep slope (10°–18°)	0.39	0.6	0	
	Steep slope (18°–30°)	1.42	0.5	0	
	Very steep slope (30°–45°)	1.45	0.3	1	
	Vertical slope (45°–90°)	1.5	1	1	
2. Slope Profile ($p_{4=}$ P_s/N_p)	Summital convexity	1.1	0.7	1	The summital convexity had high degree of losses and adversely affected (Jamwal et al. 2019)
	Rectilinear section	0.3	0.5	0	
	Free face	0.11	0.2	0	
	Basal concavity	1.17	1	1	
3. Relative relief ($p_{4=}$ P_s/N_p)	R_R 1244–3000 RR > 3000 m	0.9.3	0.5 1	0 1	The higher relative relief and avalanches both have positive correlation
4. Land use land cover (LULC) ($p_{4=}\ P_s/N_p$)	Settlements	0.15	0.2	0	The land use type barren/wasteland, scrub land providing more acceleration to avalanches (Salm 1978)
	Agricultural land	0.6	0.3	0	
	Forest cover	0.8	0.5	1	
	Barren/wasteland	1.40	1	1	
	Grass/grazing	1.30	0.8	1	
	Scrubland	1.05	0.6	0	
	Water bodies	1.17	0.7	0	
	Snow and glacier	0.10	0.1	0	
5. Slope aspect (p_5) $P5 = P_s/N_p$	Flat	0.01	0.1	0	North and south facing slopes are more vulnerable because of their direction during the time of winter and summer (Kuniyal et al. 2019)
	North	2.10	1	1	
	North East	0.71	0.4	0	
	East	0.24	0.3	0	
	South East	1.05	0.7	1	

(continued)

Table 6.1 (continued)

Parameters	Classification	Affected area in terms of land degradation Identification and	Weight score (Score/Total No. of Parameters = P_s/N_p)	Vulnerability	Avalanches incidences impacts
	South	1.10	0.8	1	
	South West	0.91	0.5	0	
	West	0.22	0.2	0	
	North West	0.97	0.6	1	
	Average = Total cells value/no. of cells	0.80	0.54	0.41	

as 1, slope of very steep slope (30°–45°) with affected area (1.45 km^2) is scored as 0.3, steep slope (18°–30°) is scored as 0.5, moderate steep slope scored as 0.6, moderate slope (0.39 km^2) is scored 0.8 and gentle slope is not affected with the avalanches and scored as 0. Tangling, Apka, Lippa, Asrang, Chakra, Spillo, Poo, Khab and Nakko village's area has a very steep slope which has poor soil texture, less vegetation-covered, high gully rills erosion, dry climate condition. Gentle slope to moderate slope found in the region of Chaura, Burang and Wangtu above the region (YashangDhar, PunagKhas, Urni, Cooling, MeruKhas, Rurag, Kibla, Karcham, Rali) has moderate steep to the steep slope (Fig. 6.3). Here forest-covered is moderate sparse and snow impact is high above the RaliRanrang, Shongtong, Barang and Tangling. Kalpa, Pangi, Khadura, Akpa, Khab areas have a very steep slope with sparse vegetation and with indicated the high risk of avalanches (Table 6.1).

Fig. 6.3 Avalanches incidences in Spillo, Poo, Khab and Nakko village's of Satluj River upper basin

6.4.3 Slope Aspect

In the northern hemisphere of temperate latitudes, the north direction slope is mostly affected during the winter. The settlement on the North Slope aspect has high vulnerability and risk north-facing (shady) slopes usually produce more avalanches and more persistent avalanche hazard in mid-winter. The south-facing slope is produced more wet avalanches during the summer season (Fohn et al. 1998). The slope aspects of North (2.10 km^2), South (1.10 km^2), Southeast (1.05 km^2) are highly affected areas with high risk and North scored as 1, South scored as 0.8, southeast scored as 0.7, respectively. And other aspects of the basin are scored such has 0.6 North West (0.71 km^2), 0.5 Southwest (0.91 km^2), 0.4 northeast (0.71 km^2), 0.3 East (0.24 km^2) and West (0.22 km^2) aspect is scored as 0.2 (Table 6.1).

6.4.4 Slope Profile

The distinctive segments such as profile are called slope elements or slope segments. A slope profile study is done on the basis of field surveys. Different types of slopes profile such as summits convexity, basal concavity, rectilinear section and free face of slope profiles are commonly found in the Satluj valley Concave elements of slopes are very commonly found in the lower portion of the Satluj valley (Fig. 6.4). The free face, rectilinear section, and summital convexity are affected with avalanches impacts (Perla 1977). The basal concavity is highly affected (1.17 km^2) and scored as 1, rectilinear section (0.30 km^2) is scored as 0.5, free face (0.11 km^2) is scored as 0.2 and semimetal convexity (1.1 km^2) is scored as 0.7 (Table 6.1). The Basal concavity area is highly affected by avalanches. The basal concavities are also affected because this section received high pressure of snow mass and leads to incidences of avalanches.

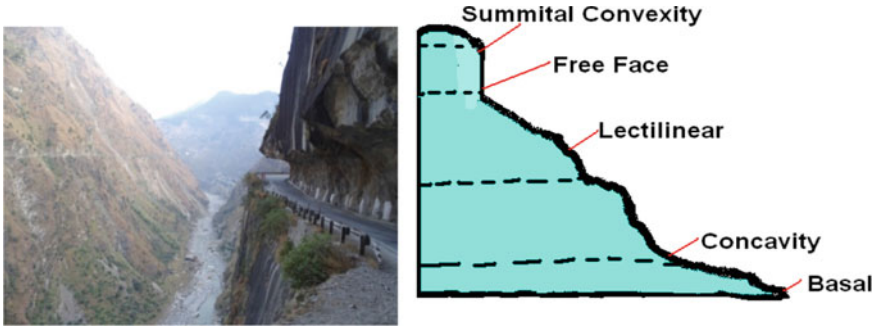

Fig. 6.4 Free face segments of hill slope has also found in upper (near to Khab) and in the areas of Powari, Shongtong and Karcham Wangtu

6.4.5 *Land Use Land Cover (LULC)*

LULC is also considered to be the major factor in influencing the movement of the avalanche. The heterogeneous structure of the mountain forest appears to play a significant role in stopping avalanches. Significant snow-mass detrainment behind tree stands appears to be the key process to stop small avalanches on steep slopes (Clung and Schaerer 1993). Barren and sparsely vegetated areas are more prone to weathering, erosion and slope instability and more susceptible to avalanches. Kinnaur district has maximum area is found under the categories of Snow-covered 2490 km^2 (39%) and wasteland 2030.63 km^2 (31%) types of land use. However, water bodies (5.3 km^2), Built-up (1.54 km^2) and agriculture (52.8 km^2) has a very low area. Other categories forest-covered 484.63 km^2 (8%) area and Grassland covered is only 1383.1 (20.58%). It is made clear from the field survey that the area of Karchamwagtu, Powari, Tangling, Kalpa, Bokta, Pangi, RarangKhas, Akpa, Rispa, Jangi, Spillo, Nako has heavy snowfall incidences during the winter season. The soil compactness is reduced during the snowfall and incidences of avalanches increased (Table 6.1; Figs. 6.5 and 6.6).

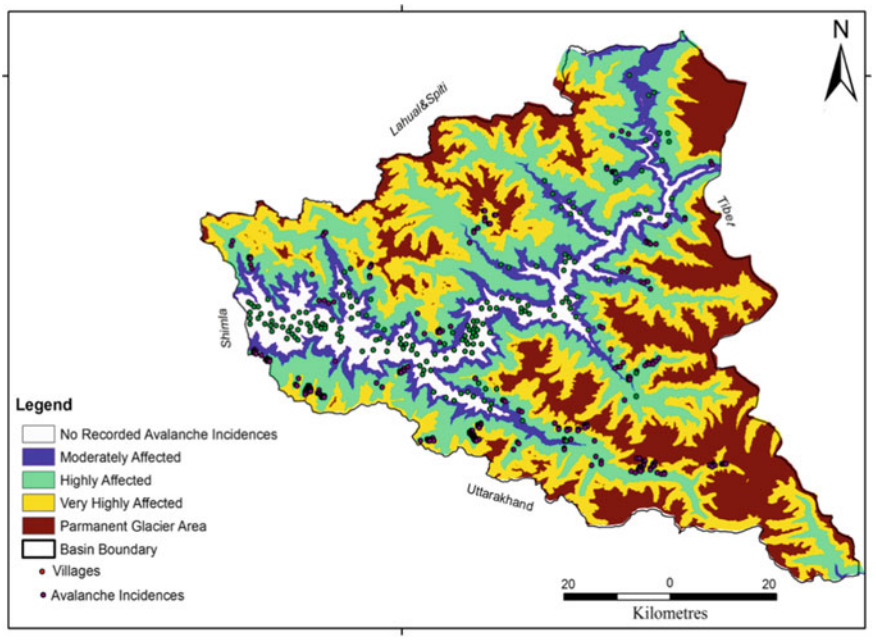

Fig. 6.5 Avalanches affected area in upper basin of River Satluj

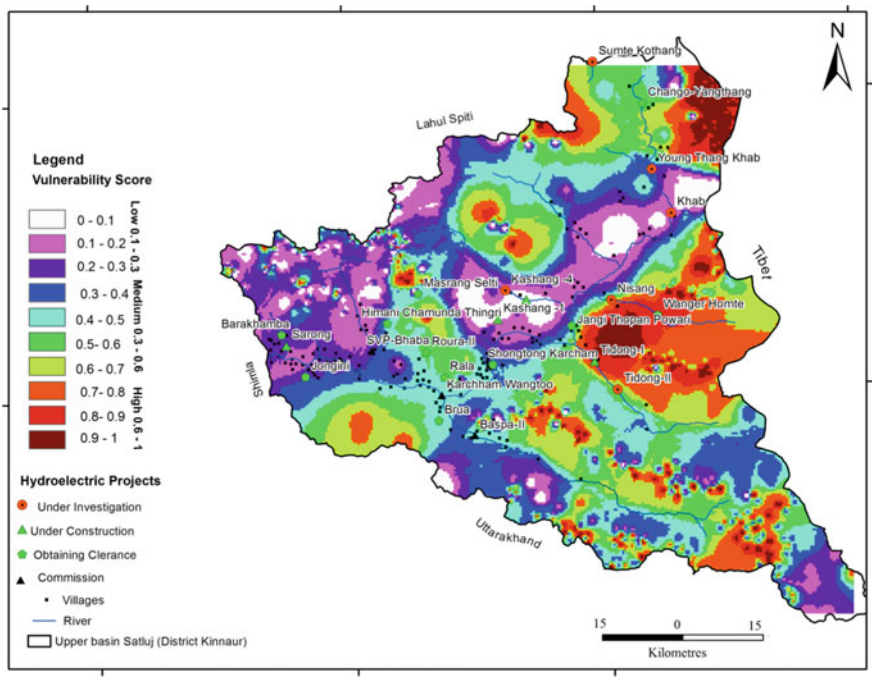

Fig. 6.6 Avalanches vulnerability in upper Satluj basin of Himachal Pradesh

6.5 Conclusion

The avalanches incidences are noticed in the upper region of the basin. The losses are highly counted on the selective trigging factors such as very steep slope, basal concavity slope profile, high relative relief >3000 m and region of sparse vegetation and wasteland is highly affected. The slope aspect of north, south, and southeast is highly affected. However, human causality and property losses are very rarely recorded. Geographic information system made clear that about 100 km^2 areas are highly damaged because of snow avalanches. Because of avalanches, forest lands are highly affected. The maximum incidences of avalanches are recorded above the 3500 m in district Kinnaur. More than 75% area of the upper basin falls under the high altitude. The 5458 km^2 (80%) area of the study region has under the high degree of slope >35°. The maximum incidences of avalanches were noticed under the slope types of higher degree. The concave slope more prone to avalanches incidences during the time of high precipitation. The physical degradation has high on the slope aspects of the north, east, southeast and south and west. The region has more barren areas (62%) then the region has more vulnerability as an avalanches point of view.

The overlay analysis reveals that the about 6% region has very high vulnerability of avalanches. Out of which 0.9% (61.7 km^2) area has high vulnerability and 5.5% (362.2 km^2) region has medium vulnerability. The remaining portion 93% (6137

km^2) of basin has low vulnerability and not recorded incidences of avalanches. All avalanches parameters analyzed average vulnerability score (0.41) indicated the low vulnerability.

Acknowledgements The Authors are thankfully to acknowledge the Director of G.B. Pant National Institute of Himalayan Environment (NIHE) and Department of Geography Kumaun University Nainital, Uttarakhand 263001, for providing research support and valuable guidance and providing GIS lab facilities to deportment of this study.

References

Bocchiola D, Bianchi JE, Marty GE, Sovilla B (2008) Regional evaluation of three-day snow depth frequency curves for Switzerland. Nat Haz Ear Sys Sci 8:685–705

Chandel V (2015) Snow avalanche as disaster in mountain environment: a case of Himachal Pradesh. Int J Geod Geosci 6(2):1578–1584

Clung DM, Schaefer P (1993) The avalanche handbook. Mountaineer, Seattle, USA

Colbeck S, Akitaya E, Armstrong R, Gubler H, Lafeuille J, Lied K, Clung D, Morris E (1990) International classification for seasonal snow on the ground, International commission for snow and ice IAHS, World Data Center, Glaciology, University of Colorado, Boulder, CO, USA

Dunning SA, Mitchell WA, Rosser NJ, Petley DN (2007) The HattianBala rock avalanche and associated landslides triggered by the Kashmir Earthquake of 8 October 2005. Eng Geo 93(3–4):130–144. https://doi.org/10.1016/j.enggeo.2007.07.003

Fohn PMB (1993) Characteristics of the weak snow layers and its interface's. In: Proceeding of the international snow science workshop, Breckenridge, USA, pp 60–170

Fohn PMB, Camponovo C, Krusi G (1998) Mechanical and structural properties of weak layers measured in situ. Ann Glaci 26:1–5

GHP (2006) State of environment report, Himachal Pradesh, Shimla. State Council for Science Technology and Environment, pp 1–137

IPCC (2012) Managing the risks of extreme events and disasters to advance climate change adaptation: a special report of Working Groups I and II. Cambridge University Press, Cambridge, UK

IUGS (1997) Quantitative risk assessment for slopes and landslides: the state of the landslide risk assessment. In: Proceeding of the international workshop on landslide risk assessment, pp 19–21

Jamwal A, Kanwar N, Kuniyal JC (2019) Use of geographic information system for the vulnerability assessment of landscape in upper Satluj basin of district Kinnaur, Himachal Pradesh, India. Geo Eco Lands 6:1–17. https://doi.org/10.1080/24749508.2019.1608410

Jurg S, Martina L (2001) Characteristics of human triggered avalanches. Cold Reg Sci Technol 33:147–162

Kuniyal JC, Jamwal A, Kanwar N, Chand B, Kumar K, Dyani P (2019) Vulnerability assessment of the Satluj catchment for sustainable development of hydroelectric projects in the north-western Himalaya. J Mount Sci 16:2714–2738. https://doi.org/10.1007/s11629-017-4653-z

Lata R, Herojeet R, Dolma K (2017) Environmental and social impact assessment: a study of hydroelectric power projects in Satluj Basin in District Kinnaur, Himachal Pradesh, India. Int J Earth Sci Eng10(02):270–280. https://doi.org/10.21276/ijese.2017.10.0219

Moges G, Bhole V (2015) Morphometric characteristics and the relation of stream orders to hydraulic parameters of River Goro: an ephemeral river in Dire-dawa, Ethiopia, Uni J Geosci 3(1):13–27

Perla R (1977) Slab avalanche measurements. Can Geotech J 14:206–213

Salm B (1978) Snow forces on forest plants. Mount For Aval 157–181

Sharma S, Kuniyal JC, Agarwal DK, Sharma JC (2008) Role of environmental impact assessment and public involvement in sustainable development of hydropower projects in the mountain-a case of the Beas valley, Himachal Pradesh, India. Ind J Power River Valley Dev 58(4):37–47
Singh S (2004) Geomorphology, 4th edn. Kalyan Publication, Allahabad, pp 381–382
Stoffel A, Meister R, Schweitzer J (1998) spatial characteristics of avalanche activity in an Alpine valley: a GIS approach. Rev Geophy 41(4):1–25
USGS (2004) Lynn Highland: landslide types and processes. http://pubs.usgs.gov/fs/2004/3072/fs-30-72

Chapter 7
Assessment of Soil Risk by RUSLE Model Using Remote Sensing and GIS in Pench River Basin, Madhya Pradesh, India

C. S. Dwivedi, Raghib Raza, A. C. Pandey, and D. C. Jhariya

Abstract This study leads to the evaluation of risks in soil erosion for highland landscapes using the RUSLE model and data obtained from remote sensing within a GIS and to propose several land-use scenarios that can reduce soil losses. Each erosion factor of the RUSLE model was computed. The Tropical Rainfall Measurement Mission (TRMM) data, provided by point scale, was examined to calculate rainfall and runoff erosivity (R) factors. Annual R values range from 1009.827 to 1283.383 MJ mm $ha^{-1}h^{-1}$, whereas the R values of the wet season are double that of the dry season. Using The Digital Elevation Model (DEM), the topographic LS factors were computed from the slope and flow accumulation algorithms. Landsat ETM + Satellite images utilized in the calculation of C factors by using the shin value which determines the proportion of each land use type within each value between 0 and 1. Erosion risks on cultivation land were moderate, whereas they were quite high on the dry crop, protection forest, and unused land types. The most severe erosion rates occurred on settlement or urban development region which had poor vegetation cover. Erosion risk and classified slope maps are useful to identify and delineate the spatial allocation of protection forest. The K-factor is calculated through the algorithm and data is used from FAO Erosion soil, in which topsoil layer of clay, silt, sandy, and organic composition is taken for the calculation. In summary, the integration of the RUSLE model and remotely sensed data provides an effective platform for the evaluation of risks in soil erosion and for the selection of appropriate land use scenarios that can reduce soil losses on a large scale.

Keywords Soil erosion · RUSLE model · Erosion risk · K-factor

C. S. Dwivedi (✉) · R. Raza · A. C. Pandey
Department of Geoinformatics, School of Natural Resource Management, Central University of Jharkhand, Ranchi 835205, Jharkhand, India
e-mail: chandra.dwivedi@cuj.ac.in

D. C. Jhariya
Department of Applied Geology, National Institute of Technology Raipur, Raipur, India
e-mail: dcjhariya.geo@nitrr.ac.in

R. B. Singh et al. (eds.), *Remote Sensing and Geographic Information Systems for Policy Decision Support*, Advances in Geographical and Environmental Sciences,
https://doi.org/10.1007/978-981-16-7731-1_7

7.1 Introduction

Soil is usually a product of process when tiny particles of endured rocks and minerals blend in with rotting plants, creatures, and other natural resources. Soil formation is a moderate cycle that takes long years. Nevertheless, the dirt that is made is continually exposed to common and artificial powers that disturb it. Soil disintegration is characterized as the wearing a method of dirt. Dirt is the topmost layer of soil and it is most beneficial on the ground which consists of natural and supplement-rich nutrients. The debasement of agrarian land by soil disintegration is an overall marvel prompting loss of surface soil which is rich in supplements, expanded overflow from more impermeable dirt, and diminished water accessibility to plants. In this manner, assessment of soil misfortune and recognizable proof of basic zone for the execution of best administration practice is vital to achieving the activities related to soil conservation. Complete land zone exposed to soil debasement associated with human-intrusion has been assessed around 2 Bha (Billion hectares). By this, around 110 Mha by water disintegration and 550 Mha by wind disintegration is assessed because of the disintegration of the land zone influenced by soil corruption (Saha 2003). In India, soil erosion majorly affects the agricultural part, shore siltation, soil debasement, and so on. To issue and forestalling further annihilation of dirt layer, several legal moves have been taken by the legislature to amend this. About 45% of the absolute topographical surface zone which is around 130 million hectares of land (Kothyari 1996), is influenced by genuine soil disintegration through the canyon and crevasse, moving development, developed badlands, sandy zones, deserts, and water-logging in this country. Exorbitant disintegration of soil with a subsequent high rate of sedimentation in the repositories and diminished ripeness has resulted in serious ecological issues for the nation with deplorable monetary outcomes.

Soil erosion manifold affects the climate and the economy (Vanacker et al. 2003). Soil erosion eliminates rich dirt and carries it into the water bodies, limiting the effectively restricted agricultural area and certainly resulting in to decrease in food production. The shipped silt in water debases the quality of it and leads to eutrophication (Pimentel 2006). Quickened soil disintegration on the one hand causes flood, dry season, and starvation (Zhao et al. 2013). Then again, a lot of dregs released into the stream influences supply and dams, expand their expenses of support, and since quite a while ago run makes them unusable (Samaras and Koutitas 2014). Understanding the status of soil disintegration helps to control the soil disintegration and natural reclamation. Albeit different specialists have attempted examinations identified with disintegration issues (Tamrakar 1993). A few models exist to anticipate the degree of water-prompted disintegration (Brady and Weil 2019). The models run from observational (USLE/RUSLE,) to physical or handle based MMF (Morgan et al. 1984), EUROSEM (Morgan et al. 1992), GUEST (Ciesiolka et al. 1995); LISEM (De et al. 1989); and shift extensively in implication and information input. For the anticipation of the mean pace of soil misfortune because of water disintegration from rural grounds, the Universal Equation (USLE) has been fruitful (Wischmeier et al. 1978a, b). In the mid-1990s, the fundamental USLE was modified to make a disintegration

expectation instrument called the Revised Universal Soil Loss Equation (RUSLE) (Renard et al. 1997a, b). The RUSLE represents how the atmosphere, geography, soil, and land-use influences the terrill soil disintegration and the stream, brought by the impacts of the raindrop. It's been widely used to gauge soil disintegration misfortune, survey soil disintegration hazard, and to deal with improvement and protection plans to manage disintegration under various land-spread conditions, for example, croplands, rangelands, and upset backwoods lands (Milward and Mersy 1999; Sahli et al. 2020). The utilization of far-off detecting and processes conducted in GIS makes soil disintegration assessment and its areal appropriation plausible with sensible expenses and better precision in bigger zones. A mix of far-off detecting by GIS and RUSLE gives the possibility to appraise the misfortune in disintegration soil on a cell-by-cell premise (Lee and Lee 2006; Xu et al. 2009).

7.2 Description of the Study Area

Figure 7.1 showing the Pench River basin is a part of the Kanhan River, which eventually join into it. The origin of this river is in Madhya Pradesh (India) particularly in the Chhindwara district and it flows across Pench National Park, a Tiger project

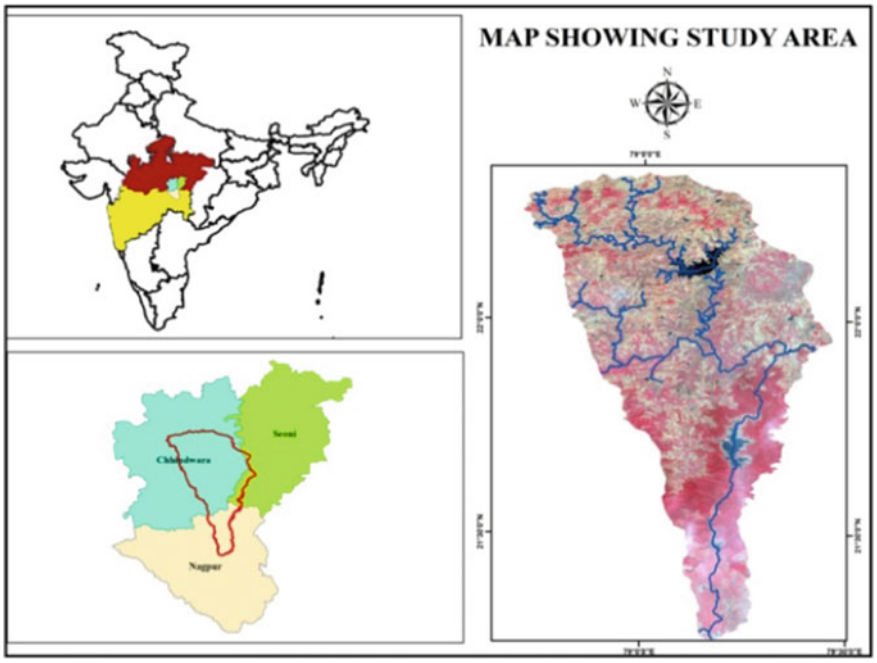

Fig. 7.1 Location of the study area

reserve of India. The Pench River comprises a total area of about 4466.54 Km^2 area. The Pench River flows through the edging areas of Seoni and Chhindwara and then merges with the Kanhan river in the Nagpur district. The Pench River is also a tributary of Banganga and it flows from north to south. While flowing through the Pench National Park, it separates the Pench reserve into two halves of the west and east Pench.

7.3 Methodology and Parameter Estimation

The extend of erosion, associated degradation of soil, and the amount of sediment eroding from a catchment area depends on interactions of complex aspects such as climate, topography, vegetative cover, soil, man-made development, and other geological condition. So, the prediction of rates of rill erosion for a long period and interrill from the ground could be possible with the widely accepted method is the RUSLE itself. This method is the idea of Wischemeier and Smith in 1965 based on 10,000 small test plots data that collected from throughout the United States with a huge time span. Around 22 m of flow length has been assigned for each test plot and evaluated similarly by combining the measurement of the soil loss as a tool for prediction. RUSLE is a modified edition of the earlier USLE (Wischemeier and Smith, 1978) which incorporates new research since 1978. The conservation planning with the RUSLE in the Agriculture Handbook 703 (Renard et al. 1997a, b; Kim et al. 2011) has been considered as an encyclopedia for its modification. The RUSLE has operated on the assumption is that the deposition and detachment of the sediments are controlled by its actual content present in the flow. The erosion of residue is not limited to the source of material, instead, it is limited by the capacity of the agent that carrying it, especially the flow rate and patterns. When the carrying capacity of the flow becomes equal to or exceeds the sediment load the detachment can be taking place (Fig. 7.2).

The basic structure of the RUSLE equation remains the same, while the application involves the changes that consider modifying its factors. USLE and RUSLE compute the average rate of erosion that can take place in the field slope in a year. The calculation behind it is shown (Eq. 7.1).

$$\mathbf{A} = \mathbf{R} \times \mathbf{K} \times \mathbf{L} \times \mathbf{S} \times \mathbf{C} \times \mathbf{P} \tag{7.1}$$

where:

A Spatial average soil loss and temporal average soil loss per unit of area
R Rainfall-runoff erosivity factor
K Soil erodibility factor
L Slope length factor

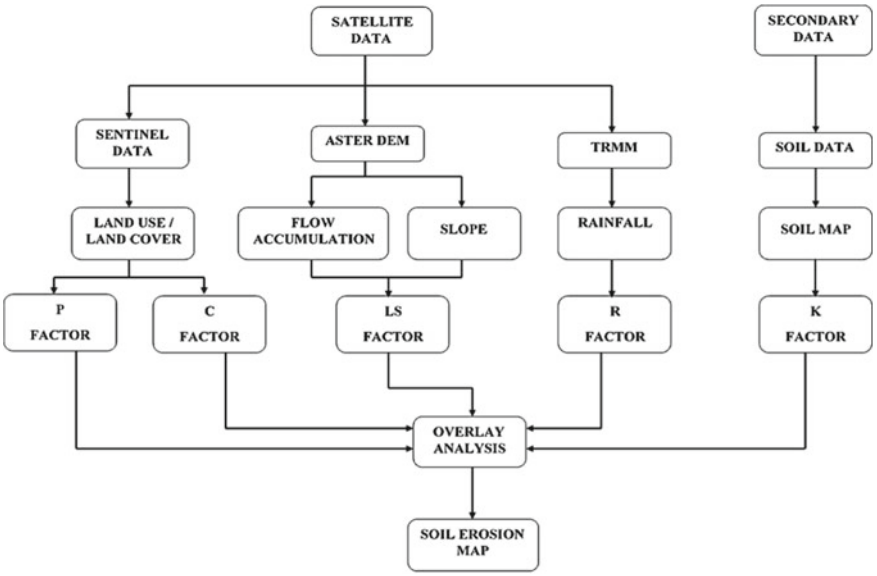

Fig. 7.2 Figure shows the adopted methodology

S Slope steepness factor
C Cover management factor
P Support practice factor

7.3.1 Slope Length Factor (L) and Slope Steepness Factor (S)

The dimension of slope length and the amount of steepness directly controls the runoff and erosion. Slope length and amount of cumulative runoff are directly proportional likewise the steepness of the land and velocities of the runoff. Even though the erosive activity is highly affected by the variation in steepness rather than the length of slope (McCool et al. 1987). The LS factor (Srinivasan R, Engel BA (1991); Engel 2005; Esa et al. 2018; Moore and Burch 1986a, b) can be estimated using the equation (Fig. 7.3):

$$\begin{aligned} \mathrm{LS} &= ([\text{Flow Accumulation}] \times 30/22.13)0.4 \\ &\times \left(\sin\left[\text{local slope gradient}\right]/0.0896\right)1.3 \end{aligned} \tag{7.2}$$

where LS is slope steepness—length factor and cell size of the unit contributing area is 30 m × 30 m.

After the application of testing methods as per Mitasova et al. (1998) to compute LS factor, the method has changed for its better result by creating an algorithm by Van

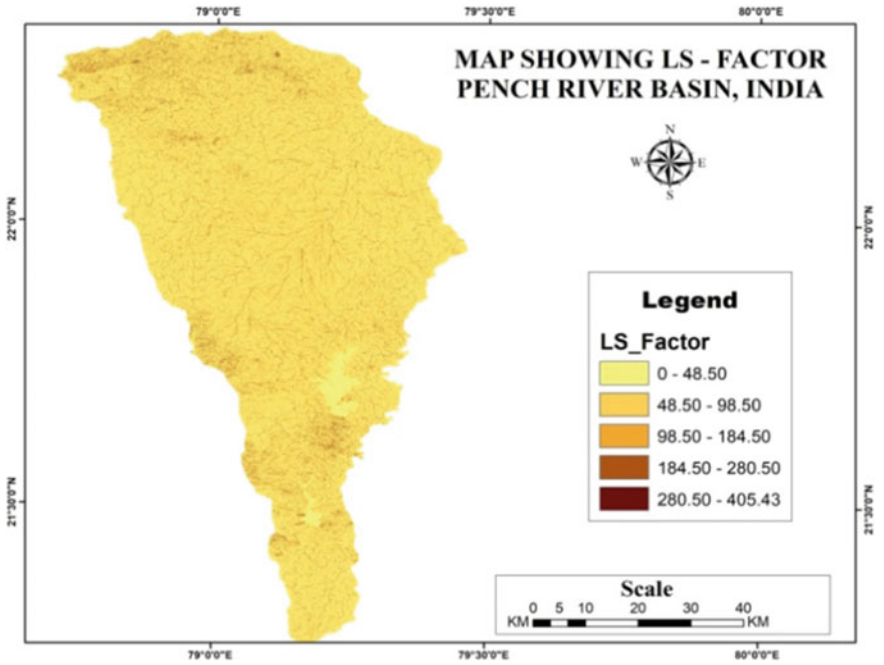

Fig. 7.3 Map representing LS—factor of the study area

Remortel et al. (2001), is developed based on the equation of Renard et al. (1997a, b). The λ and θ were computed directly under the GIS software using AML (Arc Macro Language) script under ArcInfo and DEM (Digital Elevation Model) at 30 m resolution.

7.3.2 Soil Erodibility Factor (k-factor)

An equation given by William to estimate KUSLE values is:

$$K(USLE) = K(W) = f\ (csand) * f\ (cl\text{-}si) * f\ (orgc) * f\ (hisand)$$

where:

f(csand)	Coarse Sand content of the soil
f(cl-si)	Clay to Silt ratio
f(orgs)	Content of Organic Carbon the soil
f(hisand)	High sand content in Soil

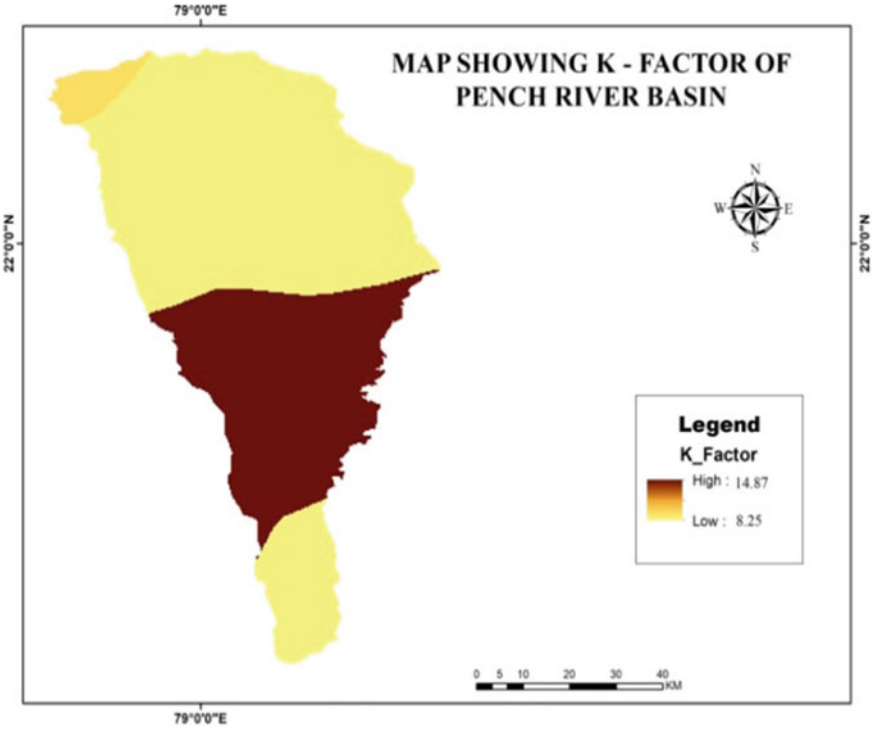

Fig. 7.4 K—factor map of the study area

K indicator in soils lowers when the f(csand) possess high coarse-sand content and with finer sand the value of K indicators for soils increases; soil erodibility factor for soils with high clay to silt ratio is provided by the f(cl-si); same as f(csand) the K value in soil reduces when the f(orgs) values are high i.e., high content of organic carbon and when the f(hisand) hold high sand content (Ndayisaba et al. 2016) (Fig. 7.4, Table 7.1):

$$f_{csand} = \left(0.2 + 0.3 \times \exp\left[-0.256 \times ms \times \left(1 - \frac{m_{silt}}{100}\right)\right]\right) \quad \text{(A)}$$

$$f_{cl-si} = \left(\frac{m_{silt}}{m_C - m_{silt}}\right)^{0.3} \quad \text{(B)}$$

$$f_{orgc} = \left(1 - \frac{0.25 \times orgC}{orgC + \exp\left[3.72 - 2.95 \times orgC\right]}\right) \quad \text{(C)}$$

$$f_{hisand} = \left(1 - \frac{0.7 \times \left(1 - \frac{m_s}{100}\right)}{\left(1 - \frac{m_s}{100}\right) + exp\left[-5.51 + 22.9 \times \left(1 - \frac{m_s}{100}\right)\right]}\right) \quad \text{(D)}$$

Table 7.1 Soil K—factor calculation

Soil unit symbol	Sand % topsoil	Silt % topsoil	Clay % topsoil	OC % topsoil	f_{csand}	$f_{cl\text{-}si}$	f_{orgc}	f_{hisand}	KUSLE	K factor
Vc	22.4	24.5	53.0	0.69	0.203	0.031	0.971	0.99	0.006	8.25
Bv	23.3	26	50.7	1.1	0.203	0.038	0.898	0.99	0.007	9.39
I	58.9	16.2	24.9	0.97	0.200	0.061	0.927	0.99	0.011	1.487

$$K = \left[2.1 \times 10^{-4} \times \mathrm{M}^{1.14}(12 - a) + 3.25(b - 2) + 2.5(c - 3)\right] \times \left(\frac{0.1317}{100}\right)$$

$$\mathbf{K = A \times B \times C \times D \times 0.1317}$$

where:

m_s the sand fraction content (0.05–2.00 mm diameter) [%];
m_{silt} the silt fraction content (0.002–0.05 mm diameter) [%];
m_c the clay fraction content (<0.002 mm diameter) [%];
orgC the organic carbon (SOC) content [%]

To ensure that the erodibility prediction model used expresses the real condition of the area under observation, the results generated from each taxonomic group must match the properties of the respective soil class in relation to the other classes, provided that each soil type has its distinct features, also erodibility values expected to differ from place to place. In tropical soils, erosional processes are mainly associated with their sandy nature (Miqueloni and Bueno 2011). However, with respect to study areas, the soil erodibility factor is directly proportional to sand levels. Therefore, to estimate the K factor under the study conditions, the most suitable model was Sharpley and Williams (1990), which shows a positive correlation with sand levels and a negative with clay and organic matter.

7.3.3 Land Cover and Crop Management Factor (C-factor)

The C factor of RUSLE mainly uses for Cover management. It represents how the roughness and surface cover affects the erosion of soil. Moreover, due to the importance of C factor on the effect of land use on soil erosion, it uses for the assessment of the impact of BMPs (Best Management Practices) on soil erosion reduction (Renard et al. 1997a, b). The cover management factor is a unitless and can be determined through two methods. The initial method involves determining event-specific values as listed in Table 7.2 for calculations.

The C value observed near the water body is very low but it is relatively high in the vegetation and agricultural region. Along with that, the proper calculation of the C factor helps engineers and designers to come up with an effective plan to control erosion that have a high probability of surviving the "gully washer". Independent of the size of the rainfall event for the calculation of the C management factor is a plus point compared to others. However, the lack of an established dataset of baseline bare soil to perform the calculation of the C factor is considered as one of the major limitations of it (Fig. 7.5).

Table 7.2 Cover management factor (C)

S. no	Land cover type	Cover management factor (C)	Applied method
1	Water body	0	
2	Forest	0.03	Trial and error
3	Vegetation	0.041	
4	Intense agriculture	0.37	NIAST (2003)
5	Spars agriculture	0.36	NIAST (2003)
6	Barren land	0.02	BCEOM (1998)
7	Settlement	0.01	Urban density
8	Waste land	0.06	Kim (2006)
9	Sandy land	0.01	

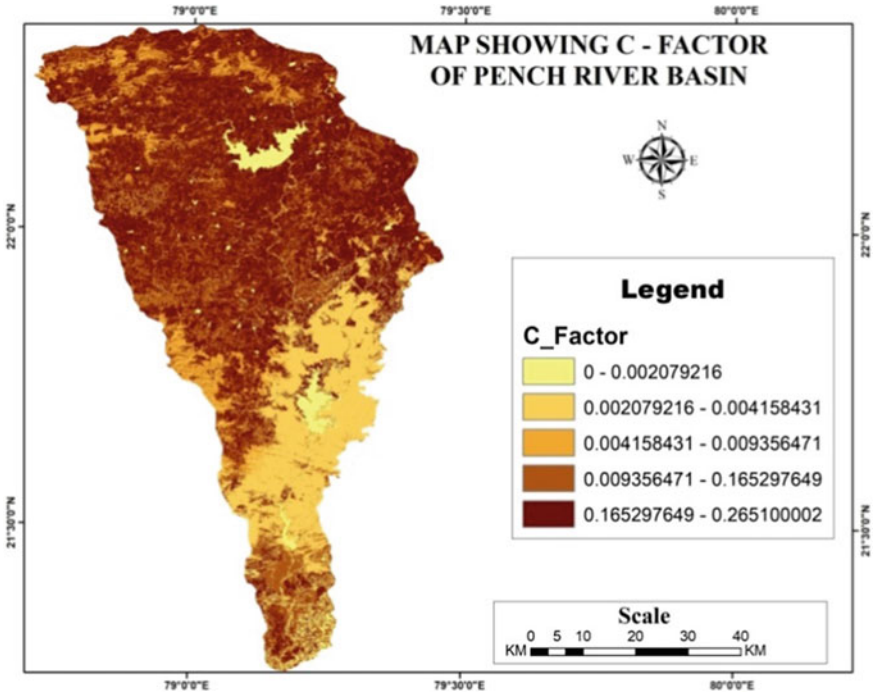

Fig. 7.5 C—Factor map of the study area

7.3.4 The Support Practice Factor (P-factor)

The effect of support practices on the average rate of erosion in the annual base can be illustrated by the P factor (unitless) of RUSLE. It is the ratio of soil loss with a support factor to that with straight row farming up and downslope. The activities like strip cropping, terracing, and contouring are pointed as supporting practice by RUSLE (Michigan State University, 2001).

The ratio of soil loss with specific support practice to straight row upslope and downslope tillage soil loss, represents as support practice factors, has mentioned in Fig. 7.6. The runoff velocity, concentration of runoff, pattern of drainage, and hydraulic forces exerted by a runoff on soil etc. can decrease P factor consists of control practices. These can be prevented by some of the supporting mechanical practices like the application of strip cropping, terracing, and contouring, etc. Here, most of the areas in the Pench watershed are covered with forest, and only 15% if it is utilized for cultivation like paddy and crop fields. Table 7.3 shows the values of support practice factor related to the agricultural activities and slope (Renschler et al. 1999).

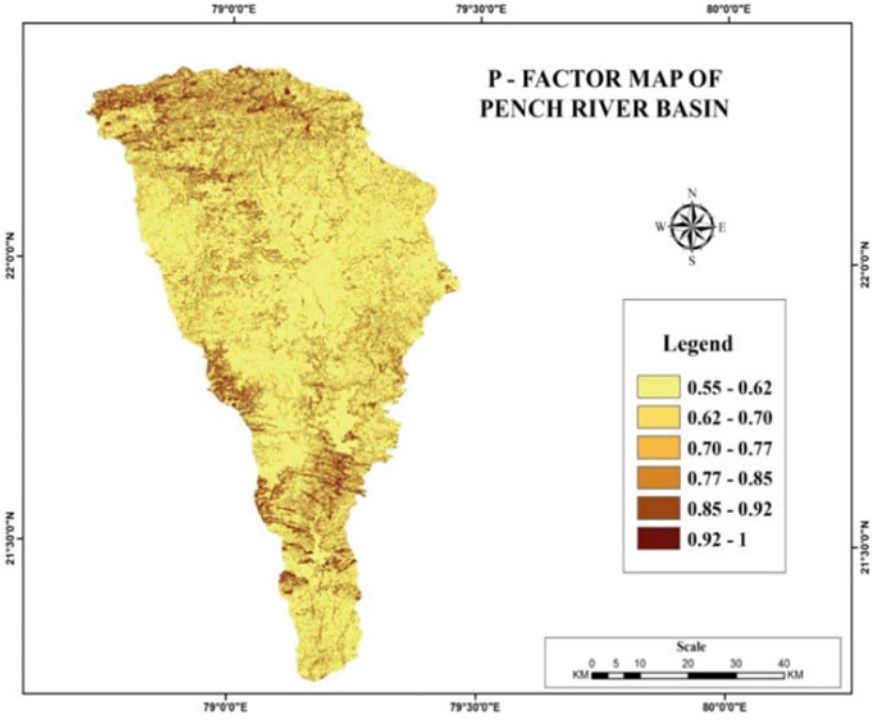

Fig. 7.6 P—Factor map of study area

Table 7.3 Support practice factor (p)

S.no	Slope %	Contouring	Strip cropping	Terracing
1	0.0–7.0	0.55	0.27	0.10
2	7.0–11.3	0.60	0.30	0.12
3	11.3–17.6	0.80	0.40	0.16
4	17.6–26.8	0.90	0.45	0.18
5	26.8>	1.00	0.50	0.20

The region of terracing with the slope in the paddy field has considered for the calculation of the support practice factor and is estimated based on its relation between contouring and slope of crop fields. Figure 7.6 represents the support practice factor (P) of the Pench watershed.

7.3.5 The Annual Rainfall and Runoff Erosivity Factor (R-factor)

Each rainfall event, its duration, magnitude, and intensity can be given all together through the rainfall erosivity factor (R-factor). In this study, the R-factor database of 13 precipitation stations in the Pench River basin has been generated from the original equation of the RUSLE R-factor.

Mean annual rainfall values for Madhya Pradesh (India) having high climate variability shown in Table 7.4. Here, Fig. 7.7 showing rainfall erosivity in the Pench River basin gives a spatial overview of strength rain on erosive activity. The interpolation model (Kriging) used for the interpolation of R factor point values has endup with a fair result. In Fig. 7.7 R-factor reflecting high value shows a strong influence of high soil loss zone, seasonality in precipitation, latitude, and also the elevation of the area on it.

7.4 Result

The cell-by-cell analysis of surface soil loss using the values of RUSLE factors in Arc GIS 10.4 using the Eq. 7.1 has applied for the determination of the rate of soil loss on an average annual basis. The result of the soil map is shown in Fig. 7.8. For the ease of presentation of output data, the map has been classified mainly into five sections (Table 7.5). The rate of annual soil loss ranked very low for plain areas to high for tributaries having a steep slopes and well over very high in some areas.

Table 7.4 Rainfall data with the station

S. no	Area	Latitude	Longitude	Annual mean rainfall
1	Winatola	21.249	79.169	1100.134
2	Newarwada	21.437	79.197	1171.901
3	Vagholi	21.57	79.312	1197.837
4	Kanhargaon	22.04	78.79	1283.383
5	Seonimegha	22.156	78.995	1190.162
6	Dharakuhi	22.342	78.981	1009.827
7	Dongoria	22.26	78.83	1073.792
8	Jaitpur	22.18	79.426	1098.342
9	Kanhargaon	21.699	79.126	1103.468
10	Kajra	22.275	78.677	1270.629
11	Bakora	22.366	79.416	1095.643
12	Saongi	21.331	79.479	1162.453
13	Sawandri	21.292	78.819	1211.009

Source mirador.gsfc.nasa.gov/TRMM

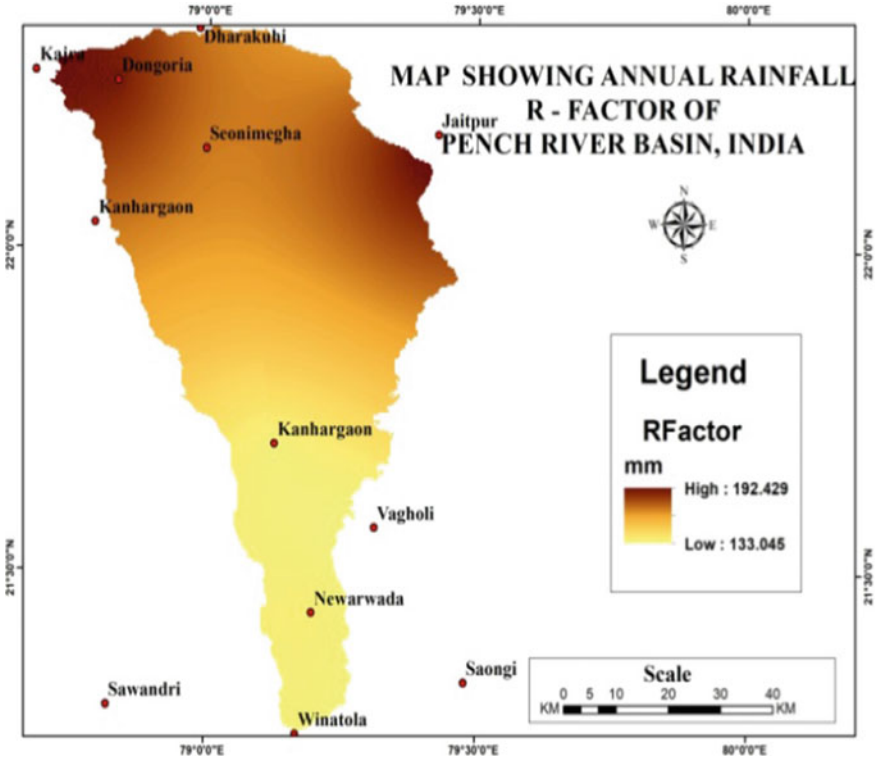

Fig. 7.7 Annual rainfall map of the study area

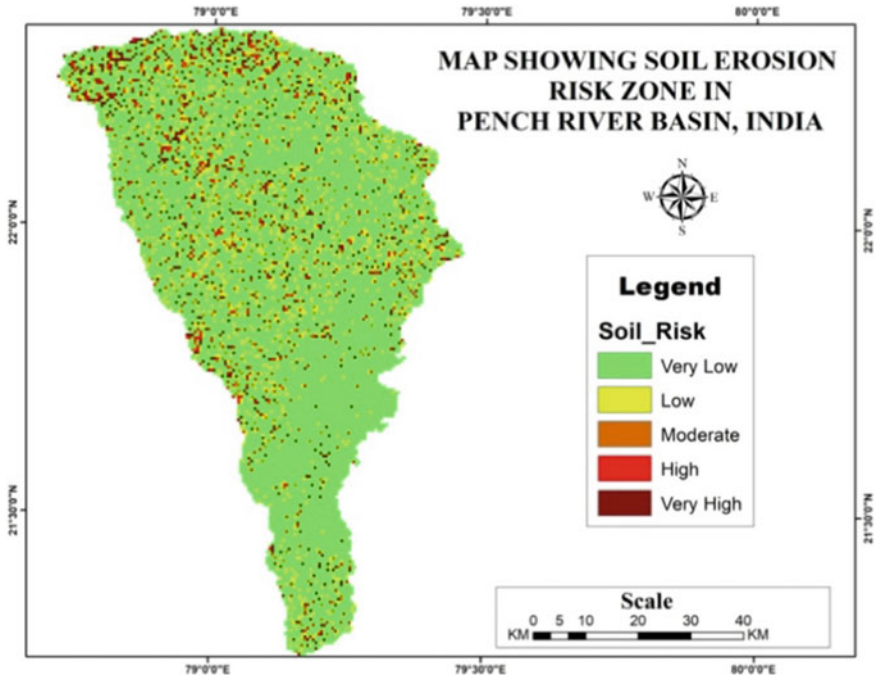

Fig. 7.8 Map showing soil erosion risk zone

Table 7.5 Annual soil loss rates and severity classes with their conservation priority in the study area

Soil loss (t ha^{-1} y^{-1})	Severity classes	Priority classes	Area (ha)	Percent of total area	Annual soil loss (tone)	% of total soil loss
0–10	Very low	V	119254.9821	29.23	24074.15	14.32
10–20	Low	IV	112342.1116	25.79	34410.9	20.18
20–30	Moderate	III	102554.0001	21.11	44266.95	24.09
30–40	High	II	100025.0154	13.15	48189.3	23.19
40 >	Very high	I	12477.9583	10.72	4267.75	18.22

7.4.1 Rainfall Erosivity Factor (R)

Studies show, the average rate of soil erosion over an area is primarily rainfall-dependent (Jain et al. 2001; Dabral et al. 2008). The characterization sediment yield over a seasonal distribution event, be more easily connected with the daily variation of rainfall and the associated deviation in the rate of soil erosion (Wang et al. 2002). The advantages of the utility of annual rainfall consist of computation simplicity, its availability, and regional steadiness of the exponent (Shinde et al. 2010). In this study rainfall data developed from the method of interpolation has been selected for

the computation of R factor. The results from R factor values have fallen between 1132.04 and 1192.42 MJ/mm$ha^{-1}hr^{-1}/year. The results clearly show that Kajra and Jaitpur regions have high rainfall as indicated from results which lie majorly in the northern zone.

7.4.2 Soil Erodibility Factor (K)

The assignment of K values to respective soil types has been conducted for the generation of soil erodibility map. It has been found that the generated K factor values are range between 8.25 and 14.87. The lower value is usually associated with soil with low permeability and moisture content, etc.

7.4.3 Topographic Factor (LS)

The Topographic factor is the representation of an erosional process that is influenced by the slope length and steepness. Inputting the flow accumulation and slope in percentage in Eq. 7.2 will give the values of the topographic factor. Also, it's been observed from the analysis that the value of LS increases from 0 to 405.43 as slope and flow accumulation increases.

7.4.4 Crop Management Factor (C)

Information regarding land use provides a better outline of the utilization of land and other aspects of cropping patterns, forest, fallow land, location of surface water bodies, wasteland, or erosional studies. Remote sensing and GIS are considered as the potential techniques to generate thematic layers of LULC of a region. According to patterns of land use in the area, it has been classified into nine major classes. The values of the C factor that has been assigned to the corresponding land-use class have listed in Table 7.2. The Crop management factor map has been produced by considering the LULC map and Crop management factor (C) (Fig. 7.5).

7.4.5 Potential Annual Soil Erosion Estimation

The annual loss of soil according to the analysis of pixel by pixel basis of the soil erosion which represents the spatial distribution of soil erosion in the study area has been carried out with the help of the RUSLE model in the GIS software. The total area of soil loss is 119254.98 ha. and the measured annual sediment load against

the RUSLE during the water year of 2017 is 24074.15 t (Table 7.5). The sediments carried by rivers have been deposited at the vented dams especially at the upstream portion and consecutively remove yearly. The high-quality sand from the deposit utilizes for construction works as construction materials.

This is one of the reasons behind the reduction of sediment load at measuring regions. However, in the present day, the soil loss can be compared with sediments yield (Esa et al. 2018). In the study area, the potential of soil loss has been classified into four major categories based on erosion rate: Very low, low, moderate, high, and very high erosion. The very high rate of erosion corresponds to high soil loss accordingly least erosional rate indicates low soil loss (Table 7.5). Rest of them falls between the erosional rate of moderate and high. It's been observed that some regions of the study area come under the high soil loss category, which may be the result of the steep slope. The map that indicates the range of severity in soil erosion is the result of consideration of four ordinal types of soil erosion. A major part of the study area falls under the categories of low erosion and the region with very high erosion and steep slope with barren terrain. Foothills of central region experience moderate erosion occurs in which has an agricultural region with mild slope.

Table 7.5 shows that the steeper slope banks of tributaries are the locations which show the high rate of soil erosion in the study area. The area covers about 23.87% of the total area and 41.21% of the total soil loss and falls under the erosional severity class of high and very high, which requires the first and second order of conservation priorities. A thorough analysis revealed that the RUSLE factor that is the steepness and length factor supports the soil erosion and high rate of soil loss in the area (Fig. 7.3). Other low soil erosion areas together comprise 76.13% of the total area and responsible for 58.79% of total low soil loss which is carried away from the study area. The high rate of soil erosion in these areas is contributed by their topographical ruggedness and poor vegetation. Thus, these are associated with high erosion potential land use which has a severity class range of high and very high in which priorities conservation of fourth and fifth.

7.5 Summary

Overland stream examination demonstrated that the overland stream from slopes will in general amass in the piedmont fields; henceforth, slant length factor was figured higher in the piedmont fields. The gathering of overland stream in the piedmont fields, essentially in the upper piece of it, has improved the dirt disintegration. Impact of higher LS factor on soil disintegration in Pench waterway bowl was balanced by regular woods spread. Normal timberland spread in the watershed expands the penetration rate and along these lines decreases surface overflow and soil disintegration (Woo and Luk 1990). Geographical and vegetation spread variables are the most significant components influencing soil misfortune in the sloping watersheds (King et al. 2005; Zhou et al. 2008). Close forests having generally excellent vegetation spread reductions surface overflow and results from low soil disintegration (Sidle

et al. 2004). Squander Land and desolate Land were anticipated to have a high rate of soil disintegration than land with scour or without clean (decrepit land). Vegetation in these territories should be improved by embracing appropriate preservation measures. Soil preservation estimates, for example, bio-designing estimates should be actualized in high-to-high hazard of soil disintegration region to save surface spillover and consequently decreasing soil misfortune for upgrading vegetation spread and improving soil efficiency in the watershed (Tiwari 2004). The investigation represented utilization of GIS in the spatial distribution of soil in a quantitative level, its disintegration to anticipate soil misfortune potential, and to find out the zone of high disintegration hazard for the application of measures in soil protection in the subwatershed. The factors that represent the soil disintegration were produced spatially and incorporated in GIS to foresee the rate of soil disintegration and were additionally grouped into the category hazard map includes the soil disintegration. The normal soil misfortune in Lithosol and Combisol fields was anticipated extremely high. Among different land spread classes, desolate land, agrarian land, and waste land were anticipated to have the most elevated normal soil loss.

7.6 Conclusions

Anticipating spatial circulation of different disintegration severities of these terrains will help in receiving proper soil protection measures to lessen soil disintegration. The study showed that the RUSLE-3D model with GIS fills as a vigorous and essential device in distinguishing spatial conveyance of soil disintegration hazard region in the watershed for soil protection arranging. Data on normal soil disintegration pace of different land use/land spread sorts assists with embracing appropriate preservation measures for shielding soils from additional disintegration. A method is an efficient tool for its application in limited resources. Therefore, this can be effectively applied in the policy implications. Due to quickened land debasement, there must be the practice of economical soil preservation methodologies in the zone where the vegetation front of the land ought to be improved to reduce the expulsion of soil natural issue. The capacity of soil for holding the water and supplement accessibility of the dirt ought to be expanded by adding organic and agronomic preservation plans to increment agrarian profitability and to the loss of limited biodiversity in the territory. The farmers sought to be remembered for all such plans as dynamic members.

References

Brady CN, Weil RR (2019) The nature and properties of soils, 14th edn. Prentice Hall, Upper Saddle River, NJ, USA, 2008; Geosciences, 9(147):17–19

BCEOM (1998), Abbay River Basin Integrated Development Master Plan Project. Report to Ministry of Water Resources, The Federal Democratic Republic of Ethiopia

Ciesiolka CA, Coughlan KJ, Rose CW, Escalante MC, Hashim GM, Paningbatan EP, Sombatpanit S (1995) Methodology for a multicountry study of soil erosion manage. Soil Technol 8:179–192

Dabral PP, Baithuri N, Pandey A (2008) Soil erosion assessment in a hilly catchment of North Eastern India using USLE, GIS and remote sensing. Water Resour Manage 22(12):1783–1798

De Roo APJ, Hazelhoff L, Burrough PA (1989) Soil erosion modelling using "ANSWERS" and Geographical Information Systems. Earth Surf Processes and Landforms 14:517–532

Esa E, Assen M, Bahir AL (2018) Implications of land use/cover dynamics on soil erosion potential of agricultural watershed, northwestern highlands of Ethiopia. Environ Syst Res

Jain SK, Kumar S, Varghese J (2001) Estimation of soil erosion for a Himalayan watershed using GIS technique. Water Resour Manage 15(1):41–54

Kim HS (2006) Soil erosion modeling using RUSLE and GIS on the IMHA watershed, South Korea. Doctoral dissertation, Colorado State University, USA

Kim JB, Saunders P, Finn JT (2005) Rapid assessment of soil erosion in the Rio Lempa Basin, Central America, using the universal soil loss equation and geographic information systems. Environ Manage 36(6):872–885

Kim J-H, Kim K-T, Lee J-W (2011) Development of soil erosion analysis systems based on cloud and HyGIS. J Korean Assoc Geogr Inf Stud

Kothyari UC (1996) Erosion and sediment problems in India. In: Proceedings of the exeter symposium on erosion and sediment yield: global and regional perspectives, July 1996, pp 531–540. IAHS Publ No 236

Lee GS, Lee KH (2006) Scaling effect for estimating soil loss in the RUSLE model using remotely sensed geospatial data in Korea. J Hydrol Earth Syst Sci 3:135–157

Lu H, Prosser IP, Moran CJ, Gallant JC, Priestley G, Stevenson JG (2003) Predicting sheetwash and rill erosion over the Australian continent. Aust J Soil Res 41:1037–1062

Milward AA, Mersy JE (1999) Adapting RULSE to model soil erosion potential in a mountainous tropical watershed. CATENA 38:109–129

Mitasova H, Mitas L, Brown WM, Johnston D (1998) Multidimensional Soil Erosion/deposition Modeling and visualization using GIS. Final report for USA CERL. University of Illinois, Urbana-Champaign, IL

Miqueloni DP, Bueno CRP (2011) Multivariate analysis and spatial variability to estimate soil erodibility of an anfisol. Revista Brasileira de Ciência do Solo, 35(6): 2175–2182

Morgan RPC, Morgan DDV, Finney HJ (1984) A predictive model for the assessment of soil erosion risk. J Agric Eng Res 30:245–253

Moore ID, Burch FJ (1986a) Physical basis of the length-slope factor in the Universal Soil Loss Equation. Soil Sci Socie America J, 50:294, 1298

McCool DK, Brown LC, Foster GR, Mutchler CK, Meyer LD (1987) Revised Slope Steepness Factor for the Universal Soil Loss Equation, Transactions of the ASAE. 30(5): 1387–1396. https://doi.org/10.13031/2013.30576.

Morgan RPC, Quenton JN, Rickson RJ (1992) EUROSEM: documentation manual; Silsoe College: Silsoe, UK, Multi-temporal soil erosion risk assessment in N. Chalkidiki using a modified USLE raster model. EARSeLe Proc 8:40–52

Ndayisaba F, Lamek N, Alphonse K, Omifolaji K, Liu T, Zhang C (2016) Deforestation effects on soil erosion in the Lake Kivu Basin, D.R. Congo-Rwanda. Forests

NIAST (2003) Agricultural utilization of organic wastes and its environmental risk assessments. National Institute of Agricultural Science and Technology, RDA, Suwon, 49–103

Pimentel D (2006) Soil erosion: a food and environmental threat. Environ Dev Sustain 8:119–137

van Remortel R, Hamilton M, Hickey R (2001) Estimating the LS factor for RUSLE through iterative slope length processing of digital elevation data. Cartography 30(1):27–35

Renard K, Foster G, Weesies G, McCool D, Yoder D (1997a) Predicting soil erosion by water: a guide to conservation planning with the revised universal soil loss equation (RUSLE). US Government Printing Office, Washington, DC

Renard KG, Foster G, Weesies G, McCool D, Yoder D (1997b) Predicting soil erosion by water: a guide to conservation planning with the revised universal soil loss equation (RUSLE), vol 703. United States Department of Agriculture, Washington, DC, USA

Renschler CS, Mannaerts C, Diekkrüger B (1999) Evaluating spatial and temporal variability in soil erosion risk—rainfall erosivity and soil loss ratios in Andalusia, Spain. CATENA 34:209–225

Saha SK (2003) Water and wind induced soil erosion assessment and monitoring using remote sensing and GIS. In: Satellite remote sensing and GIS applications in agricultural meteorology, pp 315–330

Samaras AG, Koutitas CG (2014) The impact of watershed management on coastal morphology: a case study using an integrated approach and numerical modeling. Geomorphology 211:52–63

Shinde V, Tiwari KN, Singh M (2010) Prioritization of micro watersheds on the basis of soil erosion hazard using remote sensing and geographic information system. Int J Water Resour Environ Eng 2(3):130–136

Srinivasan R, Engel BA (1991) Effect of slope prediction methods on slope and erosion estimates. Applied Engineering in Agriculture, 7:779–783. https://doi.org/10.15377/2409-5710.2016.03.02.1

Tamrakar R (1993) A comparative study of land use change In The Shivapuri integrated watershed development area between 1981–1993. Department of Soil Conservation and Watershed Management, Ministry of Forest and Soil Conservation, Kathmandu, Nepal

Vanacker V, Govers G, Barros S, Poesen J, Deckers J (2003) The effect of short term socio-economic and demographic change on land use dynamics and its corresponding geomorphic response with relation to water erosion in a tropical mountainous catchment. Ecuador Landsci Ecol 18:1–15

Wang G, Gertner G, Singh V, Shinkareva S, Parysow P, Anderson A (2002) Spatial and temporal prediction and uncertainty of soil loss using the revised universal soil loss equation: a case study of the rainfall–runoff erosivity R factor. Ecol Model 153:143–155

Wischmeier WH, Smith DD (1978a) Predicting rainfall erosion losses: a guide to conservation planning. In: Agriculture handbook 282. USDA-ARS, USA

Wischmeier WH, Smith DD (1978b) Predicting rainfall erosion losses—a guide to conservation planning. U.S. Department of Agriculture, Science and Education Administration, Hyattsville, MD, USA, p 62

Xu YQ, Shao XM, Peng J (2009) Assessment of soil erosion using RUSLE and GIS: a case study of the Maotiao River watershed, Guizhou Province, China. Environ Geol 56:1643–1652

Youcef S, Mokhtari E, Merzouk B, Laignel B, Vial C, Madani K (2020) Mapping surface water erosion potential in the Soummam watershed in Northeast Algeria with RUSLE model. J Mt Sci

Zhao G, Mu X, Wen Z, Wang F, Gao P (2013) Soil erosion, conservation, and eco-environment changes in the Loess Plateau of China. Land Degrad Dev 24:499–510

Chapter 8
Socio Economic Livelihood Vulnerability to Mountain Hazards: A Case of Uttarakhand Himalaya, India

Subodh Kumar, Pankaj Kumar, Anju Singh, Ashwani, and Manish Kumar

Abstract Large portions of the Uttarakhand state have hilly terrain, which made it more susceptible toward hazards of both kinds e.g., natural and man-made. Due to its unique topography, state is endowed with huge amount of natural resources and biodiversity. In last couple of decades anthropogenic activities in the region increased exponentially which has exposed the communities living in the region to hazards making them more sensitive. Based on the district-wise secondary data of demographic structure, availability of health facilities and various socio economic indicators, 'Exposer' of the communities toward hazards, their level of 'Sensitivity' and 'Adaptive capacity' which is their capability to cope with these challenges, are calculated. At least seven out of 13 districts have low exposer and low sensitivity while all the districts except Udham Singh Nagar have shown moderate adaptive capacity. Dehradun is most sensitive while Udham Singh Nagar is the only district, which has low adaptive capacity.

Keywords Livelihood vulnerability · Mountain hazards · Uttarakhand Himalaya

S. Kumar
Indian Administrative Service (IAS), Ministry of Chemicals and Fertilizers, Government of India, Shastri Bhawan, Delhi 110001, New Delhi, India

P. Kumar (✉) · Ashwani
Department of Geography, Delhi School of Economics, University of Delhi, Delhi 110007, India

A. Singh
Department of Geography, Aditi Mahavidyalaya, University of Delhi, Delhi 110039, India

M. Kumar
Department of Geography, School of Basic Science, Central University of Haryana, Mahendragarh, Haryana, India
e-mail: manish.ks@cuh.ac.in

R. B. Singh et al. (eds.), *Remote Sensing and Geographic Information Systems for Policy Decision Support*, Advances in Geographical and Environmental Sciences,
https://doi.org/10.1007/978-981-16-7731-1_8

8.1 Introduction

Before the appearance of Homosapiens on Earth, the purely natural system ruled our planet. Millions of years later, the human presence transformed the geophysical events such as earthquakes, volcanic eruptions, landsliding, and/or flooding into natural disasters. Human beings have been facing 'natural hazards' since the dawn of civilization. The last few decades have demonstrated an increased concern for the occurrence of natural disasters and their consequences for leaders and organizations around the world. Multifarious hazards and disasters bring about immense loss to human lives and their livelihood specially in mountain regions. These hazards could either be natural or anthropogenic. They have the characteristic of posing danger to the different social entities of our planet, nevertheless, this danger is not only the result of the process per se (natural vulnerability), it is the result of the socio economic systems and their associated vulnerabilities toward livelihood (socio economic vulnerability). There has been a continuous increase in the frequency and vulnerability of the Himalayan mountain people to hazards, disasters and heightened risks. This constant fear has further kept dweller's socio economic status and the future of their livelihood bleak. Recently, attention has been paid to the prevention, reduction and mitigation of natural disasters by creating a Scientific and Technical Committee of the International Decade for Natural Disaster Reduction (IDNDR) focusing on implementation Sendai Framework on Disaster Risk Reduction (SFDRR). The present study focus on indicator based evaluation of exposure, sensitivity and adaptive capacity of each district of Uttarakhand state. However, Socio Economic Livelihood Vulnerability (SELV) has been calculated to see nature and magnitude of vulnerability to help districts in the better management and enhancement of adaptation strategies to cope these disasters.

8.2 Conceptual Background

8.2.1 Natural Hazards

Hazards are any phenomena which pose a threat to nature, people, their life, assets and property. They have the potential of causing a disaster in future, if not monitored or prepared for, in time. A natural hazard is an agent that has the potential to cause a disaster (Cuny 1994). On the basis of origin, they are classified as geological, hydro-meteorological or biological. Some of the natural hazards faced by the mountainous people are landslides, cloud bursts, avalanches, earthquakes, animal or plant infection, disease outbreak, wildfires, mud flow, etc. It is believed that natural hazards turn into disasters when human communities face high risk and vulnerability (Harvard International, 2010). Tobin and Montz (1997, 5) explained that a natural hazard 'represents the potential interaction between humans and extreme natural events'. Because of human activities, the hazard exists, and humans are constantly

exposed to them. The landscape of the Himalaya is a result of a continuing competition between the collision of tectonic plates, which has raised the Himalaya Mountains, and denudation, which causes erosion. Glaciers and rivers deposit eroded sediments. The high rate of these processes of uplift, erosion and sedimentation creates a highly dynamic environment which is associated with earthquakes, landslides, floods, extreme temperature variation, wind and snowstorm, and drought. They impact lives, livelihoods and critical infrastructure.

8.2.2 Risk

Risks are the anticipated losses that the people face in terms of assets, livelihood resources, injuries or even demise, due to a potential peril/hazard, which occurs at a specific space and time. It includes the level up to which households or communities are prepared to overcome the unforeseen catastrophe. Risk is sometimes taken as synonymous with hazard but risk has the additional implication of chance of a particular hazard actually occurring. Thus, hazard can be defined as 'a potential threat to humans and their welfare' and risk as 'the probability of hazard occurrence'. It can be assed using the following formula:

$$\text{Risk} = \frac{\text{Hazard} \times \text{Vulnerability}}{\text{Coping Capacity}}$$

Risk is defined as the probability of harmful consequences borne by humans, socially, economically and environmentally, resulting from interactions between anthropogenic hazards and vulnerable conditions. (UNDP and Bureau of Crisis Prevention and Recovery 2010). Risk is commonly expressed as a function of exposure, the conditions of vulnerability that are present, and the magnitude and frequency of a hazard event. The type and degree of risk varies greatly between individuals of the same age and sex according to personal factors such as location, occupation and life-style. Risk can be classified into two broad categories: (i) Involuntary risks—These are risks which are not willingly undertaken. They are relatively rare but typically have a catastrophic potential impact. Most of the natural hazards fall into this category and represent the risks imposed as a result of living in a particular environment or landscape setting. (ii) Voluntary risks—These are risks which are more willingly accepted by people through their own actions. Unlike involuntary risks, they are rated more directly by individuals according to their own judgments and life-style. Man-made hazards, including risks from technology, are sometimes placed in this group.

Fig. 8.1 Various dimensions of vulnerability

8.2.3 Vulnerability

The characteristics and circumstances of a community, system or asset that make it susceptible to the damaging effects of a hazard. Vulnerability is the susceptibility of both human and natural systems to experience harm as a result of being exposed and being sensitive to a perturbation (such as a climatic hazard) and lacking sufficient responsive, adaptive and coping capacity to deal with the perturbation (IPCC 2012). Vulnerability is the result of the whole range of economic, social, cultural, institutional, political and even psychological factors that shape people's lives and create the environment that they live in (Fig. 8.1). In other words, defining vulnerability also means understanding the underlying factors or root causes of vulnerability (UNISDR 2009). The elements of vulnerability are measured through exposure, sensitivity and resilience of a bounded system at a particular spatial scale. The ability of people to deal with hazards represents indicators of socio economic vulnerability, which varies between different groups of people (Dow 1992) and across states in mountain regions. Some districts of states are better prepared while others lag behind.

8.2.4 Disaster

A disaster refers to a sudden major misfortune that disrupts the fabric of normal functioning of a society. It causes casualties, damage, loss of property, essential services, means of livelihood or infrastructure at a scale which is beyond the normal capacity of the communities to cope, if left unaided (United Nations Organization). Himalayan communities are highly prone to natural disasters and with the change in climate, there has been an upscale in the occurrence and the intensity of such events. Disaster cycle can better assess damage and risk looking into response, preparedness,

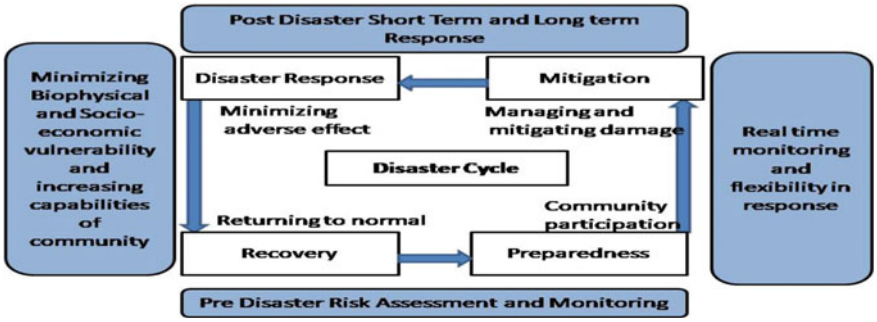

Fig. 8.2 Representation of disaster cycle

recovery and mitigation strategies of a society (Fig. 8.2). Socio economic vulnerability assessment helps in quantifying magnitude of risk a state, district or village is posing during particular disaster.

8.3 Vulnerability Scenario of Himalayan People

The people from the Himalayan region are more vulnerable to climate induced disasters like avalanches, earthquakes, cloud bursts, debris flow, flash floods, landslides, mass movements, etc. Each year, climate induced events have adverse impacts on the livelihood of the Himalayan communities. During monsoon, heavy rains occur in the entire region due to which there are roadblocks everywhere. This creates a barrier in the accessibility of people to obtain essential services or even travel from one end to another. Climate change illustrates the distinction between risk and vulnerability. It is deduced that the impact of natural disasters is felt more severely by the people who are weak socio economically as their habitats are located in vulnerable areas and they are not designed to withstand the impact of natural hazards or disasters (Fig. 8.3). This increases their risk and vulnerability. Thus, in such a condition, it is suggested that poverty and disaster management should be intricately linked. (Sharda et al. 2010).

Different coping potential is observed in the event of hazards by different communities of people. Some of the factors that come into play while adapting to and being resilient enough to hazards and disasters are the population, settlement pattern, topographic location, gender and age. Since, majority of men migrate to plain regions in search of better livelihood opportunities, women and children are left behind at home to cope and deal with disasters individually, which make them more vulnerable. According to the data of ICIMOD, about 30% of the Himalayan people suffer from food insecurity and 50% of them face malnutrition (majorly women and children), which further enhances their vulnerability during and after a catastrophe.

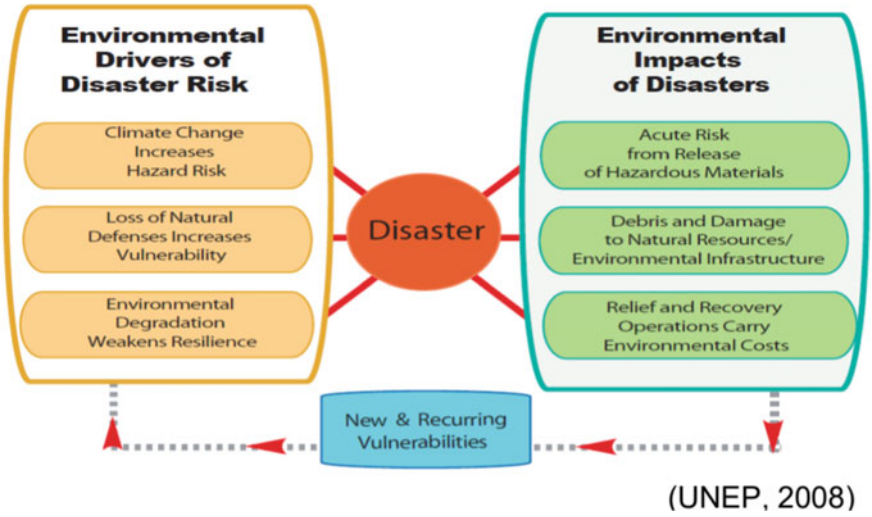

Fig. 8.3 Environmental causes and consequences of disasters (*Source* UNEP 2008)

The people of Himalayas greatly depend on the local produce and natural resources to meet their daily needs. This makes them highly dependent on the nature for sustenance. This direct dependence increases their vulnerability and risk factor to hazards and disasters. Even when it comes to the tourism industry, this problem is being faced. This is so because due to the high amount of pollutants being released by the big industrial countries and cities, the glaciers of the Himalayas are melting and turning black. This exposes their rocky surface due to which there is a decrease in the number of tourists that visit the Himalayas for adventure activities like hiking, trekking, mountain climbing, skiing, etc.

8.4 Study Area

Uttarakhand is a state in the Northern part of India, which shares international border with Tibet in the North and Nepal in the East. To the South and the West are two Indian states, Uttar Pradesh and Himachal Pradesh respectively, as shown in Fig. 8.4. The geographic extent of the state is 31.469° N, 79.062° E in the North, 30.25° N, 81.02° E in the East, 29.56° N, 77.99° E in the South and 31.06° N, 77.806° E in the West, with a total area of 53,483 Km^2 (Fig. 8.4). The diverse topography includes glaciers, large number of perennial rivers, rugged mountainous terrain and dense forests. The elevation of the region varies greatly between 300 and 8000 m. About 68.4% of the state is covered by evergreen forests and 85% by mountains (Bhambri et al. 2016; Shresthta and Zinck 2001). Nanda Devi (7816 m) is highest peak of the

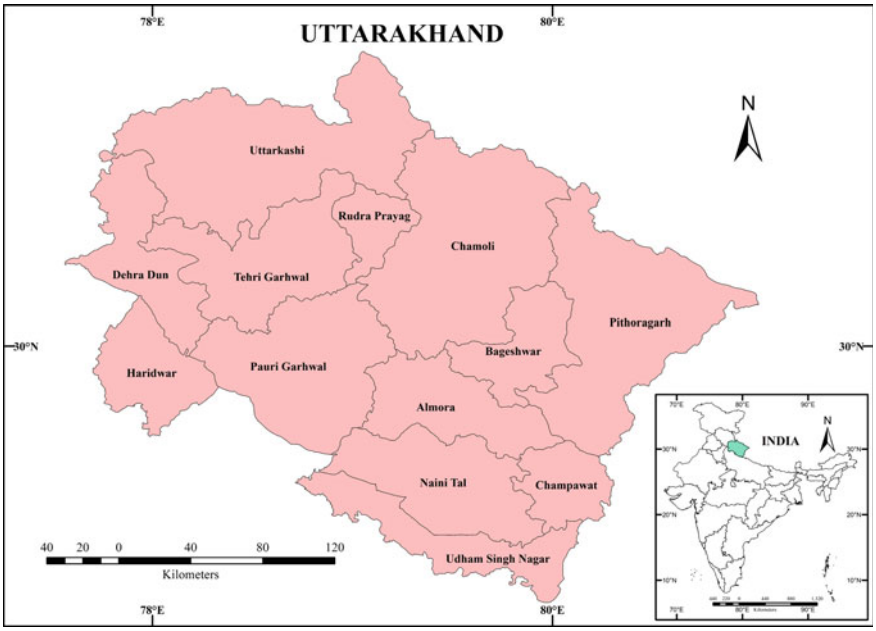

Fig. 8.4 District map of study area

state, Kamet (7756 m), Chaukhamba (7138 m), Trisul (7120 m), Nandakot (6861 m) are some other important peaks.

Most of the northern part of state is always snow covered and glaciated. Mighty rivers of Ganga and Yamuna originated from Gangotri and Yamunotri glaciers respectively. Some other important rivers are Alaknanda, Bhagirathi, Ramganga, Kosi, Saryu, Nayar and Sharda. Various dams and hydropower projects such as Tehri Dam, Srinagar hydropower project, Yamuna hydropower project, Chilla hydropower project etc. have been constructed over these rivers. State has rich biodiversity with various varieties of flora and fauna. More than 3.47 million hectares which comprise approx 71% area of the state is covered with forest. There are total 12 national parks in the state. Jim Corbett (oldest of Indian peninsula), Nanda Devi and Valley of flowers (UNESCO world heritage sites), Rajaji National park, Govind Pashu Viharand Gangotri National park are some important parks. Based on its physiographic characteristics state can be arranged into three regions namely the Himalaya, the Shivalik (Bhabhar) and the Terai.

Administratively it is a relatively small state comprising only 13 districts. For the effective administrative purposes, state has been divided into two administrative regions western part as Garhwal region (6 districts) and eastern part as Kumaon region (7 districts). Hills of the Garhwal side have steep slopes than Kumaon side. Dehradun is its winter capital and recently state announced that Gairsain town of the Chamoli district would be its new summer capital. Population of the state has been grown to 1.01 crore in 2011 with a decadal growth rate of 1.8%. Population

density of the state is 189 persons/km^2. Sex ratio is more than the national average at 963 females per thousand male and average literacy rates is 78.82%. Hindus (82.97%) and Muslims (13.95%) are major religious group. 30.23% out of total population resides in urban areas. Transhumance is commonly practiced by Bhotias in the state. Economy of the state is dependent mainly on agriculture and tourism sector. Due to difficult terrain farming is practiced through terrace cultivation. There are two types of tourism in the state e.g., religious tourism and commercial tourism. Haridwar, Rishikesh, Badrinath, Kedarnath, Nandadevi, Gangotri and Yamunotriare known mainly for religious tourism while Nainital, Mussorrie, Almora, Ranilkhet and Haldwani are quite famous for commercial tourism.

8.5 Fragility of Uttarakhand and Livelihood Vulnerability

Uttarakhand occupies a significant part of fragile Himalayan ecosystem. Its geomorphological, meteorological and geo-tectonic structure makes the state vulnerable to numerous natural disasters such as earthquakes, landslides, flash floods, glacial lake outburst floods, forest fires, avalanches etc. Over the past thirty years, the frequency and intensity of such disasters has increased alarmingly (ICIMOD 2009). Moreover, changing climate has further endangered its fragile ecosystem. Above average rise in temperature, irregular rainfall, shrinking glaciers and ascending snow line in Himalayas have made the state most vulnerable to risks associated with climate change which have further intensified disasters like cloud burst, landslide a number of other disasters (UAPCC 2014). The state is in fact among the five most disaster-prone states in India (USDMA 2007). Uttarakhand is susceptible to multiple disasters like Glacial Lake Outburst Floods (GLOFs), landslide, cloud burst, forest fires out of which earthquake is the most prominent and devastating as the state lies in the highest seismic zone of India i.e., zone iv and v. The state has seen many major seismic events in the last few decades, particularly in 1991 (Fig. 8.5) and 1999 of magnitude 6.6 and 6.8 respectively which caused huge devastation.

Glacial Lake Outburst Floods (GLOFs) and Landslide Lake Outburst Floods (LLOFs) hazards are prominent in higher reaches of Uttarakhand Himalaya. During field visit the presence of several paraglacial lakes between Bhujbas and Gaumukh suggests that in the past flash floods in Bhagirathi Valley might have taken place due to the filling of smaller lakes (Fig. 8.6). Most of the glacial lakes in the Uttarakhand Himalaya, including in the Bhagirathi Valley, are moraine dammed in origin, and ice-dammed lakes are very rare (Naithani et al. 2001). Frequency and magnitude of these natural hazards has shown increasing trend in last few decades due to fast melting of glaciers and availability of open space at snow out positions of glaciers to moraine dammed lakes.

Landslide is another major disaster caused mainly due to heavy rainfall, seismic tremors or human intervention such as mining and construction. The state sees the occurrence of landslide events each year mainly near tectonic boundaries of MBT and MCT (Figs. 8.7 and 8.8). Avalanches are common in snow covered regions of the

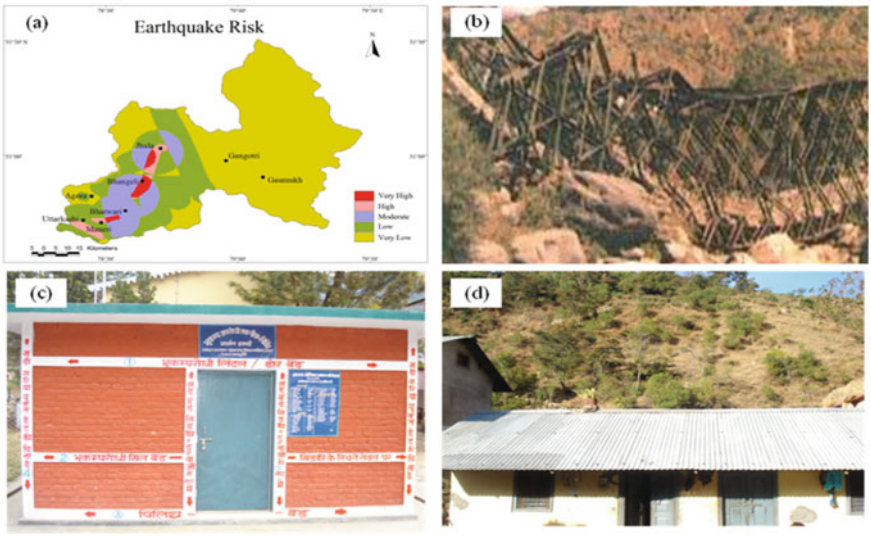

Fig. 8.5 **a** Earthquake risk vulnerability map of Uttarkashi district, **b** collapsed Bridge near Gawana after 1991 Earthquake **c** model structure of earthquake resistance house for Uttarakhand state **d** less earthquake vulnerable house in Maneri Village

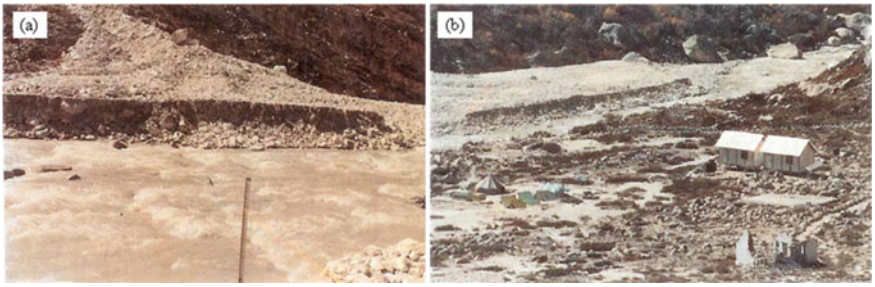

Fig. 8.6 **a** Sediments brought by Left-bank Nala formed Moraine-dammed Lake outburst on the Bhagirathi River near Bhujbas on June 6, 2000 **b** Department of Science and Technology (DST) hut and other structures at Bhujbas washed away after June 6, 2000 flashflood (Singh et al. 2002)

states particularly near Kedarnath, Badrinath, Yamnotri and Gangotri. Cloud burst is a very heavy rainfall which does not last long but causes very heavy downpour which results in flash floods. In 2013, the state saw the most disastrous form of cloud burst leading to flash floods in India which led to immense damage of life, livelihood and infrastructure. Forest fires are most common in the state and destroy large patches of dense forests every year particularly Chir-Pine forest (NIDM 2013).

All these disastrous events have adversely affected the life and property in the state. Uttarakhand flood in 2013 alone affected the lives of more than ninety lakh people from all over the country. Nearly 6000 people were recorded dead and a lot

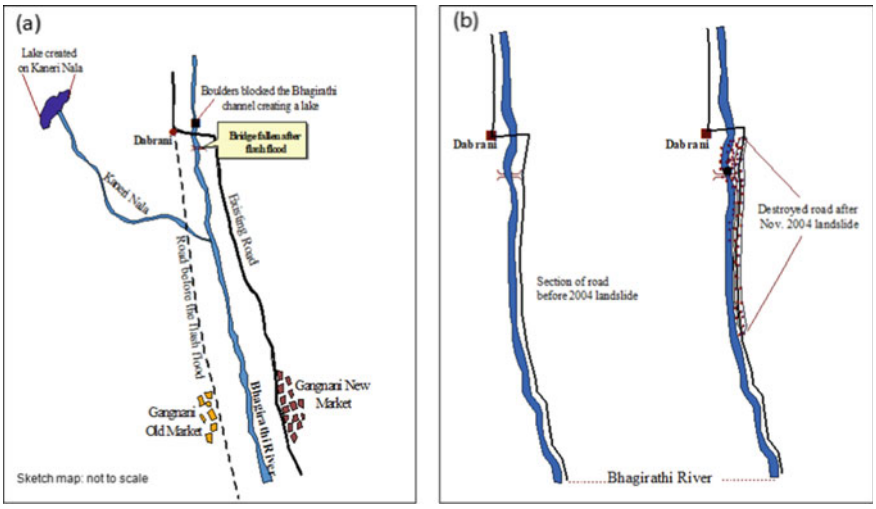

Fig. 8.7 **a** Bridge on river near Dabrani and **b** portion of road between Dabrani and Gangnani completely destroyed after 2004 landslide

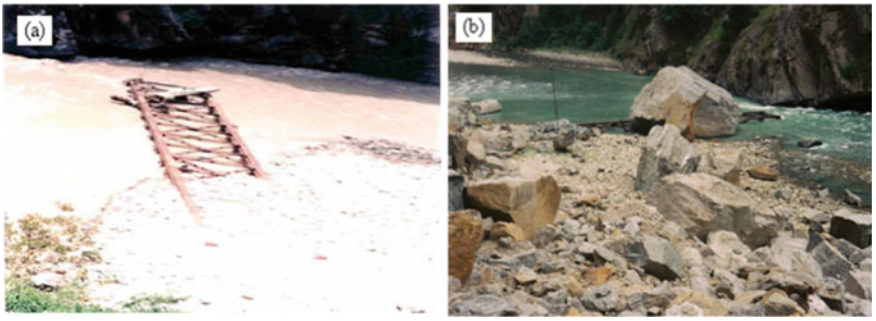

Fig. 8.8 **a** A bridge fallen in the Bhagirathi River near Dabrani after June, 1978 'D.M. Landslide and Flashflood' **b** another bridge covered by rocks after November, 2004 Landslide

more were missing or injured. A huge infrastructural damage was recorded, where around 2052 houses were totally destroyed, 1307 roads were fully damaged and as many as 147 bridges collapsed (Down to Earth, 2016). In addition to it, there was the huge loss of livelihood of local people dependent on tourism, agriculture and allied activities. Apart from human and infrastructural loss, disasters like Forest fires resulted in a huge loss of crucial forest resources. In 2016, forest fire burnt a total of 2166 km^2 area of the state out of which 87% was dense forest. Overall, about 7.35% of the total area of forest turned into ashes as a result of it (Jha et al. 2016).

Uttarakhand is primarily an agrarian state with more than 75% of population involved in agriculture which already explains its poor social and economic condition. Moreover, frequent events of disasters do not allow the people to cope with

the damage caused by it and pushe them further toward more vulnerable conditions. Poor building structure of the house, lack of adequate infrastructure, awareness and preparedness against the disasters causes more damage to lives and infrastructure in the state (DMMC Report 2012). According to vulnerability atlas of India, about 56% of the houses in the state are kutcha houses which point toward high vulnerability, considering the frequency and intensity of disasters in the state. Low levels of literacy, no alternative livelihood options, high migration, high dependency, poverty, low economic development together magnify the vulnerability of people. Overall, these disasters along with their adverse impacts on livelihood increase the socio and economic vulnerability of the people. Therefore, the study of socio economic vulnerability of districts of Uttarakhand state is very important in order to fully understand the impact of disaster on Socio Economic Livelihood Vulnerability (SELV).

8.6 Methodology

8.6.1 Data Source

The present study is primarily based on secondary data collected from reports of central and state government. Demographic indicators data of district of Uttarakhand has been collected from Census of India (https://censusindia.gov.in/2011census/population_enumeration.html), Directorate of Economics and Statistics, Planning Department, Government of Uttarakhand (http://usdma.uk.gov.in/). Sub indicators to access exposure, sensitivity and adaptive capacity of district (Table 8.1) has been compiled from reports such as Uttarakhand Economic Survey 2019–2020, Uttarakhand Human Development Report 2018, Statistical Abstract Uttarakhand 2015 2016, Population Analysis Uttarakhand 2011 and Uttarakhand Disaster Recovery Project report Disaster Risk Assessment of Uttarakhand, Uttarakhand Disaster Management Authority (http://usdma.uk.gov.in/PDFFiles/Atlas_Vol3A_20190131.pdf).

8.6.2 Methods

A different numbers of factors combined to measure the Socio economic livelihood vulnerability to climate change and its variability. Such factors would be internal or external for vulnerability. Several methods and calculations have been developed for evaluating the vulnerability to form an index. The analysis of vulnerability is discussed in the view of risk-hazard (Ribot 2009). We calculated the Socio Economic Livelihood Vulnerability Index (SELVI) by using major factors like demography, health, social indicators and economic indicators under three components (Adaptive Capacity, Exposure and Sensitivity) of LVI. And various sub-components are come under the major components (Table 8.1) to calculate the vulnerability. Table 8.1

Table 8.1 Demographic, social, health and economic indicators of districts of Uttarakhand state

	Demographic			Social					
District	Population density	Population below age 14 (%)	Population above age 60 (%)	Forest cover (%)	Migrants migrated in last 10 years	Literacy level	Share of rural population (%)	No of Bank branch per average population	Bank loan distribution in lakh
Uttarkashi	41	33.1	8.7	88.8	19,893	75.8	92.73	5157	53.7
Chamoli	49	30.7	9.9	59.4	32,020	82.7	84.69	4166	191.5
Rudraprayag	112	31.4	11.2	76.8	22,735	81.3	95.87	4405	120.1
Tehri Garhwal	170	32.4	10.7	66.2	71,509	76.4	88.69	4584	125.9
Dehradun	549	27.3	9.1	55.5	25,781	84.3	44.49	2966	401.3
Pauri Garhwal	129	29.3	12.7	57.6	47,488	82	86.21	3471	650.2
Pithoragarh	68	30.1	10.9	72.3	31,786	82.3	85.71	4560	102.8
Bageshwar	116	31	11.7	53	23,388	80	96.54	5096	51
Almora	198	30.3	12.4	50.8	53,611	80.5	89.89	4234	79.4
Champawat	147	33.4	9.1	56.7	20,332	79.8	85	4476	25.4
Nainital	225	29.6	8.3	73.1	20,951	83.9	61.05	3773	212.7
Udham Singh Nagar	649	32.7	7	33.3	6064	73.1	64.4	4936	248.3
Hardwar	801	33.6	7.3	31.1	8168	73.4	63.33	6656	105.4

(continued)

Table 8.1 (continued)

	Health			Economic				
District	No of home stay in district	Total number of Hospital	Households with an improved drinking-water source (%)	Households using improved sanitation facility (%)	District-wise estimates of poverty (%)	District-wise percentage share of marginal workers, 2011	District-wise work participation rates (%), 2011	Rural households by monthly income of highest earning member (Rs.) less than 5000
Uttarkashi	210	4	75.1	48.5	20.44	18.4	47.6	80.1
Chamoli	299	7	93.2	62.4	20.37	36.4	46.2	60.07
Rudraprayag	101	3	86.5	67.6	20.71	30.2	46.7	53.74
Tehri Garhwal	133	11	77.4	65.8	10.15	31.5	45.3	70.94
Dehradun	377	38	99.5	75.6	10.09	16.2	34.3	48.95
Pauri Garhwal	60	12	88.1	66.2	29.36	40	39.9	59.17
Pithoragarh	218	6	83.9	62.7	15.85	32.8	44.8	62.83
Bageshwar	56	3	83	67.4	24.01	36.8	47.6	66.37
Almora	126	8	83.9	65	13.62	32.6	47.9	73.3
Champawat	15	3	89.5	59.5	26.55	37	38.3	73.12
Nainital	226	20	95.9	73	8.75	21.2	39.4	61.78
Udham Singh Nagar	6	24	97.6	56.2	12.6	23.8	35.9	65.02
Hardwar	15	14	99.1	56.9	22.63	14.4	30.6	62.56

Source Table complied from Uttarakhand government reports accessed from websites https://censusindia.gov.in and http://usdma.uk.gov.in

comprises the explanation of each sub-component with a quantitative value. Each component is made up with several major components and sub-components, each of indicators are calculated on different scales, and they calculated by Eq. (8.1).

$$Risk = \frac{Hazard \times Vulnerability}{Coping\,Capacity}$$

$$\text{Index } sd = \frac{Sd - S\text{min}}{S\text{max} - S\text{min}} \tag{8.1}$$

where, Sd is the original sub-component for district d, and S_{min} and S_{max} are the minimum and maximum values particular district.

After each sub-component was standardized, then sub-components were averaged using Eq. (8.2) to calculate the value of each major component:

$$Md = \sum_{i=1}^{n} indexsdi \frac{1}{n} \tag{8.2}$$

where, Md = one of the five major components for district d.

And lastly, the three IPCC components were calculated based on Eq. (8.3).

$$LVId = \frac{\sum_{i=1}^{n} Wmi\,Mdi}{\sum_{i=1}^{n} Wmi} \tag{8.3}$$

where, *LVId* is an IPCC defined contributing factor (Adaptive capacity, Exposure and Sensitivity) for district d; *Mdi* are the major components for district d; *Wmi* are the weight of each major components and n is the number of major components in each contributing factor.

In this study, the SELVI is scaled from 0 (least vulnerable) to 1 (most vulnerable).

8.7 Results and Discussion

8.7.1 Sensitivity

Sensitivity tells us about the degree of risk for the communities living in a specific region due to its exposer to the various extreme events, both natural and anthropogenic in nature. High sensitivity increases the risk of vulnerability of the communities residing in that particular region. The major components to calculate sensitivity are 'demographic profile and health'. Sub-component of demographic profile includes total number of people below 14 years and above 60 years, population density and health includes availability of clean drinking water, sanitation facilities, basic health

facilities and total no. of hospitals available in the district. Calculation shows that Dehradun is the most sensitive (0.802) and Uttarkashi is least sensitive (0.299) district of the state. After Dehradun, Udham Singh Nagar (0.53), Haridwar (0.519) and Nainital (0.465) districts are also having quite high sensitivity rate respectively. These districts are among top four districts of the state with highest population and density due to which their overall sanitation facility and per capita health resources are also very low. Children below 14 years and elderly people above 60 years of age are most sensitive among all. Haridwar is most densely populated (801 persons/km^2) district of the state. Highest sensitivity rate of Dehradun is also because it is second most populous district of the state with population density of 549 persons per km^2 only after Haridwar district, besides that Dehradun city is also summer capital of the state, developed and quite populous. While Uttarkashi has an average of only 41 persons residing in a km^2 area. Other districts like Chamoli, Rudraprayag, TehrigarhwalPaurigarhwal, Pithoragarh, Bageshwar, Almora and Champawathas comparatively low sensitivity (0–0.4) while Nainital, Udham Singh Nagar and Haridwar has moderate sensitivity (Fig. 8.9).

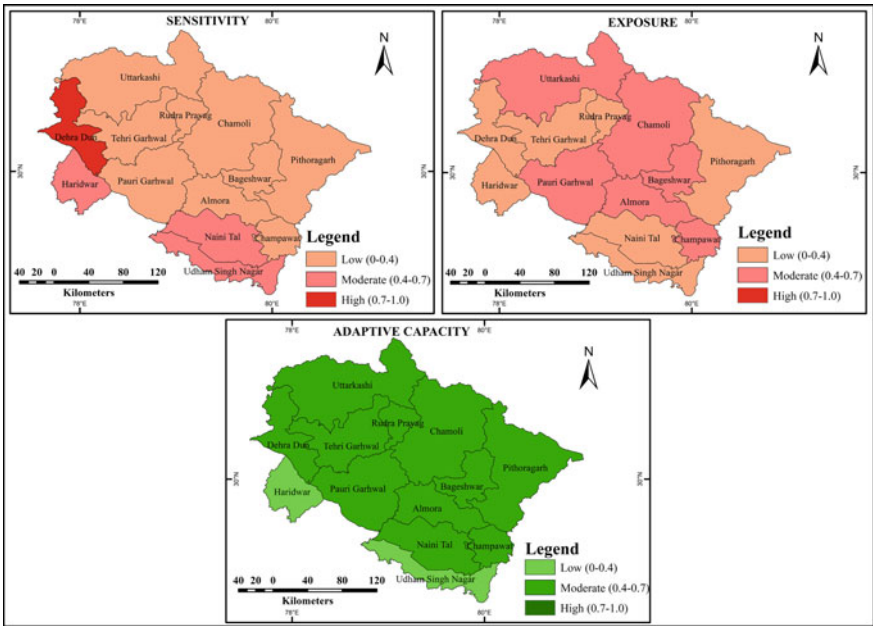

Fig. 8.9 Map of magnitude of sensitivity, exposure and adaptive capacity of districts

8.7.2 Exposure

Exposure to extreme financial and socio-political conditions could increase the risk of vulnerability for the communities residing in the region. Level of exposer can be calculated by analyzing the financial condition of the community. Here, poverty rate, share of marginal workers and their participation rate is taken into account to calculate the exposer of the district. Census of India had classified the workers into two main categories. First, main workers who got work for more than six months in a year and second, marginal workers who got work for less than six months during a year. These marginal workers do not have any job security, paid very little and often have to migrate from one place to another place in search of jobs. Majority of them are living below poverty line, this exposed them to face situations like malnutrition and starvation. Due to weaker financial condition of the family many of students are unable to complete their studies, left it midway to take up some kind of job to help their family. Very often due to lack of proper skills they became marginal worker and this vicious cycle goes on. The condition of financial uncertainty makes the communities more vulnerable. Districts like Rudraprayag (RP), Tehri Garhwal (T Garh), Dehradun (DD), Pithoragarh (PG), Nainital (NTal), Udham Singh Nagar (USN), Haridwar (HDWR) have low exposer (0–0.4) and Uttarkashi (UK), Chamoli, Paurigarhwal (P Garh), Bageshwar (Bagesh), Almora, Champawat (Champ) have moderate exposure (Table 8.2) (Fig. 8.9).

8.7.3 Adaptive Capacity

Adaptive capacity refers to the capability of any community to readjust themselves in the changed conditions smoothly. In order to reduce the risk of vulnerability, our adaptive capacity should be high. Smooth adaptability of the new and changed conditions for any community depends upon the factors such as social bonding between individuals, households and communities, their knowledge system and financial condition, common resources and their optimal use. Here, percentage of forest cover, literacy rate, share of rural population in total population, percentage migration and average no. of homestay in every district, average no. of bank branches, and total loans given, these seven sub-components have been taken as the basis to calculate the degree of adaptability of the communities living in this hilly states. Uttarkashi has the highest (0.552) while Udham Singh Nagar has the lowest (0.381) adaptive capacity among all the 13 districts of Uttarakhand. During analysis, we found that in Udham Singh Nagar forest-cover has been reduced to 33%. Literacy rate is 73.1% and no. of home stay in the district is only 6, both are lowest among all the 13 district. Compare to this 88.8% area of Uttarkashi district is covered by forest, 210 home stays, and literacy rate is 75.8%. Out of total, 69.77% population of Uttarakhand state lives in rural areas which means there is less infrastructural development. Which led to the migration of workers and skilled people. Forest cover provides various resources

Table 8.2 Value of major components and sub components

S.no	Major/Sub component	Unit	Max	Values												Min
				UK	Chamoli	RP	T Garh	DD	P Garh	PG	Bagesh	Almora	Champ	NTal	U S N	HDWR	
1	*Demography*																
1.1	Density of population	Km^2	1000	0.041	0.049	0.122	0.170	0.549	0.129	0.068	0.166	0.198	0.147	0.225	0.649	0.801	0
1.2	Population below age 14	Percent	100	0.331	0.307	0.314	0.324	0.273	0.293	0.301	0.310	0.303	0.334	0.296	0.327	0.336	0
1.3	Population above age 60	Percent	100	0.087	0.099	0.112	0.107	0.091	0.127	0.109	0.117	0.124	0.091	0.083	0.070	0.073	0
2	*Social*																
2.1	Forest cover	Percent	100	0.888	0.594	0.768	0.662	0.555	0.576	0.723	0.530	0.508	0.567	0.731	0.333	0.311	0
2.2	Literacy level	Percent	100	0.758	0.827	0.813	0.764	0.843	0.820	0.823	0.800	0.805	0.798	0.839	0.731	0.734	0
2.3	Share of rural population	Percent	100	0.927	0.846	0.958	0.886	0.444	0.862	0.857	0.965	0.898	0.850	0.610	0.644	0.633	0
2.4	Migrants migrated in last 10 years	Percent	100	0.060	0.082	0.094	0.115	0.015	0.069	0.066	0.089	0.086	0.078	0.022	0.004	0.008	0
2.5	No of home stay in district	Count	400	0.525	0.747	0.252	0.332	0.942	0.150	0.545	0.140	0.315	0.037	0.565	0.015	0.037	0
2.6	No of bank branch per average population	Count	7000	0.631	0.433	0.481	0.516	0.193	0.294	0.512	0.619	0.447	0.495	0.354	0.587	0.931	0
2.7	Bank loan distribution	Count	700	0.076	0.273	0.171	0.179	0.573	0.928	0.146	0.072	0.113	0.036	0.303	0.354	0.150	0

(continued)

Table 8.2 (continued)

S.no	Major/Sub component	Unit	Max	Values													Min
				UK	Chamoli	RP	T Garh	DD	P Garh	PG	Bagesh	Almora	Champ	NTal	U S N	HDWR	
3	*Health*																
3.1	Total number of hospital	Count	40	0.100	0.175	0.075	0.275	0.950	0.300	0.150	0.075	0.200	0.075	0.500	0.600	0.350	0
3.2	Households with an improved drinking-water source	Percent	100	0.751	0.932	0.865	0.774	0.995	0.881	0.839	0.830	0.839	0.895	0.959	0.976	0.991	0
3.3	Households using improved sanitation facility	Percent	100	0.485	0.624	0.676	0.658	0.756	0.662	0.627	0.674	0.650	0.595	0.730	0.562	0.569	0
4	*Economic*																
4.1	District-wise poverty	Percent	100	0.204	0.203	0.207	0.101	0.100	0.294	0.158	0.240	0.136	0.265	0.087	0.126	0.226	0
4.2	District-wise percentage share of marginal workers	Percent	100	0.184	0.364	0.302	0.315	0.162	0.400	0.328	0.368	0.326	0.370	0.212	0.238	0.144	0
4.3	District-wise work participation rates	Percent	100	0.476	0.462	0.467	0.453	0.343	0.399	0.448	0.476	0.479	0.383	0.394	0.359	0.306	0

(continued)

Table 8.2 (continued)

S.no	Major/Sub component	Unit	Max	Values													Min
				UK	Chamoli	RP	T Garh	DD	P Garh	PG	Bagesh	Almora	Champ	NTal	U S N	HDWR	
4.4	Rural households by monthly income of highest earning member (Rs.) less than 5000	Percent	100	0.801	0.600	0.537	0.709	0.489	0.592	0.628	0.664	0.733	0.731	0.618	0.650	0.626	0

to the communities which enhance their adaptability. Increased Banking penetration ensures financial stability and security of money and formalization of loans as people do not have to depend on money lenders. Due to its serenic beauty, Uttarakhand is the tourism hub of the north India. Many tourists live in homestays in distant rural parts of the districts and increased banking facilities in those areas also helping the tourism industry which is a major source of income in the state. Districts of Uttarkashi, Chamoli, Rudraprayag, TehriGarhwal, Dehradun, PauriGarhwal, Pithoragarh, Bageshwar, Almora, Champawat, Nainital, Haridwar have moderate adaptive capacity (0.4–0.7) while Udham Singh Nagar has low adaptive capacity e.g., 0.381 (Table 8.1) (Fig. 8.9).

8.7.4 Livelihood Vulnerability

In this method scale of livelihood vulnerability index is from 0 (Least vulnerable) to 0.5 (most vulnerable). Values ranging between '0.4 and 0.5' denote very high vulnerability and 12 out of 13 districts of Uttarakhand state lie in this range e.g., they are highly vulnerable (Table 8.3). Dehradun is the most vulnerable (0.486) while Champawat is the least vulnerable (0.396). Lower degree of sensitivity, exposer and comparatively higher degree of adaptability for the changed conditions will make the community less vulnerable (Fig. 8.9).

8.8 Conclusion

One of the main reasons behind the creation of a new state e.g. Uttarakhand on was its tough terrain and hilly topography, which needs an exclusive and special set of policies based on local requirement to develop this region. As roads were built and connectivity improved, people started making settlements in distant mountains on very high altitudes. Various projects were launched to tap huge potential for hydroelectricity, horticulture, herbal medicines and timber industries in the state. In this process many a time, the impact of these projects on the environment and biodiversity of the region is ignored. Irrational overexploitation of natural resources has led to the unbalanced development. Flourishing tourism industry in the state has put enormous pressure on resources of the state. This sudden increase in anthropogenic activities also contributed to the increased list of hazards in the state. The devastating cloudburst and flood of 2013 was a recent example. Uttarakhand came under seismic zone 4 and 5 which are highest risk zones. Apart from earthquakes, landslides, flashfloods, avalanches and droughts are other major hazards. In this situation, it is extremely important to analyze the factors which expose communities to these hazards and determine the degree of sensitivity of the region. These factors include economic condition of the community such as per capita income, type of job, job security, financial inclusion, availability of formal credit, penetration of banking

Table 8.3 Value of major components in the districts

Major comp./values	Low (0–0.4)	Moderate (0.4–0.7)	High (0.7–1)
Sensitivity	Uttarkashi Chamoli Rudraprayag, Tehrigarhwal Paurigarhwal Pithoragarh Bageshwar Almora Champawat	Nainital Udham Singh Nagar Haridwar	Dehradun
Exposer	Rudraprayag Tehri Garhwal Dehradun Pithoragarh Nainital Udham Singh Nagar Haridwar	Uttarkashi Chamoli Paurigarhwal Bageshwar Almora Champawat	
Adaptive capacity	Udham Singh Nagar	Uttarkashi Chamoli Rudraprayag Tehri Garhwal Dehradun Pauri Garhwal Pithoragarh Bageshwar Almora Champawat Nainital Haridwar	

facilities in distant region, demographic factors such as people of below 14 years and above 60 years of age in the total population, sex ratio, population growth, health related issues such as number of hospitals in every district, primary health centers, basic sanitation facilities, number of people suffering from chronic diseases etc. How a community will respond to the hazards or any such calamity, depend upon the degree of adaptive capacity of the community and the region. It includes factors such as literacy rate of the community especially female literacy rate, societal bond, poverty rate, availability of clean drinking water etc. Measurement and assessment of these factors will tell us about degree of vulnerability of any community residing in a particular region. This measurement tells us about specific factors upon which policymakers should be focusing more and help us to make informed policy decisions.

References

Bhambri R, Mehta M, Dobhal DP, Gupta AK, Pratap B, Kesarwani K, Verma A (2016) Devastation in the Kedarnath (Mandakini) Valley, Garhwal Himalaya, during 16–17 June 2013: a remote sensing and ground-based assessment. Nat Hazards 80(3):1801–1822

Cuny FC (1994) *Disasters and development*. Intertect Press

DDMC Report (2012) Investigations in the Asi Ganga valley on the aftermath of flash flood /landslide incidences in August, 2012. Disaster Mitigation and Management Centre Department of Disaster Management Uttarakhand Secretariat, Dehradun, India

Dow K (1992) Exploring differences in our common future (s): the meaning of vulnerability to global environmental change. Geoforum 23(3):417–436

Human Development Report (2008) Fighting climate change: human solidarity in a divided world

India Disaster Report (2013) National Institute of Disaster Management (NIDM), Ministry of Home Affairs, Government of India

Interagency Panel on Climate Change (IPCC) (2012) Summary for policy makers. In: Managing extreme events and disasters to advance climate change adaptation. A special report of working groups I and II of the intergovernmental panel on climate change. Cambridge University Press, Cambridge, UK and New York, USA, pp 1–19

Jha CS, Gopalakrishnan R, Thumaty KC, Singhal J, Reddy CS, Singh J, Pasha SV, Middinti S, Praveen M, Murugavel AR, Reddy SY, Vedantam MK, Yadav A, Rao GS, Parsi GD, Dadhwal VK (2016) Monitoring of forest fires from space–ISRO's initiative for near real-time monitoring of the recent forest fires in Uttarakhand, India. Current Sci 110(11):2057–2060

Naithani AK, Nainwal HC, Sati KK, Prasad C (2001) Geomorphological evidences of retreat of the Gangotri Glacier and its characteristics. Curr Sci 80(1):87–94

Ribot JC (2009) Vulnerability does not just fall from the sky: toward multi-scale pro-poor climate policy. In: Mearns R, Norton A (eds) The social dimensions of climate change: equity and vulnerability in a warming world. World Bank, Washington, DC

Sharda et al. (2010) Landslide studies in India, Glimpses of geo-science research in India, pp 98–101

Shrestha DP, Zinck JA (2001) Land use classification in mountainous areas: integration of image processing, digital elevation data and field knowledge (application to Nepal). Int J Appl Earth Obs Geoinf 3(1):78–85

Singh DS, Misra A (2002) Role of tributary glaciers on landscape modification in the Gangotri glacier area, Garhwal Himalaya, India. Current Sci 82(5):567–571

Tobin GA, Montz BE (1997) Natural hazards: explanation and integration. Guilford Press, New York

UAPCC (2014) Uttarakhand action plan for climate change. Government of Uttarakhand, India. https://forest.uk.gov.in/uploads/climate_change_information/1616764235.pdf

UN International Strategy for Disaster Reduction (UNISDR) (2009) Global assessment report on DRR. Risk and poverty in a changing climate. United Nations, Geneva, Switzerland

USDMA (2007) http://usdma.uk.gov.in/PDFFiles/Atlas_Vol3A_20190131.pdf

Chapter 9
Land Surface Temperature Retrieval of Landsat-8 Data Using Split-Window Algorithm Over Delhi City, India

Pawan Kumar Thakur, Manish Kumar, R. B. Singh, Vaibhav E. Gosavi, Bhim Chand, and Sarika Sharma

Abstract The Land Surface Temperature (LST) is important parameter measured by satellite thermal remote sensing technology and is also a key to study the energy and water exchange from local to global level; also helps in studies related to hydrological cycle, global warming, Land Use Land Cover (LULC) change and associated temperature changes, soil moisture, vegetation water stress etc. The estimation of Land Surface Temperature using Landsat-8 OLI (Operational Land Imager), through Split-Window (SW) algorithm was carried out in Delhi city of India. The Supervised classification method using Support Vector Machine (SVM) has been used and selected different types of signatures with the help of Region of Interest (ROI) in EVNI 5.3 for detection of LULC categories. The spatial distribution of LST of Landsat-8 (OLI), dated 09th February 2014 ranged from minimum of 13.72 to 25.00 °C as a maximum was observed. The estimation of LST versus LULC categories further reveals the higher vegetative cover brings down the surface temperature. It is observed that agricultural/crop area, dense and sparse vegetation are conducive in lowering the LST, whereas, built-up surfaces, bare land/soil and industrial area exhibits higher

P. K. Thakur (✉)
Forest Ecology & Climate Change Division, Himalayan Forest Research Institute, Conifer Campus Panthaghati, Shimla 171013, Himachal Pradesh, India

M. Kumar
Department of Geography, School of Basic Sciences, Central University of Haryana, Mahendergarh 123031, Haryana, India

R. B. Singh
Department of Geography, Delhi School of Economics, University of Delhi, Delhi 110007, India

V. E. Gosavi
G. B. Pant National Institute of Himalayan Environment, Kosi-Katarmal, Almora 263601, Uttrakhand, India

B. Chand
G. B. Pant National Institute of Himalayan Environment, Himachal Regional Centre, Mohal-Kullu 175126, Himachal Pradesh, India

S. Sharma
School of Education, Central University of Haryana, Mahendergarh 123031, Haryana, India
e-mail: sarikasharma@chu.ac.in

R. B. Singh et al. (eds.), *Remote Sensing and Geographic Information Systems for Policy Decision Support*, Advances in Geographical and Environmental Sciences,
https://doi.org/10.1007/978-981-16-7731-1_9

LST. For validation of LST derived from Landsat—8, the standard daily LST product of MODIS11a1 Terra has been used. The validation analysis showed the coherence between LST estimation using Landsat 8 and MODIS daily LST products. However, in general, the range of surface temperature in MODIS is observed to be higher than that of Landsat data which is due to its coarser resolution. It is inferred that for surface temperature estimation over Delhi City, Landsat-8 provides realistic results than MODIS; while for regional level studies MODIS data could be a good option.

Keywords Land surface temperature · Split-window · SVM · LULC · MODIS

9.1 Introduction

Land Surface Temperature (LST) provides the temperature of a surface. It represents the earth's 'skin' temperature. Rise in this skin temperature of the earth leads to adverse environmental conditions (Rongali et al. 2018). The LST is important parameter measured by satellite remote sensing technology and is also a key to study the energy and water exchange (Yu et al. 2014), and helps in studies related to hydrological cycle, global warming, LULC change, land-surface interaction and associated temperature changes, soil moisture, vegetation water stress etc. (Thakur and Gosavi 2018).There is increasing interest in scientific fraternity about LST as it forms the base for a variety of applications, including environmental and agricultural monitoring (Yang et al. 2014).Being a governing parameter, it is also a vital input to weather or climate prediction models, hydrological models and in agriculture sector for effective irrigation water management (Nikam et al. 2016), drought monitoring and urban heat island studies (Friedel 2012; Son et al. 2012; Maimaitiyiming et al. 2014).These aspects show significance and necessitate the precise estimation of LST.

LST is dynamic nature, both spatially and temporally and varies with the complexity of the LULC that changes naturally as well as due to socio-economic and developmental activities such as construction and industrialization. However, due to variables changes of LST, the in-situ measurement of LST is a tedious task and is uneconomic and insufficient from user's point of view (Yang et al. 2014; Nikam et al. 2016). Here comes the remote sensing technology a very handy and a vital tool to make it possible to get the LST status over large regions with a regular revisit capability (Peng et al. 2014). Remote sensing satellite with the characteristics of synoptic and repetitive coverage of earth features provides an opportunity to retrieve the LST at local to regional scale from different temporal resolution (Rozenstein et al. 2014). Using Thermal Infrared (TIR) bands of remote sensing satellites, it is possible to retrieve the LST of an area at specified time of satellite visit (Rongali et al. 2018).

At present, multiple satellite or sensors are available that provides a repetitive synoptic view in short intervals of the Earth's surface. Among them are, public domain global thermal data provider sensors such as the Moderate-Resolution Imaging Spectroradiometer (MODIS) and the National Oceanic and Atmospheric Administration's (NOAA's), Advanced Very High Resolution Radiometer (AVHRR)

which uses two Long-Wave Infrared (LWIR) bands and provides the data twice in a day with a coarser spatial resolution, i.e., 500–1000 m. The remote sensing data in LWIR band was also available from Thematic Mapper (TM) and Enhanced Thematic Mapper Plus (ETM+) onboard Landsat-5 and Landsat-7 respectively with higher spatial resolution but with a longer temporal resolution of 16 days (Rozenstein et al. 2014; Nikam et al. 2016; Jiménez-Munoz and Sobrino 2008). Advanced Spaceborne Thermal Emission and Reflection Radiometer (ASTER), Landsat TM, ETM + OLI, HJ-1B IRS and CBERS-02 IRMSS (Wan 2008; Jiménez-Muñoz et al. 2010; Li et al. 2010; Dousset and Gourmelon (2003) also used for retrieving LST. Based on data availability for relatively longer period in TIR region, Landsat satellite series (Landsat 4 to Landsat 8) provide sufficient observational information in monitoring earth's environment at the global scale (Yang et al. 2014) which can be used for retrieval of LST. The two spectrally adjacent thermal bands can be utilized to retrieve LST by using Spilt-Window (SW) algorithm for achieve higher accuracy (Nikam et al. 2016). McMillin (1975) was the first to propose SW algorithm to retrieve the sea surface temperature (SST) using the differences in the atmospheric absorbance of two adjacent LWIR bands. Prince (1984) in making transmission from SST to LST, implemented SW using AVHRR data from NOAA 7. Thereafter SW algorithm seen many modification and application in variety of studies and been regarded as most widely used algorithm for estimation of LST due to its simplicity and robustness. The present study planned keeping in view the importance of the LST and above-mentioned background. The LST has been retrieved from Landsat 8 TIRS data for the New Delhi City in India using SW algorithm and validated using MODIS datasets for comparison.

9.2 Study Area

Delhi is the National Capital Territory of India and is biggest metropolitan city in India. According to the Census of India, Delhi Municipal Corporation has a total ward of 272 in 2011 shown in (Fig. 9.1). Delhi is India's most populous city and is situated in the northern part of India. The combination of different LULC and vulnerable to atmosphere turbulence of modern city of Delhi with long history; hence has been chosen as the study area. Delhi city lies in between latitude 28° 23′ 17″ North – 28° 53′ 00″ North and Longitude 76° 50′ 24″ East—77° 20′ 37″ East and lies at an altitude between 213 and 305 m Above from Mean Sea Level (AMSL) land covering an area of 1483 km^2. It is situated on the bank of river Yamuna (a tributary of the river Ganga). It is bordered in the east by the state of Uttar Pradesh and on the north, west and south by the state of Haryana. Chakraborty et al. (2013) described Delhi city in three physiography i.e., The Yamuna flood plain (low-lying and sandy), the ridge (most dominating physiographic features of Delhi territory which is originated in Rajasthan (Aravali hills) and entering in Delhi from the south direction and extends in northeastern direction) and the plain (rest of the Delhi). The total population of National Capital Territory Delhi by the year 2011 of 18.2 million (Census of India).

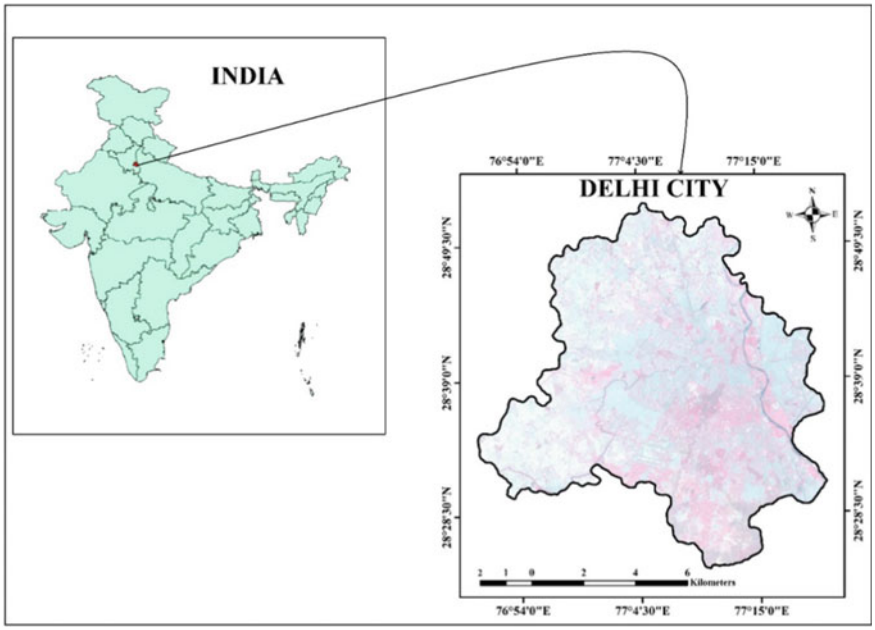

Fig. 9.1 Location map of Delhi city

The average annual rainfall is approximately 714 mm, most of which falls during the monsoon in July and August. The ambient temperature rises to as high as 47 °C, while on the other hand the cold during winters is severe and the temperature may reach as low as −0.6 °C during winter (Chakraborty et al. 2013).

9.3 Data Used and Methodology

9.3.1 Data Collection

Cloud Free Landsat 8 satellite data of February, 2014 for the study area has been downloaded from United States Geological Survey (USGS) Earth Explorer website (http://earthexplorer.usgs.gov/). All the data are pre-processed and projection to the Universal Transverse Mercator (UTM) projected system. The details of the satellite data collected are shown in Table 9.1. Landsat-8 is one of the Landsat series of National Aeronautics and Space Administration (NASA), Landsat 8 (formally the Landsat Data Continuity Mission, LDCM) was launched on an Atlas-V rocket from Vandenberg Air Force Base, California on February 11, 2013. In the present study, the TIR bands 10 and 11 were used to estimate brightness temperature and OLI spectral bands 2, 3, 4 and 5 were used to generate Normalized Difference Vegetation

Table 9.1 General information of Landsat 8 and MODIS datasets

Sensor/Satellite	No. of bands	Resolution (m/Km)	Path/Row and reference system	Date of acquisition
OLI	9	30 m	WRS-II/146/40	09-02-2014
TIR	2	100 m	WRS-II/146/40	09-02-2014
MODIS (TIR)	2	1 km	WRS-II/146/40	26-02-2014

Index (NDVI) of the study area. Customized models were built in 'Model Maker' environment of ERDAS Imagine 2020 to retrieve LST using SW algorithm.

9.3.2 Derivation of Normalized Difference Vegetation Index (NDVI) Image

The NDVI is a measure of the amount and vigor of vegetation at the surface. It is observed that healthy vegetation reflects very well in the near infrared part of the spectrum. Green leaves have a reflectance of 20% or less in the 0.5–0.7 range (Green to Red) and about 60% in the 0.7–1.3 μm range (Near Infrared). The value is then normalized to −1 NDVI +1 to partially account for differences in illumination and surface slope. The index is defined by Eq. 9.1. Estimation of NDVI using OLI sensor optical Bands after layer stacking of Band 2, 3, 4 and 5 using algorithm shown in (Eq. 9.1):

$$\mathrm{NDVI} = \frac{\mathrm{BAND\,5} - \mathrm{BAND\,4}}{\mathrm{BAND\,5} + \mathrm{BAND\,4}} \tag{9.1}$$

9.3.3 Retrieval of LST

The Landsat 8 OLI data and TIRS bands are converted to at-sensor level spectral radiance and reflectance using the rescaling factors provided in the metadata. At-sensor level radiance for Landsat 8 data is estimated using the following (Eq. 9.2):

$$\mathrm{L}_{\lambda} = (M_L \times Q_{cal} + \mathrm{A}_L) \tag{9.2}$$

where

L_{λ} is spectral radiance ($\mathrm{Wm}^{-2}\ \mathrm{sr}^{-1}\ \mu\mathrm{m}^{-1}$);
Q_{cal} is the Level 1pixel value in Digital Number (DN),
M_L is the band-specific multiplicative rescaling factor and

Table 9.2 Thermal band of sensor Landsat-8 and calibration constants for thermal band (Kelvin)

Thermal constant	Band 10	Band 11
K_1	1321.08	1201.14
K_2	777.89	480.89

A_L is the radiance multiplicative scaling factor. Similarly, the Top-of-atmosphere (TOA) reflectance from Landsat 8 data has been estimated using the following (Eq. 9.3):

$$\rho = (M_\rho \times Q_{cal} + A_\rho) \tag{9.3}$$

Where

ρ is the TOA spectral reflectance (unitless);
$M\rho$ is the reflectance multiplicative scaling factor and
$A\rho$ is the reflectance additive scaling factor. Values of M_L, A_L, $M\rho$ and $A\rho$ for each band are Landsat 8 OLI and TIRS can be obtained from metadata file.

The effective at-sensor Brightness Temperature (TB) also known as black body temperature is obtained from the spectral radiance using Plank's inverse function. TB is the microwave radiation radiance traveling upward from the top of Earth's atmosphere. The calibration process has been done for converting thermal DN values of thermal bands of TIR to TB. For finding TB of an area the Top of Atmospheric (TOA) spectral radiance of (L_λ) was needed. TB for both the TIRs bands was calculated by adopting Eq. 9.4.

$$T_B = \frac{K_2}{\text{In}(1 + \frac{K_1}{L_{\lambda i}})} \quad \text{(Unit : Kelvin)} \tag{9.4}$$

where K_1 and K_2 are thermal calibration constants for each TIRS bands represented by i, and values of these constant given in Table 9.2 are used from metadata files of Landsat 8 data.

9.3.4 Process of Split-Window (SW) Algorithm

LST was calculated by applying a structured mathematical algorithm viz., SW algorithm. The simplified formulation of this algorithm suggested by Jimenez-Munoz and Sobrino et al. (2008) is as follows Eq. 9.5:

$$\text{TS} = \text{TB10} + \text{C1} \times (\text{TB10} - \text{TB11}) + \text{C2} \times (\text{TB10} - \text{TB11})2$$

Table 9.3 SW coefficient values (*Source* Skokovic et al. 2014)

Constant	Value
C0	− 0.268
C1	1.378
C2	0.183
C3	54.300
C4	− 2.238
C5	− 129.200
C6	16.400

$$+ \text{C0} + (\text{C3} + \text{C4} + \text{w}) \times (1 - \varepsilon) + (\text{C5} + \text{C6} + \text{w}) \times \Delta\varepsilon \quad (9.5)$$

where,

LST	Land Surface Temperature (°K)
C0 to C6	Split-Window Coefficient values used by Skokovic et al. (2014) in Table 9.3
TB10 and TB11	brightness temperature of band 10 and band 11 (°K)
ε	Mean LSE of TIR bands
w	Atmospheric water vapor content
Δε	Difference in Land Surface Emissivity (LSE) estimated using formulation of Yu et al. (2014) and Nikam et al. (2016)

9.4 Result and Discussion

9.4.1 Density of Urban Area of Delhi Municipal Corporation During February 2014 Using Landsat-8 (OLI)

Delhi Municipal Corporation prepared new wards map according to Census of India 2011 included 272 Wards, 8 Cantonments and 9 New Delhi Municipal Council (NDMC) areas. Built-up density was calculated from the ward wise and it has been divided into five categories in percentage, from Very Low (0.03–0.33), Low (0.34–0.59), Medium (0.60–0.77), High (0.78–0.90), Very High (0.91–100) Density respectively shown in (Fig. 9.2). The high-density wards are mainly in the eastern and central parts of Delhi, whereas the very low built-up density wards are in the suburbs of the City, located in the northern, southern and western part of Delhi City. These latter areas were formerly agricultural and vegetated lands are still being converted into residential, commercial, multi-complexes, shopping mall and industrial area etc. Therefore, these wards have less population density. All density categories are also shown increased in built-up density in Delhi Municipal Corporation. High built-up density is attributed to population growth mainly, Central Delhi and north east part of

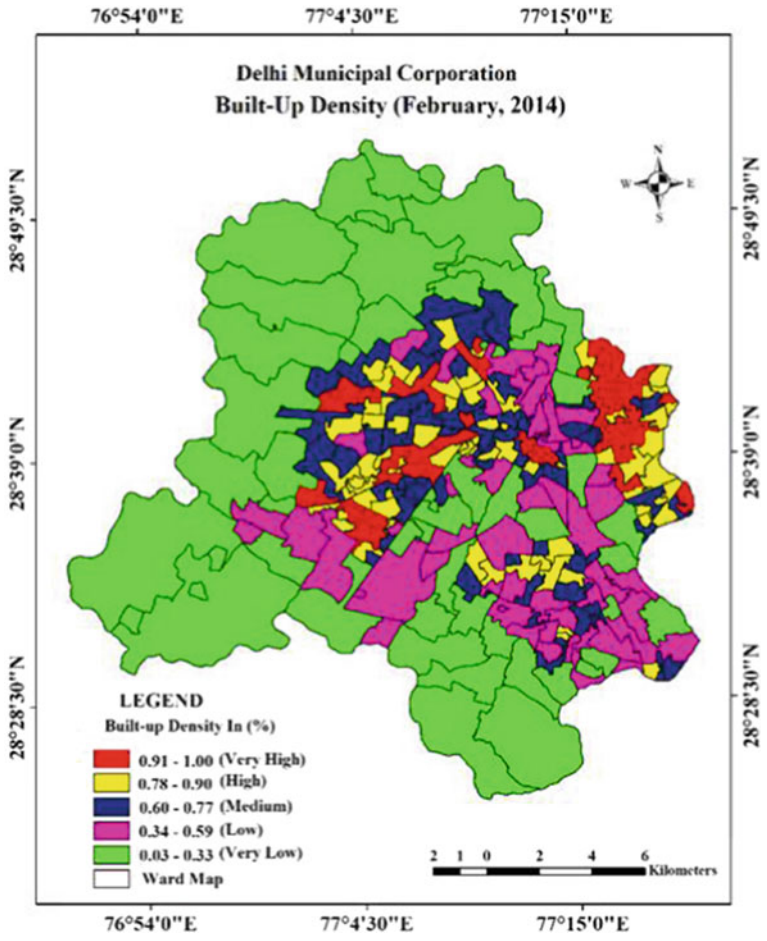

Fig. 9.2 Built-up density of Delhi city, Landsat-8 (OLI), image February, 2014

Delhi City because the reason of migrant population, for better medical, educational and employment facilities from different region and surrounding Delhi National Capital Region (DNCR). Analysis shown that Delhi Municipal Corporation has very high built-up density (88 to 99%) in the north–east part of Delhi i.e., in ward no 242, 247, 248, 250, 252, 255 to 263. Other side of central Delhi wards no 82, 83, 85, 86 and 88 also observed very high built-up density in very compact manner, which could be the possible reason for the raised LST in those wards area. Very low density was observed in wards no 2, 175 and 176 in (2–29%) mainly these areas are mostly covered in agriculture land, dense vegetation and sparse vegetation (Fig. 9.3). High built-up density implies that the land is being used for urbanization at a faster rate, which indicates that per capita consumption of land has increased rapidly over the last few decades. The per capita land consumption refers to the utilization of all lands

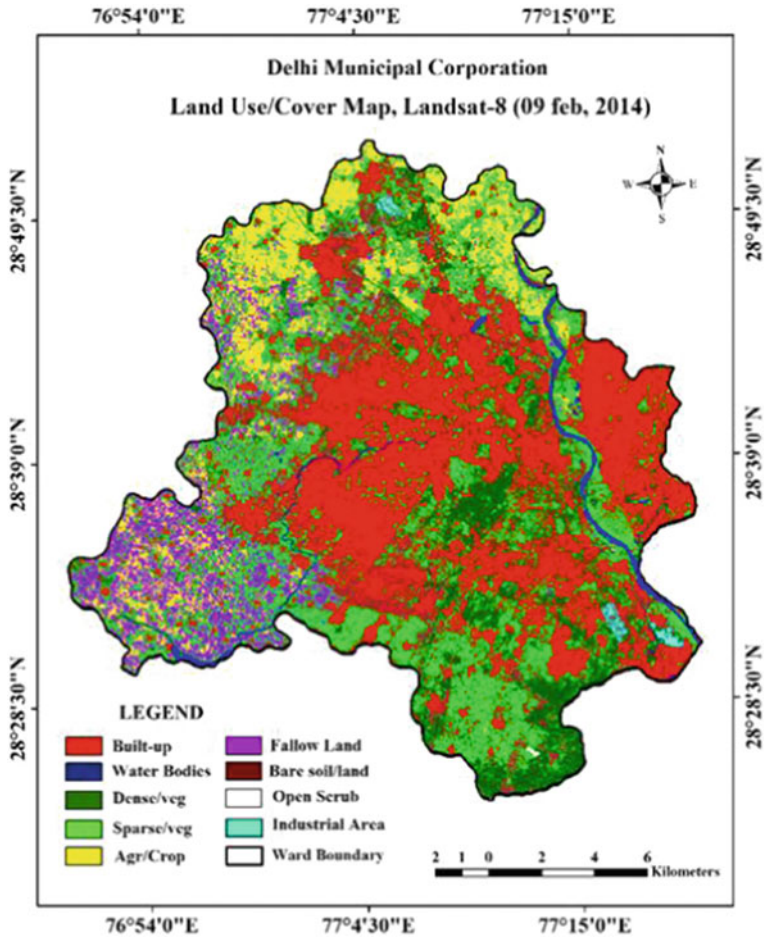

Fig. 9.3 Supervised classification using SVM of Landsat-8 (OLI), image 09th February, 2014

for development activities (e.g., commercial, industrial, educational, recreational and residential establishments) per person.

9.4.2 Landsat-8 (OLI): Land Use Land Cover (LULC) Categories in February 2014 of Delhi City

The LULC classification has been done using the standard classification scheme. Datasets of Landsat-8 (OLI), (09th February, 2014) have been taken for the LULC classification. The supervised classification method, SVM has been used on original bands and same SVM classification technique has been used with employed the

Table 9.4 Land Use Land Cover categories of the Delhi city in February 2014

LULC categories	Area in km^2	Area in percent
Built-up area	485.83	32.76
Water bodies	19.55	1.32
Dense vegetation	160.52	10.82
Sparse vegetation	377.46	25.45
Agriculture/Crop	135.71	9.15
Fallow land	143.79	9.69
Bare soil/Land	154.17	10.39
Open scrub	0.88	0.06
Industrial area	5.25	0.35
Total area	1483.16	100.00

ROI components, since this reduces data redundancy and correlations between spectral bands. The LULC in the year of 2014 using Landsat-8 (OLI) shown in (Table 9.4 and Fig. 9.3). The most of the LULC changes development is observed in and around south eastern part of Delhi, urban structures like multinational office buildings, multiplexes, shopping malls, apartments and residential have come up in Delhi areas. New developments like shopping malls, apartments and industrial area have been developed in and around north eastern Delhi and the same increase in urban structures are also observed in southern part and north eastern part of Delhi City.

The accuracy assessment was also done for above LULC analysis. For accuracy assessment of images average 30 samples per class which counts to 300 for each hybrid classified image were taken. Minimum number of samples for each class was set to 25. These points were generated using stratified random sampling method and laid on the images. The sampled points were exported from ERDAS Imagine 2020 and the ground truthing for the points was done using the Google earth imagery of the same time period used for classification. The SVM overall accuracy of all classes of 91.08% and kappa coefficient 0.88%, in Envi 5.3. The overall classification accuracy of classified image is given in (Table 9.5).

Table 9.5 Overall classification accuracy and Kappa statistics

Satellite and months	Classification accuracy	Kappa statistics
Landsat-8 (09th February, 2014)	91.08%	0.88

Table 9.6 Atmospheric up-welling, down-welling and transmission

Path	Row	Date	T	$I\uparrow$	$I\downarrow$
146	40	09/02/2014	0.92	0.56	0.96

9.4.3 Atmospheric Up-Welling, Down-Welling Radiances and Transmittance Retrieving

Atmospheric up-welling, down-welling radiances and transmittance values are extracted from online based Atmospheric Correction Parameters Calculator (ATMCORR) (available to the public at http://atmcorr.gsfc.nasa.gov/in since 2003) for the time when satellite pass (by date and time). ATMCORR uses National Center for Environmental prediction (NCEP) atmospheric data to provide global atmospheric data for altitudes. In order to provide global coverage, NCEP uses a course 1° by 1° grid spatial resolution and six-hour interval (0:00, 6:00, 12:00 and 18:00 UTC) temporal resolution. The values of atmospheric parameter for calculation of ground radiance used for LST estimation in the present study are given in (Table 9.6) for Landsat-8 TIR bands.

9.4.4 Estimation of Land Surface Temperature (LST) Using Landsat-8 (OLI), on 09th February, 2014 for Delhi City

LST for Landsat-8 (OLI) data has been estimated over the region using inverse Planck's law and the satellite derived surface emissivity values. Metropolitan areas like Delhi City are the main engines of urban growth in India. Rapid and haphazard urban growth and accompanying population pressures, result in changes in urban LULC; loss of productive agricultural land and open green spaces; loss of surface water bodies; depletion of groundwater; micro-climate change and air, water and noise pollution. Delhi has witnessed exceptional population growth during the past few decades.

The growing environmental concerns in urban areas, especially in cities like Delhi is increasing urban surface temperature due to change of natural surface regime during recent time. The present work is an attempt to assess the urban surface temperature in Delhi using Remote Sensing (RS) and Geographic Information System (GIS) techniques and to study the temperature variability of different LULC categories. Landsat-8 and MODIS datasets of thermal bands were used to estimate the LST. The spatial distribution of LST of Landsat-8 (OLI), of dated 09th Feb 2014 shown in (Fig. 9.4). The LST ranged from 13.72 °C (min) to 25.00 °C (max) with a mean of 19.36 °C and mean Standard Deviation (SD) of 1.79. It is observed in the image; west and south–west part exhibits high temperature mainly due to waste land/bare soil and fallow land. Some of the high temperature zones are also seen in the central

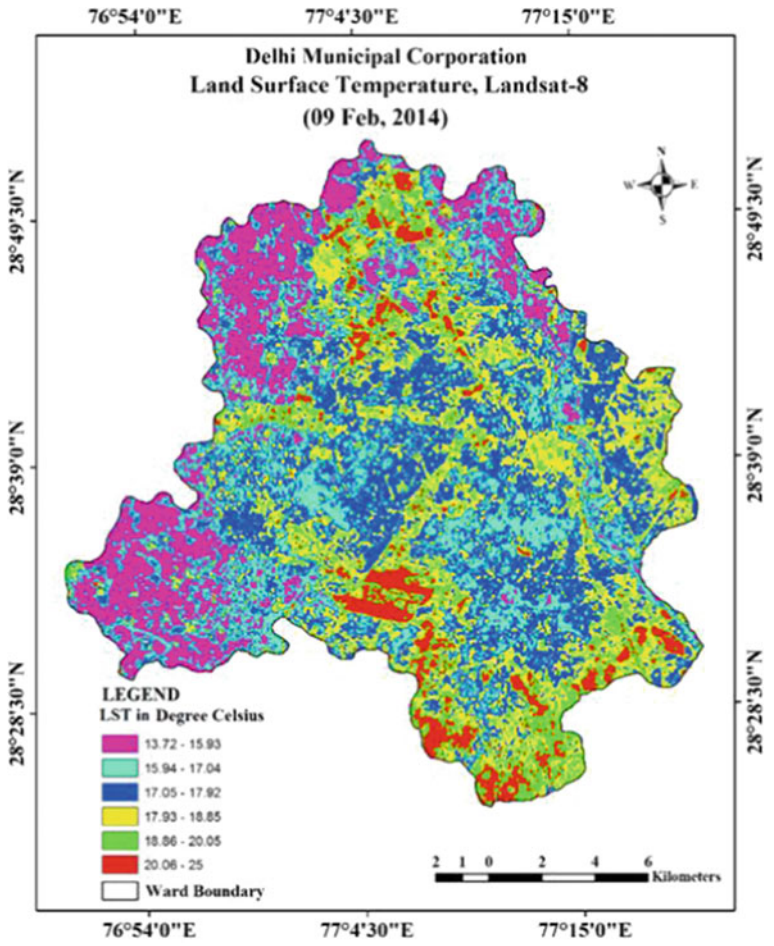

Fig. 9.4 LST derived from SWA method using Landsat 8 TIRS images of February 09, 2014 (Path 146/Row 40) dates

part of the image mainly due to commercial/industrial land use (corresponding to Fig. 9.3 of LULC).

9.4.5 Land Surface Temperature (LST) of Different Land Use Land Cover (LULC) Categories of Landsat-8 (OLI), 09th February, 2014

Table 9.7 shown the estimated LST values for different LULC categories. The minimum and maximum LST values for bare soil/land are 13.72 °C and 24.72 °C

Table 9.7 Statistics of Land Surface Temperature of different LULC categories of Landsat-8 (OLI), 09th February, 2014

Land Use Land Cover Categories	Min. temp	Max. temp	Mean	SD
Built-up area	14.37	25.00	17.94	0.91
Water bodies	14.08	23.61	16.70	1.10
Dense vegetation	14.26	23.68	18.24	1.35
Sparse vegetation	14.05	23.77	17.58	1.27
Agriculture/crop	14.02	22.11	15.64	0.92
Fallow land	14.08	22.30	16.09	0.99
Bare soil/land	13.72	24.72	18.71	1.37
Open scrub	14.51	21.97	18.88	1.57
Industrial area	16.81	24.04	19.79	1.17

with mean values of 18.71 °C and SD 1.37 respectively. For agriculture/crop land the minimum and maximum LST comes to 14.02 °C and 22.11 °C with mean of 15.64 °C and SD of about 0.92. whereas in industrial area the LST estimation comes to 16.81 °C and 24.04 °C as a minimum and maximum temperature with mean of 19.79 °C and SD 1.17 respectively. Other land use categories such as built-up area has minimum temperature of 14.37 °C with maximum up to 25.00 °C with mean temperature value of 17.94 °C. It is clearly seen from the LST analysis that bare soil/land, open scrub and industrial area exhibits higher mean value of the temperature which is attributed to open land which exposed directly to the sunlight and to developmental activities in industrial area. Mean temperature of other LULC categories are at lower side as compare to bare soil/land, open scrub and industrial area which is attributed to the fact that these land types are covered with certain covers which prevent their direct exposure to sunlight.

9.4.6 Ward Wise Distribution of Land Surface Temperature, Landsat-8 (OLI) of 09th February, 2014

The ward wise distribution of LST of Landsat 8 on 09th February, 2014 has been examined. It is observed during the daytime image that wards in west and south–west part have high surface temperature corresponding to fallow land and bare land/soil. The trend in daytime wherein the central and eastern parts of the image have high surface temperature corresponding to built-up, industrial areas and open scrub land. Wards in the north eastern part, exhibit lower surface temperatures in daytime corresponding to agricultural cropland. It is observed in (Fig. 9.5) that highest mean surface temperatures are found in the wards of NDMC -5 with 19.89 °C, Moti Nagar (ward no 99) with 19.36 °C, Karam Pura (ward no 100) with 19.61 °C, Raja Garden (ward no 101) with 19.37 °C, Hari Nagar (ward no 111) with 19.14 °C, Maj. Bhupender Singh

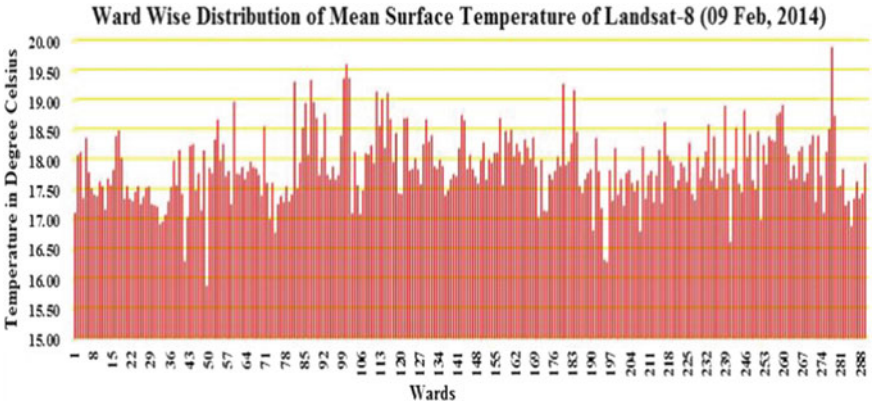

Fig. 9.5 Ward wise distribution of mean surface temperature of Landsat-8 (09th February. 2014)

Nagar (ward no 115) with 19.12 °C, Mahavir Nagar (ward no 113) with 19.02 °C. Lowest mean surface temperature was found in the wards of Rohini North (ward no 49) with 15.88 °C, Guru Hari Kishan Nagar (ward no 41) with 16.30 °C, East of Kailash (ward no 194) with 16.32 °C, Govindpuri (ward no 195) with 16.29 °C, Chitranjan Park (ward no 190) with 16.81 °C. (Details statistics of ward wise LST in Appendix).

9.4.7 Relationship Between Vegetation Density and LST of Landsat-8 (OLI), of 09th February, 2014

This section deals with the relationship between the LST of LULC and NDVI density. The regression coefficients were computed between NDVI cover of each LULC and its LST using MINITAB statistical software to calculate the scatter plot of each NDVI data product. The value of NDVI for Landsat-8 (OLI) data for February, 2014 ranges from 0.12 (low) to 0.52 (high) indicating the amount of vegetation (Fig. 9.6). LST of Landsat-8 (OLI), of 09th February 2014 was also calculated. The LST ranged from 13.72 °C (min) to 25.00 °C (max) with a mean of 17.57 °C and SD of 1.79. It is inferred from NDVI estimation that the LST has a negative strong correlation with NDVI. Table 9.7 shows the correlation between LST and NDVI. Few numbers of pixels were taken in respective LULC categories in order to have pure pixels which were used in computation of correlation. It is observed that NDVI values trend to be negatively correlated with the LST of all LULC classes (with the exception of water). The strongest negative correlation between LST and NDVI values is found in dense vegetation followed sparse vegetation built-up, agricultural cropland.

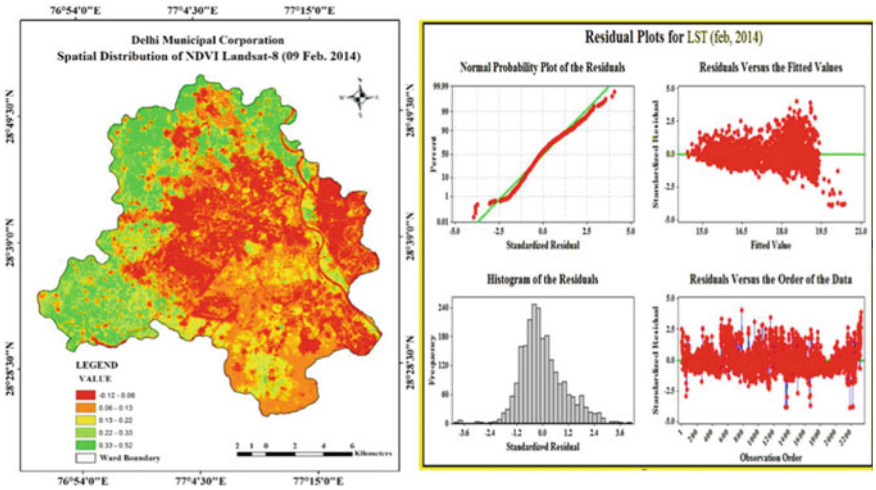

Fig. 9.6 Spatial distribution of fitted line scatter plot of Landsat-8 (OLI) February, 2014

9.4.8 Correlation Between Land Surface Temperatures (LST) and Normalized Difference Vegetation Index (NDVI)

Strong correlation between LST with NDVI is observed with the R^2 of 56.25 deviation of 1.21 of (09th February 2014). The regression coefficient between LST with NDVI for dense vegetation (forest area), sparse vegetation (grass land, scrub and green spaces) and agriculture/crop. Regression coefficient between surface temperatures with NDVI is highest over dense vegetation, followed by sparse vegetation, built-up area and agriculture land and fallow land are included all residual plot for normal probability plot of 99.99% shown in (Fig. 9.7).

9.4.9 Validation of Land Surface Temperature (LST) Using MODIS (Terra) Data in February 2014

The LST maps for 2014 MODIS 11a1 (Terra) clearly show high amplitude of surface temperature in 2014 to LULC changes attributing mainly to increase in urban built-up area (combination of settlement and industrial area). By observing the MODIS derived LST maps of Delhi city, it is observed that the maximum LST is observed over urban built-up and open space which is in coherence with Landsat 8 LST analysis. The surface temperature over industrial and settlement are high in the months of February, 2014. The same trend is followed and observed in Landsat-8 Thermal datasets. In general, the range of surface temperature in MODIS is observed to be higher than

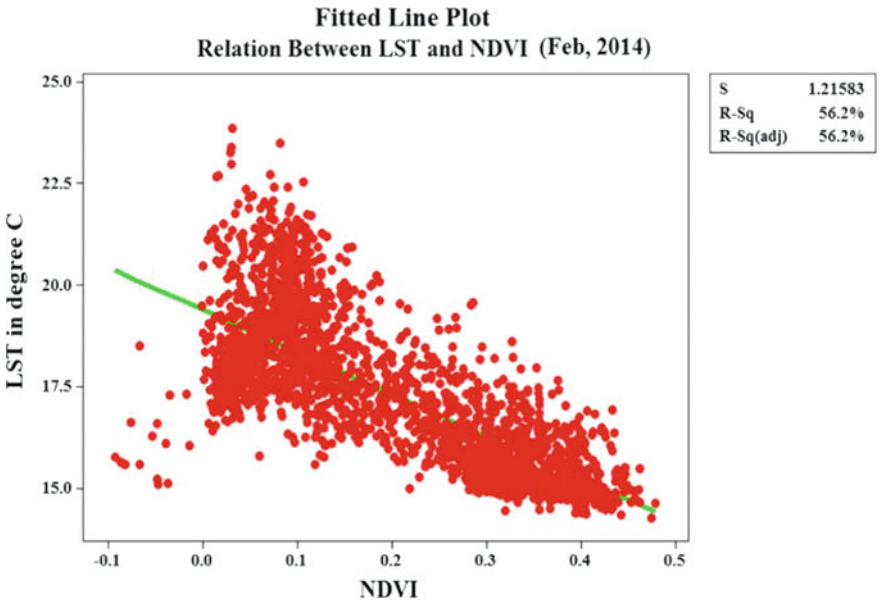

Fig. 9.7 Relation between LST and NDVI of Residual plot of Landsat-8 (OLI) 9th February. 2014

that of Landsat data which is due to its coarser resolution. It is inferred that for surface temperature estimation over Delhi, Landsat 8 provides realistic results than MODIS; while for regional level studies MODIS data could be a good option. The daytime LST using MODIS datasets for 09th February, 2014 shown in (Fig. 9.8). The estimated LST ranges from 15.36 to 27.87 °C with mean value 23.58 °C and SD of 1.94. Highest LST was observed in Built-up region followed by open scrub and industrial area whereas lowest LST in agriculture land, fallow land and water bodies. This increased LST over built-up and industrial area is due to emission of Green House Gases (GHG's) and other pollutant which prevent the out-going long-wave radiations to escape from earth's atmosphere, increased impervious surface and hence rise in emissivity.

9.4.10 Comparison of Mean Surface Temperature in Landsat-8 (OLI) and MODIS 11a1 Terra (February 2014) in Delhi City

The time of all the satellite datasets taken in the study were during the month of February 2014. In order to study the LST for different LULC categories, satellite data of Landsat-8 and, MODIS 11a1 were used. It was observed that (Fig. 9.9) water bodies, agricultural, dense and sparse vegetation exhibits lower surface temperature

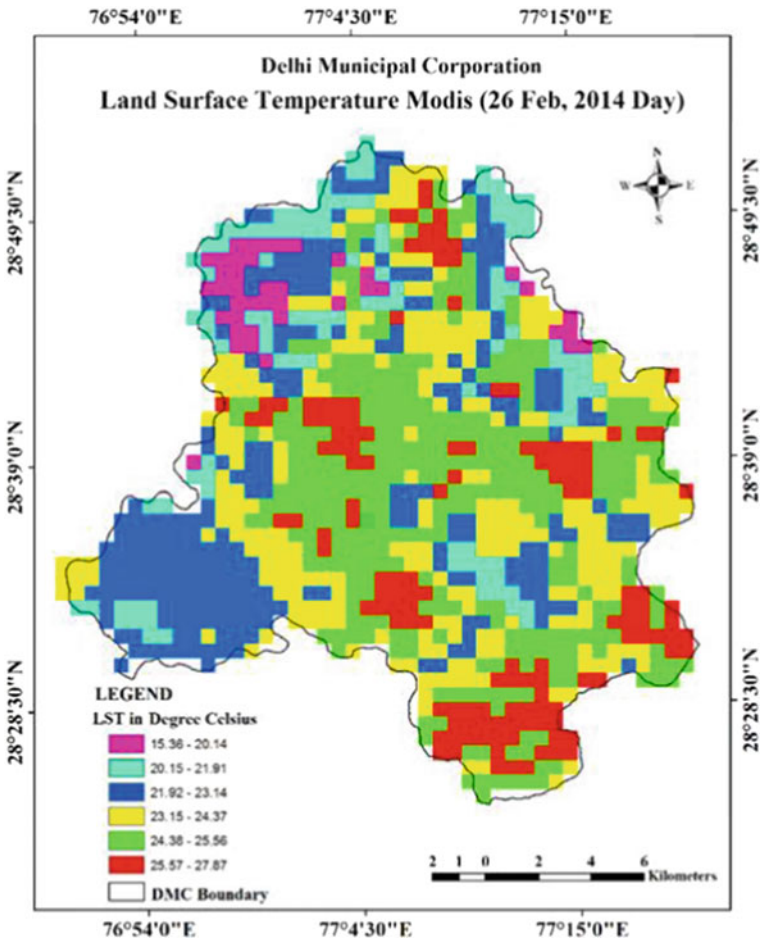

Fig. 9.8 Spatial distribution of Land Surface Temperature using MODIS 11a1, 26th February 2014-Daytime

as compare to industrial area, built-up area and bare soil/land. However, the LST of agricultural land doesn't follow usual trend of low temperature and showing temperature range on higher side as compare to other similar vegetative covers. The reflection of the barren and partially open soil was on higher side and the same has been reflected in the LST estimated of agricultural land for Landsat 8 and MODIS datasets. This study of comparison of mean LST of different LULC categories using Landsat 8 and MODIS showed that the both datasets follow similar trend in estimating LST for different LULC categories; however, the estimated LST using MODIS Daily LST products observed to be on much higher side than that of the Landsat 8 datasets, because the reason is satellite pass time in particular area.

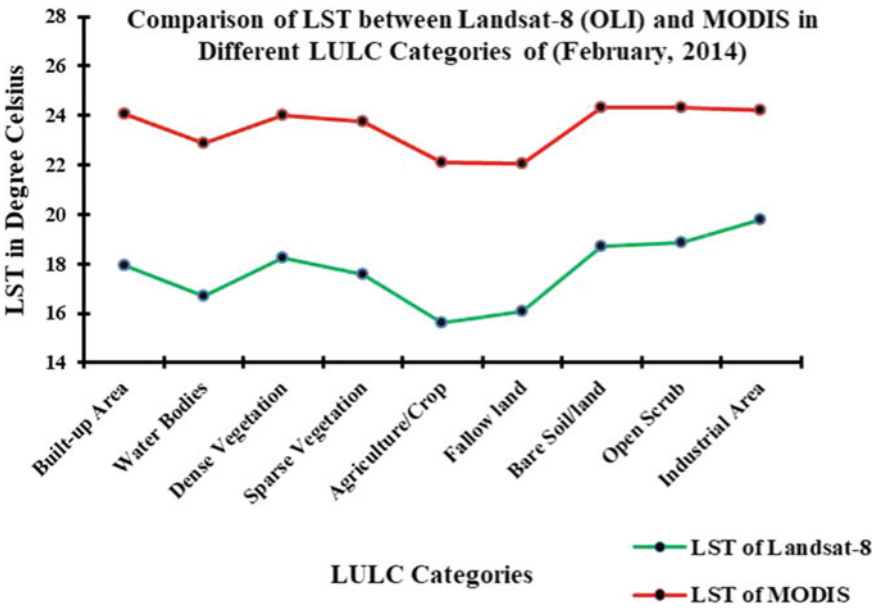

Fig. 9.9 Comparison of mean LST in different LULC of Landsat-8 (OLI) and MODIS for February 2014

9.5 Summary and Conclusion

The present study showed that hyper spectral thermal remote sensing offers great potential for advances in urban environment research. Earth surface temperature, including water surface temperature and LST, refers to the temperature of the critical layer by which the earth surface interacts with the atmosphere. Therefore, the present study has been undertaken to evaluate the potential of satellite datasets (Landsat-8 (OLI) and MODIS 11a1 Daily LST Products) to estimated LST and to analyze the temperature variability of different LULC categories of Delhi city in February 2014. Classification of image was done with SVM techniques for making LULC map of Delhi city using Landsat-8 data with 30 m spatial resolution. To study the LULC effect on LST, MODIS and Landsat-8 data were used in the year of February, 2014. SW algorithm is a fully operational algorithm; a dynamic mathematical tool provides the LST information using brightness temperature of two adjacent LWIR regions. Land surface emissivity was estimated using NDVI threshold method. In this study, it was found that minimum and maximum LST ranged from 13.72 to 25.00 °C for Landsat-8 data; whereas, 15.36 to 27.87 °C for MODIS (Terra) data in different LULC categories. Both datasets accurately simulate or estimate the behavior of LST for different LULC categories of Delhi city. However, the estimated surface temperature using MODIS is observed to be on higher side than that of Landsat-8 data. The reason attributed to coarser resolution of MODIS data as compare to

Landsat-8 data. The relationship reveals that the higher vegetation amount brings down the surface temperature in that land cover type. In other words, agricultural cropland, dense vegetation, sparse vegetation and some built-up patches. LULC are conducive to lowering of daytime surface temperature. It is observed that fallow land, waste land/bare soil, industrial and high exhibits high daytime surface temperature, while water bodies and vegetated areas lowest. It can be concluded that, Landsat-8 datasets provide accurate results for LST estimation over Delhi city, which can be used for further research that can be built upon on extracted temperature. However, for regional studies and to have general idea, one can use of MODIS datasets as a good alternate option.

Appendix

Ward Wise Distribution of Land Surface temperature (LST) from Landsat-8 (OLI) 09th February, 2014

Ward number	Ward name	Minimum	Maximum	Mean	SD
1	Narela	14.41	21.42	17.11	1.85
2	Bankner	17.13	19.82	18.08	0.47
3	Alipur	14.66	22.67	18.13	1.68
4	Bakhtawarpur	15.06	21.05	17.36	0.83
5	BalswaJahagirpuri	15.68	20.74	18.37	0.83
6	Mukandpur	16.75	20.59	17.79	0.55
7	Burari	16.88	18.83	17.52	0.38
8	Jahroda	16.51	18.78	17.42	0.37
9	MalkaGanj	16.51	19.16	17.39	0.45
10	Timarpur	16.36	19.29	17.63	0.41
11	Mukharji Nagar	16.65	18.84	17.55	0.38
12	G T B Nagar	16.53	18.69	17.16	0.30
13	Dheerpur	16.87	19.60	17.69	0.49
14	Adarsh Nagar	16.05	19.01	17.57	0.34
15	SaraiPipalthala	16.55	20.11	17.83	0.56
16	Jahangir Puri_I	16.83	20.86	18.40	0.94
17	SamaypurBaddi	16.78	21.15	18.49	0.88
18	LibasPur	16.35	20.09	18.04	0.68
19	Bhalswa	16.25	18.48	17.35	0.36
20	Jahangirpuri_II	16.62	19.39	17.56	0.36
21	Rohini	16.54	19.07	17.35	0.40
22	Rithala	16.16	18.79	17.30	0.41

(continued)

(continued)

Ward number	Ward name	Minimum	Maximum	Mean	SD
23	BudhVihar	16.43	18.78	17.46	0.31
24	Vijay Vihar	16.38	18.81	17.56	0.35
25	PoothKalan	16.60	18.49	17.26	0.28
26	Sahibabad DaulatPur	16.12	20.95	17.38	0.59
27	Begumpur	16.81	20.08	17.53	0.49
28	Bawana	16.27	21.26	17.55	0.75
29	Karala	14.84	20.73	17.25	0.69
30	Mundaka	15.96	18.56	17.23	0.39
31	NangloiJat West	15.01	19.21	17.21	0.49
32	Nilothi	15.90	18.86	16.92	0.49
33	PratapVihar	16.42	17.86	16.97	0.22
34	Nithari	16.47	18.85	17.08	0.41
35	KirariSuleman Nagar	16.71	18.54	17.30	0.35
36	Prem Nagar	16.96	20.34	17.54	0.46
37	Sultaanpuri East	15.86	21.19	17.99	0.82
38	Mangolpuri North	16.80	18.73	17.57	0.33
39	SultanpurMazra	16.82	20.85	18.16	0.93
40	Sultanpuri South	16.91	18.37	17.42	0.28
41	Guru HariKishan Nagar	13.80	22.06	16.30	0.99
42	PeeraGarhi	14.42	20.75	17.04	1.13
43	Nangloi East	16.06	20.92	18.23	0.83
44	Quammruddin Nagar	15.11	23.07	18.26	1.22
45	Rohini South	15.65	18.85	17.49	0.42
46	Mangolpuri East	16.13	20.80	17.77	0.67
47	Mangolpuri	14.69	21.27	17.15	0.95
48	Mangolpuri West	16.63	20.94	18.16	0.59
49	Rohini North	14.32	21.98	15.88	0.98
50	Rohini Central	15.09	22.04	17.86	1.04
51	Rohini East	16.85	21.67	17.77	0.84
52	Naharpur	15.20	21.53	18.34	1.01
53	Pitampura South	16.36	21.89	18.67	1.23
54	Pitampura North	16.92	20.92	17.99	0.71
55	Shalimar Bagh North	17.02	20.86	18.26	1.06
56	Shalimar Bagh South	16.78	20.31	17.72	0.52
57	PaschimVihar South	16.72	20.09	17.81	0.80
58	PaschimVihar North	16.04	18.71	17.25	0.44
59	Rani Bagh	17.07	22.89	18.98	1.01

(continued)

(continued)

Ward number	Ward name	Minimum	Maximum	Mean	SD
60	SaraswatiVihar	15.76	20.66	17.77	0.80
61	Tri Nagar	16.47	19.38	17.75	0.44
62	Rampura	16.78	21.08	17.88	0.69
63	Kohat Enclave	15.51	22.12	17.67	1.01
64	Shakarpur	15.70	20.94	17.80	1.02
65	Nimidicolony	16.82	20.57	17.97	0.58
66	Sawan Park	16.94	19.39	17.87	0.42
67	wazirpur	16.64	21.38	17.85	0.64
68	Ashok Vihar	16.56	20.29	17.74	0.53
69	Kamla Nagar	16.01	19.20	17.40	0.37
70	RanaPratapBagh	17.50	20.24	18.56	0.51
71	Sangam Park	16.71	18.58	17.61	0.34
72	Model Town	15.65	18.78	17.01	0.53
73	Shastri Nagar	16.81	19.10	17.61	0.35
74	Inderlok Colony	15.42	18.86	16.77	0.67
75	KishanGanj	16.16	18.72	17.25	0.35
76	Deputy Ganj	16.11	20.63	17.38	0.72
77	Kashmiri Gate	15.72	18.59	17.29	0.55
78	ManjuKa Tilla	16.51	19.30	17.55	0.45
79	Jama Masjid	16.44	19.05	17.30	0.42
80	Chandni Chowk	16.08	19.55	17.41	0.51
81	Minto Road	17.42	22.09	19.31	0.93
82	Kuanch Pandit	15.67	20.03	17.52	0.73
83	Bazar Sita Ram	16.19	21.77	17.95	0.99
84	Turkmaan Gate	16.03	21.89	18.54	1.27
85	Idgah road	16.46	22.14	18.95	1.23
86	Ballimaran	16.17	21.58	18.08	1.02
87	Ram Nagar	15.78	22.61	19.34	1.26
88	Qasabpura	13.72	22.18	18.97	0.96
89	Pahar Ganj	16.84	21.03	18.70	0.77
90	Modal Basti	16.72	19.85	17.74	0.45
91	Karol Bagh	17.11	19.58	18.04	0.44
92	Dev Nagar	15.94	22.15	18.77	1.15
93	Baljeet Nagar	16.56	19.64	17.75	0.58
94	West Patel Nagar	16.75	19.31	17.67	0.48
95	East Patel Nagar	17.06	18.92	17.89	0.46
96	New Ranjit Nagar	16.96	19.45	17.67	0.48

(continued)

(continued)

Ward number	Ward name	Minimum	Maximum	Mean	SD
97	Kirti Nagar	16.18	19.93	17.74	0.60
98	Manasarovar Garden	16.59	20.41	18.41	0.75
99	Moti Nagar	17.53	21.92	19.36	1.23
100	Karam Pura	17.70	21.95	19.61	1.00
101	Raja Garden	17.26	22.34	19.37	0.98
102	Raghubir Nagar	16.08	18.45	17.10	0.43
103	Panjabi Bagh	15.42	24.75	18.13	1.16
104	Madipur	16.29	19.54	17.57	0.49
105	Rajouri Garden	15.63	20.71	17.09	0.72
106	Tagore Garden	16.02	19.26	17.49	0.48
107	Vishnu Garden	16.74	20.67	18.11	0.74
108	Khyala	16.75	22.06	18.09	0.75
109	Janak Puri North	17.21	19.93	18.24	0.53
110	Nangal Raya	16.81	19.70	17.95	0.63
111	Hari Nagar	16.44	25.00	19.14	1.00
112	Subhash Nagar	17.32	20.19	18.57	0.57
113	Mahavir Nagar	17.12	22.19	19.02	0.76
114	Tilak Nagar	17.50	19.97	18.20	0.44
115	Maj.Bhupender Singh Nagar	17.23	20.28	19.12	0.67
116	Vikspuri East	14.59	24.04	18.68	1.75
117	Janakpuri West	15.46	21.32	17.96	0.84
118	Janak Puri South	17.33	19.77	18.45	0.53
119	Milap Nagar	15.57	20.02	17.43	0.88
120	SitaPuri	14.65	20.08	17.42	1.08
121	Kunwar Singh Nagar	15.09	23.40	18.70	1.46
122	Hastsal	15.86	22.56	18.71	1.17
123	VikasPuri	17.20	18.89	17.82	0.37
124	Vikas Nagar	16.20	20.98	17.84	0.71
125	Mohangarden	17.23	19.70	18.03	0.53
126	Nawada	17.05	19.42	17.84	0.52
127	Uttam Nagar	16.63	19.72	17.59	0.59
128	BindaPur	17.28	20.19	18.26	0.60
129	Dabri	16.70	24.95	18.68	1.19
130	Manglapuri	17.48	20.39	18.30	0.54
131	Sagarpur	16.93	20.96	18.41	1.01
132	sagarpur west	16.55	19.89	17.89	0.51
133	Chhawala	17.32	19.49	17.84	0.37

(continued)

(continued)

Ward number	Ward name	Minimum	Maximum	Mean	SD
134	Nangli Sakravati	15.59	20.08	18.00	0.78
135	Kakrola	16.72	19.80	17.89	0.56
136	Matiala	15.71	19.82	17.40	0.67
137	Roshanpura	15.93	19.44	17.49	0.66
138	NAzafgarh	16.53	20.28	17.67	0.60
139	DichaonKalan	17.10	20.39	17.76	0.57
140	Khera	15.28	21.19	17.72	0.92
141	Bijwasan	15.60	22.30	18.19	0.68
142	Rajnagar	16.76	21.37	18.75	0.87
143	Kapashera	17.05	21.24	18.66	0.60
144	Mahipalpur	16.85	20.12	17.85	0.42
145	Palam	17.10	19.40	18.08	0.42
146	Saad Nagar	17.04	21.37	17.84	0.58
147	Mahavir Enclave	16.87	19.42	17.72	0.41
148	Madhu Vihar	17.09	18.62	17.60	0.22
149	Rajendra Nagar	17.41	19.15	18.00	0.37
150	Poosa	15.70	21.35	18.29	0.88
151	Inder Puri	15.64	19.22	17.67	0.65
152	Naraina	17.07	19.57	18.01	0.34
153	Darya Ganj	17.05	19.12	17.95	0.33
154	Nizamuddin	17.33	18.86	18.11	0.32
155	Lajpat Nagar	17.19	19.30	18.12	0.37
156	Bhogal	17.45	20.80	18.71	0.71
157	Kasturaba Nagar	16.20	21.00	17.58	0.71
158	Kotla Mubarak Pur	17.59	20.15	18.48	0.55
159	Andrews Ganj	17.06	20.17	18.29	0.49
160	Amar Colony	17.52	19.99	18.50	0.53
161	Malviya Nagar	16.98	19.64	18.06	0.53
162	Village Huaz Rani	16.54	20.36	18.27	0.60
163	Safdarjung Enclave	17.33	20.56	18.13	0.61
164	HauzKhas	17.14	19.37	17.92	0.41
165	Vasant Vihar	17.05	20.75	18.34	0.59
166	Munirika	17.39	19.94	18.21	0.44
167	R K Puram	17.47	19.19	18.02	0.37
168	Nanakpura	15.61	22.61	18.37	0.94
169	Lado Sarai	17.18	19.53	17.88	0.44
170	Mehrauli	14.75	20.83	17.03	1.14

(continued)

(continued)

Ward number	Ward name	Minimum	Maximum	Mean	SD
171	VasantKunj	17.42	19.16	18.00	0.32
172	Kishan Garh	14.94	20.49	17.15	0.79
173	Said UlAjaib	14.76	19.01	17.13	0.81
174	Chhatarpur	17.09	18.68	17.75	0.28
175	Aya Nagar	16.89	19.19	17.67	0.38
176	Bhati	17.22	18.67	17.81	0.24
177	Sangam Vihar	17.00	19.91	18.05	0.54
178	Devli	17.15	18.92	17.89	0.32
179	Tigri	15.95	22.45	19.28	1.11
180	Dakshinpuri Extn	17.25	18.72	17.91	0.24
181	Khanpur	16.52	20.72	17.97	0.59
182	Ambedkar Nagar	17.14	22.06	18.28	0.68
183	Madangir	17.72	21.97	19.16	1.00
184	PushpVihar	17.10	21.28	18.47	0.79
185	Tuglakabad Extn	16.94	19.64	17.56	0.37
186	Sangam Vihar West	16.90	18.49	17.44	0.29
187	Sangam Vihar Central	17.08	18.25	17.67	0.26
188	Sangam Vihar East	16.72	19.10	17.78	0.36
189	Chirag Delhi	17.43	18.84	17.84	0.25
190	Chitranjan Park	14.33	22.49	16.81	1.47
191	ShahpouJat	16.98	21.45	18.37	1.04
192	Greater Kailash_I	16.93	19.42	17.80	0.54
193	Sriniwaspuri	14.33	21.65	17.18	1.30
194	East of Kailash	14.02	22.04	16.32	1.59
195	Govindpuri	14.25	20.76	16.29	1.19
196	Kalkaji	14.32	22.88	17.82	1.66
197	Tughlakabad	14.55	22.07	17.31	1.39
198	PulPehladpur	14.75	21.23	18.20	1.25
199	Tekhand	15.77	19.70	17.41	0.59
200	Harkesh Nagar	16.07	20.77	17.68	0.76
201	Jaipur	15.21	19.30	17.23	0.70
202	MithaPur	16.91	19.78	17.77	0.47
203	Badarpur	16.89	20.95	17.83	0.65
204	Moladband	16.73	19.96	17.61	0.57
205	Zakir Nagar	16.67	18.85	17.47	0.49
206	Okhla	16.67	19.99	17.65	0.59
207	MadanpurKhadar	14.04	22.78	16.80	1.60

(continued)

(continued)

Ward number	Ward name	Minimum	Maximum	Mean	SD
208	Sarita Vihar	16.62	20.50	18.22	0.78
209	MayurViharPhase_I	16.23	19.30	17.35	0.56
210	Dallupura	16.23	20.73	17.74	0.67
211	Trilokpuri	16.34	20.80	17.81	0.70
212	New Ashok Nagar	16.07	19.99	17.29	0.67
213	Kalyan Puri	16.70	20.58	17.74	0.70
214	Khichdipur	16.63	22.83	18.17	0.97
215	Kundli	16.71	18.85	17.27	0.41
216	Gharoli	16.83	20.69	18.63	0.76
217	Vinod Nagar	16.50	21.07	18.07	0.79
218	Mandawali	15.51	22.07	17.99	1.14
219	MayurViharPhase_II	16.44	19.88	17.90	0.75
220	Patpad Gunj	16.42	18.57	17.52	0.32
221	Kishan Kunj	16.94	19.51	17.66	0.38
222	Laxmi Nagar	16.57	20.24	17.95	0.67
223	Shakarpur	16.45	20.67	17.88	0.83
224	Pandav Nagar	16.44	19.84	17.62	0.65
225	Anand Vihar	16.67	21.34	18.28	0.98
226	Vishwas Nagar	16.12	19.87	17.42	0.55
227	IP Extn	16.52	19.07	17.32	0.37
228	Preet Vihar	16.63	20.49	18.05	0.64
229	Krishna Nagar	15.56	20.19	17.70	0.71
230	Geeta Colony	16.31	20.37	17.87	0.70
231	Ghondli	17.20	19.66	18.14	0.37
232	Anarkali	16.93	20.49	18.59	0.79
233	Dharmpura	16.30	19.35	17.65	0.44
234	Gandhi Nagar	17.18	20.09	18.39	0.63
235	Azad Nagar	16.64	18.99	17.51	0.41
236	Raghubarpura	16.69	20.18	17.85	0.55
237	Shahdara	16.65	20.61	17.70	0.50
238	Jhilmil	17.26	21.60	18.90	1.23
239	Vivek Vihar	16.49	20.21	17.77	0.53
240	Dilshad Colony	14.23	20.99	16.62	1.24
241	Dilshad Garden	16.73	18.78	17.84	0.36
242	New Seema Puri	17.07	21.10	18.53	0.70
243	NandNagri	16.39	20.14	17.60	0.61
244	Sundar Nangri	16.39	20.21	17.45	0.57

(continued)

(continued)

Ward number	Ward name	Minimum	Maximum	Mean	SD
245	Durgapuri	16.77	21.69	18.83	0.87
246	Ashok Nagar	16.76	19.86	18.05	0.55
247	Ram Nagar	17.55	20.39	18.43	0.51
248	Welcome Colony	15.62	20.21	17.65	0.95
249	Chouhan Bangar	15.31	20.54	17.50	0.73
250	Jaffrabad	17.29	19.97	18.48	0.54
251	New Usmaanpur	14.30	20.37	16.99	1.23
252	Maujpur	15.68	19.93	18.25	0.81
253	Bhajanpura	16.42	19.62	17.92	0.52
254	Brahampuri	17.59	19.08	18.39	0.30
255	Ghonda	17.92	18.82	18.33	0.16
256	Yamuna Vihar	17.71	19.12	18.31	0.25
257	Subhash Mohalla	17.78	20.37	18.75	0.44
258	Kardampuri	18.22	19.30	18.79	0.21
259	Janta Colony	17.81	19.83	18.92	0.42
260	Babar Pur	17.41	19.74	18.23	0.44
261	Jeevanpur	17.05	19.96	18.10	0.55
262	Gokalpur	16.28	20.64	17.67	0.56
263	Saboli	16.88	19.57	17.91	0.41
264	Harsh Vihar	16.07	19.52	17.69	0.53
265	Shiv Vihar	17.11	20.17	18.14	0.75
266	Karawal Nagar East	16.75	22.22	18.22	1.18
267	Nehru Vihar	16.02	19.37	17.64	0.53
268	Mustafabad	16.30	20.27	17.77	0.53
269	KhajuriKhas	16.90	20.35	18.26	0.75
270	TukhMirpur	17.11	20.54	18.41	0.77
271	Karawal Nagar West	14.69	19.35	17.29	0.69
272	Sonia Vihar	17.08	20.67	18.40	0.66
10001	NDMC-1	15.67	21.52	17.74	1.06
10002	NDMC-2	15.79	19.75	17.11	0.56
10003	NDMC-3	16.09	21.14	18.13	0.93
10004	NDMC-4	16.15	21.05	18.52	0.90
10005	NDMC-5	16.50	23.25	19.89	1.32
10006	NDMC-6	16.81	21.47	18.74	0.92
10007	NDMC-7	16.12	19.72	17.54	0.72
10008	NDMC-8	15.81	20.32	17.56	0.65
10009	NDMC-9	16.62	20.06	17.85	0.59

(continued)

(continued)

Ward number	Ward name	Minimum	Maximum	Mean	SD
5001	CANT-1	14.97	19.94	17.23	0.60
5002	CANT-2	16.24	20.12	17.31	0.52
5003	CANT-3	15.85	20.21	16.88	0.44
5004	CANT-4	16.58	18.64	17.35	0.37
5005	CANT-5	16.60	19.66	17.64	0.50
5006	CANT-6	16.43	18.37	17.35	0.30
5007	CANT-7	15.75	21.05	17.43	0.82
5008	CANT-8	17.12	19.83	17.95	0.56

References

Chakraborty SD, Kant Y, Mitra D (2013) Assessment of land surface temperature and heatfluxes over Delhi using remote sensing data. J Environ Manage 148:143–152

Dousset B, Gourmelon F (2003) Satellite multi-sensor data analysis of urban surface temperatures and landcover. ISPRS J Photogramm Remote Sens 58(1–2):43–54

Friedel MJ (2012) Data-driven modeling of surface temperature anomaly and solar activity trends. Environ Modell Softw 37:217–232. http://atmcorr.gsfc.nasa.gov/, http://earthexplorer.usgs.gov/.

Jiménez-Muñoz JC, Sobrino JA (2008) Split-window coefficients for land surface temperature retrieval from low-resolution thermal infrared sensors. IEEE Geosci Remote Sens Lett 5:806–809. https://doi.org/10.1109/LGRS.2008.2001636

Jiménez-Muñoz JC, Sobrino JA (2010) A single-channel algorithm for land-surface temperature retrieval from ASTER data. Geosci Remote Sens Lett IEEE 7(1):176–179

Li H, Liu QH, Zhong B (2010) A single-channel algorithm for land surface temperature retrieval from HJ-1B/IRS data based on a parametric model. In 2010 IEEE international on geoscience and remote sensing symposium (IGARSS), pp 2448–2451

Maimaitiyiming M, Ghulam A, Tiyip T (2014) Effects of green space spatial pattern on land surface temperature: Implications for sustainable urban planning and climate change adaptation. ISPRS J Photogramm Remote Sens 89:59–66

McMillin LM (1975) Estimation of sea surface temperatures from two infrared window measurements with different absorption. J Geophys Res 80(36):5113–5117

Nikam BR, Ibragimov F, Chouksey A, Garg V, Aggarwal SP (2016) Retrieval of land surface temperature from Landsat 8 TIRS for the command area of Mula irrigation project. Environ Earth Sci 75:1169

Peng SS, Piao SL, Zeng ZZ (2014) Afforestation in China cools local land surface temperature. Proc Natl Acad Sci 111(8):2915–2919

Prince JC (1984) Land surface temperature measurements from the split window channels of the NOAA 7 Advanced very high resolution radiometer. J Geophys Res Atmos 89(D5):7231–7237

Rongali G, Keshari AK, Gosain AK, Khosa R (2018) Split-window algorithm for retrieval of land surface temperature using Landsat 8 thermal infrared data. J Geovisual Spat Anal. https://doi.org/10.1007/s41651-018-0021-y

Rozenstein O, Qin Z, Derimian Y, Karnieli A (2014) Derivation of land surface temperature for Landsat-8 TIRS using a split window algorithm. Sensors 14(4):5768–5780

Skokovic D, Sobrino JA, Jimenez-Munoz JC, Soria G, Julien Y, Mattar C, Jordi C (2014) Calibration and validation of land surface temperature for Landsat 8—TIRS sensor. Land product validation and evolution, ESA/ESRIN Frascati (Italy), pp 6–9, January 28–30, 2014

Sobrino JA, Reillo S, Cueca J, Prata AJ (2008) Algorithms for estimating surface temperature from ASTR-2 data. http://earth.esa.int/pub/ESA_DOC/gothenburg/101sobri.pdf.

Son NT, Chen CF, Chen CR (2012) Monitoring agricultural drought in the lower Mekong basin using MODIS NDVI and land surface temperature data. Int J Appl Earth Obs Geoinf 18:417–427

Thakur PK, Gosavi VE (2018) Estimation of temporal land surface temperature using thermal remote sensing of Landsat-8 (OLI) and Landsat-7 (ETM+): a study in Sainj River Basin, Himachal Pradesh, India. Environ We Int J Sci Tech 13(2018):29–45

Wan ZM (2008) New refinements and validation of the MODIS land-surface temperature/emissivity products. Remote Sens Environ 112(1):59–74

Yang L, YunGang C, XiaoHua Z, ShengHe Z, GuoJiang Y, JiangYong H, XiuChun Y (2014) Land surface temperature retrieval for arid regions based on Landsat-8 TIRS data: a case study in Shihezi, Northwest China. J Arid Land 6(6):704–716

Yu X, Guo X, Wu Z (2014) Land surface temperature retrieval from Landsat 8 TIRS-comparison between radiative transfer equation based method, Split-Window algorithm and single channel method. Remote Sens 6(10):9829–9852

Chapter 10
Investigation of Land Use and Landcover Changes and Its Relationship with Land Surface Temperature and Ground Water Temperature Over Bangalore City

Surya Deb Chakraborty, Yogesh Kant, K. Mruthyunjaya Redd, and P. Jagadeeswara Rao

Abstract Urban heat redistribution is mainly result of surface energy process. Surface energy process is also contributed in urban environment. Urban heat island (UHI) is mainly defined when urban temperature is elevated compared to surrounding rural area. Both in above and below the ground UHI is observed. This is happened due to conductive heat transport. How the Land surface temperature and ground water temperature are affected by the urban land use in Bangalore is the primary plan of investigation. Landsat data of 1999 and 2009 are used to understand the LU/LC changes. In this present study we used satellite derived Land surface temperature and field collected Ground water temperature which was analyzed using interpolation method and Supervised Classification Change Detection technique applied for change analysis. Here investigation was done for a period of one decade (1999/2009) on LST changes over different land use. Moreover, relationship between NDVI and LST was also considered. To understand urban surface, we estimated Normalized Difference Built-Up Index (NDBI) and Built up Area Index (BUAI); with this we are trying to find relationship with ground water temperature. Changing land use pattern, mostly expansion of built-up area has effect over land surface temperature in Bangalore urban district. The correlation between LST and the Ground water temperature

S. D. Chakraborty (✉)
Agricultural Science and Application Division, Department of Space, National Remote Sensing Centre, ISRO, Balanagar 500037, Hyderabad, India

Y. Kant
Marin and Atmospheric Science Division, Indian Institute of Remote Sensing, ISRO, Dehradun, India
e-mail: yogesh@iirs.gov.in

K. M. Redd
Rural Development and Watershed Management Division, National Remote Sensing Centre, ISRO, DOS, Balanagar 500037, Hyderabad, India
e-mail: reddy_km@nrsc.gov.in

P. J. Rao
Department of Geo-Engineering & Resource Development Technology, College of Engineering, Andhra University, Visakhapatnam, India

R. B. Singh et al. (eds.), *Remote Sensing and Geographic Information Systems for Policy Decision Support*, Advances in Geographical and Environmental Sciences,
https://doi.org/10.1007/978-981-16-7731-1_10

(GWT); has been studied on 2009 data and found 80% correlation between them. In result, it is showing that GWT is less than LST but wherever LST is high there GWT is also high. In city core area like residential, outside industrial and road, GWT and LST both show high but near to lake or park area both show low temperature. Results show that during years 1999 to 2009 that LST and GWT directly affected due to rapid urban growth which reflects over built-up area enlarged from 39 to 57%. We can understand that urbanization has an impact on both on LST and GWT. The study showed that land use land cover change has important role of increasing GWT which is a marker of the strength of urban heat island effect and can be utilized to evaluate the extent of the urban heat island effect.

Keywords Ground water temperature · Land surface temperature · Built up area index · Sub surface urban heat island · Remote sensing

10.1 Introduction

The urban heat island effect in core urban are like CBD and housing areas which increases strength of the heat waves. The large number of man-made urban structure is mainly made of tar and concrete which covers urban areas. The human urban–rural contrast and urban heat island represented by temperature gradient, the nonporous material such as asphalt and concrete replace land surface which is the main cause of deforestation. This increases rainwater runoff and reduces evaporation (Carlson 1986). The thermal characteristic of urban surface is a significant information for urban organizers and modelers for improving city site quality creation more eco-accommodating. In present time urban heat island (UHI) spectacle is occurring in all layers of present time urban areas, for example, environment, surface and subsurface. There are numerous issues identified related to this spectacle. UHI has a positive impact on regional atmospheric pollution and increased mortality rates because of heat waves. In case of SUHI which is directly responsible increases ground water temperature and it puts stress on underground ecosystem. From the study of Cheon et al. (2014), we found that mean air temperature is firmly identified with the yearly mean ground water temperature because of conductive heat transport measure. In another study (Menberg et al. 2014) clarify that surface air temperature affects subsurface ground water temperature (GWT). Yet it's still confusing of the connection process between air and ground water temperature.

At present time, satellite remote sensing is opening a new door to measure surface temperature. Air temperature, surface temperature and ground surface temperature are correlated with each other but it's not yet accurately resolute. From the study of Chakraborty et al. (2015), Pongracz et al. (2010), Peng et al. (2011), we understand that LST which is derived from satellite are easy to access spatial and temporal condition of UHI in different cities of India, Europe and worldwide. In other side, GWT measurement in existing ground water monitoring wells using interpolation

measurement process is costly and tedious method to study subsurface urban heat island (Ferguson and Woodbury 2007).

In the investigation of Osaka japan by Huang et al. (2009), demonstrated that urban estimated well temperature was generously raised in contrast with those forecasted from meteorological time series. House, manure system and underground subway tunnels are the major anthropogenic sources of the causes of this irregularities. There are numerous investigations discovered which were attempted to appraise GWT from over the ground estimation, for example, LST.

Without satellite information, because of time delay among above and subterranean temperature, more profound GWT was hard to quantify. Anthropogenic heat fluxes effect into subsurface is not preferred by Zhan et al. (2014). In numerous investigations it appeared that building, underground tunnel, sewage system elevated thermal temperature in underground. Therefore, need to improve the estimation of urban GWT urban bodies and buildings is under observation.

The principle goal of the examination is to understand how land use and land cover change put an impact over GWT and LST over Bangalore city. The extraordinary change in land use/land cover related with human exercises is viewed as an incredible main impetus in nearby atmosphere and climate changes. Urban Heat Island (UHI) intensity is closely related to LU/LC patterns over time. Therefore, accurate detection of LU/LC changes associated with urbanization and LST, GWT distribution is critical to environmental monitoring, management and planning. Therefore, for this research, much emphasis is placed on determining the urban LU/LC changes and their impact on GWT and LST patterns. The current examination targets identifying the effect of Land Use/Land Cover Changes of Bangalore Urban District on its Land Surface Temperature and Ground water temperature. For this purpose multitemporal LANDSAT TM Images of 1999 and 2009 are used for post classification (supervised classification) change detection. This emphasizes the change in Built-up, Water bodies of other land use classes. The LST retrieved from multitemporal LANDSAT TM Images of 1999 and 2009, GWT data was collected from field which is available for the year 2009.

10.2 Study Area

10.2.1 Location of the Study Area

The population density of Bangalore is almost 20,000 people per km^2 and more than 8 million people staying under the greater Bangalore corporation. The geographical span area of Bangalore city is almost 713 m^2 which is situated at an altitude of 894 m (MSL). 12° 39′ N and 13° 18′ N latitude and 77° 22′ E and 77° 52′ E longitude (Fig. 10.1) where Bangalore is situated in between. Presently the city is facing water scarcity because of rapid increase of population due to industrialization and migration from rural Karnataka and rest of the country relatively in short time span.

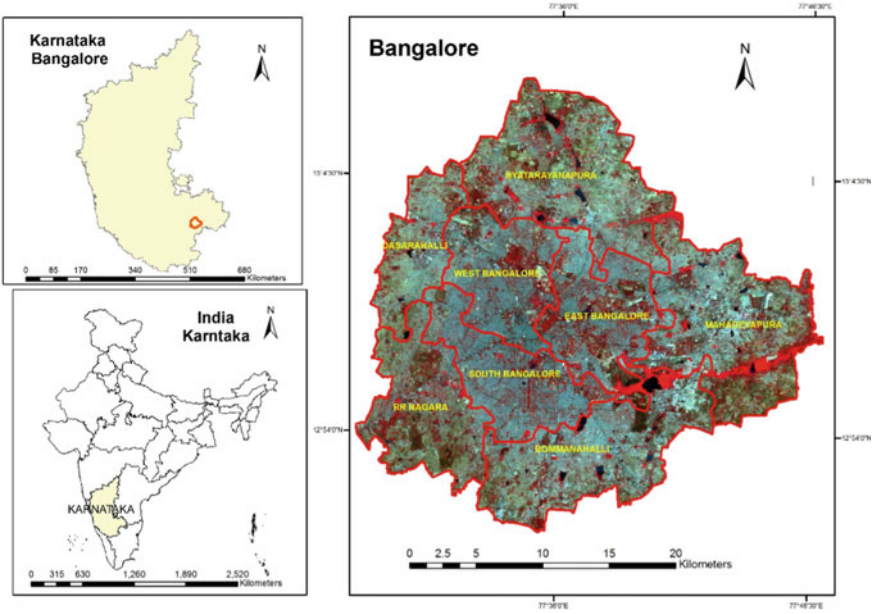

Fig. 10.1 Showing study area Bangalore, India

10.2.2 Rainfall in the Study Area

Bangalore city experiences both SW and NE monsoon rainfall. However SW monsoons are prominent. The average rainfall is around 800–900 mm per year. As per meteorological department data (residual mass curve analysis of rainfall data) from 1901, the average rain tend to be rising in the first two decades and fell in the consequent years up to 1950, thereafter a rise occurred in 1980s and, presently it is on rise.

10.2.3 Geological and Hydrological Settings of the Study Area

The aquifer setup, geography and chronological behavior of groundwater level are the major points to understand the hydrological setup. The essential for the peninsular granitic complex pattern which is mainly Precambrian Granite and Gneiss of the Indian Precambrian Shield are founded surrounding terrains of Bangalore district. Migmatite and gneiss are prevailing, however there is a zone of granite and granodiorite exactly 20 km wide moving in a north–north-west bearing over the far western part of the area.

Minor regions of charnockite happen in the far south western aspect of the area, and there are some little extended assemblages of amphibolite's. Central part we mostly found the trend of schist aligned along a north south. Several dolerite dykes to the north, west and southwest are observed in Bangalore city according to the Geological and Mineral map of Karnataka and Goa. The dominant strike direction we found in northeast and smaller structure of strike we found in easterly side. The dimensions of the dykes are indicated by Hunse and Farooqi (1995) in a report on groundwater of Bangalore Urban District. They additionally allude to lineaments, obviously connected with cracking (or potentially the dolerite dykes), with a grouping of strike in a north-upper east arrangement, and with a length going from 5 to 30 km.

10.3 Material and Method

The surface temperature was assessed utilizing Landsat TM-5 datasets over various Land use (LU)/Land Cover (LC) of Bangalore territory more than 10 years of time span. On other side Ground water temperature data was collected from field work in 2009 (Table 10.1, Fig. 10.2).

10.3.1 Methodology

To remove geometric and atmospheric error geometric correction and atmospheric FLAASH correction was applied over all Landsat satellite images. Landsat image of 1999 and 2009 datasets are used to achieve land use (LU) and landcover (LC) classification. LU/LC are classified in four classes like vegetation, built-up, waterbody and others. NDVI, surface emissivity and surface temperature all these biophysical parameters are retrieved from these data sets. On the other hand ground water temperatures are collected from different wells. 77 wells GWT data are collected from field which was collected during field visit. GWT and LST, considering in same scale for that we use geostatistical tool in ArcGIS. GWT are interpolated using IDW technique under Geostatistical tool in Arc GIS.

Here 1999 and 2009 summer (March) (April) data is used to estimate surface temperature over various land use/land cover. Radiance was calculated over visible and near infrared bands after pre-processing and subsets over Landsat-5 images. Value is needed to derive at pixel level to get effective results in surface temperature and surface emissivity. Emissivity was mostly observed uniform in the spectral range

Table 10.1 Data used for GWT and LST

Dataset used	Year (1999)	Year (2009)
	Landsat TM-5	Landsat TM-5
		Ground water temperature

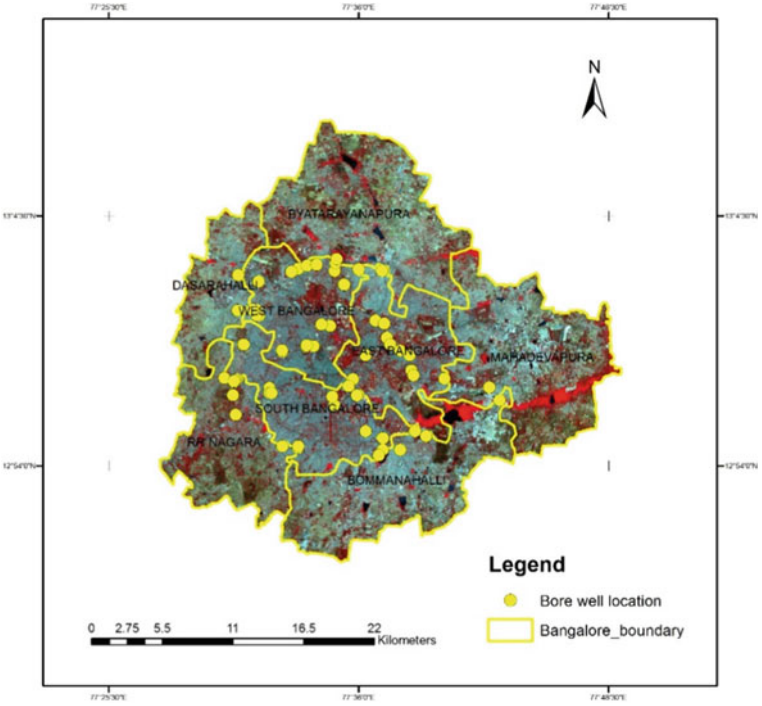

Fig. 10.2 Showing borehole location GWT collected in area of Bangalore, India

between 8 and 14 μm. To estimate pixel base emissivity the proportion of vegetation cover in conjunction with NDVI was taken care.

$$\varepsilon = \mathrm{a} + \mathrm{b} * \ln(\mathrm{NDVI}) \tag{10.1}$$

where a = 1.0094 and b = 0.047 where, NDVI $= \frac{(\rho_{NIR} - \rho_{Red})}{(\rho_{NIR} + \rho_{Red})}$ p = reflectance

Thermal band 6 in Landsat TM imagery is used to estimate spectral radiance which is mentioned above (NASA 2004). This is the viable at-satellite temperatures of the saw Earth-atmosphere framework under a suspicion of solidarity emissivity and utilizing pre-launch alignment constants (Mansor and Cracknell 1994). The conversion of digital number of thermal bands into spectral radiance are mainly followed by Landsat user's handbook (Mansor and Cracknell 1994). Temperature is estimated as,

$$\mathrm{T} = \frac{K_2}{\ln\left(\frac{\varepsilon K_1}{\mathrm{L}_\lambda}\right) + 1} \tag{10.2}$$

where $K_1 = 607.76$ mWcm^{-2}sr^{-1} μm^{-1}, $K_2 = 1260.56$ K 2, L_λ = radiance, ε = emissivity.

After estimated LST we use Arc GIS to extract same place LST value where GWT data is available. Then we use geostatistical tool in ArcGIS to interpolate LST using IDW Geostatistical tool.

Increased job opportunity in cities is the main cause of increase in population density which effected on the expansion of building area. The impermeable land in urban area increases like roads, buildings, sewer tunnels. This change has an impact on physical geographic environment of cities which is main cause of the Urban Heat Island Effect.

To understand the urban built-up land use class, Normalized Difference Built-Up Index is a good indicator. Unique spectral response of built-up lands that have higher reflectance in MIR wavelength range than in NIR wavelength range based on this principle this index developed. Using reflectance value from MIT and NIR bands of the satellite image NDBI was calculated. NDBI is given as

$$\text{NDBI} = (\text{MIR - NIR})/(\text{MIR} + \text{NIR}) \tag{10.3}$$

where MIR is represented as middle infra-red band and NIR is represented as near infra-red band.

For the LANDSAT TM Imagery the TM5 (MIR) and TM4 (NIR) bands are used for estimating the NDBI.

But NDBI has some disadvantages. Barren land and low-density vegetation area, both of these two kinds of land also reflect as an urban built-up area in results. So as to upgrade the consequence of urban built-up areas extraction (Liu et al. 2018) BUAI was assessed.

$$\text{BUAI (Built Up Area Index)} = \text{NDBI - NDVI} \tag{10.4}$$

In NDVI non-vegetated area is mainly occupied with built-up land, barren land and waterbodies. Here in this methodology we used BUAI to enhance our results over urban built-up area.

10.3.2 Results and Discussion

The LU/LC classification for LANDSAT TM Datasets for 1999 and 2009 was carried out by taking four classes namely Built-Up, Vegetation, Water bodies and others. The datasets was classifying using the supervised Classification-maximum likelihood method. In first steps training sets are created on the basis of ground truth and spectral signature then classified it into four classes. An overall accuracy of 88.74% (Kappa Coefficient: 0.8480) for Feb 1999 datasets and 87.15% (Kappa Coefficient: 0.8275) for Jan 2009 datasets was obtained during the accuracy assessment. The

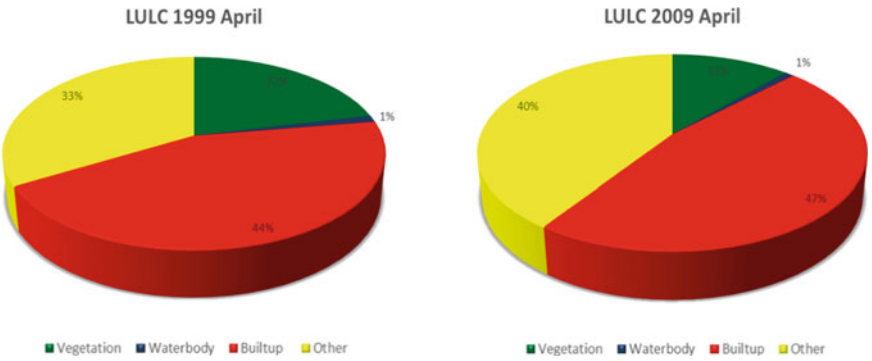

Fig. 10.3 Showing LU/LC statistic of 1999 and 2009

classified map of LU/LC of Bangalore Urban District for 1999 and for 2009 is shown in (Fig. 10.4). The LU/LC maps show different LU/LC classes such as Built-up, Vegetation, Water bodies' agriculture and dry/other open lands. The maps also delineate the greater Bangalore region from the outskirts.

We can observe from the (Fig. 10.3) that the built class are increasing in last 10 years from 44 to 47%. Due to emerging electronics city in the Anekal taluk south eastern region of Bangalore showing more expansion in built-up. In northern part built-up expansion is toward the New International Airport at Dvanahalli in Bangalore Rural district which is very near to Bangalore North Taluk. The built-up extension toward Bangalore East is credited due to the development of the ITPL in Whitefield in the Bangalore East Taluk. The built-up extension toward Bangalore West is because of the settlements coming near the Peenya Industrial Area and also the increase in the number of industries in that region. According to census urban population in Bangalore has increased by 46.86% and population density to have increased from 2985 per km^2 in 2001 to 4378 per km^2 in 2011 are the major causes behind urban expansion.

The increase in the Built-up and other land use class but a decrease in the Vegetation and Water body's classes can be clearly appreciated in the Fig. 10.3. These figures show the percentage wise distribution of the area of different LU/LC classes of Feb 1999 and Jan 2009 respectively. The increasing urbanization and industrialization may be attributed as the reasons for the loss of vegetation and water bodies. Figure 10.4 shows the LU/LC classification of the year 1999 and 2009.

Here LST values were retrieved from the emissivity and radiance value for both the Landsat TM datasets of April 1999 and 2009. The LST maps of April 1999 and 2009 have been shown in Fig. 10.5. In both the images of LST 1999 and 2009 showing significant increase in surface temperature of over Bangalore urban district, the LST maps indicate a surprising higher Land Surface Temperature in the outskirts compared to the Greater Bangalore Region for both the temporal data. This is a fact that there are more urban green space and water bodies and wetlands in the heart of the city which keeps the city cooler compared to the outskirts.

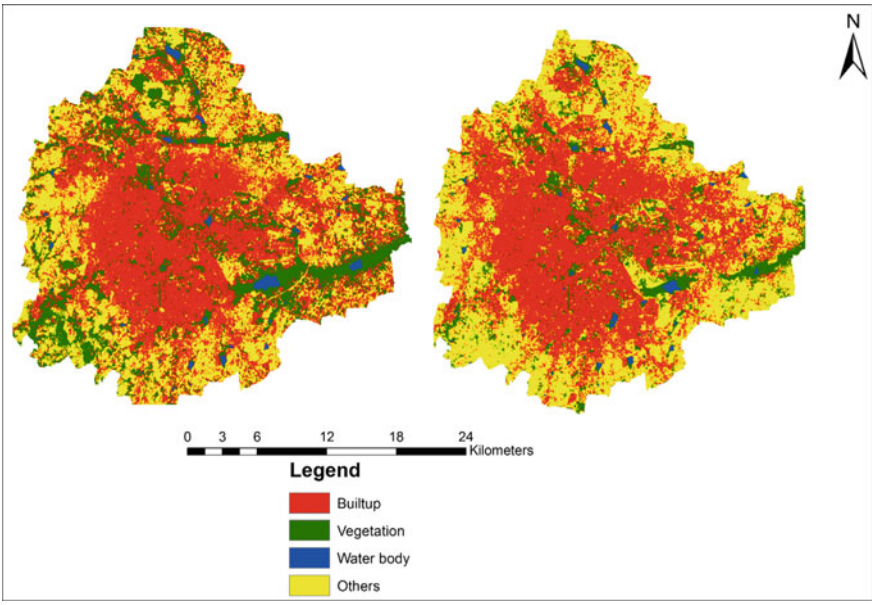

Fig. 10.4 Showing LU/LC of Bangalore 1999 and 2009

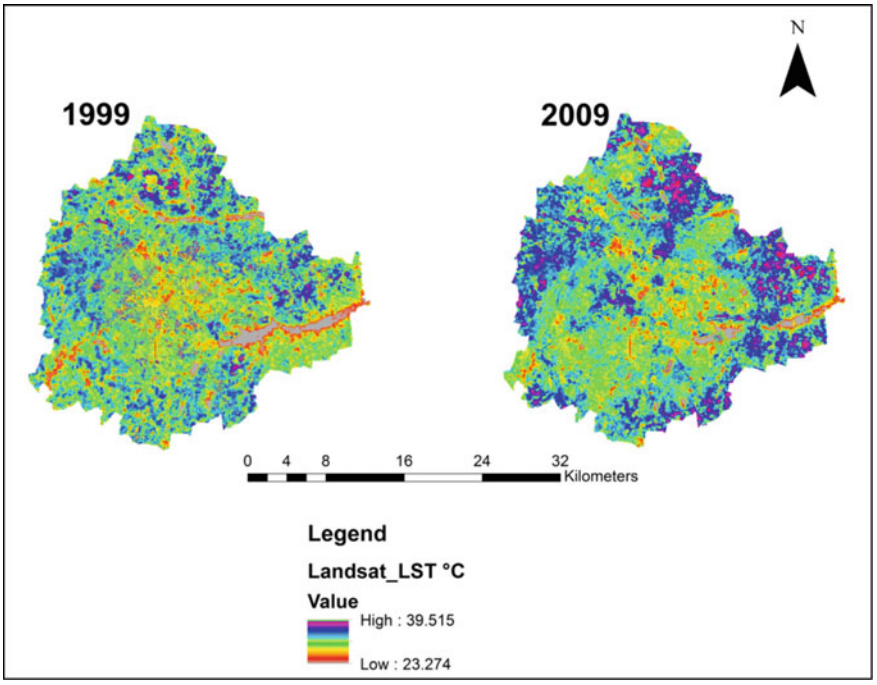

Fig. 10.5 Showing Land surface Temperature of Bangalore 1999 and 2009

Outskirts have more vacant lands, mining activities and urban agglomeration affecting on the loss of vegetation. From the study of Abinakudige (2011) we observed similar condition of lower LST value in the heart of the city compared to the outskirts.

Ground Water Temperature (GWT) and Land Surface Temperature (LST) over Bangalore city affected by LU/LC change are also focused in this study. A map of GWT and LST are created using ArcGIS Geostatistical tool for fair comparison. To understand the relationship between GWT and LST, Correlation coefficient are performed. Even relationship between GWT and LST of the different land use land cover has been studied here.

From the Fig. 10.6 we observed that in the 2009 showing that wherever LST is high in the same place GWT is also showing high. We observed that north western part of western Bangalore and southern part of Bayataranpura showing high LST and high GWT in 2009 images. As in this area urbanization is higher than city inside because inside city parks and gardens makes city cooler than outside. In 2009 southern part of Bangalore which is the near boundary of Bomanahalli and Mahadevapura temperature is showing high in both LST and GWT because of rapid urbanization effect.

From the Fig. 10.7 it was proved that there is very strong correlation between LST and GWT. In the year 2009 we observed positive correlation between GWT and LST. R^2 value is 0.8338 in 2009 which is showing very high. As we have already seen that in (Chakraborty et al. 2015) paper on Delhi that urbanization has impact on LST. We

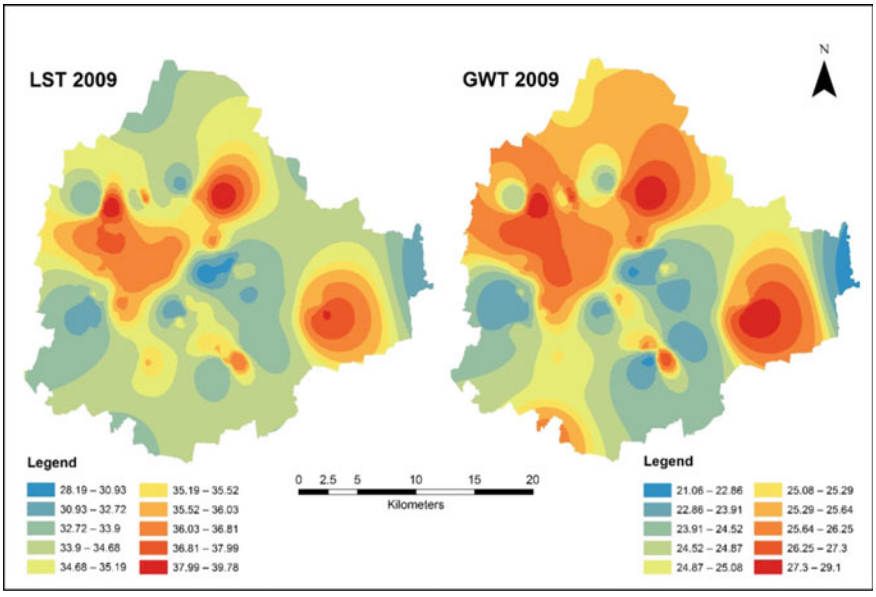

Fig. 10.6 Showing LST and GWT of Bangalore 2009

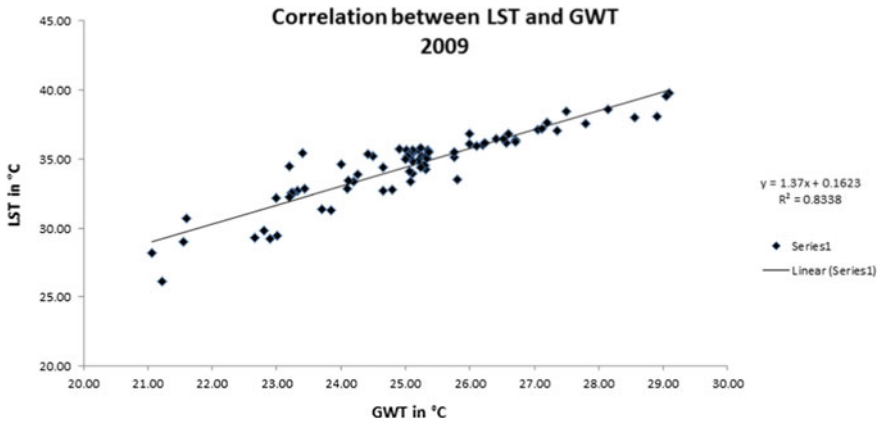

Fig. 10.7 Showing correlation between LST and GWT of Bangalore 2009

Table 10.2 LU/LC comparison with GWT and LST 2009

Land use/Land cover	Ground water temperature 2009	Land surface temperature 2009
Built up	27.20	37.61
Open land	29.05	39.57
Fallow land	23.20	34.44
Shrub land/parks/forest	21.20	29.37
Water body	21.06	28.19

can establish relationship with LST and GWT which proved that urbanization has also effect on GWT (Table 10.2).

Here we try to find out how built-up area is affecting over LST and GWT. For that we calculate NDBI to focus on built-up area. Here we observed that last 10 years huge population boom inside Bangalore city which was going to effect on LU/LC change. This increased population density is the main cause of increasing built-up area in Bangalore. We found strong indication increasing built-up from satellite derive LU/LC and NDBI from both 1999 and 2009 images. NDBI has some disadvantages if we purely are using it. Our idea is to focus on urban built-up areas extraction and for that to enhance our result we used BUAI. We found very positive correlation between BUAI with LST and GWT.

Last 10 years Bangalore showed huge change in built-up area which mainly affected over LST and GWT. From the Figs. 10.8 and 10.9 we mainly estimated NDBI and BUAI (Built-up area index) of the year 1999 and 2009. We consider BUAI is better indicator than NDBI. Here we observed south eastern part of Bangalore near Bellendur, Kadabeesanahalli and Marathahalli village (red marked in Figs. 10.8 and 10.9), this area near to HAL airport we found huge changes in BUAI due to high

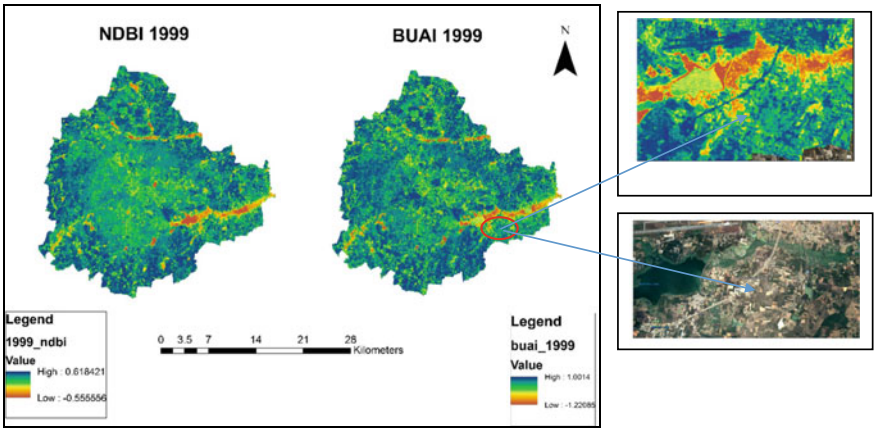

Fig. 10.8 Showing NDBI and BUAI of Bangalore 1999

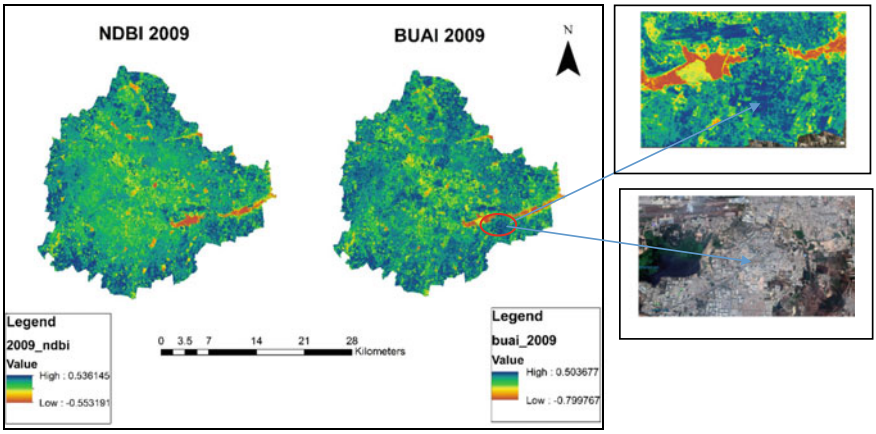

Fig. 10.9 Showing NDBI and BUAI of Bangalore 2009

construction of built-up area. Due to high construction of built-up area in last 10 years also affected in high LST and GWT value.

A sample point method using 50 randomly selected points were used to understand the connection between LST and GWT to NDBI and BUAI derived from Landsat TM-5 1999, 2009 respectively. Here GWT is only concentrated over year 2009 as availability of data sets, which was collected by ground survey. Good positive correlation found between LST, GWT and BUAI is clearly understood from the three transect lines in Figs. 10.10 and 10.11. It was observed from results that BUAI detected high same scenario were found over LST and GWT. The correlation

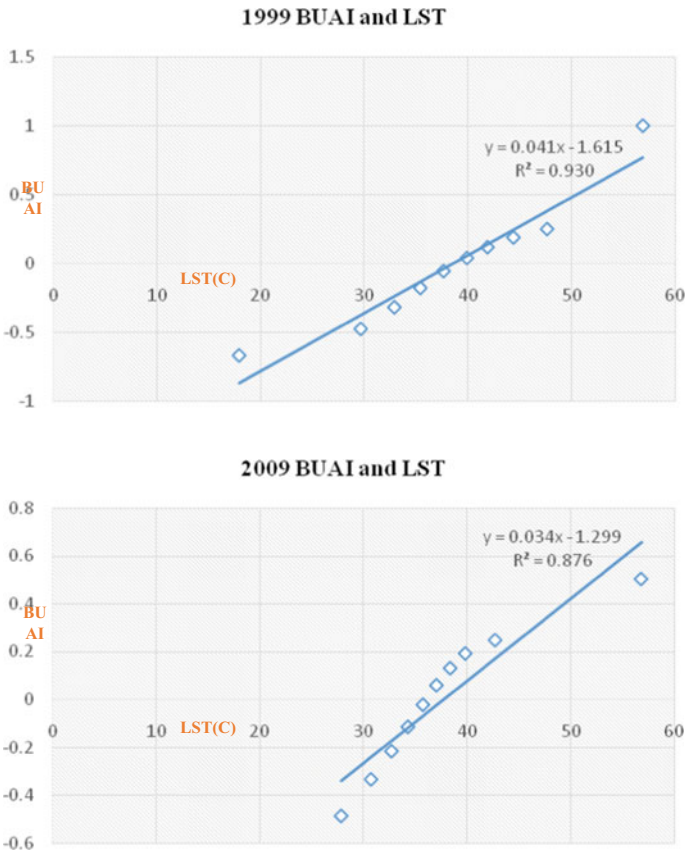

Fig. 10.10 Showing correlation between BUAI and LST of Bangalore 1999 and2009

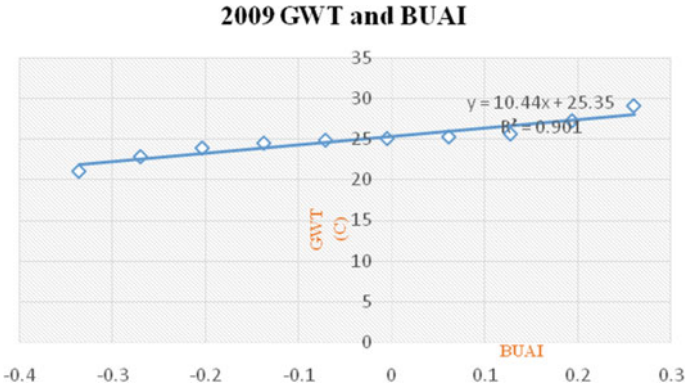

Fig. 10.11 Showing correlation between GWT and BUAI of Bangalore 1999 and2009

coefficient of $R^2 = 0.9305$, $R^2 = 0.8765$, between BUAI (Built-up area index) and LST (land surface temperature) over the year 1999 and 2009 showed very positive relationship. Correlation coefficient of $R2 = 0.9018$ over 2009 found between BUAI and GWT which detected as positive correlation in results.

10.4 Conclusions

In this study multi-temporal remote sensing data are used to understand land/use and land cover changes as well as surface temperature changes and investigate the relationship with GWT in Bangalore city. Rapid changes in land use classes like built-up has an impact over LST and GWT, this study was attempted to understand that. This study is considering four classes, those are built-up, vegetation, water body and others. If we see the result, then we observed that built-up area is increased by 44–47% in last 10 years. Here we found there is strong relationship between NBDI and BUAI with LST which proved that this increased built-up has affected on increasing LST value. The similar trend we found over GWT. We can take that GWT is a good indicator for urban heat island study. We observed that built-up area is showing higher LST in both the years 1999 and 2009. We also observed that under built-up area GWT is showing higher value than non-built up area. We also observed that Bangalore city expanding its boundary mainly outskirt area of the city removing the vegetation area and converting in built-up area less vegetated area mostly concrete area found with higher LST and GWT value. Even we found very strong positive relationship between NDBI, BUAI and LST. So, this study gives us a basic understanding how huge construction in Bangalore city is affecting on LST and GWT value. In the last 10 years Bangalore city lost its parks, gardens and lakes. It is understandable from this study that for mitigating Urban Heat Island effect city parks and lakes are taking major role. So, it is important to protect existing country parks and lakes to mitigate urban heat gradually in a long term. Bangalore city authority should focus more to protect its parks and lakes which will mitigate its temperature. City also take adoption of green building project more. Instead of using thermal power city should move toward sustainable energy consumption like sun energy. It's also focused to clean its lake from pollution. Electric vehicles should be encouraged more inside the city.

References

Carlson TN (1986) Regional-scale estimates of surface moisture availability and thermal inertia using remote thermal measurements. Remote Sens Rev 1:197–247

Cheon JY, Ham BS, Lee JY, Park Y, Lee KK (2014) Soil temperatures in four metropolitan cities of Korea from 1960 to 2010: implications for climate change and urban heat. Environ Earth Sci 71(12):5215−5230

Chakraborty SD, Kant Y, Mitra D (2015) Assessment of land surface temperature and heat fluxes over Delhi using remote sensing data. J Environ Manage 143−152

Ferguson G, Woodbury AD (2007) Urban heat island in the subsurface. Geophys Res Lett 34(23):L23713

Huang S, Taniguchi M, Yamano M, Wang CH (2009) Detecting urbanization effects on surface and subsurface thermal environment–a case study of Osaka. Sci Total Environ 407(9):3142–3152

Hunse TM, Farooqi MA (1995) Groundwater development perspective in Bangalore District, Karnataka. Central Groundwater Board, South west Region Technical Report, Series D

Mansor SB, Cracknell AP (1994) Monitoring of coal fire using thermal infrared data. Int J Remote Sens 15(8):1675–1685

Menberg K, Blum P, Kurylyk BL, Bayer P (2014) Observed groundwater temperature response to recent climate change. Hydrol Earth Syst Sci 18(11):4453–4466

NASA, Landsat Project Science Office (2004) Landsat 7 Science data users hand book, Chapter: 11, Data products. http://www.gsfc.nasa.gov/IAS/handbook/handbook_htmls

Peng S, Piao S, Ciais P, Friedlingstein P, Ottle C, Bréon F-M, Nan H, Zhou L, Myneni RB (2012) Surface urban heat island across 419 global big cities. Environ Sci Technol 46(2):696–703

Pongracz R, Bartholy J, Dezso Z (2010) Application of remotely sensed thermal information to urban climatology of Central European cities. Phys Chem Earth 35(1–2):95–99

Zhan W, Ju W, Hai S, Ferguson G, Quan J, Tang C, Guo Z, Kong F (2014) Satellite-derived subsurface urban heat island. Environ Sci Technol 48(20):12134–12140

Chapter 11
Land Use Land Cover Change Detection and Its Impact on Land Surface Temperature of Malana Watershed Kullu, Himachal Pradesh, India

Shivani Parmar, Pawan Kumar Thakur, Monika Chauhan, and Renu Lata

Abstract Land Surface Temperature (LST) is an important phenomenon in global warming, forest fire, glacier melting, global environmental change, and human-environment exchanges. In the present study, an attempt has been made to quantitatively evaluate and detect the Land Use Land Cover (LULC) change analysis and the associated changes in the LST of Malana Watershed, in district Kullu, Himachal Pradesh of the Indian Himalayan Region (IHR). Due to various natural phenomena and anthropogenic activities. i.e., hydropower development and roads construction, the LULC pattern of the earth's surface is undergoing a fleeting change. To assess the LULC change pattern, satellite imageries were acquired for the years 2001 of Landsat-7 Enhanced Thematic Mapper Plus (ETM+), 2011 of Landsat-5 Thematic Mapper (TM), and 2017 of Resourcesat-2, Linear Imaging Self-Scanning Sensor (LISS -IV). The Supervised classification method using the Support Vector Machine (SVM) algorithm was applied in Environmental Visualization Imagine (ENVI) 5.3 and ERDAS Imagine 2015 and the study area was classified in total 8 LULC classes viz. glacier, water bodies, built-up, forest green, vegetation, agricultural land, barren land, open/rocky land. From 2001–2017, the results revealed that the study area has undergone a substantial increase and decrease in the LULC change pattern. Glaciers, forest green, and vegetation areas have declined from 2001 to 2017; for which the main causing factors include an increase in atmospheric temperature and anthropogenic activities. The current research study indicate that the area has witnessed a substantial increase and decrease in the LULC for different categories. There has been a considerable decrease in the glacier area from 39.19 km^2 (in 2001) to 32.97 km^2 (in 2017) and the area under Built-up/settlements categories has been increased from 0.1 km^2 (in 2001) to 0.14 km^2 (in 2017). For the estimation of LST, thermal bands of the Landsat series satellites were used with both mathematical algorithm such as Single Channel (SC) and Split Window (SW) algorithm.

S. Parmar · R. Lata
G. B. Pant National Institute of Himalayan Environment, Himachal Regional Centre, Mohal-Kullu, Himachal Pradesh 175 126, India

P. K. Thakur (✉) · M. Chauhan
Forest Ecology and Climate Change Division, Himalayan Forest Research Institute, Conifer Campus, Panthaghati, Shimla, Himachal Pradesh 171 013, India

R. B. Singh et al. (eds.), *Remote Sensing and Geographic Information Systems for Policy Decision Support*, Advances in Geographical and Environmental Sciences,
https://doi.org/10.1007/978-981-16-7731-1_11

Normalized Difference Vegetation Index (NDVI) was estimated for deriving Land Surface Emissivity (LSE). The spatial distribution of LST of Landsat-7 ETM+ (18th October 2001) ranged from minimum 263.54 Kelvin (K) to maximum of 292.23 K, Landsat-5 TM (22nd October 2011) ranged from minimum 265.13 K to maximum of 288.61 K and for Landsat-8 OLI, (06th October 2017) ranged from minimum 264.89 K to maximum of 294.75 K. A decrease in the glacial area attributes to an increase in the barren and open/rocky areas as reflected in the results. Built-Up and agricultural land witnessed an increase in the area owing to the developing tourism in Parbati valley and altitudinal expansion of the horticultural area. The area under water bodies also increased accounting for the variation in the flow of the river.

Keywords Land use land cover · Land surface temperature · Landsat-8 · SVM · Split window

11.1 Introduction

Land surface temperature (LST) is one of the most important parameters in the interaction from land surface to atmospheric interaction (Cristobal et al. 2008; Kuenzer and Dech 2013; Li et al. 2013a). The distribution of LST can provide useful information about the surface physical properties and climate which plays a role in the culmination of various attributes like the green cover, hydrological components, glacier melting, water stress, topography, soil, groundwater, and anthropogenic structures on the earth's land surface and immediate subsurface on the environmental studies (Lambin et al. 2003). The importance of LST in various scientific fields as mentioned earlier, LST acts as a governing parameter in water and energy exchange between land and atmosphere. Therefore, its application in studying the impacts of change in Land Use Land Cover (LULC) on surface temperature is of great importance in the context of climate change and in the era of development. The LULC is the purposive engagement of the land management approach put on the land cover by deliberate human expansion. Thus urban development strictly depends upon the LULC of that area. Mountain systems constitute a significant fraction of the continental area of about 20% and provide life support to 10% of the world's population. These systems typically display a rapid change in vegetation, hydrology, and climate in relatively small scales. Snow, glaciers, and permafrost in cold mountains are highly sensitive to climatic change and thus provide crucial information on climate change and its impacts on natural resources and the socio-economic condition of people.

Growing anthropogenic activities around the world are inducing large-scale modification of the Earth's land surface thus posing a profound impact on the functioning of global systems (Lambin et al. 2001). Changes in land cover patterns can directly affect energy and mass transitions. For illustration, when deforestation occurs, there is less cloud development due to less transpiration thus leading to less precipitation in turn affecting the whole water cycle further causing a considerable impact on the climate. One of the most visible human modifications of the terrestrial ecosystem

is the alteration of the LULC which significantly affects the local, regional and global environment (Mitsuda and Ito 2011; Mahmood et al. 2010; Weng 2001). The consequence can be seen in the form of soil degradation (Islam and Weil 2000), loss of biodiversity (de Koning et al. 2007), rampant urban sprawl (Jat et al. 2008; Martinuzzi et al. 2007; Yu and Ng 2007; Mundia and Aniya 2006; Sudhira et al. 2004), it was found that there is outstripped increase in built up area in Shimla City of Himachal Pradesh state in India, which is attributed to construction of new buildings on forest and vegetation lands (Thakur et al. 2020), land deterioration by the tourism industry and agricultural expansion (Shalaby and Tateishi 2007), prominent variation in biogeochemical and hydrological cycles (Foley et al. 2005; Meyer and Turner 1996; Ojima et al. 1994), changes in the global carbon cycle, increase in the concentration of atmospheric CO_2, and a gradual slump in ecosystem services together resulting in colossal and sometimes irreversible damage to the global environment (Lead, CO 2018).

These changes can extremely modify the prevailing conditions of the near-surface atmosphere over the cities by affecting the degree of absorption of solar radiation, albedo, surface temperature, evaporation rates, the transmission of heat to the soil, storage of heat, wind turbulence (Mallick et al. 2008), modify energy and water balance processes (Oke 2002). According to United Nations (2010); LST is likely to rise at a rapid rate exposing approximately 69% world's population by 2050 to this vulnerability. In a developing country like India, since urbanization is accelerating at a very high rate both in intensity and areal coverage area, the impact has also been increasing manifolds. With the emergence of geo-spatial techniques like Remote Sensing (RS) and Geographic Information System (GIS), LULC mapping and its analysis have become fairly easy. For better management of resources, RS and GIS tools were used in many studies to deduce the industrial, agricultural, and residential areas (Malczewski 2004; Rawat and Kumar 2015; Butt et al. 2015; Marina and Bogdan 2016). The remotely sensed data have been used to extract information from several image analyses and change detection techniques (Lu et al. 2004, 2011). GIS, on the other hand, enables the integration of information extracted from remote sensing for clear interpretation and modelling of LULC (Mesev and Walrath 2007).

LST is a parameter that plays an important role in the geophysical studies (Quattrochi and Luvall 1999; Kalma et al. 2008; Kustas and Anderson 2009; Weng et al. 2004; Feizizadeh and Blaschke 2012; Mallick 2014; Song et al. 2015). It provides the temperature of a surface, and its help in studies related to hydrological cycle, global warming, LULC change, land-surface interaction from surface to atmosphere and associated temperature changes, soil moisture, vegetation water stress etc. (Thakur and Gosavi, 2018). A rise in LST, can lead to an imbalance in the environmental conditions such as the melting of snow, receding glacier, change in the rainfall pattern, and changes in the vegetation of land surface and climatic conditions. In polar regions, the melting of glaciers and ice sheets can result in flooding and a rise in sea level. In monsoon countries, an increase in the LST can lead to uncertain rainfall. It also affects the vegetation of the whole earth's surface thus causing a considerable change in the LULC pattern over the years. The local climate of an area evolves with the natural and anthropogenic activities change occurring in that area thus changing the LULC

of an area. Therefore, it gets important to develop an appropriate algorithm for the precise estimation of LST (Rongali et al., 2018). An estimation of LST will thus help to address a lot of integrative issues in earth sciences, climatology, environmental sciences, global climate change, glaciology, hydrology, etc. Since high-resolution satellite data is available conveniently, remote sensing techniques may prove to be a preferred substitute to conventional methods (Owen et al. 1998).

Landsat 5 TM sensor and Landsat 7 ETM+ sensor embedded on the satellite provided thermal data using just one Long Wave Infrared (LWIR) band with a higher spatial resolution (Nikam et al. 2016). Initially, a SC algorithm was developed to derive LST (Qin et al. 2001; Jimenez-Munoz and Sobrino 2003; Sobrino et al. 2004; Jimenez-Munoz et al. 2009). Along with remote sensing data, this method also requires atmospheric parameters which can only be retrieved through complex atmospheric transmittance/radiance codes (Li et al. 2013b) to be involved in the Radiative Transfer Equation (RTE). It is due to this reason that the applicability of this method is restrained (Jimenez-Munoz and Sobrino 2006). To overcome this restrain and to improve the accuracy of LST retrieved from remote sensing data, Sobrino et al. (1993) developed an algorithm, which employs two thermal bands typically located in the atmospheric window between 10 and 12 μm popularly known as SW algorithm. Further, the SW algorithm does not require accurate atmospheric profiles and the algorithm is suitable for various sensors with no less than two Thermal Infrared (TIR) channels within the atmospheric window. However, this algorithm requires a prior knowledge of the pixel emissivity in each TIR channel. The premise of SW algorithm is that the radiance attenuation for atmospheric absorption is proportional to the radiance difference of simultaneous measurements at two different wavelengths, each subjected to different amounts of atmospheric absorption (Jimenez-Munoz and Sobrino 2008).

The main disadvantage of this algorithm are that it can lead to variation in performance and corrupt the accuracy in the presence of high total column Water Vapour (WV) or at large viewing zenith angles (McMillin 1975; Becker and Li 1990; Sobrino et al. 1994; Wan et al. 1996). Keeping in view the importance of the LST and available data products/platforms for retrieving the LST, present study was conducted in Malana watershed, Kullu district, in Himachal Pradesh of IHR. A change in LST over different LULC categories is derived from Landsat-7 ETM+ for October 2001 and Landsat-5 TM for October 2011 were used SC algorithms and Landsat-8 OLI (Operational Land Imager) for October 2017 was used SW algorithm.

11.2 Study Area

According to the Census of India 2011 the total population of 1722 of which 888 are males while 834 are females, Malana is a medium size village and the oldest democratic culture, located in the North-East of Kullu district, Himachal Pradesh. Considered as one of the ancient villages in Kullu district it is popularly known as the Republic of Malana. It is about 130 km long narrow valley, situated

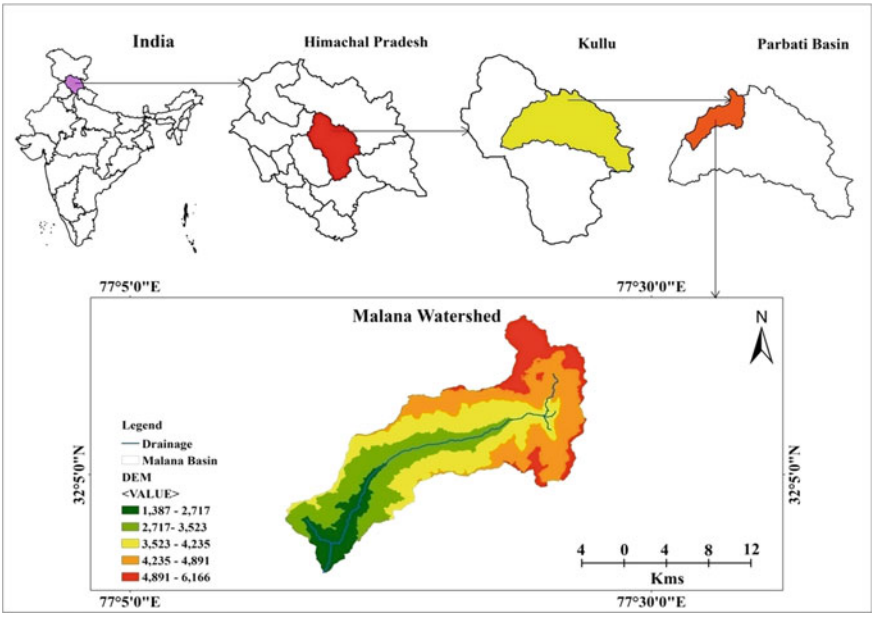

Fig. 11.1 Location map of the study area

between latitudes 32°0′6.666″ to 32°12′54.533″ N and Longitudes 77°14′18.423″ to 77°23′53.627″ E between the elevation of 1387–6166 meters (m) Above Mean Sea Level (amsl) shown in Fig. 11.1. The climate in Malana is warm and temperate with an average temperature being 11.5 °C and average rainfall being 1622 mm. Winters witness much less rainfall than summers. The Malana Glacier is at the headwaters of the Malana River which feeds the Malana Hydropower Plant 108 MW that lacks a significant reservoir. The Malana River then flows into the Parbati River.

11.3 Materials and Methods

11.3.1 Method for LULC Classification

11.3.1.1 Specifications of the Data Used

LULC dynamics were analyzed using the following data given in Table 11.1.

Table 11.1 Specification of the data used in the present study

Satellite	Sensor	Path/Row	Resolution (m)	No. of bands	Map projection and datum	Date of acquisition and acquired from	Remarks
Landsat-7	Enhanced thematic mapper plus (ETM+)	WRS-II/147/38	30 m	2, 3, 4, 5 and TIR band 6	Universal Transverse Mercator (UTM), World Geodetic System 1984 Datum (WGS 1984)	18–10-2001 USGS website	TIR bands for LST retrieval and other bands for LULC change detection
Landsat-5	Thematic mapper (TM)	WRS-II/147/38	30 m	2, 3, 4, 5 and TIR band 6	UTM, WGS (1984)	22–10-2011 USGS website	TIR bands for LST retrieval and other bands for LULC change detection
Resourcesat-2	Linear imaging self -scanning sensor (LISS IV)	95/48	5.8 m	3	UTM, WGS (1984)	31–10-2017 National Remote Sensing Centre (NRSC), Hyderabad	Green, Red, and NIR bands for LULC change detection
Landsat-8	Operational land imager (OLI)	WRS-II/146/40	30 m	2, 3, 4, 5, 6, 7 and TIR bands 10 and 11	UTM, WGS (1984)	06–10-2017 USGS website	TIR band for LST retrieval

11.3.1.2 Geometric and Radiometric Correction

For minimizing the influence of seasonal variation, all three images were selected from the same season. Images of October month were chosen since during this period the ice and snow cover is minimum and the area is relatively cloud-free which facilitates clear visibility of various geomorphologic and surface features thus helping in identifying and demarcating boundaries and calculating the corresponding areas. Since the raw satellite data contains geometric distortions it is imperative to rectify them for correct measurement of area, precise localization and, integration of multi-source (Zhang and Zhang 2007). The error-free images are obtained after being corrected radiometrically (noise reduction, haze reduction, histogram matching) and geometrically to Universal Transverse Mercator (UTM) coordinate system (Kumar and Anbalagan 2016). For land-use change detection the proper geo-rectification is essential and the accuracy of geo-rectification should be within 1–2.5 Pixels (Zhang and Zhang 2007). False Color Composite (FCC) images are then created for 2001, 2011, 2017 of the study area for better interpretation and classification.

11.3.1.3 Study Area Extraction

After the required rectification, the Landsat images are layer stacked (in ERDAS Imagine 2015) to create a multi-band attribute image, where each band represents a different attribute. The LISS—IV image is mosaicked (in ERDAS Imagine 2015). The study area is then extracted by using an Area of Interest (AOI) file derived from a vector dataset of the study area's boundary. The subset images are then re-projected using the data management tool (in ArcGIS 10.5). All the images are then co-registered to the UTM (WGS 1984, Zone 43 N) Projected Coordinate System (PCS). The methodology of the LULC process is shown in Fig. 11.2.

11.3.1.4 Image Classification

The images are then classified to create LULC maps using Supervised Classification in ERDAS Imagine 2020 with the help of SVM algorithm in ENVI Classic 5.3. SVM minimizes the classification error on unseen data without foregoing assumptions made on the probability distribution of the data (Mantero et al. 2005). The classification categories are followed by Bhuvan Geoportal prepared by the Indian Space Research Organization (ISRO) which is an established geoportal restricted to Indian topography. For each of the predetermined LULC categories (Table 11.2), training samples were selected by establishing polygons around representative sites. Spectral signatures were obtained for specific land cover types from the satellite imagery, which were recorded by using the pixels enclosed by these polygons. A satisfactory and acceptable spectral signature is the one ensuring "minimal confusion" among the different categories of the land covers to be mapped (Gao and Liu 2010). The major challenge while classifying the satellite images using the

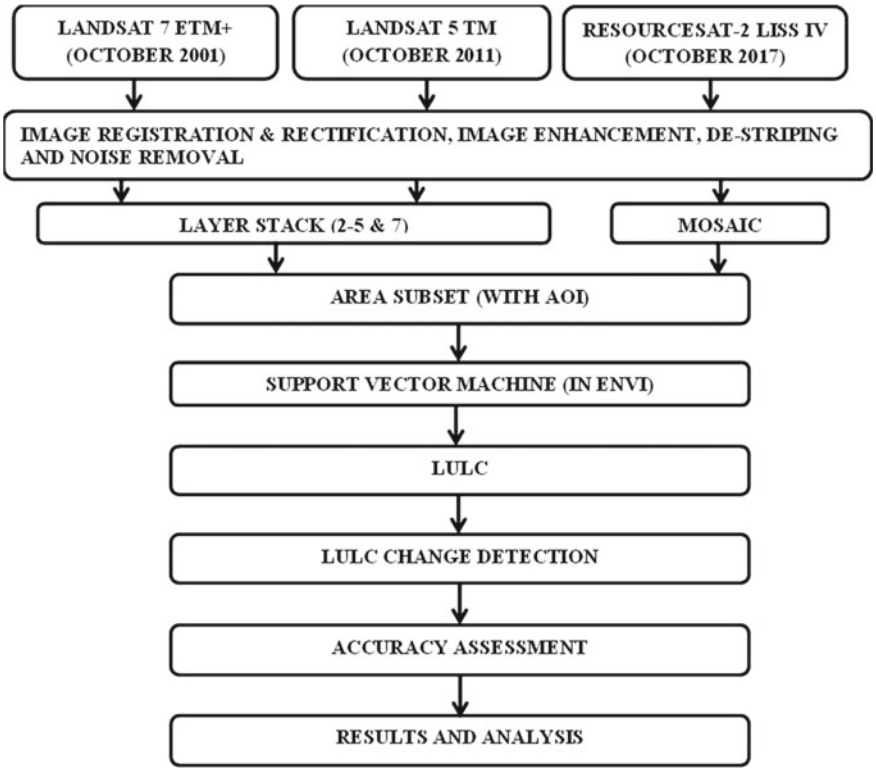

Fig. 11.2 Flowchart of the LULC analysis

Table 11.2 Description of LULC Classes

LULC categories	Description
Glacier/snow	Snow/glacier—covered area, glacial lakes, debris glacier
Waterbodies	Rivers, lakes, reservoirs, streams etc
Forest green	Dense green forest (coniferous forest)
Vegetation	Sparse vegetation, grasslands, scrublands
Agriculture/scrubland/grassland	Cropped area, fallow land, and plantations (apple, pear, pomegranate)
Built-up/settlements	Human habitation area (Residential, commercial, developmental)
Barren land	Uncultivated area,
Open/rocky land	Exposed areas, open land rocky with no vegetation

SVM method is to select the most suitable kernel function type (Radial Basis Function—RBF, Linear, Polynomial, or Sigmoid) and its parameters, which affects the performance of SVM. The commonly used kernel is RBF and polynomial, in the literature for the remotely sensed image classification (Pal and Mather 2005). The SVMs need user-defined parameters that influence the kernels function performance. Hence, the classification accuracy of SVMs depends upon the choice of the parameters and kernels (Ustuner et al. 2005). For improving the classification accuracy, reduction of misclassifications, and detecting the changes in ERDAS Imagine 2015 post-classification comparison technique was used (Mengistu and Salami 2007). The misclassified pixels were rectified using the recode techniques/option available in the software ERDAS Imagine 2015 for doubtful areas.

11.3.1.5 Accuracy Assessment

A stratified random method was used to represent different land cover classes of the area to carry out an accuracy assessment of land cover maps extracted from satellite images.

Generally, classification accuracy refers to the comparison of two datasets, one being the results obtained by the analysis of remotely sensed data and the second based on the reference information, referred to as "ground truth" (Congalton 1991). For this accuracy assessment, 350 pixels (50 per category) were first generated using a stratified random sampling scheme for each of the three LULC maps. A cross—tabulation was performed between the class values and the ground truth with the results being presented as an error matrix. The Producer's accuracy weighs the omissions errors, which relates the authentic rightly classified pixels in a category with the number of pixels classified in the same category during the training step. User's accuracy designates the probability of some classified pixels inconsonant with the same category in the reference data, relating the authentic right classification pixels in a category with the same group of pixels classified on the actual classification (Congalton 1991). They are obtained using the following formula.

$$\text{Producer's accuracy } (\%) \;=\; 100\% \text{ error of omission/lapse}$$

$$\text{User's accuracy } (\%) \;=\; 100\% \text{ error of commission/inadvertence}$$

A nonparametric kappa test was used to determine the classification accuracy as it accounts for all the elements in the error matrix rather than just the diagonal elements (Rosenfield and Fitzpatirck-Lins 1986). The overall accuracy for 2001, 2011, and 2017 was computed respectively (Table 11.10). A change matrix (Weng 2001) is also produced in ERDAS Imagine 2013 software. Furthermore, both overall kappa (accompanied by its variance) and class estimated kappa coefficients were also evaluated.

The value of Kappa can range from −1 to +1, where +1 amount to complete agreement between the two data sets and <1 amount to less than perfect agreement. Negative values are bogus and occurs rarely. Kappa statistic (Cohen, 1960) provides better interclass discrimination than overall accuracy (Foody, 1992; Ma and Redmond, 1995). The calculation of Kappa statistic K is as follows (Eq. 11.1):

$$K = \frac{\text{Total sum of correct} - \text{sum of all the (row total column total)}}{\text{Total squared} - \text{sum of the all the (row total column total)}} \quad (11.1)$$

We rarely get a perfect agreement. A good level of agreement is elucidated in different ways by separate people. Monserud and Leemans (1992) suggested that values < 0.4 amount to poor or very poor agreement, values from 0.4 to 0.55 amount to a fair agreement, values from 0.55 to 0.7 amounts to good agreement, values from 0.7 to 0.85 amount to very good agreement, and values higher than 0.85 amount to excellent agreement between images.

11.3.2 LST Extraction from Thermal Band

The present study employs the SC algorithm to estimate Top of Atmospheric (TOA) Spectral Radiance of TIRS Band 6 for Landsat TM and Landsat ETM + sensor of bands 2–5 and SW algorithm to obtain LST using Landsat 8 TIRS data (10 and 11 bands). In conjunction with TIRS, data from OLI are also required for the extraction of LST. Firstly, Landsat 8 OLI sensor bands 2, 3, 4, and 5 are layer stacked, and by employing bands 4 and 5 the NDVI image is developed. Using the NDVI image, Fractional Vegetation Cover (FVC) is calculated by taking the fraction of the area covered by the vegetation, and the FVC image is developed. The FVC image is then used to generate the land surface emissivity (LSE) image. LSE is an important surface property that indicates the material composition of the earth, especially for the silicate minerals, despite it varying with viewing angle and surface coarseness (Sobrino et al. 2001, 2005). The estimation of LSE requires the emissivity of the soil and vegetation for bands 10 and 11. The LSE images of bands 10 and 11 are obtained individually. Secondly, Landsat 8 has two TIRS bands. The TB is approximated for bands 10 and 11. The thermal digital number (DN) values of raw thermal bands 10 and 11 of TIRS are converted into the TOA spectral radiance after employing the thermal calibration process. Lastly, SW coefficient values and TB is used for LST estimation. The flowchart of the proposed SW algorithm to estimate LST is shown in Fig. 11.3.

11.3.2.1 Normalized Difference Vegetation Index (NDVI) Estimation

To correlate surface temperature with the vegetation, NDVI is calculated using Landsat data and employing the formula (Townshend and Justice, 1986): given in

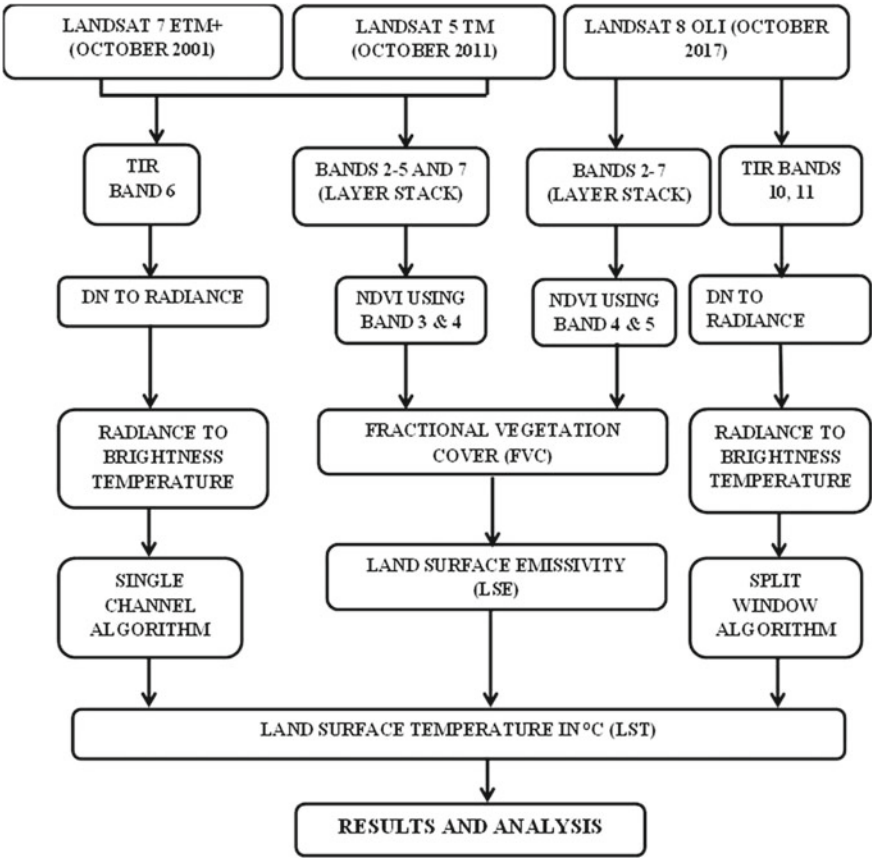

Fig. 11.3 Flowchart of the LST Retrieval

Eq. 11.2 by ERDAS IMAGINE 2020.

$$\mathbf{NDVI} = \frac{\mathbf{NIR} - \mathbf{Red}}{\mathbf{NIR} + \mathbf{Red}} \tag{11.2}$$

where, NIR means near—infrared band and R means red band. For Landsat TM and ETM + data bands 3 and 4; and for Landsat OLI, data bands 4 and 5 were used to calculate NDVI. It indicates the density of the green stretch of an area i.e. vegetation. The value of NDVI always results in a number that varies from (negative) −1 to (positive) +1. A zero means no vegetation; values from 0 to +1 indicate vegetation cover and the value close to 1 indicate a high density of vegetation.

The NDVI is approximated using OLI sensor optical bands (4 and 5), ETM+ and TM optical bands (3 and 4) from the composite of bands (2, 3, 4 and 5) using the formula given in Eq. 11.2.

$$\text{For Landsat 8 (OLI), NDVI} = \frac{\text{Band 5} - \text{Band 4}}{\text{Band 5} + \text{Band 4}} \tag{11.3}$$

$$\text{For Landsat 7 (ETM+) and Landsat 5 (TM),} \quad \text{NDVI} = \frac{\text{Band 4} - \text{Band 3}}{\text{Band 4} + \text{Band 3}} \tag{11.4}$$

It ranges from $-1 < \text{NDVI} < +1$.

11.3.3 Thermal Calibration and Generation of FVC Image

The NDVI image is reclassified into soil and vegetation, and their separate values are calculated using ArcGIS 10.5. The FVC is calculated using Eq. 11.5, and the FVC image is developed. The SW algorithm then uses this FVC image to develop the LSE image.

$$\text{FVC} = \frac{\text{NDVI} - \text{NDVI soil}}{\text{NDVI vegetation} - \text{NDVI soil}} \tag{11.5}$$

11.3.3.1 Land Surface Emissivity (LSE)

The LSE image is generated from the FVC image obtained using Eq. 11.6. The generation of LSE image requires emissivity values of the soil and vegetation of the bands 10 and 11, and these values are given in Table 11.3 are referred from Yu et al. (2014). The LSE images of bands 10 and 11 are generated individually as follows:

$$\text{LSE} = \varepsilon_s \text{X} (1 - \text{FVC}) + \varepsilon_v \text{X FVC} \tag{11.6}$$

where, ε_s is emissivity of the soil, ε_v is emissivity of the vegetation, and FVC is fractional vegetation cover.

Table 11.3 Emissivity values

Emissivity	Band 10	Band 11
E_s	0.9668	0.9668
E_v	0.9747	0.9896

Source Yu et al. (2014)

11.3.3.2 Conversion of the Digital Number (DN) to Spectral Radiance (Lλ) Using Single Channel Algorithm

Following the principle of thermal electromagnetic radiation, which states that all matter with a temperature above absolute zero (K) emits thermal radiation which is transmitted in the form of electromagnetic waves, the signals received by the thermal sensors (ETM+) can be converted to at-sensor radiance. The spectral radiance (Lλ) is calculated using the following equation (Eq. 11.7) in ERDAS Imagine 2020 software.

$$\mathbf{L\lambda} = \frac{\mathbf{L_{MAX}} - \mathbf{L_{MIN}} * \mathbf{DN} - 1 + \mathbf{L_{MIN}}}{\mathbf{Q_{CALMAX}} - \mathbf{Q_{CALMIN}}} \tag{11.7}$$

where;

L_{MAX} the spectral radiance that is scaled to Q_{CALMAX} in W/(m^2 * sr * μm).
L_{MIN} the spectral radiance that is scaled to Q_{CALMIN} in W/(m^2 * sr * μm).
Q_{CALMAX} the maximum quantized calibrated pixel value (corresponding to L_{MAX}) in DN = 255.
Q_{CALMIN} the minimum quantized calibrated pixel value (corresponding to L_{MIN}) in DN = 1 L_{MAX} and L_{MIN} are obtained from the Metadata file available with the image.

11.3.3.3 Conversion of Spectral Radiance (Lλ) to At-Satellite Brightness Temperatures (TB)

The emissivity corrected surface temperature has been calculated for Band 10 and Band 11 of Landsat 8, following Eq. 11.9 Artis and Carnahan (1982).

$$\mathbf{T_B} = \frac{\mathbf{K2}}{\mathbf{In}\left(1 + \frac{\mathbf{K1}}{\mathbf{L\lambda}}\right)} \quad (\mathbf{Unit}: \ \mathbf{Kelvin}) \tag{11.8}$$

where:

TB At-satellite brightness temperature (K)
Lλ Spectral Radiance in $W \cdot m^2 \cdot sr^{-1} \cdot \mu m^{-1}$
K1 and K2 K2 and K1 are two pre-launch calibration constants given in (Tables 11.4 and 11.5).

Table 11.4 K1 and K2 values for Landsat 8 TIRS bands

Thermal Constant	Band 10	Band 11
K1	1321.08	1201.14
K2	777.89	480.89

Table 11.5 K1 and K2 value for Landsat 7 ETM+ and Landsat 5 TIRS bands

Sensor	K1	K2
Landsat 7 ETM +	666.09	1282.71
Landsat 5 TM	607.76	1260.56

The final Land Surface Temperature (LST) in Kelvin is estimated by the following Eq. 11.9.

$$\mathbf{LST} = \frac{\mathbf{TB}}{1 + (\lambda \mathbf{TB}/\mathbf{p}) * \mathbf{lne})} \tag{11.9}$$

where:

Lλ the wavelength of the emitted radiance which is equal to 11.5 μm,
E the spectral emissivity,
P h.c/σ,
Σ Stefan Boltzmann's constant which is equal to $5.67 \times 10^{-8} \mathrm{Wm}^{-2}\ \mathrm{K}^{-4}$,
h Plank's constant (6.626×10^{-34} J S),
c velocity of light (2.998×108 m/s).

In this present study, the spectral emissivity coefficient is taken as unity. For all the calculations at the pixel level of the image, models were developed using the spatial model maker of ERDAS Imagine 2020.

11.3.3.4 Split Window (SW) Algorithm for LST

LST was calculated by applying a meticulous mathematical SW algorithm first proposed by McMillin (1975) who retrieved sea surface temperature (SST) using the difference in atmospheric absorption of two adjacent LWIR bands. Researchers have thereafter implemented and modified the SW algorithm for different purposes. The proposed SW algorithm resort to the atmospheric window in the range of 10–12 μm wavelengths for the TIRS bands (10 and 11). The base of the SW algorithm is the radiance attenuation for atmospheric absorption, which is proportional to the difference in radiance of concurrent measurements at two different wavelengths, each of them based on varying amounts of atmospheric absorption. For the present study, the following formulation (Eq. 11.10) given by Jimenez-Munoz and Sobrino (2008) was used:

$$\begin{aligned}\mathbf{TS} = {} & \mathrm{TB10} + \mathrm{C1} \times (\mathrm{TB10} - \mathrm{TB11}) + \mathrm{C2} \times (\mathrm{TB10} - \mathrm{TB11})2 + \mathrm{C0} \\ & + (\mathrm{C3} + \mathrm{C4} + \mathrm{w}) \times (1 - \varepsilon) + (\mathrm{C5} + \mathrm{C6} + \mathrm{w}) \times \Delta\varepsilon \end{aligned} \tag{11.10}$$

where:

Ts is the land surface temperature (°K);

TB10 and TB11	are brightness temperature of band 10 and 11 of Landsat 8 (°K) respectively;
ε	is mean land surface emissivity ($0.5 \times [\varepsilon 10 + \varepsilon 11]$) of TIR bands;
w	is atmospheric water vapor content (g/cm^2);
$\Delta\ \varepsilon$	represents the difference in land surface emissivity ($\varepsilon 10 - \varepsilon 11$) and
C0–C6	are split window coefficients

Split—window coefficients values were given by Skokovic et al. (2014) for TIRS of Landsat 8, available in the public domain and the same has been used here (Table 11.6). Therefore, a very simple yet robust SW algorithm was selected to retrieve LST using Landsat 8 TIRS data.

LMAX and LMIN are obtained from the Metadata file available with the image and are given in the Table. 11.7, 11.8 and 11.9.

Table 11.6 Split Window coefficient values for TIRS of Landsat 8

Constants	Value
C0	− 0.268
C1	1.378
C2	0.183
C3	54.300
C4	− 2.238
C5	− 129.200
C6	16.400

Table 11.7 Landsat-8 (OLI) Sensor thermal band and calibration constant values of Lλ

Band no	Satellite/Sensor	L_{MAX}	L_{MIN}
10	Landsat8/OLI high gain	22.00180	0.10033
10	Landsat8/OLI low gain	22.00180	0.10033
11	Landsat8/OLI high gain	22.00180	0.10033
11	Landsat8/OLI low gain	22.00180	0.10033

Table 11.8 Landsat-7 (ETM+) Sensor thermal band and calibration constant values of Lλ

Band no	Satellite/Sensor	L_{MAX}	L_{MIN}
6.1	Landsat7/ETM+ high gain	12.65	3.200
6.2	Landsat7/ETM+ low gain	17.04	0.000

Table 11.9 Landsat-5 (TM) Sensor thermal band and calibration constant values of Lλ

Band no	Satellite/Sensor	L_{MAX}	L_{MIN}
6	Landsat 5 TM	15.3030	1.2378

11.4 Results and Discussions

11.4.1 Land Use Land Cover (LULC) Analysis

Considering the interest of the study, eight LULC classes have been generated. The ultimate classification products provide an impression of the major LULC features of Malana watershed for 2001–2017 (Fig. 11.4a–c).The classified images were assessed for accuracy based on a random selection of 50 reference pixels for each time period. The overall accuracies of the classified images 2001, 2011, and 2017 were found to be 94.07%, 91.15%, and 91.73%, with Kappa coefficients of 0.9289, 0.8950, and 0.9036 respectively. (Table 11.10).

11.4.2 Change in LULC Area From 2001–2017

The statistics summary of area calculations offer an extensive data set of area under different LULC categories from 2001–17, with their increasing and decreasing trend of LULC in terms of the overall landscape (Figs. 11.5 and 11.6). The results indicate that the study area has witnessed substantial increase and decrease in the land use pattern for different categories (Table 11.11). There has been a considerable decrease in the glacier area from 39.19 km^2 (in 2001) to 32.97 km^2 (in 2017). The constantly increasing surface temperature due to global warming could be a major cause of this decrease. Snow cover is related to atmospheric temperature and studies by Shekhar et al. (2010) has detailed the seasonal temperature variations and their impact on snowfall in Indian Himalayan region. There is a likelihood relationship between the decrease in snow cover and an increase in bare rock area and vice versa. The area under the water body has increased from 0.81 km^2 (in 2001) to 0.84 km^2 (in 2017). This change can be accounted for the variation in the flow of the river and melting of glaciers which would lead to an increase in glacier-fed river flows/lakes. The area under Built-up category has increased from 0.1 km^2 (in 2001) to 0.14 km^2 (in 2017). This increase can be accounted for the developing tourism in Parvati valley owing to which the village core areas have expanded; guesthouses and homestays are being constructed. Better road connectivity to higher altitudes is also boosting up the settlement growth. The forest cover area has essentially decreased from 52.14 km^2 (in 2001) to 46.48 km^2 (in 2017). Various studies have indicated that climate change (The Intergovernmental Panel on Climate Change (IPCC) 2001) and anthropogenic factors (Negi et al. 2012) such as deforestation can affect forest cover. Cutting down

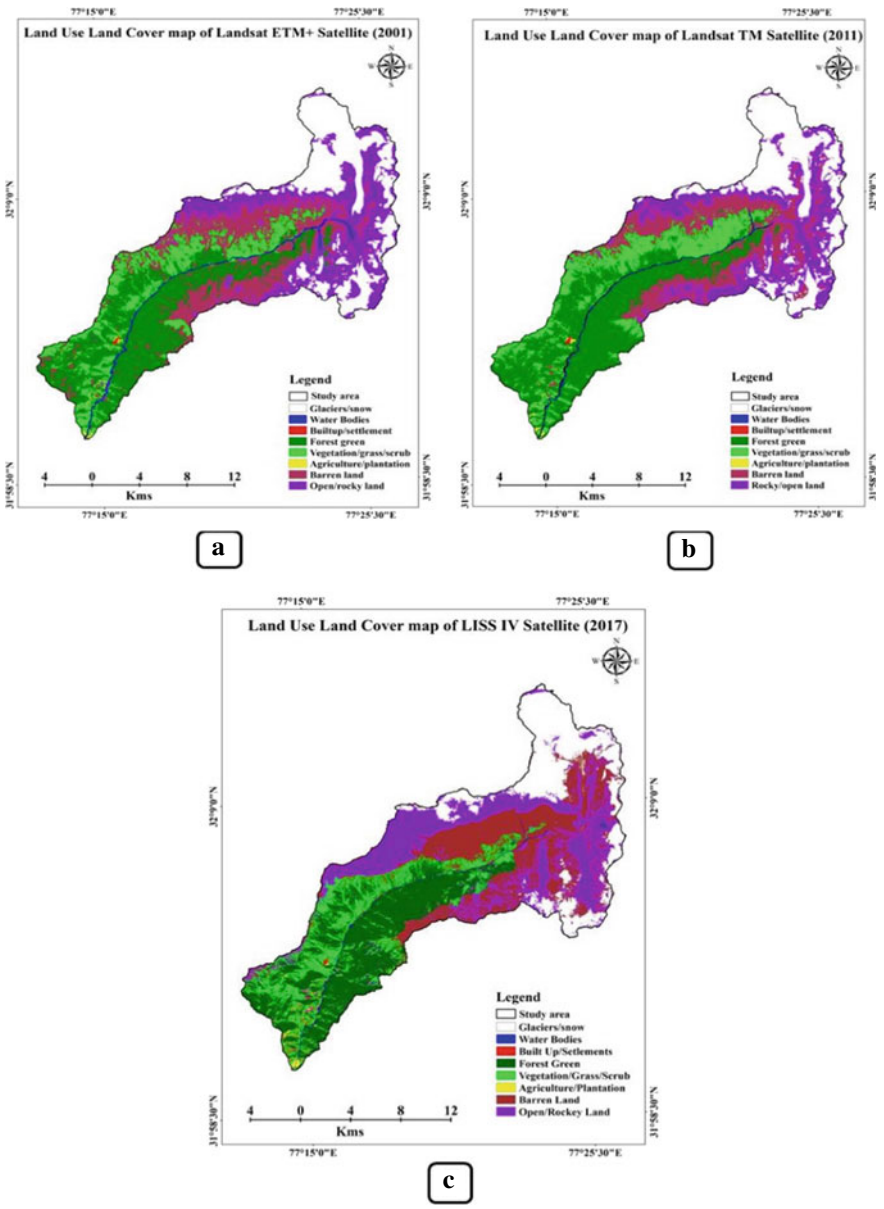

Fig. 11.4 LULC maps obtained by using supervised classification **a** 2001 **b** 2011 **c** 2017

Table 11.10 Overall classification accuracy and Kappa statistics from 2001–2017

Year	User's accuracy (%)								Producer's accuracy (%)								Overall Accuracy (%)	Kappa coefficient
	G	W	B	F	V	A	Ba	O	G	W	B	F	V	A	Ba	O		
2001	100	85.71	100	91.30	100	75	90.48	90.45	100	100	100	91	82	100	95	100	94.07	0.9289
2011	100	72	100	97.78	90	81.25	93.33	92	96.67	94.74	100	91.67	85.71	92.86	84.85	92	91.15	0.8950
2017	100	100	100	95.83	73.08	100	86.36	100	10/snow0	100	100	95.83	100	100	79.17	72.22	91.73	0.9036

Here, G—glacier; W—water bodies; B—built-up; F—forest green; V—vegetation; A—agriculture; Ba—barren land; O—Open/rocky land

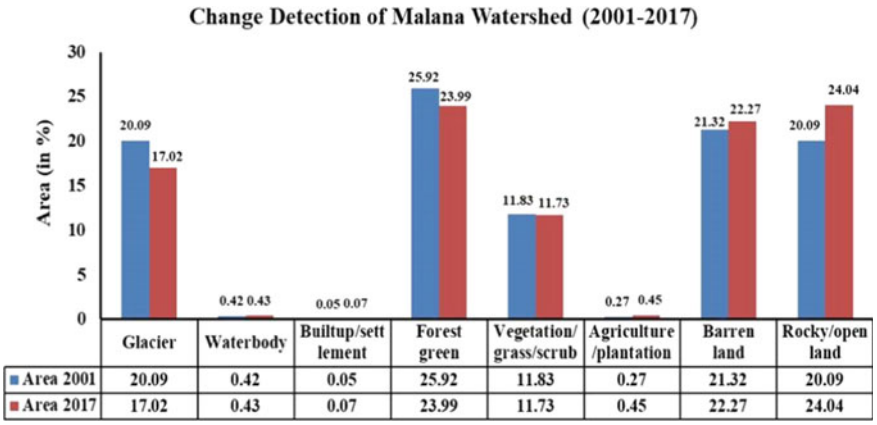

Fig. 11.5 Graph depicting the status of LULC categories from 2001–2017 (in %)

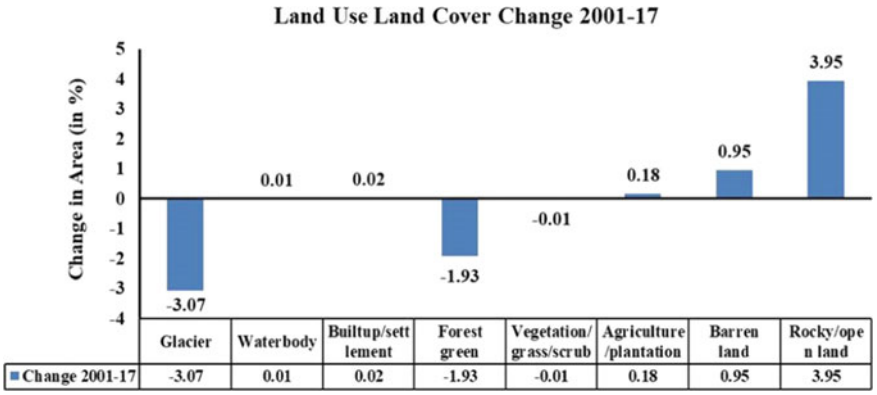

Fig. 11.6 Graph depicting the status of LULC change from 2001–2017

Table 11.11 Statistics of change in LU/LC area from 2001–2017

LULC Category	Area (2001)		Area (2011)		Area (2017)		Change in area 2017–2001 (in %)
	(in km^2)	(in %)	(in km^2)	(in %)	(in km^2)	(in %)	
Glacier/snow	39.19	20.09	38.97	19.98	32.97	17.02	−3.07
Water bodies	0.81	0.42	0.81	0.41	0.84	0.43	0.01
Built-up/settlement	0.1	0.05	0.11	0.06	0.14	0.07	0.02
Forest green	50.57	25.92	51.97	26.64	46.48	23.99	−1.93
Vegetation	23.08	11.83	25.18	12.91	22.72	11.73	−0.01
Agriculture	0.53	0.27	0.54	0.27	0.88	0.45	0.18
Barren land	41.59	21.32	37.7	19.33	43.16	22.27	0.95
Open/rocky land	39.2	20.09	39.79	20.4	46.58	24.04	3.95

of trees for built-up/settlement and an altitudinal shift in agriculture and horticulture might have led to this decrease. The vegetation cover has decreased from 26.32 km^2 (in 2001) to 22.72 km^2 (in 2017). This change can also be attributed to different anthropogenic activities. The agricultural area has increased from 0.53 km^2 (in 2001) to 0.88 km^2 (in 2017). The increased area under agriculture is mostly related to the expansion of the horticulture area to higher elevations which can be possibly related to socioeconomic factors (Sah and Mazari 1998). The area under barren and open/rocky land has increased from 36.68 km^2 (in 2001) to 43.16 km^2 (in 2017) and 39.2 km^2 (in 2001) to 46.58 km^2 (in 2017) respectively. This increase can be attributed to the decrease in glacier cover area and forest/vegetation cover area.

11.4.3 Land Surface Temperature (LST) Change Analysis

Figure 11.7a, b shows the NDVI image of the Malana watershed as on 18 October 2001, 22 October 2011 respectively estimated from Band 4 and Band 3 of the ETM+ and TM sensors and Fig. 11.7c shows the NDVI image as on 06 October 2017 estimated from band 4 (RED) and band 5 (NIR) of the OLI sensor using ERDAS Imagine 2020. It is evident from this figure that the NDVI value varies from −0.42 to 0.62, −0.51 to 0.70, and −0.20 to 0.54 for the year 2001, 2011, and 2017 respectively. The NDVI value ranges from +1 to −1; where the higher NDVI values closer to +1 indicates the healthy and green vegetation cover area and the lower NDVI values closer to -1 indicates water body or glacier covered area. These NDVI images were then used as an input for reclassification and the reclassified images for soil and vegetation were obtained separately. The NDVI values for soil and vegetation were calculated and respectively were put into Eq. 11.7 in order to obtain the FVC image and then LSE image was obtained by using Eq. 11.8.

In the LST products derived using SC algorithm from Landsat-7 ETM+ (2001) and Landsat-5 TM (2011), the highest value observed was 292.23 K and 288.61 K respectively and the lowest value observed was 263.54 K and 265.13 K respectively (Fig. 11.8a, b). In the LST products derived using SW algorithm from Landsat-8 for October 2017, the highest value observed was 294.75 K, whereas, the lowest LST value observed 264.89 K (Fig. 11.8c). The highest LST values were observed in south and west side which comprise of forest land and built-up area with development activities (like Malana Hydropower Project); and the lowest values were observed in north and east side which comprises of glacier covered land of the study area. The mean LST was observed to be 19.62 °C and standard deviation of 4.95 for October 2017 LST estimates. The highest and lowest values of LST represent the hot/warm and cold/snowy/glacial areas in the study area. The change in the LST follows the same trend over the study period of 16 years i.e., a change of ±3–5 °C.

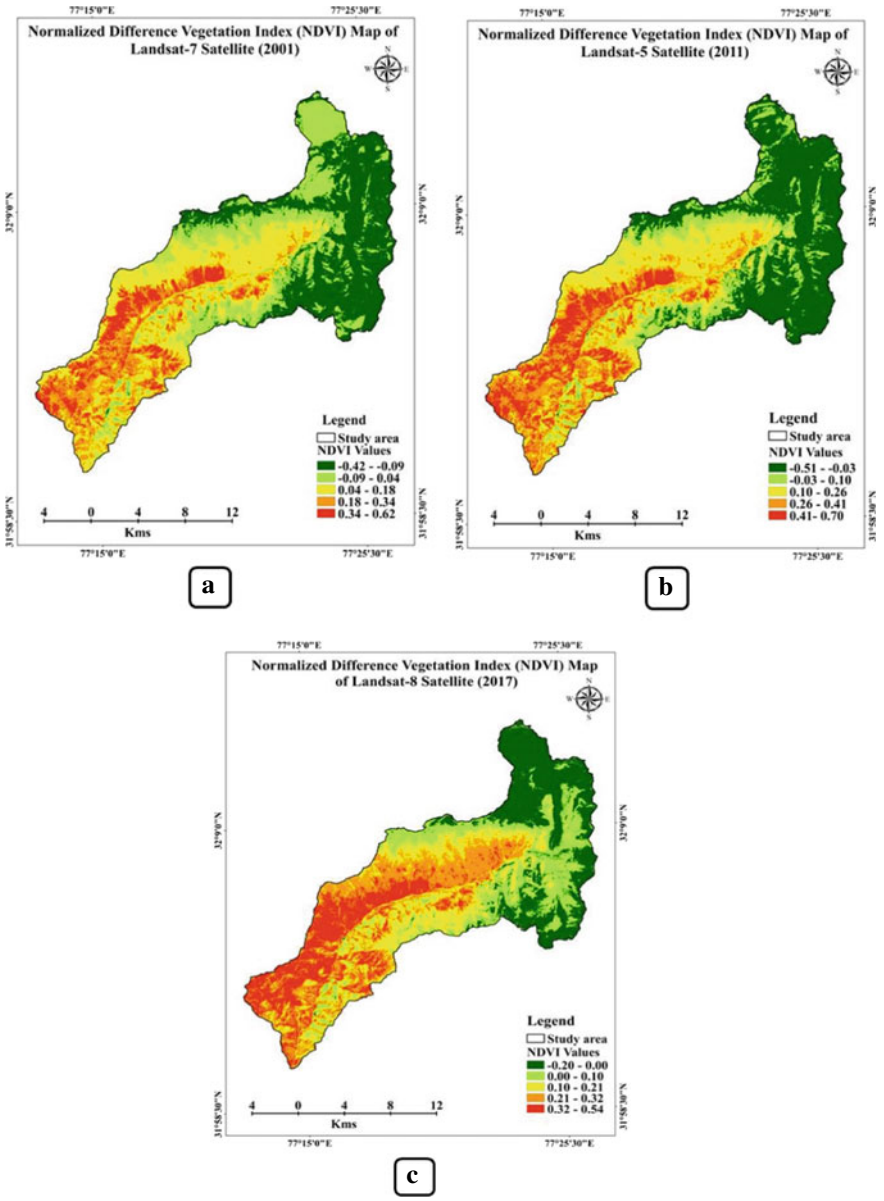

Fig. 11.7 NDVI maps derived from **a** Landsat-7 ETM+ Satellite (2001), **b** Landsat-5 TM Satellite (2011), **c** Landsat-8 OLI Satellite (2017)

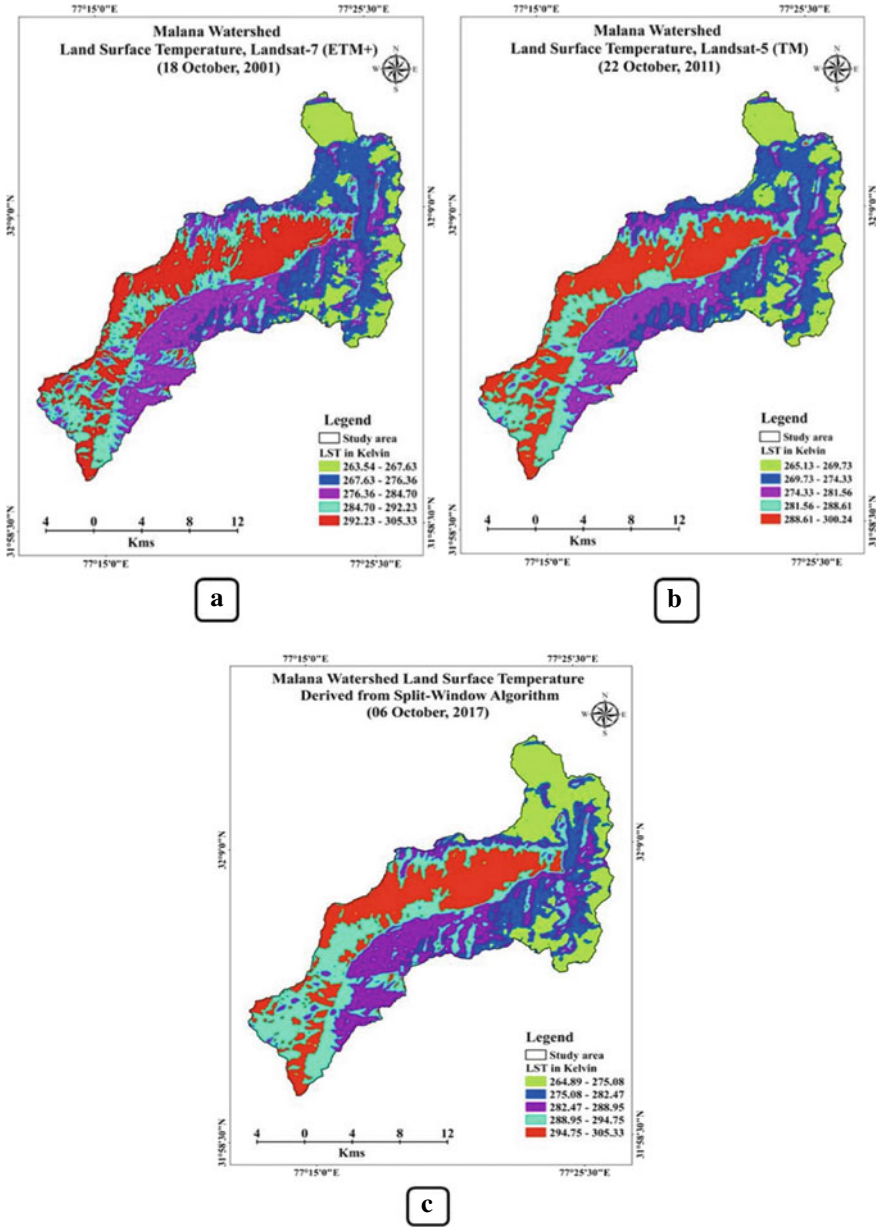

Fig. 11.8 LST maps derived from SC algorithm **a** Landsat-7 ETM+ (2001), **b** Landsat-5 TM (2011); LST derived from SW algorithm **c** Landsat-8 OLI (2017)

11.4.4 Statistics of LST of Different LULC Categories for the Year 2001, 2011, and 2017

The statistical information of LST in different LULC classes for the year 2001, 2011, and 2017 is calculated using the zonal statistics tool (in Spatial Analyst toolbar) of ArcGIS 10.5. Table 11.12 shows the calculated statistics for the year 2001. The minimum mean temperature among all the categories is exhibited by glacier/snow category which is 267.89 K (standard deviation 4.04) and the maximum mean temperature is shown by vegetation and agricultural area which is 296.98 K (standard deviation 3.46) and 295.39 K (standard deviation 2.53) respectively shown in (Fig. 11.9).

Table 11.13 shows the calculated statistics for the year 2011. The minimum mean temperature among all the categories is exhibited by glacier/snow category which is 266.86 K (standard deviation 3.98) and the maximum mean temperature is shown

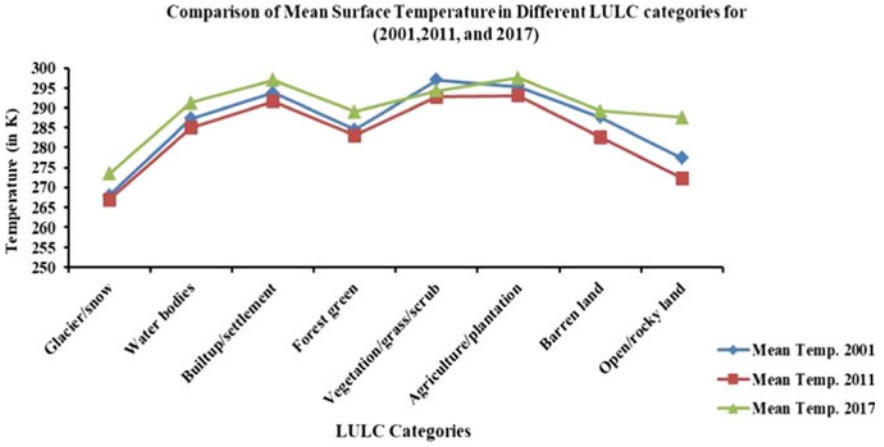

Fig. 11.9 Graph depicting the mean surface temperature in different LULC categories

Table 11.12 Statistics of LST over LULC categories for 2001 (Landsat-7 ETM+)

LULC categories	Min temp	Max temp	Mean Temp	SD
Glacier/snow	256.27	288.61	267.89	4.04
Water bodies	274.08	302.94	287.32	5.06
Built-up/settlement	287.52	299.01	293.79	1.91
Forest green	261.42	303.90	284.46	5.41
Vegetation/grass/scrub	275.32	305.33	296.98	3.46
Agriculture/plantation	289.70	302.45	295.39	2.53
Barren land	261.42	303.90	287.75	8.29
Open/rocky land	254.74	300.99	277.30	9.26

by vegetation and agricultural area which is 292.81 K (standard deviation 3.41) and 293.10 K (standard deviation 2.17) respectively.

Table 11.14 shows the calculated statistics for the year 2017. The minimum mean temperature among all the categories is exhibited by glacier/snow category which is 273.40 K (standard deviation 5.45) and the maximum mean temperature is shown by Built-up and agricultural area which is 297.04 K (standard deviation 2.28) and 297.51 K (standard deviation 2.65) respectively.

Table 11.15 compares the mean surface temperature over different LULC categories for all the three years. It was observed that during the entire time period of our study i.e., 2001–2017 glacier/snow covered area exhibited the minimum mean temperature among all the other categories and Built-up and agricultural land exhibited the maximum mean temperature The satellite images are taken for October month during which the agricultural land turns into fallow land and therefore the reflection of the soil is on the higher side. In our study area, developmental activities involves the construction of Hydropower projects (Malana-I, 86 MW and Malana-II, 100 MW), power stations, which thus also reflect the sun's rays on a higher side thus increasing the temperature.

Table 11.13 Statistics of LST over LULC categories for 2011 (Landsat-5 TM)

LULC categories	Min temp	Max temp	Mean temp	SD
Glacier/snow	254.04	284.55	266.86	3.98
Waterbodies	273.98	295.96	285.03	3.49
Built-up/settlement	286.92	295.52	291.60	1.23
Forest green	267.42	298.12	283.08	5.16
Vegetation/grass/scrub	275.56	300.66	292.81	3.41
Agriculture/plantation	286.92	298.55	293.10	2.17
Barren land	259.14	300.24	282.61	8.34
Open/rocky land	253.38	296.83	272.32	7.12

Table 11.14 Statistics of LST over LULC categories for 2017 (Landsat-8 OLI)

LULC categories	Min temp	Max temp	Mean temp	SD
Glacier/snow	262.98	299.17	273.40	5.45
Waterbodies	274.53	299.24	291.29	3.28
Built-up/settlement	289.34	302.69	297.04	2.28
Forest green	274.51	301.41	289.06	3.34
Vegetation/grass/scrub	263.45	302.80	294.27	3.24
Agriculture/plantation	287.05	303.43	297.51	2.65
Barren land	263.30	305.33	289.21	9.01
Open/rocky land	262.88	303.05	287.64	8.64

Table 11.15 Statistics of comparison of mean surface temperature over different LULC categories for (2001, 2011, and 2017)

LULC categories	Mean temp. 2001	Mean temp. 2011	Mean temp. 2017
Glacier/snow	267.89	266.86	273.40
Water bodies	287.32	285.03	291.29
Built-up/settlement	293.79	291.60	297.04
Forest green	284.46	283.08	289.06
Vegetation/grass/scrub	296.98	292.81	294.27
Agriculture/plantation	295.39	293.10	297.51
Barren land	287.75	282.61	289.21
Open/rocky land	277.30	272.32	287.64

11.5 Conclusion

In this study, it was proven that the supervised classification of multi-temporal satellite images is an effective tool to quantify current land use as well as to detect changes in a changing environment. Landsat-7 ETM+, Landsat-5 TM, Landsat-8 OLI and LISS IV satellite images of 2001, 2011, and 2017 were used for the analysis. The observed changes varied from one LULC category to another over the period of analysis (2001–2017). Some categories/classes experienced decrease while some experienced an increase in the LULC area. This study advocates that multi-temporal satellite data is very useful for studying the LULC change pattern of an area which acts as a fundamental base of a successful land-use strategy required for the progressive development of any area. Whereas we examined that the area under glacier has been decrease from 39.19 km^2 (in 2001) to 32.97 km^2 (in 2017), meanwhile, the area under Built-up/settlements has increased from 0.1 km^2 (in 2001) to 0.14 km^2 (in 2017). Knowledge about LULC has become important to overcome the problems associated with climate change such as biogeochemical cycles, loss of productive ecosystems, biodiversity, degradation of environmental quality, loss of agricultural lands, destruction of wetlands. The main reason behind the LULC changes includes rapid population growth, rural-to-urban migration, reclassification of rural areas as urban areas, lack of valuation of ecological services, poverty, ignorance of biophysical limitations, and use of ecologically incompatible technologies. The findings of the study also indicate the existence of a strong relationship between LULC change and LST. We will further propose the results of LST to find out headwater contribution, and glacier melting scenario due to climate change in the Malana watershed. The results of the study will come out as a positive scientific addition for the people of Malana as it provides important information regarding soil and water conservation further helping the decision makers and strategists in natural resources management at a micro-level for the sustainable development.

Acknowledgements The authors would like to thank USGS Earth Explorer for online freely available of Landsat series data and National Remote Sensing Centre (NRSC), Hyderabad, India for

providing the high resolution LISS - IV data. The authors are thankful to the Director, G. B. Pant National Institute of Himalayan Environment Kosi-Katarmal, Almora, Uttarakhand for providing the facilities in Himachal Regional Centre Mohal-Kullu, Himachal Pradesh. Authors would also like to acknowledge the Director, (Dr. S. S. Samant) Himalayan Forest Research Institute, Conifer Campus, Panthaghati, Shimla, Himachal Pradesh, where we could modify and finalize the present work.

References

Artis DA, Carnahan WH (1982) Survey of emissivity variability in thermography of urban areas. Remote Sens Environ 12(4):313–329

Becker F, Li Z-L (1990) Towards a local split window method over land surfaces. Int J Remote Sens 11(3):369–393

Butt A, Shabbir R, Ahmad SS, Aziz N (2015) Land use change mapping and analysis using Remote Sensing and GIS: a case study of simly watershed, islamabad, pakistan. Egyptian J Remote Sensing Space Sci 18(2):251–259

Congalton RG (1991) a review of assessing the accuracy of classifications of remotely sensed data. Remote sensing environ 37(1):35–46

Cohen J (1960) A coefficient of agreement for nominal scales. Educ Psychol Measur 20(1):37–46

Corner RJ, Dewan AM, Chakma S (2014) Monitoring and prediction of land-use and land-cover (LULC) change. In: Dhaka megacity. Springer, Dordrecht, pp 75–97

Cristobal J, Ninyerola M, Pons X (2008) Modeling air temperature through a combination of remote sensing and GIS data. J Geophys Res 113:1–13

De Koning L, Merchant AT, Pogue J, Anand SS (2007) Waist circumference and waist-to-hip ratio as predictors of cardiovascular events: meta-regression analysis of prospective studies. Eur heart J 28(7): 850–856

Feizizadeh B, Blaschke T (2012) Thermal remote sensing for land surface temperature monitoring: Maraqeh County, Iran 2.Methods and data. In: IEEE international symposium on geoscience and remote sensing, pp 2217–2220. https://doi.org/10.1109/IGARSS.2012.6350808

Foley JA, DeFries R, Asner GP, Barford C, Bonan G, Carpenter SR, Snyder PK (2005) Global consequences land use sci 309(5734):570–574

Gao J, Liu Y (2010) Determination of land degradation causes in Tongyu County, Northeast China via land cover change detection. Int J Appl Earth Obs Geoinf 12:9–16

IPCC (2001) https://www.ipcc.ch/ipccreports/tar/wg1/pdf/WGI_TAR_full_report.pf, 51(54):123–128

Islam K, Weil RR (2000) Soil quality indicator properties in mid-Atlantic soils as influenced by conservation management. J soil water conservation 55(1): 69–78

Jat MK, Garg PK, Khare D (2008) Monitoring and modelling of urban sprawl using remote sensing and GIS techniques. Int J A earth Observation and Geo Inf 10(1):26–43

Jimenez-Munoz JC, Cristobal J, Sobrino JA, Soria G, Ninyerola M, Pons X (2009) Revision of the single-channel algorithm for land surface temperature retrieval from Landsat thermal-infrared data. IEEE Trans Geosci Remote Sens 47(1):339–349

Jimenez-Munoz JC, Sobrino JA (2003) A generalized single-channel method for retrieving land surface temperature from remote sensing data. J Geophys Res Atmos 108(D22):1–9

Jimenez-Munoz JC, Sobrino JA (2006) Error sources on the land surface temperature retrieved from thermal infrared single channel remote sensing data. Int J Remote Sens 27(5):999–1014

Jimenez-Munoz JC, Sobrino JA (2008) Split-window coefficients for land surface temperature retrieval from low-resolution thermal infrared sensors. IEEE Geosci Remote Sens Lett 5(4):806–809

Kalma JD, McVicar TR, McCabe MF (2008) Estimating land surface evaporation: a review of methods using remotely sensed surface temperature data. Surv Geophys 29:421–469. https://doi.org/10.1007/s10712-008-9037-z

Kuenzer C, Dech S (2013) Thermal infrared remote sensing: sensors, methods, applications. Remote Sens Digital Image Proces 17:429–451

Kumar R, Anbalagan R (2016) Landslide susceptibility mapping using analytical hierarchy process (AHP) in Tehri reservoir rim region, Uttarakhand. J Geol Soc India 87(3):271–286

Kustas W, Anderson M (2009) Advances in thermal infrared remote sensing for land surface modelling. Agric Meteorol 149:2071–2081. https://doi.org/10.1016/j.agrformet.2009.05.016

Lambin EF, Geist HJ, Lepers E (2003) Dynamics of land-use and land-cover change in tropical regions. Annu Rev Environ Resour 28(1):205–241

Lambin EF, Turner BL, Geist HJ, Agbola SB, Angelsen A, Bruce JW, …, George P (2001) The causes of land-use and land-cover change: moving beyond the myths. Glob Environ Chang 11(4):261–269

Lead CO (2018) The Carbon Cycle and Atmospheric Carbon Dioxide. Livshin I (ed.) (2019). Artificial Neural Networks with Java: tools for building neural network applications Apress

Li ZL, Tang BH, Wu H, Ren H, Yan G, Wan Z, Trigo IF, Sobrino JA (2013a) Satellite-derived land surface temperature: current status and perspectives. Remote Sens Environ 131:14–37

Li Z-L, Wu H, Wang N, Qiu S, Sobrino JA, Wan Z, Tang B-H, Yan G (2013b) Land surface emissivity retrieval from satellite data. Int J Remote Sens 34(9–10):3084–3127

Lu D, Moran E, Hetrick S, Li G (2011) Land-use and land-cover change detection. In: Advances in environmental remote sensing sensors, algorithms, and applications. CRC Press Taylor & Francis Group, New York, pp 273–290

Lu D, Mausel P, Brondizio E, Moran E (2004) Change detection techniques. Int J Remote Sens 25(12):2365–2401

Ma Z, Redmond RL (1995) Tau coefficients for accuracy assessment of classification of remote sensing data. Photogramm Eng Remote Sens 61(4):435–439

Martinuzzi S, Gould WA, González OMR (2007) Land development land use and urban sprawl in Puerto Rico integrating remote sensing and population census data. Landscape and urban planning 79(3–4):288–297

Mahmood T, Malik SA, Hussain ST (2010) Biosorption and recovery of heavy metals from aqueous solutions by Eichhornia crassipes (water hyacinth) ash BioResources 5(2):1244–1256

Malczewski J (2004) GIS-based land-use suitability analysis: a critical overview. Prog Plan 62(1):3–65

Mallick J (2014) Land characterization analysis of surface temperature of semi-arid Mountainous City Abha, Saudi Arabia using remote sensing and GIS. J Geogr Inf Syst 06:664–676. https://doi.org/10.4236/jgis.2014.66055

Mallick J, Kant Y, Bharath BD (2008) Estimation of land surface temperature over Delhi using Landsat-7 ETM+. J Ind Geophys Union 12(3):131–140

Mantero P, Moser G, Serpico SB (2005) Partially supervised classification of remote sensing images through SVM-based probability density estimation. IEEE Trans Geosci Remote Sens 43:559–570

McMillin L (1975) Estimation of sea surface temperatures from two infrared window measurements with different absorption. J Geophys Res 80:5113–5117

Mengistu DA, Salami AT (2007) Application of remote sensing and GIS inland use/land cover mapping and change detection in a part of south western Nigeria. Afr J Environ Sci Technol 1(5):99–109

Mesev V, Walrath A (2007) GIS and remote sensing integration: in search of a definition. Wiley, Chichester, pp 1–16

Meyer WB, Turner BL (1996) Land-use/land-cover change: challenges for geographers. Geo J 39(3):237–240

Mitsuda Y, Ito S (2011) A review of spatial-explicit factors determining spatial distribution of land use/land-use change. Landscape Ecol Eng 7(1):117–125

Mundia CN, Aniya M (2006) Dynamics of landuse/cover changes and degradation of Nairobi City, Kenya Land Degrad Develop 17(1):97–108
Monserud RA, Leemans R (1992) Comparing global vegetation maps with the Kappa statistic. Ecol Model 62(4):275–293
Nikam BR, Ibragimov F, Chouskey A, Garg V, Aggarwal SP (2016) Retrieval of land surface temperature from Landsat 8 TIRS for the command area of Mula irrigation project. Environmental Earth Sciences 75:1169
Oke TR (2002) Boundary layer climates. Routledge
Owen TW, Carlson TN, Gillies RR (1998) An assessment of satellite remotely-sensed land cover parameters in quantitatively describing the climatic effect of urbanization. Int J Remote Sens 19:1663–1681. https://doi.org/10.1080/014311698215171
Ojima DS, Galvin KA, Turner BL (1994) The global impact of land-use change. Bio Sci 44(5):300–304
Pal M, Mather PM (2005) Support vector machines for classification in remote sensing. Int J Remote Sens 26(5):1007–1011
Qin Z, Karnieli A, Berliner P (2001) A mono-window algorithm for retrieving land surface temperature from Landsat TM data and its application to the Israel-Egypt border region. Int J Remote Sens 22(18):3719–3746
Quattrochi DA, Luvall JC (1999) Thermal infrared remote sensing for analysis of landscape ecological processes: methods and applications. Landsc Ecol 577–598.https://doi.org/10.1002/9781118801628.ch03
Rongali G, Keshari AK, Gosain AK, Khosa R (2018) Split-window algorithm for retrieval of land surface temperature using Landsat 8 thermal infrared data. J Geovisual Spat Anal 2(2):14
Rosenfield G, Fitzpatrick K (1986) A coefficient of agreement as a measure of thematic classification accuracy. Photogram Eng Remote Sens 52(2):223–227
Rawat JS, Kumar M (2015) Monitoring land use/cover change using remote sensing and GIS techniques: a case study of Hawalbagh block, districtAlmora, Uttarakhand, India. Egypt J Remote Sens Space Sci https://doi.org/10.1016/j.ejrs.2015.02.002
Sah MP, Mazari RK (1998) Anthropogenically accelerated mass movement, Kulu Valley, Himachal Pradesh, India. Geomorphology 26(1–3):123–138
Shalaby A, Tateishi R (2007) Remote sensing and GIS for mapping and monitoring land cover and land-use changes in the Northwestern coastal zone of Egypt. Appl Geogr 27(1):28–41
Shekhar MS, Chand H, Kumar S, Srinivasan K, Ganju A (2010) Climate-change studies in the western Himalaya. Ann Glaciol 51(54):105–112
Sobrino JA, Caselles V, Coll C (1993) Theoretical split-window algorithms for determining the actual surface temperature. Il Nuovo Cimento C 16(3):219–236
Sobrino JA, Li ZL, Stoll MP, Becker F (1994) Improvements in the split-window technique for land surface temperature determination. IEEE Trans on Geoscience and Remote Sensing 32(2):243–253
Sobrino JA, Jiménez-Muñoz JC, Verhoef W (2005) Canopy directional emissivity: comparison between models. Remote Sens Environ 99(3):304–314
Sobrino JA, Raissouni N, Li ZL (2001) A comparative study of land surface emissivity retrieval from NOAA data. Remote Sens Environ 75(2):256–266
Song L, Liu S, Kustas WP, Zhou J, Ma Y (2015) Using the surface temperature-albedo space to separate regional soil and vegetation temperatures from ASTER data. Remote Sens 7:5828–5848. https://doi.org/10.3390/rs70505828
Sobrino JA, Jiménez-Muñoz JC, Paolini L (2004) Land surface temperature retrieval from LANDSAT TM 5 Remote Sensing environ 90(4):434–440
Sudhira HS, Ramachandra TV, Jagadish KS (2004) Urban sprawl: metrics, dynamics andmodelling using GIS. Int J Appl Earth Obs 5:29–39
Townshend JR, Justice CO (1986) Analysis of the dynamics of African vegetation using the normalized difference vegetation index. Int J Remote Sens 7(11):1435–1445

Thakur PK, Gosavi VE (2018) Estimation of Temporal Land Surface Temperature using Thermal Remote Sensing of Landsat-8 (OLI) and Landsat-7 (ETM+): A study in Sainj River Basin, Himachal Pradesh, India. Environ We Int J Sci Tech 13:29–45

Thakur PK, Kumar M, Gosavi VE (2020) Monitoring and modelling of urban sprawl using geospatial techniques—a case study of Shimla City, India. In Geoecology of Landscape Dynamics Springer, Singapore pp 263–294

UN (2010) World urbanization prospects: the 2009 revision population database

Ustuner M, Sanli FB, Dixon B (2015) Application of support vector machines for land use classification using high-resolution Rapid Eye images: a sensitivity analysis. Eur J Remote Sens 48(1):403–422

Wan ZM, Dozier JA (1996) A generalized split-window algorithm for retrieving land-surface temperature from space. IEEE Trans Geosci Remote Sens 34(4):892–905

Weng Q (2001) A remote sensing-GIS evaluation of urban expansion and its impact on surface temperature in the Zhujiang Delta. China. Int J Remote Sens 22(10):1999–2014

Weng Q, Lu D, Schubring J (2004) Estimation of land surface temperature-vegetation abundance relationship for urban heat island studies. Remote Sens Environ 89:467–483. https://doi.org/10.1016/j.rse.2003.11.005

Yu X, Guo X, Wu Z (2014) Land surface temperature retrieval from Landsat 8 TIRS-comparison between radiative transfer equation based method, split window algorithm and single channel method. Remote Sens 6(10):9829–9852

Chapter 12
Spatio-Temporal Changes in Metropolitan Cities of India: A Comparative Study of Delhi and Mumbai

Sanjit Kumar, Kushala Devi, Manish Kumar, Sourav Bhadwal, Nitin Chauhan, and Naresh Kumar Verma

Abstract India witnessed a significant transformation in urban area from last few decades. Most of the million cities emerged rapidly in a very short period. Migration is one of the most important factors due to which most of the cities are transforming into one lakh cities and million cities. This study is based on the comparative analysis of urban transformation of Delhi (Administrative Capital) and Mumbai (Economic Capital) metropolitan cities of India. The study analyzes the changes among the major attributes of urban place (i.e., water, greenery and built-up). Traditional outfit of these cities has changed drastically over the years. Understanding the trends of urbanization in these cities is very important for planners and decision makers. Geo-spatial techniques are used to carry out spatial and temporal variation. In this study, spatial pattern of urban place with focus on built-up area has been studied with the help of land use/land cover maps extracted from the temporal satellite imageries. The Shannon's entropy is calculated in this process to find the actual change and pattern of change taken place in these cities where built-up is taken as spatial phenomena. An attempt is made to draw relationship between built-up and its other causing elements by using statistical techniques (Stepwise-Regression). Landscape metrics as quantitative measures are carried out in this paper to examine the spatial structures and patterns of landscape in these cities.

Keywords Urban transformation · Spatial and temporal analysis · Shannon's entropy · Stepwise regression

S. Kumar (✉) · K. Devi · N. Chauhan
Haryana Space Applications Centre, CCS HAU Campus, HISAR 125004, India

M. Kumar · S. Bhadwal
Department of Geography, School of Basic Sciences, Central University of Haryana, Mahendergarh, Haryana 123031, India
e-mail: manish.ks@cuh.ac.in

N. K. Verma
Special Center for National Security Security Studies, Jawarharlal Nehru University, New Delhi, India
e-mail: nkverma@mail.jnu.ac.in

R. B. Singh et al. (eds.), *Remote Sensing and Geographic Information Systems for Policy Decision Support*, Advances in Geographical and Environmental Sciences,
https://doi.org/10.1007/978-981-16-7731-1_12

12.1 Introduction

In present scenario, most of the metropolitan cities of developed and developing countries are changing rapidly. These cities are growing in every aspect of spatial phenomena such as area, population and density. These cities are experiencing changes in physical conditions also due to change in population over time. Urban areas are transforming every day due to the facilities it provides to its population. Population of small towns and cities are magnetized to the metropolitan cities like Delhi and Mumbai for better and efficient facilities. Unsatisfactory nature of human beings somehow changes the shape and texture of urban places. Urban places have always shown significant role in the transformation of society from ancient time to present. Landscape spatial patterns are connected with dynamic process (Wu et al. 2001; Nagendra and Pareeth 2006). Cities are growing in both aspect; population as well as area. Unmeasured flow of population toward these cities is also expanding its boundaries. Boundaries of these metropolitan cities are expanding in the fringe areas. This rapid growth of urban places in a developing country like India results positive growth in share of urban population from 109 million in 1971 (19.90%) to 388 million in 2011 (31.30%). Urban area contributes for less portion of the total land surface on earth, rapid changes in the urban areas significantly transformed natural set-up and created huge environmental and social impacts (Berling and Wu 2004; Grimm et al. 2000). It is very important to monitor and plan the expansion of urban place especially in this case where people from all parts are marking their presence in these fragile cities. A great amount of work has been done in the field that enables researcher to review a vast amount of literature. Sinha (2017) has carried out LU/LC change and change detection through post classification comparison in his study on urban sprawl in Gautama Budh Nagar District, Uttar Pradesh. Geospatial techniques such as GIS and Remote Sensing has been used to carry out these types of research. Bhagwat (2011) analyzed the change in land use and land cover by evaluating statistics of four different time classified data of Kathmandu Metropolitan with the help of Geospatial Techniques. He suggested that analysis based on land use statistics and transition metrics are very meaningful to analyze change taken place in any city. Yuan et al. (2005) has used multi-time (1986, 1991, 1998, 2002) Landsat TM satellite image to map and monitor land cover change for twin cities of Metropolitan Area of Minnesota. Urban area has increased between 1986 and 2002 by 9.1% (23.7–32.8%) which is common trend for the metropolitan cities like this. Rawat et al. (2014) have done a study on five towns of Uttarakhand i.e., Ramnagar, Nainital, Bhimtal, Almora and Haldwani and extracted land use land cover changes which took place in these towns over 20 years. Satellite data of 1990–2010 has been used to carry out the result of this study which shows conversion of agricultural and vegetation land into built-up area. Mehta et al. (2012) used geospatial techniques i.e., Remote Sensing and GIS to understand and analyze changes that occur in arid environment of Kutch region in Gujarat between 1999 and 2009. Amin et al. (2012) monitored a significant change in land use land cover of Srinagar city in Kashmir

Valley by studying land use land cover maps by processing satellite images of 1990–2007. Besides methodologies of change detection, statistical techniques are also used by integrating geospatial techniques to quantify, estimate, map and monitor the urban change and urban expansion. Two major types of methods are used in quantifying, assess, mapping and monitoring urban change is Shannon's Entropy. Shannon's entropy is basically a mathematical model to estimate the unorganized changes that occur at any geographical area. Shannon's Entropy (Hn) is used to calculate degree of spatial concentration of geographic phenomena (Xi) for any "n" spatial units. Entropy can also be apply to identify the degree of urban change or growth with respect to development in a city either compact or dispersed in nature. In most of the work related to geospatial technologies built-up area is generally taken as base variable to quantify urban change. The main objective of this study is to extract, understand, analyze and compare the changes that took place in both the cities (Mumbai and Delhi) from 2001 to 2011. These methods are also applied to find out the actual result of urban change taken in both the metropolitan cities.

12.2 Study Area

Delhi is the administrative capital of India and one of the most grown metropolitan city in India. Delhi is the second most populous city of world and the largest city in terms of total area. Delhi is also known by NCT (National Capital Territory). Delhi along with other satellite towns have got the status of National Capital Region. The geographical extent of Delhi is 28.61°N 77.23°E, and lies in Northern India. Delhi borders Haryana on the north, west and south whereas Uttar Pradesh in the east. Yamuna is the only one river which is flowing the through Delhi. Delhi and Uttar Pradesh are separated by Hindon River flowing through. Delhi is surrounded by The Delhi Range from three sides which originates from the Aravali range in the south. This Delhi ranges reaches a height of 318 m (1043 ft.) and is the prominent feature of this region.

Mumbai is India's most populous city and also the administrative capital of Maharashtra State. Mumbai is often known as Economical Capital of India. The city is located at western side of Maharashtra as well as India and lies between 18° 53′ and 19° 16′ N latitudes and between 72° 46′ and 72° 57′ E longitudes. The city has forest area in the northern part and also at the coast of Arabian sea. Thus, the changes in built-up area has been mainly in the south, south-east and eastern part of Mumbai. Mumbai is the largest city in the state whereas this is the only city in the state which has million plus population. The city is experiencing highest population growth rates. The city will also experience spatial expansion in the coming future due to the economic growth which will eventually attract population. The location of both the cities in India has been depicted in Fig. 12.1.

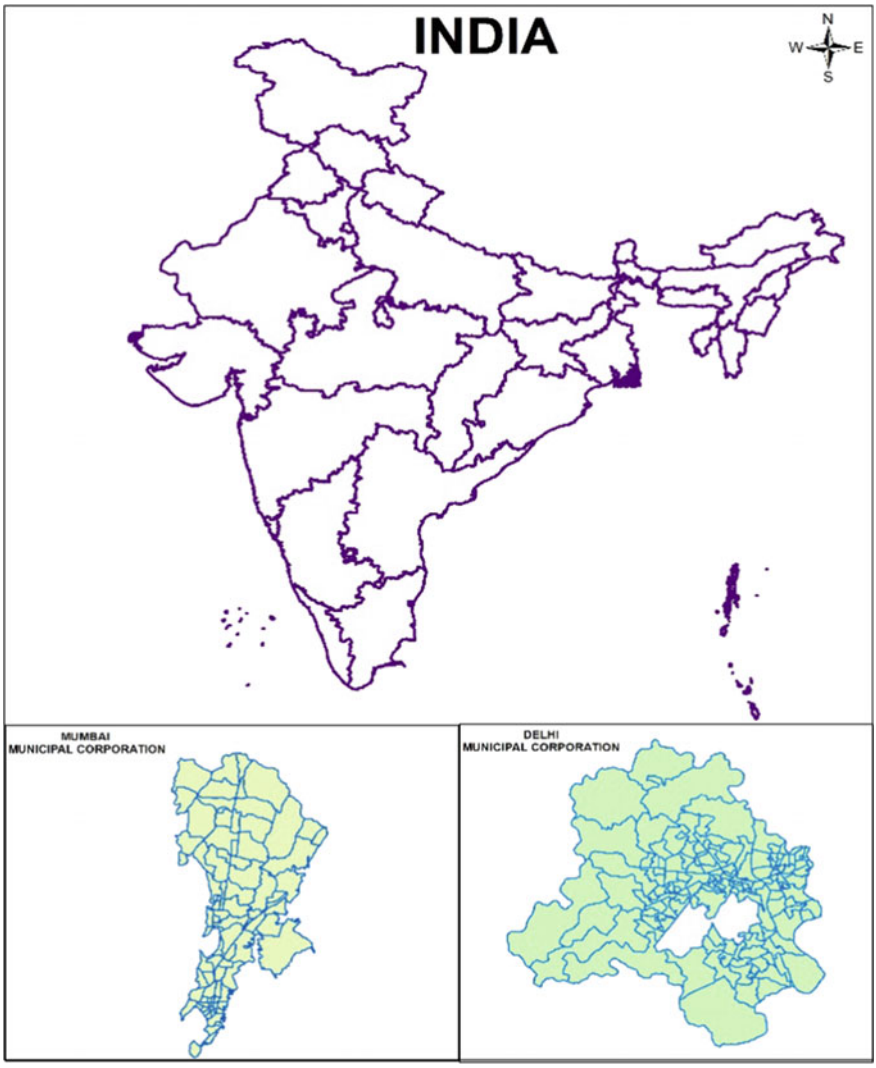

Fig. 12.1 Study area map

12.3 Materials and Methods

12.3.1 Database

This study is based on primary and secondary source of database. Demographic data have taken from Census of India (2011). Ward map of Delhi and Mumbai is also taken from Census of India. Urban transformation or changes in urban area is carried

Table 12.1 Radiometric characteristic (Landsat 4–5 TM)

Satellite	Spectral resolution (nm)	Band	Spatial resolution (m)
Landsat 4–5 TM	Band 1:0.45–0.52	Blue	30
	Band 2:0.52–0.60	Green	30
	Band 3: 0.63–0.69	Red	30
	Band 4: 0.76–0.90	Near IR	30
	Band 5: 1.55–1.75	Mid IR	30
	Band 6: 10.4–12.5	Thermal	
	Band 7: 2.08–2.35	Mid IR	30

out with the help of temporal satellite imagery (February 2001 and January 2011). Satellite images are downloaded from Earth Explorer (USGS) through Internet.

The Thematic Mapper (TM) is very advanced, multispectral scanning sensor designed to provide higher resolution, narrow and sharper spectral variation, enhanced geometric conformity and a high radiometric accuracy and resolution than earlier MSS Data (Table 12.1, Fig. 12.2).

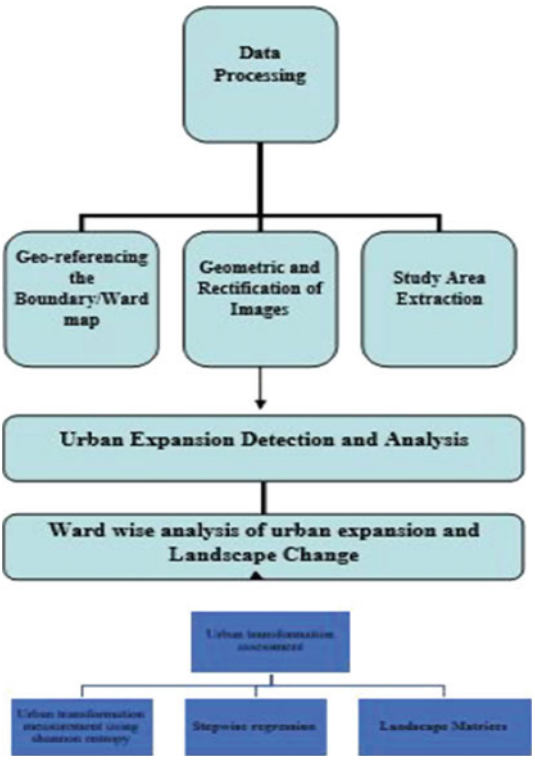

Fig. 12.2 Schematic diagram of methodology

12.3.2 Image Classification

Geometric correction and Rectification is done for better interpretation and classification result, False Colour Composite (FCC) images were created for 2001 and 2011 of the study area. The geo-rectified image was enhanced to better identification of features on earth surface. Image interpretation technique is used for FCC image to extract different features in the study area by using unsupervised classification. Some of the misclassified area with respect to pixel is also corrected through recode in ERDAS Imagine 15. Four major land use/cover types are identified and used in this study, namely; built-up area, vegetation, water bodies, non-built-up area.

12.3.3 Change Detection

To performing overall change taken place with respect to LU/LC, To find out actual change and significant result post classification method used in this case. Exact pixel wise change has been observed through change matrix. Temporal satellite data has been used for overall loss and gain of each land use and land cover class between 2001 and 2011. This information from all the classes has been compiled to generate land use land cover maps. To analyze the actual changes in land cover over period few change detection techniques are used. Post classification method is often used to detect urban change detection of any area (Jensen 1996). Rectified imagery of each date is independently classified to match their respective classes based on the reflectance value. The resulting classes based on the grouping of all pixels are overlaid in its initial stage to compare land cover maps of the cities.

12.3.4 Ward Wise Analysis of Urban Transformation

For analysis and comparison of total land use changes took place in these metropolitan cities. Built-up area from each image has been extracted for further analysis. To carry out ward wise information about the urban land use changes, images of urban and built-up land of all the 88 wards in Mumbai Municipal Corporation and 134 wards in Delhi Municipal Corporation were extracted from the classified images. Digitization of outline boundaries of each ward was employed for extraction of built-up area and total area. These areas were later incorporated in ward wise entropy assessment in order to find out exact compactness and dispersion in both the cities.

12.3.5 Urban Transformation Analysis

12.3.5.1 Urban Transformation Measurement Using Shannon's Entropy

Urban area change is a complex phenomenon and causes environmental as well as social impacts. It can be caused by population growth, topography, proximity to major resources, services, and infrastructure. Many attempts have been made to measure urban sprawl by measuring Shannon's entropy within a GIS. Shannon's Entropy is used to measure the degree of spatial concentration and dispersion, as defined by geographical variables. In other words, Shannon's entropy is a measure to determine the compactness or dispersion of built-up land growth in the urban areas. To find out the compactness or dispersion of the urban development, an integrated analysis has been carried out. To measure the compactness or dispersion of urban built-up, Shannon's entropy method was adopted (Yeh 2001; Li and Yeh 2004; Lata et al. 2001; Sudhira et al. 2004). H_n can be used to measure the degree of spatial concentration or dispersion of geographical variable among n zones. The Shannon's entropy (H_n) is given by,

$$\mathbf{H_n} = -\Sigma \mathbf{Pi} \log (\mathbf{P_i})$$

where $P_i = X\mathrm{i}/\Sigma X\mathrm{i}$, and xi is the density of land development, which equals the amount of built-up area divided by the total amount of land in the ith of n total zones $n =$ Total number of zones.

The value of entropy ranges from 0 to log n. If the distribution is very compact then the entropy value would be closer to 0 and when the distribution is much dispersed the value will be closer to log n. Large value of entropy indicates the occurrence of urban sprawl. This methodology was adopted to study the distribution of built-up in different wards, around the core, and along the National Highway. To analyze the sprawl of Mumbai city, the study area was divided into 88 and 134 zones based on the administrative wards of Delhi and Mumbai City. The ward boundaries were digitized from the scanned map of Mumbai Municipal Corporation. Two types of thematic layers are needed for calculation of densities of land development in each zone. The ward boundaries formed one layer and the built-up area formed the other layer. The overlay of boundaries layer on the built-up layer can clip the built-up area of individual wards and villages. The density of built-up area was calculated by dividing the built-up area of each ward from its total area. In general, the sprawl is affected by some location factors, such as distance to urban centres and roads.

12.3.6 Stepwise Regression

Step-by-step regression was used to trace the impact on the positive growth of dependent aspect like the built-up of the independent variable. The density of the population, the literacy of women, non-agricultural workers, the absolute population and the variable dependent are independent variables, and they account for the proportion between the areas of the buildings and the walls.

12.3.7 Landscape Matrices

Utilizing "landscape metrics as quantitative measures of spatial structures and patterns gives the ability to describe urban land use features, structures and patterns of a landscape" (Herold et al. 2002). Most of the landscape metrics correlate with each other. For this study the most widely applied methods such as landscape metrics extracted from the classified images was used. These are the following metrics which we focused to find these metrics.

12.4 Result and Discussion

To study the spatial–temporal changes in urban place over the past 10 years, Satellite Imageries are maps of 2001–2011 as mentioned in the above section (database) were procured and processed according to the detailed methodologies mentioned in the earlier section. In order to analyze the urban change pattern and to identify the causing factors behind these urban changes various approaches were adopted for built-up statistics for the city as a whole, ward wise, zone wise and distance wise.

12.4.1 Land Use/cover Status of Delhi and Mumbai

Figures 12.3 and 12.4 depicts spatial distributional pattern of land use/cover of Delhi (541.12 ml^2) and Mumbai (152.63 ml^2) for the year 2001 while 2011. Table 12.2 and 12.3 reveal that in 2001, about 45.76% (247.67 ml^2) area was under built-up area in Delhi, whereas about 60.51% (92.37 ml^2) area was under built-up in Mumbai. Likewise, 50.43% (272.67 ml^2) and 34.42% (34.42 ml^2) area was under vegetation, 2.76% (14.98 ml^2) and 0.65% (1 ml^2) under open space and 5.56% (1.02 ml^2) and 4.39% (6.71 ml^2) area was covered by water body in Delhi and Mumbai, respectively. In 2011, the contribution of urban area under Delhi increased by 22.37% (23.62 ml^2) but Mumbai experienced a slow change in urban area in comparison to 2001 i.e.,

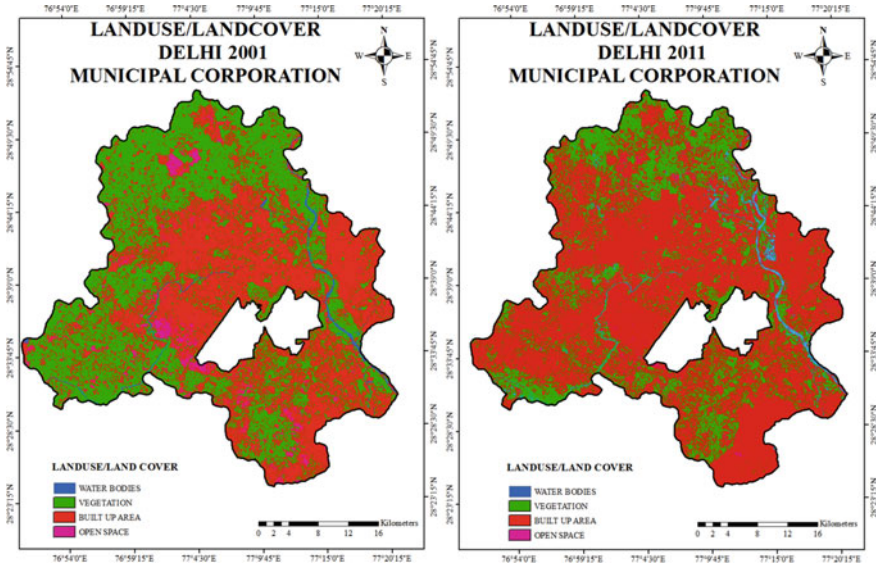

Fig. 12.3 Land use/cover of Delhi, 2001and 2011

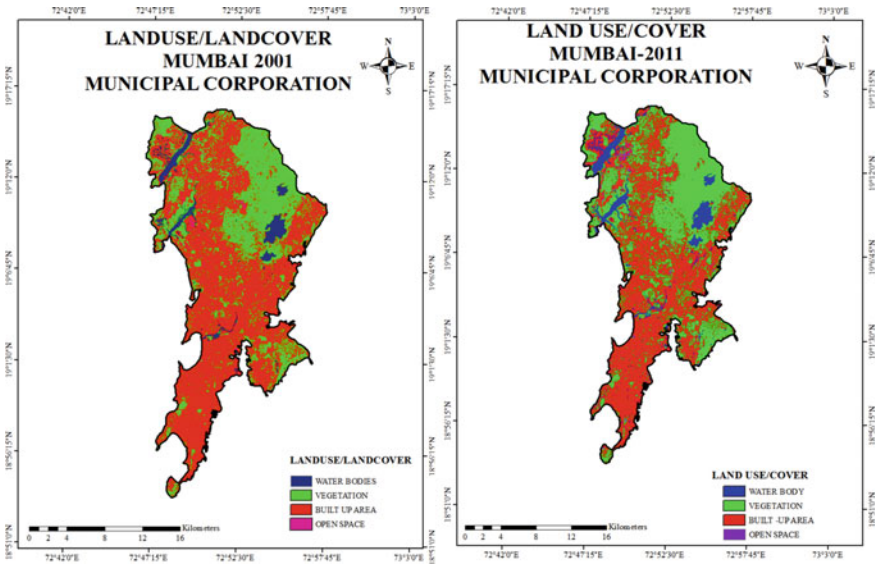

Fig. 12.4 Land use/cover of Mumbai, 2001 and 2011

Table 12.2 Area and amount of change in different land use/cover categories in Delhi, 2001–2011

Land use/cover categories	2001		2011		Change 2001–2011	
	ml^2	%	ml^2	%	ml^2	%
Water body	5.56	1.02	10.16	1.870	−2.50	0.85
Vegetation	272.91	50.43	157.92	29.180	−22.39	−21.25
Built up	247.67	45.76	368.680	68.130	23.62	22.37
Open space	14.98	2.76	4.37	0.800	−0.52	−1.96

Table 12.3 Area and amount of change in different land use/cover categories in and Mumbai, 2001–2011

Land use/cover categories	2001		2011		Change 2001–2011	
	ml^2	%	ml^2	%	ml^2	%
Water body	6.71	4.40	6.97	4.56	−2.50	0.85
Vegetation	52.55	34.43	44.83	29.40	−22.39	−21.25
Built up	92.37	60.52	100.36	65.80	23.62	22.37
Open space	1.00	0.66	0.47	0.30	−0.52	−1.96

5.23% (7.99 ml^2). On the other hand, vegetation cover of Delhi depleted at very high rate in these 10 years and was left with only 29.18% (157.92 ml^2).

Mumbai underwent through the same scenario but the rate of change is bit slow at 29.4% (44.83 ml^2). The proportion of water body increased in both the metropolitan cities reached at 1.87% (10.16 ml^2) and 4.56% (6.97 ml^2) in Delhi and Mumbai respectively. Open space of both the metropolitan cities decreased in 2011 down with −1.96% and −0.35% in Delhi and Mumbai, respectively.

12.4.2 Land Use/cover Change

The data presented in Tables 12.2 and 12.3 depict that both positive and negative changes occurred in the land use/cover pattern in Delhi and Mumbai. During the last decades, the built-up area has increased from 247.67 ml^2 in 2001 to 368.68 ml^2 and 92.37 ml^2 in 2001 to 100.36 ml^2 in 2011 which accounts for 22.37% and 5.23% of the total sprawl area of Delhi and Mumbai. The vegetation cover has been decreased from 272.90 ml^2 in 2001 to 157.92 ml^2 in 2011 in Delhi and 52.55 ml^2 in 2001 to 44.83 ml^2 in 2011. This decrease in vegetation accounts for 21.25% and 5.05% in Delhi and Mumbai, respectively. Similarly, decrease in water bodies and open space land may also be seen from the table. The change in land use/cover under various categories have been clearly depicted (Figs. 12.5, 12.6, 12.7 and 12.8).

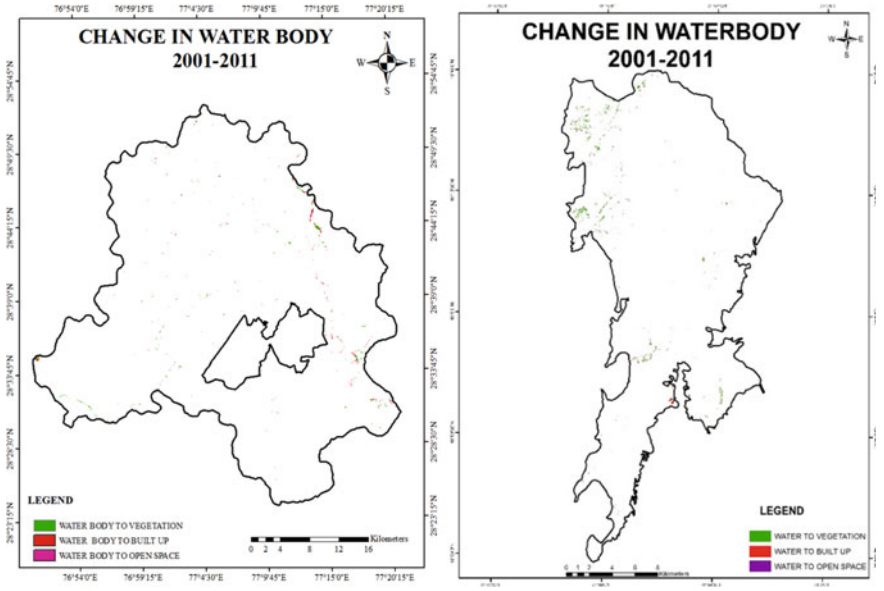

Fig. 12.5 Change in water body in Delhi and Mumbai (2001–2011)

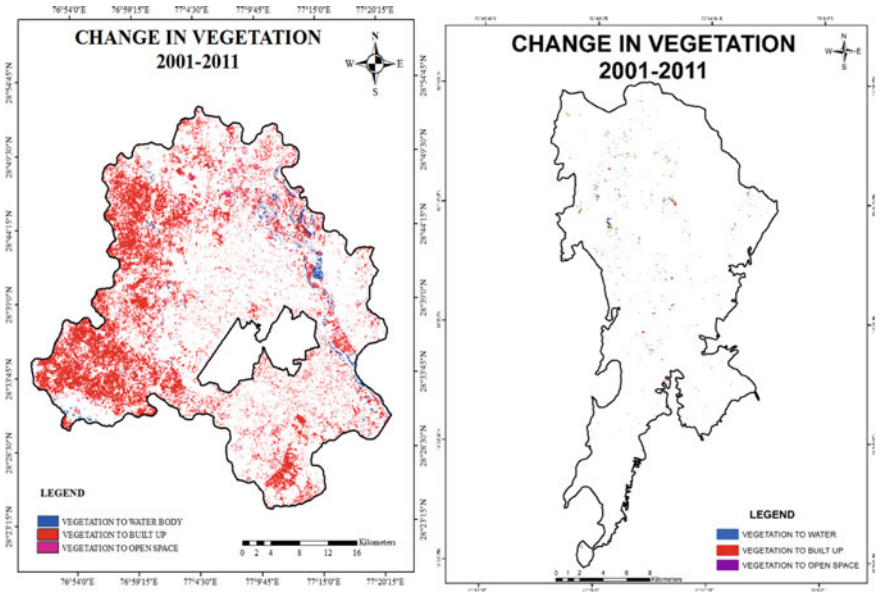

Fig. 12.6 Change in vegetation in Delhi and Mumbai (2001–2011)

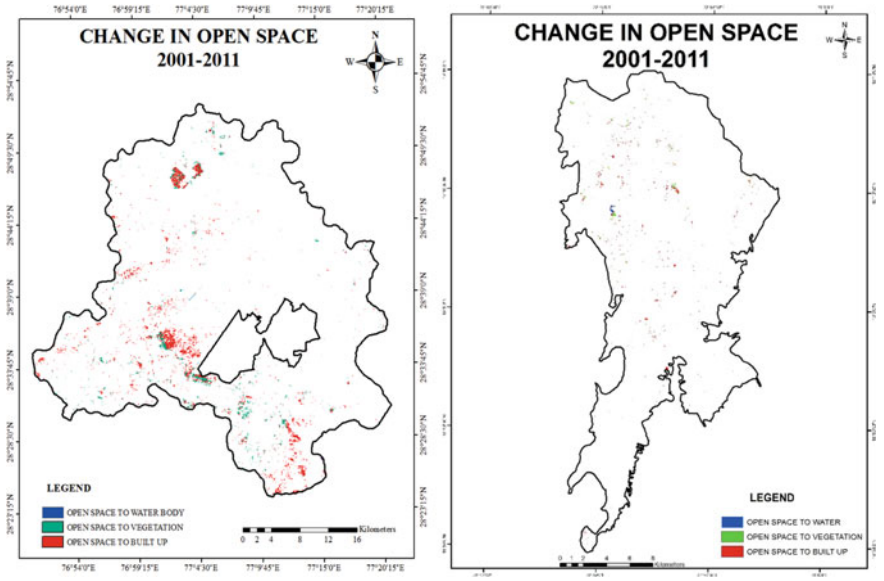

Fig. 12.7 Change in open space in Delhi and Mumbai (2001–2011)

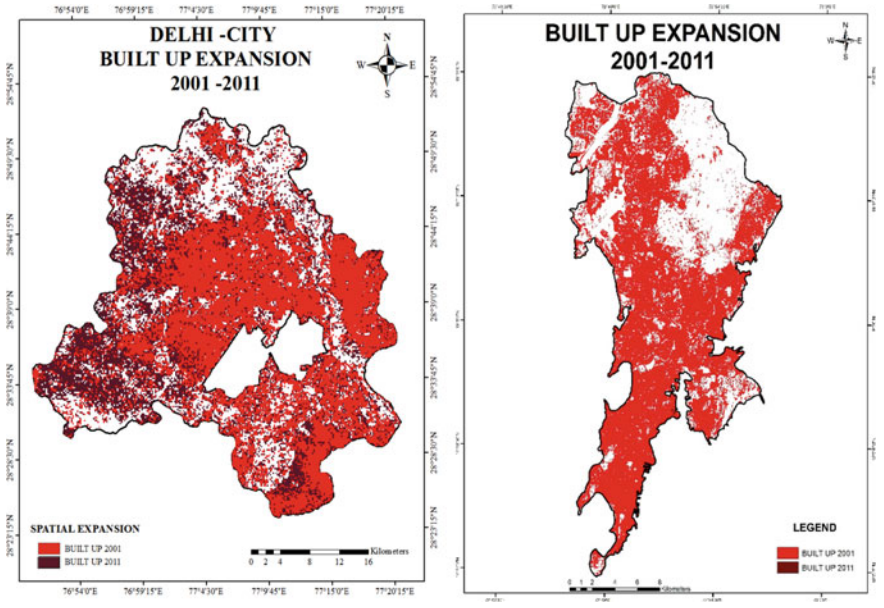

Fig. 12.8 Expansion of built-up area in Delhi and Mumbai (2001–2011)

Table 12.4 Land use/cover change matrix showing land encroachment in Delhi, 2001–2011

Land use/cover categories Year 2011	Year 2001				
	Water body	Vegetation	Built up	Open space	Sum_2011
Water body	3.91	6.18	0.00	0.07	10.16
Vegetation	0.89	152.67	0.00	4.37	157.93
Built up	0.72	110.76	247.67	9.51	368.66
Open space	0.05	3.29	0.00	1.02	4.36
Sum_2001	5.56	272.91	247.67	14.97	

Table 12.5 Land use/cover change matrix showing land encroachment in Mumbai, 2001–2011

Land use/cover categories Year 2011	Year 2001				
	Water body	Vegetation	Built up	Open space	Sum_2011
Water body	5.69	1.23	0.00	0.04	6.96
Vegetation	0.70	43.89	0.00	0.23	44.82
Built up	0.30	7.09	92.37	0.58	100.35
Open space	0.01	0.32	0.00	0.15	0.47
Sum_2001	6.70	52.53	92.37	0.92	

To understand land encroachment for different land categories during the last one decade, a change detection matrix (Tables 12.4 and 12.5) was prepared which reveals that:

- About 110.76 and 7.09 ml^2 area of vegetation covered has been converted into built-up land, 3.293 and 0.32 ml^2 area under barren land and 6.181 and 1.23 ml^2 area under water body in Delhi and Mumbai respectively;
- About 4.37 and 0.22 ml^2 area of barren land has been converted into vegetative area, 9.51 and 0.58 ml^2 into built-up area and 0.070 and 0.044 ml^2 into water body in Delhi and Mumbai;
- About 0.887 and 0.7 ml^2 area of water body has been converted into vegetation cover and 0.048 and 0.007 ml^2 area under barren land whereas 0.717 and 0.304 ml^2 area has been encroached by built-up in Delhi and respectively.

12.4.3 Urban Sprawl Measurement: Shannon Entropy

For each ward, the entropy of the urban areas was calculated in 2001 and 2011. The entropy shows that the patterns of urban change/growth between the study area have changed substantially internally. Usually, urban growth/change in the entire region is quite evident. The municipal area Delhi and Mumbai grew nearby in all the wards, the growth threshold ($\text{Log}(n) = \log(134) = 2.12$) and ($\text{Log}(n) = \log(88) = 1.94$) were almost reached. Increased or closer to log (n) means that the development spread or

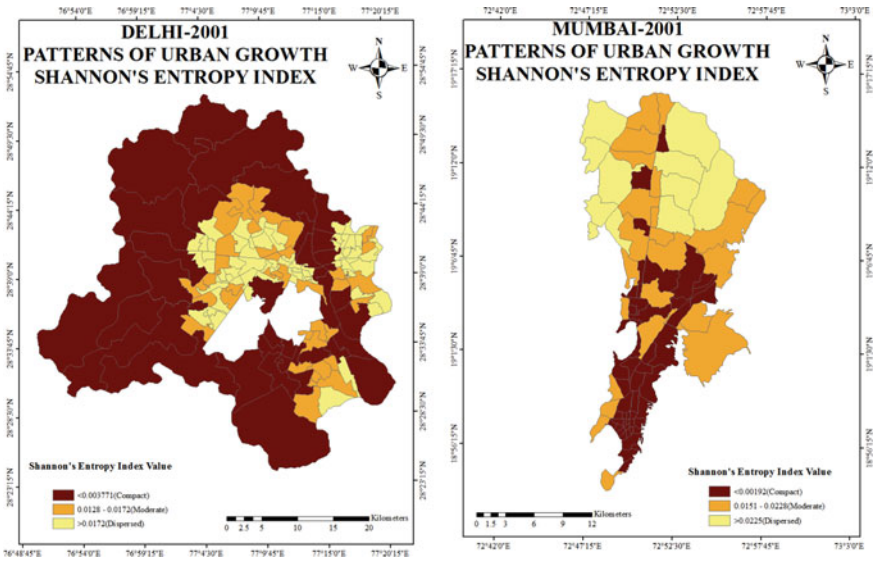

Fig. 12.9 Patterns of urban growth in Delhi and Mumbai, 2001 (Shannon's entropy index)

dispersed or sparse. The lower the entropy values, both aggregated and compact is the development. In 2011, the lower ward entropy values show aggregated or compact growth in the region as a whole. During the study period (2001–2011), the wards in Delhi, Mumbai grew phenomenally and the entropy value in 2011 has been higher (Figs. 12.9 and 12.10).

12.4.4 Correlates and Determinants of Urban Growth

There are a variety of factors that influence urban development. Due to a lack of data, it is difficult to include all of those factors in a quantitative analysis. As a result, this analysis includes the factors for which data was provided by the Census of India and satellite. Stepwise regression was used to estimate the contribution of these factors in urban growth because it tells us the contribution of an added or deleted variable in explaining the dependent variable by looking at changes in the R^2 value (Mahmood 1977). The determinants of urban growth were studied using ward level data from 2001.Other years did not have ward-level population data for the same municipalities as 2001. As previously stated, the built-up density or percentage of built-up area has been regarded as the most important indicator of urban growth, and thus it has been used as a dependent variable in the analysis, as shown in Tables 12.6 and 12.7. The determinants of urban growth are broken down into four categories, each of which explains 78.8% of the variation in urban growth. This proportion has been deemed very significant in regression analysis. The population density, which represents the

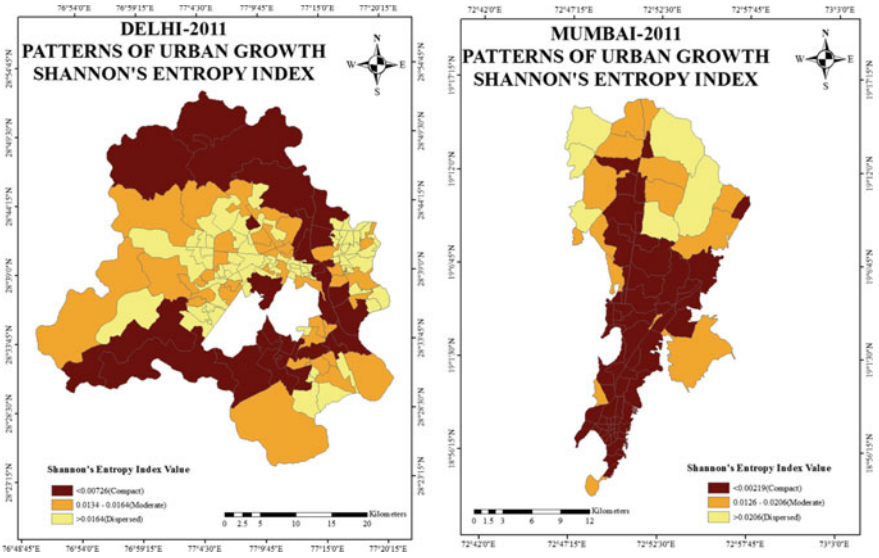

Fig. 12.10 Patterns of urban growth in Delhi and Mumbai, 2011(Shannon's entropy index)

Table 12.6 Model summary of stepwise regression-Delhi

Model	R	R Square	Increase in R Square	Adjusted R Square	Increase in adjusted R Square	Std. error of the estimate
1	0.813	0.748		0.755		1.083092082
2	0.902	0.823	0.075	0.819	0.74	0.902471038
3	0.913	0.831	0.007	0.825	0.006	0.887713476
4	0.911	0.834	0.004	0.827	0.002	0.882215120
5	0.916	0.838	0.004	0.829	0.002	0.877487146
6	0.913	0.841	0.003	0.830	0.001	0.873613483
7	0.913	0.851	0.000	0.828	−0.002	0.879048537

Table 12.7 Model summary of stepwise regression-Mumbai

Model	R	R Square	Increase in R Square	Adjusted R Square	Increase in adjusted R Square	Std. error of the estimate
1	0.871	0.758		0.755		1.093092082
2	0.913	0.833	0.075	0.829	0.74	0.912471038
3	0.917	0.841	0.007	0.835	0.006	0.897713476
4	0.919	0.844	0.004	0.837	0.002	0.892215120
5	0.921	0.848	0.004	0.839	0.002	0.887487146
6	0.923	0.851	0.003	0.840	0.001	0.883613483
7	0.923	0.851	0.000	0.838	−0.002	0.889048537

basic characteristic of city growth, i.e., a large population in a small area, explains the highest proportion. Female literacy rate is the second most important explanatory variable, indicating the educational importance of Delhi and Mumbai in city growth. The third variable is the percentage of female workers in the secondary and tertiary sectors, which is an indicator of the city's employment opportunities. For the rural and other migrants, these opportunities act as a "pull factor." Absolute population is the model's final indicator, and it represents the role of wards in city growth.

a. Predictors: (Constant), No_HH
b. Predictors: (Constant), No_HH, alpha
c. Predictors: (Constant), No_HH, alpha, TOT_WORK_P
d. Predictors: (Constant), No_HH, alpha, TOT_WORK_P, total pop
e. Predictors: (Constant), No_HH, alpha, TOT_WORK_P, total pop, LIT_gap
f. Predictors: (Constant), No_HH, alpha, TOT_WORK_P, total pop, LIT_gap, sex_ratio
g. Predictors: (Constant), No_HH, alpha, TOT_WORK_P, total pop, LIT_gap, sex_ratio, bita

12.4.5 Spatial/Landscape Metrics

The process of urban growth in Delhi and Mumbai has also been measured with the help of spatial or landscape metrics. It could be seen that percentage of built-up area increased from 45.76 and 60.51% in 2001 to 68.13 and 65.8% in 2011 for Delhi and Mumbai respectively (Table 12.2). In absolute terms, built-up area increased from 247.67 and 92.37 ml^2 in 2001 to 368.68 and 100.36 ml^2 in 2011 i.e., it increased near to half of 2001 in Delhi whereas in Mumbai it increased in very less amount about 10^{years}. This indicates that there has been rapid growth in Delhi as far as horizontal urban growth of built-up, on the other hand in Mumbai urban growth in terms of built-up area is very less in comparison to Delhi. Core area of Delhi sharply increased from 247.67 to 368.68 ml^2 between 2001 and 2011.On the other hand, Mumbai experiences fraction of changes in core area (Tables 12.8 and 12.9).

The quick growth in the core region is attributable to both an increase in built-up area and a decrease in the number of patches. From 2000 to 2011, not only did

Table 12.8 Spatial /landscape change (ml^2) in Delhi

Metrics	2001	2011	Δ%2001–2011
CA	247.67	368.68	48.86
NP	82.79	50.44	− 39.074
LPI	0.32	0.12	108.034
ED	0.20	0.18	− 5.731
FRAC_AM	0.0051	0.005	3.71
ENN_MN	0.24	0.21	− 8.537
Contagion	0.20	0.22	9.247

Table 12.9 Spatial/landscape change (ml^2) in Mumbai

Metrics	2001	2011	Δ%2001–2011
CA	92.37	100.36	8.6472
NP	14.11	11.64	− 17.5006
LPI	0.10	0.11	11.3172
ED	0.15	33.3911	− 17.6390
FRAC_AM	0.0052	0.0051	− 1.4090
ENN_MN	0.57	0.23	− 59.5946
Contagion	0.20	0.22	7.0985

the largest patch area grow, but so did the percentage (LPI) of the largest patch area to total built-up area, which increased from 45.76% in 2000 to 68.130% in 2011, indicating that almost all of Delhi's built-up area in 2011 has become a single interconnected patch. While the overall built-up area in Mumbai expanded from 60.52% in 2000 to 65.80% in 2011, the majority of built-up patches remained in single patches. Similarly, in both cities, all other landscape features have changed dramatically over the decades. The rest of 165 built-up patches had an area of just 478 hectares contributing to less than 4% of built-up area in 2011. Thus, the area and edge metrics indicates that there has been rapid increase in built-up area as well as largest patch area between 2001 and 2011.

12.5 Conclusion

This study shows that the metropolitan cities such as Delhi and Mumbai somehow indicate the same trend of changes which occurred in last one decade. Remote sensing data means satellite imageries, temporal data is used to extract the amount of changes in both the metropolitan cities. Facilities offered by these cities automatically attract people from nearby small towns. These two metropolitan cities are approximately proving the concept of "Primate City" given by Mark Jafferson. The core area of the city has become more compact than earlier and surrounding region getting clusters. Somewhere sprawl has been expanded beyond city boundary limits. The most expansion happened along major roads as well as outer part of the city, the flow of migrations not only all India. In order to restrict consequences of urban change, there is need of proper management of new built-up. No doubt in upcoming years Delhi and Mumbai becomes one of very large city of World.

References

Allefsen RA (1962) City hinterland relationship in India. University of California Press

Berling-Wolff S, Wu J (2004) Modeling urban landscape dynamics: a case study in Pheonix, USA Urban Ecosyst 7(3)
Bhagwat R (2011) Application of remote sensing and GIS, landuse/land cover change in Kathmandu metropolitan city. Nepal J Theor Appl Inform Technol 23(2):80–86
Grimm NB, Grove JG, Pickett ST, Redman CL (2000) Integrated approaches to long-term studies of urban ecological systems: Urban ecological systems present multiple challenges to ecologists—Pervasive human impact and extreme heterogeneity of cities, and the need to integrate social and ecological approaches, concepts, and theory. BioScience 50(7):571–584
Herold M, Scepan J, Clarke KC, (2002) The use of remote sensing and landscape metrics to describe structuresand changes in urban land uses. Environ Plann A 34(8):1443–1458
Jat MK, Garg PK, Khare D (2008a) Modeling of urban growth using spatial analysis techniques: a case study of Ajmer city (India). Int J Remote Sens 29(2):543–567
Jat MK, Garg PK, Khare D (2008b) Monitoring and modelling of urban sprawl using remote sensing and GIS techniques. Int J Appl Earth Observ Geoform 10(1):26–43
Jensen J (1996) Introductory digital image processing. Prentice Hall, New Jersy
Joshi PK, Lele N, Agarwal SP (2006) Entropy as an indicator of fragmented landscape. Curr Sci 91(3):276–278
Lata KM, Sankar RCH, Krishna PV, Badrinath KVS, Raghavaswamy (2001) Measuring urban sprawl: a case study of Hyderabad. GIS Dev 5:8–13
Li X, Yeh AGO (2004) Analyzing spatial restructuring of land use patterns in a fast growing regionusing remote sensing and GIS. Landscape Urban Plann 69(4):335–354
Mahmood A (1977) Statistical methods in geographical studies. Rajesh Publications, New Delhi
Mehta A, Sinha VK, Ayachit G (2012) Land use/land cover study using remote sensing and GIS in an arid environment. Bull Environ Sci Res 1(3–4):4–8
Nagendra H, PareethS GR (2006) People within parks-forest villages, land cover change and landscape fragmentation in the Taboda Andhari Tiger Reserve, India. Appl Geogr 26(2):96–112
Rawat JS, Kumar M, Biswas V (2014) Land use/cover dynamics using multi-temporal satellite imagery: a case study of Haldwani Town area, district Nainital, Uttarakhand, India. Int J Geomgeosci 4(3):536–543
Sinha SK (2017) Urban sprawl in Gautam Budh Nagar District, Uttar Pradesh. Ann Nat Assoc Geogr India 36(1):89–102
Sudhira HS, Ramachandran TV, Jagadish KS (2004) Urban sprawl: metrics dynamics and modelling using GIS. Int J Appl Earth Observ Geoinform 5:29–39
Wu F (2001) China's recenturban development in the process of land and housing marketisation and economicglobalisation. Habitat Int 25(3):273–289
Yeh A (2001) Measurement and monitoring of urban sprawl in a rapidly growing region using entropy. Photogramm Eng Remote Sens 67(1):83–90
Yuan F, Sawaya KE, Loeffelholz BC, Bauer ME (2005) Land cover classification and change analysisof the Twin Cities (Minnesota) Metropolitan Area by multitemporal Landsatremote sensing. Remote Sens Environ 98(2–3):317–328

Chapter 13
Assessment of Particulate Pollutants (PM_{10} and $PM_{2.5}$), Its Relation with Vegetation Cover and Its Impacts on Apple Orchards in Kullu Valley, Himachal Pradesh, India

Bhim Chand, Pawan Kumar Thakur, Renu Lata, Jagdish Chandra Kuniyal, and Vijay Kumar

Abstract Present study is an attempt to estimate the effects of roadside dust pollution on apple trees of Mohal (1146 m), Raison (1359 m) and one control site, Beasar (2181 m), Kullu Valley, Himachal Pradesh. In both Mohal and Raison sites, PM_{10} and $PM_{2.5}$ are showing the increasing trend which is affecting the apple farming and production in the area. When the dust particles settle down on the stigma of flower it stops an anther to contact with stigma, which affects the pollination. Thus, the dust particle affects the flower of plant during the time of pollination. Particulate pollutants PM10 (<10 μm) and $PM_{2.5}$ (<2.5 μm) have been monitored in and around of apple orchards. Average PM_{10} concentration has found low (20.9 ± 1.7 μg m^{-3}) at control site Beasar, whereas it shows high value (88.1 ± 2.0 μg m^{-3}) at Raison. Mohal has relatively higher PM_{10} concentration with a mean value of 104.2 ± 1.1 μg m^{-3}. In Mohal and Raison sites, the particulate pollutants have μcrossed the permissible limit (100 μg m^{-3}) as prescribed by National Ambient Air Quality Standards (NAAQS). There is negative correlation with NDVI values and pollutants concentration. It is also made clear from HYSPLIT model and CALIPSO analysis that the sources of pollutants are mainly local in nature. The Air Quality Index (AQI) study reveals that air quality of Mohal falls under good condition. But during spring season, the pollutants cross the permissible limit which affects the pollination process of apple trees.

B. Chand (✉) · R. Lata · V. Kumar
G. B. Pant National Institute of Himalayan Environment, Himachal Regional Centre, Mohal-Kullu 175126, Himachal Pradesh, India

P. K. Thakur
Forest Ecology & Climate Change Division, Himalayan Forest Research Institute, Conifer Campus Panthaghati, Shimla 171013, Himachal Pradesh, India

J. C. Kuniyal
G. B. Pant National Institute of Himalayan Environment, Kosi-Katarmal Almora 263601, Uttarakhand, India

R. B. Singh et al. (eds.), *Remote Sensing and Geographic Information Systems for Policy Decision Support*, Advances in Geographical and Environmental Sciences,
https://doi.org/10.1007/978-981-16-7731-1_13

Keywords Particulate pollutants · PM_{10} · $PM_{2.5}$ · Kullu valley · Apple orchards

13.1 Introduction

Apple farming and its production is directly related to climatic condition of a particular region. At present, the traditional apple farming is under stress due to changes in climate (Basannagari and Kala 2013). Presence of particulate pollutants even in a small quantity can affect the environment by influencing the thermal properties of the environment. Radiative effect is shown by these gases by which they absorb the long wave radiation and reduce the outgoing at the top of atmosphere and this leads to increase in temperature (Wang et al. 1976). Atmospheric pollutants are released into the environment by natural and anthropogenic sources like agricultural, industrial, transportation, residential and natural sources (Bernard et al. 2001; Ramanathan and Feng 2009). Air pollution not only affects the air quality but also its acute and chronic effect can create various health problems in human being (Oberdörster et al. 2004). Especially, particulate matter ($PM_{2.5}$) plays foremost role in creating depression, anxiety and many other neurological problems in human being (Calderón-Garcidueñas et al. 2002; Oberdörster et al. 2004). These particulate matters also affect atmospheric process like reduce visibility, effect precipitation pattern and cloud formation and also play an important role in making rain, clouds and fog acidic in nature (Celis et al. 2004; Khoder 2002). According to Gajananda et al. (2005), the level of air pollution is increasing over the sensitive areas of northwestern part of the Himalayas due to high anthropogenic activities as they monitored the Total Suspended Particulate (TSP), size-separated atmospheric aerosols and Aitken Nuclei (AN) at Mohal (Kullu) and Manali tourist complex since 1996.

The mountain environment is one of the most weak biological systems to the environmental change as are the mountain networks, particularly those essentially rely upon animal husbandry, marginal agriculture and agriculture items. Currently, the Himalayan mountain environment is confronting the difficulties made because of expanding aridity, hotter winter season, inconstancy in precipitation and unexpected frosts and storms (Renton 2009; Dash and Hunt 2007) which generally influence the whole scope of biodiversity, including farming and cultivation crops (Renton 2009; Kala 2013). However, the Himalaya harbors rich biodiversity and is one of the weakest mountain biological systems to environmental change (Xu et al. 2009; Bawa et al. 2010), there is scarcity of orderly examination of environmental change and its effects on the Himalayan biological systems, biodiversity and neighborhood individuals' occupations (Shrestha et al. 2012). Farmers of Indian Himalayan Region (IHR) develop many natural product crops, including pomes (apple and pear) and stone natural products (peach, plum, apricot and cherry) in significant amount, (Ghosh et al. 1999) yet apple has the preference over all other agricultural crops (Kala 2007). The main aim of this study is to know the status and source of particulate pollutants and their effects on apple plantations.

13.2 Study Area

The present study deals with ambient air quality status in and around the apple orchards area in Kullu valley. Kullu is a broad open valley formed by the Beas River situated between Manali and Larji. Kullu valley is famous for its temples, beauty and its majestic hills covered with pine and deodar forest and sprawling apple orchards. Ambient air quality was monitored at Mohal Latitude—31° 54′ 54.15″ N and Longitude—77° 07′ 25.42″ E at the Altitude of 1146 m, Beasar (control site) Latitude—32°01′41.34″ N Longitude—77°05′34.73″ E at the Altitude of 2181 m third site Raison: Latitude—32°03′25.14″ N Longitude—77°08′06.91″ E at the Altitude of 1359 m (Fig. 13.1).

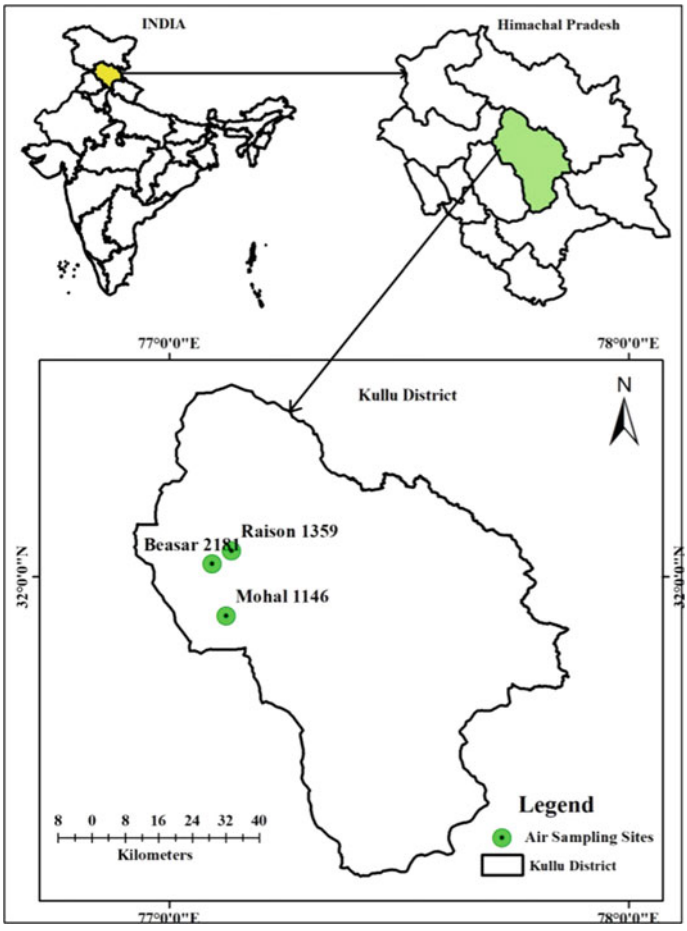

Fig. 13.1 Location of the study area in the Kullu valley, Himachal Pradesh

13.3 Methodology

Current study has been carried out during the winter, spring and summer seasons in 2019 (January to June 2019). The air quality status of Beasar and Raison sites was monitored only in summer season. Respirable Dust Sampler (RDS; Envirotech NL-460) was used to observe PM_{10} under ambient air quality monitoring based on filtration-gravimetric method with Whatman filter paper (20.3 × 25.4 cm). Fine Particulate Sampler (APM-550 make Envirotech) was used for $PM_{2.5}$. The Whatman Glass Micro Fibre Filter paper (GF/A (47 mm) was used to expose $PM_{2.5}$. Samples were exposed on 24 hourly bases during winter season (January to March 2019), spring season (April 2019) and summer season (May to June 2019).

13.3.1 Air Quality Index (AQI)

Air Quality Index (AQI) was computed to know the overall pollution status. The AQI was calculated from the method used by Bhaskar and Mehta (2010) as follows:

$$AQI = \left(\frac{M_{ob}}{M_{st}}\right) \times 100$$

where, M_{ob} = observed value of air pollutants, M_{st} = standard value of acceptable limit of NAAQS.

13.3.2 Normalized Difference Vegetation Index (NDVI)

Normalized Difference Vegetation Index (NDVI) was calculated in the two selected sites with the help of Remote Sensing (RS) and Geographic Information System (GIS). Cloud Free Landsat-7 and Landsat-8 satellite data of October 2003 and October 2019 had been downloaded from the United States Geological Survey (USGS) Earth Explorer website. All the data were pre-processed and projected to the Universal Transverse Mercator (UTM) projected system. The details of the satellite data collected are shown in Table 13.1. Landsat-7 and Landsat-8 are the satellites of the Landsat series launched by NASA. In this study, bands 2–7 and 2–5 of Landsat-8 and Landsat-7 were, respectively, used to calculate different indices.

Table 13.1 General Information of Landsat-7 (ETM+) and Landsat-8 (OLI) datasets (2003–2019)

Sensor/Satellite	No. of bands	Resolution (m)	Path/Row and reference system	Date of acquisition
ETM +	7	30	WRS-II/146/40	10-05-2003
TIR	2	30	WRS-II/146/40	10-05-2003
OLI	9	30	WRS-II/146/40	28-10-2019
TIR	2	100	WRS-II/146/40	28-10-2019

13.3.3 Derivation of NDVI Image

NDVI images are calculated from NIR and Red bands of the Landsat 8 sensor. Using NDVI maps, we can separate vegetation from the non-vegetation area. The NDVI is related to healthy vegetation because the infrared band is high radiance reflecting and observing as well in the part of the spectrum. Green leaves have a reflectance of 20% or less in the 0.5 to 0.7 range (Green to Red) and about 60% in the 0.7 to 1.3 μm range (near Infrared). The value is then normalized to –1 NDVI + 1 to partially account for differences in illumination and surface slope. The index is defined by Eqs. 13.1 and 13.2. Estimation of NDVI using Landsat-7 and Landsat-8 sensor optical band after layer stacking, mosaicking and subsetting with the help of area of interest (AOI), band 2, 3, 4, 5 and 7 using the algorithm.

$$\text{For Landsat} - 7(\text{ETM}+) \qquad \text{NDVI} = \frac{\text{BAND 4} - \text{BAND 3}}{\text{BAND 4} + \text{BAND 3}} \tag{13.1}$$

$$\text{For Landsat} - 8(\text{OLI}) \qquad \text{NDVI} = \frac{\text{BAND 5} - \text{BAND 4}}{\text{BAND 5} + \text{BAND 4}} \tag{13.2}$$

13.4 Results and Discussion

Is one of the major negative results due to the road construction and other developmental activities particularly during construction stage are one of the major sources of air pollution.

13.4.1 PM_{10} Concentration at Mohal

During winter season, the highest ever concentration of PM_{10} (162.6 μg m^{-3}) was observed on January 16, 2019 (Fig. 13.2). The low concentration of PM_{10} was observed as 25.7 μg m^{-3} on February 25, 2019. Average concentration of PM_{10}

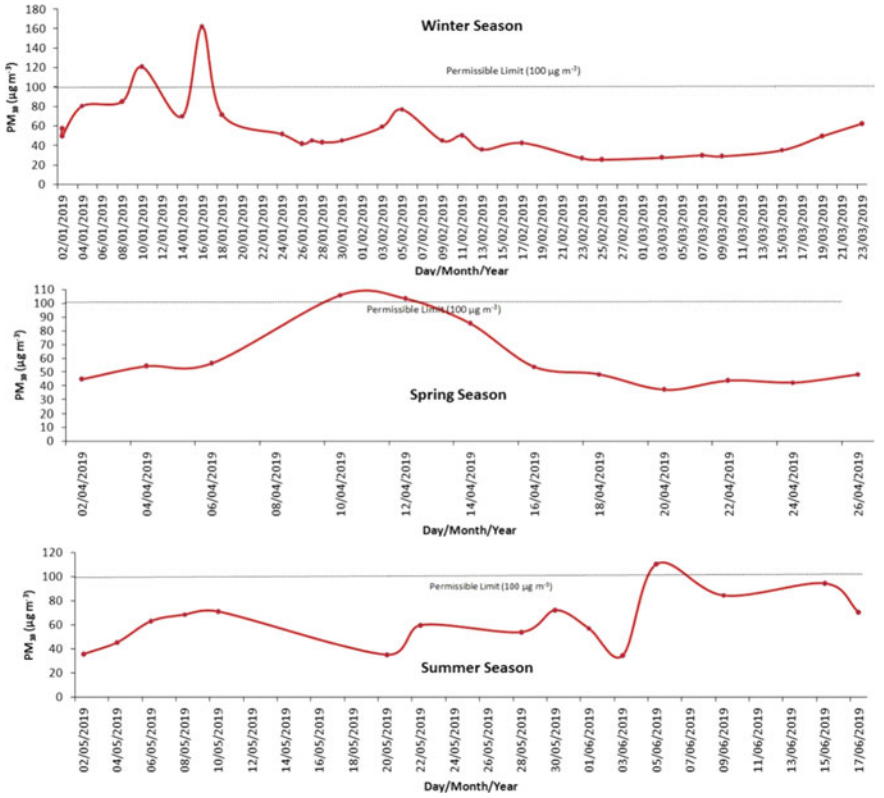

Fig. 13.2 PM_{10} Concentration at Mohal during different season

was observed 56.6 ± 5.8 μg m^{-3}. While the status of PM_{10} during spring season was observed 106.3 μg m^{-3} as maximum on April 10, 2019 and 37.2 μg m^{-3} minimum on April 20, 2019 (see Fig. 13.2). The average concentration of PM_{10} was observed 60.4 ± 6.9 μg m^{-3}. On the other hand, during summer season, the highest ever concentration of PM_{10} (110.6 μg m^{-3}) was observed on June 05, 2019 (see Fig. 13.2). This value of PM_{10} was observed minimum 34.7 μg m^{-3} on June 03, 2019. The average concentration of PM_{10} was observed 63.9 ± 6.9 μg m^{-3}. It is observed that the background values of six samples were beyond the acceptable limit (100 μg m^{-3}) as prescribed by NAAQS, especially in case of the spring season when the flowering on the apple trees was on its peak which affects the pollination.

13.4.2 PM_{10} Concentration at Raison and Beasar

PM_{10} concentration at Raison and Beasar sites were observed only in summer season, ranged between 9.6 μg m^{-3} and 31.8 μg m^{-3} with the mean value of 20.9 ± 1.7 μg m^{-3} at Beasar. Highest ever concentration of PM_{10} (31.8 μg m^{-3}) was observed on June 28, 2019. On the other hand, the Raison site PM_{10} concentration ranged between 34.7 μg m^{-3} and 112.3 μg m^{-3} with the mean value of 64.9 ± 6.2 μg m^{-3} at Raison site (Fig. 13.3).

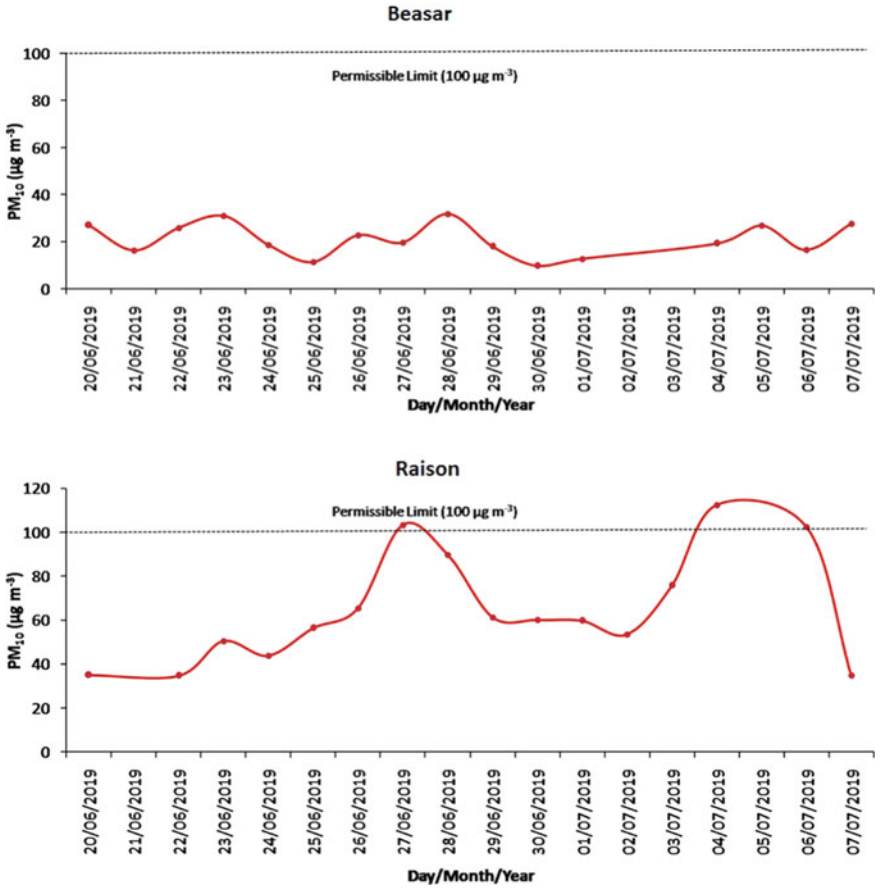

Fig. 13.3 PM_{10} Concentration at Beasar and Raison during summer season

13.4.3 $PM_{2.5}$ Concentration at Mohal

During winter season, the $PM_{2.5}$ concentration ranged between 10.4 $\mu g\ m^{-3}$ and 53.3 $\mu g\ m^{-3}$ with the mean value of 22.7 $\pm$ 1.8 $\mu g\ m^{-3}$. During spring season, the highest ever concentration of $PM_{2.5}$ (51.3 $\mu g\ m^{-3}$) was observed on April 24, 2019 (Fig. 13.4), the low concentration of $PM_{2.5}$ was observed as 5.6 $\mu g\ m^{-3}$ on April 14, 2019. The average concentration of $PM_{2.5}$ was recorded as 23 $\pm$ 3.4 $\mu g\ m^{-3}$. While the status of $PM_{2.5}$ during summer season was observed 42.1 $\mu g\ m^{-3}$ as maximum on May 04, 2019 and 18.4 $\mu g\ m^{-3}$ minimum on June 03, 2019 (see Fig. 13.4). The

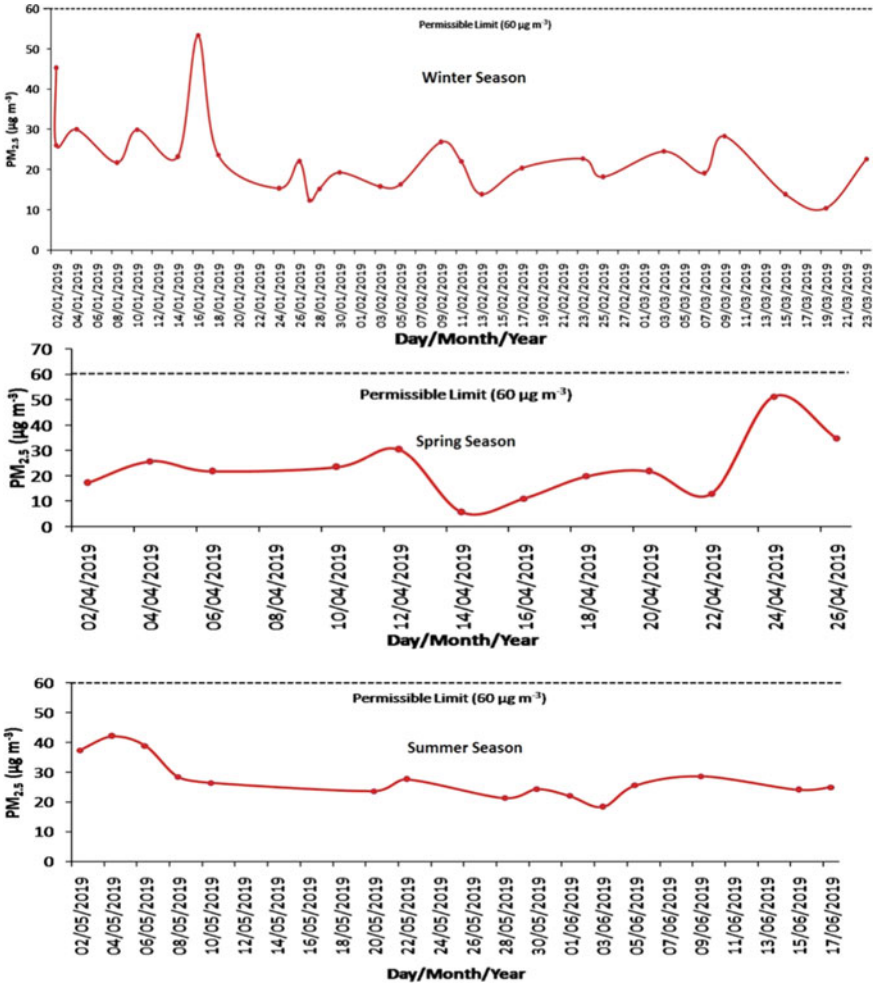

Fig. 13.4 $PM_{2.5}$ Concentration at Mohal during different season

average concentration of $PM_{2.5}$ was observed 27.6 ± 3.1 μg m^{-3}. All these values were within the permissible limit as per NAAQS (see Fig. 13.4).

13.4.4 $PM_{2.5}$ Concentration at Raison and Beasar

The $PM_{2.5}$ concentration ranged between 10.3 μg m^{-3} and 40.6 μg m^{-3} with the mean value of 21.6 ± 1.9 μg m^{-3} at Raison. Highest ever concentration of PM_{25}(40.6 μg m^{-3}) was observed on June 20, 2019. On the other side, the Beasar (Control) site PM_{10} concentration ranged between 3.1 μg m^{-3} and 17.2 μg m^{-3} with the mean value of 10 ± 0.9 μg m^{-3} (Fig. 13.5).

13.4.5 PM_{10} and $PM_{2.5}$ Concentration Compare with Control Sites Beasar

The control site Beasar is an apple orchard sites which undisturbed area by National Highway and other development activities. The PM_{10} concentration of Mohal and Raison was observed to have higher concentration (Mohal 112.2 μg m^{-3}) as

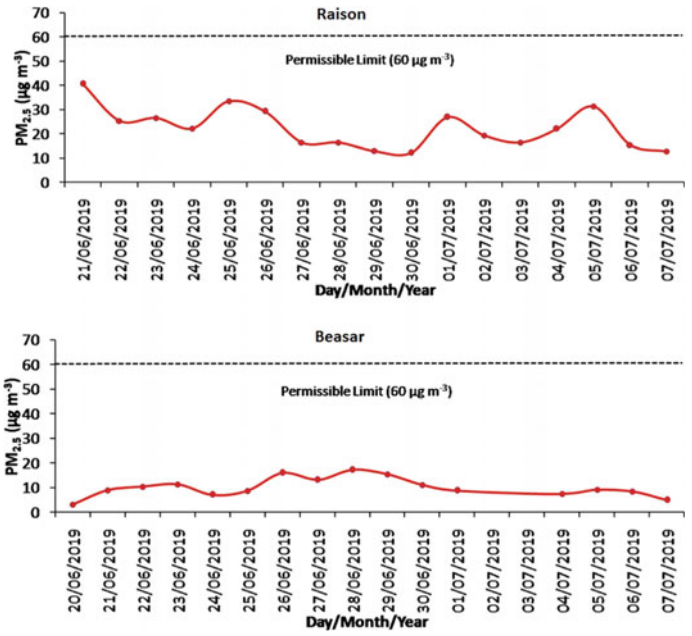

Fig. 13.5 $PM_{2.5}$ Concentration at Raison and Beasar during summer season

compared to control site (31.8 $\mu g\ m^{-3}$). On the other hand, $PM_{2.5}$ concentration was also higher 53.3 $\mu g\ m^{-3}$ at Mohal and Raison as compared to Beasar.

13.4.6 Normalized Difference Vegetation Index NDVI and Pollutants

When we compare and evaluate the NDVI values and pollutants concentration in the two selected sites, one of them was Beasar which was control site and second monitoring sites was Mohal. During the study, it was found that the NDVI value was high at Beasar (0.28–0.53), on the other hand in the same site, the particulate pollutants' concentration was low (31.8 $\mu g\ m^{-3}$) as compared to Mohal. The NDVI value was found low (0.11–0.2) at Mohal (Fig. 13.6) while the concentration of pollutants was high (112.2 $\mu g\ m^{-3}$) as compared to Beasar, it means where there is more greenery, there will be less pollutants and where there is less greenery, there will be more pollutants. There is negative correlation between NDVI and pollutants.

13.4.7 Back Trajectories, CALIPSO and Pollution Sources

Using Hybrid Single-Particle Lagrangian Integrated Trajectory (HYSPLIT) model derived by National Oceanographic and Atmospheric Administration (NOAA), the seven days back trajectories were drawn to highlight long-range transport source during pollution episodes. The trajectories were drawn one episode's value during winter season (i.e., January 16, 2019) at Mohal and during spring season episode value on April 10, 2019 at Mohal during the occasion of high pollution days.

In and around Mohal site, the maximum values of particulate pollutants were observed as 162.6 $\mu g\ m^{-3}$ on January 16, 2019, where the back trajectory was coming from Morocco, Homoda Desert. The trajectory, thereafter, passed through Algeria, Libya near Sahara Desert, Iraq, Afghanistan, Islamabad (Pakistan), Pathankot (India), Kangra district of Himachal Pradesh (India) and ultimately reached at Mohal (Fig. 13.7a). Meanwhile, observation through CALIPSO indicated that the vertical distribution of dust particles was mainly below 8 km at Tibetan Plateau and Irkustsk (Russia) (Fig. 13.8). Therefore, it is made clear that the entire observations throughout the trajectories have revealed that they did not pass through the Tibetan Plateau and Irkustsk (Russia) region and were not contributing directly to pollution which indicate that these episodes resulted from the local pollutants.

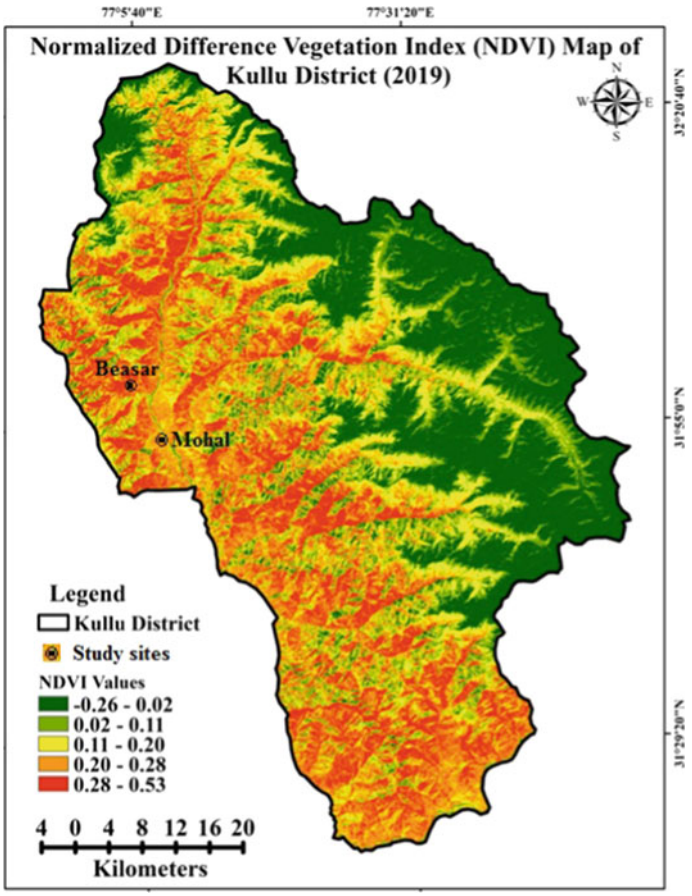

Fig. 13.6 Normalized difference vegetation index of Kullu valley

During the spring period, the CALIPSO image (see Fig. 13.8) indicated that the vertical distribution of dust aerosols at Koppal district of Karnataka (India), the back trajectory shifted from the Western Sahara, Algeria, Libya and passed through Iran, Afghanistan, Pakistan, Kangra (India) and ultimately reached at Mohal (see Fig. 13.7b). However, the trajectories did not cross over the vertical distribution of smoke, aerosols and these observations indicated that there was no other external source contributing to particulate pollution at Mohal.

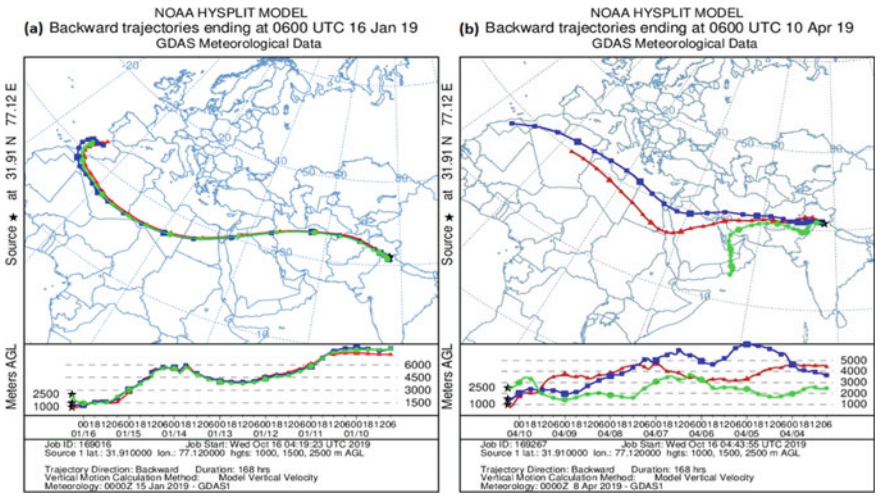

Fig. 13.7 Back trajectories using HYSPLIT Model to relate with highest particulate pollutants for: **a** Winter season **b** Spring season

13.5 Air Quality Index (AQI)

The AQI is one of the major tools which are used to determine the overall air quality status and general trends based on the specific standards. This index indicates the environmental status in the form of air quality and also informs the general public to understand how clear or pollute air they breathe daily. According to Environmental Protection Agency (EPA), it is divided into six different limits (Table 13.2).

It is clear from Fig. 13.9 and Table 13.2 that the values of AQI are in the good range for sampling sites which are under good category.

13.6 Conclusion

The concentration of particulate pollution was observed high at Mohal and Raison as compared to Beasar control site. Because the Mohal and Raison are nearby National Highway (NH3); therefore, the concentration of pollutants was higher as compared to the control site. The concentration of PM_{10}at Mohal and Raison was above the permissible limit (100 $\mu g\ m^{-3}$) prescribed by NAAQS. However, it is noted that concentrations of PM 2.5 at all the sites were well within the permissible limit. The NDVI value was highest at Beasar and lowest at Mohal, whereas the concentration of pollutants was opposite, highest concentration at Mohal and lowest at Beasar. It is also understood from HYSPLIT and CALIPSO analysis that there is local source of pollutants. The AQI study reveals that air quality of Mohal falls under good condition. However, the concentration of the PM10 was above the acceptable limit during spring

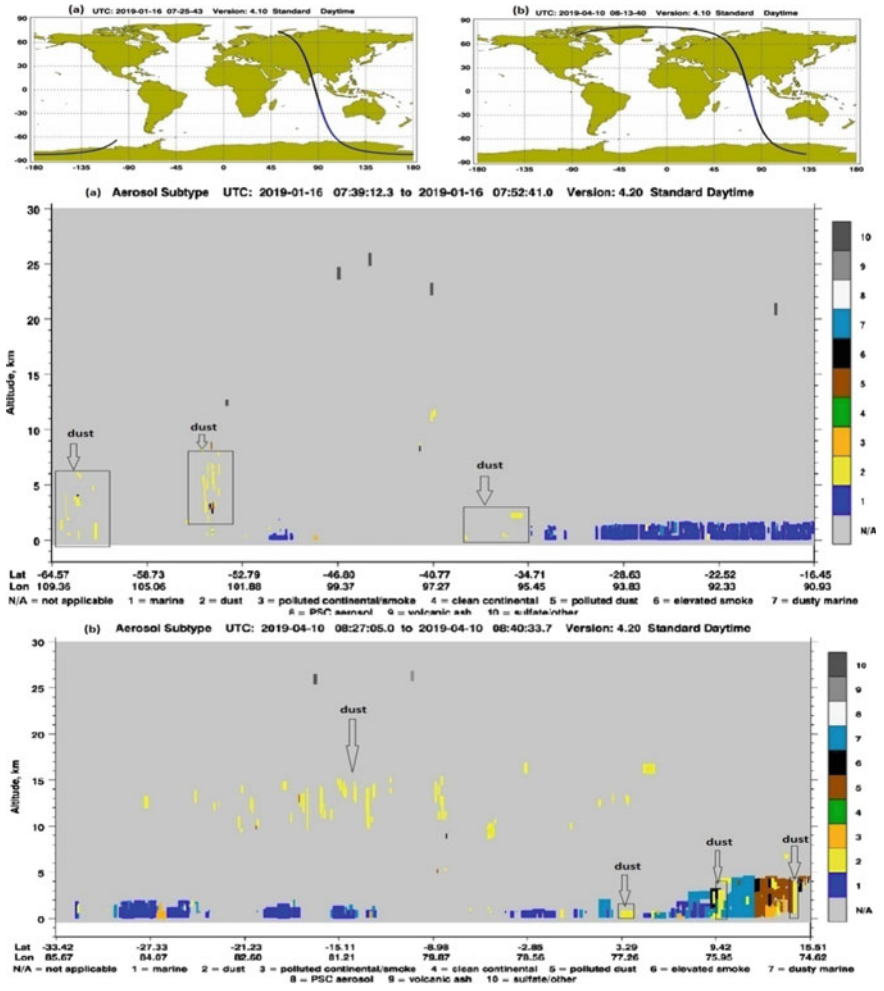

Fig. 13.8 CALIPSO Model to relate with highest particulate pollutants during winter and spring season

Table 13.2 AQI values and level of health concerns

Sr. no	AQI Value	Level of health concern (AQI)
1	0–50	Good
2	50–100	Moderate
3	101–150	Unhealthy for sensitive group
4	151–200	Unhealthy
5	200–300	Very unhealthy
6	301–500	Hazardous

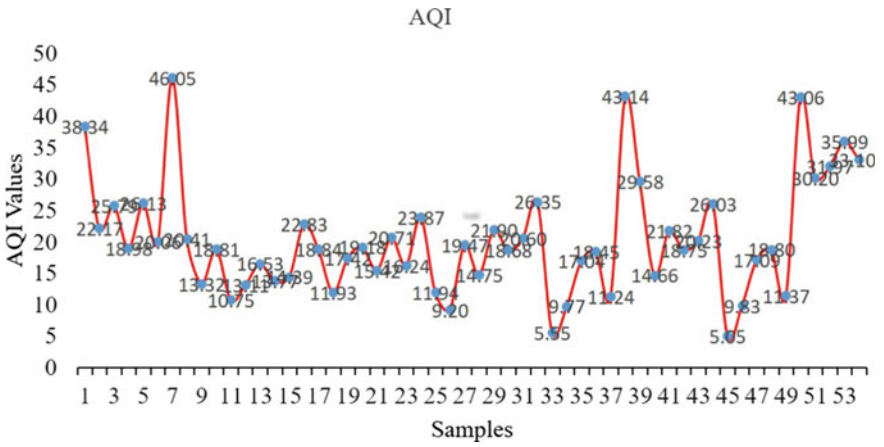

Fig. 13.9 Air quality index (AQI) in selected sites during study period

season when flowering in apple orchard at peak level which might not be so good from viewpoint apple orchards.

Acknowledgements The authors sincerely acknowledge the Director, G.B. Pant National Institute of Himalayan Environment, Kosi-Katarmal, Almora, Uttarakhand for providing facilities to the Himachal Regional Centre of the Institute, Mohal-Kullu, Himachal Pradesh-175 126 which could make this study possible.

References

Basannagari B, Kala CP (2013) Climate change and apple farming in Indian himalayas: a study of local perceptions and responses. PLOS ONE 8(10):e77976

Bawa KS, Koh LP, Lee TM, Liu J, Ramakrishnan P (2010) China, India, and the environment. Science 327:1457–1459

Bernard SM, Samet JM, Grambsch A, Ebi KL, Romieu I (2001) The potential impacts of climate variability and change on air pollution-related health effects in the United States. Environ Health Perspect 109(2):199

Bhaskar BV, Mehta VM (2010) Atmospheric particulate pollutants and their relationship with meteorology in Ahmedabad. Aerosol Air Qual Res 10:301–315

Calderón-Garcidueñas L, Azzarelli B, Acuna H, Garcia R, Gambling TM, Osnaya N, Rewcastle B (2002) Air pollution and brain damage. Toxicol Pathol **30**(3):373–389

Celis JE, Morales JR, Zaror CA, Inzunza JC (2004) A study of the particulate matter PM_{10} composition in the atmosphere of Chillan, Chile. Chemosphere 54:541–550

Dash SK, Hunt JCR (2007) Variability of climate change in India. Curr Sci 93:782–788

Gajananda K, Kuniyal JC, Momin GA, Rao PSP, Safai PD, Tiwari S, Ali K (2005) Trend of atmospheric aerosols over the north western Himalayan region, India. Atmos Environ 39(27):4817–4825

Ghosh SP (1999) Deciduous fruit production in India. In: Papademetriou MK, Herath EM (Eds) Deciduous fruit production in Asia and the Pacific. Thailand: Regional Office for Asia and the Pacific, Food and Agricultural Organization, pp 38–56

Kala CP (2007) Local preferences of ethnobotanical species in the Indian Himalaya: Implications for environmental conservation. Curr Sci 93:1828–1834

Kala CP (2013) Climate change and challenges of biodiversity conservation. In: Kala CP, Silori CS (Eds) Biodiversity, communities and climate change. The Energy and Resources Institute, New Delhi, pp 259–269

Khoder MI (2002) Atmospheric conversion of sulfur dioxide to particulate sulfate and nitrogen dioxide to particulate nitrate and gaseous nitric acid in an urban area. Chemosphere 49:675

Oberdörster G, Sharp Z, Atudorei V, Elder A, Gelein R, Kreyling W, Cox C (2004) Translocation of inhaled ultrafine particles to the brain. Inhal Toxicol 16(6–7):437–445

Ramanathan V, Feng Y (2009) Air pollution, greenhouse gases and climate change: global and regional perspectives. Atmos Environ 43(1):37–50

Renton A (2009) Suffering the science: climate change, people and poverty. Oxfam briefing paper number 130. Oxfam International, Oxford

Shrestha UB, Gautam S, Bawa KS (2012) Widespread climate change in the himalayas and associated changes in local ecosystems. PLOS ONE 7(5):e36741

Wang WC, Yung YL, Lacis AA, Mo TA, Hansen JE (1976) Greenhouse effects due to man-made perturbations of trace gases. Science 194(4266):685–690

Xu J, Grumbine R, Shrestha A, Eriksson M, Yang X (2009) The melting Himalayas: cascading effects of climate change on water, biodiversity, and livelihoods. Conserv Biol 23:520–530

Chapter 14
The Magnitude of Transformation in Land Use Land Cover of Kalyan-Dombivli, Smart City

Astha Smarth Kapur, Pankaj Kumar, G. Areendran, and Krishna Raj

Abstract Kalyan-Dombivli is a twin city in a municipal corporation, with its headquarters located in Kalyan in Thane district in the Indian state of Maharashtra. Besides carrying the impression of a rich cultural heritage and societal vibrance, the historic significance of the city which dates back to the British era is particularly enthralling. Due to its highly educated population (91% literacy rate), it is often called the second cultural capital of Maharashtra after Pune and boasts of a pioneering status in providing E-governance solutions to its residents. A time period of approximately three decades has been considered in order to determine the level of current physical and economic development in the city, an attempt has also been made to substantiate the same, providing sufficient amount of evidence, in the backdrop of GIS and Remote Sensing. To estimate the extent and pattern of change in the land-use and cover of the area, two satellite imageries of the years 1990 and 2017 are selected, over which, hybrid pixel classification is run, and ten classes of varying land-use/cover are created. On its basis, LULC maps have been generated. The subsequent results are pretty much in line with the ongoing increase in population and the developmental activities indicating maximum growth in built-up from 12.7% in 1990 to 31.8% in 2017 and corresponding shrinkage in fallow lands and wastelands from 34% in 1990 to 8% in 2017 and 17% in 1990 to 6% in 2017, respectively. This, to a large extent implies that, the area in a few years may be optimally developed so as to be successfully delineated as a smart city.

Keywords Kalyan-Dombivli · Hybrid pixel classification · Land-use land cover · Normalized difference vegetation index

A. S. Kapur (✉) · P. Kumar
Department of Geography, Delhi School of Economics, University of Delhi, Maurice Nagar, New Delhi, India

G. Areendran · K. Raj
Indira Gandhi Conservation and Monitoring Centre (IGCMC), WWF-India, Lodi Estate, New Delhi, India
e-mail: gareendran@wwfindia.net

K. Raj
e-mail: kraj@wwfindia.net

R. B. Singh et al. (eds.), *Remote Sensing and Geographic Information Systems for Policy Decision Support*, Advances in Geographical and Environmental Sciences,
https://doi.org/10.1007/978-981-16-7731-1_14

14.1 Introduction

Portions of land on the surface of the earth, may be termed as territories belonging to a country, state, district, tehsil or a village and can be occupied by natural components or can be attributed to umpteen number of uses which are of significance to mankind, but essentially all these portions collectively form the land resource. The resource that is a home to almost all types of activities those are associated with humans and other living creatures alike. Land cover fundamentally links and influences the human and physical environment. Any change in herein, can simply be designated as a primary cause affecting the global ecological system that influences the world climate (Vitousek 1994). Due to its widespread availability, humans since times immemorial have always utilized the land resource in manners that make their lives comfortable, be it the era of gathering foods from the forests or cultivation of crops, or the era of construction of offices, industries or residences by clearing the vegetation which even created room for primary, secondary and tertiary activities. Now this land, due to its capability of being able to support both natural covers and myriad land-uses, possesses indescribable amount of vitality for us, and we on our part need to tend it and plan our daily activities judiciously on it. This is known as land-use planning, for which purpose, humans, using their intelligence and wit have devised several usable, comprehensive and authentic methods of successfully carrying out their enterprises, within the boundaries of their territories and in the limited spaces made available to them by their respective governments, without disturbing the delicate balance of the surrounding ecology.

One among these methods involves the use of Remote Sensing and Geographical Information System (GIS) technology. This art, a few calibrated experts have been able to master and it has been trickling down to the common man ever since. The result is satellite-based and computer-aided assessment of land, its existing land covers and uses as well as designing of measures that create scope for enhancement, advancement and optimum expansion, particularly in areas which are designated as cityscapes which are essentially recognized for having a predominance of land-use, over land cover. As in this case, where the current study revolves around the city of Kalyan and Dombivli falling under the jurisdiction of Kalyan-Dombivli Municipal Corporation (KDMC) that has been categorized as a 'Smart City' by the Government of India. This paper deals with the utilization of the Remote Sensing and GIS techniques for providing a suitable analysis of the area with all its land usages and covers. It is most appropriate to commence from the very beginning of this study and thus the paper shall progress through all the steps undertaken, in a chronological fashion, covering the minute details for attempting a logical analysis of the prevalent land-use land cover patterns and the transformations that have occurred over a period of, a little less than three decades, from 1990 to 2017.

14.2 Scope and Objectives

The maps of land-use and cover thus generated shall prove to be highly beneficial in order to come up with lucrative land-use planning ideas and with accountable conclusions to promote a healthy balance between the components of a smart city to reach a situation wherein there is a proportionate allocation of the facilities to the residents. Moreover, urban expansion brings about phenomenal modification in the existing forested tracts, agricultural areas and scrublands, hence, these maps shall pave the way for sustainable land-use planning with minimum threat to the natural environment. The key objective of the study is to generate maps showcasing the land-use and cover of the area under KDMC, with special emphasis on Kalyan and Dombivli City, for two years namely 1990 and 2017, using satellite images, so as to be in a position to be able to assess the magnitude of change that has taken place therein during this time span of 27 years through the method of change detection. And also to calculate the NDVI for the study area, to assess the extent of change in vegetation.

14.3 Study Area

The present study revolves around Kalyan-Dombivli Municipal Corporation Area, situated in Thane District of Maharashtra. Its areal extent is 113.22 km^2. Its latitudinal and longitudinal boundaries span an area of 19°4′–19°14′ N and 72°9′–73°17′ E, respectively. Its northern boundary is flanked by Ulhās Creek and Ulhās and Kalu Rivers. KDMC, prominently covers 8 major township settlements, namely—Kopar, Dombivli, Thakurli, Kalyan, Vithalwadi, Shhard, Ambivli and Titwala. Out of these, Kalyan and Dombivli have seen maximum development and provide residences to a huge number of people who have their offices in Greater Mumbai and Mumbai Suburban. Kalyan-Dombivli contributes approximately 40% to the GDP of the entire state and is regarded as a part of the Mumbai Metropolitan Region (MMR) (KDMC-CDP 2012).

14.4 Materials and Data Used for Land-Use/Land Cover Mapping

For gaining a successful understanding of the land cover, the dynamics and patterns of land utilization, it is imperative to first understand the importance of having and protecting land cover. Only then will the efforts of predicting the impacts of land cover change become meaningful. Since land cover is highly dynamic in nature, thus, it can be understood only with the help of accurate data. This purpose is well served by Remote Sensing, since it is an attractive source of thematic images that

Table 14.1 Details of landsat 5 TM and landsat 8 OLI/TIRS images

S. No	Satellite	Path and row	Date of pass	Characteristics
1	Landsat 5 TM	148 and 047	9th March 1990	Spatial resolution = 30 m No. of bands = 7
2	Landsat 8 OLI/TIRS	148 and 047	30th January 2017	Spatial resolution = 30 m No. of bands = 11

demonstrate the Earth's surface as it actually is (Foody 2002). Hence, for appropriate use in the current study, good quality, cloud-free data, in the form of two satellite images i.e. Landsat 5 with Thematic Mapper (TM) Sensor on board, Path-148 and Row-047 and Landsat 8 with both Operational Land Imager and Thermal Infra-Red Sensors (OLI-TIRS) on board Path-148 and Row-047 for the dates 9th March 1990 and 30th January 2017, respectively, both having a spatial resolution of 30 m each, were downloaded from the USGS Earth Explorer website of NASA (National Aeronautics and Administration) and projected in the Universal Transverse Mercator (UTM) projection (Zone 43 N) in the World Geodetic System (WGS) 1984 datum. Although images of the winter and the spring season i.e. January and March have been chosen but since the area is primarily urban and the process of urbanization per se continues, thus the images of different seasons i.e. winter and spring are not of much consequence. Besides, the areal extent of the green cover for both the seasons has been productively measured. The details of satellite data are shown in Table 14.1.

14.4.1 Software Used

ERDAS IMAGINE 2014 software is an essential and user-friendly application for carrying out various techniques of Remote Sensing. Software ARCMAP VERSION 10.2.1 is a user-friendly application, primarily used to create maps, perform spatial analysis and manage geographic data in an automated scenario. GOOGLE EARTH PRO is a software that readily assists the user in GIS data-related operations like digitization for map creation, visualization, manipulation and exporting of data.

14.5 Methodology

First of all, the shapefile of the study area, acquired from the Kalyan-Dombivli Municipal Corporation office was projected in UTM projection Zone 43 N, WGS 1984 and was geo-referenced. The cloud-free satellite images of the years 1990 (Fig. 14.1) and 2017 (Fig. 14.2), containing the study area were downloaded and layer stacked.

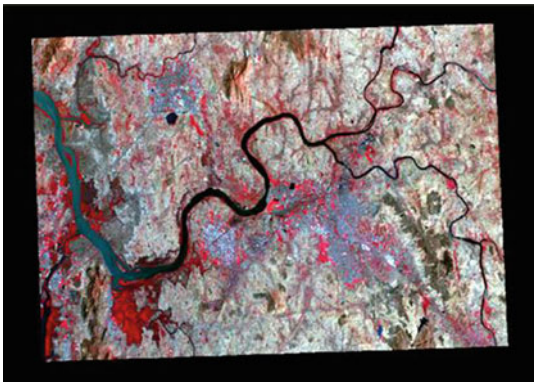

Fig. 14.1 Image 9th March 1990 (downloaded from USGS Website)

Fig. 14.2 Image 30th January 2017 (downloaded USGS Website)

14.5.1 Method and Procedure

Hybrid Pixel Land-use/Land Cover Classification (using Unsupervised Classification Technique).

This type of classification is attempted by grouping together those pixels that possess spectral similarity, and the resultant classified image is then regarded as a thematic map that highlights the land-use and land cover of the region (Foody 2002). To reach this stage, a number of steps were followed that is the subset of the study area/Area of Interest (AOI) was extracted from the imagery and finally *Unsupervised Image Classification* was run for the multiband imageries. The *ISODATA (Iterative Self-Organizing Data Analysis Technique) Algorithm* is used by Erdas to perform the Unsupervised Classification. It is named as iterative since it repeatedly performs the entire classification and recalculates the statistics. Thus, the output is in the form of a thematic raster layer. It self organizes the pixels present in the image, such that, it locates the clusters inherent in the dataset. This approach is followed in those cases wherein the user wishes to separate those classes that are liable to

be confused with some other class. For instance, shadow, water and dark vegetation are quite often mistaken for each other. It also helps in the identification of detailed subclasses in the final classified image. The minimum spectral distance formula is made use of, in the *ISODATA* clustering method, to form clusters. The ISODATA clustering method uses the minimum spectral distance formula to form clusters. It begins with either arbitrary cluster means or means of an existing signature set, and each time the clustering repeats, the means of these clusters are shifted. The new cluster means are used for the next iteration. Clustering of the image is repeated till the time the execution of maximum number of iterations has taken place or maximum percentage of unchanged pixels has been reached. To ease out the interpretation of the image subset, so that corresponding colours can be assigned to the respective pixels, the colour scheme is selected as False Color Composite (FCC), and the band combination is selected as 4, 3 and 2 for both Landsat Image subsets. By selecting the Unsupervised Classification option, the software allocates the necessary statistics to the image, for classification into various physical features on the basis of different colours. By clicking and selecting various pixels in the image and manually assigning discreet colours to the features present therein, optimum recognition of the land-use land cover classes becomes possible. As a pixel is selected, simultaneously its corresponding class gets highlighted in the attribute table. Thus, a befitting name is entered in the table for the given pixel. On completion of the classification for all the classes, the process of *'Recoding and cleaning'* of the image subset is initiated. This is done so as to limit the classes to a number that is convenient to handle and easily relatable, and furthermore, the image is cleaned in a manner that excess colour is removed or merged into the existing classes to provide a discreet and understandable view of the surface of the study area after the final categorization. For those land-use and cover classes, that are difficult to differentiate from each other, AOIs are carved out through digitization for those specific features and these are then recoded into the requisite class for both the Landsat Image subsets. Then the geo-referenced shapefile of the study area is clipped from the image subset. This clipped portion is then used for preparation of LULC maps for the two given years (Figs. 14.3 and 14.4). Table 14.2 denotes the LULC classes used for identifying the changes that occurred in a time span of 27 years from 1990 to 2017. A total of ten classes were used in the classification.

14.5.2 Change Detection

It is pretty obvious that readily perceptible changes in LULC have occurred in the study area within a considerable time gap of 27 years. Hence, the change detection technique comes in quite handy in this situation. The change though is evident from the satellite image itself, but in order to arrive at accurate conclusions, it became requisite to proceed through the above procedures and finally prepare a matrix to appropriately and sufficiently showcase the magnitude and extent of occurrence of

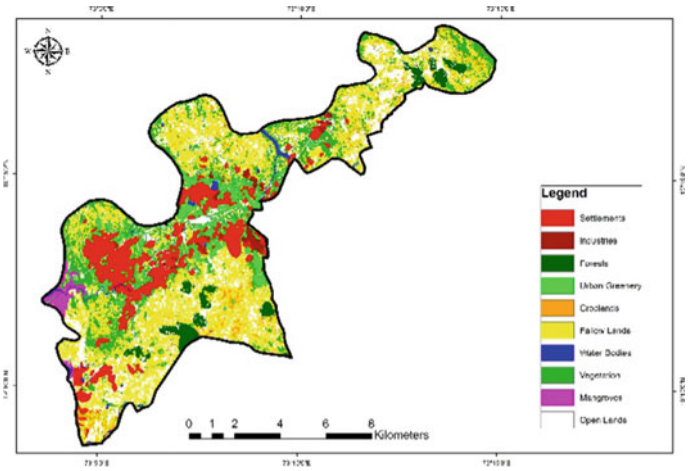

Fig. 14.3 Land-use/cover map of KDMC, 1990

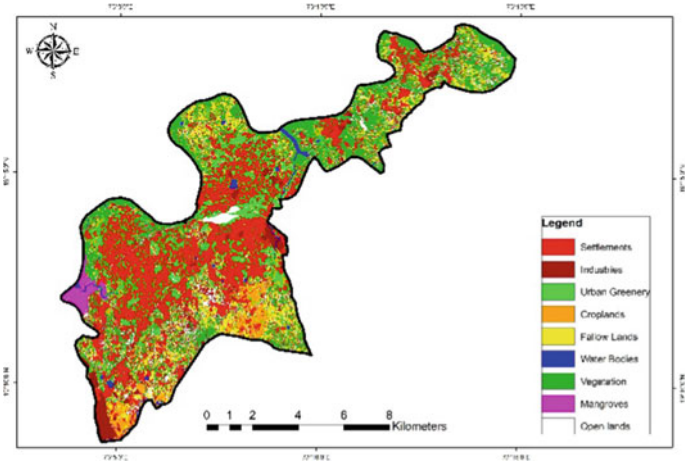

Fig. 14.4 Land-use/cover Map of KDMC, 2017

the change to provide a better understanding of the same. For correctly detecting the change in LULC, a change detection matrix has been created.

14.5.3 Accuracy Assessment

There may arise disagreements between the two data sets i.e. the remotely sensed data and the LULC map derived from it. These are collectively termed as errors (Congalton

Table 14.2 LULC classes for 1990 and 2017

Land-use land cover class	General description
Settlements	Buildings used for residential purposes
Industries	Buildings used for commercial purposes
Forests	An area at the fringe of settlements, and crown density of less than 10% of the canopy cover
Urban greenery	Land dedicated to parks, gardens or green areas between habitations
Cropped-land	Land used for current cultivation, with crops
Fallow land	The lands used for cultivation but left uncropped for one or more seasons
Water bodies	An area covered with water, in the form of lakes, ponds, canals and rivers
Vegetation	Landscape dominated by scrubs, having a tendency of intermixing with cropped areas
Mangroves	An evergreen vegetation type that grows along tidal creeks in coastal areas in the tropics
Open lands	Lands left vacant or used for commercial purpose like roads, railways etc.

1991; Smedes 1975). Thus, accuracy assessments are essentially vital for any user of the LULC classification techniques so as to judge the level of precision and to arrive at satisfying outcomes. It also provides scope for further rectification. Till the time the accuracy of any classification is assessed, it is not considered complete (Lillesand and Kiefer 2000). There are several options available for accuracy assessment, but Cohen's KAPPA Analysis is preferred in this case for checking the accuracy of the Unsupervised LULC classification. It is a discreet multivariate measure of agreement, used in several classifications. The overall classification accuracy came out to be 82.00%.

14.5.4 NDVI Calculation

With the completion of the LULC classification, began the segment of the Normalized Difference Vegetation Index (NDVI) calculation. The Normalized Difference Vegetation Index (NDVI) is a numerical indicator which is widely applicable in vegetation studies, as it optimally indicates the extent of pasturelands, crop yields, healthy and unhealthy vegetation, carrying capacities of range lands and the like. It is highly advantageous for analysing the remotely sensed vegetation measurements and to identify the presence of live green vegetation in the observed target. It is computed using the visible red and the near-infrared bands of the electromagnetic spectrum. Healthy vegetation absorbs most of the visible light that falls on it and

reflects majority of the near-infrared light. Contrary to this, unhealthy or sparse vegetation reflects most of the visible light and absorbs the near-infrared light. (Holme et. al, 1987). A larger difference between the near-infrared and the red reflectance points to the fact that there is a higher incidence of vegetation in that particular region. Thus for the present study, NDVI for both the images Landsat 5 TM and Landsat 8 OLI/TIRS is calculated with the help of the formula:

NDVI = (NIR - RED) / (NIR + RED) or
NDVI = (Band 4 – Band 3) / (Band 4 + Band 3) in case of Landsat 5 TM

For Landsat 8 OLI/TIRS the following formula was used:

NDVI = (NIR - RED) / (NIR + RED) or
NDVI = (Band 5 – Band 4) / (Band 5 + Band 4)

Finally, the study area being clipped from the resultant image is reclassified to restrict the number of classes to 5 for 1990 image and 4 for 2017 image and bring out precise depiction of NDVI. The colour scheme of the obtained areas is then changed to the most befitting one for the appropriate demarcation and precise understanding of the vegetation for the specified area (Figs. 14.5 and 14.6). The values for NDVI range between −1 and + 1. The area covered by vegetation, after calculation came out to be 18.68 sq. km. for 1990 and 12.68 sq. km for 2017. This emphatically indicates that the green cover has systematically declined over the area especially in the Kalyan-Dombivali twin city, so as to make room for construction activities and facilities that are a prerequisite in a smart city. Albeit, the practices of environmental conservation have not been totally compromised, and the importance of green cover in such an upcoming urban area has not been undermined.

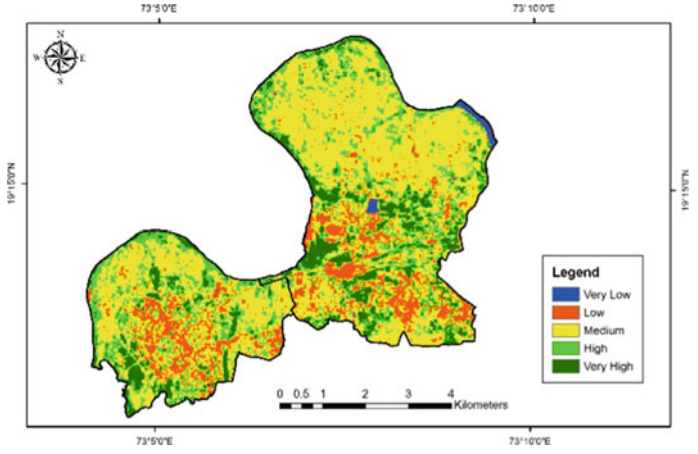

Fig. 14.5 Kalyan-Dombivli NDVI, 1990

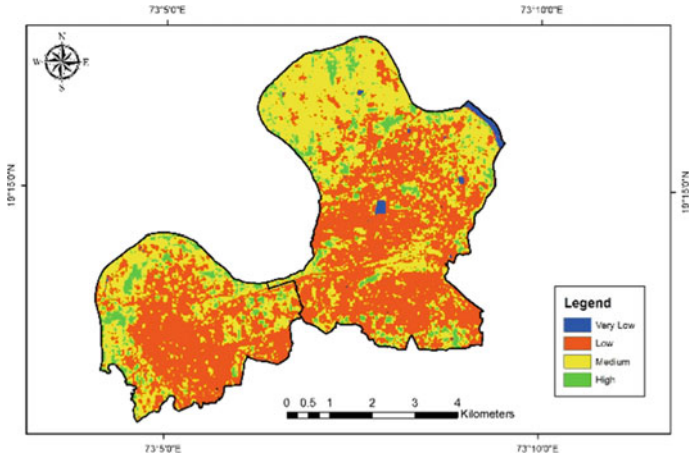

Fig. 14.6 Kalyan-Dombivli NDVI, 2017

14.6 Results and Discussion

As is quite evident from Figs. 14.1 and 14.2, the subsets for the years 1990 and 2017 have been carved out from Landsat 5 TM and Landsat 8 OLI/TIRS, respectively. Land-use/cover maps have been generated, as can be seen in Figs. 14.3 and 14.4. These maps clearly indicate changes in LULC that have taken place over the last 27 years, but in order to be precise with the changes, a table of change detection has been created, showcasing the 10 classes (Tables 14.3 and 14.4).

The Tables 14.3 and 14.4 indicate likely changes in the LULC of the region. The most conspicuous ones stand highlighted in the tables. These include the categories

Table 14.3 Land-use/cover KDMC, 1990

Class name	Area in Sq. Kms	Area in %
Settlements	14.37	12.70
Industries	1.26	1.11
Forests	3.96	3.50
Urban greenery	5.20	4.59
Croplands	5.65	4.99
Fallow lands	38.42	33.93
Water bodies	1.30	1.15
Vegetation	22.39	19.77
Mangroves	1.56	1.38
Open lands	19.33	17.08
Total	113.22	100.00

Source: *Land-use Map of KDMC, 1990*

Table 14.4 Land-use/cover KDMC, 2017

Class name	Area in Sq. Kms	Area in %
Settlements	35.99	31.79
Industries	6.23	5.51
Forests	0.00	0.00
Urban greenery	12.61	11.14
Croplands	9.13	8.07
Fallow lands	9.04	7.98
Water bodies	1.32	1.17
Vegetation	30.36	26.81
Mangroves	1.34	1.19
Open lands	6.97	6.15
Total	113.22	100.00

Source Land-use Map of KDMC, 2017

of settlements plus industries which can collectively be termed as the built-up in the region. This category points to the maximum swell, owing to in-migration of population from the heavily congested parts of Mumbai in search of bigger, better and cost-effective houses, plus employment opportunities in the industries, as the cities of Kalyan and Dombivli lie in close proximity. The built-up class has witnessed a rise of 23.5% in 2017 from 1990. There is a complete loss of forests, which had a crown density of less than 10% of the canopy cover. But this may be attributed to the expansion of the cityscape and conversion of the forested tracts into croplands or lands with light vegetation in the form of scrub. Furthermore, the 26% decline in fallow lands in 2017 and 11% fall in open or vacant lands clearly point to the fact that there is rapid urbanization in the area and in order to cater to the food requirement and demand of space for settlements of the growing population, the fallow and vacant areas have been consumed majorly by the builders for establishing residences, and entrepreneurs for establishing service industries or shopping complexes, partially by the cropped lands to meet the food requirements, and also by the vegetation and urban greenery for beautification of the area. The open/ vacant lands, fallow lands and forests can be seen prominently diminishing, for this is the price required to be paid for rising urbanization! From the two maps of Kalyan and Dombivli (Figs. 14.7 and 14.8), a remarkable expansion in the built-up area can be perceived.

These point to the fact that there has been a considerable increase in the construction activity in 27 years, which is attributable to the influx of population from the crowded parts of Mumbai and suburbs due to provision of affordable housing, basic amenities, inviting infrastructure and peaceful ambience. Majority of the population residing here belongs to the literate middle-income group.

The graph in Fig. 14.9 represents the amount of area occupied by the different types of land-uses and covers in KDMC. Out of the total area of 113.22 km^2, maximum area 38.42 km^2 was occupied by fallow land, indicating that in the year 1990, the area was primarily agrarian and the population was predominantly engaged in primary

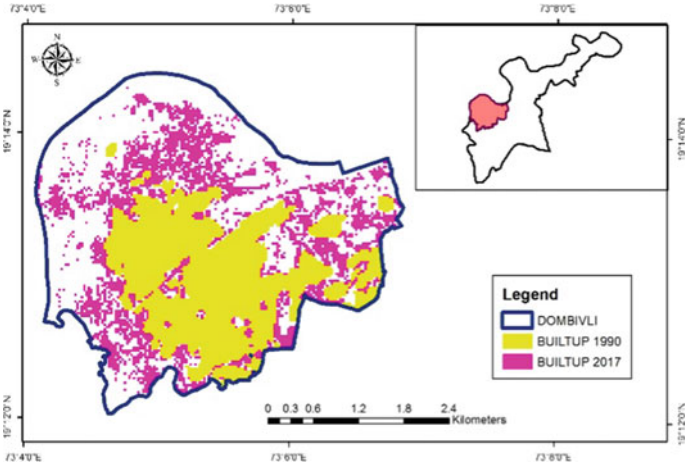

Fig. 14.7 Built-up increase, Dombivli, Since-1990

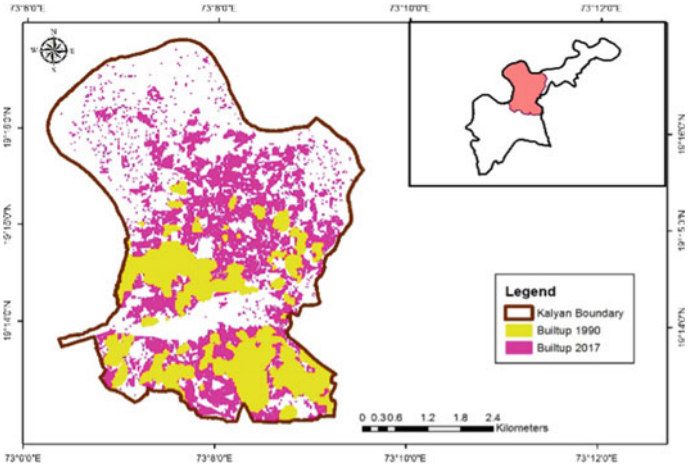

Fig. 14.8 Built-up Increase, Kalyan, Since-1990

activities, and the second highest area was under scrubland vegetation which also points to the presence of primary sector activities and the least area was occupied by industries suggesting minimal engagement in secondary and tertiary activities. The 14.37 sq. km area under settlements housed this agrarian population along with some immigrant population from the neighbouring areas. On the other hand, the graph of LULC of KDMC in 2017 brings to light an overwhelming rise in the area under settlements, as the subregion in a time span of a little less than three decades has acted as a magnet for attracting a tremendous population towards itself, especially those people who came looking for better opportunities in terms of residences,

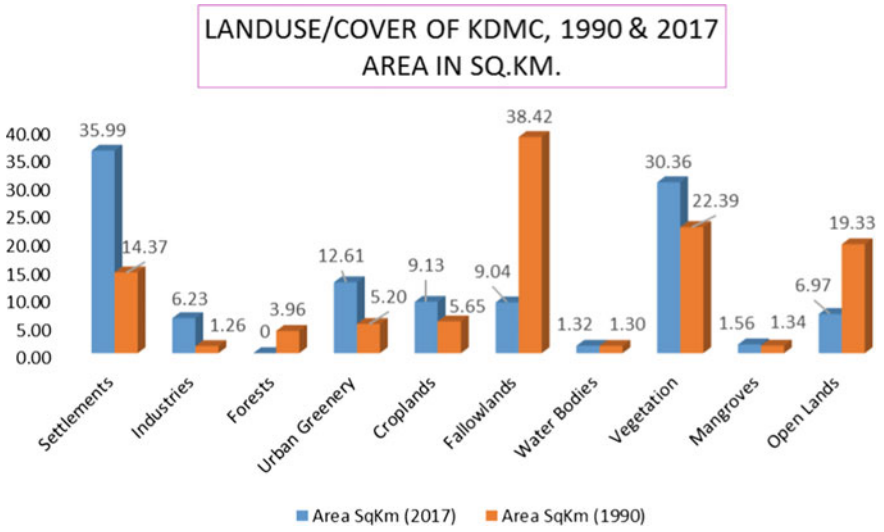

Fig. 14.9 Land-use/cover of KDMC, 1990 and 2017

infrastructure and economy. Moreover, there has been a significant rise in the area under industries i.e. 6.23 sq. km from 1.26 sq. km, this is sufficient to showcase the level of involvement of the people in the secondary sector and also points to a shift in the pattern of employment and their sources of livelihood. The forests have been depleted to make room for construction activities, agriculture and at places these have been replaced by plain vegetation. On comparing the two years, it becomes evident that though there has been a drastic increase in land uses, but it has not been so at the expense of land cover to a superior degree thus keeping the environmental aspect in view and giving it due importance. The urban greenery has duly swelled to prevent KDMC from turning into a concrete jungle.

Maps of Dombivli for 1990 and 2017 (Figs. 14.10 and 14.12) and their corresponding pie charts (Figs. 14.11 and 14.13) of the same years (1990 and 2017) reveal the reality of the ongoing change in the LULC in Dombivli in the last 27 years. There has been a remarkable rise in the settlements from 34% in 1990 to 49% in 2017. The industries have also grown by 1% to synergize the employment scenario. The improvement in urban greenery has perfectly blended with the built up, offering spaces for healthy living. The agricultural lands have been pushed away to the peripheral areas, and the open lands that were lying vacant have been judiciously used as lands of financial worth.

An attentive look into the scenario of LULC in Kalyan unfurls a similar pattern as can be seen in the case of Dombivli (Figs. 14.14 and 14.16). Herein, the rise in residences has been brisk and greater in comparison to its twin city, marking a 21% rise from 1990, and there has been a corresponding increment in the urban greenery as well. The industries have grown by 2% which primarily include service industries, municipal workshops, bus depots and treatment plants. The open and

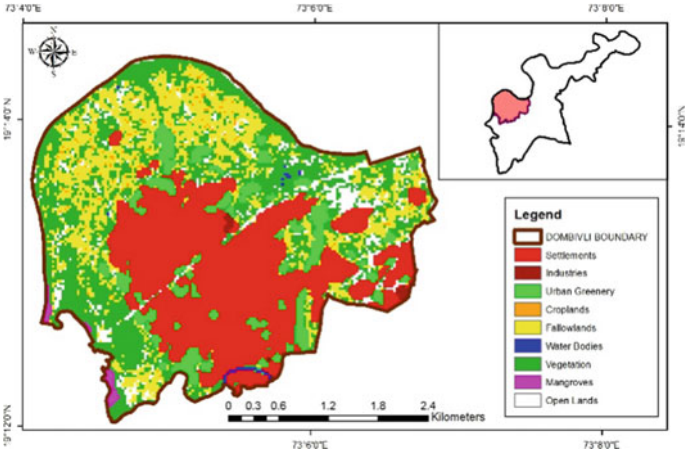

Fig. 14.10 Land-use/cover of Dombivli in 1990

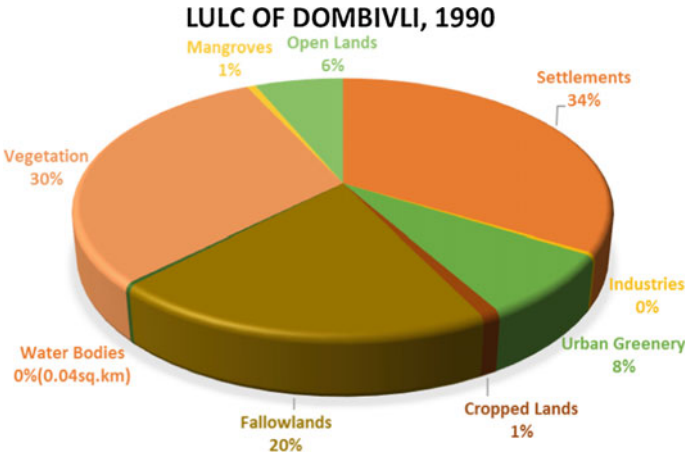

Fig. 14.11 Pie chart showing LULC of Dombivli, 1990

vacant lying lands which in 1990 were sporadic but plentiful in Kalyan, now support plush greenery, residential buildings and structures of public utility (Figs. 14.15 and 14.17). Worth mentioning is the fact that the water bodies in the form of ponds and lakes have been given their due importance and even practices of beautifying them are underway to convert them into spots of recreation and tourist attraction.

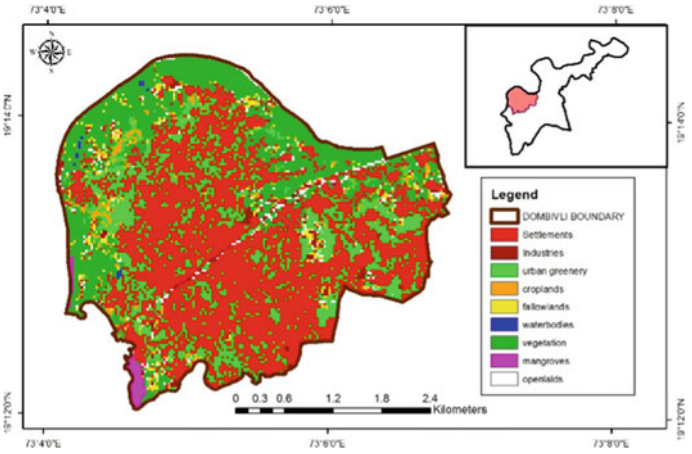

Fig. 14.12 Land-use/cover of Dombivli in 2017

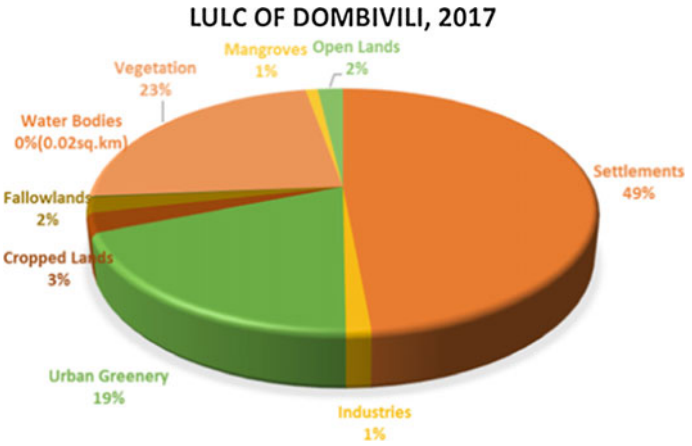

Fig. 14.13 Pie chart showing LULC of Dombivli, 2017

14.7 Conclusion

From the above data, observations and discussions, it can logistically be concluded that the land-use and cover of the area in question have drastically changed, wherein land-use, in comparison to land cover has overwhelmingly expanded, converting it from an area of predominantly agrarian nature to one with organized urbanization. This change owes its existence to improvements in technology, in incomes and occupations which in turn has significantly altered the standard of living of the existing residents and those who moved in from other parts of Maharashtra in search of better accommodation. The area also supports several rented settlements and hotels suitable

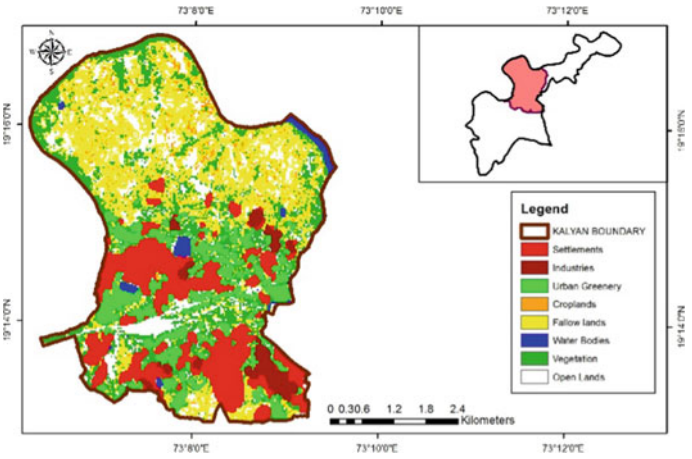

Fig. 14.14 Land-use/cover of Kalyan in 1990

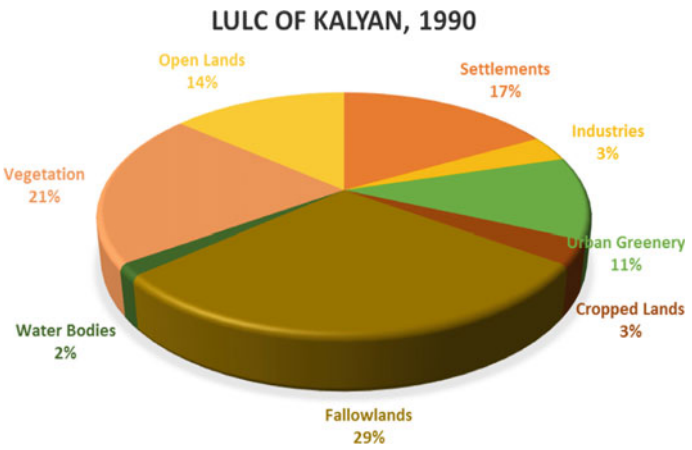

Fig. 14.15 Pie chart showing LULC of Kalyan, 1990

for the low, middle and high income bearers. Besides this, the presence of the municipal corporation headquarters and regional office makes the area administratively sound. There has been a welcome expansion of the cityscape which is inclusive of the facilities of comfortable as well as luxurious living. The marketplace is flooded with all types of commodities ranging from those of daily needs like grocery, to clothes of international brands. Not excluding repair shops, warehouses, even multiplexes and malls. The most striking feature about the population is that 91% of it is educated and a majority of the people belongs to the middle-income category who are extremely aware about their surroundings and government policies. As far as the Normalized Difference Vegetation Index (NDVI) is concerned, a net decrease of

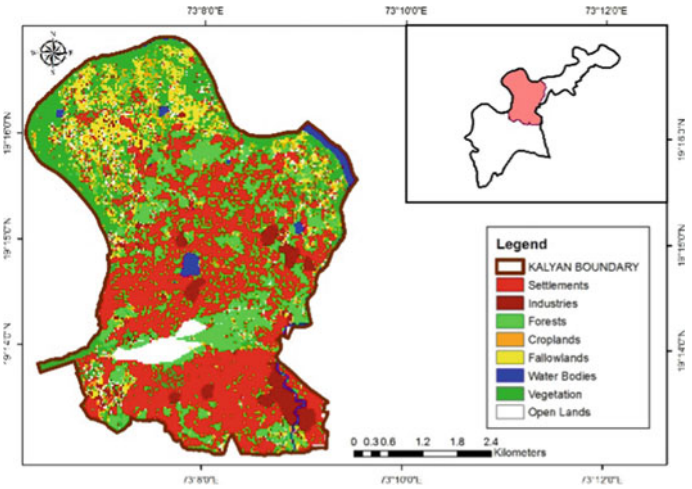

Fig. 14.16 Land-use/cover of Kalyan in 2017

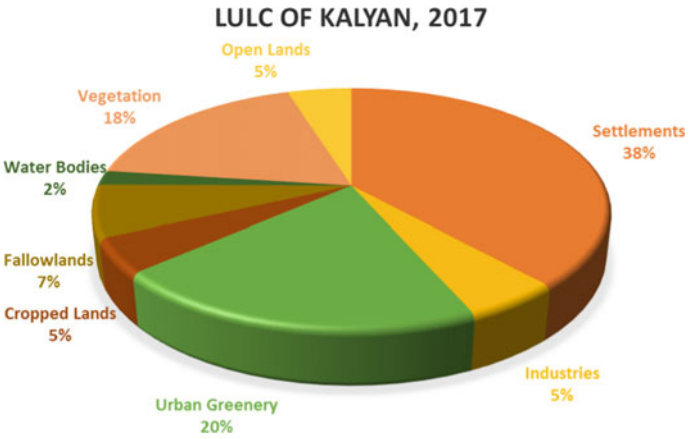

Fig. 14.17 Pie chart showing LULC of Kalyan, 2017

6 sq. km from 1990 to 2017 has been recorded. But nevertheless, there has been a visible upgradation of the greening activities around the buildings in the region. Thus in a nutshell, it can be concluded that with further investment, proper funding and improved citizen participation, the area shall see speedy returns in terms of becoming a smart city as projected by the central government and urban local bodies.

Acknowledgements For any research procedure to reach a successful conclusion, several factors and resource persons play a vital role. Similarly, this paper is an articulation and embodiment of the consistent and efficacious efforts and timely inputs in the form of guidance which was genuinely and abundantly provided by my mentor and guide Dr. Pankaj Kumar (Assistant Professor, Delhi

School of Economics, University of Delhi) as well as Dr. G. Areendran (Dr. G. Areendran, Director and Head of IGCMC division, WWF-India) and Dr. Krishna Raj (Senior Program Officer IGCMC division, WWF-India) who paved the way for me to learn the necessary software in WWF and made accessible several data (apart from whatever I collected during field surveys) required to produce the desired outcomes. Their contribution in this paper is undeniable and profound.

References

Anonymous. https://www2.le.ac.uk/departments/physics/research/eos/format-eo/2014-example-outputs/land-classification-tutorial.

Census of India (2011) Village and town directory, series-28, part XII-A, district census handbook. Census of India, Thane, Maharashtra

Congalton RG (1991) A review of assessing the accuracy of classifications of remotely sensed data. Rem Sens Environ 37:35–46

Foody GM (2002) Status of land cover classification accuracy assessment. Rem Sens Environ 80:185–201

George J et al (2016) Land use/land cover mapping with change detection analysis of Aluva taluk using remote sensing and GIS. Int J Sci Eng Technol 4(2):383–389

Holme A et al (1987) The development of a system for monitoring trend in range condition in the arid shrub-lands of Western Australia. Aust Rangeland J 9:14–20

Kafi KM et al (2014) An analysis of LULC change detection using remotely sensed data: a Case study of Bauchi City. IOP Conf Series: Earth Environ Sci 20:1–9. https://doi.org/10.1088/1755-1315/20/1/01205

KDMC (2012) Revised city development plan. Kalyan-Dombivli Municipal Corporation, Thane, Maharashtra

Lillesand TM, Kiefer RW (2000) Remote sensing and image interpretation, 4th edn. Wiley, New York

Mallupattu PK et al (2013) Analysis of land use/land cover changes using remote sensing data and GIS at an urban area, Tirupati, India. Sci World J 2013:6

NRSC. http://bhuvan.nrsc.gov.in/gis/thematic/tools/document/LULC250/0405.pdf

Roderick M et al (1996) Calibrating long term AVHRR derived NDVI imagery. Rem Sen Environ 58:1–12

Smedes HW (1975) The truth about ground truth. In Proceedings 10th international symposium on remote sensing of environment, pp 821–823.

USGS. https://landsat.usgs.gov/what-are-band-designations-landsat-satellites

USGS. https://earthexplorer.usgs.gov/

Vitousek PM (1994) Beyond global warming: ecology and global change. Ecology 75:1861–1876

Chapter 15
Assessment of Tiger Tourism in India: A Case Study of Ranthambore Tiger Reserve, Rajasthan, India

Bhanwar Vishvendra Raj Singh and Anjan Sen

Abstract Our "Future Earth" depends on the ecosystem services and green planet. But nowadays, the depletion of biodiversity resources is rapidly increasing all over the globe. In biodiversity, each organism has a contribution in sustaining the balance of nature. In this context, Tiger is an icon of healthy wildlife which is considered as a vital factor for maintaining the Universal Food Chain System. Among various tiger reserves, Ranthambore is unquestionably the most popular tiger reserve. It is situated in the transition zone between a semi-arid desert condition and seasonally wet peninsular India. It is estimated that the Ranthambore Tiger Reserve (RTR) provides flow benefits worth ₹ 8.3 billion (₹ 0.56 lakh/hectare) annually. According to NTCA Report (2015), important ecosystem services originating from RTR include gene-pool protection (₹ 7.11 billion per year), provisioning of water to the neighboring regions (₹115 million per year), provisioning of habitat and refuge for wildlife (₹ 182 million per year), generation of cycling of nutrients (₹ 34 million per year), and sequestration of carbon (₹69 million per year).Additionally, the Ganesh Temple is visited by close to ten lakh pilgrims every year. The study comes out with an economic valuation of Tiger tourism in RTR. The research also studies how the tiger economy is contributing to the environment and economy of nearby regions. It is an important source of revenue throughout the forest ecosystem. In-situ conservation of RTR is an important method of conserving biodiversity. Therefore, humanity should protect, conserve, restore, and sustainably develop all eco resources across the globe so that it is available to the coming generation.

Keywords Tiger habitat · Tiger tourism · Forest ecosystem · Biodiversity conservation

B. V. R. Singh (✉)
Assistant Professor, Department of Geography, Faculty of Earth Sciences, Mohanlal Sukhadia University, Udaipur 313001, India

A. Sen
Professor, Department of Geography, Delhi School of Economics, University of Delhi, Delhi 110007, India

R. B. Singh et al. (eds.), *Remote Sensing and Geographic Information Systems for Policy Decision Support*, Advances in Geographical and Environmental Sciences,
https://doi.org/10.1007/978-981-16-7731-1_15

15.1 Introduction

In the twenty-first century, our economy is regulated by availability and access to environmental resources. But human intervention has rapidly increased the exploitation of natural resources all over the world, due to huge pressure from anthropogenic activities. Therefore, Land Use and Land Cover (LULC) is changing every day, which has the most adverse impact on environmental properties. Consequently, these results create phenomena like climate change, environmental degradation, overpopulation, genetic engineering, pollution, and resource depletion. These are bringing modifications in vegetation, biodiversity, air, water, soil, and land productivity (Xiubin 1996), which is very harmful to the human being and future earth.

Presently, there has been a decline in biodiversity over the last four decades, attributed largely to habitat fragmentation and land conversion (Butchart et al. 2010; Krauss et al. 2010; Zapfack et al. 2002).The Intergovernmental Panel on Climate Change (IPCC) estimated that 1.86 billion tons of carbon are emitted annually due to LULC owing to tropical deforestation, which is an active contributor to global warming and resultant climate change.

Therefore, the best option to utilize natural resources is a sustainable development approach. For example, eco-tourism has a unique method to generate sources of revenue without any damage to physical properties. It is a well-known fact that each country has a unique assemblage of natural resources, providing numerous advantages viz. promotion of cultural services, increase in carbon storage and sequestration, poverty alleviation, watershed protection, natural hazard regulation, sustaining food security and agriculture services, improvement of medical services and eco-tourism.

In this paper, the major focus is on eco-tourism activities like a "Tiger Economy". Tiger is an iconic wild animal, enjoying a unique status, of being among the largest carnivore in Asia, occupying an eminent position in the food chains the apex predator in the region, and also revered as a powerful cultural symbol. The Royal Bengal Tiger can be found across eastern parts of South Asian countries of India, Bangladesh, Nepal, and Bhutan.

But all is not going well with the big cats. The tiger is of the most endangered of large mammals and also within its species. The "Royal Bengal Tiger" is particularly confined in small scattered pockets in South Asia. India holds over seventy% of the world's tiger population and has the best chance of saving the population of this magnificent animal in the wild. The country has taken a pioneering initiative to conserve its national animal through Project Tiger since 1973, by establishing 47 tiger reserves. It covers over 2% of the country's geographical area, approximately 10% of the recorded forest area, and more than 40% of the country's total protected area.

Ranthambhore Tiger Reserve (RTR) has good potential for contributing to the local economy of Sawai Madhopur District in Rajasthan. According to NTCA Report (2015), important ecosystem services originating from RTR include gene-pool protection (₹ 7.11 billion per year), provisioning of water to the neighboring regions (₹ 115 million per year), provisioning of habitat and refuge for wildlife (₹

182 million per year), generation of cycling of nutrients (₹ 34 million per year), and sequestration of carbon (₹ 69 million per year). Additionally, the Ganesh Temple is visited by close to 10 lakh pilgrims every year.

15.2 Study Area

Ranthambhore Tiger Reserve (RTR) is named after "Ranthambhore Fort", the great historical monument, now designated a world heritage site by the UNESCO (Hill Forts of Rajasthan). It has immense natural beauty, as the majestic fort of Ranthambhore is situated amid the national park, on top of a hill. The Ranthambhore Tiger Reserve lies between latitudes 24°41′ N 26°22′ and longitudes 76°16E–77°14 E. The reserve is situated in the southeastern part of Rajasthan in the districts of Sawai Madhopur and Karauli district. The river Banas divides the reserve into two parts, the northeastern part being the Kaila Devi Sanctuary and southeast part the Ranthambhore National Park.

The Ranthambhore Tiger Reserves spread over 1,394.5 Sq. Km. as Ranthambhore National Park, Kaila Devi Wildlife Sanctuary, and Sawai Man Singh Wildlife Sanctuary and others are the main area for tiger and wildlife herbivore population. The park is located on the Western bank of mighty river Chambal. It's also dry-deciduous "dhok" (*Anogeissus pendula*, Edgew) forest and the vegetation of Ranthambhore is considered as Tropical Dry Deciduous Forest. It is a unique example of natural and historical richness in the semi-arid area and denuded tract of Sawai Madhopur and Karauli District of eastern Rajasthan. (Fig. 15.1).

15.3 Research Methodology

The present research is based on both qualitative and quantitative methods, which are built on primary and secondary database sources. Data has been collected from a variety of organizations such as the National Tiger Conservation Authority (NTCA), The Ministry of Environment and Forests (MOEF), Van Vibhag, Government of Rajasthan, Ranthambhore Tiger Reserve Authority, and several other NGOs.

In this study, the two main databases collected from the authority were total visitors and total income, in the past 16 financial years (2000–01 to 2015–16). Additionally, an ecosystem evaluation process was constructed from the analytical models, the "GIS-based spatial simulation models". These simulation models can understand the local ecosystem features in a better way, thus elevating the overall valuation. Such a mapping of ecosystem services can deliver very useful controlling recommendations for tiger reserve management to optimize benefits from the tiger reserve (NTCA Report 2015).

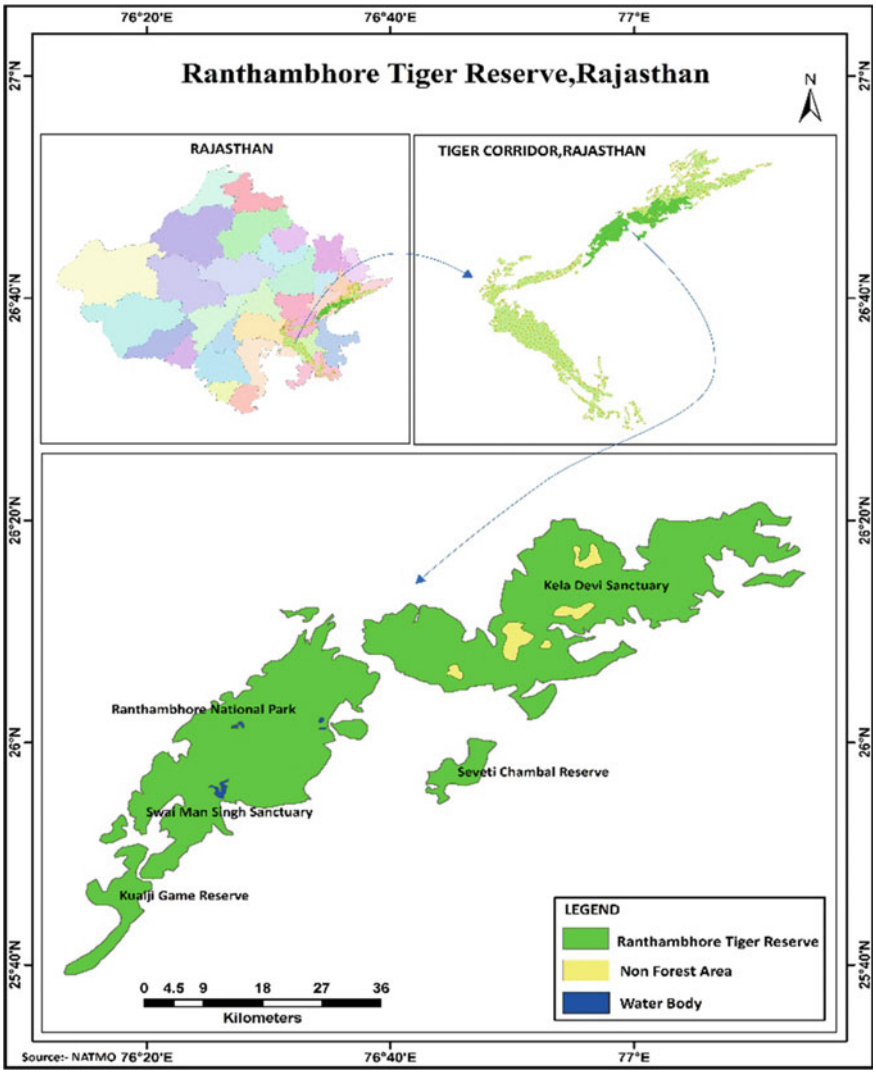

Fig. 15.1 Location map of Ranthambhore tiger reserve, India

The author has used ArcGIS-10 software and MS Excel to generate a relationship between visitors and revenues, as it is assumed that a direct relationship exists between tourist inflow and source of income. (Fig. 15.2).

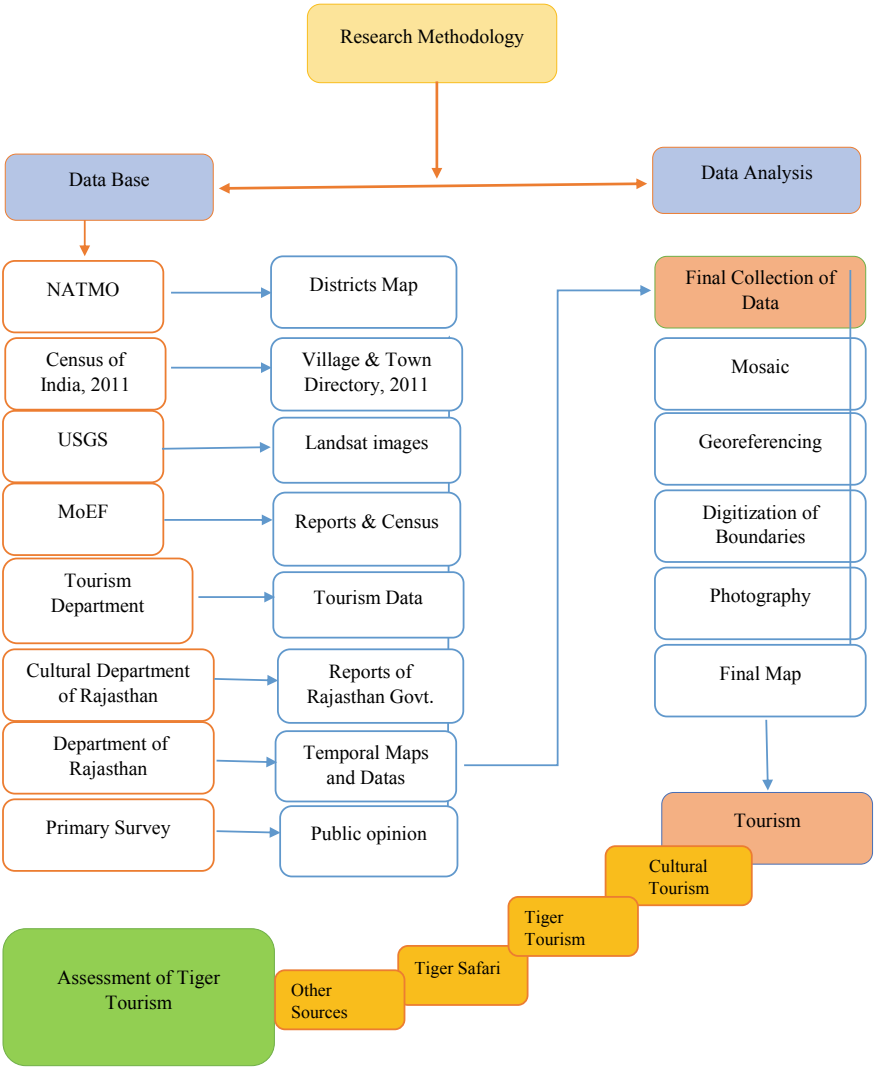

Fig. 15.2 Research methodology

15.4 Result and Discussion

Eco-tourism is a part of culture services in an ecosystem. Tiger tourism is increasing very rapidly in RTR, as it is considered as among the world's best places for sight-seeing a tiger. Presently, RTR has around 65 tigers, and one of them "Machali Tigress", who died recently, acquired a lot of fame. Another tiger "T-24 ÚSTAD"

too became very famous after it attacked the forest guard and killed him. Therefore, the authority shifted him to the Biological Park of Udaipur Rajasthan.

Recently, UNESCO declared Ranthambhore Fort as a world heritage site, which along with several large and small temples inside RTR is a major attraction for tourists and pilgrims. The principal temples in RTR are Ganesh Temple inside the Ranthambhore Fort, Keladevi Mata Temple, Soleshwar Mahadev Temple, Amareshwer Mahadev Temple, Khatola Mahadev Temple, and Kamaldhar Mahadev Temple. It is estimated that about 7–8 lakh pilgrims visit the Ganesh Temple annually (NTCA Report 2015).

India's Ranthambhore Tiger Reserve is among the most famous tiger habitats in the world. Therefore, it is visited by several tourists from across the globe, which is a huge source of revenue for the state's economy. And, this source is deemed as a green economy', which is a dynamic example of sustainable development sandwiched between environment and economic resources. One can easily appreciate how much tiger habitat is providing ecosystem services, for the regional development of RTR.

Ecosystem service of RTR, there are a lot of services such as Provisioning services such as food, freshwater, wood-timber, and fuel. As a condition of forest habitat like a dry deciduous and terrain as a semi-arid landscape, which is more suitable for food and wood for local stakeholders as well as Regulating services such as climate regulation, food regulation, and water purification flourish through forest habitat. Finally, most prominent services are a Cultural service such as esthetic, spiritual, educational, and recreational as a Tiger safari, which is most famous and sustainable practices of RTR ecosystem services.

In this flowchart (Fig. 15.3), how ecosystem services are giving benevolence to all stakeholders, in the context of RTR is the best example for the sustainable development of natural resources.

With several tourists visiting the tiger reserve and the world heritage fort, it has become a source of livelihood resource for both the local as well as outside stakeholders, to fulfill the basic needs of natural resources from the tiger economy.

Figure 15.4 indicates a gradual increase in the tourist's inflow in the past fifteen years. In 2000–01, very few tourists arrived due to various reasons—economic, social, and environmental, besides the availability of very few connectivities from around the world.

Since then, the government has focused on the conservation of biodiversity, which has led to an increase in the tiger population in India. Today, India has 70% of the world's tiger population, and this number is gradually increasing. While the number of students (scholars and researchers) have largely remained the same; the number of foreign tourists increased from 2000–01 to 2010–11 but has stagnated in the next five years. This is attributed to the global recession in international tourist movements. However, the arrival of domestic tourists has seen a reverse trend, increasing steadily and consistently, from less than 50,000 in 2000–01 to nearly 3,00,000 in 2015–16, an increase of over six-fold. This trend in the growth of the tiger economy is a very positive sign of the management of the tiger economy.

Figure 15.5 shows the total revenue collected from tiger tourism, which had three components—entry fee, eco-development surcharges, and other charges.

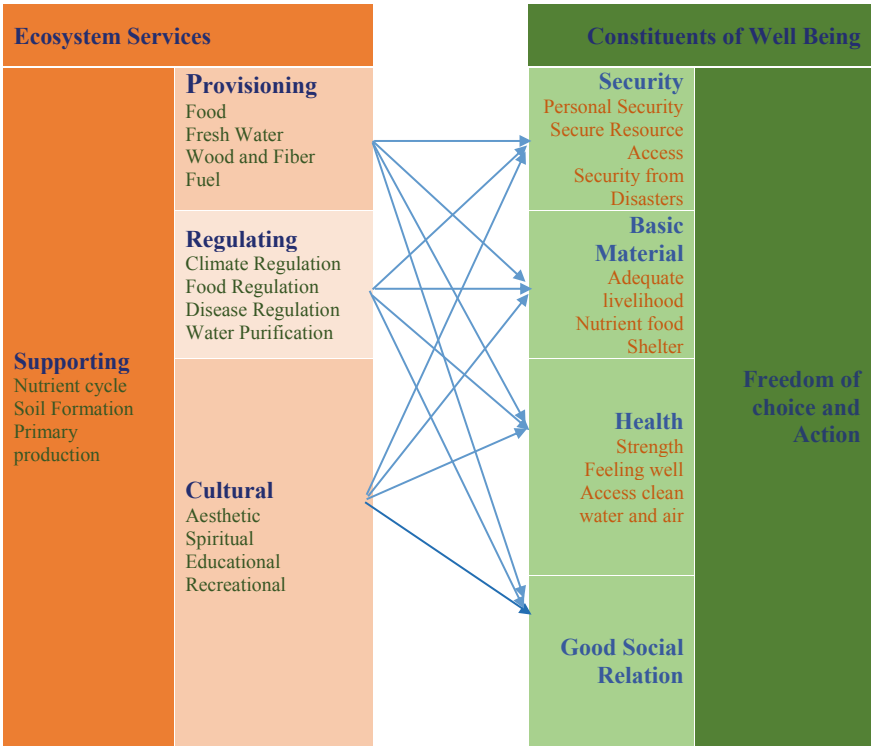

Fig. 15.3 Linkage between Ecosystem services and human well-being in RTR. Source: (MEA, 2005)

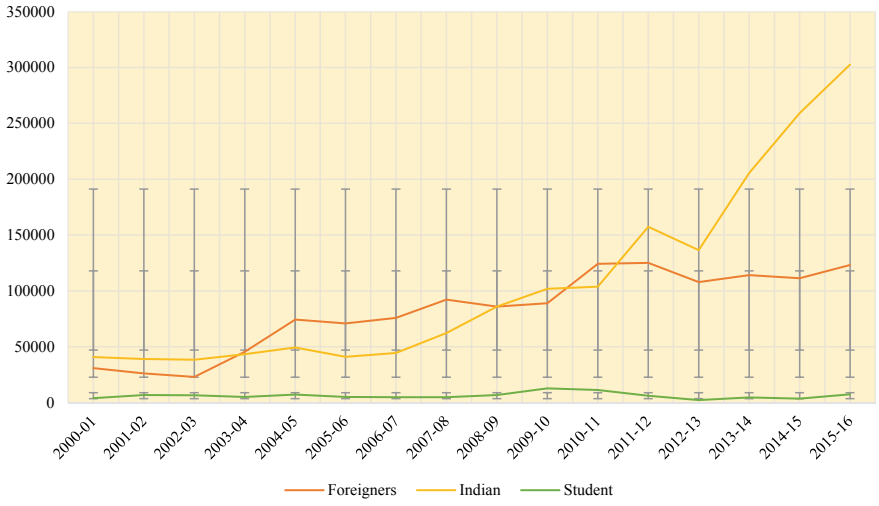

Fig. 15.4 Tourist arrivals in Ranthambhore tiger reserve, 2001–2016

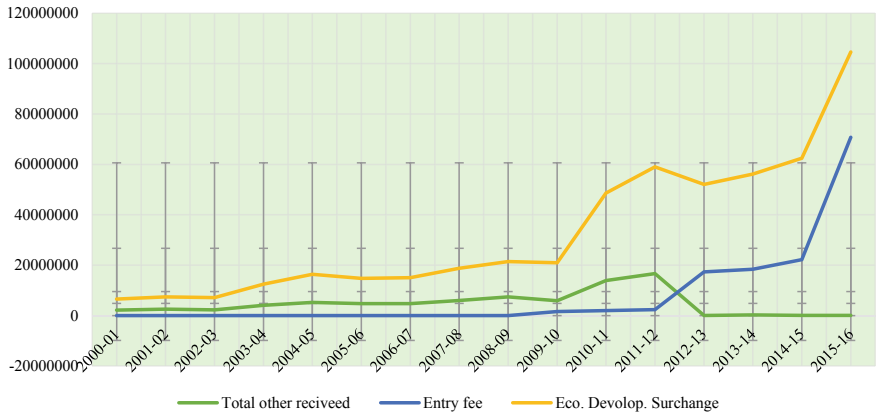

Fig. 15.5 Revenue from tiger tourism of Ranthambhore tiger reserve, 2001–2106

According to the graph, the amount collected as eco-development surcharges has consistently remained the largest component and has witnessed an acceleration in its growth since 2010–11, owing to an overall increase in the number of tourists.

The entry fee, which was introduced only in 2009–10, lagged initially but jumped in 2015–16, also due to an overall increase in the number of tourists. This translates into the fact that, tiger tourism activities are increasing day by day due to better management of tiger reserve as well as flourishing cultural sites.

But anthropogenic activities and infrastructure are encroaching on tiger corridors links and threatens to isolate its critical population. The rapid growth of tourism—both in terms of several tourists and also infrastructure is unsustainable and irreparable. It can be safely concluded that in its current form, tiger tourism is a serious threat to RTR ecosystem.

(Fig. 15.6) is a wheel diagram, which compares the tourist arrival and revenue generated per year as a%age of the total in all the previous sixteen years (2000–16). For example, the year 2000–01 received 2% of all tourists, but generated 1% of total revenue; while the year 2015–16 received 14% of all tourists, but generated 24% of total revenue. Over the years, the proportion of revenue generated is greater than tourist arrivals, which is a positive sign for better conservation of biodiversity, which augers well for eco-tourism.

But most visitors come for tiger safari, as Ranthambhore Tiger Reserve is globally well-known as a tiger habitat; and according to BBC, it is the best place for tiger sightseeing. RTR is situated on top of a hill of the Vindhyan system and plays a critical role as the junction of the tiger movement. The neighboring town of Sawai Madhopur has known the world over as the tiger destination, and wildlife tourism is the most important economic industry in the district. The current lodging house capacity of the town is approximately 3,000 tourist beds apart from the tourism industry in the Sawai Madhopur town, many people from local communities are involved in eco-tourism activities in RTR areas. Besides, more than 100 people from

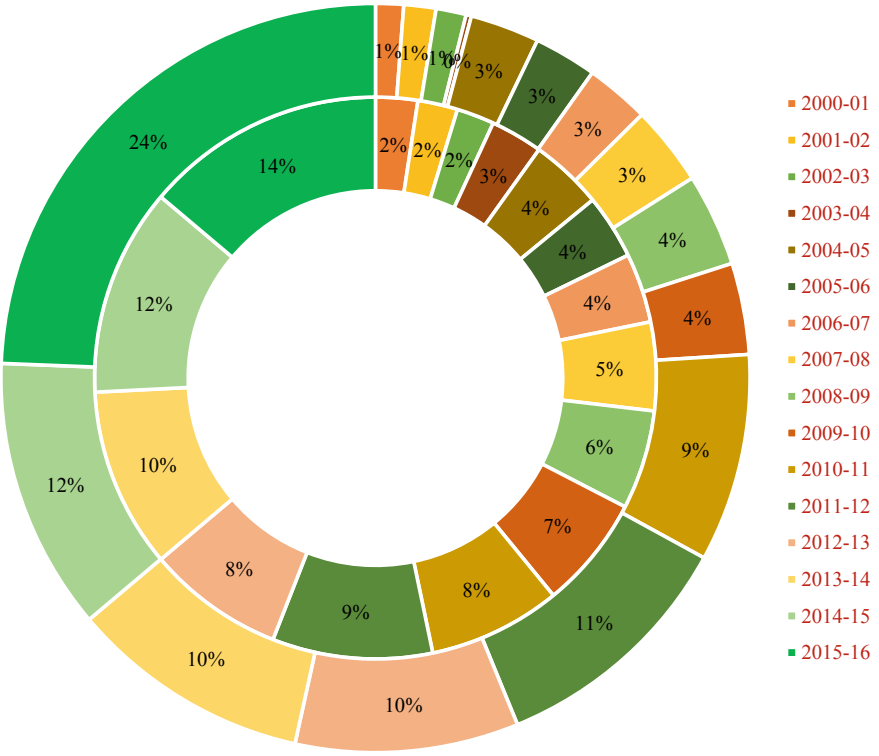

Fig. 15.6 Comparison of tourists and revenue strengths of RTR, 2001–2016 total tourists arrivals (inner circle) total revenue of in RTR (outer circle)

the local community have been selected and trained as Nature Guides, who earn their livelihood from tourism in RTR resources.

Figure 15.7 shows the variety of taxes generated for the state economy from tiger tourism, which is advantageous for government and local people. These benefits are uplifting socio-economic standard of native people.

As India entered a new tax regime of "One Nation One Tax", from 1st July 2017, all these taxes will be merged into one common format, the Good and Service Tax (GST). Next (Fig. 15.8), some of the glimpses below show a tiger tourism-related activities in RTR, In these all activities, tiger tourism is most prominent cultural services in terms of direct benefits but as well as other services are flourishing such as natural resources, agriculture, husbandry, and others activities.

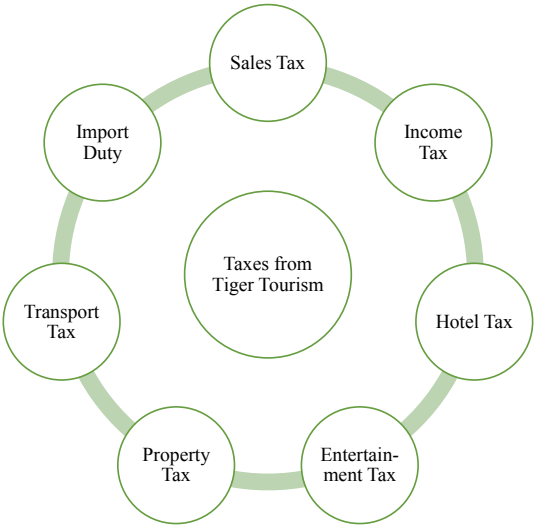

Fig. 15.7 Sources of revenue from tiger tourism, 2001–2016

Fig. 15.8 Glimpses of Ranthambhore tiger tourism. **Source**: (Compiled by Scholar, 2017)

15.5 Conclusion

Apart from conserving wildlife and biodiversity of RTR, tiger reserves also provide a variety of resources and are associated with economic, social, cultural, and spiritual

benefits, which are also termed as ecosystem services. Tiger reserves support human life by protecting agricultural genetic material by being nurseries; and providing cheap and clean water for drinking and irrigation. Tiger reserves not only help in mitigating natural disasters such as floods and cyclonic storms but also resources of many medicines and drugs. In addition to natural and cultural resources, tiger reserves are also an important driver of tourism, for both local and outside stakeholders.

Finally, from rag pickers to hotel tycoons, all are fully dependent on tiger tourism, which is a unique pattern and best model for the sustainable development of biodiversity resources with in-situ conservation methods. It fulfills the basic needs of local communities and outside stakeholders, who are involved in direct and indirect tiger tourism activities. That's the best way for sustainable development of bio-resources. Therefore, the focus should be to restore the environmental resources, which would be helpful for the economy, society, and environment, leading to holistic regional development in RTR areas.

References

http://envfor.nic.in/division/wildlife. Accessed 7 May 2017.
http://forest.rajasthan.gov.in/content/raj/forest/forest-department/en/departmental-wings/forest-devlopment/districtwise-forest-blocks-google-earth.html. Accessed 21 June 2017.
http://forest.rajasthan.gov.in/content/raj/forest/forest-department/en/home.html. Accessed 17 June 2017.
http://projecttiger.nic.in/. Accessed 5 June 2017.
http://projecttiger.nic.in/content/44_6_TigerReserve.aspx. Accessed 5 June 2017.
http://projecttiger.nic.in/Ntcamap/108_1_43_mapdetails.aspx. Accessed 7 May 2017.
http://www.sustainablescale.org/CconepttualframeworkUnderstandingScale/measurigSclae/MilleniumEcosystemAssesment.aspx. Accessed 1 May 2017.
Butchart SH, Walpole M, Collen B, Van Strien A, Scharlemann JP, Almond RE, Watson R (2010) Global biodiversity: indicators of recent declines. Science, 328(5982):1164–1168
Krauss J, Bommarco R, Guardiola M, Heikkinen RK, Helm A, Kuussaari M, Steffan DI (2010) Habitat fragmentation causes immediate and time-delayed biodiversity loss at different trophic levels. Ecology letters, 13(5): 597–605
MEA (2005) Living beyond our means: natural assets and human well-being: Statement from the board. Millennium Ecosystem Assessment
Ntca.gov.in. (2015) NTCA Report 2015 Available at: [Accessed 5 June 2017]
Zapfack L, Engwald S, Sonke B, Achoundong G, Madong BA (2002) The impact of land conversion on plant biodiversity in the forest zone of Cameroon. Biodiversity & Conservation 11(11):2047–2061
Xiubin L (1996) A review of the international researches on land use/land cover change. Acta Geograph Sinica 51:558–565

Chapter 16
Inventory and Phenological Assessment of Apple Orchards Using Various Remote Sensing Techniques for Shopian District of Jammu and Kashmir State, India

Arvind Pandey, R. Hebbar, Sarita Palni, Jiwan Singh Rawat, and Uday Raj

Abstract Horticultural crops are one of the vital role players in the field of economic development in Indian hilly regions. Among all, apple is one of the important horticulture crop in the North-West Himalaya, and 60% of apple production comes from Kashmir state in India. The identification and monitoring of apple becomes essential for proper assessment and planning for large production of apple. Now-a-days, Remote Sensing and GIS have been emerging as the newest and more advanced technique for crop monitoring, crop inventory and the assessment of its production. Keeping in view, the present work deals with the identification of apple-producing areas and assessment of phenology patterns of apple trees in Shopian district of Jammu and Kashmir which is a leading producer of apple in the whole world. The IRS-P6 LISS-IV, Cartosat-1 and LANDSAT-8 data were used for phenology and classification. Top of Atmospheric (TOA) correction and various digital classification algorithms viz., supervised MXL, Unsupervised ISODATA and NDVI threshold were used for estimation of the apple orchard area and NDVI profile for phenology pattern across the years. In comparison to other classification techniques, Supervised classification technique was found most suited with having accuracy ranging between 90 and 95% for all stages of apple trees. On the basis of spectral response and NDVI response, apple orchards were distinguishable amidst the other crops/vegetation types. Generated normalized difference vegetation index value was found to be 0.65 for apple orchards for LISS-IV and the results are used for finding the phenology of apple tree. Using the above NDVI threshold value, the apple orchards are classified with an accuracy range of 75–80%. It shows the unique spectral and phenology feature of apple and highlighted the seasonal change. This method is also very useful for other

A. Pandey (✉) · S. Palni · J. S. Rawat
Department of Remote Sensing and GIS, Soban Singh Jeena University, Almora, Uttarakhand, India

R. Hebbar · U. Raj
Regional Remote Sensing Centre, NRSC/ISRO, ISITE Campus, Marathahalli, Bengaluru 560037, India
e-mail: hebbar_kr@nrsc.gov.in

U. Raj
e-mail: udayraj@nrsc.gov.in

R. B. Singh et al. (eds.), *Remote Sensing and Geographic Information Systems for Policy Decision Support*, Advances in Geographical and Environmental Sciences,
https://doi.org/10.1007/978-981-16-7731-1_16

orchard inventory and estimation of productivity. Besides, this also provides a trend in any abnormal seasonal change on horticulture area which may help in providing pre-information about health and effect on overall production of orchard.

Keywords Remote sensing · Apple orchards phenology · supervised and unsupervised classification · NDVI

16.1 Introduction

The scenario of horticultural activities in the country has been changing rapidly both in terms of production and productivity. India stands at the second position in terms of fruits and vegetables production in the whole world and is the leader in several horticultural crops such as mango, papaya, banana, cashew nut, areca nut, potato (Kaul 1997). Proper planning of these crops basically requires reliable and precise data depicting area under production and total production at different spatial hierarchies (block, tehsil, district and state) (Tompkins et al. 2010). Hence, availability of reliable statistical database at micro level is one of the most critical requirements for efficient policy planning for proper development and management of resources (Sadoulet and Janvry 1995). In Asia and Europe, the history of growing apples dates back to over thousand years (Sadoulet and Janvry 1995). Origin of apple is known to be from Central Asia, where its wild ancestor, ***Malus sieversii*****,** can still be found till today (Harris et al 2002; Way et al. 1991). Apple tree (***Malus domestica***) is a type of deciduous tree (family—Rosaceae), mainly known for its sweet, pomaceous fruit (Ramírez and Davenport 2013). Apple is cultivated in the whole world as a fruit tree, and it is the most widely grown species among the genus ***Malus***. Apple trees do not attain much height and remain small if grafted onto roots (rootstock) but can grow hugely if they are grown from seeds. There are more than 7,500 known varieties of apples worldwide, which result in a range of desired characteristics (Suresha et al. 2012). Different cultivars are usually bred for different purposes and tastes, including cooking, eating uncooked and production of cedar and apple vinegar. In 2010, about 69 million tons apples were grown worldwide and almost half of this total was produced alone by China (Lima et al. 2010). The United States is the second-leading producer, with more than 6% of world production. Turkey, Italy, India and Poland follow the lead after US, respectively, in terms of apple production.

At present, satellite data with medium resolution is being operationally used for mapping and monitoring of agricultural crop (Becker-Reshef et al 2010). Many research works on remote sensing and geospatial technological applications for site-specific management of fruit and nut crops, guidelines for their phenological observation have been carried out by various scholars (Panda et al. 2010; Koch et al. 2007; Polgar and Primack 2011). However, in Himalayan areas, systematic examinations for investigating the utility of Remote Sensing data for horticultural fruit and crops grown by plantation techniques are restricted (Usha and Singh 2013). Advanced object-based classifiers have indicated promising outcomes for differentiation of

high-resolution information for monitoring, mapping and planning of nature-based resources. Object-based image classification technique is an incredible and promising strategy for grouping of high-resolution satellite images by changing image pixels into objects using both textural and logical data (Hebbar et al. 2014). Johansen et al. (2009) demonstrated the use of high-resolution data for depiction of banana plantations utilizing a combination of object-based classification and post-classification visual editing. With progression in space innovation, accessibility of high-resolution information and advanced classifiers, Remote Sensing can play a crucial part in the inventory of horticultural crops. In this context, this current investigation was proposed to investigate the expected utilization of high-resolution data for identifying and outlining horticultural crop types by using semi-automatic classification method *vis-à-vis* conventional visual interpretation techniques.

The major objectives of the study were (i) to study the phenology of apple orchards using temporal data, (ii) to study the inventories of apple orchards using multi-sensor data and (iii) accuracy deviation of classified data.

16.2 Study Area

Shopian was initially known as 'Sheen-e-van' which means 'forest of snow' is a historical town located within 33°42′37.27″ N to 74°56′28.77″ E (Fig. 16.1). It has remained a very important city from the time period of Mughal rulers (Schofield, 2000). The total area of this subdivision is 307.42 km^2 of which 196.93 km^2 area of cultivable nature. From 1872 to 1892 A.D onwards, Shopian was one among 6 Wazarat headquarters in Kashmir. Shopian district is positioned in the foothills of Pir Panjal mountain range and most of its terrain is hilly. The district is also recognized as 'Apple Bowl' of the state as it is famous for horticulture sector. Fruit production in this district is estimated to be 2 lakhs metric tons per annum. Shopian is also home for walnuts (Bhat and Lone 2017).

16.3 Data Used

Cartosat-1 data with 2.5 m PAN and LISS-IV data with 5.8 m resolution multiple data with three band (Green, Red and NIR band) are used for classification of apple orchards. Landsat-8 multiple temporal data with 30 m multiple, 15 m PAN and 30 m thermal data with 11 bands were used for temporal change assessment from June to January. Temporal data are used for determination of phenology of apple orchards and classification of apple orchards (Table 16.1, Fig. 16.2).

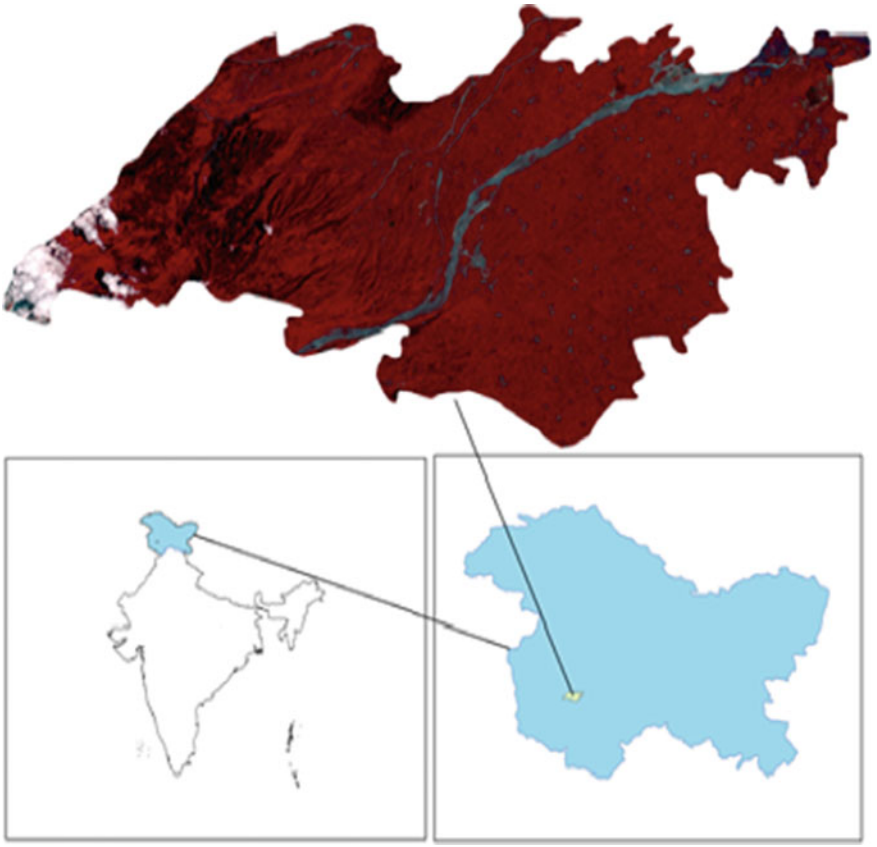

Fig. 16.1 Study area

Table 16.1 Characteristics of satellites data

Satellite	Resolution	Sensor	Revisit time (days)
Cartosat-1 IRS-P5	2.5 M (PAN)	PAN-AFT	5
LISS-IV (IRS-R2)	5.8 m (multi)	L4FX	5
Landsat-8	30 m (multi and thermal)15 m (PAN)	OLI and TIRS	16

16.4 Methodology

Methodology adopted in this study aims to determine the phenology of apple orchards using Landsat-8 multi-temporal data, inventory of apple orchards using multi-sensor data and consoled accuracy of classified data with high-resolution satellite imagery (Fig. 16.3).

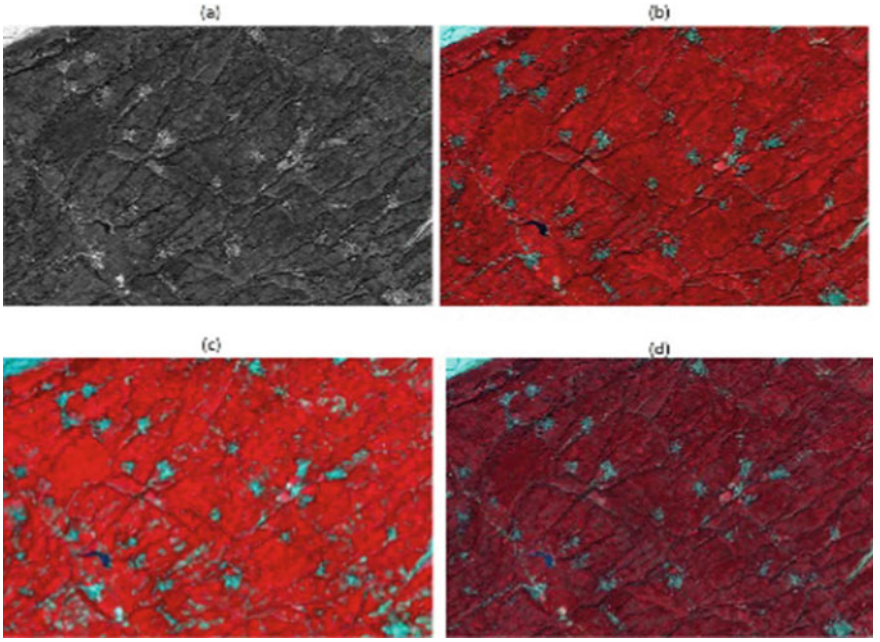

Fig. 16.2 Satellite images used for the study. **a** Cartosat-1 (2.5 m PAN data). **b** LISS-IV multiple data (5.8 m). **c** Landsat-8 multiple data (30 m). **d** Fused Image of Cartosat-1 PAN and LISS-IV multiple data

Three datasets i.e., Landsat-8, Cartosat-1 and LISS_IV have been used to carry out this work. The data of Landsat-8 have been pre-processed by calculating the ToA. It is then layer stacked so that a particulate image can be used. After this, the study area is subset from the layer-stacked image. The subset image is then used for doing the supervised and unsupervised classification to create NDVI spectral profiles for determining the apple orchard phenology profile.

Similarly, Cartosat-1 and LISS-IV images are also pre-processed by ortho-rectifying the both images and then fusing them together. The fused image is then classified by using the methods of supervised as well as unsupervised classification. NDVI is also calculated from the fused image. The supervised and unsupervised images of all the three datasets are then used to validate the output results so that the final classified map can be produced.

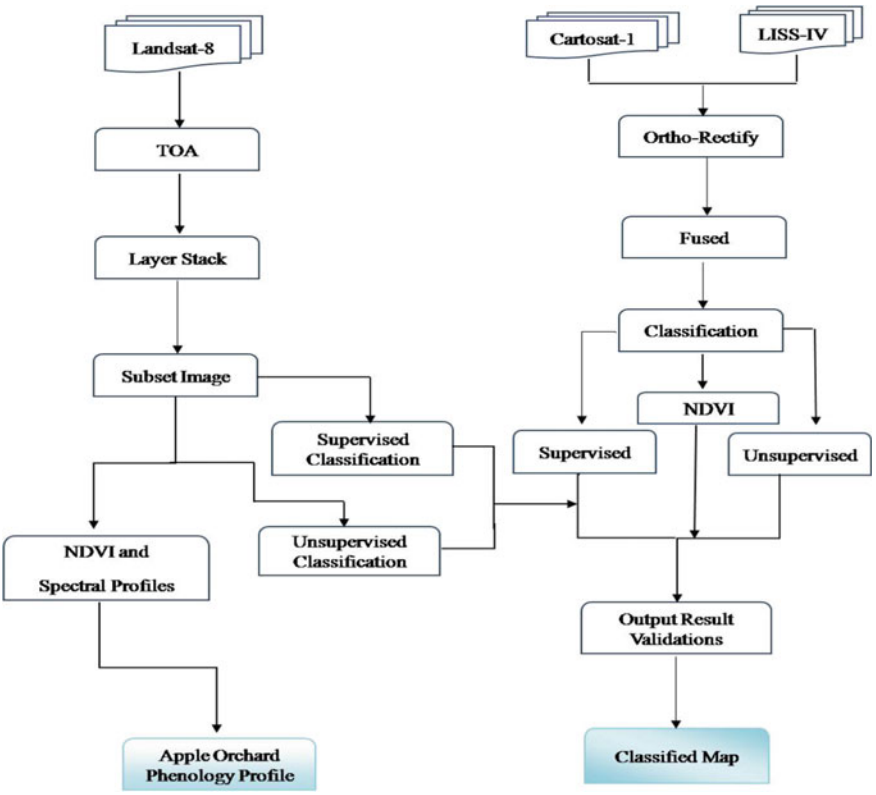

Fig. 16.3 Methodology used for phenology and classification of apple orchards

16.5 Results and Discussions

16.5.1 Spectral Profile of Apple Orchards, Forests and Agriculture Area in NIR Band

Spectral profiles have taken after Top of Atmospheric (TOA) correction of Landsat-8 data. The profile considered here indicates the spectral reflectance in NIR band. In NIR band, the green color reflects maximum; hence, NIR band is used for comparison of Apple, Forest and Agriculture reflectances. Figure 16.4 shows the various reflectance value across the months in Apple orchards, Forests and Agriculture. The following graph was drawn for above figure to describe the temporal changes in terms of spectral reflectance. It is observed from the graph that the spectral profile of apple is different from the spectral profile of forest and agriculture due to high density of orchards.

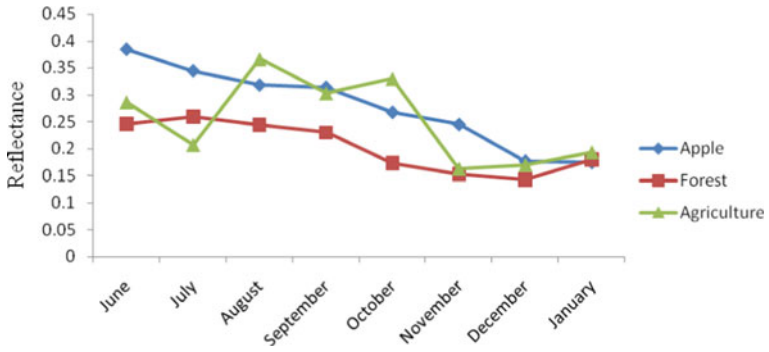

Fig. 16.4 NIR reflectance of the Apple orchards, forests and agriculture (June 2014 to January 2015)

16.5.2 NDVI

Most of vegetation indices (VI) incorporate the information accommodated in two spectral bands i.e., Red and Near-infrared. These indices are set up so as to limit the impact of outer components on spectral data and to determine the characteristics of canopy, for example, leaf area index (LAI) and portion of absorbed photosynthetic active reflectance (Xu and Guo 2014).

NDVI value differs across the months (Fig. 16.5), where red color indicates the distribution of apple orchards. These images show the monthly changes of vegetation in the area. In the month of June, we can see the maximum red color in image and after that it is decreasing continuously. From June to August, monsoon period prolongs hence the proportion of green leaves is maximum and after that it decreases continuously.

16.5.3 NDVI Difference in Among Months

The below Fig. 16.6 indicates the NDVI profile of apple forest and agriculture. The graph indicates that the NDVI response of apple is different from the forest and agriculture. Classification of apple can be done easily with the help of NDVI response.

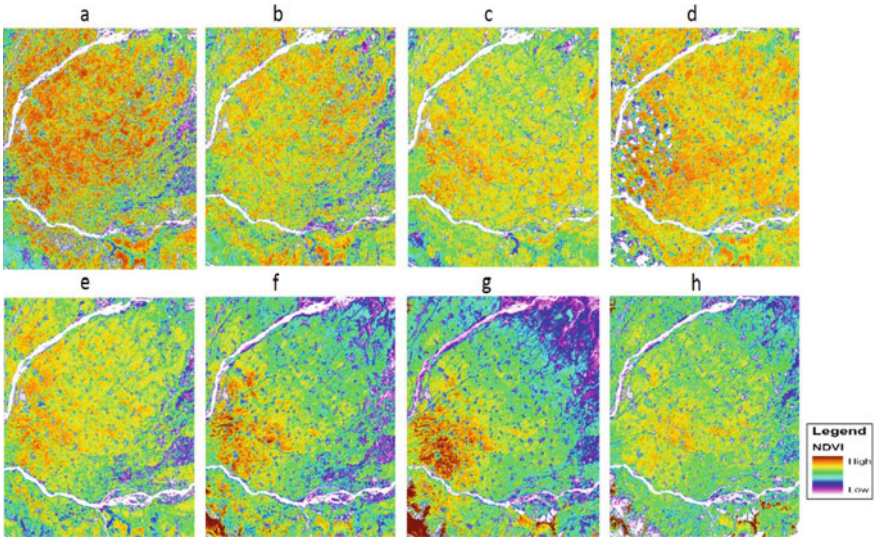

Fig. 16.5 NDVI Changes (temporal change of NDVI (**a**) June, (**b**) July, (**c**) August, (**d**) September,(**e**) October, (**f**) November, (**g**) December and (**h**) January month NDVI)

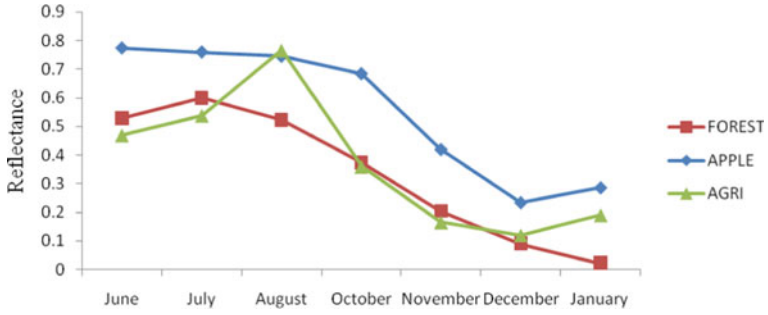

Fig. 16.6 NDVI difference in the month June to January

16.6 Classified Image Result

After spectral profile, we did the classification of the fused image (Cartosat-1 and LISS-IV), Landsat-8 image and NDVI images. With the help of classification, we get the following result.

16.6.1 Classification

For the assessment of phenological pattern and vegetation classification, three different satellite imageries, Cartosat-1, LISS-IV and Landsat-8 were used. Landsat-8 images were used for assessment of phenological pattern with the help of spectral reflectance of apple trees. Fused images of Cartosat-1 and LISS-IV were used for classification of apple orchards, whereas LISS-IV images were used for calculation of NDVI classification, based on threshold values. In this study, we have five classified images which are LISS-IV fused image, Landsat-8 layer stack image and NDVI image. To find out high accuracy in classification, three different methods, e.g., Supervised classification, Unsupervised classification and NDVI Threshold value classification were used (Fig. 16.7).

16.7 Classification Result

In this study, the apple orchards were classified into three age classes viz., Young age, Middle age and Mature age trees.

i. Young apple trees—young apple trees are 0–3 years trees which are young plantations.

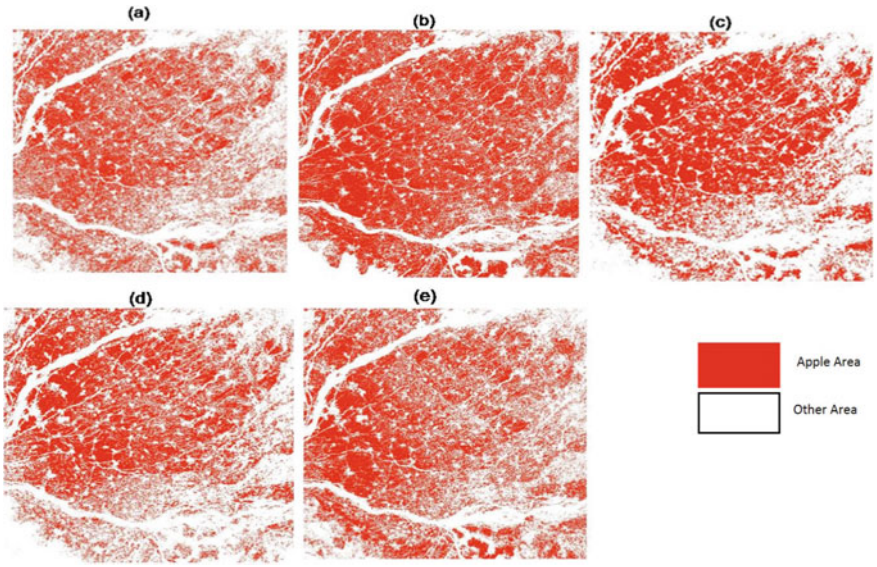

Fig. 16.7 Result of classification images. **a** Supervised classification (Cartosat-1 and LISS-IV fused image). **b** Unsupervised classification (Cartosat-1 and LISS-IV fused image). **c** Supervised classification (Landsat-8). **d** Unsupervised classification (Landsat-8). **e** NDVI classification

ii. .Middle apple trees—middle apple trees are 3–5 years trees.
iii. Mature apple trees—mature apple trees are above 5 years.

16.7.1 Classification of Mature Age Trees

With the help of very high-resolution imagery, we take some area of apple mature trees and compare with the classified image.

In Table 16.2, the area of 41.13 hectare is the area of young age apple tree which is identified from the very high-resolution imagery for shape file area. LISS-IV and Cartosat-1 fused image data for Supervised and Unsupervised classification give 37.64 hectare and 34.47 hectare area, respectively, which are 0.91% and 0.83% classified. After that Landsat-8 data are used for supervised and unsupervised classification and it resulted in 35.38 hectare and 32.07 hectare areas which are 0.86% and 0.77% area of classified image in comparison with the very high-resolution imagery area. NDVI image data used for classification with the help of threshold value, and nearly 33.89 hectare areas are resulted which are 0.82% of classified with the very high-resolution imagery area.

16.7.2 Classification of Middle Age Trees

With the help of very high-resolution imagery, we get some random area of middle age apple trees and compared it with the classified image.

In Table 16.3 shows the 31.1 hectare area of young age apple tree which is identified from the very high-resolution imagery. With the help of LISS-IV and Cartosat-1 fused image data for supervised and unsupervised classification area of 29.6 hectare and 28.1 hectare area fall under classified, which are 0.95% and 0.90%. The Landsat-8 data are used for supervised and unsupervised classification and got 24.03 hectare and 25.72 hectare areas which are 0.77% and 0.82% of classified in comparison with the very high-resolution imagery area. Finally, NDVI image data are used for classification with the help of threshold value and 24.47 hectare areas, which are 0.78%, classified with the very high-resolution imagery area.

Table 16.2 Apple mature age trees classification result

S. No	Classification images	Shape file area (mature age) (Ha.)	Classified area (Ha)
1	LISS-IV (supervised)	41.13	37.64
2	LISS-IV (unsupervised)	41.13	34.47
3	Landsat-8 (supervised)	41.13	35.38
4	Landsat-8 (unsupervised)	41.13	32.07
5	NDVI	41.13	33.89

Table 16.3 Apple middle age trees classification result

S. No	Classification Images	shape file area (middle age) (Ha)	Classified area (Ha)
1	LISS-IV (supervised)	31.1	29.6
2	LISS-IV (unsupervised)	31.1	28.1
3	Landsat-8 (supervised)	31.1	24.03
4	Landsat-8 (unsupervised)	31.1	25.72
5	NDVI	31.1	24.47

16.7.3 Classification of Young Age Trees

With the help of very high-resolution imagery, we got some random area of young-aged apple trees and compared it with the classified image.

In Table 16.4, the 26.21 hectare area of young age apple tree which is identified from the very high-resolution imagery. With the help of LISS-IV and Cartosat-1 fused image data for supervised and unsupervised classification and 17.01 hectare and 19.29 hectare area, which are 0.64% and 0.73% classified. The Landsat-8 data are used for supervised and unsupervised classification and got 14.11 hectare and 11.59 hectare areas which are 0.53% and 0.44% are classified compared with the very high-resolution imagery area. The NDVI image data are used for classification with the help of threshold value and got 10.68 hectare areas which are 0.40% classified with the very high-resolution imagery area. The accuracy assessment achieved through classification is 0.91% and by Kappa Coefficient is 0.81.

16.8 Accuracy Assessment

LISS-IV supervised classification gives the better classified image in comparison with other classifications. LISS-IV fused data showed the 0.64 to 0.95% classification accuracy in Mature, Middle and Young age apple orchards. Supervised classification gives better result for Middle age apple orchards. The Table 16.5 showing the

Table 16.4 Apple young age trees classification result

S. No	Classification of images	Shape file area (young age) (hectare)	Classified area (hectare)
1	LISS-IV (supervised)	26.21	17.01
2	LISS-IV (unsupervised)	26.21	19.29
3	Landsat-8 (supervised)	26.21	14.11
4	Landsat-8 (unsupervised)	26.21	11.59
5	NDVI	26.21	10.68

Table 16.5 LISS-IV supervised classification in different age

S. No	Classification of images (LISS-IV supervised)	Shape file area (young) (hectare)	Classified area (hectare)	Accuracy %
1	Mature age (above 5)	41.13	37.64	0.91
2	Middle age (3–5)	31.1	29.6	0.95
3	Young age (0–3)	26.21	17.01	0.64

Table 16.6 LISS-IV Unsupervised classification in different age

Sl. No	Classification of (LISS-IV unsupervised)	Shape file area (young) (hectare)	Classified area (hectare)	Accuracy %
1	Mature age (above 5)	41.13	34.47	0.83
2	Middle age (3–5)	31.1	28.1	0.90
3	Young age (0–3)	26.21	19.29	0.73

classification result of supervised classification of Mature, Middle and Young age apple orchards.

LISS-IV unsupervised classification gives the better classified image in comparison with Landsat-8 and NDVI classifications. LISS-IV fused data are given a range of 0.73 to 0.83% of classification accuracy in Mature, Middle and Young age apple orchards. Unsupervised classification gives better result for Middle age apple orchards. In the Table 16.6, the classification result of unsupervised classification of Mature, Middle and Young age apple orchards is shown.

16.8.1 Landsat-8 Supervised Classification

Landsat-8 supervised classification gives the good classified image for mature age apple orchards compared with other classifications. Landsat-8 data are given 0.53–0.86% classification accuracy in Mature, Middle and Young age apple orchards. Supervised classification gives better result for mature age apple orchards. The Table 16.7 shows the classification result of supervised classification of Mature, Middle and Young age apple orchards.

Table 16.7 Landsat-8 Supervised classification in different age

Sl. No	Classification of landsat-8 (spervised)	Shape file area (young) (hectare)	Classified area (hectare)	Accuracy %
1	Mature age (above 5)	41.13	35.38	0.86
2	Middle age (3–5)	31.1	24.03	0.77
3	Young age (0–3)	26.21	14.11	0.53

Table 16.8 Landsat-8 unsupervised classification in different age

Sl. No	Classification of landsat-8 (unsupervised)	Shape file area (young) (hectare)	Classified area (hectare)	Accuracy %
1	Mature age (above 5)	41.13	32.07	0.77
2	Middle age (3–5)	31.1	25.72	0.82
3	Young age (0–3)	26.21	11.59	0.44

16.8.2 Landsat-8 Unsupervised Classification

Landsat-8 unsupervised classification gave good classified image for Middle age apple orchards compared with NDVI classification. Landsat-8 data are given 0.44–0.77% classification accuracy in Mature, Middle and Young age apple orchards. Unsupervised classification gives better result for Middle age apple orchards. The Table 16.8 shows the classification result of unsupervised classification of Mature, Middle and Young age apple orchards.

16.8.3 NDVI Classification

NDVI classification has given good classified image for mature age apple orchards compared with Landsat-8 classification. NDVI data are given 0.40 to 0.82% classification accuracy in Mature, Middle and Young age apple orchards. NDVI classification gave better result for mature age apple orchards. In the Table 16.9, the classification result of unsupervised classification of Mature, Middle and Young age apple orchards are shown.

Table 16.9 Landsat-8 NDVI classification in different age

Sl.No	Classification of NDVI	Shape file area (young) (hectare)	Classified area (hectare)	Accuracy %
1	Mature age (above 5)	41.13	33.89	0.82
2	Middle age (3–5)	31.1	24.47	0.78
3	Young age (0–3)	26.21	10.68	0.40

16.9 Discussion

Phenology plays an important role in overall growth and assessment of plant (Sharma and Panigrahy 2007). In this study, we calculated phenology of apple tree and classified the apple orchards with the help of visual interpretation. We have high-resolution image of Cartosat-1 and LISS-IV images which is useful for supervised and unsupervised classification. With the help of spectral profile, we calculated NDVI and after that NDVI threshold values. We used the classified NDVI images. Phenological stages are defined by the Landsat-8 imagery and fused image of Cartosat-1 and LISS-IV data. They are useful for classification of apple orchards. In this study of apple phenological stages which are calculated by Landsat-8 data are then matched with the original natural activity of apple trees. In the NDVI result, the months from June-2014 to October-2014 show the maximum RED colors which indicate apple orchards. In the November month, NDVI and spectral profile show considerable decrease in reflectance values due to falling of leaves. With the help of NIR reflectance, we were able to easily find apple orchard areas. With the help of high-resolution data and fused image, the apple orchards are classified. The results are compared visually and the accuracy is tabulated. From classification techniques, accuracy of the Cartosat-1 and LISS-IV fused image of about 0.91% is produced for mature apple trees, 0.95% for middle apple trees and 0.64% for the young apple trees.

16.10 Conclusion

Remotely sensed data can be utilized successfully in detection, mapping and planning of horticulture crops. In this study, we have proposed a strategy based upon the unique spectral and phenology feature of apple and have focused on the season-wise changes among uncovered leaf falls, ground spread and growing apple plants. To examine the characteristics of apple planning results, supervised classification and unsupervised classification techniques were chosen and compared. The present study was done to investigate the capability of high-resolution LISS-IV and Cartosat-1 data for mapping and Landsat-8 information for phenology of horticultural plantations. Spectral data and NDVI data are utilized for classification of apple plantations. The classification technique was evaluated by very high-resolution images. The results of apple orchards delineation have classification accuracy of 85–92 percent. Other improvement in precision and accuracy could be accomplished utilizing spectral and NDVI threshold value classification of merged data. This study demonstrated potential for spectral, NDVI, Supervised and Unsupervised classification process for delineation of apple orchards. Evaluation and comparison show that inventory of apple orchards by supervised classification method can achieve the highest accuracy. The classification results of apple orchards for satellite data used are in agreement, including the approach of NDVI and spectral reflectance in phenology of apple orchards.

Acknowledgements We thank Director of Regional Remote Sensing Center-South (RRSC-S), Bengaluru for providing required support to conduct the study and thank to NRSC/ISRO for data support.

References

Becker-Reshef I, Justice C, Sullivan M, Vermote E, Tucker C, Anyamba A, Small J, Pak E, Masuoka E, Schmaltz J, Hansen M (2010) Monitoring global croplands with coarse resolution earth observations: the global agriculture monitoring (GLAM) project. Remote Sensing 2(6):1589–1609

Bhat TA, Lone TA (2017) Potential and prospects of J&K economy. Educreation Publishing, New Delhi

Harris SA, Robinson JP, Juniper BE (2002) Genetic clues to the origin of the apple. Trends Genet 18(8):426–430

Hebbar R, Ravishankar HM, Subramoniam SR, Uday R, Dadhwal VK (2014) Object oriented classification of high-resolution data for inventory of horticultural crops. Int Arch Photogramm Remote Sens Spatial Inf Sci 40(8):745–749

Johansen K, Phinn S, Witte C, Philip S, Newton L (2009) Mapping banana plantations from object-oriented classification of SPOT-5 imagery. Photogramm Eng Remote Sens 75(9):1069–1081

Kaul GL (1997) Horticulture in India-production, marketing and processing. Ind J Agric Econ 52(3):561–573

Koch E, Bruns E, Chmielewski F-M, Defila C, Lipa W, Menzel A (2007) Guidelines for plant phenological observations. World Climate Data and Monitoring Programme, Geneva

Lima ÁM, Cerqueira MA, Souza BW, Santos ECM, Teixeira JA, Moreira RA, Vicente AA (2010) New edible coatings composed of galactomannans and collagen blends to improve the postharvest quality of fruits–Influence on fruits gas transfer rate. J Food Eng 97(1):101–109

Panda SS, Hoogenboom G, Paz JO (2010) Remote sensing and geospatial technological applications for site-specific management of fruit and nut crops: a review. Remote Sensing 2(8):1973–1997

Polgar CA, Primack RB (2011) Leaf-out phenology of temperate woody plants: from trees to ecosystems. New Phytol 191(4):926–941

Ramírez F, Davenport TL (2013) Apple pollination: a review. Sci Hortic 162:188–203

Sadoulet E, De Janvry A (1995) Quantitative development policy analysis, vol 1. Johns Hopkins University Press, Baltimore

Schofield V (2000) Kashmir in conflict: India, Pakistan and the unending war. IB Tauris, London

Sharma A, Panigrahy S (2007) Apple orchard characterization using remote sensing and GIS in Shimla district of Himachal Pradesh. In Proceedings of remote sensing and photogrammetry annual conference 2007, pp. 11–14.

Suresha M, Shilpa NA, Soumya B (2012) Apples grading based on SVM classifier. Int J Comput Appl 975:8878

Tompkins JA, White JA, Bozer YA, Tanchoco JMA (2010) Facilities planning. Wiley, New York

Usha K, Singh B (2013) Potential applications of remote sensing in horticulture—a review. Sci Hortic 153:71–83

Way RD, Aldwinckle HS, Lamb RC, Rejman A, Sansavini S, Shen T, Watkins R, Westwood MN, Yoshida Y (1991) Apples (Malus). Genetic Resour Temperate Fruit Nut Crops 290:3–46

Xu D, Guo X (2014) Compare NDVI extracted from Landsat 8 imagery with that from Landsat 7 imagery. Am J Remote Sens 2(2):10–14

Chapter 17
Geospatial Technology in Sustainable Forest Management in Molakalmuru Taluk of Karnataka State, India

M. C. Manjunatha and H. T. Basavarajappa

Abstract Geospatial approaches address cost-beneficial, convenient and genuine data moreover by temporal domain for natural resource management and developmental planning. Forest conservancy and its impact on environment have gained importance in national and international program. Extreme changes on forest cover around the globe had recorded by fast jump up in population, varying in land use activities, forest fires, pressure on economic mineral deposits, reduced rain conditions and climate change. Forest degradation is a matter of grave concern and prime focus that immensely required for forest sustainable management through systematic planning. According to 1999 assessment of the Karnataka Forest Department, Molakalmuru taluk holds 21% spread of forest cover which includes open deciduous; dense/closed deciduous; forest plantations and scrub forest. The study focuses on timely designing and management of forest lands to satisfy future desires. Mapping of forest lands and its detection is explored using topographic maps of 1:50,000 scale; geo-rectified satellite data of IRS-LISS-III through GIS software. The ultimate output outlines the forest land exploitation using geospatial tools for its sustainability.

Keywords Geospatial technology · Forests · CDA · Molakalmuru

17.1 Introduction

Forest is one among the major resources that takes crucial role in sustaining the ecological equilibrium and environmental system continuously disappearing at an alarming rate (Roy et al. 2002). Forests are the large area dominated by medicinal plants, timber, construction purposes, agricultural implements, carts and accessories, firewood & charcoal, aromatic, oil yielding, fodder, dye, detergents and soap, resin

M. C. Manjunatha (✉)
Department of Civil Engineering, Maharaja Institute of Technology, Thandavapura, Mysuru 571302, Karnataka, India

H. T. Basavarajappa
Department of Studies in Earth Science, Centre for Advanced Studies in Precambrian Geology, University of Mysore, Mysuru 570006, Karnataka, India

R. B. Singh et al. (eds.), *Remote Sensing and Geographic Information Systems for Policy Decision Support*, Advances in Geographical and Environmental Sciences,
https://doi.org/10.1007/978-981-16-7731-1_17

and gum, flavoring agents, vegetables, cereals and millets, pulses, pickles, fruits, fiber, green manure, other commercial crops, sacred trees, basket making, mat weaving and roof thatching (FAO 2001). India would need 325 million tons of food grain to feed its projected population of 1.4 billion by 2025 (Roy 2009). Deforestation will increase region greenhouse emission and different trace gases; presumably influencing the climatic conditions, as a result of the absorption of carbon is higher in forest regions than within the agricultural lands (Fearnside 2000). Satellite-based mapping of vegetation cover is also a major demand for numerous planning and designing schemes at the topographic extent (Singh et al. 2002). Moreover, depicting the exact locations of vegetation varieties and human land activities carries valuable data for regular monitoring of terrains and sustains their multifariousness, human interruptions and varying environmental conditions (NLULC 2006; Tiwari and Singh 1984; Tiwari 1994).

The development, maintaining and management of forest assets require comprehensive understanding of the forests concerning their standard and location overtime, so as to achieve the balance between the implementation and restoration strategies (Kushwaha 2005). The extent of information depends greatly on the spatial and spectral resolution of the satellite imagery acquired. Four regular characteristic features derived from satellite Remote Sensing (RS) data are canopy shape, tree size categories, percent of crown and vegetation structure (Roy et al. 2002). Geospatial approach is a powerful tool with decision making will successfully uplift governance, empower sustainable development, serve in better business action plans to bring people for location-based information. Technology is employed comprehensively in India for forest identification, exploring groundwater zones, ocean productivity, environmental impact analysis, land and water sustainability and natural disaster monitoring (Geospatial Today 2013). Geospatial tools show tremendous approach in fast spatial and temporal monitoring of tropical forest resources as support system for decision makers (Rai 2013). Geospatial methods offer immense role in collection, analysis and storing all kinds of geospatial data particularly prerequisite for forest appraisal (Roy et al. 2002).

17.2 Location

The study area located in 14°34′–15°02′ Northing and 76°35′–76°52′ Easting measuring an area of 738.23 km^2 (Fig. 17.1) (Manjunatha and Basavarajappa 2015). Study area enjoys moderate climate throughout the year with temperature ranging from 20 to 31 °C (CGWB 2013). Most of the rain is recorded throughout SW monsoon of 541.5 mm in 28 rainy days. 90% of the population is depending on agricultural practices. The major crops grown are bajra, groundnut, horse gram, small millets and jowar (CGWB 2013). Molakalmuru is the heart for silk textiles having immense values. The net sown area of the taluk is only 43.81% due to low, erratic and undependable rainfall (CGWB 2013).

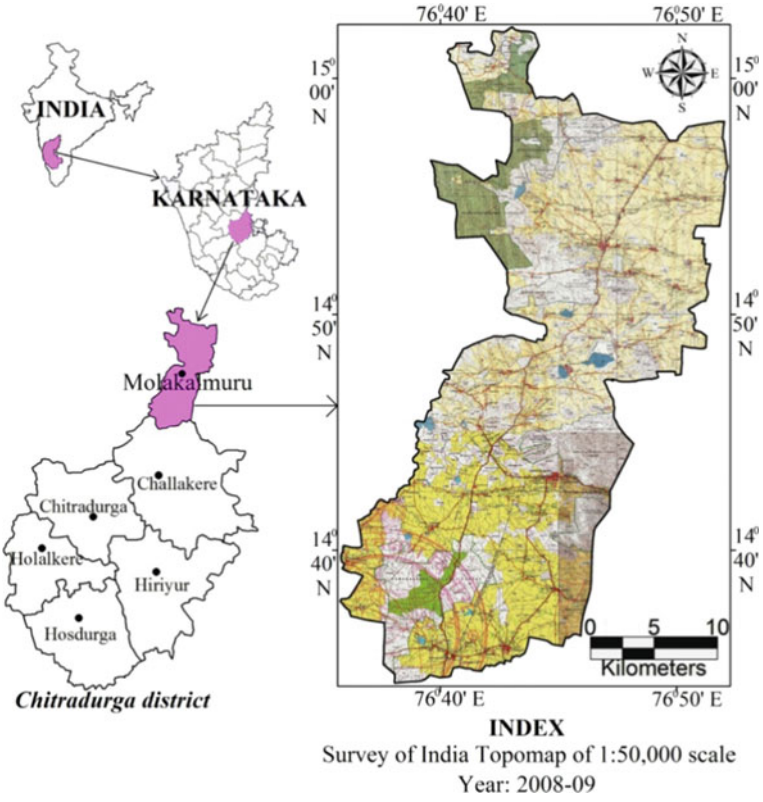

Fig. 17.1 Location and Topo map of Molakalmuru taluk

17.2.1 Physiography

The northern parts of Molakalmuru are considered predominantly as central hilly forest zone; whereas southern parts are considered as eastern Vedavathi plains (Babu 2013). Undulating topography, interspersed with patchy ranges, detached clusters and isolated low ranges of rocky hills, barren hills are noticed all along the northern parts (Manjunatha and Basavarajappa 2015; CGWB 2013). Molakalmuru chiefly consists of crystalline schists, granitic gneisses with younger granites and hardly older basic intrusive (Radhakrishna and Vaidyanathan 2011). Ample parts of soils are exposed and few places are noticed with thin cover of grasses (Babu 2013). These cover larger parts of forests in the study area with complete barrenness of various massive rocky hills of irreversible phases are recorded (Sathyan 1967). About 75% of the taluk covers granite hillocks and dying State Reserved Forests and the remaining 25% is partly dry land cultivated (CGWB 2013).

17.3 Database and Methodology

The study involved Indian Remote Sensing (IRS-1C/1D), PAN + LISS-III satellite data (Bands: 2, 3 and 4) to achieve the spatial and temporal changes of forest area. Satellite data are digital mosaic information of earth's land features which have immense value in forest study and monitoring (Rai 2013). Geospatial technology enables upgraded drawing and timely observing of forest resources for better results (Franklin 2001). Forest lands with its categories are digitized supported the quality schemes given by National Remote Sensing Agency (NRSA 2007; Manjunatha 2017). Limited field visits are carried out to map Ground Control Points (GCP) of each forest boundary using Garmin GPS of 3 m resolution that are later overlaid on SoI Topo map.

Satellite images are geo-rectified by adopting the permanent earth surface features of major roads, power-lines, settlements, co-ordinates and forest boundaries derived from SoI topo maps (Basavarajappa et al. 2016). Forest maps are first digitized by SoI topographic sheets during the year 1975–78 and 2008–09 (Manjunatha 2017) (Figs. 17.4 and 17.5). The contrast in the satellite data in the form of Size, Texture, Shape, Pattern, Association and Shadow is involved to measure types of forest cover using ArcGIS and Erdas Imagine software (Manjunatha et al. 2015). Supervised classification investigations are executed on multispectral and multi-temporal satellite data in GIS environment (Manjunatha and Basavarajappa 2015; Manjunatha 2017) (Fig. 17.2a).

17.3.1 Data Used

a. **Topo maps:** 57A/12; 57B/9, 10, 13, 14 during 1975–78 and 2009–10, Survey of India (SoI) of 1:50,000 scale, Bengaluru.

b. **Satellite Data used:** IRS-1C/1D; LISS-III of 23.5 m Resolution (D43E12, D43K09, 10, 13, 14) [Acquisition year: 2000–01] and Panchromatic data of 5.8 m resolution [Acquisition year: 2005–06] (Manjunatha 2017) (Fig. 20.2a), NRSC, Hyderabad.

c. **Software:** Erdas Imagine v2013 and Arc GIS v10 (Manjunatha 2017).

d. **Thematic maps:** Rivers and Tanks; Reserved Forest Cover and its Classification.

e. **GPS:** Exact forest boundaries are recorded during extensive field visits using Garmin-etrex 10 of 3m resolution (Manjunatha 2017).

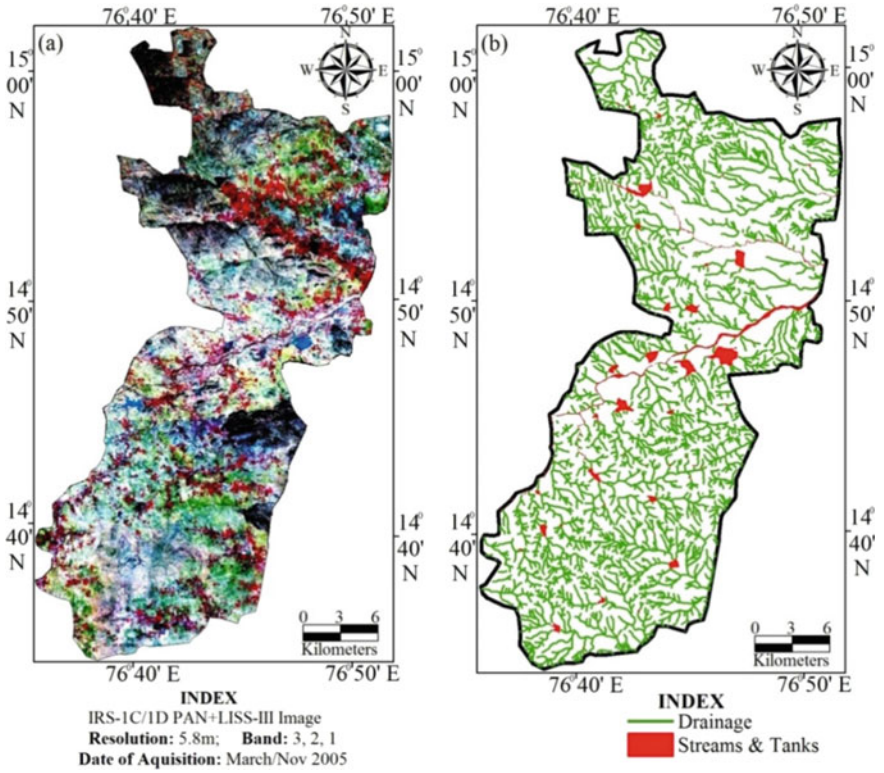

Fig. 17.2 **a** IRS-PAN + LISS-III image. **b** Drainage and tanks of Molakalmuru taluk

17.4 Rivers and Tanks

Janaga halla (Chinna Hagari) river and Gunderi halla stream drains major parts of Molakalmuru taluks receive the main drainage from the western portions offering irrigation facilities (Sathyan 1967) (Fig. 17.2b). Gangammana halla is a small stream which drains minor parts of north-eastern region (CGWB 2013). Flowing on the western region of the study taluk boundary, Gunderi halla then enters the heart of Ramapura village and takes a flip within the north-easterly direction, falling into the Vedavati stream within the orbit of the Bellary district (Sathyan 1967). Rangayyana Durga Dam offers irrigation facilities in western parts of Molakalmuru taluk (CGWB 2013). Gangammana halla stream flows toward south-west from its catchment area near Kelagina Kanive Village and yields water requirement of more than ten villages on the lower side which finally merges with Vedavathi river (Manjunatha et al. 2018). It is further stated that the availability of water at Gangammana halla can be assessed only during rainy season. Two important hill streams flow toward Northwestern direction in the taluk, flow into Janaga halla, a few miles on the far side of taluk boundary (Thakur 2016). Several other minor streams also find their way into the

Janaga halla. Several anicuts have been constructed all along the basin to impound water (Sathyan 1967). Granites, granitic-gneisses and amphibolite gneisses are the most water bearing formations within the study area (Ravikumar et al. 2014; CGWB 2013).

17.5 Mapping of Forest Cover

Visual Image Interpretation Technique (VIIT) been globally utilized for forest survey (Anonymous 1983) and monitoring satisfactorily by Remote Sensing (RS) data with high spatial resolution. Horizontal plantation measuring 7–8 m in width and pack of 3–4 trees are effectively recognizable (Roy et al. 2002). Acquiring the temporal data provides information regarding phenological conditions such as, deciduous or evergreen forests. The multispectral satellite data in digital form can be analyzed through computers using digital image processing software and categorized into different forest cover types (Roy et al. 2002).

Forests are mostly outlined as a plant community chiefly of trees and alternative woody vegetation cover with a tree cluster beyond 10 percent and area greater than 0.5 ha (FAO 2001; Singh et al. 2006). Forest lands are primarily consisting of dense vegetation cover, medicinal plants and variety of large vegetation types able to yield timber and forest materials (Saxena et al. 1993; Basavarajappa et al. 2014; Manjunatha 2017). In Molakalmuru taluk, reserved forest lands are dispersed as fragmented blocks and include both natural forests and man-made forests (plantations) (Kayet et al. 2019; CFD 2012). The study area includes 7 State Reserved Forest namely, Bandravi, Hire Adavi, Kamarakaval, Konasagara, Krishnarajapura, Sanjivarayana kote and Santegudda State forests (Fig. 17.3a) with an approximate area of 155.04 km^2 (1978) being reduced by numerous major and minor agents (Manjunatha 2017) (Figs. 17.4, 17.5, 17.6, Table 17.1).

17.6 Mapping of Forest Classification

Classification studies of LU/LC portray numerous perspectives of natural resources which keep changing due to its demand (Roy et al. 2002). Multiple land uses on a single land parcel with respect to standardize the LULC information are very much required to analyze land classification system. Forests are categorized into open deciduous; dense/closed deciduous; forest plantations and scrub forest supported by the crown cover/density/location and structure for two periods of time (Fig. 17.3b). The larger imagery scale or higher sensor resolution helps in differentiating forest types more accurately (Roy et al. 2002). Generally, supervised classification techniques using maximum likelihood algorithm are considered adequate (Roy et al. 2002). However, both supervised and unsupervised method i.e., hybrid technique

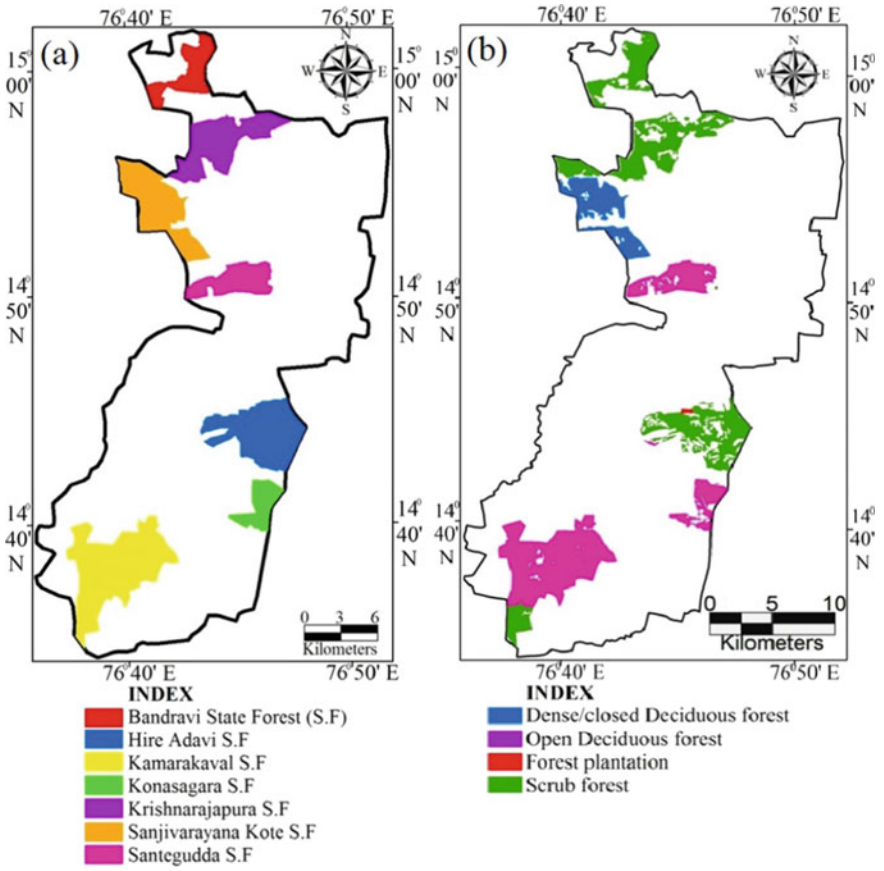

Fig. 17.3 **a** Reserved forest. **b** Forest classification map of Molakalmuru taluk

produces best outcome (Kushwaha and Madhavan Unni 1989). Satellite data acquisition of a particular time period in a year, once most variations occur by phenological changes such as date of emergence of flowers and leaves, leaf fall, species phase change etc. enhance the satellite image potentiality in delineating the forest types.

17.6.1 Deciduous Forest

Represented as the forest land that chiefly contains deciduous species and wherever the trees shed their leaves once in every year (Basavarajappa et al. 2014). Vegetation density, type, structure and its composition of forest lands along with deteriorating phases assist to explore the deciduous type under sustainable limits of precision (Pant et al. 1992). Multi-temporal data, particularly of October and March/April

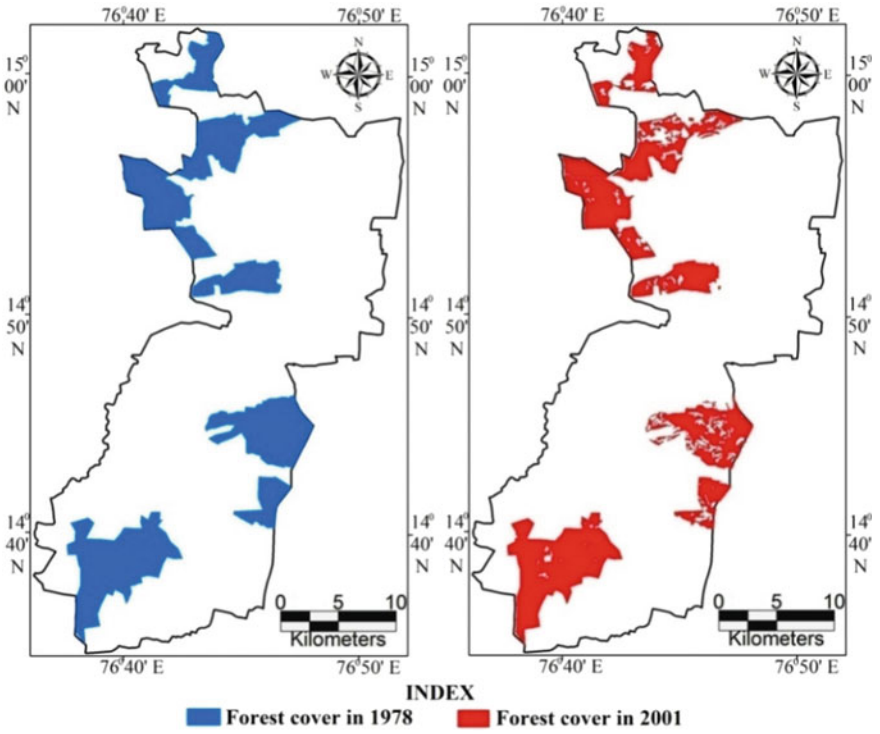

Fig. 17.4 Temporal mapping of forest covers during 1978 and 2001

seasons help in their discrimination from other forest types (Basavarajappa et al. 2014). It represents dark red to red tone, mainly rich in timber trees like teak wood, rose wood, honne, bamboo on Standard False Color Composite (FCC) (Fig. 17.3b). Dense/ closed deciduous forest are noticed all along the medium relief of hill slopes occupy the major parts of Sanjivarayana Kote State Forest (S.F), Vaderahalli, SW parts of Chinivaladagudda and Southern parts of Jalipente villages (CFD 2012). Open deciduous forests are noticed in Northern parts of Chikkanahalli, SW parts of Hire Adavi S.F, major parts in Konasagara S.F, Adavimallapura, SW parts of Nerlahalli, major parts of Kamarakaval S.F and Eastern parts of Harvinadoddi village.

17.6.2 Forest Plantation

These are forest areas artificially planted with trees economic importance of forest resources (Basavarajappa et al. 2014). The common indigenous and exotic trees of forest plantations are teak, sal, deodar and others (Manjunatha et al. 2018). Full grown plantations are normally difficult to differentiate from natural forests; however, new

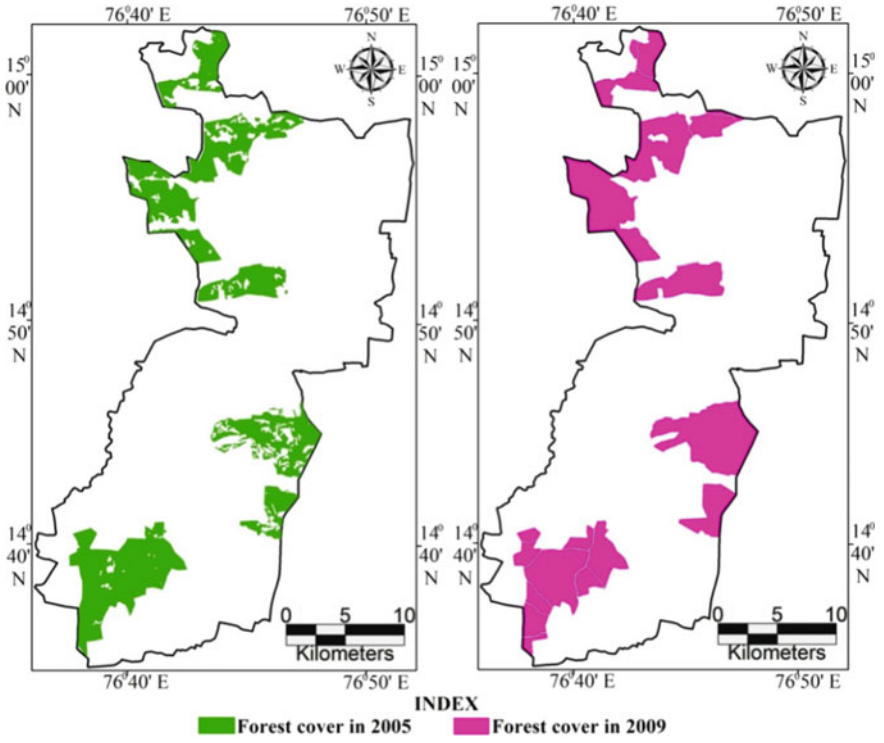

Fig. 17.5 Temporal mapping of forest covers during 2005–2009

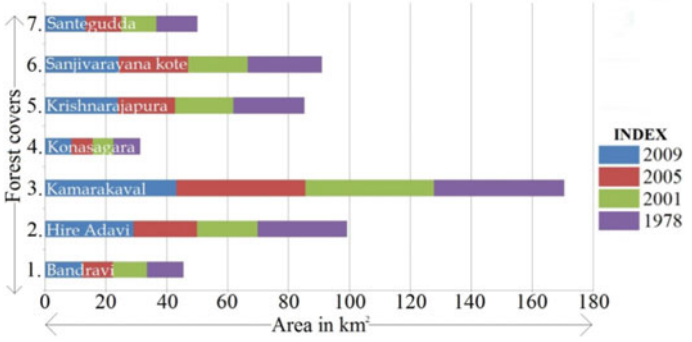

Fig. 17.6 Bar chart representing the temporal mapping of forest covers

and young plantations can be readily separated from the contiguous forested areas (Basavarajappa and Dinakar 2005). It depicts light red to red tone on Standard False Color Composite (Dinakar 2005) (Fig. 17.3b). A huge mass of forest plantations

Table 17.1 Temporal mapping of forest covers in Molakalmuru taluk

Sl. no	Name of the forest	Area in km^2 (1978)	Area in km^2 (2001)	Area in km^2 (2005)	Area in km^2 (2009)
1	Bandravi S.F	12.1229	10.1699	11.1589	12.1644
2	Hire Adavi S.F	29.0800	20.9275	19.8554	29.2613
3	Kamarakaval S.F	43.2716	42.2774	42.1890	42.6838
4	Konasagara S.F	8.7105	7.0458	6.7978	8.7816
5	Krishnarajapura S.F	24.0071	18.7014	19.2166	23.3181
6	Sanjivarayana kote S.F	24.2959	22.6714	19.5859	24.4314
7	Santegudda S.F	13.5518	11.6456	11.3378	13.5756
	Total	155.0400	133.4390	130.1414	154.2162

was noticed on foot hills of almost all the major forest cover with elevations in the northern parts of Hire Adavi S.F.

17.6.3 Scrub Forest

Scrub forest is associated with barren rocky/stony waste and scrub formed due to inadequate and erratic rainfall (Basavarajappa et al. 2014). The condition is drought and extreme heat in summer season precludes hardly any profitable forest (Manjunatha and Basavarajappa 2017). On Standard False Color Composite, it represents light red tone to brown tone relying on canopy shelter (Dinakar 2005) (Fig. 17.3b). These were encountered in major parts of Bandravi S.F; Krishnarajapura S.F and Hire Adavi S.F, Southern parts of Kamarakaval S.F, Northern parts of Sanjivarayana Kote S.F and few patches in Eastern parts of Santegudda S.F.

17.7 Change Detection Analysis (CDA)

Forest covers an area of 155.04 km^2 in 1975–78 has been degraded to 133.43 km^2 (2001) because of human encroachment at all forest border limits by agricultural overlap (Manjunatha 2017), grazing animals, illegal cut of trees and illegal quarrying activities (Manjunatha et al. 2018) (Fig. 17.4). Approximately 21 km^2 of the forest land been reduced from 1975 to 2001 observed by Change Detection Analysis (CDA) (Manjunatha 2017) (Fig. 17.7; Table17.2). Illegal granitic-gneiss quarries are observed along the northern parts of Bandravi S.F, Krishnarajapura S.F and NE parts of Kamarakaval S.F. Gradual increase in population increased the agricultural activities noticed all along the State Forest boundaries of Bandravi, Hire

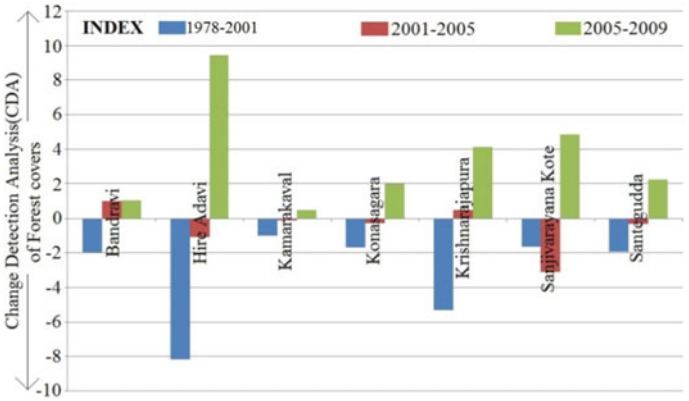

Fig. 17.7 Column graph showing Change Detection Analysis (CDA) of forest lands (Manjunatha 2017)

Table 17.2 Change Detection Analysis (CDA) of forest covers in Molakalmuru taluk

Sl. no	Forest covers	1978–2001	2001–2005	2005–2009
1	Bandravi S.F	−1.9530	+0.9890	+1.0055
2	Hire Adavai S.F	−8.1525	−1.0721	+9.4059
3	Kamarakaval S.F	−0.9942	−0.0884	+0.4948
4	Konasagara S.F	−1.6647	−0.2480	+1.9838
5	Krishnarajapura S.F	−5.3057	+0.5152	+4.1015
6	Sanjivarayana kote S.F	−1.6245	−3.0855	+4.8455
7	Santegudda S.F	−1.9062	−0.3078	+2.2378

Adavi, Konasagara, Krishnarajapura and Santegudda (Manjunatha and Basavarajappa 2017). Metalled and Unmetalled roads are identified to be passing through Bandravi S.F, Krishnarajapura S.F, Santegudda S.F, Hire Adavi S.F, Kamarakaval S.F; while only unmetalled roads are observed in Sanjivarayana Kote S.F and Konasagara S.F which later may lead into more illegal granite/gneiss quarrying activities, illegal cut of trees, agricultural sprawl, grazing domestic animals and other impacts (Manjunatha et al. 2018).

17.8 Results and Discussion

Approximately 21 km^2 area of forest been reduced in 2001 when correlated with the data of 1975 (Manjunatha 2017). The entire forest land in the study area measures about 155.04 km^2 in 1975–78 has been degraded to 133.43 km^2 (2000–01) due to human intrusions through agricultural sprawl, over-grazing, deteriorate pasturelands

on steep slopes, unsuccessfully monitored forest lands, illicit cutting of trees, illegal mining activities and its waste dumping (Manjunatha et al. 2018). The taluk is one of the most backward taluks facing lack of basic infrastructure, unemployment, poverty, lack of skills, illiteracy, health care centers (Nagesha and Ajeya 2018). The Forests of Molakalmuru vary from dry mixed deciduous type occur in patches in certain blocks with primarily scrub forests tending to thorny bushes in the driest localities (Babu 2013).

The taluk holds 98.28 hectares of permanent pastures and other grazing lands within the notified State Forest cover (CGWB 2013). These pastures may face scarcity of fodder for the domestic animals which need feeding during extreme summer conditions. Deforestation was noticed recently due to the intensity of over-grazing, forest fires and other anthropogenic factors (Manjunatha and Basavarajappa 2017). A variety of assorted massive rocky hills of irreversible phases are observed in Hire Adavi S. F covering large portion of forest barrenness (Babu 2013). Extreme edaphic condition is one of the types of degraded forests occurs in poor and shallow soil associated with vast area of bare and rocky localities (Babu 2013). Illicit cutting of trees was commonly observed by the vicinity of village peoples to fulfill their needs of fuel, small timbers for huts and houses and agricultural implementations (CFD 2012). Over-grazing are observed by the large population of cattle, goat and sheep especially in Hire Advai forest premises which affecting the natural regeneration status causing deterioration of wild life habitat (CFD 2012). Geospatial approach by forest authorities has regularly increased, encouraged in vast part which suits the information require for forest regeneration practices (Wulder and Franklin 2003).

17.9 Reclamation Strategies

In India, forest covers an area of 21.54% (ISFR 2017) but the total expected is 33% as per India's forest policy (Geospatial Today 2013). Forest Survey of India (FSI) has taken up various implemental strategies to reclaim reserved forest cover in many states of the Country (Geospatial Today 2013). Karnataka Forest Department Authority came up with many regeneration programs along with local village peoples to retain the forest resources during recent years (Manjunatha and Basavarajappa 2017). Rotational grazing, controlling fire hazards combined with rigid protection avoiding soil erosion and enriching moisture regime were practiced periodically by the Forest Department Authorities (CFD 2012), but still it needs more regeneration programs to reclaim natural forest resources in the study area. Illegal mining lands were demarcated and maintained to enlarge the forest covers in the study area. Artificial mode of sowing seeds in the bushes also helps in regeneration (CFD 2012). Plantations in large areal extent of encroachments of agricultural activities, grazing lands and mining area should be implemented.

17.10 Conclusion

SoI topomap and IRS LISS-III Satellite images are effectively utilized to bring out temporal changes of Forest covers through GIS software. More than 24 km^2 area of forest cover has been restored and reclaimed through periodic implementation programs by Forest Authorities (2008–09). An accurate mapping of forest cover and its classification analyses are the meaningful data for natural resources sustainability. Geospatial technologies come in handy for effective management and add immense value to planning and development analysis for forest regeneration and act as support system to achieve sustainable goals.

Acknowledgements The authors are indepthly acknowledged to Prof. Krishne Gowda Y.T, Principal, Maharaja Institute of Technology Thandavapura, Mysuru; Prof. P. Madesh, Chairman, DoS in Earth Science, CAS, University of Mysore, Mysore; CGWB, SoI, Bengaluru; ISRO-NRSC, Hyderabad; and UGC-MRP No.42-73(SR)/2012-13, dt:12.03.2012, New Delhi for financial support.

References

Anonymous (1983) Nationwide mapping of forest and non-forest areas using Landsat false color composite for the period 1972–75 and 1980–82, Technical report, National remote sensing agency (NRSA), vol 1, pp 1–36

Babu G (2013) A note of the floristic diversity and ethno-botany of Chitradurga district, Foundation of Revitalization of Local Health Traditions, Centre of Excellence of Union Ministry of Environment and Forests, Bangalore

Basavarajappa HT, Dinakar S (2005) Land use/ land cover studies around Kollegal, Chamarajanagar district using remote sensing and GIS techniques. J Indian Mineral 1:89–94

Basavarajappa HT, Dinakar S, Manjunatha MC (2014). Analysis of land use/ land cover classification around Mysuru and Chamarajanagara district, Karnataka, India using IRS-1D, PAN+LISSIII Satellite data. Int J Civil Eng Technol (IJCIET) 5(11):79–96

Basavarajappa HT, Manjunatha MC, Maruthi NE (2016) Land use/land cover change detection analysis in Hosadurga taluk of Chitradurga district, Karnataka, India using Geo-informatics technique. J Int Acad Res Multidiscip (IJARM) 4(2):304–314

CFD (2012) Working plan Chitradurga forest division, PWPR-II, Govt. of Karnataka, Bengaluru, pp 1–439

CGWB (2013). Central Ground Water Board, Govt. of India, Ministry of Water Resources, Groundwater Information Booklet, pp 1–31

Dinakar S (2005) Geological, geomorphology and land use/land cover studies using remote Sensing and GIS around Kollegal Shear Zone, South India, Unpub thesis, University of Mysore, pp 1–191

FAO (2001) Global forest resources assessment 2000. Italy, Rome

Fearnside PM (2000) Global warming and tropical land-use change: greenhouse gas emissions from biomass burning, decomposition and soils in forest conversion, shifting cultivation and secondary vegetation. Clim Change J 46:115–158

Franklin SE (2001) Remote sensing for sustainable forest management. CRC Press, Boca Raton, Florida

Geospatial Today (2013) Empowering India through Geospatial Technologies, Federation of Indian Chambers of Commerce & Industry and Gateway Media Pvt Ltd, Hyderabad, pp 1–224

ISFR (2017) India state of forest report, http://fsi.nic.in/isfr2017/isfr-forest-cover-2017.pdf, pp 1–36
Kayet N, Pathak K, Chakrabarty A, Singh CP, Chowdary VM (2019) Forest health assessment for geo-environmental planning and management in hilltop mining areas using Hyperion and Landsat data. Environ Sci Pollut Res. https://doi.org/10.1007/s11356-020-09795-w
Kushwaha SPS (2005) Geospatial technology for forest resources management. Int J Ecol Environ Sci, International Scientific Publications, New Delhi, 31(1):9–20
Kushwaha SPS, Madhavan Unni NV (1989) Hybrid interpretation for tropical forest classification. Asian-Pacific Remote Sens J 1(2):69–75
Manjunatha MC (2017) Applications of hyperspectral remote sensing and GIS on NE-SW transects of Chitradurga District, Karnataka, India, Unpub thesis, University of Mysore, pp 1–204
Manjunatha MC, Basavarajappa HT (2015) Spatial data integration of lithology, geomorphology and its impact on Groundwater prospect zones in Precambrian terrain of Chitradurga district, Karnataka, India using geomatics application. Global J Eng Sci Res Manage 2(8):16–22
Manjunatha MC, Basavarajappa HT (2017) Anthropogenic pressure on forest cover and its change detection analysis using geo-informatics in Holalkere taluk of Chitradurga district, Karnataka, India. Int J Sci Res Sci Technol (IJSRST) 3(1):71–76
Manjunatha MC, Basavarajappa HT, Jeevan L (2015). Geomatics analysis on land use land cover classification system in Precambrian terrain of Chitradurga district, Karnataka, India. Int J Civil Eng Technol (IJCIET) 6(2):46–60
Manjunatha MC, Maruthi NE, Siddaraju MS, Basavarajappa HT (2018) Temporal mapping of forest resources in Hosadurga taluk of Karnataka State, India using geo-informatics. J Emerg Technol Innov Res (JETIR) 5(11):124–132
Nagesha B, Ajeya G (2018) Role of self help groups in rural development—a study. Int J Trend Sci Res Dev (IJTSRD) 2(4):1454–1459
NLULC (2006) National land use and land cover mapping using multi-temporal AWiFS data, Natural Resources Census, Project Report 2004–05, NRSA/LULC/1:250K/2006-2
NRSA (1995). Integrated mission for sustainable development, technical guidelines, National remote sensing agency, Department of Space, Govt. of India, Hyderabad
NRSA (2007) National remote sensing agency, Manual of Nationwide land use/land cover mapping using satellite imagery, part-1, Balanagar, Hyderabad
Pant DN, Das KK, Parth Sarathi Roy (1992) Mapping of tropical dry deciduous forest and landuse in part of Vindhyan range using satellite remote sensing. J Indian Soc Remote Sens 20(1):9–20
Radhakrishna BP, Vaidyanathan R (2011) Geology of Karnataka. Geological Society of India, Bengaluru
Rai PK (2013) Forest and land use mapping using remote sensing and geographical information system: a case study on model system. Environ Skeptics Critic 2(3):97–107
Ravikumar P, Deljo Davis, Sharika Mathew, Somashekar RK, Prakash KL (2014). Spatio-temporal variation in radon concentration in groundwater with respect to rock types: a case study from Chitradurga District, Karnataka. J Geol Soc India 83:156–164
Roy PS (2009) Natural resource management and geo-information science. In: 10th ESRI India user conference, geography in action, pp 1–13
Roy PS, Dutt CBS, Joshi PK (2002) Tropical forest resource assessment and monitoring. Trop Ecol 43(1):21–37
Sathyan BN (1967) Chitradurga district, Mysore State Gazetteer, pp 1–26
Saxena KG, Rao KS, Purohit AN (1993) Sustainable forestry-prospects in India. J Sustain Forestry 1:69–95
Singh TP, Singh S, Roy PS (2002) Vegetation mapping and characterization in West Siang District of Arunachal Pradesh, India—a satellite remote sensing-based approach. Curr Sci 83(25):1221–1230
Singh IJ, Mizanurahaman M, Kushwaha SPS (2006) Assessment of effect of settlements on growing stock in Thano range of Dehradun forest division using RS & GIS. J Indian Soc Remote Sens 34(2):209–217

Thakur H (2016) Chandravalli—an early historic settlement in Karnataka, India. Anc Hist Archeol 3(3):49–54

Tiwari AK, Singh JS (1984) Mapping forest biomass in India through aerial photographs and nondestructive field sampling. Appl Geogr 4(2):151–165

Tiwari AK (1994) Mapping forest biomass through digital processing of IRS-IA data. Int J Remote Sens 15(9):1849–1866

Wulder M, Franklin S (eds) (2003) Remote sensing of forest environments: concepts and case studies. Kluwer Academic Publishers, Dordrecht, Boston, London

Chapter 18
Application of GIS Technology in Detection of Crime Hot Spots and Vulnerable Areas of Jalandhar Commissionerate

Harcharan Singh and Vinay Maitri

Abstract The huge number of crimes in knowable areas was noted in many records in Jalandhar Police Commissionerate. These crime hot spots are first in rating examples of the possible unused quality value of place in the observations of crime. Crimes are increasing in day to day life in the major cities as compare to the satellite towns and regional areas. It can also relate that the cities areas with working class population are relatively higher crimes than where the people from HIG (high income group) and LIG (lower income groups) live together with high economic disparities. Mainly this thing is related to the different types of people or nature of people in specific areas, class of people, type of city or area in the city, distance of basic services from the specific location, distribution of spaces etc. Mainly there is a strong relation in between the different types of crimes and locations (Specific locations), type of development (around the particular location) also plays a vital role in increasing the chances of major crime happenings at particular location. One major important thing is that there is a relation of crime hot spot areas with their surrounding physical built up and existing environment, which make easy for the offenders or criminals to do crimes and escape easily from the locations after committed the criminal activities. There are some crime studies that look at the spatial distribution of crime with its relationship between physical built up and surrounding environment, which clearly focus on certain land uses and hot spots that are directly connected with the occurrence of different types of crimes. This study in Police Commissionerate Jalandhar is based on three major questions, how to identify and mark the crime hot spots, what are the tool and technique required to assess the status of crime in the city, the type of physical built up has any significance on crime occurrences and future status of crimes in the city. It highlights the vulnerable areas (crime hot spots) in Jalandhar Commissionerate having high number of crimes and its causes for their occurrence and its final outcomes/recommendations through which it can be prevent from repetitions in coming future. The study focuses on the identification of crime

H. Singh (✉)
Alumni, GRD School of Planning, GNDU, Amritsar 143005, Punjab, India

V. Maitri
Department of Transport Planning, School of Planning & Architecture, New Delhi 110002, India

R. B. Singh et al. (eds.), *Remote Sensing and Geographic Information Systems for Policy Decision Support*, Advances in Geographical and Environmental Sciences,
https://doi.org/10.1007/978-981-16-7731-1_18

hot spots with relation to the snatching points and vulnerable areas under different police stations of Jalandhar Police Commissionerate.

Keywords GIS Technology · Crime hot spot analysis and spatial data analysis · Buffer analysis · Crime mapping

18.1 Introduction

A crime hot spot is a specific location or particular part within a (knowable) known area, with a high number of recorded Criminal events. Cities crimes and physical built-up environment are correlated to each other, by which the physical planners or geospatial city planners are able to understand the causative factor and can control the rate of crime by using the planning tools and techniques (technology). The GIS-based mapping along with identified crime hot spots offers to crime analysts, the graphic representations of crime-related issues, which help them to consider that where and why the crimes were occurred and identify the root causes of their chances of future happening and how it can improve the attempts of the police force to tackle the possible crimes and it mainly gives the basic information about the crime affected areas or sensitive areas. Mapping of crime hot spot along with its proper geospatial locations helps the city police to enhance their modes and methods of protecting citizens in more effective and efficient manner. Simply these maps display the crime related information spatially regarding where the crimes can possibly occur. It will help in the planning and policing mechanism such as: giving directions about proper police patrolling, quick action, better knowledge of paths, possible movement pattern of criminals in the Crime sensitive areas. The policy makers in police departments of Jalandhar Commissionerate can use these maps to observe basic trends in criminal activity in different areas and help them to make policies regarding controlling and solving the possible activities of the criminals in crime sensitive areas. For better understanding.

Suppose that the boundaries are network units of a fixed size and start. There is a rule for hot spot place start at any network unit might be the coming here-after: If the unit were not a hot spot place in the earlier time stretch of time but the number of crimes of a pointed out printing letters now goes over limits a given details of edge, limit value, then the unit becomes a hot spots during the current stretch of time.

Hot spots are, by definition, small in part using seeing check-out of pin maps and edge, limit counts for hard and soft crimes, Sherman and Weisburd (1995) taken to be hot spot in Minneapolis Minnesota, of no more than one having an effect equal to the input solid mass of a street a part in which a police officer can easily see and be seen.

Geographic Information System (GIS) uses geography and computer-generated mapping as a connection technique that merges different data all together and prepares information of great mass, size, amounts of location-based news in understandable format. GIS-generated maps and information helps police personnel to take

necessary decisions effectively for mitigation or preventive measures carefully by right coming first. It will observe based on historical events, and predict the possible future crime status and their possible locations. GIS can also be used to know the possible upcoming major threats, and helps to the responders to take the position for making strategy for tackling, sending troops or whilst en route to a small event to help in moving army, ships, in fighting system and in defence mechanisms. GIS helps make out possible unused quality suspects to increase persons making observations person likely of wrongdoing base when no leads are clear (Johnson 2000). GIS technology basically helps to find out the geospatial facts based on the repetition of crimes on particular points or locations in the city. It enables the users to level the facts and view the facts fullest of danger to the one example question under discussion or special work. It is used earth over by police division of an organization, both greatly sized and small, to make ready mapping answers for crime observations. The present work space is a base level reasoning scaled-copy for the putting into effect of GIS in the Indian policing. This work space also out-lines things in the way, chances and current steps on the point to the application of GIS technology and tries to make some carefully worked designs for its putting into effect in Indian police divisions of an organization. GIS software helps to co-ordinate the pointed location-based facts from number times other starting points. GIS mapping helps the police department to understand the situation of any crime into their ambit with efficient way.

18.2 Aim and Objective

The main aim of study is to identify the crime hot spots in the Jalandhar Commissionerate area for better policing strategies. The major objectives are to map the crime hot spot areas in the Police Commissionerate Jalandhar and to suggest the outcome methods in reference to the physical environment of that location to prevent those areas from turning out crime hot spots in coming future.

18.2.1 Limitations

The boundary of Commissionerate created combining 14 police stations located in the area using GIS tools, Google earth imagery and Primary surveys/interviews data and observations by the author. The limitations of time, unavailability of some data/information and observation/ finding of Interviews lead author to create these figures in the research paper (refer all tables and figures) for the study purpose. This map is created purely for the study purpose only and does not have any legal authentication by any government body.

18.3 Study Area

Jalandhar Commissionerate System came into existence in Jalandhar city (in Jalandhar District, Punjab in India) on 15th Feb 2010. Jalandhar is situated in the centre of Punjab as shown in Fig. 18.1 Administratively Jalandhar Police Commissionerate is divided into 14 conventional police stations and 2 special Police stations i.e., women police station and NRI police station. There are five sub-divisions and two zones (city 1 and city 2). There are mainly 7 police stations in each zone, so the 2 zones mainly consist of $7 + 7 = 14$ Police stations.

18.3.1 Crime Hot Spots

The Crime hot spots are mainly based on the relation of place and time of the Crime with its spatial references, with special attention on the areas those facilitates or supports the criminals for doing crimes, also their behaviour. In the big cities like as Jalandhar, the crime hot spots are mainly like as tourists spots, Innocent public/crowded areas like as Market etc., Religious places, Political leaders, Security forces, Religious Gathering, Vital Installation like as airport, railway station and bus stand, Government property and Historical buildings, and in some of the special urban forms in the city. This sort of knowledge can be very helpful in making the several kind of spatial models and analysis that are taking over for hot spots points

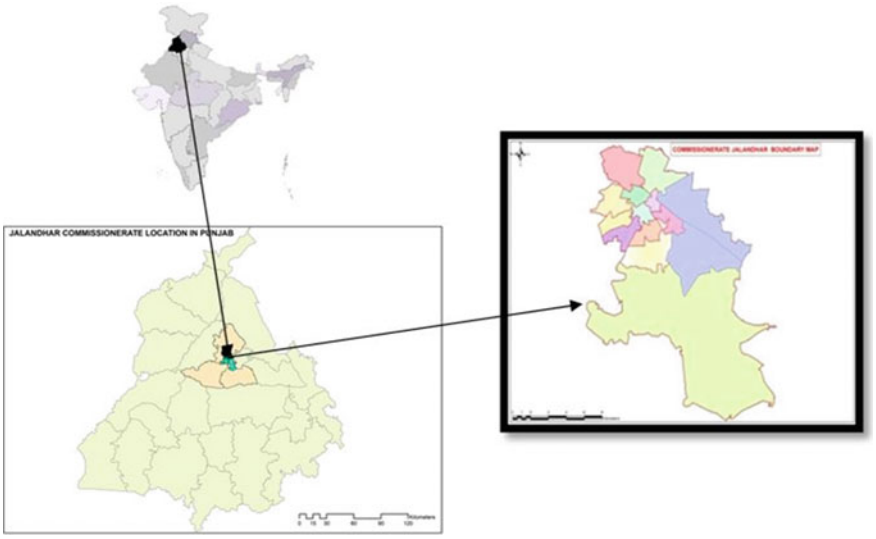

Fig. 18.1 Location of Jalandhar Police Commissionerate in Punjab (in India) (*Source* Map is prepared by Author)

with buffer ring (round circles) marks. There are some major two techniques of analysis of these Crime hot spots are as following.

18.3.2 Expressive Analysis

This type of analysis based on the geospatial data of the hot spots at different locations in the city. This data should imbricate an in-harmony rule wiring for putting in order stock-still areas into non-hot spots and hot spots at variegated stages of development. Then observers will have a largest wiring for noting random stochastic events, such as regression to the middle, half way between, from ordered hardening of soft-crime hot spots to increasingly serious crimes.

18.3.3 Analysis Based on the Point Patterns

In this method the crime hot spots are to be shown by using the points on these hot spots with different sizes or shapes (like as round shape, square shape etc.). In this the points are to be placed on the location of the crime hot spot and the size of the point determine the level of that particular hot spot (level of place is determined with the N number of crimes occurred on that particular point/location). The shape of the points is very helpful to determine different types or category of crimes occurred on that particular location and point like as crime related to property, crime related to human being etc.

18.3.4 Technical Security Arrangements Already Followed by the Punjab Police Department for Reducing the Crime in Sensitive Areas

There are different types of technical security arrangements, which are mainly followed by the Punjab Police Department for controlling the criminal activities and reducing the chances of escaping the offenders after committed the crimes like as installation of CCTV cameras on sensitive areas or places along with 24 $\times$ 7 h monitoring team on these cameras, demarcation of vulnerable Points in the city and alert the PCR /Police Mobile team (On two wheelers and four wheelers) for patrolling in the pre-demarcated, selected or allotted areas, formation of Intelligence team in Punjab Police for gathering the information of crime affected areas or for pre crime research at internal level of selected areas, provide regular training to the armed forces in Punjab Police with disaster management techniques and regular upgrading

the mobile applications for better interaction in between public and police like as Know your Police App, Sanjh etc.

18.3.5 Criminals and Offenders Use to Do Several Activities to Make a Place as Vulnerable Place or Crime Hot Spot

Criminals and offenders are mainly use to do different activities for make the specific locations as crime hot spot locations and vulnerable areas like as creation and spreading Nuisance, Rumours and Dis-content any particular place, loitering around important/prohibited areas and installations, taking Photographs/videography of different locations or places, infiltration into institutions/organizations of national importance and alluring/Enticing/Blackmailing innocent individuals for their own ends. Mainly the offenders or criminals use to do criminal activities on vacant lands, open spaces, dark streets during the night and near the pubs, bars and night clubs.

18.3.6 Data Used

The study mainly relied on data obtained from the crime records (FIR) of Jalandhar Commissionerate police station. Data pertaining to the property offence were taken main vulnerable points and main Snatching Points from Feb. 2010 to 2017 only, where the same crime (Snatching) is occurred with multiple times from last from 6–7 years. The incident data are classified as Chain Snatching, Mobile Snatching and other Snatching activities with their detail information as incident location address, time of occurrence.

The map of Jalandhar Police Commissionerate is prepared by using Google earth (Satellite view) map, know your Police mobile application and primary survey on the ground conducted by the author with team on the basis of updated list of the areas in each Police station of Police Commissionerate Jalandhar.

18.4 Methodology

The study is divided in three phases; first phase is collection of required data. The study of crime hot spots in Jalandhar Commissionerate Police Stations Limit includes the collection of specific data from secondary sources like as http://jalandharpolice.gov.in/website concerning the requirements of materials. The availability of crime records from Jalandhar Commissionerate Police station is very much helpful; also the

socio-economic profile of Jalandhar Commissionerate area from concerned offices is important for the completion of the study.

Second phase includes the analysis of various data, issues and finding the problematic areas with reference to vulnerable areas or points in case of snatching crimes from data compilation. The conversion of information into geospatial or georeferenced point of view i.e. indicating the crime incidents on map with the proper geospatial techniques by GIS tools, the preparation of maps for proper understanding of crime incidents in the study area. The existing data of Jalandhar Commissionerate area from concerning office are important; as it indicates the various factors that trigger the rising of crimes in the area past from 2010 up to 2017.

Third phase includes the identification of causative factors drawn from the existing status, findings and the conclusion. The prepared map with multiple buffer technique helps in visualizing the places or crime hot spots with different buffer zones. Information gathered from the number of crime incidents with GIS technology and mapping to analyse the Snatching point's data on ground by using buffer technique at various different distances, in which (Snatching points and Vulnerable Points in the city) are well arranged in the attribute table of shape file with the help of GIS software like as Tables 18.1 and 18.2.

These maps help to understand the crime pattern in the area, and also describe about the major root causes of this type of crimes in reference to the physical built up and land uses. This mapping representation gives a visualization in the form of pictures, that will help in viewing, knowledge of where and why crimes take place and can get well the attempts to fight against crime and can help police keep safe (out of danger) to the citizens more effective manner. Through GIS-based analysis and -generated 'visual representation made the photographic memory more active to understand and remember the characteristics of area, like some special type of crimes records i.e. snatching related crimes, physical built up of the area and surrounding network (Fig. 18.2).

18.4.1 Inter Relationship Between Existing Land Use and Snatching Crime in Jalandhar Commissionerate

Jalandhar Commissionerate's continuous growth in population outcomes in the many social illnesses (bigger crime rates). The offenders mainly try to allocate the time to select the specific and suitable location where they can commit crimes with less risk factor in the shortest time. The offenders mainly try to allocate the time to select the specific and suitable location where they can commit crimes with less risk factor in the shortest time. Land use pattern planning of the particular fields plays a crucial role in the quality and effectiveness of the extensive plan of the town and also has effectiveness in controlling or reducing crime in the town of Jalandhar. There are many variables that are listed as growth issues in towns, as Jalandhar City in Punjab faces problems in developing nations, such as rising unemployment

Table 18.1 Snatching points under along different land use in Jalandhar Commissionerate

Sr. no	Places	Land use
1	Ambedkar Nagar	Residential land use
2	Dilbagh Nagar	Residential land use
3	Shastri Nagar Market Harbans Nagar	Commercial land use
4	Tilak Nagar and Deol Nagar	Institutional land use
5	Lakshmi Narayan Mandir, Model House, Bhargo Camp	Mixed land use
6	Tower Enclave Phase 1, Bhargo Camp	Residential land use
7	Model House, Bhargo Camp	Mixed land use
8	Model House Main Market	Mixed land use
9	HP Petrol Pump, Near Nari Niketan, Bhargo Camp	Mixed land use
10	Adda Bhargo Camp	Mixed land use
11	Nari Niketan Road, Bhargo Camp	Residential land use
12	Sahibzada Ajit Singh Nagar, Jalandhar City	Mixed land use
13	Mata Rani Chowk, Model Town	Mixed land use
14	Near Guru Ravidass Chowk, Jalandhar City	Commercial land use
15	Near Kartar Nagar Chowk, Jalandhar City	Mixed land use
16	Near Atta Chakki, Model House, Jalandhar City	Mixed land use
17	Tara Wali Gali, Model House, Jalandhar City	Residential land use
18	Near RK Dhaba, Bhargo Camp	Commercial land use
19	Kwality Food, Kapurthala Road	Commercial land use
20	Sham Nagar Road, Jalandhar City	Commercial land use
21	Near Balbir Hospital, Jalandhar City	Commercial land use
22	Near DAV Flyover, Jalandhar City	Institutional land use
23	Vikas Puri Mohalla, Jalandhar City	Residential land use
24	Khingra Gate, Jalandhar City	Commercial land use
25	Near Tanda Railway Crossings, Jalandhar City	Commercial land use
26	Near Janta Hospital Road	Commercial land use
27	Dhan Mohalla, Jalandhar City	Residential land use
28	Near Ravidass School, Kishanpura	Mixed land use
29	Damoria Pull, Near Jalandhar City Railway Station	Mixed land use
30	KMV College	Institutional land use
31	Sweet Shop, Vikas Puri, Jalandhar City	Commercial land use
32	Tanda Railway Crossing	Commercial land use
33	Ganesh Nagar, Dakoha	Residential land use
34	Mohalla Jagatpura	Residential land use
35	Ali Mohalla	Residential land use
36	Rainak Bazar, Jyoti Chowk	Commercial land use

(continued)

Table 18.1 (continued)

Sr. no	Places	Land use
37	Urban Estate Phase 1 and 2	Residential land use
38	Near PNB Chowk	Commercial land use
39	Avtar Nagar, Jalandhar City	Residential land use
40	Government School, Rehmanpur	Institutional land use
41	Deep Nagar Market	Commercial land use
42	Rama Mandi Market	Commercial land use
43	Ranjit Enclave, Deep Nagar, Jalandhar	Residential land use
44	Khusropur	Residential land use
45	Bhullar Colony, Dakoha	Residential land use
46	Opposite Petrol Pump, Guru Gobind Singh Avenue, Jalandhar	Mixed land use
47	Fauji Wali Gali, Rama Mandi	Residential land use
48	Ladhewali	Residential land use
49	Near AksharDham Mandir, Surya Enclave	Mixed land use
50	Old Jawahar Nagar	Mixed land use
51	BMC Chowk	Commercial land use
52	BMC Chowk to Shastri Market Road	Commercial land use
53	Vijay Nagar, Jalandhar	Residential land use
54	DAV Flyover	Institutional land use
55	Near Guru Gobind Singh Stadium	Recreational ground
56	Mohalla Maan Singh Nagar	Residential land use
57	Near Prithvi Planet	Commercial land use
58	GTB Nagar	Mixed land use
59	Ujala Nagar, Basti Sheikh	Residential land use
60	Basti Danishmandan	Residential land use
61	Green Model Town	Residential land use
62	Opposite Vishal Tool Factory, Basti Danishmandan	Mixed land use
63	Mayor World School, Jalandhar	Institutional land use
64	Dushehra Ground, Jalandhar Cantt	Open space
65	Civil Hospital	PSP land use
66	Harman Timber Store, Reru Pind	Mixed land use
67	Global Hospital, Jalandhar	Mixed land use
68	Majit Singh Nagar	Mixed land use
69	Masand Chowk	Residential land use
70	V-Mart, Nakodar Chowk	Commercial land use
71	Baba Deep Singh Nagar	Residential land use
72	Doaba Chowk to Preet Nagar Chowk	Residential land use

(continued)

Table 18.1 (continued)

Sr. no	Places	Land use
73	Basti Guzan	Residential land use
74	Ghaa Mandi	Mixed land use
75	Near Lyallpur Khalsa College, Jalandhar	Institutional land use
76	Near Chunmun Chowk	Mixed land use
77	Garden Colony	Residential land use
78	Garha Road Opposite Bus Stand	Commercial land use
79	Cool Road	Mixed land use
80	New Jawahar Nagar	Mixed land use
81	Shaheed Udham Singh Nagar	Residential land use
82	Krishna Nagar	Residential land use
83	Arjun Nagar	Residential land use
84	Prabhakar Palace, Near BSF Chowk	Commercial land use
85	Ladowali Road	Mixed land use
86	Alaska Chowk	Commercial land use
87	Flour Mill Chowk	Commercial land use

Source Primary Survey

in the town, the emergence of informal economy and housing, violence, crime and social disorders, etc. The physical environment of the urban area plays a crucial role in committing all kinds of offenses, as bad land use planning and displacement at particular places contribute to social ills such as theft and snatching of offender operations. The geospatial analysis of crime trends in towns attempts to develop convenient policies and techniques to fight social anarchy and deter crime through the use of geospatial analytical instruments and techniques. Criminals and offenders are doing a lot of rational stuff, predominantly they prefer to commit offences by using less effort, which means lower risk factor and get the greatest advantages from it. This rational strategy is used by analysts and scientists to discover methods to put obstacles against these offences (Clarke 1983, 1992; Clarke and Cornish 1985). From this point of perspective, one thing is to make it very clear that crime occurs when the criminals come into touch with any crime destination in the appropriate location, Where the likelihood of detection are small and the chances of safe departure without apprehension are high. In brief, the site's physical environment or natural guardian plays an important part in the occurrence of crime. Existing land use and physical use are essential to influencing the incidence of crime. Existing land use and physical built up have an impact on the criminal's ability to assess some particular site appropriate for the conduct of crime.

Mainly the crimes committed by the perpetrators are extremely dependent on the people previous operations and current activities in his/her daily lives, as individuals who primarily develop or indulge in drug addiction commit offenses such as robbery and snatching.

Table 18.2 Vulnerable points under various police stations in Jalandhar Commissionerate

Sr. no	Name	Type	Police station
1	Shaheed Bhagat Singh Interstate Bus Terminal	Bus Stand	Ps Div 7
2	Punjab Institute of Medical Science	PIMS Hospital	Ps New Baradari
3	Reliance Shopping Mall	Shopping Mall	Ps Div 7
4	PAP Sports Complex	Sports Ground	Ps New Baradari
5	Lyallpur Khalsa College	LKC College	Ps New Baradari
6	PAP Line	Public-Semi Public Area	Ps Cantt
7	Army Area	Army Cantt	Ps Cantt
8	Viva Collage Mall	Shopping Mall and PVR	Ps Cantt
9	Military Hospital	Army Hospital	Ps Cantt
10	Army Golf Course	Sports Course	Ps Cantt
11	Nikku Park	Recreational Park	Ps Div 6
12	Guru Gobind Singh Stadium	Sports Stadium	Ps Div 6
13	Model Town	Shopping Area	Ps Div 6
14	Dushehra Ground	Open Space	Ps Cantt
15	GNDU Regional Campus	University Regional Campus	Ps Rama Mandi
16	Indian Oil Corporation	Oil Tanks	Ps Rama Mandi
17	Kanya Maha Vidyalaya	Women College	Ps Div 8
18	Doaba College	College	Ps Div 3
19	Devi Talab Mandir	Religious Place	Ps Div 3
20	Jalandhar City Railway Junction	Railway Station	Ps Div 3
21	SD College For Women	College	Ps New Baradari
22	Jalandhar Cantt Railway Station	Railway Station	Ps Cantt
23	Govt. Technical College For Girls	College	Ps New Baradari
24	Commissioner Office	Court Complex and Commissioner Office	Ps New Baradari
25	Court Complex	Government Area	Ps New Baradari
26	Tehsil Complex	Tehsil Complex	Ps New Baradari
27	Cuoro Mall	Shopping Mall and PVR	Ps Div 7
28	Hong Kong Stadium	Sports Stadium	Ps Div 7
29	Shere Punjab Kabaddi Academy	Sports Academy	Ps Div 1
30	DAV College	College	Ps Div 1
31	Meharchand Polytechnic College	Polytechnic College	Ps Div 1
32	Surjit Hockey Stadium	Hocky Stadium	Ps Div 1

(continued)

Table 18.2 (continued)

Sr. no	Name	Type	Police station
33	Gandhi Stadium	Sports Stadium	Ps Div 1
34	DAV Engineering College	Daviet College	Ps Div 1
35	DAV Institute Of Physiotherapy	Physiotherapy Institute	Ps Div 2
36	Hansraj Mahila Vidyalaya	HMV College	Ps Div 2
37	Gulab Devi Hospital and Nursing College	Hospital and College	Ps Div 2
38	Doordarshan Kendra Jalandhar	Doordarshan Kendra	Ps Div 4
39	TV Tower Jalandhar	TV Tower	Ps Div 7
40	MBD Mall	Shopping Mall and PVR Cinema	Ps New Baradari
41	Hotel Radisson	Hotel	Ps New Baradari
42	Guru Nanak Mission Hospital	Hospital	Ps Div 4
43	Nehru Garden Company Bagh	Company Bagh	Ps Div 3
44	Civil Hospital	Government Hospital	Ps Div 4
45	CT Institute Of Engineering and Management	College	Ps Sadar
46	Focal Point Industrial Area	Industrial Area	Ps Div 8
47	Trinity College	College	Ps Rama Mandi
48	Apeejay College Of Fine arts	College	Ps New Baradari
49	Government Sports College	Sports College‘	Ps Basti Bawa Khel
50	St. Soldier Institute Of Management and Technology	Educational Institute	Ps Basti Bawa Khel
51	KCL College	College	Ps New Baradari

Source Primary Data

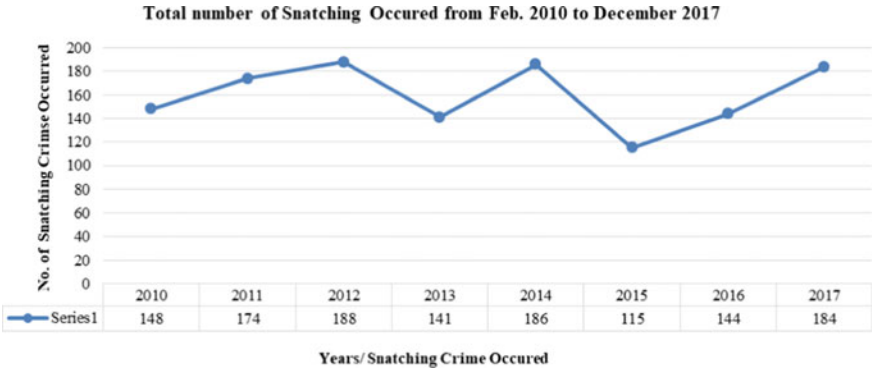

Fig. 18.2 Shows the snatching crime occurred in Jalandhar Commissionerate (From 2010 to 2017) (*Source* Jalandhar Commissionerate)

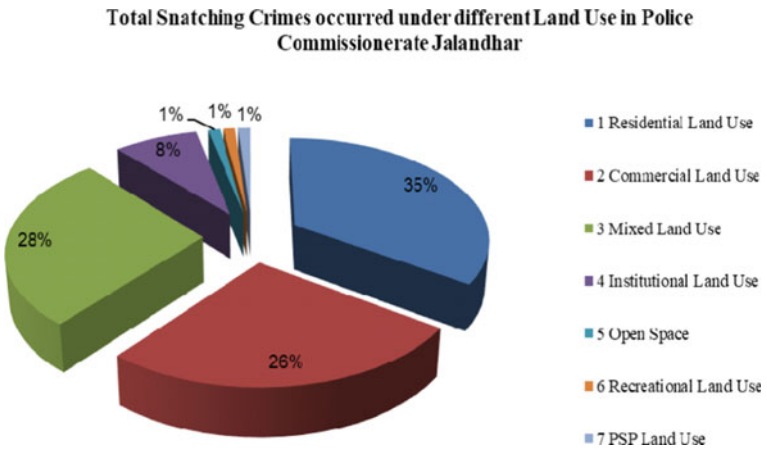

Fig. 18.3 Total Snatching crimes occurred in different Land Use in Police Commissionerate Jalandhar (*Source* Secondary Data)

Mainly because people do wrong in their lives, it is the primary root cause of criminal possibilities for perpetrators because there are many kinds of offenses, such as property crimes, snatching and robbery activities, which are greater in places where there is a demobilization location of market/shopping areas (commercial land use area) and commercial developments in the ribbon primarily involve criminal operations such as burglaries, snatching and theft, but residential land use regions or key residential regions primarily involve criminal operations such as snatching.

In Police Commissionerate Jalandhar, the maximum snatching crimes were occurred in residential land use, commercial land use and mixed use land use as shown in Table 18.1 by name of the areas and in Fig. 18.3 in percentage of snatching crimes occurred in Jalandhar Commissionerate in different land use. But in some extent this type of crime activities were also happened in Institutional land use, Open spaces and PSP land uses.

Most of the residential land use, commercial land use and mixed land use areas in Jalandhar Commissionerate are not well planned as per the given norms and standard of URDPFI and PUDA as well. Due to this haphazard growth in most of the areas, there is a lack of chances of proper monitoring on the streets and areas by the patrolling Police through their two wheelers and four wheelers vehicles. Which tends to increase the chances of many types of crimes to be occurred in Jalandhar Police Commissionerate. It also gives most of the advantage to the offenders or criminals to practise their criminal activities with easy ways like as snatchings in the residential, commercial or mixed land use areas. Into this type of physical built up and partially planned areas the offenders easily get way to enter into the locations, Easier way to target the person or property by the offenders at particular place, less visibility of offenders during crime from other surrounding people, congestion at the place or location and to understand all the possible shortcut routes or best routes to escape from the location just after the crime is committed to. So this thing proves the

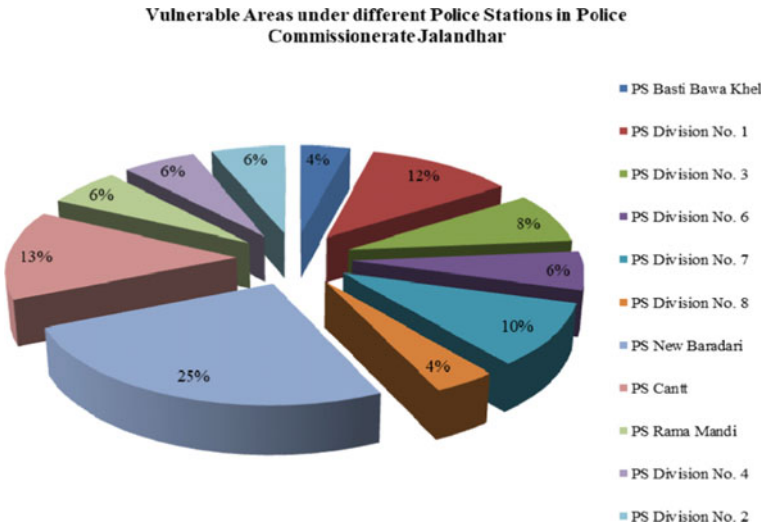

Fig. 18.4 Vulnerable areas under different police stations in police commissionerate Jalandhar (*Source* Secondary Data)

relationship between the physical built up/ land use and crime incidents occurred in some specifically locations.

Most of the vulnerable areas or points in Police Commissionerate Jalandhar are came to existence under the jurisdiction of Police station division no. 7, Police station division no. 1, Police station Cantt and Police station New Baradari as shown in below Table 18.2 and as percentage shown in Fig. 18.4.

The main reason in PS division no. 1 the non-conforming land uses together that here the Industrial land use very high and haphazardly merged with residential, they are non-conforming land uses, and has negative impact on surrounding. In Industrial units, there small worker works, variety of people from different background work there, some of them work on daily purposes, causing social mix and lack of belongingness hence trigger the mentality to indulge in unsocial activities, such as theft in Houses, drugs, snatching, negligence and other criminal activity. In PS New Baradari the snatching activity is very high, having commercial and residential activity the core area acting as regional market, attracts the regional population and different strata of population congregate in market space to access the services and Market, but it is also congested, streets are narrow as well as encroached. That attracts the criminal activities. Theft at housing dwelling, forcibly theft and Snatching, these are the major crimes here, also policing is very difficult, here proper arrangement of surveillances is more required. In PS Cantt the places like as Deep Nagar market, Dushehra ground havelinked with the Phagwara road or Ludhiana road passing from the Cantt area, which also connected with open spaces and rural areas also. Through which the offenders get easy way or multi ways/ paths to escape from the crime hot spot locations after committed the criminal activities on bikes especially. In PS

division no. 7 from one side it is connected with village Sabana and secondly it is connected with Urban Estate 1 and 2, which has one of the upper MIG and HIG areas of Jalandhar, where most of the offenders and criminals are used to enter for snatching purposes from the people who use to live in urban areas and its surroundings because the people who use to live in the HIG and upper MIG areas are the main target of these snatchers. Especially the females who use to walk on the pedestrian paths and parks during evening time and in day time whilst their movement at on neighbourhood level for daily works.

18.5 Results and Discussions

There are identified total 301 different crime hot spot areas in Jalandhar Commissionerate for their Vulnerability to crimes specifically Snatching Crimes occurred at these locations (as shown in Table 18.3). Maximum crime related to snatching is occurred in that particular hot spots and their relevant data had collected from the secondary data of Jalandhar Police Commissionerate in reference to snatching crime and by implemented the GIS techniques on it for their analysis. According to the distribution of crime events will be understand that almost all parts of the Jalandhar Commissionerate are acted vulnerable, and happening wrong operations. Except for a few pockets the complete work of the Jalandhar city is witnessing less crime events. The other analyses are based as following.

18.5.1 GIS-Based Vulnerable Areas Mapping

In the present study, the data from last one-year facts had been observed for analysis the crime hot spot for Snatching crime. Here the points are identified and buffer areas are marked, at various different levels of distances in metres by using GIS techniques giving findings for hot spot areas of crime events within the limits of Jalandhar Commssionerate police stations. In harmony with to the divisions of an organization of two different zones of Jalandhar City 1 and Jalandhar City 2 Crime Branch (CCB), Jalandhar, The crime facts were put in order under the group of snatching attacks in day and night. To observe the hot spots in the selected part in each crime spots have been placed, rectified ground truthing of these points (coordinates of the location) from Google maps, whilst locating these points, where the crime has took place, the time of crime happened, the day and house details are also been included to understand the relationship between the crime and its occurrence. Maps emphasize on the areas where high number of crimes had occurred. This information focuses based on the locational attributes and highlights the concerned sensitive areas (vulnerable area), their immediate surrounding who also have the influence of the criminal activities i.e., the affected zones and its radius of influence. Those required high preventive measure to deal with large number of crimes. This kind of evolved

Table 18.3 High, moderate and less affected areas in reference to snatching crime vulnerability after GIS-based analysis

Sr. no	High	Moderate	Less
Police Station Division No. 1			
1	DAV College	Mehar Chand Polytechnic College	Greater Kailash
2	Shere Punjab Kabaddi Academy	Dav Institute Of Physiotherapy	Bhagat Singh Colony
3	DAV Institute Of Engineering and Technology	Ram Nagar	Moti Nagar
4	Surya Vihar (Residential Area)	Friends Colony	
5	Sham Nagar (Residential Area)	Hukam Chand Colony	
6	Rose Park Colony	Dayanand Colony	
Police Station Division No. 2			
7	Transport Nagar	Jatt Pura	Gurdev Nagar
8	New Patel Chowk	Charanjit Pura	Hardev Nagar
9	Jail Road Compound Area (Commercial Area)	Mitha Bazar	Guru Nanak Nagar
10	Neela Mahal		
11	New Prem Nagar		
12	Sangat Nagar		
Police Station Division No. 3			
13	Central Town (Commercial Area For Mobile Phone Shops)	Doaba College	Attari Bazar
14	Chahar Bagh	Dhan Mohalla	Damoria Pull
15	Partap Bagh	Rajindra Nagar	
16	Bajwa Colony		
17	Jodhewal Basti		
18	Kot Kishan Chand Area		
Police Station Division No. 4			
19	Pucca Bagh	Civil Hospital	Ali Mohalla
20	LIC Office	Makhdoom Pura	
21	Bidharath Nagar Colony	Hansraj Stadium (Recreational Area)	
22	Patel Hospital		
23	Sky Lark Hotel		
24	Shastri Nagar (Commercial Area)		

(continued)

Table 18.3 (continued)

Sr. no	High	Moderate	Less
25	Civil Line		
Police Station Division No. 5			
26	Ujala Nagar	New Ashok Nagar	Gobind Nagar Extension
27	Basti Sheikh	Satkartar Nagar	Hargobind Nagar
28	Basti Danishmandan		Balbro Nagar
29	Tej Mohan Nagar		Kot Sadiq
Police Station Division No. 6			
30	Model Town	Lal Nagar	Rishi Nagar
31	Guru Gobind Singh Stadium	Avtar Nagar	Waryam Nagar
32	GTB Nagar (High Area/High Class Area)	Rameshwar Nagar	
33	Dada Nagar		
34	Nm Town		
Police Station Division No. 7			
35	Urban Estate Phase 1	Bank Colony	Isharpuri Colony
36	Urban Estate Phase 2	Dashmesh Avenue	Universal Colony
37	Green Woods Enclave	Garha	Khurla Kingra
38	Cuoro Shopping Mall and Cinema		Mithapur
39	TV Tower Jalandhar		
Police Station Division No. 8			
40	Reru Pind	New Kailash Nagar	New Kailash Nagar
41	Doaba College To Preet Nagar	New Gobind Nagar	Aman Nagar
42	Preet Nagar	Sodal Nagar	Hari Singh Nagar
43	Shiv Nagar		
Police Station New Baradari			
44	Bus Stand	Police Line	Shantipura
45	Lodawali Area	Lyallpur Khalsa College	Kirti Nagar
46	Raga Motors	KCL College	
Police Station Basti Bawa Khel			
47	Basti Guzan	Raja Garden Colony	Paras Estate
48	New Harbans Nagar	Basti Bawa Khel	Krishna Nagar
49	Dilbagh Nagar	GRD Enclave	Babu Labh Singh Nagar
50	Ambedkar Nagar	JP Nagar	
51	Virdi Colony		

(continued)

Table 18.3 (continued)

Sr. no	High	Moderate	Less
52	Raj Nagar		
Police Station Sadar			
53	Saprai	Charnanpur	Dhina Village
54	Jamsher Khas	Chitewani	
Police Station Cantt			
55	Deep Nagar	Allahdin Pur	New SA Colony
56	Rehmanpur	Paragpur	Alipur
57	Mandakini Resort, Kot Kalan		Cantt
58	Khusropur		
Police Station Rama Mandi			
59	National Avenue	Joginder Nagar	Professor Colony
60	Dakoha	Rama Mandi	Ganesh Nagar
61	Sainik Vihar	Baba Budha Ji Nagar	Guru Nanak Nagar
62			Railway Colony
Police Station Bhargo Camp			
63	Orthonova Hospital	Bootan Mandi	Ishwar Nagar
64	Ravidass Nagar	Tower Enclave	New Dashmesh Nagar
65	Laxmi Naraya Mandir (Model Town Area)		
66	New Kartar Nagar Colony		
67	Tilak Nagar		

Source Primary Data

pictures of sensitive areas will help in locating the crime; can help police to keep safe (out of danger) citizens more efficiently.

In (Fig. 18.5), it mainly shows the vulnerable crime hot spots of specific crime i.e. snatching crime. According to the given data, Police Station Division no. 6 has high number of snatching crime hot spot areas, which are near to 58 in numbers. PS Division no. 4 has near to 45 number of snatching crime hot spot areas. In PS Division no. 1, PS Sadar and PS Division no. 5 has less number of snatching crime hot spot areas into their jurisdictions. This vulnerable snatching points or crime hot spots in the jurisdictions of different police stations are well mapped in (Figs. 18.6 and 18.7) as given below with help of GIS tools.

The Map in (Fig. 18.6) shows the least to most vulnerable area for Snatching crimes in Jalandhar Commissionerate in different Police Station jurisdictions. This analysis is based on occurrence of crimes in which light in colour area shows the less vulnerable areas and the Dark colour areas show the high vulnerable areas for Snatching crimes in the specific Police Stations jurisdictions. The core area is highly affected from the snatching crime; it is market area and old residential area, crowded

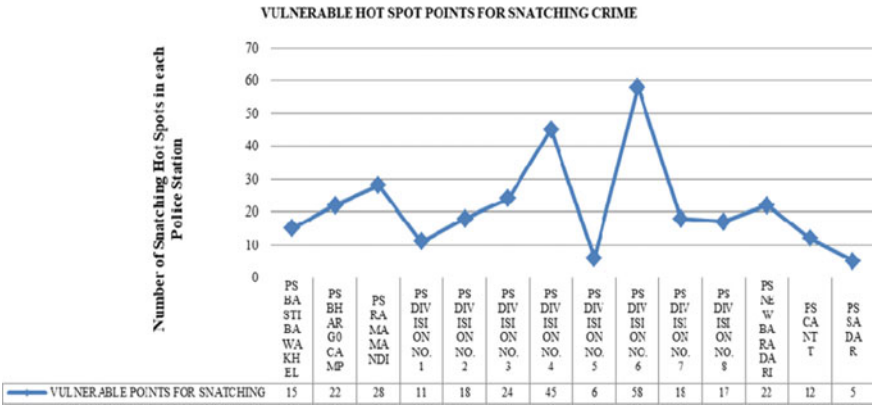

Fig. 18.5 Vulnerable snatching points in various police stations in Jalandhar Commissionerate (*Source* Secondary Data)

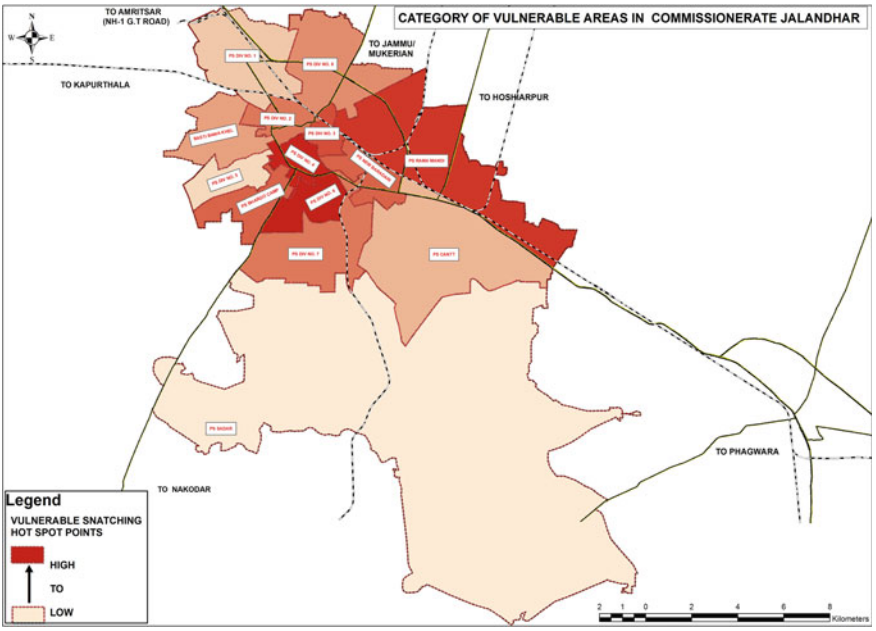

Fig. 18.6 Vulnerable snatching points show in different categories from low to high in police stations of Jalandhar Commissionerate (*Source* Prepared by the author)

with narrow and encroached streets. These conditions aid to the crime in this area. By this visual representation technique of mapping, it is easy to understand about the Status of crime (high, moderate and low), identification of vulnerable areas for Specific crimes (snatching crimes) in every Police Station Jurisdiction.

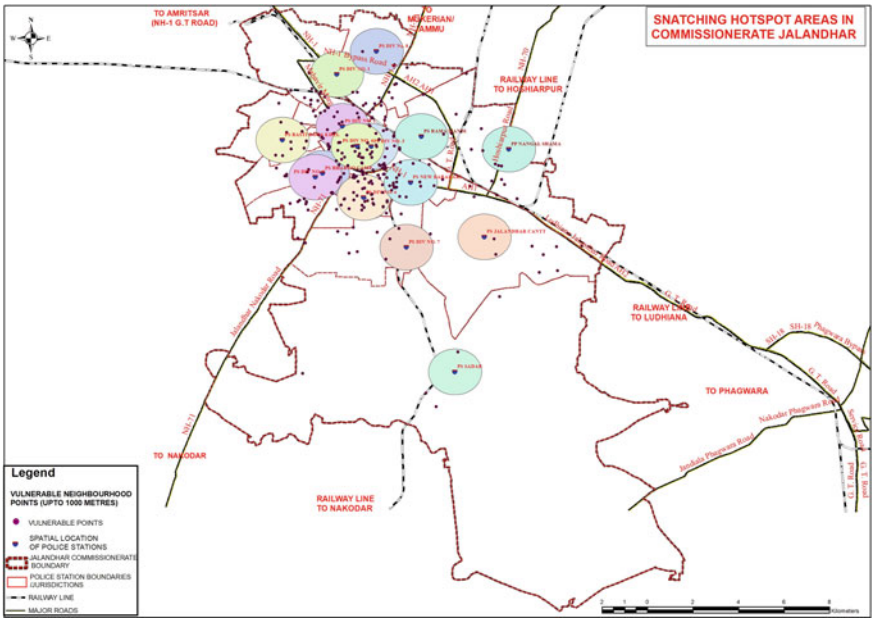

Fig. 18.7 Vulnerable snatching hot spot areas in Jalandhar Commissionerate (Nadir taken from Locations of the Police Stations) (*Source* Prepared by the author)

The map in Fig. 18.7 shows the vulnerable Snatching points and the geospatial catchment area around the pointed location of the Police Stations mainly up-to neighbourhood level (1 km^2). Most effective and rapid response by police in this catchment. It shows that being the presence of Police Station location at specific point in Jalandhar Jurisdiction, the number of crimes (vulnerable Snatching crimes points) are occurring within the catchment area of each Police Station, which indicates towards the negligence and ineffective services by the Police for public in specific Police station; i.e., PS Division no. 3, PS Division no. 4 and PS Division no. 6 have more number of crimes hot spots but it comes under its neighbourhood catchments indicating the ineffective policing. That indicates, these above three mentioned Police stations need to enhance their patrolling techniques into their Police Station Jurisdictions for controlling their occurrence of crime enhances their effectiveness and quick response and eradicate the menaces of crimes.

18.5.2 Hot Spot Analysis on GIS

Crime Hot spots mean the geographical areas where the frequency of crime occurrence is unusually very high. The results are based on limited time, observations made on the hot spots where the "snatching" crimes had occurred. According to

Fig. 18.7 the occurrence of snatching crimes is high in year 2012, 2014 and highest in 2017. There are a number of different ways to do this, and a map was made come into existence with geospatial observation on GIS software like as give buffer to the points to show their influence at their neighbourhood distance.

18.5.3 Buffer Analysis Technique

Buffers are the bands, parts of interest around the selected thing (Harries 1999) as shown in Fig. 18.8. The size, range, degree of these bands, parts depend up on the influence zone around the hot spot area. Short-time store bands, parts were got ready for the Police station placing. The 5 different rings in the map were outlined at a space (times) between every distance of 200 m each. The inner ring covers the first 200 m from the central crime hot spot and by each ring the difference is started to increase by 200 m each (200, 400, 600, 800 and 1000 m). It is also showing that of being conscious of snatching crime will take place well away from the police station.

With the help of the buffer technique in GIS at different level of distances (Neighbourhood level, which is mainly up to 1 Km^2) shown in the Figs. 18.8 and 18.9, one thing has observed that the most of the Snatching crime was occurred at neighbourhood distances from the Police stations or different police stations of Jalandhar Commissionerate.

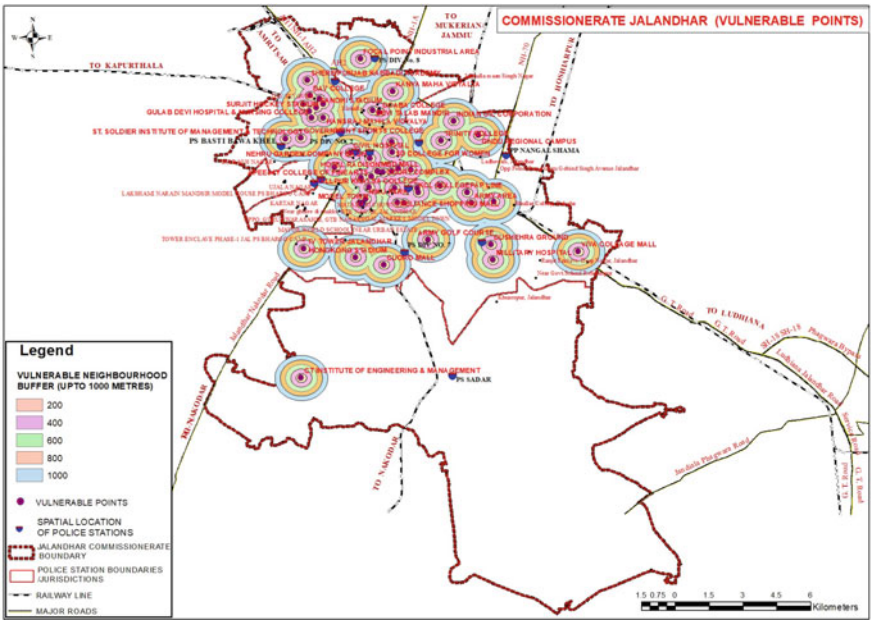

Fig. 18.8 Vulnerable areas in Jalandhar Commissionerate (*Source* Prepared by the author)

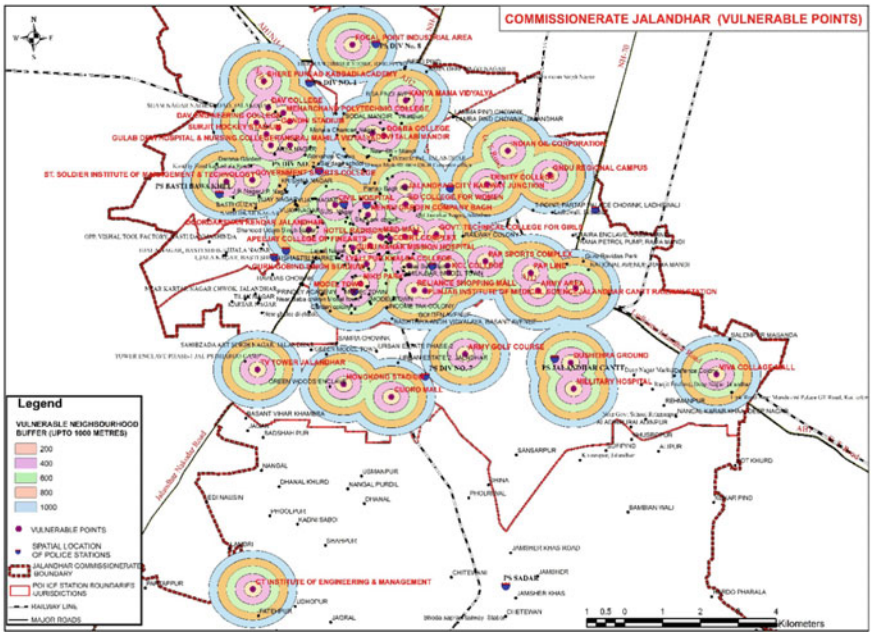

Fig. 18.9 Vulnerable points in Jalandhar Commissionerate (*Source* Prepared by the author)

Figures 18.9 and 18.10 maps are showing the vulnerable areas and its buffers in Jalandhar Commissionerate, it shows the distance of police stations and probable area where crime can occur. It gives the impact area of the criminal and its effect by different colour bands. In this map it shows that PS Div. no. 6, PS Div. no. 4 and PS Basti Bawa Khel lies in between 200 to 400 m^2 from the vulnerable crime hot spot. The PS Rama Mandi, PS Div. no. 2 and PS Cantt lies in between 600 and 800 m^2 from the Crime hot spot areas and PS Div. no. 7 and PS Div. no. 5 lies in between 1000 m^2. from the Major Crime hot spot areas. PS Sadar and PP Nangal Shama lies beyond the Neighbourhood distance/level from the major Crime hot spot areas. Here it indicates that the majority of Crimes are occurring within the neighbourhood limits and they are occurring due to lack of policing, appropriate planning and lack of quick and Effective response.

Figures 18.10 and 18.11 show the enlarge (Zoom) version of Fig. 18.9. It shows the detail of the core area, analysis of the core areas, which comes under these rings (Showing distance from the crime hot spot), the KML file (Generated from GIS Software) is overlaid on the Google earth directly or through GIS Software as shown in Figs. 18.12 and 18.13 respectively. These representation would be very helpful for the Police Department to find the core areas and streets, comes under these rings at various different distances. It can also analyse the influence or effect of the location of Police station near the hot spot location of the crimes, in which they are happening anywhere in the city, whether a police station is present or not in

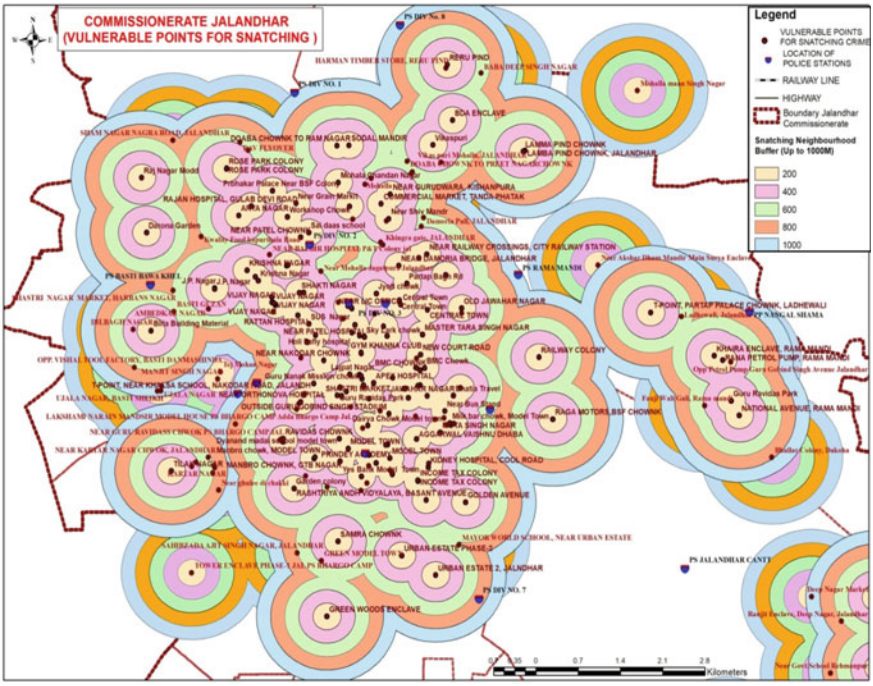

Fig. 18.10 Buffers show the Snatching Hot Spot (2010–2017) in Jalandhar Commissionerate (*Source* Prepared by the author)

that place. It is to be noted that policing needs more rapid or quick response that will make the difference in the occurrence of crimes in these areas, least approachable areas get high frequency of crime occurrence or vice versa. As an outcome of that, those stations become ineffective and area becomes more vulnerable i.e., open for occurrence of more number of crimes. Criminals seem to take more chances in these areas where there is any narrow opening, less crowded, isolated areas those are less approachable and take more time to execute any quick response.

From the identification of hot spot areas and the demarcation of these on areas on maps i.e., crime mapping helps to improve the policing mechanism such as day and night patrolling schedule in the area, the peak timing of occurrence of crime and its shifts during the years, more efficient and quick response to eradicate the crime favourable situations, and enhance the sense of alertness with in the area police for quick response.

In the map in Fig. 18.9 shows the same Crime hot spot (vulnerable areas or geospatial points) shows the information of Figs. 18.12 and 18.13 (Maps) on the Google satellite imagery for better understanding about the crime hot spots for Snatching crime in relation to the development and build environment. Because It gives better understanding of built-up density, Street network and hot spots for mainly examines

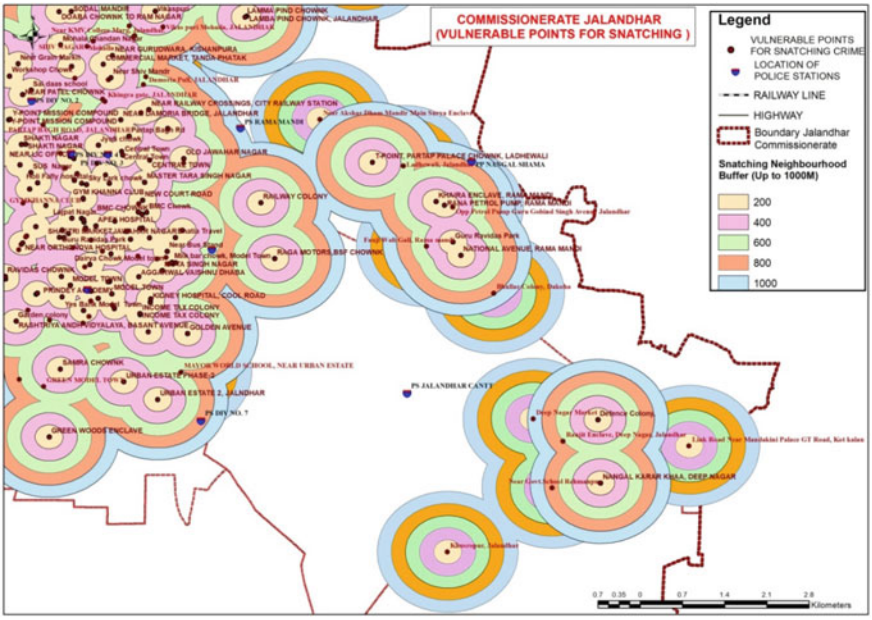

Fig. 18.11 Buffers show the Snatching Hot Spot (2018) in Jalandhar Commissionerate (*Source* Prepared by the author)

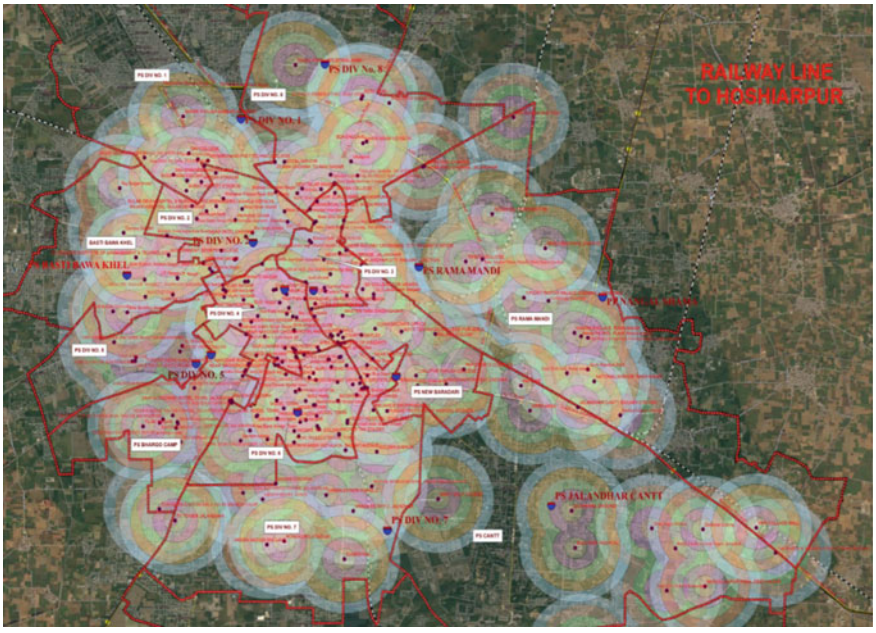

Fig. 18.12 Buffers show the Snatching Hot Spot on Google satellite view image (*Source* Prepared by the author)

SNATCHING CRIME HOT-SPOT BUFFER ANALYSIS ON GOOGLE IMAGE

(a)

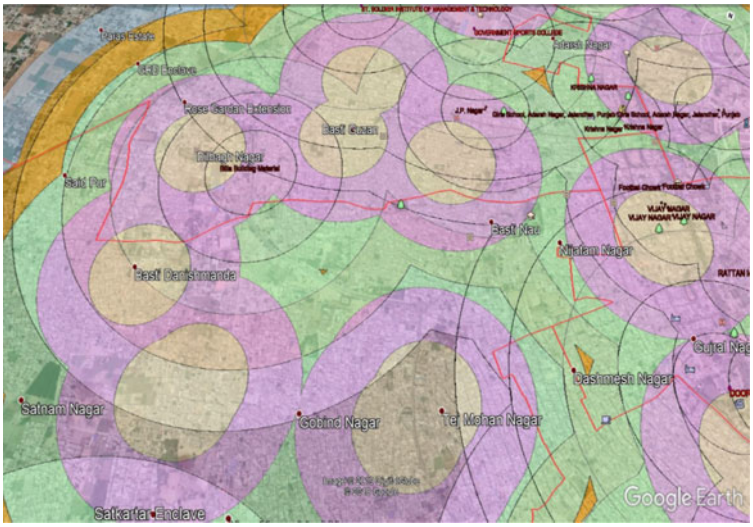

(b)

Fig. 18.13 **a** Buffers Show the Snatching Hot Spot on Google Image and **b** In this map, it shows the enlarged (Zoom) image (HIG and MIG area in Jalandhar Commissionerate) of neighbourhoods showing the Snatching crime hot spots on the Google Satellite Imagery with multi buffer rings. **c** In this map, it shows the whole image (HIG and MIG area in Jalandhar Commissionerate) of neighbourhoods showing the Snatching crime hot spots on the Google Satellite Imagery with multi buffer rings (*Source* Prepared by the author by itself)

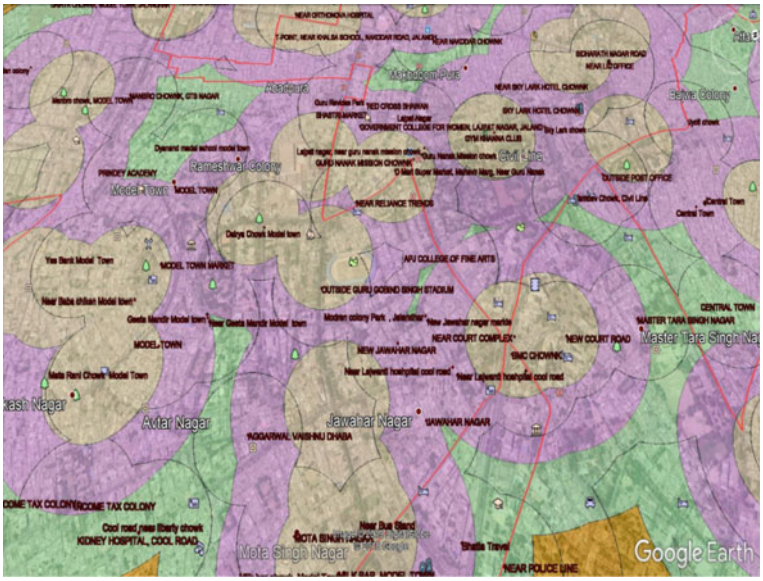

(c)

Fig. 18.13 (continued)

the relation of these and highlights the high to low influence areas under crime hot spots points on real ground features.

In Fig. 18.13a, b maps show the enlarged (Zoom) image of neighbourhoods showing the snatching crime hot spots on the Google Satellite Imagery (HIG and MIG area in Jalandhar Commissionerate) as shown in Fig. 18.13c. It shows the Core areas of Jalandhar which are highly affected area by crimes (Majority of hot spot areas or geospatial hot spot crime areas on satellite view maps (Google Maps) by using buffer technology with GIS Technology on GIS software), which helps to analyse and examine the crime hot spot areas more effective and efficient way. It represents the relation of Hot spots and Built-up density, and different distance levels from the major hot spot points. In this map representation gives the understanding that more isolated spaces as well as the highly crowed space have become more vulnerable to the snatching crime.

18.5.4 Findings

By using the GIS technology through ArcGIS software's and satellite view Google maps as shown in the figure (from Figs. 18.12 and 18.13), these Tables showing the Police stations and identified areas of Highly affected, Moderate affected and Less

affected areas, the Highly affected areas are the high vulnerable areas (Hot Spots of Crimes) and Less affected areas are less vulnerable areas.

18.5.5 Recommendations

Use computer-aided simulation techniques to model patterns of crime and to make precise forecasts of possible occurrences of crime and use GIS to study the interrelationships of variables affecting crime-related growth in cities and to make accurate predictions of crime occurrences and security resource allocation decisions. Develop custom GIS applications and programs that can analyse variables such as land use, zoning, construction codes and security of the neighbourhood and circumstances of accommodation. In general, the shelter designs and the residential area housing/block development plans make the area safer or less vulnerable to criminal activity. Mainly in the buildings of residential areas with less entrance to their homes, fewer floors and better views of the outside have less fear of the inhabitants and less risk of victimization. In Jalandhar, the buildings with proper building barriers and street patterns help residents monitor the entries of drug dealers and distributors who drive through the city because these people are mainly engaged in snatching activities to fulfil their financial requirement for drugs. In Jalandhar Commissionerate well-designed houses involve planting in and outside their homes, where certain significant indicators are present in the majority of Jalandhar resident areas. That determines the relationship between the site of the crime and the incidence of the crime in any particular place, such as in the case of suspects or criminals, using tall shrubs (inside and outside the homes), Alcoves and Blind corners in the streets to avoid or flee after a snatching type or theft type crimes have been committed and even the multiple street exit points also encourage offenders to commit the crime on the streets (Defensible space by Newman 1972).

Understand the factors that affect crime chances through the link between land use and crime possibilities by using GIS as instrument for proactive crime prevention choices. At the neighbourhood level, if there is mixed land use with high-volume streets and attractors and non-residential land use, such as shopping streets, in any particular area, such as the Jyoti chowk market in Jalandhar city where the movement of non-residential communities, local commuters for shopping purposes and attractors is more closely related to the residents of the area, the probability of certain crimes such as snatching and burglaries in this form of location is more attributable to the correlation between physical characteristics and crime rate. In the newly developed areas in Jalandhar Commissionerate such as near Surya enclave, new development near Khusropur village and new development in the colonies on Nakodar and Kapurthala road (where the maximum plots are still vacant) should take steps to prevent crime and avoid crime. This thing is keep in mind that the secure closure of public, semi-public and, in particular, private vacant lands or parcels in specific areas in any region or city should be essential, otherwise these types of areas could be the main places for the commission of offenders crimes or for the planning of offenders

groups, mainly after evening. GIS-based crime hot spot analysis guides the Police department of Jalandhar Commissionerate to manage or use their limited resources (Human as resources in police department) as according to the effective level of hot spot (High, Moderate or less).

18.6 Conclusion

This paper is giving the three major answer that was highlighted in the introduction, as the Identification Crime Hot spots on the bases of Occurrence of Crime, and analysed with the help of GIS technique which relate the Data and represent it into the spatial dimension (i.e., mapping), relation to the type of development, Built-up Density and identification of areas which falling into the Vulnerable zones (the Probabilistic locations for occurrence of crime in Future, mentioning less to high vulnerable areas).

First, by attributing the data of occurrence of crime on to the jurisdictions map of Jalandhar Commissionerate into a GIS Software, gives a clearer picture that how many areas are falling in the jurisdictions of various Police Stations those are highly affected by the occurrence of crime, relation to the neighbourhood approach clarifies that the crime with in the neighbourhood limits is due to lack of patrolling negligence and ineffectiveness, lack of awareness, Reports are not registered in that areas, people are not aware to report on time and least quick/Rapid responses, made by the police Stations. As these areas are those areas which get the immediate responses. The buffer analysis gives the overlapped picture of the crimes in the city. The city core is highly crucial in term of crimes and its influence is overlapping to the surrounding, where other police station works. Due to this it helps to police administration for the intra-Department coordination amongst the various police stations and gives opportunity to work on the city together, understand the pattern of crime, now after identification of these areas it can become ideal areas by using the better police practices. The overlay buffer map on Google Imagery helps to understand the relation of occurrence of crime, its influence zone and its built-up density, gives clearer picture (isolated spaces as well are the highly crowed space are become more vulnerable to the snatching crimes) and in this analysis identifies the highly affected areas and least affected areas also direction of the crimes. It also identifies the probable areas those could be affected by the crimes in future. Under each police station boundary there are many sensitive areas for different crimes, such as Bhargo Camp and Model House area under PS Bhargo Camp, Basti sheik area under Basti Bawa Khel and Ali Mohalla under PS Division No. 4 etc., where the crime rate is as high as in other areas. These types of areas require special attention from the Police Department by drawing up certain spatial schemes and planning to monitor the occurrence of criminal activities in sensitive areas on the basis of identified crime hot spot areas.

So, GIS technology with crime hot spot analysis study also helps to identify the terrorist activities, movements and other major crime locations. By plotting different snatching crimes all together creates a pattern, which helps to tackle the problem

and after identification of these vulnerable/crime hot spot locations and provides its outcome in user understandable digital format or maps, which give opportunity to police department to work in very effective and efficient manner.

Acknowledgements The author thankfully acknowledges the name of Sh. PK Sinha (IPS), Commissioner of Police (Jalandhar Commissionerate) for providing the guidance and Crime data from February 2010–2017 for the purpose of research. The author also thankful to the ADCP Security and Headquarter Sh. Gautam Singal (PPS) for providing his great assistance, guidance and support in this research.

References

Clarke RV (1983) Situational crime prevention: Its theoretical basis and practical scope. Crime and Justice 4:225–256. http://www.jstor.org/stable/1147510

Clarke RV (1992) Situational crime prevention, Harrow and Heston, New York

Clarke R, Cornish D (1985) Modeling offenders' decisions: a framework for policy and research. In: Tonry M, Morris N (eds) Crime and justice: an annual review of research, vol 6. University of Chicago Press, Chicago, pp 147–185

Harries K (1999) Mapping crime-principle and practice. Washington DC, Crime Mapping Research Center, National Institute of Justice, U.S Department of Justice

Johnson CP (2000) Crime mapping and analysis using GIS. In: Geomatics: conference on geomatics in electronic governance, pp 1–5

Newman O (1972) Defensible space. MacMillan, New York

Sherman L, Weisburd D (1995) General deterrent effects of police patrol in crime "Hot Spots": a randomized, controlled trial. Justice Q 12:625–648. https://doi.org/10.1080/07418829500096221

Chapter 19
Quantifying Land Use/Land Cover Change and Landscape Fragmentation Over the Intanki National Park, Nagaland (India) Using Geo-Informatics

Mhaphruovizo Liezietsu, Mukesh Kumar, Arnab Kundu, Subongchiten Jamir, Ankush Vinod Lal, Neeraj Kumar, Dipanwita Dutta, and Deepak Lal

Abstract Land use/land cover (LULC) change is an extremely significant driving component of ecological degradation in tropical regions where forests are under risk due to various anthropogenic activities. The present study appraises changing pattern of LULC (1999–2017) over the Intanki National Park (INP) in Nagaland (India) using Landsat imageries. Moreover, the study attempts to assess the evaluation of forested landscape at the patch, class and landscape levels of study region. At the class level, distinctive measurements of forest and non-forest classes during the period were compared. The study reveals that several patches were developed in the southern part of that INP while the north-eastern region has lost majority of its forest. The forest constituted 95% in 1999 which was reduced to 84% in 2017. The accuracy assessment of LULC maps derived from satellite imageries indicated > 87% concurrence with the test dataset. This study will be helpful for policy makers to realize the landscape arrangement and plan the region for sustainable growth.

Keywords Degradation · landscape change · remote sensing · fragmentation metrics · INP (India)

M. Liezietsu · M. Kumar · S. Jamir · N. Kumar · D. Lal
Centre for Geospatial Technologies, Sam Higginbottom University of Agriculture, Technology and Sciences, Prayagraj, Uttar Pradesh, India
e-mail: deepakl@shiats.edu.in

A. Kundu (✉)
Department of Geo-Informatics, P.R.M.S. Mahavidyalaya, Bankura University, Bankura, West Bengal, India

A. V. Lal
Department of Civil Engineering, Sam Higginbottom University of Agriculture, Technology and Sciences, Prayagraj, India
e-mail: ankush.vlal@shiats.edu.in

D. Dutta
Department of Remote Sensing and GIS, Vidyasagar University, Midnapore, West Bengal, India

R. B. Singh et al. (eds.), *Remote Sensing and Geographic Information Systems for Policy Decision Support*, Advances in Geographical and Environmental Sciences,
https://doi.org/10.1007/978-981-16-7731-1_19

19.1 Introduction

Land cover change is a key variable that effects and links numerous parts of the physical and human environments. Land cover has established a key variable of the earth's structure that usually has shown a nearby relationship with physical environment and the human actions (Bell and Walker 2005; Srivastava et al. 2014). Throughout the years many programs such as LULC change and International Geosphere Biosphere Program (IGBP) have been conducted to tackle human-induced processes on land cover changes. Land cover modifications like landscape ecology focus on the connections between spatial outline and natural practices on a landscape level which shows relationship between landscape structures, utility and changes eventually (Wu and Hobbs 2007; Wu 2008). LULC is firmly associated characteristics of the earth's surface. Land use has an effect on land cover and changes in land cover influence land use. Land use is defined as the way people utilize the land and its assets (e.g. agriculture, grazing, urban development etc.). Accurate information on land use is vital to identify the drivers of land cover change and it's effect on land. In twentieth century, rapid LULC changes by human actions occurring in tropical and sub-tropical countries are constantly transforming landscapes, in that way threatening worldwide sustainability and most importantly, the livelihood. Land transformation, habitat loss and fragmentation are distinctive processes of landscape transform. Landscape ecology is an exceptionally interdisciplinary stream that integrates bio-physical and systematic approaches transversely natural and social science and involves spatial investigation and modeling to the front of environmental research (Li and Wu 2004). The earth surface is experiencing a steady landscape transform coming about from a diversity of natural and man-made disturbances. In addition, natural disturbances consist of flames, storms, floods and volcanic eruptions. Human conflicts can expect numerous structures, for example, contamination, rotation, habitat damage and fragmentation. The global ecosystems have been transformed significantly either to handle agriculture or to built-up systems owing to the essential needs of people (Botequilha Leitáo et al. 2006). Land cover adjustments, in which land cover may have been modified however the class stays unaltered (e.g. degraded grassland, thinned forest), might be spoken to by ordinary post-classification association techniques for change detection. Although nearly all classification strategies have determined on the utilization of spectral dimension, the spatial domain additionally contains significant information to help in change detection.

From a biodiversity point of view, fragmentation, loss and debasement of habitat are broadly measured as the most significant driving variables and thus this has been a major topic of research (Hanski 2005; Fischer and Lindenmayer 2007). The term fragmentation indicates the concurrent decrease in continuous forest zones and sub-division of the entire forested area into tiny non-contiguous patches (Laurance 2000; Midha and Mathur 2010). Landscape fragmentation is generally caused by infrastructure development, population raise, forest cover reduction, alteration of landscape for agricultural purposes to meet the essential needs of people. Land cover fragmentation analyses are performed to understand the effect of land cover changes

within a landscape through estimating a variety of metrics to depict fragmentation and spatial allocation. The spatio-temporal dynamics will help to identify the social and bio-physical processes fueling these changes (Brown et al. 2000). Owing to its interaction with physical, ecological and man-made processes and considering the effects of anthropogenic activities on natural and quasi-natural habitats, preservation and sustainability of land cover has become a matter of great concern (De Groot 2006). Moreover, evaluating the spatial extent of LULC change and its cumulative impacts especially over restricted areas is perceived as an important topic of research in recent period.

A variety of indices have been developed in the previous decades to quantify landscape and landform changes. These indices comprise patch density and size, edge, shape, area, nearest neighbor, diversity and interspersion, which give practical information about the composition and pattern of landscape. The correlation between ecological information and outcome of these indices can be helpful for estimating changes in landscape formation with time (Olsen et al. 2006). Landscape indices can likewise be utilized to portray how anthropogenic activities influence landscape formation (Li et al.2000; Tang et al. 2006). An additional significant benefit of utilizing landscape metrics is to distinguish the variations among the indices and match up to them multi-temporarily (Botequilha Leitáo and Ahern 2002). Reed et al. (1996) identified the effects of fragmentation which include habitat loss for a few plant and animal species, habitat formation for others, reduced connectivity of the residual vegetation, decreased patch size, increased space between patches and an increase in edge at the expense of inner habitat. Griffith et al. (2000) assessed the principal components analysis (PCA) on landscape prototype metrics derived from a Kansas land cover data base at three different spatial resolutions.

FRAGSTATS software program was utilized in this study for landscape metrics estimation. FRAGSTATS was developed to compute a broad diversity of landscape metrics for categorical map outline. It is an independent program developed in Microsoft visual C++ for use in the windows operating system (McGarigal et al. 2002). Cumming and Vernier (2002) used FRAGSTATS to assess the landscape pattern metrics in northeast Alberta (Canada). Ashish et al. (2004) conducted a study to investigate the potentiality of ETM + data on land use mapping of Chamestap region, Mazandaran (Iran). Goparaju et al. (2005) showed the changing biodiversity of Vindhyan highlands in the Indian dry tropical forests. In their study, Matsushita et al. (2006) described the varying characteristics of landscape formation over the lake Kusumigaura basin of Japan during the period 1979–1996 using FRAGSTATS and GIS . Cushman et al. (2008) identified individual segments of class and landscape level formation in various landscapes with distinct geographical characteristics. Midha and Mathur (2010) studied fragmentation in two diverse regions viz. Dudhwa National Park and Katerniaghat Wildlife Sanctuary and found forest management activities (development of road network and plantations) and measured their extent by selected metrics at the forest class level. Thapa et al. (2016) studied the effect of climate variation on biodiversity and ecological practices in Nepal region. Singh et al. (2016) utilized contemporary techniques, i.e., EO and GIS with fragmentation study to compute changes of landscape in the Rajaji National Park (RNP) from 1990 to

2009. Kumar et al. (2018) addressed the landscape fragmentation and transformation since 1976–2014 over the Usri watershed (India) using satellite remote sensing. This research intends to address the potentiality of two widely used methodologies for LULC research: land cover changes and landscape fragmentation study. The various strategies utilized for change detection and fragmentation analyses were examined and assessed with satellite datasets and then compared to existing techniques by LULC classification.

19.2 Study Region

Intanki or Ntangki is a National Park located in Peren district of Nagaland (India). The district is bounded by the state of Assam in the west, Dimapur district to the northeast, Kohima district to the east and Manipur state to the south. Intanki National Park is situated in the north-western part of Peren at 25°31′N 93°44′E with a whole area of 2,300 sq. km. (Fig. 19.1). The altitude of the district varies from 800 to 2500 m above sea level. The Intanki Wildlife sanctuary was declared as a National Park in the year of 1993. It was also declared as an elephant reserve on February 2, 2005. The maximum temperature recorded in the park is 35 °C and the minimum recorded temperature is 4 °C and the place receives heavy rainfall from June to October with an average of 1500 mm annually. INP is made up of thick rain forests making a perfect habitat for all types of animals and birds. The park has a large number of mountains & hills and the altitude of the place ranges around 677 m. Some parts of the national park also have semi tropical and deciduous vegetation. Entire Park is covered with lush grass and semi tropical tress. Mountains, cliffs and valleys within the park are unique places for camping, trekking and present good opportunities for sightseeing. There are a number of tree species such as sal, deodar, litchi, teak, mahogany, palms, rattan, bamboo, *Cymbidium tigrinium*, *Shoreaassamica* present in the park. Animals like gibbon, golden langur, elephant, barking deer, sambar, porcupine, mithun, hornbill, tiger, sloth bear, black stork, white-breasted kingfisher, python and monitor lizard were found in the park. The park serves as a reserve for the famous Amur falcons (*Falco amurensis*) which migrate to as far as South Africa.

19.3 Materials and Methods

19.3.1 Data Used

Landsat datasets for 1999 and 2017 were obtained from USGS (http://www.usgs.gov/in) of the similar season to minimize any seasonal and phonological variations inland cover. Top of image atmospheric (ToA) calibration for data set was applied to come out with biasing factors and keep away from getting out come initiated from

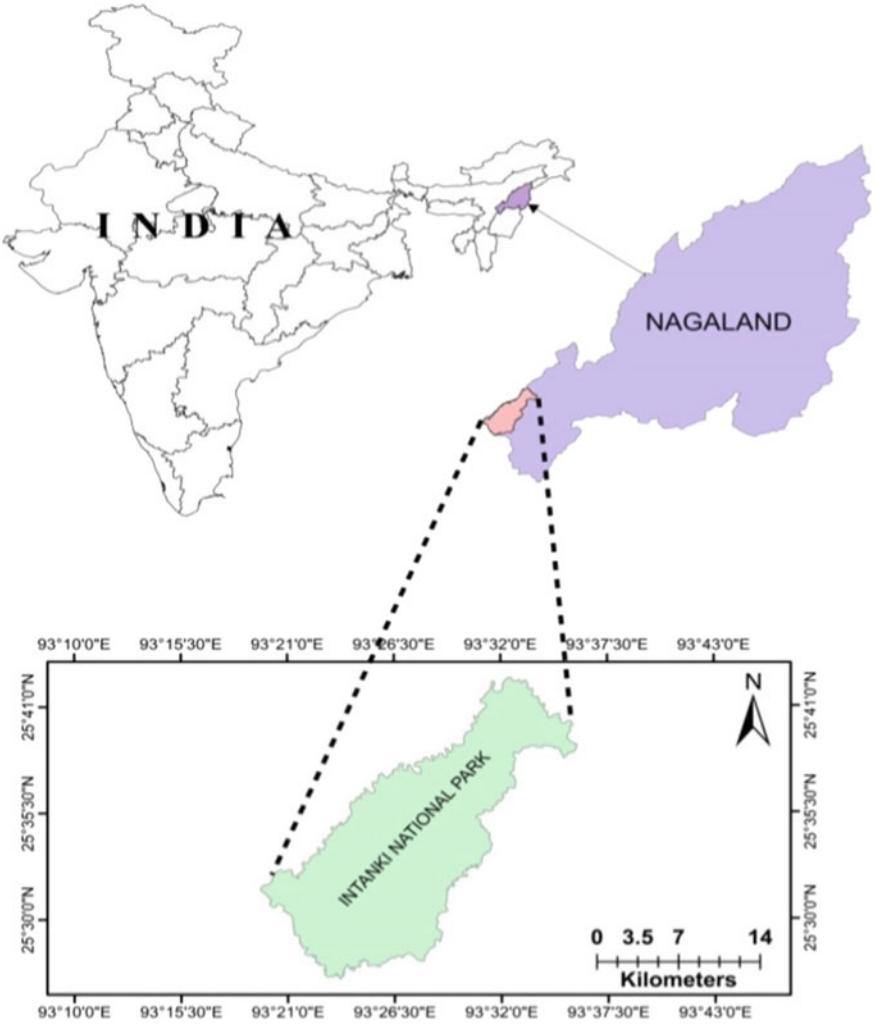

Fig. 19.1 Location of study area

the diverse sun angle and the atmosphere (Singh et al. 2016; Kumar et al. 2018). The details of satellite data set have been shown in Table 19.1.

Table 19.1 Particulars of satellite data

Year	Datasets	Band	Resolution (m)	Scale
18th Jan 1999	Landsat 5	1,2,3,4	30	1:50,000
04th Feb 2017	Landsat 8	2,3,4,5	30	1:50,000

Table 19.2 Detail descriptions of LULC classes

LULC classes	Description
Open land	Contain open soil, rock, sand, agriculture field and settlements
Dense forest	Tree species with canopy over more than 40%
Open forest	Tree species with canopy over 10–40%

19.3.2 Methodology

19.3.2.1 LULC Classification of Study Area

LULC maps were prepared from the training areas by supervised classification applying the Maximum Likelihood Classifier (MLC)-based methodology. This method has been successfully used by numerous researchers (Strahler 1980; Srivastava et al. 2014; Kumar et al. 2018). Training polygons are recognized areas applied to classify the rest portion of the image (Jensen 1996). Supervised classification was carried out with ERDAS IMAGINE 10 to find out the LULC classes. As per FAO classification system (FAO 2010; 5.3), three LULC classes were set up for image classification shown in Table 19.2.

So as to decide the accuracy of the diverse classified images a stratified random sampling methodology was utilized for determination of ground control points (GCP). An aggregate of 150 ground control points were chosen. For every sample point, changes were independently evaluated. The information of change for various classified image has been determined by Survey of India topographic maps, Survey of published literature and interviews with forest officers, classified map published by NRSC and ground truth information. Accuracy assessment of both the images was executed, derived from overall accuracy, producer's accuracy, user's accuracy and Kappa coefficient (Jensen 1996).

19.3.2.2 Landscape Metric Analysis

In this analysis, landscape metrics at patch and class level were determined for the classified images using FRAGSTATS. It can calculate several (more than 100) spatial metrics for every cover up class just as for the whole landscape. Be that as it may, a considerable lot of them are exceptionally connected (McGarigal and Marks 1995; Riitters et al. 1995). Therefore, only 8 metrics were used in this study which was based on review of previous studies (Forman 1995; Riitters et al. 1995; Griffith et al. 2000; Southworthet al. 2004; Günlü et al. 2009; Midha and Mathur 2010; Kumar et al. 2018; Gabril et al. 2019). The NP, PLAND, PD, ED, LSI, IJI, MESH and LPI were selected to quantify the change of study region (Table 19.3).

Table 19.3 Metrics used at class level to measure fragmentation (McGarigal and Marks 1995; Kumar et al. 2018)

Percentage of landscape–PLAND (%)	PLAND equals the percentage the landscape comprised of the corresponding patch type
Number of patches-NP	Total number of patches in this class
Patch Density-PD (per unit per ha)	Ratio of number of patches and the area of investigated
Largest patch index LPI (ha)	Ratio of largest patch area to investigated area
Edge DensityED (m/ha)	Total length of edge involving the corresponding land use/land cover class divided by total area (ha)
Landscape shape indexLSI	Average complexity of the landscape as a whole
Interspersion-juxtaposition indexIJI	Degree of interspersion of patches of this class, with all other classes
Effective Mesh SizeMESH (ha)	Landscape Division Index expresses the probability that two randomly placed landscapes are in the same patch and the MESH corresponds to area defined by the division index; division is a probability while MESH is an area

19.4 Results and Discussion

19.4.1 Classification and Accuracy Assessment of LULC Images

The accuracy estimation of LULC maps derived from satellite imageries was shown in Table 19.4. It will in general be seen that the utmost overall classification accuracy was accomplished for 1999 image (87.50%) followed by 2017 (92.50%).

The classified maps for the year 1999 and 2017 were produced using supervised classification and are illustrated in Fig. 19.2. The LULC information for the forest classes of INP for both the years studied are given in Table 19.5. It may be seen that the total forest cover of the INP for the year 1999 constituted 95% of forest which has reduced to 84% in 2017.

It can also be seen that the area of dense forest has decreased from 17,912.3 ha to 16,838.71 ha and also the area of open forest has decreased drastically from 10,921.2 ha to 8580.52 ha. About 10% of open forest and 4% of dense forest has decreased over the last 19 years. The area of open land has increased due to human activities such as deforestation, agricultural practices, housing, fuel etc. The Increase in agriculture land is credited to ascend in human populace in light of the fact that 80%

Table 19.4 Accuracy assessment of LULC

Years	Overall accuracy (%)	Kappa coefficient
1999	87.50	0.83
2017	92.50	0.90

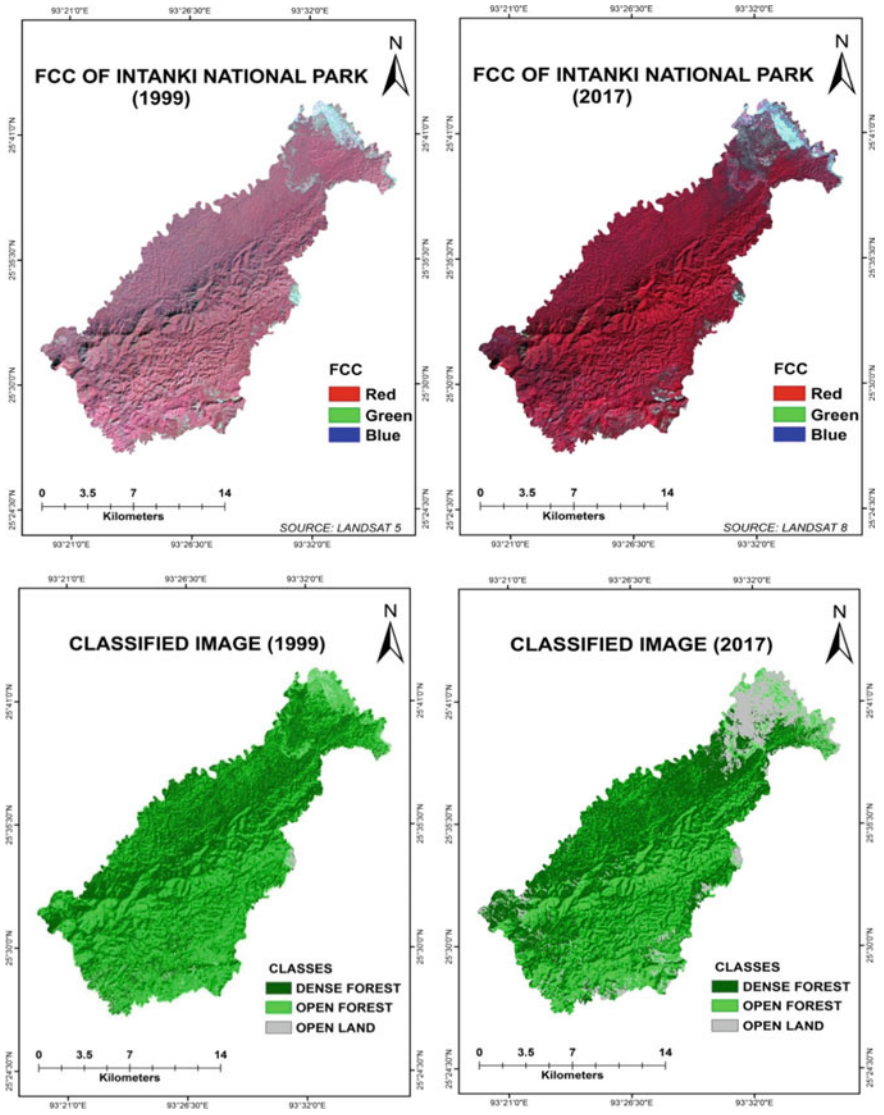

Fig. 19.2 False color composite (FCC) and classified images (1999 and 2017)

of the number of inhabitants in the area despite everything relies upon agribusiness and related enterprises for monetary turn of events and food. The area has increased double its amount from 1324.9 ha to 4739.2 ha, i.e. it has exponentially increased by over 10% during the last 19 years. Several patches have appeared in the southern part of the National Park while the north-eastern region has lost majority of its forest.

Table 19.5 Area statistics of different LULC classes (1999 and 2017)

Class	1999		2017	
	Area (ha)	% Area	Area(ha)	% Area
Dense forest	17,912.3	59.39	16,838.71	55.83
Open forest	10,921.2	36.21	8580.52	28.45
Open land (settlement/barren land/agriculture)	1324.89	4.39	4739.16	15.71
Total	30,158.39	100	30,158.39	100

Table 19.6 Landscape metrics of class level

Date	Class Type	PLAND	NP	PD	ED	LSI	IJI	MESH	LPI
1999	Dense forest	25.54	149	0.18	16.07	22.33	36.29	4644.40	24.23
1999	Open forest	11.65	480	0.60	16.12	33.61	37.61	44.00	1.44
1999	Barren land/settlement	0.79	131	0.16	1.66	13.01	83.38	0.27	0.12
2017	Dense forest	23.85	152	0.19	13.86	19.94	67.94	3807.84	21.94
2017	Open forest	8.56	419	0.53	12.26	29.42	49.69	22.73	1.04
2017	Barren land/settlement	5.60	193	0.24	5.03	14.95	87.35	1.10	3.71

19.4.2 Fragmentation and Landscape Metrics

Forests of the region changed gradually in 1999 to 2017 in terms of landscape fragmentation. As need be, it is pivotal to comprehend the example of forest transformations. The landscape metrics-based study of the two years by LULC classes gave information with respect to how patterns of forest cover altered with time. It has been seen that the number of patches (NP) for dense forest increase during 1999 to 2017 (Table 19.6). The quantity of patches is a superior index of fragmentation: as the region of the landscape is stable, further patches equate to additional fragmentation. The percentage of land (PLAND) of dense and open forest decreased while the barren and settlements has increased from 0.799 to 5.60. The largest patch index (LPI) of dense forest has diminished from 24.23 to 21.94 and the barren and settlement land increased from 0.12 to 3.71 while there were little changes in open forest.

19.5 Conclusion

Spatio-temporal LULC changes along with landscape fragmentation in the INP were examined over a period of 18 years. The outcomes show that supervised classification can be utilized to create satisfactory classified maps. FRAGSTATS study indicated that landscape has been increasingly fragmented in considered period. Analysis of the result exhibited that changes occur in dense as well as open forest throughout the studied period. Since 1999 there was an increase in settlement and barren land

due to deforestation for agricultural practices resulting in increased fragmentation of forest cover. The dense forest in the western region of INP flourished while the north region forest cover was declined in 2017. Investigation of the metrics described that landscape formation in study zone had changed significantly over the 18 year study period, ensuing in fragmentation of the landscape as showed through the huge patch numbers and the littler patch sizes because of substantial timber deduction, illicit cutting and out of control stand treatments. Hence, the outcome of this study will be valuable to the forest maintenance officers/forest executives, wildlife conservators to comprehend the landscape pattern of the study area.

Acknowledgements Authors affirm their earnest gratitude to USGS (http://www.usgs.gov/) for making available of satellite datasets and FRAGSTATS developer for accomplish this study.

References

Ashish D, Hoogenboom G, McClendon RW (2004) Land-use classification of gray-scale aerial images using artificial neural networks. Transactions of the ASAE 47:1813–1819

Bell M, Walker MJC (2005) Late quaternary environmental change: physical and human perspectives. Routledge, 2nd Edition. pp. 368

BotequilhaLeitão A, Miller J, Ahern J, McGarigal K (2006) Measuring landscapes. Island, Washington, DC

BotequilhaLeitáo L, Ahern J (2002) Applying landscape ecological concepts and metrics in sustainable landscape planning. Landsc Urban Plan 59:65–93

Brown DG, Duh JD, Drzyzga SA (2000) Estimating error in an analysis of forest fragmentation change using North American Landscape Characterization (NALC) data. Remote Sens Environ 71:106–117

Cumming S, Vernier P (2002) Statistical models of landscape pattern metrics, with applications to regional scale dynamic forest simulations. Landsc Ecol 17:433–444

Cushman SA, McGarigal K, Neel MC (2008) Parsimony in landscape metrics: Strength, universality, and consistency. Ecol Indicat 8:691–703

De Groot R (2006) Function-analysis and valuation as a tool to assess land use conflicts in planning for sustainable, multi-functional landscapes. Landsc Urban Plan 75:175–186

The Food and Agriculture Organization (FAO) of the United Nations (2010) Global Forest Resources Assessment 2010. Main report 1-378

Fischer J, Lindenmayer DB (2007) Landscape modification and habitat fragmentation: a synthesis. Global Ecol Biogeog 16:265–280

Forman RT (1995) Some general principles of landscape and regional ecology. Landsc Ecol 10:133–142

Gabril EMA, Denis DM, Nath S, Paul A, Kumar M (2019) Quantifying LULC change and landscape fragmentation in Prayagraj district, India using geospatial techniques. Pharm Innov J 8:670–675

Goparaju L, Tripathi A, Jha CS (2005) Forest fragmentation impacts on phytodiversity-An analysis using remote sensing and GIS. Curr Sci 88:1264–1274

Griffith JA, Mantinko EA, Price KP (2000) Landscape structure analysis of Kansas at three scales.Landsc Urban Plan 52:45–61

Günlü A, Kadıoğulları AI, Keleş S, Başkent EZ (2009) Spatiotemporal changes of landscape pattern in response to deforestation in Northeastern Turkey: a case study in Rize. Environ Monit Assess 148:127–137

Hanski I (2005) Landscape fragmentation, biodiversity loss and the societal response. EMBO Rep 6:388–392
Jensen JR (1996) Introductory Digital Image Processing: A Remote Sensing Perspective. Prentice Hall, pp. 316
Kumar M, Denis DM, Singh SK, Szabó S, Suryavanshi S (2018) Landscape metrics for assessment of land cover change and fragmentation of a heterogeneous watershed. Remote Sens Appl Soc Environ 10:224–233
Laurance WF (2000) Mega-development trends in the Amazon: implications for global change. Environ Monit Assess 61:113–122
Li H, Wu J (2004) Use and misuse of landscape indices. Landsc Ecol 19:389–399
Li X, Lu L, Cheng G, Xiao H (2000) Quantifying landscape structure of the Heihe River Basin, north-west China using FRAGSTAT. J Arid Environ 48:521–535
Matsushita B, Xu M, Fukushima T (2006) Characterizing the changes in landscape structure in the Lake Kasumigaura, Japan using a high-quality GIS dataset. Landsc Urban Plan 78:241–250
McGarigal K, Marks BJ (1995) Spatial pattern analysis program for quantifying landscape structure. General Technical Report PNW-GTR-351 US Department of Agriculture, Forest Service, Pacific Northwest Research Station.pp 122
McGarigal K, Cushman SA, Neel MC, Ene E (2002) FRAGSTATS: spatial pattern analysis program for categorical maps. Amherst: Computer software program produced by the authors at the University of Massachusetts. Available from http://www.umass.edu/landeco/research/fragstats/fragstats.html
Midha N, Mathur PK (2010) Assessment of forest fragmentation in the conservation priority Dudhwa landscape, India using FRAGSTATS computed class level metrics. J India Soc Remote Sens 38:487–500
Olsen LM, Dale VH, Foster T (2006) Landscape patterns as indicators of ecological change at Fort Benning, Georgia, USA. Landsc Urban Plan 79:137–149
Reed RA, Johnson-Barnard J, Baker WL (1996) Fragmentation of a forested Rocky Mountain landscape 1950–1993. Biol Conserv 75:267–277
Riitters KH, O'Neill RVO, Hunsaker CT, Wickham JD, Yankee DH, Timmins SP, Jones KB, Jackson BL (1995) A factor analysis of landscape pattern and structure metrics. Landsc Ecol 10:23–39
Singh SK, Srivastava PK, Szabo S, Petropoulos GP, Gupta M, Islam T (2016) Landscape transform and spatial metrics for mapping spatiotemporal land cover dynamics using earth observation data-sets. GeocartoInt 32:113–127
Southworth J, Munroeb D, Nagendra H (2004) Land cover change and landscape fragmentation comparing the utility of continuous and discrete analyses for a western Honduras region. Agricul Ecosyst Environ 101:185–205
Srivastava PK, Mukherjee S, Gupta M, Islam T (2014) Remote sensing applications in environmental research. (Eds) Switzerland: Springer Verlag, pp. 212
Strahler AH (1980) The use of prior probabilities in maximum likelihood classification of remotely sensed data. Remote Sens Environ 10:135–163
Tang J, Wang L, Yao Z (2006) Analyzing urban sprawl spatial fragmentation using multi-temporal satellite images. Gisci Remote Sens 43:218–232
Thapa GJ, Wikramanayake E, Jnawali SR, Oglethorpe J, Adhikari R (2016) Assessing climate change impacts on forest ecosystems for landscape-scale spatial planning in Nepal. Curr Sci 110:345–352
Wu J (2008) Landscape ecology. In: Jorgensen SE (ed) Encyclopedia of Ecology. Elsevier, Oxford, p 2780
Wu J, Hobbs R (2007) (Eds.) Key Topics in Landscape Ecology. University Press, Cambridge. pp. 297

Chapter 20
Impact of Sprawl on Development Pattern of Bengaluru City

Vivekananda Biswas, Dinesh Kumar Tripathi, and Manish Kumar

Abstract Using multi-temporal satellite imagery, the present study illustrates the Spatio-temporal dynamics of sprawl and its impact on Bengaluru City of Karnataka, India. Urban sprawl is the uncontrolled and uncoordinated outgrowth of towns and cities. The process of urban sprawl can be described by a change in the pattern over time, like a proportional increase in built-up surface to population leading to rapid urban spatial expansion. Landsat satellite imageries of five different periods, i.e., Landsat MSS of 1973, TM of 1991, 2001, 2011, and 2016 from Global Land Cover Facility (GLCF), quantify the changes in the Bengaluru town from over 40 years. Supervised Classification methodology has been employed using the Maximum Likelihood Technique in ERDAS 9.3. The study area images were categorised into five different classes, viz. built-up area, vegetation, agricultural land, water bodies, and sand bar. The results indicate that during the last four decades, the Bengaluru town area's built-up area and the vacant area increased. The paper also highlights the importance of digital change detection techniques and calculates urban sprawl's impact on proper land use planning for sustainable development.

Keywords Land use/Land cover · Spatio-temporal · Multi-temporal satellite imagery · Remote sensing

V. Biswas (✉)
Department of Urban Land Development and Management, Ethiopian Civil Service University (ECSU), Addis Ababa, Ethiopia

D. K. Tripathi
Rana Pratap Post Graduate College, Sultanpur 228001, UP, India

M. Kumar
Department of Geography, School of Basic Sciences, Central University of Haryana, Mahendergarh 123031, Haryana, India
e-mail: manish.ks@cuh.ac.in

R. B. Singh et al. (eds.), *Remote Sensing and Geographic Information Systems for Policy Decision Support*, Advances in Geographical and Environmental Sciences,
https://doi.org/10.1007/978-981-16-7731-1_20

20.1 Introduction

The potential urban population growth in developed countries would be relatively moderate since population growth rates in these developed countries are low and over 80% of their population already constitutes urban population. Developing economies, on the other hand, are in the midst of transition, with the fastest growth rates. The development away from primary sector employment, high overall population growth, and growing urbanisation rates all contribute to the unusual growth of many urban agglomerations in a number of developing countries (Grubler 1994).

Urban development, which grows according to dwelling, industry, and business sectors, extends beyond city limits, causing the occupation of agricultural lands and forests, in tandem with the rapid rise in population. Urban sprawl is known as uncontrolled and unplanned growth as a result of urban development (Zhang 2004; Sudhira and Ramachandra 2007). Urban sprawl, which is apparently desired for urban growth, is not suitable for either urban development or the rural setting. In other words, urbanisation which is carried out in an unorganised and unregulated manner tends to have negative consequences that hamper regional long-term development (Bhatta 2010: 8). After the 1960s, many cities around the world, especially in metropolitan areas, saw urban development and sprawl as major issues (Squires 2002; Pengiun 2011).

The regions of urban sprawl, which are characterised as regions that have lost their rural characteristics but cannot be classified as urban, contain unique uncertainties that result in a variety of problems such as unplanned urban growth and non-agricultural use. As a result, a hinterland between rural and urban areas can be described as urban sprawl. Urban sprawl is defined by Gordon and Richardson (1997) as leapfrog development1, while DiLorenzo (2000) defines it as cancer or virus formation. Wilson et al. (2003) and Galster et al. (2001) argue that explaining rather than identifying would be more appropriate in defining urban sprawl. Global socio-economic forces combine with local environmental and spatial constraints to produce general characteristics of urban sprawl in Europe. Transportation, land prices, personal choice of dwelling, demographic patterns, cultural traditions and constraints, the increasing appeal of the and practises of local and regional land utilisation policies are examples of socio-economic forces at the macro and mid-levels. Regardless of this interaction, urban sprawl continues to build transport infrastructure rapidly and increases personal mobility (EEA 2006).

In second-world countries, the greatest challenge for science, engineering, and technology in the twenty-first century is to provide basic amenities such as adequate housing, sanitation and health, and transportation services in a habitable urban climate. One of the possible obstacles to such construction is sprawl.

Along these routes, a considerable amount of upsurge could eventually be seen. In most parts of India, this type of expansion caused by a road network between urban, semi-urban, and rural centres is very common and permanent. Since planners are unable to envision this form of development trend, these areas are devoid of infrastructure. Since this increase cannot be classified under either urban or rural

centres, it is generally left out of all government surveys (including national population censuses). The investigation of such development trends is critical from the perspective of regional planning in order to provide basic services in these areas.

This investigation gains prominence and significance as a result of the Prime Minister of India's pet project, the "Golden Quadrilateral of National Highways Development Project," which aims to connect villages, towns, and cities by building four-lane roads. The planning machinery will plan for suitable infrastructure facilities before visualising the trends and patterns of development (water, electricity, sanitation, etc.). This type of research exposes the type, scale, and nature of sprawl in a given area, as well as the factors that contribute to it. Developers and town planners will be able to predict development trends and promote different infrastructure facilities with this information. An attempt is made in this direction to understand the sprawl trend, measure sprawl along roads in terms of Shannon's entropy, and project the rate of change in the built-up region over a span of nearly three decades using spatial and statistical data from GIS. To increase the effect of urban sprawl order, only a few research studies have been conducted. The findings of the study would help in determining the feasibility of regulating urban sprawl. Examine the effect of sprawl on urban planning and the master plan's implications.

20.2 Study Area

Bengaluru is the state of Karnataka's political, cultural, commercial, manufacturing, and knowledge capital. Bengaluru was notified (established) in December 2006, covering 741 km^2 and agglomerating the district, neighbouring municipal councils, and outgrowths.

Throughout the year, the city has a nice and healthy atmosphere. It is known as India's "Garden City" because of its tree-lined streets, numerous parks, and abundance of greenery. Bengaluru has shown a ray of hope in the field of technological advancement and thus it is also conferred with the title of Silicon Valley of India, and in fact, it is one of the country's technical innovation centres, scoring 13 out of a possible 164 points (United Nations Development Programme 2001) as shown in Fig. 20.1.

Bangalore is nearly equidistant from the eastern and western coasts of the South Indian peninsula, at 12° 59′ north latitude and 77° 57′ east longitude. It is located at a height of 920 m above sea level. In the last ten years, the average annual cumulative rainfall has been about 880 mm, with around 60 rainy days per year. Summer temperatures vary from 18 to 38 °C, while winter temperatures range from 12 to 25 °C. As a result, Bangalore has a pleasant climate throughout the year.

Hebbal, Koramangala, Challaghatta, and Vrishabhavathi are the four watersheds that Bangalore is situated on. Because of the region's undulating terrain, several tanks have been built to provide for conventional irrigation and drinking needs.

Increased vehicular traffic (see section on Infrastructure in the Urban Agenda) has resulted into an increase in the discharge of suspended particulate matter (SPM)

Fig. 20.1 Study area map

and oxides of carbon, nitrogen, and sulphur into the atmosphere in recent years. The urban heat island effect has been caused by air pollution and reduced tree cover, resulting in temperature fluctuations and unexpected showers in the late afternoons.

20.2.1 Major Suburbs Centre in the Study Area Bengaluru

20.2.1.1 Yelanhanka

Yelanhanka is located on Bengaluru's northern side. With a population of 2.87 lakhs, the total area is 38.7 km^2. In the last five years, there has been a lot of development.

20.2.1.2 Kengeri

Kengeri is located on Bengaluru's northwestern outskirts. The city has a total area of 62 km^2 and a population of 5.54 lakhs. Contribute to the economy of the city.

20.2.1.3 Electronics City

Bengaluru's electronic city is located on the city's southern outskirts. The total area is 36 km^2, with a population of 2.1 lakhs. I.T. hubs and industries are well-known.

20.2.1.4 White Field

It is situated on Bengaluru's eastern outskirts. The total area is 38 km^2, and the population is 2.2 lakhs. I.T. is well-known. There are 86 I.T. firms and 24 others with a total of 90,000 workers.

20.3 Objectives

The main objectives of the present paper are

- To evaluate the concept of urban sprawl and its characteristics.
- To assess the urban trends in the study area.
- To determine impact of urban sprawl on growth in terms of land consumption, land use reform, infrastructure, and the environment.
- To formulate planning strategies for mitigating the impact of sprawl on development.

20.4 Methodology

Effective land use/land cover classification is one of the prerequisites for understanding land use/land cover dynamics. In order to land use/land cover classification and change detection, Landsat satellite data (Multispectral Scanner System-MSS and Thematic Mapper-TM) for the year 1972 1991, 2001, 2011, and 2016 were acquired by Global Land Cover Facility (GLCF) at 60 and 30 m resolution. All acquired images became 30 m spatial resolution after applying resolution merge operation to satellite image of 1972. To better understand the process of land use/land cover change over the last four decades (1973–2016), change detection and urban sprawl area, as well as change matrix[9] extracted through the images. With the help of these multi-temporal imageries, the growth of urban sprawl and magnitude of change were analysed in the ERDAS Imagine 2014, ENVI 4.3, and ArcGIS 10.3 remote sensing and GIS packages. Firstly, different bands of the imagery were stacked to produce a false-colour composite and the area of interest was extracted from the image through the image sub-setting process. To detect and analyse the land use/land cover categories, digital image classification was performed through Supervised Classification process using Maximum Likelihood Algorithm incorporating field training data and image characteristics. The land use/land cover categories of built-up area, vegetation

cover, agricultural land, vacant land, and water bodies were extracted. Further, all categories of land use/ land cover and selected parameters were analysed in GIS environment to formulate the planning strategies and recommendations.

20.5 Results and Discussions

20.5.1 Land Use/Land Cover Pattern

To understand land use/land cover pattern of the study area, satellite remote sensing data of Landsat MSS of 1973, TM of 1991, 2001, 2011, and 2016 were used. The results obtained through the analysis of multi-temporal satellite imageries amd same images were used to required maps and statistics were generated (Figs. 20.2a, b, 20.3a, b, c; Tables 20.1, 20.2, 20.3 and 20.4) Five categories of land use/land cover were identified in the study area viz. (i) built-up (ii) vegetation (iii) agriculture (iv) vacant land and (v) water body.

In the year 1973, 1.93% (5012.28 ha) under built-up area, 46.61% (120866.2 ha) under vegetation, 41.12% (106,631 ha) under agricultural land, 3.80% (9864.99 ha) under vacant land, and 6.53% (16926.75 ha) under water body during the year 1973 (Fig. 20.2a).

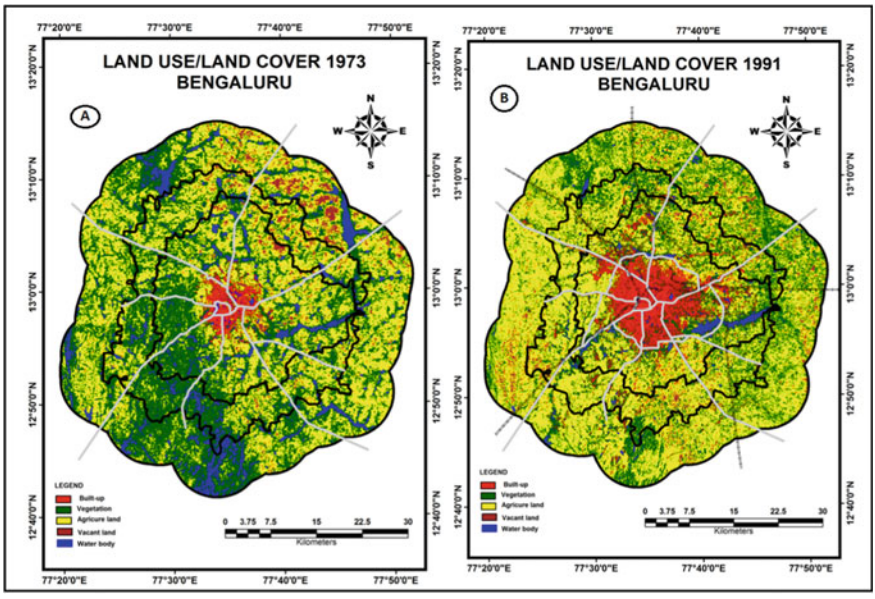

Fig. 20.2 **a**, **b** Land use/land cover status of the town area—1973 and 1991 (Based on land sat thematic mapper satellite imagery)

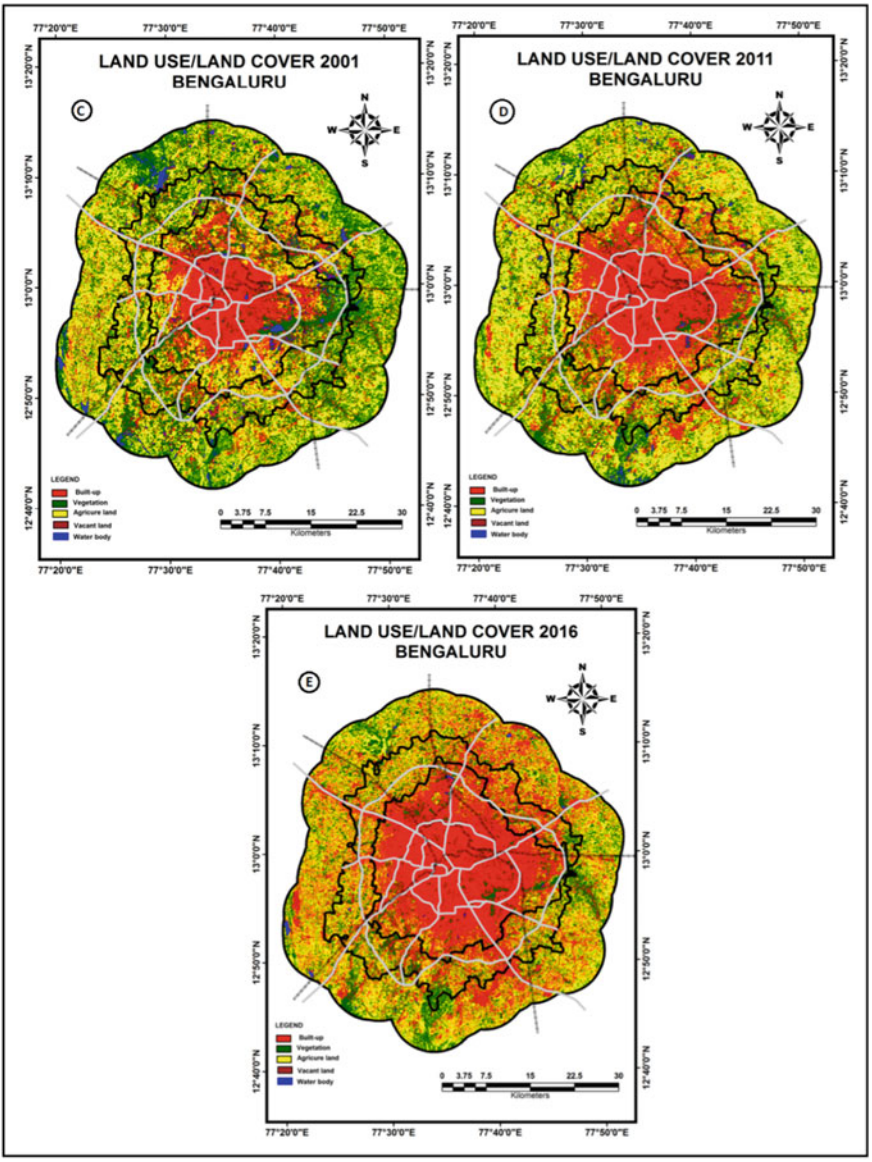

Fig. 20.3 **a**, **b**, **c** Land use/land cover status of the town area—in 1973 and 1991 (Based on land sat thematic mapper satellite imagery)

Table 20.1 Area of LU/LC categories in the sprawling area in 1973 and 1991

Land use/land cover categories	1973		1991		Change 1973–1991	
	Ha	%	Ha	%	Ha	%
Built-up area	5012.28	1.93	22958.91	8.87	17946.63	6.94
Vegetation	120866.2	46.61	85861.71	33.16	−35004.5	−13.45
Agricultural land	106,631	41.12	136872.36	52.85	30241.36	11.73
Vacant land	9864.99	3.80	8409.33	3.25	−1455.66	−0.55
Water body	16926.75	6.53	4861.8	1.88	−12,065	−4.65
Total	259301.3	100	258964.11	100	259301.3	0.00

Table 20.2 Area of LU/LC categories in the sprawling area in 1991 and 2001

Land use/land cover categories	1991		2001		Change 1991–2001	
	Ha	%	Ha	%	Ha	%
Built-up area	22958.91	8.87	53437.05	20.63	30478.14	11.76
Vegetation	85861.71	33.16	91331.73	35.27	5470.02	2.11
Agricultural land	13872.36	52.85	103789.1	40.08	−33083.3	−12.77
Vacant land	8409.33	3.25	5999.13	2.32	−2410.2	−0.93
Water body	4861.8	1.88	4407.12	1.70	−454.68	−0.18
Total	258964.11	100	258964.1	100	30478.14	0.00

Table 20.3 Area of LU/LC categories in the sprawling area in 2001 and 2011

Land use/land cover categories	2001		2011		Change 2001–2011	
	Ha	%	Ha	%	Ha	%
Built-up area	53437.05	20.63	75849.57	29.29	−22412.5	−8.66
Vegetation	91331.73	35.27	65196.99	25.18	26134.74	10.09
Agricultural land	103789.1	40.08	11021.6	43.64	−9232.5	−3.56
Vacant land	5999.13	2.32	2481.75	0.96	3517.38	1.36
Water body	4407.12	1.70	2414.16	0.93	1992.96	0.77
Total	258964.11	100	258964.11	100	0.00	0.00

Table 20.4 Area of LU/LC categories in the sprawling area in 2011 and 2016

Land use/land cover categories	2011		2016		Change 2011–2016	
	Ha	%	Ha	%	Ha	%
Built-up area	75849.57	29.29	107872.8	41.68	−32023.2	−12.39
Vegetation	65196.99	25.18	48410.21	18.70	16786.78	6.48
Agricultural land	113021.6	43.64	93060.16	35.96	19961.44	7.68
Vacant land	2481.75	0.96	8798.715	3.40	−6316.97	-2.44
Water body	2414.16	0.93	676.2375	0.26	1737.923	0.67
Total	258964.11	100	258964.11	100	0.00	0.00

During 1991, the sprawl area under these land categories was found 8.87%(22958.91 Ha) under built-up area, 33.16% (85861.71 Ha) under vegetation, 52.85% (136872.36 Ha) under agricultural land, 3.25% (8409.33 Ha) under vacant land, and 1.88% (4861.8 Ha) under water body (Fig. 20.2b).

During 2001, the sprawling area under these land categories was found 20.63% (53437.05 Ha) under the built-up area, 35.27% (91331.73 Ha) under vegetation, and 40.08% (103789.1 Ha) under agricultural land, 2.32% (5999.13 Ha) under vacant land, and 1.70% (4407.12 Ha) underwater body (Fig. 20.3a).

During 2011, the sprawl area under these land categories was found 29.29% (75849.57 Ha) under built-up area, 25.18% (65196.99 Ha) under vegetation, 43.64% (113021.6 Ha) under agricultural land, 0.96% (2481.75 Ha) under vacant land, and 0.93% (2414.16 Ha) under water body (Fig. 20.3b).

During 2016, the sprawl area under these land categories was found 41.68% (107872.8 Ha) under built-up area, 18.70% (48410.21 Ha) under vegetation, 35.96% (93060.16 Ha) under agricultural land, 3.40% (8798.715 Ha) under vacant land, and 0.26% (676.2375 Ha) under water body (Fig. 20.3c).

20.5.2 Trends of Land Conversion to Built-Up Area

To accumulate the land encroachment and land use/land cover change, a land use/land cover matrix was prepared. The land use matrix of the town area is registered in Table 21.5–21.8, and the change maps are presented in Figs. 21.4–21.7. Table 20.5 and Fig. 20.4 reveal described the conversion of other land use to built-up from 1973 to 1991. 6.89% of vegetation has converted into built-up, 7.05% agricultural land, 7.15% vacant land, and 8.4% of water body have also converted to the built-up area. From 1973 to 1991, the maximum amount of water body has decreased because of dumping and illegal construction in Bengaluru.

To understand the land encroachment and land use/land cover change, a land use/land cover matrix was prepared. The land use matrix of town area is registered in Table 21.6, and the change maps are presented in Fig. 20.5 reveal that: Table 20.6 and

Table 20.5 Land use/Land cover change matrix showing land encroachment under the different categories of land (in %) in Bengaluru sprawl area from 1973 to 1991

Land use/land cover categories		The year 1973					Total area in (Ha) 2001
The year 1991	Built-up area	100	6.89	7.05	7.15	8.4	22958.91
	Vegetation	0	37.55	27.42	29.08	50.16	85,862
	Agricultural land	0	52.86	59.89	45.56	28.35	136,872
	Vacant Land	0	0.93	4.98	17.31	1.64	8409
	Water body	0	1.77	0.66	0.9	11.46	4862
	Class total	100	100	100	100	100	258,964

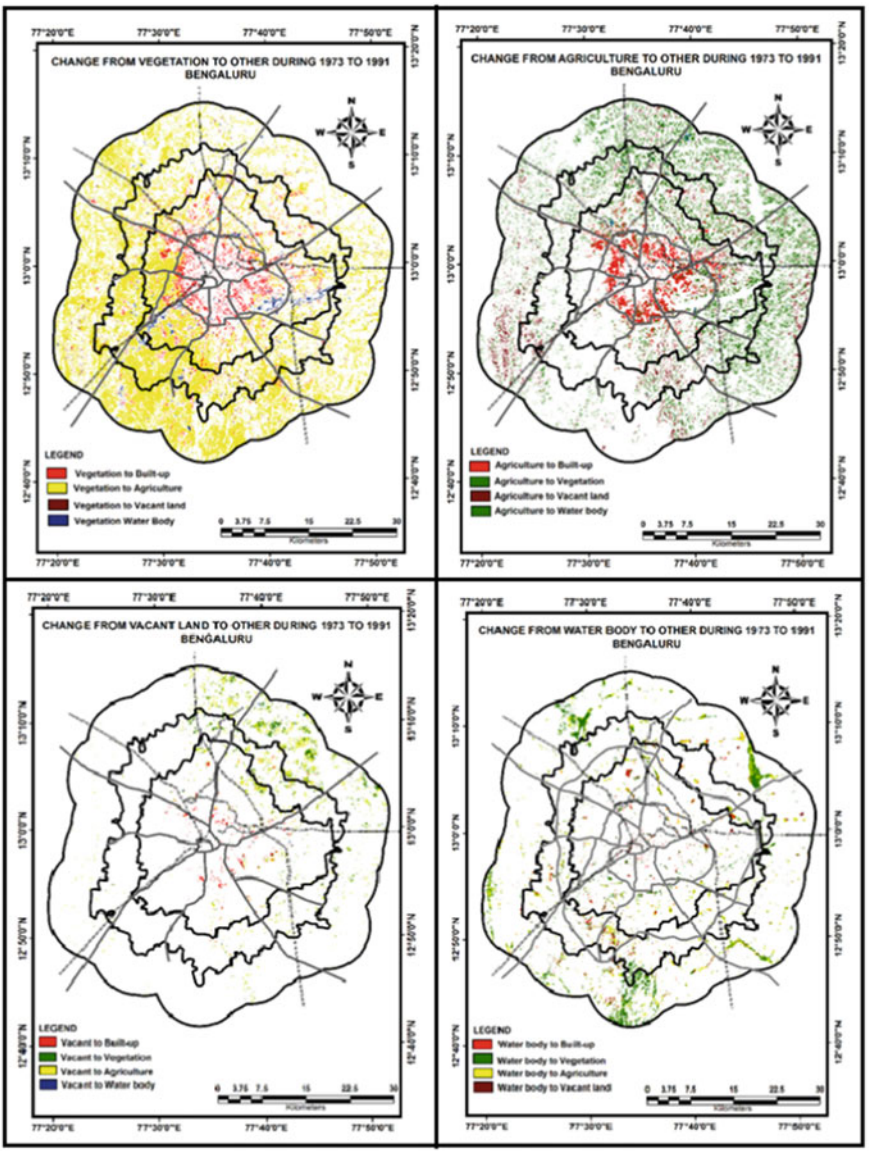

Fig. 20.4 Land use/land cover change matrix map showing land encroachment under the different land categories in the Bengaluru sprawl area from 1971 to 1991

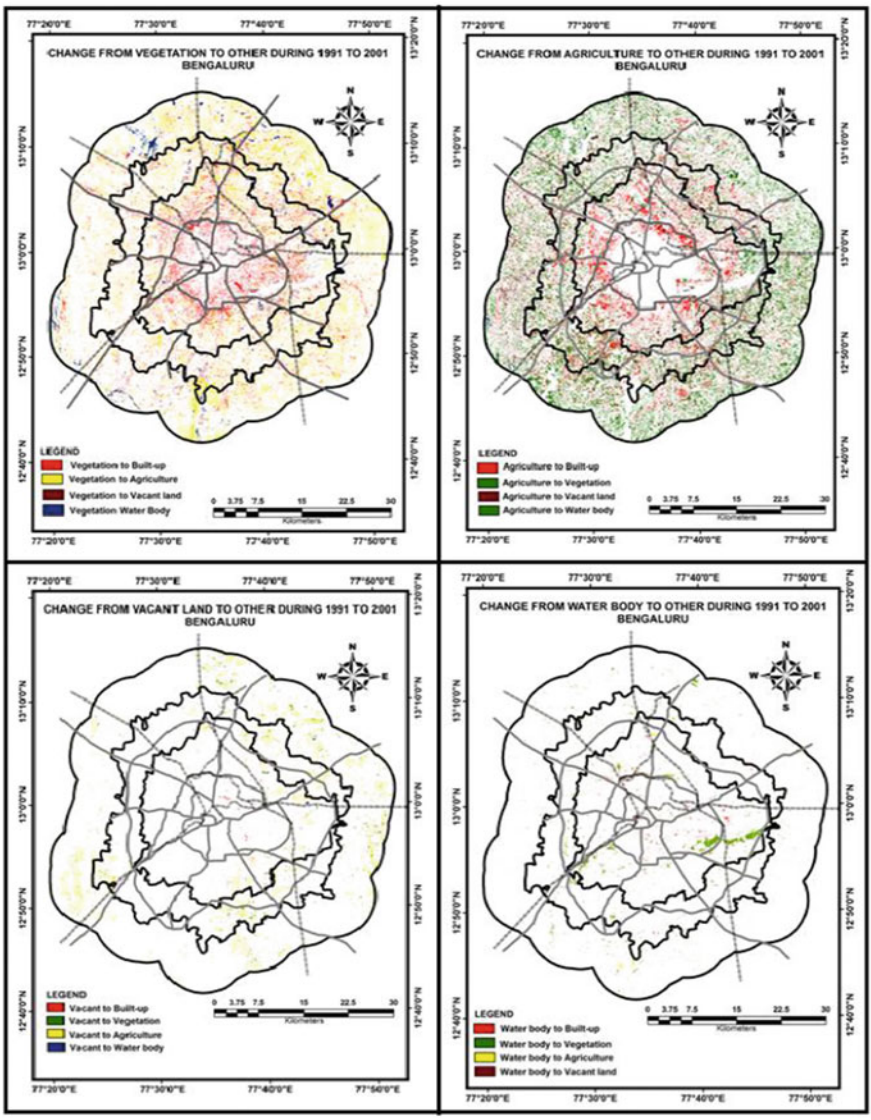

Fig. 20.5 Land use/Land cover change matrix map showing land encroachment under the different land categories in the Bengaluru sprawl area from 1991 to 2001

Fig. 20.5 have described the conversion of other land use to built-up from 1991 to 2001. There, 15.82% of vegetation has converted into built-up, 11.55% agricultural land, 4.03% vacant land, and 15.29% of water bodies have also converted to built-up areas. From 1973 to 1990, the maximum amount of vegetation and water body has decreased because of dumping and illegal construction in Bengaluru.

Table 20.6 Land use/Land cover change matrix showing land encroachment under the different categories of land (in %) in Bengaluru sprawl area from 1991 to 2001

Land use/land cover categories		The year 1991					Total area in (Ha) 2001
The year 2001	Built-up area	100	15.82	11.55	4.03	15.29	53,437
	Vegetation	0	57.61	27.79	10.75	60.33	91,332
	Agricultural land	0	23.2	57.59	55.2	8.28	103,789
	Vacant Land	0	0.37	2.32	29.59	0.19	5999
	Water body	0	3	0.75	0.42	15.9	4407
	Class total	100	100	100	100	100	258,964

Table 20.7 Land use/Land cover change matrix showing land encroachment under the different categories of land (in %) in Bengaluru sprawl area from 2001 to 2011

Land use/land cover categories		The year 2001					Total area in (Ha) 2011
The year 2011	Built-up area	100	8.8	12.32	9.26	23.36	75,850
	Vegetation	0	49.61	17.27	4.64	38.25	65,197
	Agricultural land	0	39.41	68.51	75.51	31.65	113,022
	Vacant Land	0	0.6	1.23	10.49	0.63	2482
	Water body	0	1.58	0.67	0.1	6.12	2414
	Class total	100	100	100	100	100	258,964

Table 20.7 and Fig. 20.6 have described the conversion of other land use to built-up from 2001 to 2011. 8.8% of vegetation has converted into built-up, 12.32% agricultural land, 9.26% vacant land, and 23.36% of the water body have also converted to a built-up area. From 2001 to 2011, the maximum amount of water and agricultural land has decreased because of dumping and illegal construction in Bengaluru.

Table 20.8 and Fig. 20.7 have described the conversion of other land use to built-up from 2011 to 2016. Where there 9.26% of vegetation has converted into built-up, 22.28% agricultural land, 26.15% vacant land, and 7.76% of water body have also converted to the built-up area. From 2011 to 2016, the maximum amount of vacant land and agricultural land has decreased because of Bengaluru's construction.

20.5.3 Potential and Strategies

20.5.3.1 Land Use

Land use strategies are the same for the five zones because the conversion of crop and vegetation land occurs in all the zones.

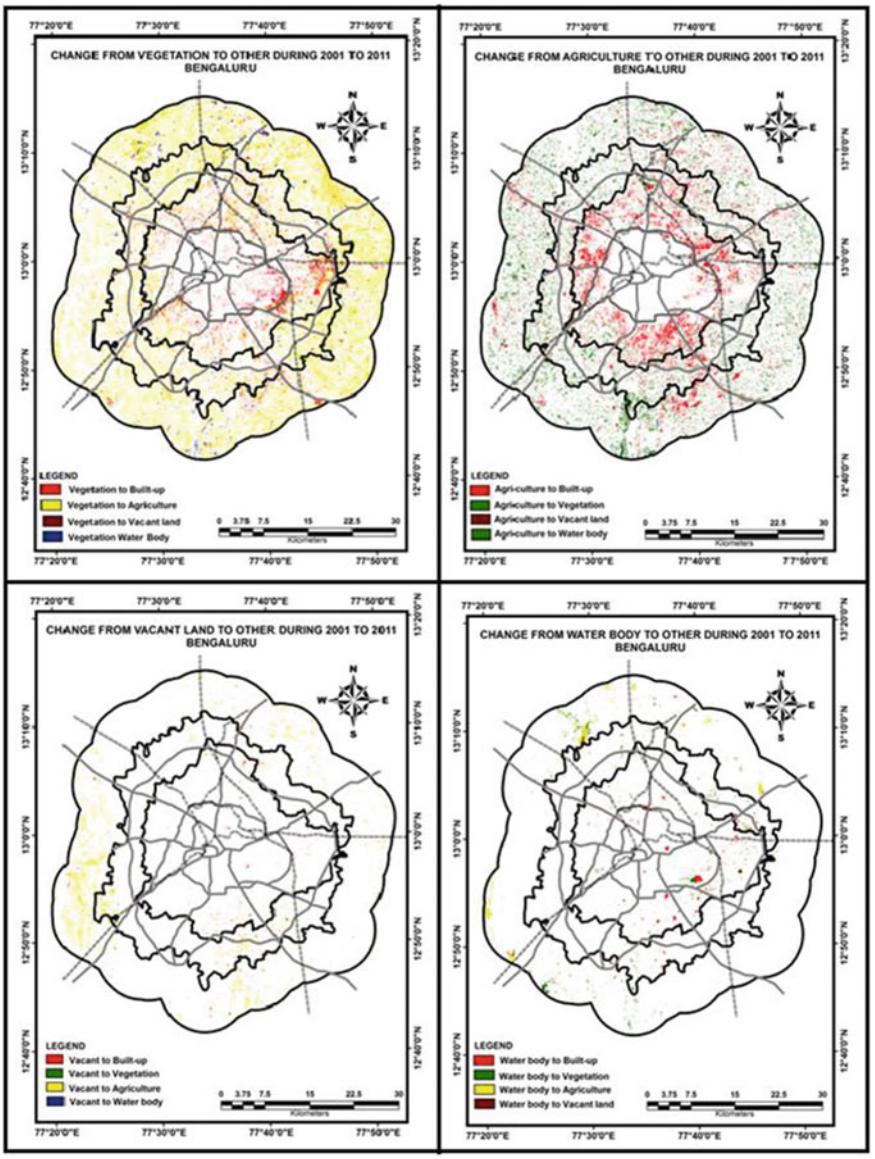

Fig. 20.6 Land use/Land cover change matrix map showing land encroachment under the different categories of land in Bengaluru sprawl area from 2001 to 2011

Table 20.8 Land use/Land cover change matrix showing land encroachment under the different categories of land (in %) in Bengaluru sprawl area from 2011 to 2016

Land use/land cover categories		The year 2011					Total area in (Ha) 2016
The year 2016	Built-up area	100	9.26	22.28	26.15	7.76	107,873
	Vegetation	0	52.41	11.41	1.26	56.09	48,410
	Agricultural land	0	36.15	60.39	19.48	34.21	93,060
	Vacant land	0	1.79	5.57	52.42	1.75	8799
	Water body	0	0.39	0.35	0.69	0.19	676
	Class total	100	100	100	100	100	258,818

20.5.3.2 Monitoring Land Use

There should be proper land use monitoring because the fertile cropland is converting to the built-up area. Vegetation is also transforming into a built-up area that should be appropriate to check by the authority. The fertile land, water body, and vegetation area should be conserved.

20.5.3.3 Development Plan

There should be a proper development plan for every zone. The sole authority should be the Bangalore Development Authority (BDA).

20.5.3.4 Protect Biodiversity

The waterbody is decreasing abruptly, and the natural forest is also degrading. So, there should be a provision to declare such an area into protected or reserved space. The sole authority should be BDA.

20.5.3.5 Environment

The central potentials are low local solid waste generation facility to rainwater harvesting for storing rainwater. There are many spaces for planting trees to control air pollution. The main strategies are the existing dense forest should be kept in a protected forest area. Arrange eco-awareness programmes in the sprawling site. A rainwater harvesting system should have in every house to preserve rainwater. There should be community participation because they face.

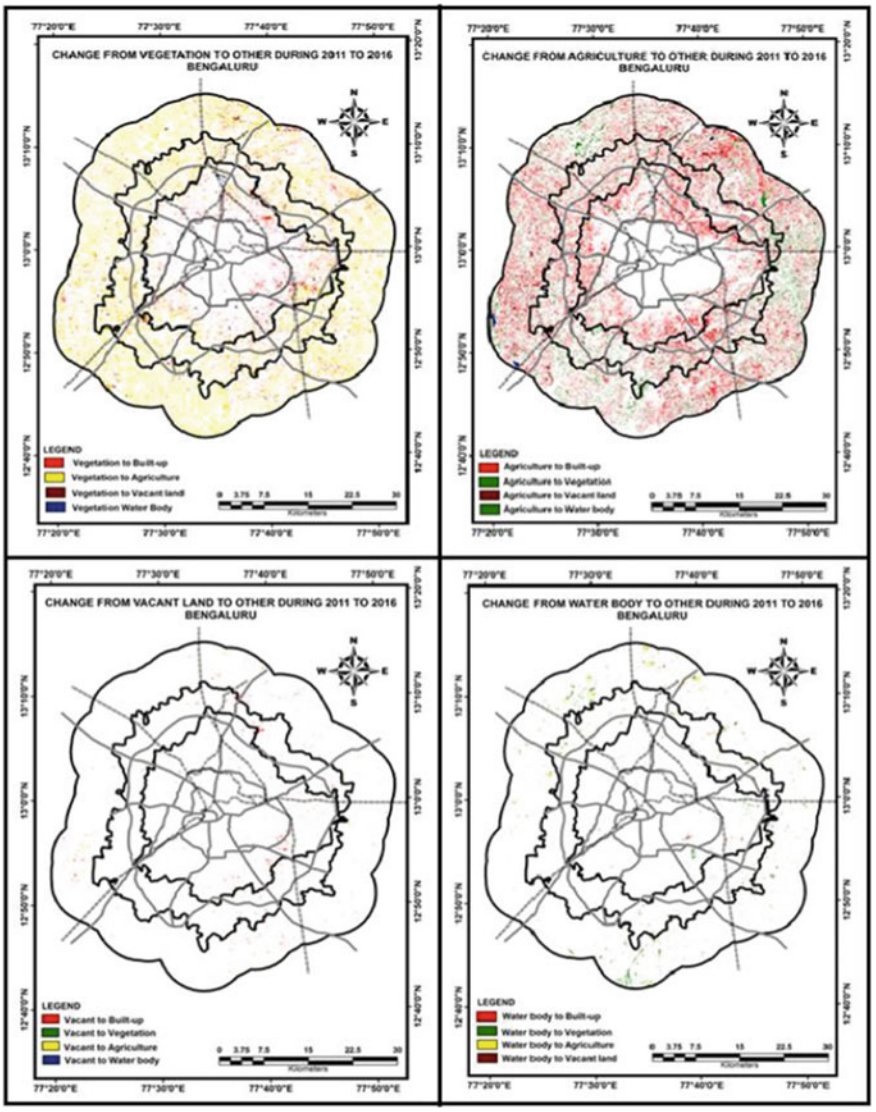

Fig. 20.7 Land use/Land cover change matrix map showing land encroachment under the different land categories in the Bengaluru sprawl area from 2011 to 2016

20.5.3.6 Socio-Economic

There are so many socio-economic potentials are available in the sprawling area. Local community participation. Availability of human resources, ability to capacity building, and opportunity to generate income.

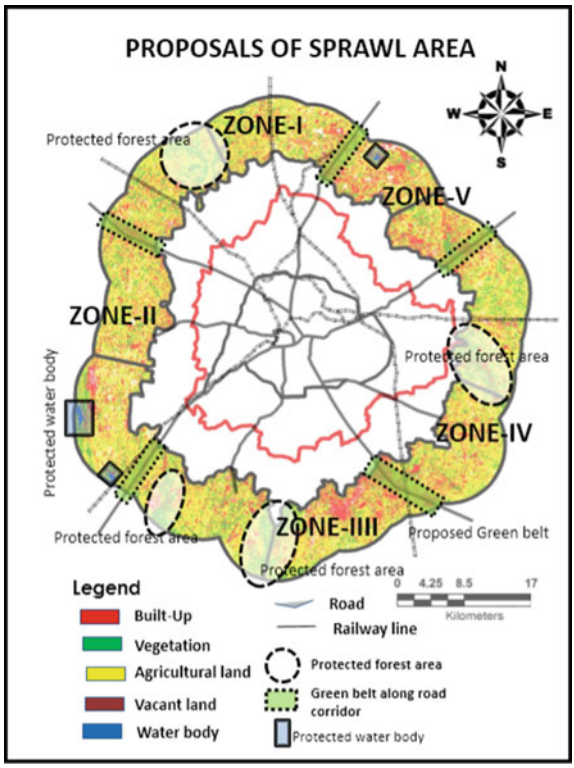

Fig. 20.8 Proposal map of sprawl area Bengaluru

20.5.3.7 Physical Infrastructure

There is no water supply, sewerage and sanitation, and drainage system. So, there should be a proper pipe water supply in all the zones. There should be sewerage and sanitation and stormwater drainage system. The road network is not right in the sprawling area, so there should be a good road network (Fig. 20.8).

20.6 Conclusion and Recommendations

Urban sprawl is a global phenomenon in metropolitan and megacities and it impacts land use, physical infrastructure, socio-economic activity, and quality of life. It is very evident with the previous studies that very few research has been carried in common to assess the type of built-up land areas and conversion from different uses to built-up in sprawl areas of megacities. The present study reveals the rate of increase in sprawl mainly outward from the boundary of Banglore Development Authority (BDA) in nearly last four decades (1973–2016). Growth rate of non-built-up to built-up area conversion is very high and increasing very rapidly.

Given the likely built-up 2021 as well as the predicted 2031 trend, it is necessary to revise the master plan 2035 to incorporate changes. It is also necessary to evolve planned development in order to prevent haphazard development. It is also necessary to evaluate the environmental impact on growth. It is also critical to evaluate infrastructure in order to plan for future growth.

References

Bhatta B (2010) Analysis of urban growth and sprawl from remote sensing data. Springer, Canada, ISSN 1867-2434

DiLorenzo W (2000) The myth of suburban sprawl, USA Today. 128:54–56

EUROPEAN ENVIRONMENT AGENCY (EEA) (2006) Urban Sprawl in Europe: The Ignored Challenge. European Commission, https://www.eea.europa.eu/publications/eea_report_2006_10

Galster G, Hanson R, Wolman H, Coleman S, Freihage J (2001) Wrestling sprawl to the ground: defining and measuring an elusive concept. Housing Policy Debate 12(4):681–717

Grubler A (1994) Technology. In: William B, Meyer BL, Turner II (Eds.) Changes in land use and land cover: a global perspective. Cambridge University Press, Cambridge, UK

Gordon P, Richardson HW (1997) Are compact cities a desirable planning goal? Am Plan Assoc 63(1):95–106. http://www.eea.europa.eu/publications/eea_report_2006_10

Pengiun Z (2011) Managing urban growth in a transforming China: evidence from Beijing. Land Use Policy 28:96–109

Squires GD (2002) Urban sprawl: causes, consequences, and policy responses. The Urban Institute Press, Washington, DC

Sudhira Hs, Ramachandra Tv (2007) Characterising urban sprawl from remote sensing data and using landscapemetrics. In: Proceedings of 10th international conference on computers in urban planning and urban management, Iguassu Falls, PR Brazil

Wilson EH, Hurd JD, Civco D, Arnold CL (2003) Development of a geospatial model to quantify, describe and map urban growth. Remote Sens Environ 86(3):275–285

Zhang B (2004) Study on urban growth management in China. Xinhua Press, China

Chapter 21
Using Remote Sensing Technique to Investigate Land Use/ Land Cover Changes in Varanasi District (UP), India

Varun Narayan Mishra, Rajendra Prasad, Praveen Kumar Rai, Mărgărit-Mircea Nistor, and Prafull Singh

Abstract Updated information of land use/land cover (LULC) is considered as a key component for various planning and management activities. The changes that occurred in LULC strongly affect the climate, ecosystem and its services from regional to global levels. Therefore, monitoring of LULC change is vital to understand various environmental transform processes and proper management of natural resources. The present study investigates the LULC changes in Varanasi District, India, by using Landsat TM/OLI satellite images of years 1988 and 2015. A supervised classification of images was performed and classified into seven major LULC categories as per the landscape of study area. The overall classification accuracies were found 86.94% (kappa coefficient = 0.848) and 89.25% (kappa coefficient = 0.875) for classified products of 1988 and 2015 respectively. The results indicate that during 1988–2015, sparse vegetation, built-up, and sand have been increased by 1.69% (2591.45 ha), 6.31% (9677.67 ha), and 0.14% (207.12 ha) while agricultural land, dense vegetation, fallow land, and water bodies have been decreased by 3.66% (5603.79 ha), 1.35% (2069.52 ha), 2.08% (3182.29 ha), and 1.06% (1620.63 ha), respectively. The study area under investigation experienced growth in built-up area at the cost of loss in agricultural land. This work also highlights the significance

V. N. Mishra
Centre for Climate Change and Water Research, Suresh Gyan Vihar University, Jaipur, Rajasthan, India
e-mail: varunnarayan.mishra@mygyanvihar.com

R. Prasad
Department of Physics, Indian Institute of Technology (BHU), Varanasi, UP, India
e-mail: rprasad.app@itbhu.ac.in

P. K. Rai (✉)
Department of Geography, K. M. C. Language University, Lucknow, UP, India

M.-M. Nistor
Department of Hydrogeology, Earthresearch Company, Cluj-Napoca, Romania

P. Singh
Department of Geology, School of Earth, Biological and Environmental Sciences, Central University of South Bihar, Gaya, Bihar, India
e-mail: psingh17@amity.edu

R. B. Singh et al. (eds.), *Remote Sensing and Geographic Information Systems for Policy Decision Support*, Advances in Geographical and Environmental Sciences,
https://doi.org/10.1007/978-981-16-7731-1_21

of remote sensing approach for investigating the nature and location of ongoing changes.

Keyword Remote sensing · LULC · SVM · Change detection

21.1 Introduction

Land use documents how people are using the land with special emphasis for economic activities. While land cover indicates how much of earth's surface is covered by forests, wetlands, vegetation, agriculture, and water. These two terms are often used interchangeably (Dimyati et al. 1996). An updated and timely information on LULC assists in monitoring the dynamics of LULC as a result of anthropogenic activities and increasing population. In general, LULC change is referred as the modification of earth's surface by anthropogenic disturbances (Ellis 2011). The effects of these anthropogenic disturbances on environment are considered as key components of environmental change (Riebsame et al. 1994). Therefore, monitoring and understanding the change in LULC are essential for sustainable natural resource management and number of planning activities (Dickinson 1995; Zhu and Woodcock 2014; Mishra and Rai 2016a, b). A large amount of data about the Earth's surface is required for monitoring of the changes in LULC effectively. Currently, remote sensing technology has been proven an effective way for getting time series data of earth's surface, which are valuable in LULC change studies. It has been also broadly used in updating LULC maps. Application of remote sensing images made possible to study the changes in LULC rapidly at lower cost with better accuracy and reported by many researchers (Foody 2003; Singh et al. 2012; Zhu and Woodcock 2014; Mishra and Rai 2016a, b; Vishwakarma et al. 2016). At present, the availability of multi-temporal remote sensing images by Landsat satellites at no cost provides valuable information for monitoring the change in LULC. In a number of studies, multi-temporal Landsat images have been utilized effectively for analyzing and monitoring LULC change (Otukeiand Blaschke 2010; Zhu and Woodcock 2014; Mishra et al. 2014b; Mishra and Rai 2016; Somvanshi et al. 2018).

A suitable classification method is also required to produce reliable and utilizable LULC maps from remote sensing images. In the last few years, several classification methods such as maximum likelihood, artificial neural network, decision tree, support vector machines, object-based methods, sub-pixel-based methods have been used in the field of remote sensing (Lu and Weng 2007). Support vector machine (SVM) is an advance nonparametric method and based on machine learning theory proposed by Vapnik and Chervonenkis (1971). In recent years, SVM has been utilized broadly for remote sensing image classification (Kumar et al. 2015; Mishra and Rai 2016a, b; Mishra et al. 2014a, 2017; Singh and Rai 2018). In several studies, the performance of SVM has been compared and found to be superior in comparison with other classification methods (Kumar et al. 2015; Mishra et al. 2017; Singh and Rai 2018).

So, the high potential of SVM has attracted a lot of attention for image classification in remote sensing community.

In the present work, SVM classification method was used to perform LULC classification at different years with the aim of investigating LULC changes over the time period of 1988–2015 in Varanasi District, UP, India. In particular, this study is focused on investigating the dynamics of LULC changes. This kind of analytical study can be used significantly as a planning tool for proper land use management and policy making.

21.2 Study Area

In this work, Varanasi District of Uttar Pradesh, India, is chosen as the study area. It is located between 25°10′30″ N to 25°35′15″ N latitude and 82°40′50″ E to 83°12′18″ E longitude covering an area of around 153290.61 ha. It is one of the oldest living cities in the world and is situated at the bank of holy river Ganga. Literally, the meaning of Varanasi is the land between river Varuna and Assi. Varanasi District is bounded by River Gomati and Jaunpur District in the north, Chandauli District in the east, and SantRavidas Nagar Bhadohi in the west. It is very eminent for being a hotspot of religion and cultural activities for over many years. It is agriculturally productive region due to its location in Indo-Gangetic plain. The location of study area is shown in Fig. 21.1.

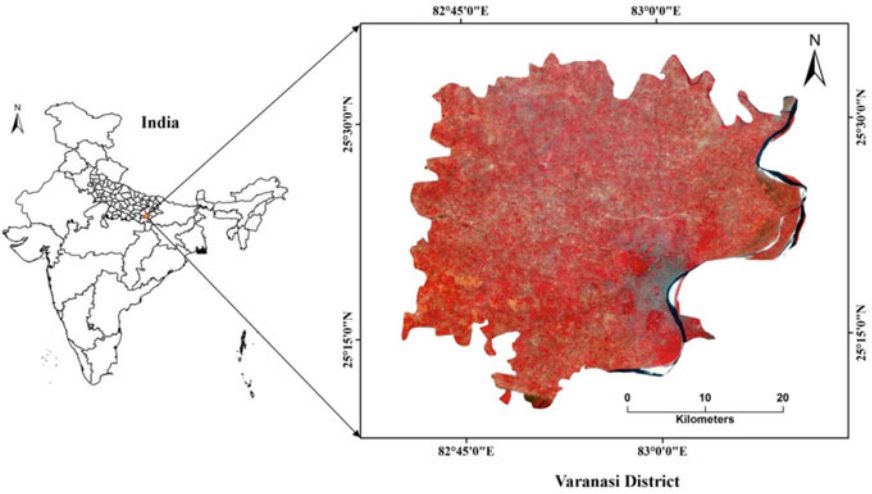

Fig. 21.1 Location map of the study area as seen on Landsat-8-OLI satellite image

21.3 Materials and Methods

In the present study, Landsat images were used to map LULC classes of Varanasi for different time periods. Remote sensing images by Landsat-5 Thematic Mapper (TM) and Landsat-8-Operational Land Imager (OLI) sensors acquired in years 1988 and 2015, respectively, were utilized. The path/row of remote sensing images is 142/42 and 142/43. The required remote sensing images were downloaded from USGS Earth Explorer website (http://earthexplorer.usgs.gov/).

21.3.1 Image Preprocessing

The preprocessing and interpretation of remote sensing images are performed using ENVI (v5.1) software to produce LULC maps. Both the remote sensing images were first imported and layer stacked to generate false color composite (FCC). It is necessary to perform geometric correction to produce LULC maps showing real word coordinate. The image-to-image registration method was used to co-register both the images. First-degree polynomial equation and nearest neighbor resampling method were used during image transformation process. The co-registered remote sensing images are in the Universal Transverse Mercator (UTM) coordinate system (Zone 44, North) with datum World Geodetic System (WGS) 1984, and the pixel size is 30 m. The FCCs are utilized for the creation of training signatures for classification purpose.

After the creation of training signatures for each LULC class, the separability analysis using transformed divergence (TD) method was used to inspect the quality of training signatures prior to image classification. Its values range from 0 to 2.0 and indicate how well the selected training signatures are statistically separated from each other. Commonly, TD value greater than 1.9 or below 1.7 shows a good and poor separability, respectively, between two classes. For this study, the separability analysis shows the range of values (from 1.75 to 2.0, where average divergence is 1.96) for Landsat-5 TM data of 1988 and (from 1.76 to 2.0, where average divergence is 1.99) for Landsat-8-OLI data of 2015, respectively.

21.3.2 LULC Classification Using SVM

The preprocessed Landsat TM/OLI images were classified using a supervised SVM classification method available in ENVI software in order to classify various LULC features. The LULC maps for years 1988 and 2015 were derived by classifying individual Landsat images. In the present study, seven major LULC classes such as agricultural land, dense vegetation, sparse vegetation, built up, fallow land, water bodies, and sand were identified and classified.

SVM is a nonparametric supervised classification method based on statistical learning theory proposed by Vapnik and Chervonenkis (1971). The aim of SVM method is the construction of an optimal separating hyperplane of linearly separable classes in decision boundary space. Nonlinear problems can be overcome by using kernel functions even with complex training samples (Vapnik 2000). It transforms nonlinear problems into linear one and maps the original input space into a new higher dimensional feature space (Vapnik 2000; Kumar et al. 2015). Thus, radial basis function (RBF) kernel is chosen as the most appropriate choice because it needs less computational work and can also handle the nonlinear relationship capably between the training samples and the whole data set. For RBF kernel, two parameters, i.e., penalty parameter (C) and gamma parameter (γ), are set to a value of 100 and 0.14, respectively.

21.3.3 Assessment of Classification Accuracy

The error matrix approach was used to assess the accuracy of classified products obtained from SVM classification method. The assessment of classification accuracy is performed by computing the overall classification accuracy (OA), producer's accuracy (PA), user's accuracy (UA), and kappa coefficient (Kc) (Congalton and Green 1999). The OA, PA, UA, and K_C are computed using the equations, respectively, given as follows:

$$\mathrm{OA} = \frac{1}{\mathrm{N}} \sum_{\mathrm{i}=1}^{\mathrm{r}} \mathrm{n_{ii}} \tag{21.1}$$

$$\mathrm{PA} = \frac{\mathrm{n_{ii}}}{\mathrm{n_{icol}}} \tag{21.2}$$

$$\mathrm{UA} = \frac{\mathrm{n_{ii}}}{\mathrm{n_{irow}}} \tag{21.3}$$

$$\mathrm{K_c} = \mathrm{N} \sum_{\mathrm{i}=1}^{\mathrm{r}} \mathrm{n_{ii}} - \sum_{\mathrm{i}=1}^{\mathrm{r}} \frac{\mathrm{n_{icol}} \mathrm{n_{irow}}}{\mathrm{N}^2} - \sum_{\mathrm{i}=1}^{\mathrm{r}} \mathrm{n_{icol}} \mathrm{n_{irow}} \tag{21.4}$$

where n_{ii} is the number of pixels correctly classified in a category; N is the total number of pixels in the confusion matrix; r is the number of rows; and n_{icol} and n_{irow} are the column (reference data) and row (predicted classes) total, respectively.

21.3.4 LULC Change Investigation

A post-classification detection method was used to perform LULC change investigation. A pixel-based change matrix was produced to interpret the changes more efficiently. The classified images of two different dates were compared using cross-tabulation method in order to determine qualitative and quantitative characteristics of the changes between 1988 and 2015. The annual rate of change (rt) for each LULC class is also calculated using equation given by (Puyravaud 2003)

$$\mathrm{rt} = \frac{1}{(t_2 - t_1)} \times \ln\left(\frac{A_2}{A_1}\right) \times 100 \tag{21.5}$$

where A_1 and A_2 are the areas (in ha) of a LULC class at years t_1 (initial time) and t_2 (later time), respectively. A positive value indicates increase, while negative value indicates decrease in the area of a particular LULC type.

21.4 Results and Discussion

LULC classification results are obtained corresponding to the Landsat images of 1988 and 2015 using SVM method and shown in Fig. 21.2a, b. The distribution of class-wise area for years 1988 and 2015 is given in Table 21.2.

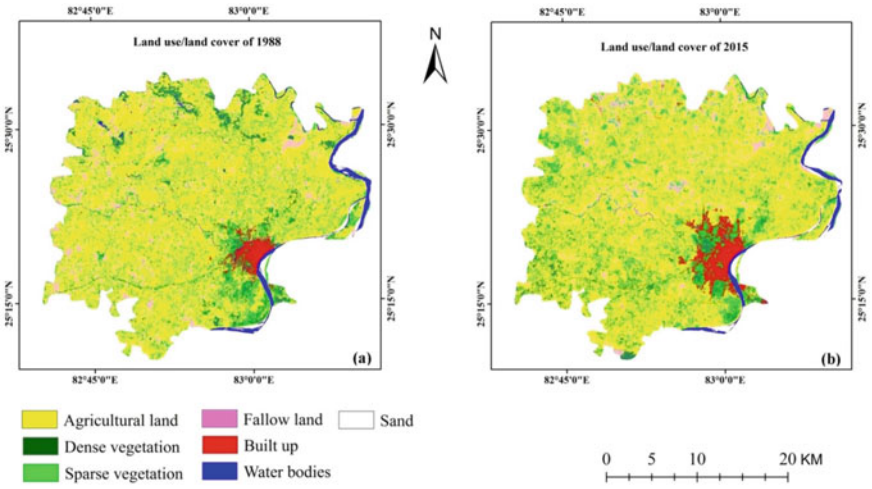

Fig. 21.2 LULC status of the Varanasi District for years **a** 1988; and **b** 2015 based on SVM

Table 21.1 Accuracy assessment results of LULC maps of years 1988 and 2015

Year	1988		2015	
LULC class	PA (in %)	UA (in %)	PA (in %)	UA (in %)
Agricultural land	83.78	84.55	88.29	89.91
Dense vegetation	89.36	91.30	89.32	90.20
Sparse vegetation	86.61	87.39	88.39	90.00
Fallow land	84.91	79.65	85.71	84.96
Built up	88.29	90.74	88.99	88.99
Water bodies	88.35	94.79	92.39	94.44
Sand	87.76	81.90	92.71	87.25
OA (in %)	86.94		89.25	
Kc	0.848		0.875	

21.4.1 LULC Status

The accuracy assessment of LULC classification results showed an OA of 86.94% (Kc = 0.848) for 1988 and 89.25% (Kc = 0.875) for 2015, respectively. The detailed statistics of PA and UA of different LULC classes achieved for different years are listed in Table 22.1.

Figure 21.2a represents spatial distributional pattern of LULC of the Varanasi District for the year 1988 while Fig. 21.2b for the year 2015. It reveals that in 1988, about 63.01% (96,586.41 ha) area was under agricultural land, 5.65% (8663.60 ha) under dense vegetation, 11.67% (17,882.37 ha) under sparse vegetation, 14.72% (22,568.04 ha) under fallow land, 1.74% (2670.51 ha) under built up, 2.59% (3968.30 ha) under water bodies, and 0.62% (951.39 ha) under sand. In 2015, the area under these LULC classes was found about 59.35% (90,982.62 ha) area was under agricultural land, 4.30% (6594.08 ha) under dense vegetation, 13.36% (20,473.82 ha) under sparse vegetation, 12.65% (19,385.75 ha) under fallow land, 8.06% (12,348.18 ha) under built up, 1.53% (2347.67 ha) under water bodies, and 0.76% (1158.51 ha) under sand (Table 21.1).

21.4.2 LULC Change

Table 21.2 shows that both positive and negative changes occurred in LULC pattern of the Varanasi District during the period under investigation. During 1988–2015, the agricultural land has decreased from 96586.41 ha in 1988 to 90982.62 ha in 2015 which accounts for 3.66% of the total study area. The dense vegetation has decreased from 8663.60 ha in 1988 to 6594.08 ha in 2015 which accounts for 1.35%. The sparse vegetation has increased from 17882.37 ha in 1988 to 20473.82 ha in 2015 which accounts for 1.69%. The fallow land has decreased from 22568.04 ha in 1988 to

Table 21.2 Area and amount of change in LULC classes during 1988 to 2015

Year	1988		2015		Change 1988–2015		
LULC class	Area (ha)	Area (%)	Area (ha)	Area (%)	Area (ha)	Area (%)	Rate of change (%)
Agricultural land	96,586.41	63.01	90,982.62	59.35	-5603.79	-3.66	-0.221
Dense vegetation	8663.60	5.65	6594.08	4.30	-2069.52	-1.35	-1.011
Sparse vegetation	17,882.37	11.67	20,473.82	13.36	2591.45	1.69	0.501
Fallow land	22,568.04	14.72	19,385.75	12.65	-3182.29	-2.08	-0.563
Built up	2670.51	1.74	12,348.18	8.06	9677.67	6.31	5.671
Water bodies	3968.30	2.59	2347.67	1.53	-1620.63	-1.06	-1.944
Sand	951.39	0.62	1158.51	0.76	207.12	0.14	0.729
Total	153,290.61	100	153,290.61	100	0.00	0.00	

19385.75 ha in 2015 which accounts for 2.08%. The built-up area has increased from 2670.51 ha in 1988 to 12348.18 ha in 2015 which accounts for 6.31%.The water bodies have decreased from 3968.30 ha in 1988 to 2347.67 ha in 2015 which accounts for 1.06%. The sand-covered area has increased from 951.39 ha in 1988 to 1158.51 ha in 2015 which accounts for 0.14%. To understand land intrusion for different LULC classes during 1988–2015, a change detection matrix was prepared and shown in Table 21.3. A diagrammatic representation of LULC changes during 1988–2015 in Varanasi District is shown in Fig. 21.3.

Table 21.3 LULC change matrix showing transitions (in pixels) during 1988 to 2015

Year 2015								
	LULC class	Agricultural land	Dense vegetation	Sparse vegetation	Fallow land	Built up	Water bodies	Sand
Year 1988	Agricultural land	3,104,808	129,000	553,326	443,621	33,357	1781	0
	Dense vegetation	96,933	60,493	92,323	28,665	13,418	1238	0
	Sparse vegetation	524,682	87,248	235,247	70,436	35,549	1052	0
	Fallow land	528,451	4795	48,155	299,835	2020	4698	4746
	Built up	2404	3915	23,097	2810	202,068	1230	395
	Water bodies	4283	4419	6548	10,087	1474	77,668	9196
	Sand	0	0	374	7510	2	4549	36,831

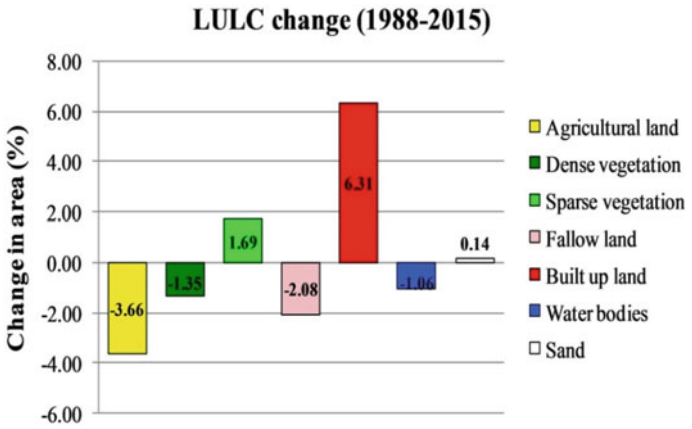

Fig. 21.3 Diagrammatic illustration of LULC changes (in %) during 1988–2015

21.5 Conclusions

The present study is conducted in one of the highly populated Varanasi District of Uttar Pradesh, India. It reveals efficacy of multi-temporal remote sensing images in investigating spatial and temporal phenomena. The major land cover classes available in study area are agricultural land and vegetation. The agricultural land has decreased by 3.66% (5603.79 ha) due to conversion in sparse vegetation and built-up area. The second major land cover class in the study area is dense vegetation which was decreased by 1.35% (2069.52 ha) due to conversion in sparse vegetation and built up land. The other major land cover class is fallow land which has also been decreasing. The built-up area has increased by 6.31% (9677.67 ha) due to mostly expansion of the city area. In contrast to other cities, Varanasi is composed of both planned and unplanned urban groups in close locality. So it can be possible to have diverse green spaces in the planned and unplanned urban groups of Varanasi District. The planned urban group includes BHU campus, cantonment area, and DLW. However, it is assumed that the remaining part of the area is unplanned urban group. This part experienced and spontaneous and rapid urban expansion leading to dense settlements in the core areas of Varanasi District. The urban area has continued to develop along the southward and westward side of Ganga River. These areas are subject to dense exacerbated urban settlement example with less green spaces, traffic obstruction, and intense pollution. Therefore, the present work demonstrates the usefulness of Landsat images for spatiotemporal analysis of LULC change at lower cost with better accuracy. This study can also have potential to contribute toward the sustainable development and land use planning of an area from local to global scales.

References

Congalton RG, Green K (1999) Assessing the accuracy of remotely sensed data: principles and practices. CRC/Lewis Press, Boca Raton

Dickinson RE (1995) Land processes in climate models. Remote Sens Environ 51:27–38

Dimyati M, Mizuno K, Kitamura T (1996) An analysis of land use/cover change using the combination of MSS Landsat and land use map: a case study in Yogyakarta, Indonesia. Int J Remote Sens 17:931–944

Ellis E (2011) Land-use and land-cover change. In: Cleveland CJ (Ed) The encyclopedia of earth, environmental information coalition, national council for science and the environment, April 18, 2010

Foody G (2003) Remote sensing of tropical forest environments: towards the monitoring of environmental resources for sustainable development. Int J Remote Sens 24:4035–4046

Kumar P, Gupta DK, Mishra VN, Prasad R (2015) Comparison of support vector machine, artificial neural network and spectral angle mapper algorithms for crop classification using LISS IV data. Int J Remote Sens 36(6):1604–1617

Lu D, Weng Q (2007) A survey of image classification methods and techniques for improving classification performance. Int J Remote Sens 28(5):823–870

Mishra VN, Kumar P, Gupta DK, Prasad R (2014a) Classification of various land features using RISAT-1 dual polarimetric data. Int Arch Photogramm Remote Sens Spat InfSci XL-8:833–837

Mishra VN, Rai PK, Mohan K (2014b) Prediction of land use changes based on land change modeler (LCM) using remote sensing: a case study of Muzaffarpur (Bihar), India. J GeogrInst Jovan Cvijic 64:111–127

Mishra VN, Rai PK (2016a) A remote sensing aided multi-layer perceptron-Markov chain analysis for land use and land cover change prediction in Patna district (Bihar), India. Arab J Geosci 9:1–18

Mishra VN, Rai PK (2016b) Evaluation of land use/land covers classification accuracy using multitemporal remote sensing images. Forum Geogr 15(1):45–53

Mishra VN, Prasad R, Kumar P, Gupta DK, Srivastava PK (2017) Dual-polarimetric C-band SAR data for land use/land cover classification by incorporating textural information. Environ Earth Sci 76(1):26

Otukei JR, Blaschke T (2010) Land cover change assessment using decision trees, support vector machines and maximum likelihood classification algorithms. Int J Appl Earth Observ Geoinf 12:S27–S31

Puyravaud JP (2003) Standardizing the calculation of the annual rate of deforestation. For EcolManag 177:593–596

Riebsame WE, Meyer WB, Turner BL (1994) Modeling land-use and cover as part of global environmental change. Clim Change 28:45–64

Singh S, Rai PK (2018) Application of earth observation data for estimation of changes in land trajectories in Varanasi District, India. J Landsc Ecol 11(1):5–18

Singh P, Thakur JK, Kumar S, Singh UC (2012) Assessment of land use/land cover using geospatial techniques in a semi-arid region of Madhya Pradesh, India. In: Thankur JK (eds) Geospatial techniques for managing environmental resources, pp 152–163

Somvanshi SS, Bhalla O, Kunwar P, Singh M, Singh P (2018) Monitoring spatial LULC changes and its growth prediction based on statistical models and earth observation datasets of GautamBudh Nagar, Uttar Pradesh, India. Environ Dev Sustain 22:1073–1091

Vapnik VN (2000) The nature of statistical learning theory. Springer

Vapnik VN, Chervonenkis AY (1971) On the uniform convergence of relative frequencies of events to their probabilities. Theor Probab Appl 16(264):1971

Vishwakarma CS, Thakur S, Rai PK, Kamal V, Mukharjee S (2016) Changing land trajectories: a case study from India using remote sensing. Eur J Geogra 7(2):63–73

Zhu Z, Woodcock CE (2014) Continuous change detection and classification of land cover using all available Landsat data. Remote Sens Environ 144:152–171

Chapter 22
Geo-Spatial Database for Village Resources: A Case Study of Selected Villages from the Central Himalaya

R. C. Joshi and Masoom Reza

Abstract A resource database is created including spatial and non-spatial information in a GIS platform. This work is carried out as a part of a pilot research project funded by Department of Science and Technology, Government of India. Ten villages are selected from the outer and lesser Himalayan domain of the Central Himalaya. Using high-resolution geo-coded satellite data, cadastral maps are geo-referenced and a base map is created to incorporate collected information. Satellite data, census 2011, field survey, a detailed digital land parcels wise database is created and incorporated in the cadastral map. Information of each land parcels, i.e., land use/land cover (LULC), soil characteristics, rainfall, house, spring water discharge, road and other infrastructural facilities is collected. Socio-economic survey of each household is also conducted. This work is very important for planning and management of village resources and creation of infrastructure for the sustainable development.

Keywords Village resource · Cadastral maps · LULC · Soil · Water · Rainfall · Infiltration · Socio economic data

22.1 Introduction

In India the village level planning lacks the availability of accurate and reliable data. Most of the villages came into existence unplanned; therefore, a systematic study is needed to create a database for planning and development. In his study Batjes (1995) stated that in the last 2–3 decades, the development in the field of technology and research can be seen; hence, authentic and reliable data are generated with help of government and NGO's. The responsibility to maintain database or information in villages has given to local level administration for better implementation of plans, schemes and other services.

Village resource database is very important to the planner and administrator to initiate development projects. So it is necessary to have an updated and accurate

R. C. Joshi · M. Reza (✉)
Department of Geography, D.S.B. Campus, Kumaun University, Nainital 263002, Uttarakhand, India

R. B. Singh et al. (eds.), *Remote Sensing and Geographic Information Systems for Policy Decision Support*, Advances in Geographical and Environmental Sciences,
https://doi.org/10.1007/978-981-16-7731-1_22

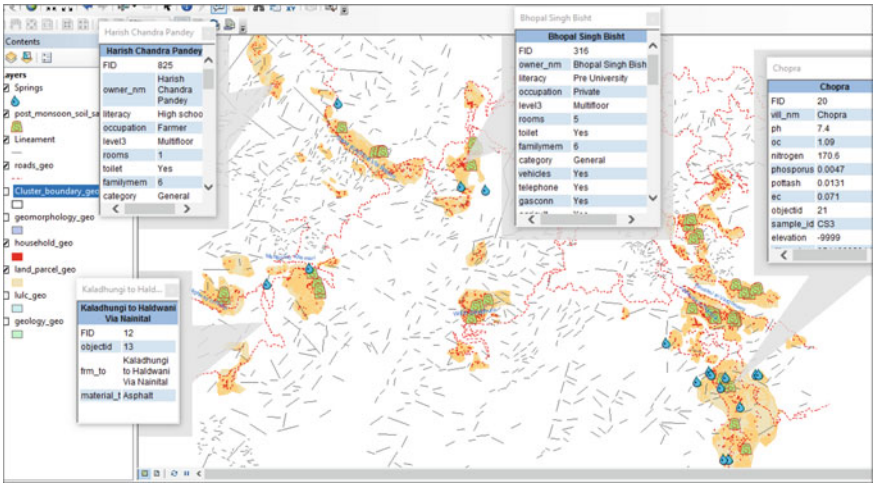

Fig. 22.1 Geo-spatial database of village resources in a GIS platform

database comprising resources and infrastructural facility available in the village. In this work, an attempt is made to incorporate spatial and non-spatial data at village level. Database is developed using satellite data, census 2011, detailed field survey and land parcels wise digital database is created and incorporated in the cadastral map (Fig. 22.1).

22.2 Study Area

The study area is situated in the central Himalayan region along the Main Boundary Thrust (MBT) consisting Siwalik and Lesser Himalayan region within an altitude of 930 m to 2560 m above mean sea level. The spatial extension of study area ranges in between 79°22′18 to 79°30′27 E. longitude and 29°18′31 to 29°23′46 N. latitude. The study area consists of 43 villages in ten (10) Gram Panchayat namely, Bajoon, Bhalyuti, Chopra, Devidhura, Gethia, Jeolikote, Khurpatal, Mangoli, Nalni and Sariatal of Nainital Tehsil, Nainital District, Uttarakhand (Fig. 22.2).

22.3 Objective

The main objective of the present research is to create a geospatial database for village resources which is carried out keeping in view the following objectives:

- To identify and delineate land use/land cover of the study area
- To identify the chemical characteristics of soils and map preparation

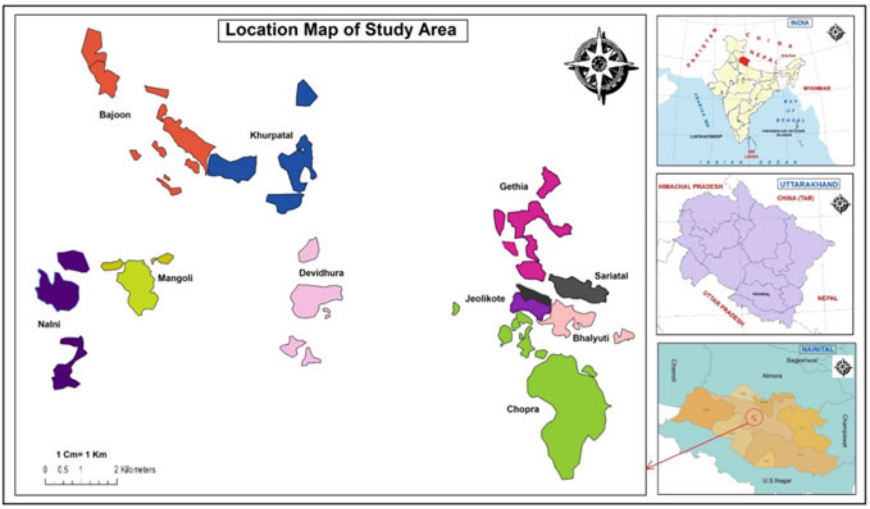

Fig. 22.2 Location map

- To identify the source of potable water and measurement of total amount of water available in a year.
- To analyse spring water quality and to record the high-resolution rainfall data.
- To conduct household survey for the collection of information regarding quality of human resource

22.4 Database and Methodology

- Quickbird data, Survey of India toposheet and cadastral maps are used to delineate the land use/land cover data. For geo-referencing of cadastral map, geocoded satellite data are used.
- The cadastral maps (1955–60) are used to delineate the village boundary and to validate the other infrastructure such as roads and foot tracks.
- The water samples are collected from the natural perennial spring for analysis. The regular water discharge is also measured to understand the amount and nature of flow of water in correlation with changing season. Heavy metal water quality analysis is made at the Centre for Studies on Bay of Bengal, Andhra University, Visakhapattanam.
- Rainfall data has been collected using rainfall data logger installed in Bajoon village.
- Five (05) soil samples from different altitude of the each village are collected to understand the variation in the soil characteristics. Soil analysis is carried out at Soil Lab. Tea Cultivation, Bhowali, Uttarakhand.
- House hold survey has done to collect the information about human resource.

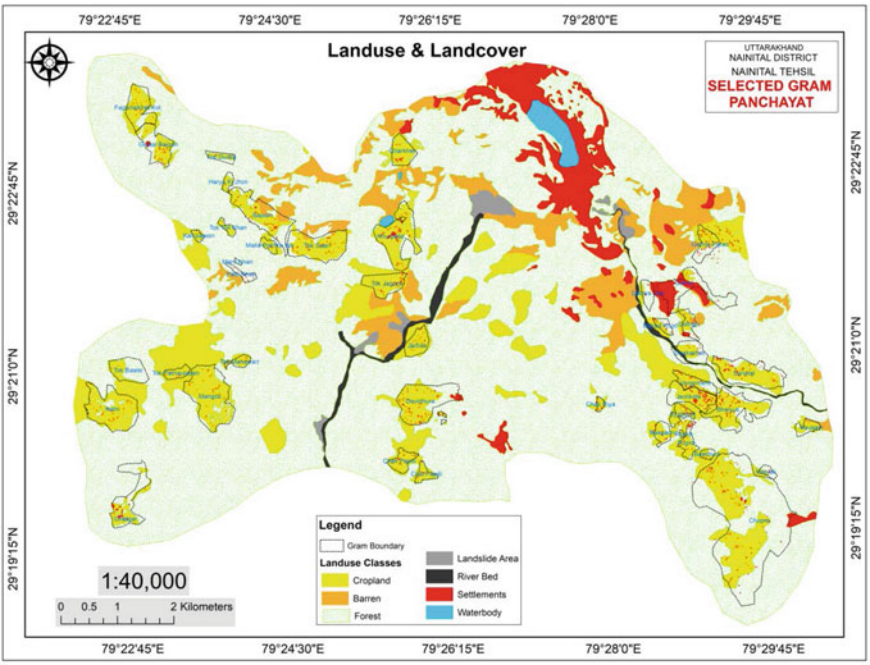

Fig. 22.3 Land use/land cover

22.5 Land Resources

Using HRSI data, village-wise land use/land cover (LULC) is delineated and ground truth survey is made. Cadastral maps are also taken into consideration for finalization of map. LULC classification is based on NRSC level II. Identified classes are agriculture, barren, built-up, forest, river bed and waterbody (Fig. 22.3). In general, highest area coverage is under agriculture followed by forest cover (Table 22.1).

22.6 Soil Quality

The chemical analysis of soil includes nitrogen, organic carbon, phosphorus, pH and potassium content. Availability of nitrogen in study area is ranging from 130 to 265 kg/hectare. The maximum amount of concentration of nitrogen found in the Lesser Himalayan villages, i.e., Bajoon, Khurpatal, and Gethia. Organic carbon is one of the important soil chemical properties which help in good agricultural growth. Analysis shows it ranges from 0.63 to 4.37. In the Siwalik villages, i.e., Nalni, Mangoli, Chopra and Bhalyuti, it is ranging from 0.63 to 1.89. Remaining villages whose maximum area lies in the Lesser Himalaya, O C value ranges from

Table 22.1 Gram panchayat wise LULC class

	LULC class (area in hectare)					
Gram	Agricultural	Barren)	Built-up	Forest	River bed	Water body
Bajoon	74.5	5.6	2	53.4	–	–
Bhalyuti	35.2	0.93	0.62	15.4	–	–
Chopra	141.8	–	3.5	164.2	–	–
Devidhura	70.5	–	2.9	16.3	0.05	–
Jeolikote	12.5	–	3.5	58.6	–	–
Sariatal	43.3	–	1	14.8	0.02	–
Mangoli	68.4	–	0.46	10.2	–	–
Nalni	66.4	–	1.2	43.9	–	–
Khurpatal	111.7	1.8	2.4	15.9	–	0.2
Gethia	12.5	5.8	3.5	59.6	0.7	–

1.89 to 4.36. Soil pH of the area is ranging from 5.6 to 7.9 and forming alkaline to moderately acidic. It is found that Bajoon, Bhalyuti and Chopra Gram Panchayat has both alkaline to acidic pH values. The concentration of phosphorus and potassium in soil is almost equal in whole area, but it is slightly higher in some parts of higher elevation area in comparison to low altitude area. The value of phosphorus ranges from 0.002 to 0.01, whereas potassium values are in between 0.004 and 0.05. The spatial variation of EC is almost same except Bhalyuti village. (Fig. 22.4).

22.7 Water Resource

More than 30 perennial natural water springs scattered in study area fulfils the water need of villagers. The spring water is very rich with many minerals which are good for agricultural growth as well as drinking purpose (Joshi and Reza 2018). In general, a small concrete tank is built at the mouth of the springs to store adequate amount of water. In some villages, the water from storage tank is also being supplied through pipeline to households for drinking purpose. The villagers also utilize spring water for the cultivation of vegetable where there is sufficient amount available. In Khurpatal, a small perennial drainage water is channelized through concrete canal all over the fields. Installation of pipeline and construction of water tank in villages is also done under the scheme/project "SWAJAL"—Uttarakhand Rural Water Supply and Sanitation Sector Program (twelfth Five-Year Plan 2012–2017, Report). This project helps thousands of people in rural hill area of Uttarakhand to access drinking water and also builds toilets for needy.

Till now, the availability of drinking water in springs is fulfilling the need of dwellers. Round the year water supply is enough for village population, but increasing population and climate change is a matter of concern for regional and local levels

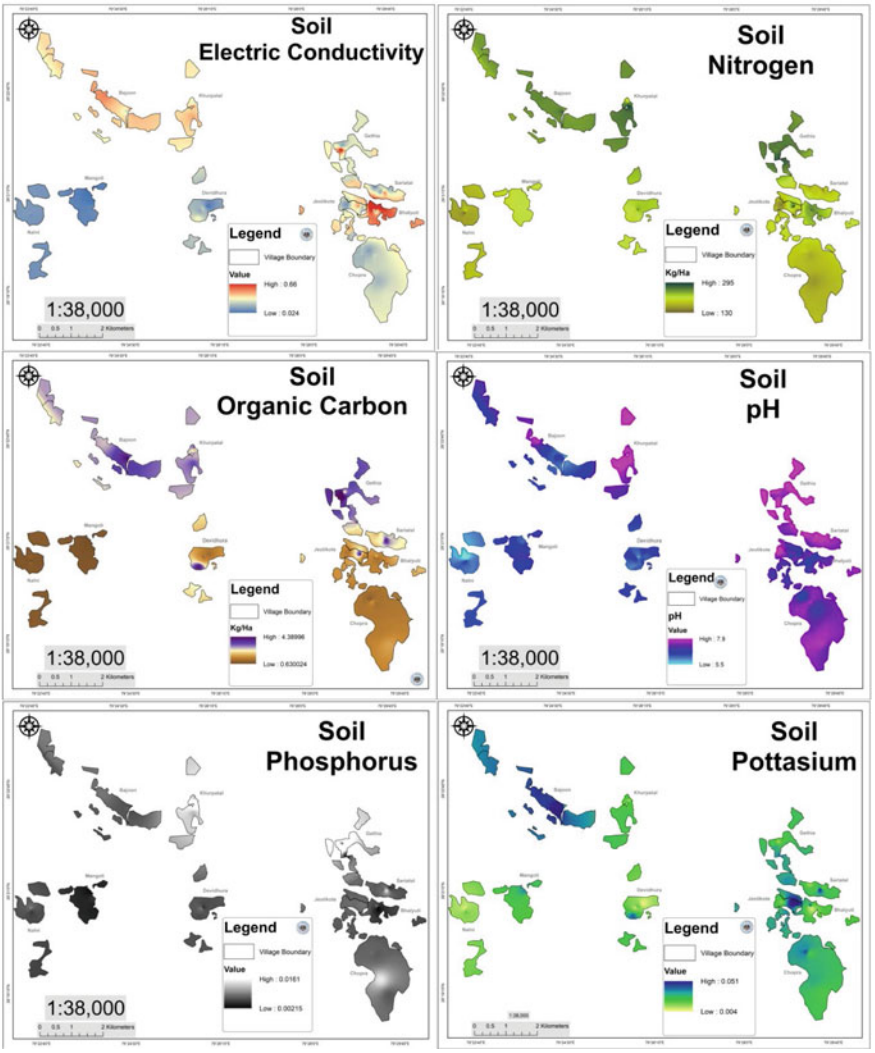

Fig. 22.4 Soil map

also. (Bhatt and Poonam Pandey 2005) Decreasing water supply due to drying of perennial sources in hills of Uttarakhand is also one of the reasons (Mamgain and Reddy 2015).

Traditionally, in the study area, drinking water was fetched from natural springs, collecting it in the ponds. However, later on, spring water was brought to their houses through pipes by people from their own efforts. Today, with the help of government funded schemes, water is being provided by pipe lines. The government is spending a significant resource to the sector for the development of infrastructure and capacities

for the successful operation of drinking water supply schemes in rural areas. The map (Fig. 22.5) indicates the status of drinking water availability and location of springs in the villages (Table 22.2).

Water quality analysis comprises six (6) parameters, i.e., lithium, aluminium, ferrous, zinc, gallium and strontium. Among the all villages Gethia is having very high values of lithium (92.193) and strontium (455.398) which is very high in comparison to other area but still is potable. The strontium level in drinking water should not be more than 4 mg/l. And it cannot use in any food products such as beverages and drinks is given by US EPA (Human Health Hazards, Fact Sheet 2015).

Rainfall

As compared to 2017, the rainfall data show there is a deficit of 153 mm of rainfall in the month of June 2018 and in the month of July 2018, 846 mm of rain deficit was recorded. The monthly deficit analysis has showed the monsoon is delayed a month in the year 2018. Deficit of rainfall, i.e. 38.9% and 75% recorded in the month of June and in July, respectively. In the month, January and February, 2019, rainfall recorded as 105 and 109 mm, respectively. In comparison to last year, i.e. 2018 in January and February, there is an increase in rainfall of 84.8 mm and 94.2 mm, respectively. (Fig. 22.6).

As per the data recorded till now, it is observed that the pattern of rainfall distribution has been changed in this region, and it is also analysed that there is deficit

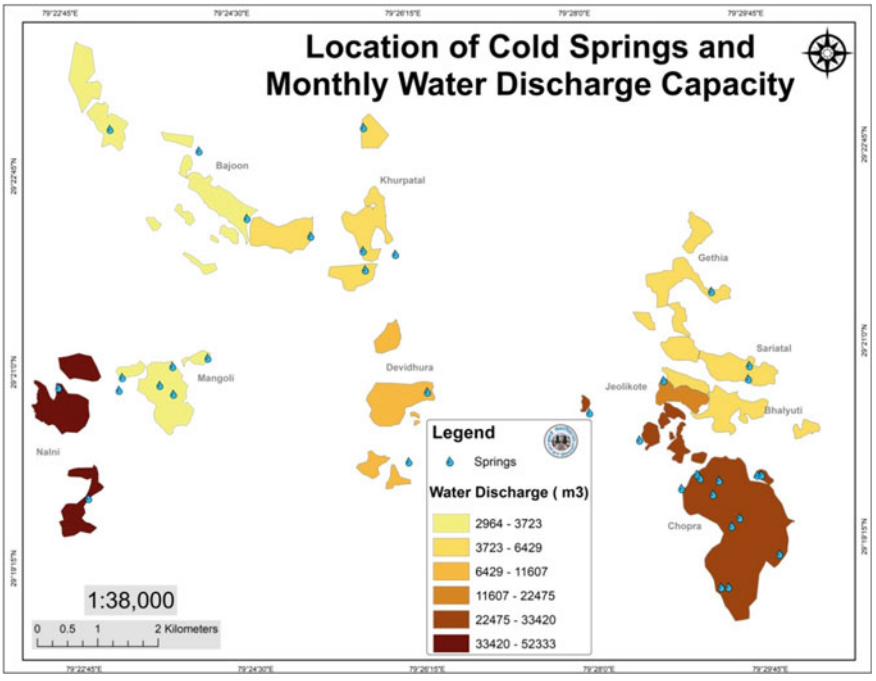

Fig. 22.5 Water discharge

Table 22.2 Spring water quality

Concentration of chemical in Spring water						
Village	Li (μg/l)	Al (μg/l)	Fe (μg/l)	Zn (μg/l)	Ga (μg/l)	Sr (μg/l)
Bajoon	2.358	7.874	6.004	4.159	4.314	81.349
Bhalyuti	1.788	5.117	3.915	1.733	5.423	100.966
Chopra	2.099	4.739	6.968	19.400	1.736	37.995
Devidhura	2.203	9.745	10.496	3.925	16.400	182.625
Gethia	92.193	7.103	3.526	4.486	3.033	455.398
Jeolikote	2.015	10.371	8.681	1.983	12.180	191.918
Khurpatal	6.041	5.556	2.779	3.551	1.782	212.082
Mangoli	2.775	6.311	11.904	2.303	13.017	185.355
Nalni	2.318	6.623	4.045	2.160	2.727	46.789
Sariatal	8.719	5.088	4.429	3.546	6.517	172.141

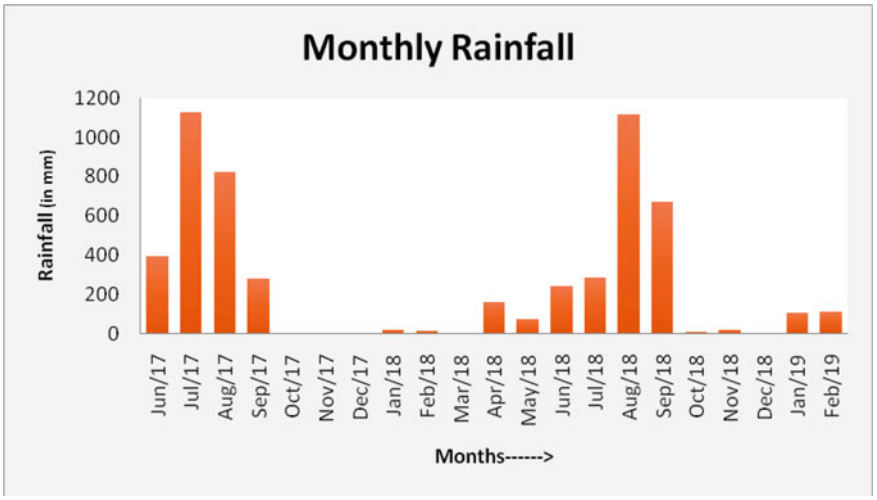

Fig. 22.6 Monthly rainfall

in rainfall in the recorded years. The two districts of Uttarakhand—Nainital and Bageshwar—have also recorded on an average 13.05 cm of rainfall deficit in the last 102 years observed by IMD (Mishra 2017).

22.8 Human Resource

Total population of study area of all Gram Panchayat is 7135 persons. The geographical area is 11.32 Km^2. The geographical area of Gram Panchayat includes all revenue area comprising land parcels whether it is for commercial or personal. The reserve forest area is excluded from the Gram Panchayat boundary. In most of the villages, houses are built beside each others. Among all Gram Panchayat, Gethia has highest number of population as well as Households, i.e., 1332 persons and 321 Households. Followed by Chopra Gram Panchayat the population is 1212 but in comparison to area, Chopra has large geographical area among all Gram Panchayat. The lowest population is recorded in Nalni Gram Panchayat, i.e., 340 and households are 68. The area which is well connected with roads and other services having good number of population and lowest population concentration resides in area which has fewer infrastructures. (Fig. 22.7) and (Table 22.3).

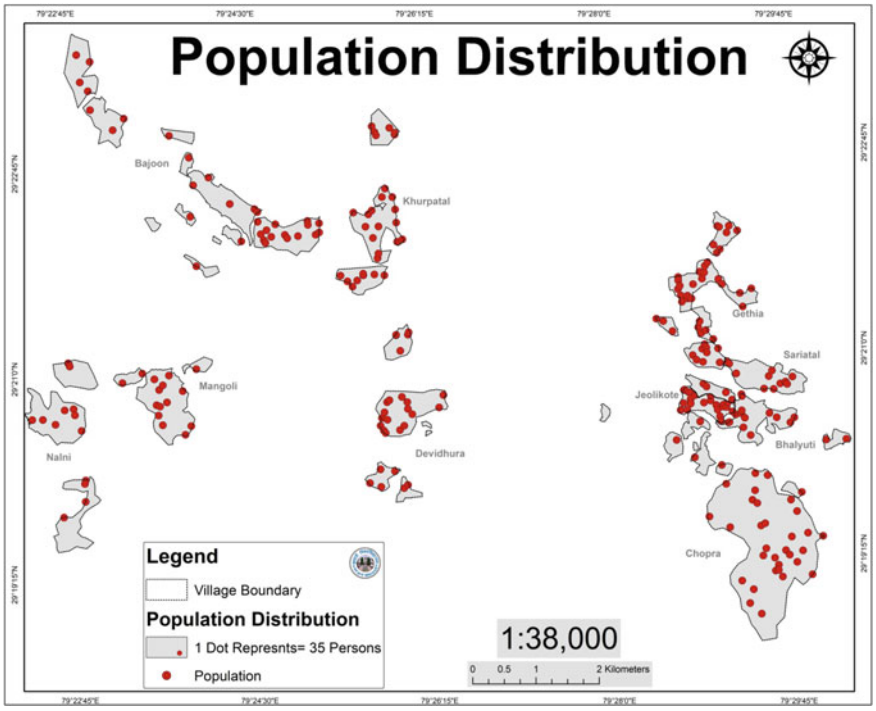

Fig. 22.7 Village-wise population

Table 22.3 Village-wise population and number of households studied

Gram panchayat	Population	No. of households
Bajoon	607	128
Bhalyuti	452	106
Chopra	1212	229
Devidhura	689	69
Gethia	1332	321
Jeolikote	502	90
Khurpatal	1162	237
Mangoli	422	60
Nalni	340	68
Sariatal	417	82
Total	7135	1390

22.9 Conclusion

Village resource database is developed using physical and economic data collected from toposheet, cadastral map, satellite data and primary data. It will be helpful to the resource planner and executive officer to visualize the present status of villages. GIS platform makes easy and provide services to store both spatial and non-spatial information in one domain; it also makes easy to access and modify the information while necessary. The data/information stored in a digital database is more safe and secure. GIS database can also be used to compare and identify the changes occurred over time period. An example of digital interactive map prepared for this work is very important for planning and management of village level resources (Fig. 22.8).

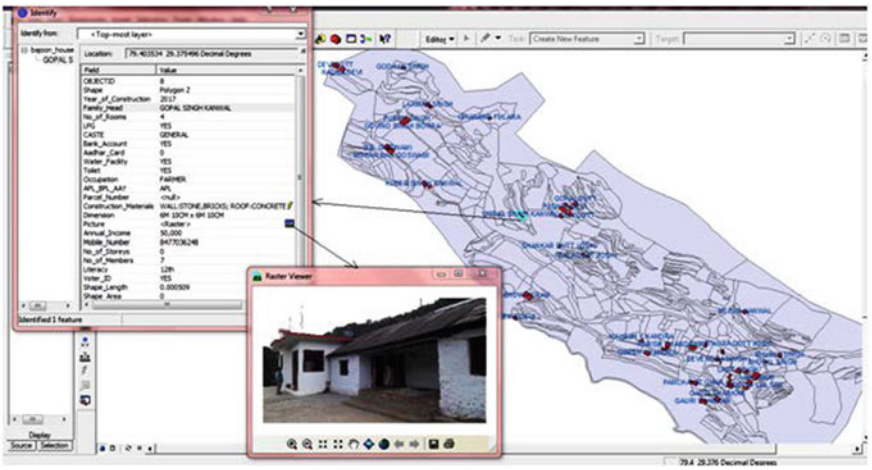

Fig. 22.8 Attribute Table in a GIS domain with land parcels and owners information

Acknowledgements Village information system is an initiative undertaken by Natural Resource Data Management System (NRDMS) division of Department of Science & Technology (DST), New Delhi. Authors are grateful to Prof. P. Rajendra Prasad, Dr. Bhoop Singh and Dr. A. K. Singh for their help to bring out this work. This work forms a part of the research project funded by DST, New Delhi.

References

Anonymous—Twelfth Five Year Plan 2012–2017, Report of the working group on rural domestic water and sanitation, Ministry of Drinking Water and Sanitation, Government of India, September 2011

Anonymous—Human Health Hazards, Fact Sheet (2015) Wisconsin division of public health, Bureau of Environmental and Occupational Health (608):266–1120

Batjes NH (1995) A global dataset of soil pH properties, International soil reference and Information centre. ISSN 0923-3792; 27, p 9

Bhatt V, Poonam Pandey J (2005) Water crisis in Uttarakhand. A report by 'Research Foundation for Science, Technology and Ecology' for National Commission for Women, January 2005, pp 27–55

Census of India (2011) http://www.censusindia.net

Joshi RC, Masoom Reza (2018) Buiding geodatabase on village information system using geopatial technology: an example of Bajoon Village, Central Himalaya, India. IJCRT 6(2):563–577. ISSN 2320-2882

Mishra A (2017) Changing temperature and rainfall patterns of Uttarakhand. Int J Environ Sci Nat Resour 7(4):1–6. ISSN 2572-1119

Mamgain RP, Reddy DN (2015) Out-migration from hill region of Uttarakhand: issues and policy options. Project Report of Giri Institute of Development Studies, sponsored by NIRD, Hyderabad

Chapter 23
Effect of Urban Expansion on Groundwater Crisis: A Comparative Assessment of Nainital, Mussoorie and Shimla Hill Cities

Rupsa Sarkar, A. C. Pandey, and C. S. Dwivedi

Abstract The growing livelihood opportunities in big cities and commercial townships in Himalayan regions are attracting more and more rural population to shift to urban areas. The rapid expansion of urban areas and concomitant population growth exert huge demand for potable water. The water crisis is more acute in the hilly regions owing to paucity of surface water sources and meagre groundwater potential in hard rocky terrain. The present study compares the urban sprawl and LULC changes in the exponentially growing hill townships of Shimla, Mussoorie and Nainital over a period of past 20 years with the help of remote sensing and Geographic Information System (GIS). Further, Groundwater Potential Zones (GWP zones) are delineated and categorized into four: good, moderate, low and poor, which are correlated with the urban expansion. The results indicated that with the increase in the urban area over the years in these cities, the groundwater recharge has decreased with resultant shifts of moderate and low groundwater zones to poor zones. Water harvesting structures for augmenting recharge in these cities have been suggested based on geo-informatics technique.

Keywords Urban sprawl · LU/LC change · GWP zones delineation · Water harvesting structures

23.1 Introduction

Himalayas are newly formed mountains nearly 50 m years ago as a result of collision of the Indian plate with the Eurasian plate. Despite it being tectonically alive, the Himalayan states of the country like Himachal Pradesh and Uttarakhand have seen massive urban expansion in the last few decades (Anbalagan 1993). Although most of the urban sprawl witnessed are unplanned and unregulated, it causes several changes in the environment (Walker 2011). One of the several negative changes includes, the

R. Sarkar · A. C. Pandey (✉) · C. S. Dwivedi
Department of Geoinformatics, School of Natural Resource Management, Central University of Jharkhand, Ranchi 835205, Jharkhand, India

R. B. Singh et al. (eds.), *Remote Sensing and Geographic Information Systems for Policy Decision Support*, Advances in Geographical and Environmental Sciences,
https://doi.org/10.1007/978-981-16-7731-1_23

changes in the Himalayan watersheds causing the aquifers to dry up and inefficient to recharge due to human disruption. This in turn contaminates the groundwater and makes it unfit for use leading to poor health of both flora and fauna. The agriculture is destroyed, livelihood disrupted, sanitation is compromised and human health becomes insecure (Tiwari et al. 2018).

Apart from changes in the river and groundwater regimes, high population density in a region can cause various problems: If there is an increase in soil sealing, it makes ground impermeable and leads to flooding; If the consumption is high, it leads to groundwater shortage and groundwater pollution (Azzam et al. 2014). Lately, as a result of good transportation facilities and better connectivity, and marketing media, even the remote areas have started facing over exploitation of resources. There needs to be a strict Urban Land-use Policy rules against over-use of natural resources to limit unregulated building of settlements and for business (Ghosh 2007).

There are various ecological effects of urban sprawl which include, increased potential for flooding and soil erosion due to impervious surfaces, decrease in groundwater for wells and irrigation, increased human and pet exposure to diseases, risks of water, air and e-waste pollution and risk to life and property from wildfires (Kamila and Chandra Pal 2015).Urban sprawl can have significant and usually negative impacts on water resources as a result of land use modifications. Urbanization has various effects on land use and leads to changes like falling of forests, replacing them with human settlement, which in turn makes all the pervious surfaces impervious and modifies the drainage channels, thus causing ground water shortages. Consequently, this human interference changes the hydrologic behaviour of a catchment (Karthiyayini et al. 2016).

The water scarcity in the Himalayan region owing to high runoff and scanty recharge of localized aquifer system is well known. The crisis for potable water is increasing year after year in the major hilly townships due to increased tourist influx. This entails a systematic study on urban sprawl and land use changes on groundwater resources in select Himalayan cities exhibiting huge water crisis during summer and winter seasons.

23.2 Study Area

Shimla, Mussoorie and Nainital are hill townships of northern India, lying on the foothills of western Himalaya. While Shimla lies in Himachal Pradesh, Nainital and Mussoorie lie in neighbouring Uttarakhand state. These states are bordered by Jammu and Kashmir on the North, Punjab to West, Tibet and Nepal on East and Uttar Pradesh on Southeast (Fig. 23.1).

Shimla is situated at an average altitude of 2206 m, Mussoorie at 1880 m and Nainital at 2084 m above sea level. Temperatures in Shimla typically range from −4 to 31 °C over the course of a year, with an average annual precipitation of 1575 mm. The

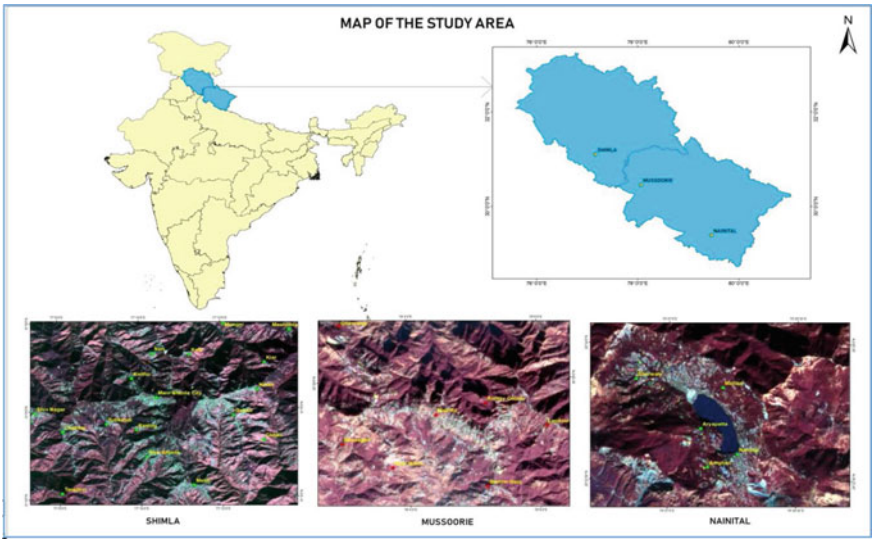

Fig. 23.1 Map of the study area for Shimla, Mussoorie and Nainital

average annual temperature of Mussoorie is 14.9 °C and precipitation is 2206 mm. In Nainital, the average annual temperature is 13 °C, while the precipitation has an average of about 1636 mm annually. Shimla, Mussoorie and Nainital receive snowfall in the months of January every year.

23.3 Data Used and Methodology

23.3.1 Data Used

Multi-temporal data was used in this research, description is given below under the name of Table 23.1.

Table 23.1 Data used in the study

Year	Satellite imagery used
1998	LANDSAT TM
2008	LANDSAT TM
2018	SENTINEL 2A
2011	ASTER DEM

23.3.2 Methodology

23.3.2.1 Area Changes with Supervised Classification

Built-up area was calculated through supervised classification of satellite data in Erdas Imagine software using Spectral Angle Mapper. Supervised classification is a process in which the user provides the software with training samples according to which the rest of the image is put into desired classes. In mountainous regions, limited LULC classification can be employed, namely, forest, built up, agriculture, water bodies and barren land. Training data sites are selected from each LULC regions classified and their spectral signatures are used in order to classify the rest of the area by assigning the values in an algorithm. This study uses all supervised classifications and finds Spectral Angle Mapper (SAM) to be most effective of all in terms of accuracy as it determines the spectral similarity between two spectra by calculating the angle between the spectra and treating them as vectors in a space with dimensionality equal to number of bands. SAM also minimizes the albedo effects.

23.3.2.2 Comparative Assessment to Calculate Sprawl

For all the years 1998, 2008 and 2018, the area calculation was done by reclassification of the LULC calculated and layout of map showing the sprawl was produced. Further, to do the comparative assessment, graphs were generated showing the changes for all the three years in all the three cities.

23.3.2.3 Relating Sprawl to Elevation Change

A contour map was prepared of all the years using DEM data. Then the sprawl area lying between each range was extracted through clipping and reclassification. The map was plotted in Excel to see the elevation changes of the sprawl over the years.

23.3.2.4 Relating Sprawl to the Change in Population

The population data as per the Census of India for 1991, 2001, 2011 was related to the sprawl changes using Graphs in Excel in order to see the trends and reasoning behind the sprawl, which can be later related to the reason behind groundwater crisis.

23.3.2.5 Thematic Map Preparations

Thematic maps are used to map a certain feature of any geographic area. In this study, the thematic maps used are LULC map, geology map, slope map, lineament density

map and drainage density map. These maps are reclassified to assign weightage. Ground Water Potential Assessment can be done by extracting various parameters and after which a weighted overlay is performed. The various parameters are as follows:

Land use: The hill townships of Shimla, Mussoorie and Nainitalis found to have crop land, water bodies, built-up, barren land and forest. Crop lands are more likely to have better groundwater potential than built-up land because the land surface resists the permeability of precipitated water. This affects the recharge of the groundwater regime. Similarly, barren lands are least suitable to be GWP Zones.

Slope: Slope of a land surface determines the groundwater recharge capability. Land surface which has steep slope is a poor groundwater recharge zone, while surface which has gentle slope is characterized as good groundwater recharge zone. As over study areas are hilly, slope plays an important factor.

Lineament density: Lineaments are areas of rocky terrain that result in faulting and fracturing. Thus, they make ground water recharge easy by increasing permeability (Kumar et al., **2011**). This is suggestive that when the density of lineaments in an area is more, it indicates the presence of groundwater. Lineament was delineated using TIN preparation that was then opened in ArcScene for better 3D view for mapping lineaments.

Drainage density: Drainage density is an expression of the closeness of water channels. Areas having high drainage density suggest a greater surface runoff and are not suitable for groundwater development. Yet, availability of drainage is a better possibility than no drainage at all.

Average Precipitation: Average annual precipitation of any region is the main contributor of groundwater, apart from the streams and rivers in the area. But the area under consideration is so small that there is no variability of average rainfall within any of the townships.

Relief: Elevation of an area plays an important role in the presence and distribution of groundwater. The higher the relief, the lesser the prospect of finding groundwater.

23.3.2.6 Groundwater Potential Zone Mapping Using Weighted Overlay Analysis

The thematic maps are reclassified into 4 classes and assigned ranks to each sub-class ranging from 1 to 5, with 1 being the best at water recharging and 5 being poor at water recharging. The weight derivation for each thematic map is done on ArcGIS 10.3 software to delineate GWP zones. The result obtained was in four zones of Poor, Low, Moderate and High. (Table 23.2).

The working formula for weighted overlay analysis is: Output layer $= \Sigma$ (Input layer $\times$ Weighted assigned/100) Where, sum of weights of all input layers $= 100$.

Table 23.2 Weight assignment to factors for potential groundwater zone mapping

S. no	Factors	Weightage (%)	Classes	Rank
1	Relief map	25	<1400	1
			1400–1800	2
			1800–2200	3
			>2200	4
2	Slope map	22	0–7	1
			8–15	2
			16–30	3
			>30	4
3	Lineament density	20	High	1
			Moderate	2
			Low	3
			No	4
4	Drainage density	18	High	1
			Moderate	2
			Low	3
			No	4
5	Land use map	15	Cropland/water body	1
			Forest	2
			Built-up	3
			Barren land	4

23.3.2.7 Area Calculations with Reclassification and Graphical Representation

Further after the delineation of the 4 zones, the areas are reclassified and area calculation is done to get the correlation between the changes in zones over the years as an effect of sprawl in the region. Then the changes in each zone in 1998, 2008 and 2018 were graphically represented to see the correlation. Then comparative assessments of the three cities were done in percentage.

23.3.2.8 Mapping Groundwater Recharge Structures

Groundwater recharging can be performed artificially by installing various harvesting structures on the water streams to intervene and create storage for dry seasons, recharge deep aquifers through injecting structures and improve the management of ground water resources and increase time for infiltration (Raviraj et al. 2017). Various artificial water harvesting structures include Check dams, Nala bunds, Farm ponds, Percolation tanks and Recharge pits.

Check dams are larger artificial harvesting structures, designed for construction over a water body of higher stream order and at least the area coverage of 0.25 km^2. They are built in order to check for extra availability of water during monsoon period and not only store rain water for using during post-monsoon seasons, but also help recharge of ground water reservoir situated in the close to region.

Nala bunds are low-budget small bunds suitable for catchments with (1st to 3rd) lower-order streams that have been deepened by erosion. The main function of these bunds is to stabilize the erosion by regularly providing moisture and stabilizing the gully.

Farm Ponds are formed by leaving a portion of land, to collect and store the excess water. They are constructed across flat topography and low permeability, or can be located across stream courses and flat topography.

Recharge pits are built to provide water to the fields during the time of crisis by building an embankment across a river/stream passing through agricultural areas.

Percolation tanks are the tanks built near streams with stream order of 3rdand 4th. It blocks the surface runoff in the barren land areas, holds water flowing from the catchment area and then helps percolation of stored water in the aquifer with a view to raise groundwater level. Areas with adequate fractures facilitate good groundwater recharge and are suitable for construction of percolation tanks.

23.3.3 Methodology Flowchart

See Fig. 23.2.

23.4 Result and Discussion

23.4.1 Changes in Land Use Land Cover Over Years 1998, 2008 and 2018

Land use is the man-made features on the surface of the earth such as built-up area, railways, roads, agriculture, while Land cover is the natural features such as forest, water bodies, waste land. These natural and man-made features can form a reference base for applications in this study ranging from watershed delineation to urban sprawl.

The LULC graphs were plotted for the years 1998, 2008 and 2018, in order to know that as the sprawl increased which land cover feature got replaced. (Figs. 23.6, 23.7 and 23.8).

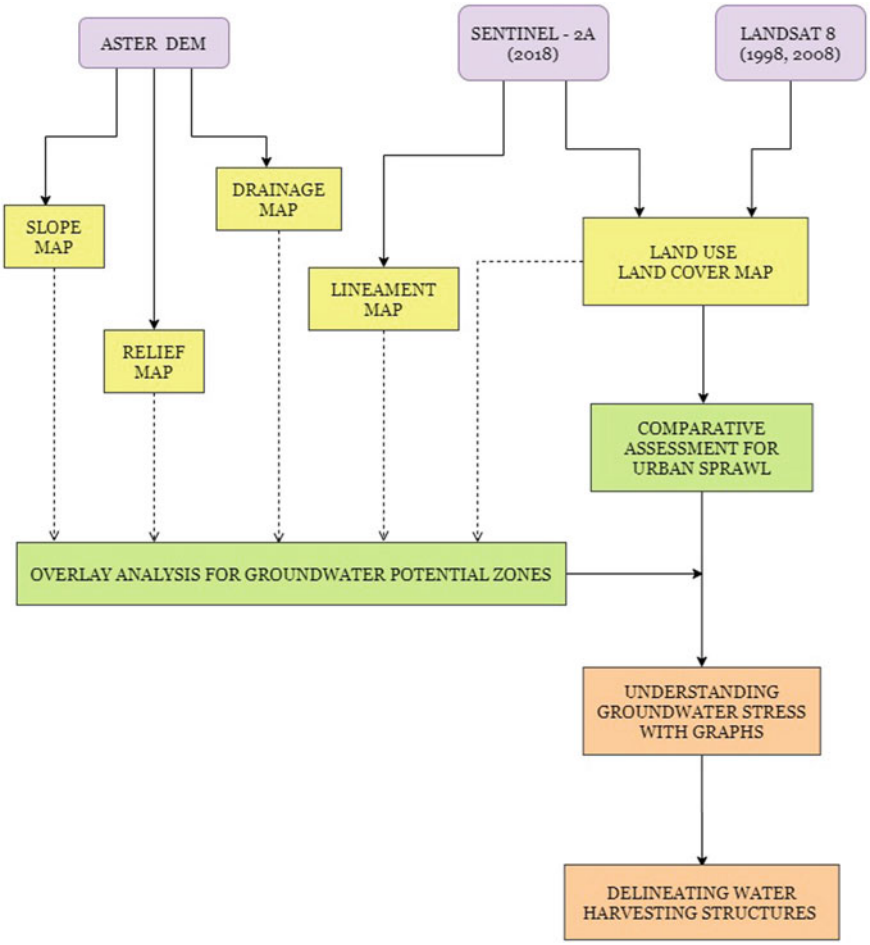

Fig. 23.2 Methodology flowchart

In all the three cities, it was seen that with the rapid increase in the built-up, there was a rapid decline in forest. Also we see slight increase in agriculture possibly due to increase in population. None the less, barren land remains the same for all the three townships of Shimla, Mussoorie and Nainital (Figs. 23.3, 23.4 and 23.5). In order to increase the built-up in these cities, forest cover was majorly harmed and replaced. In 20 years, the forest area cleared for built-up was seen to be about 10 km^2 in Shimla, 3 km^2 in Mussoorie and 2 km^2 in Nainital (Figs. 23.6, 23.7 and 23.8).

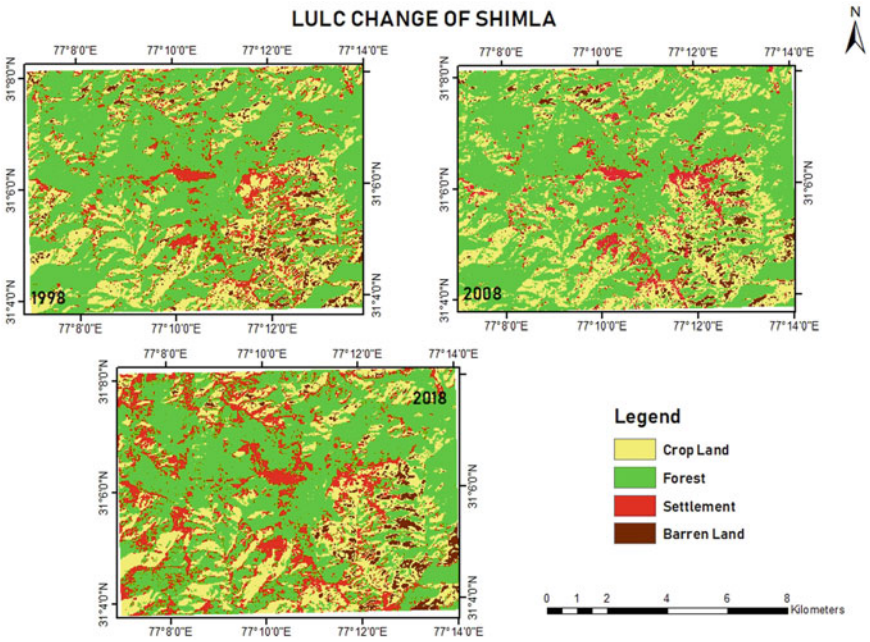

Fig. 23.3 Change in LULC over the year 1998, 2008 and 2018 in Shimla City

23.4.2 Change in Area Under Each Elevation Range Over the Years

Contours were mapped in ArcGIS, and the study area of each year was clipped and justified into 8 elevation classes based on the range, which was then reclassified to get the area.

In Shimla, it was seen that the elevation ranges from 1400 to 2500 m. Initially in 1998, more than 2.5 km^2 area was on the elevation 2000–2200 ^{m} because higher elevations had cooler weather during the summer season. But over the years, the change in area in that elevation range is subtle. In 2008, more built-up change is seen to take place in the elevation ranges from 1600 to 1900. More than 1 km^2 of built-up increase can be seen in 2008 at an elevation 1500–1600 ^{m}. Likewise, more than 1 km^2 change in 1600–1700 and 1.5 km^2 change in the range 1800–1900, from the year 1998 to 2008. This can be due to the crisis of groundwater at higher relief areas. In 2018, it was seen that only elevations that majorly experienced sprawl were the lower elevation regions which varied from 1400 to 1800 m, while the higher elevation area nearly remained the same with minor changes. (Fig. 23.9).

Similar variations as observed in Shimla can be seen in the case of Mussoorie and Nainital where initially most of the area lied in higher elevations i.e., between 1901 to 2000 m in Mussoorie and 2001 to 2350 m in Nainital. But in the township of Nainital, even in the later years, very subtle changes are seen in the lower elevation

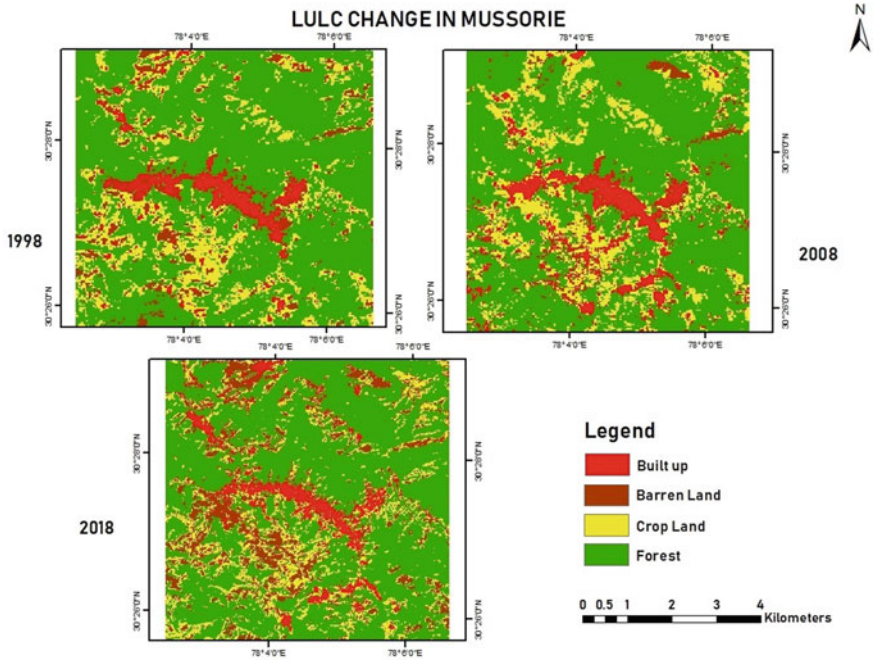

Fig. 23.4 Change in LULC over the year 1998, 2008, 2018 in Mussoorie City

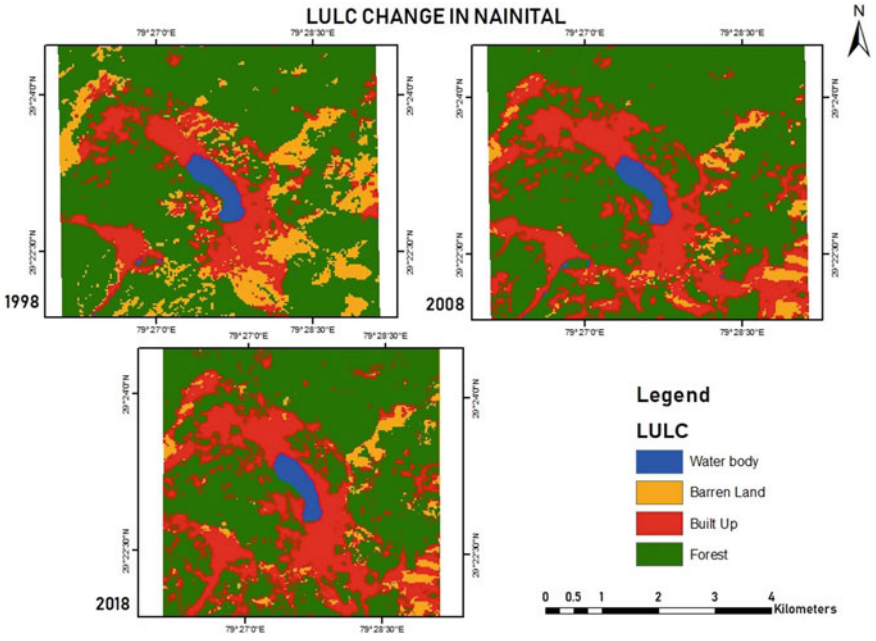

Fig. 23.5 Change in LULC over the year 1998, 2008, 2018 in Nainital City

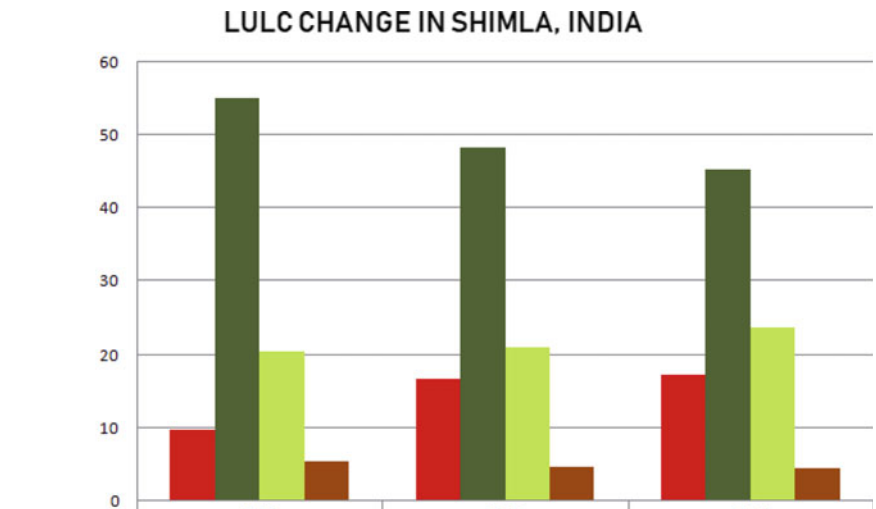

	1998	2008	2018
BUILT UP	9.6948	16.7067	17.2436
FOREST	54.9846	48.2577	45.1825
AGRICULTURE	20.5207	21.0546	23.5938
BARREN LAND	5.4128	4.5939	4.593

Fig. 23.6 Graph showing change in LULC in Shimla City

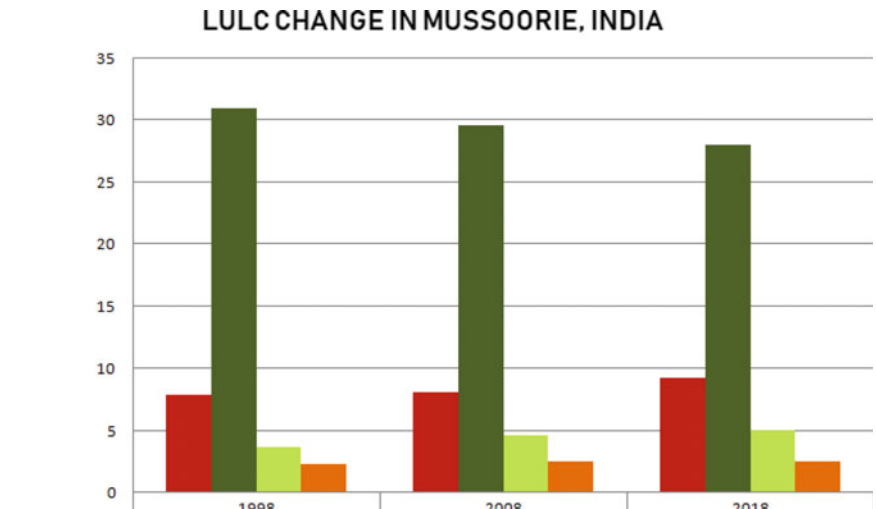

	1998	2008	2018
BUILT UP	7.8802	8.0485	9.2119
FOREST	30.8493	29.5023	27.9779
AGRICULTURE	3.6929	4.6453	5.0595
BARREN LAND	2.3337	2.56	2.5068

Fig. 23.7 Graph showing change in LULC in Mussoorie City

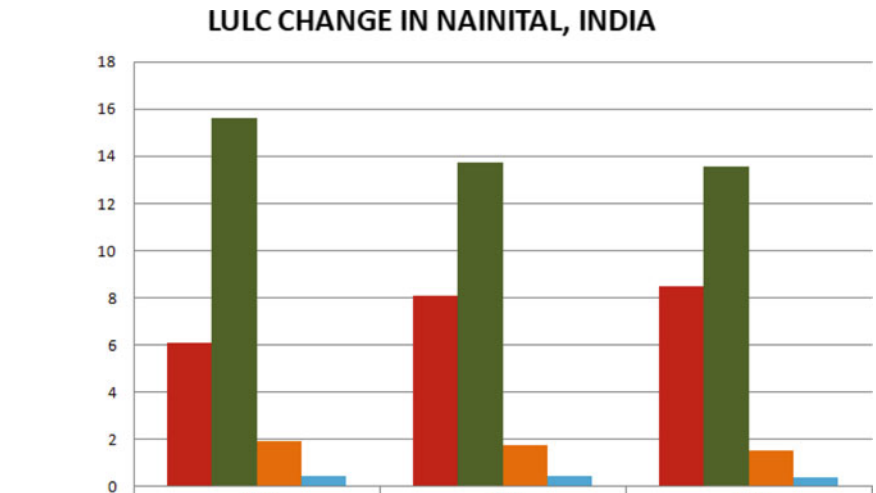

	1998	2008	2018
BUILT UP	6.0805	8.1032	8.5006
FOREST	15.6111	13.726	13.5777
BARREN LAND	1.9181	1.7904	1.5628
WATER BODY	0.4491	0.4392	0.4177

Fig. 23.8 Graph showing change in LULC in Nainital City

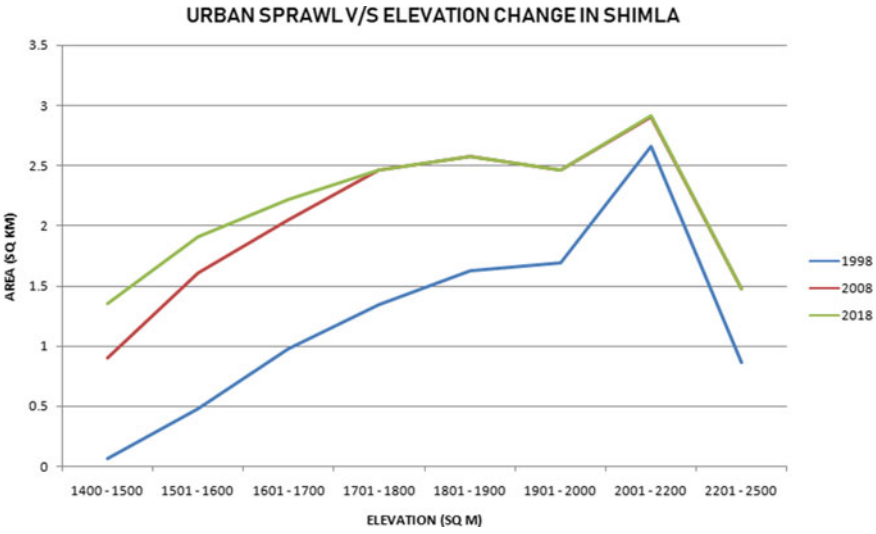

Fig. 23.9 Area under each elevation range in 1998, 2008, 2018 in Shimla

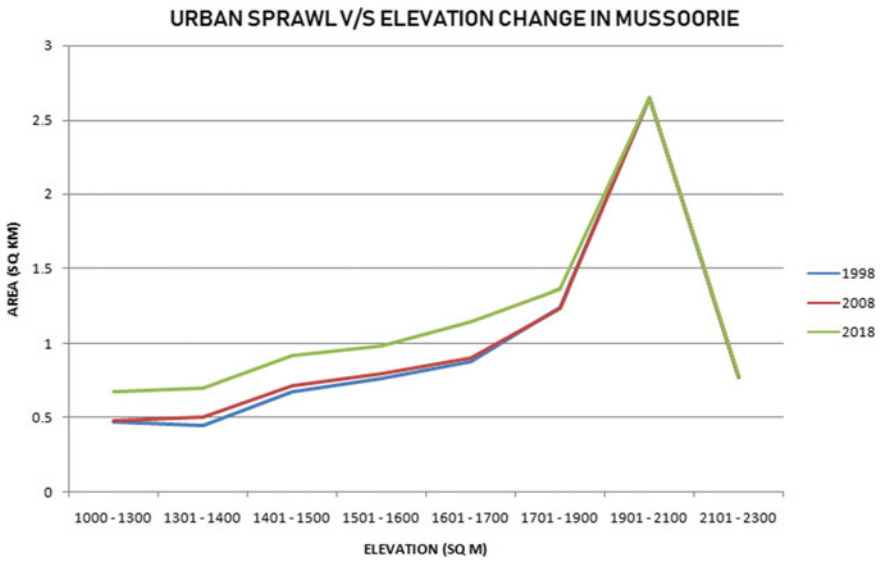

Fig. 23.10 Area under each elevation range in 1998, 2008, 2018 in Mussoorie

ranging 1300–1500. Most abrupt change is seen between the years 1998 to 2008 where the sprawl elevation changes from 0.5 km^2 to about 1.25 km^2 in 1500 to 1600 m elevation (Fig. 23.10). This is because Naini Lake lying at a lower elevation is surrounded by slopes around which the sprawl has occurred. But in Mussoorie, the main township at a range 1900–2100 m has seen no major growth in built-up from 1998. Unlike Shimla and Nainital, Mussoorie has seen more elevation changes in the later years between 2008 and 2018, as the major population growth is seen in those years (Fig. 23.11).

23.4.3 Preparation of Thematic Layers for Weighted Overlay Analysis

Five thematic maps of each study area (Shimla, Mussoorie and Nainital) were made and categorized into 4 classes each in order to perform the weighted overlay analysis (Figs. 23.12, 23.13, 23.14, 23.15, 23.16 and 23.17).

- Slope map
- Relief map
- Land Use map
- Drainage density map
- Lineament density map.

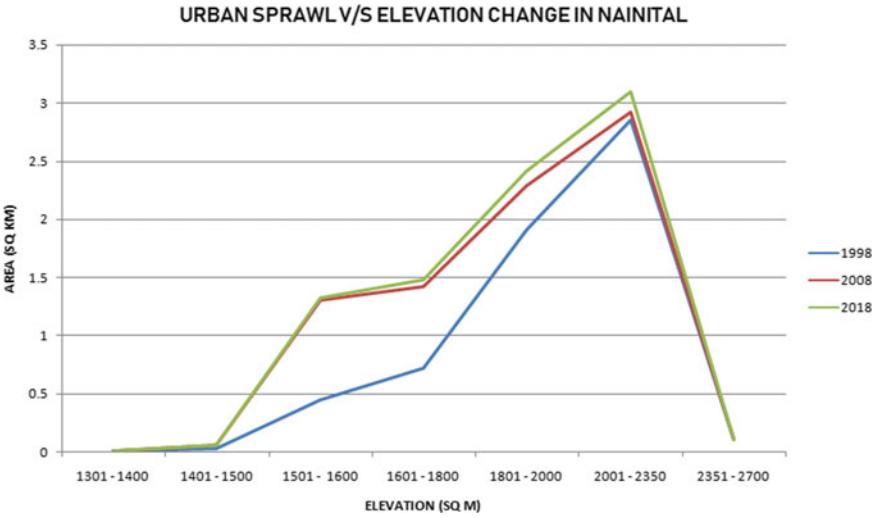

Fig. 23.11 Area under each elevation range in 1998, 2008, 2018 in Nainital

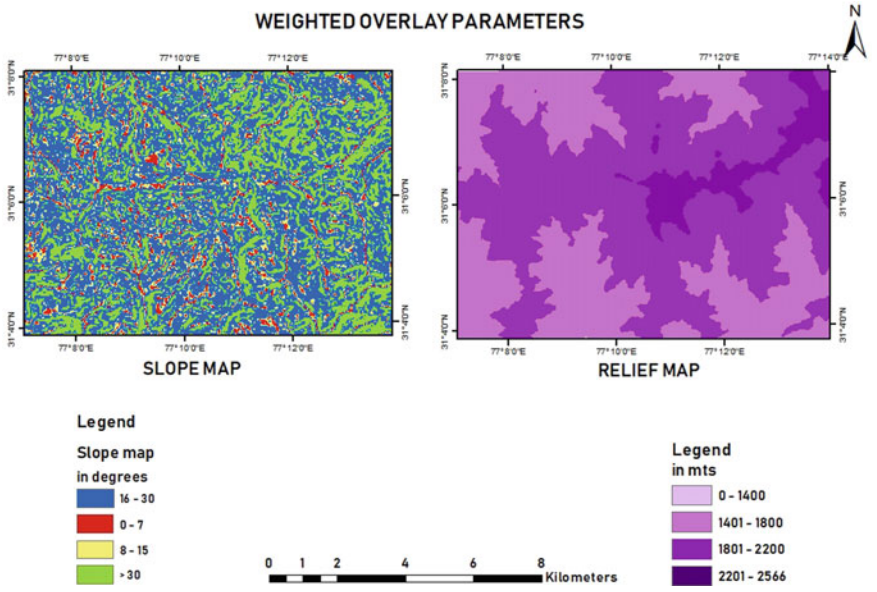

Fig. 23.12 Slope map and relief map of Shimla

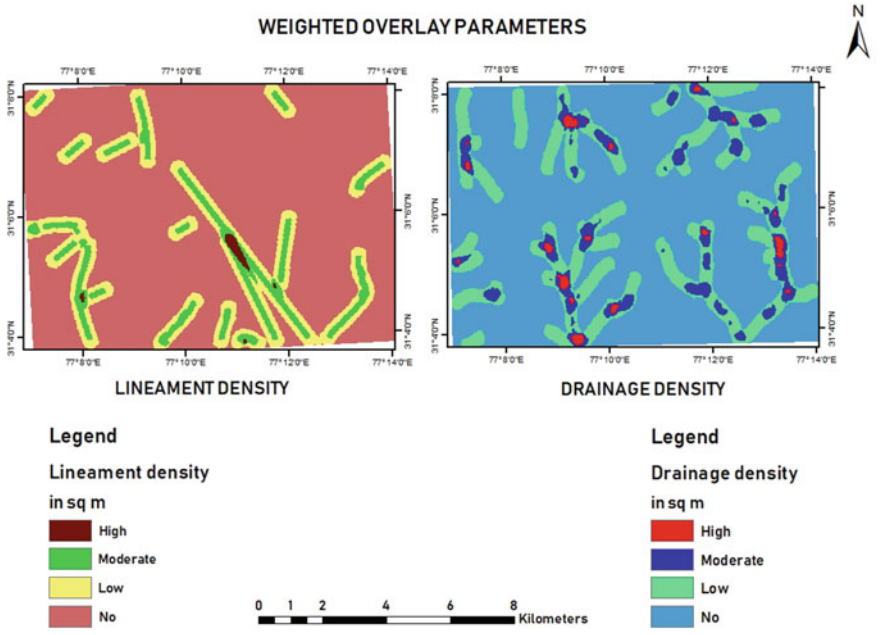

Fig. 23.13 Lineament density map and drainage density map of Shimla

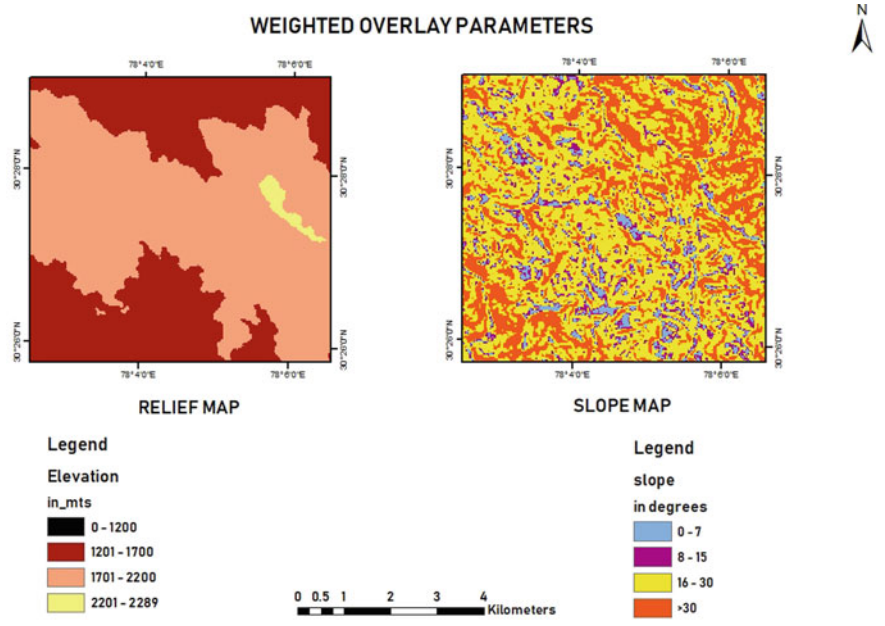

Fig. 23.14 Slope map and relief map of Mussoorie

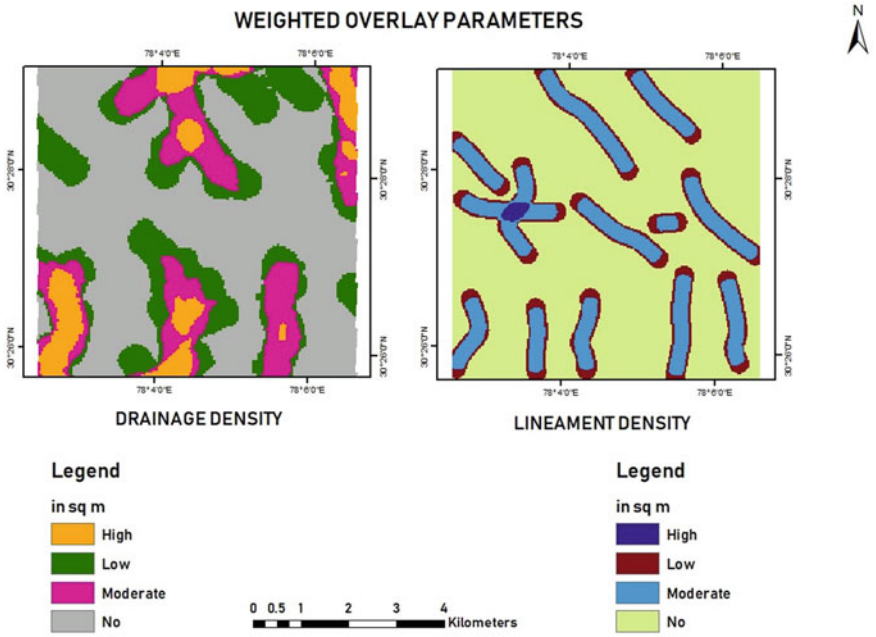

Fig. 23.15 Drainage density map and lineament density map of Mussoorie

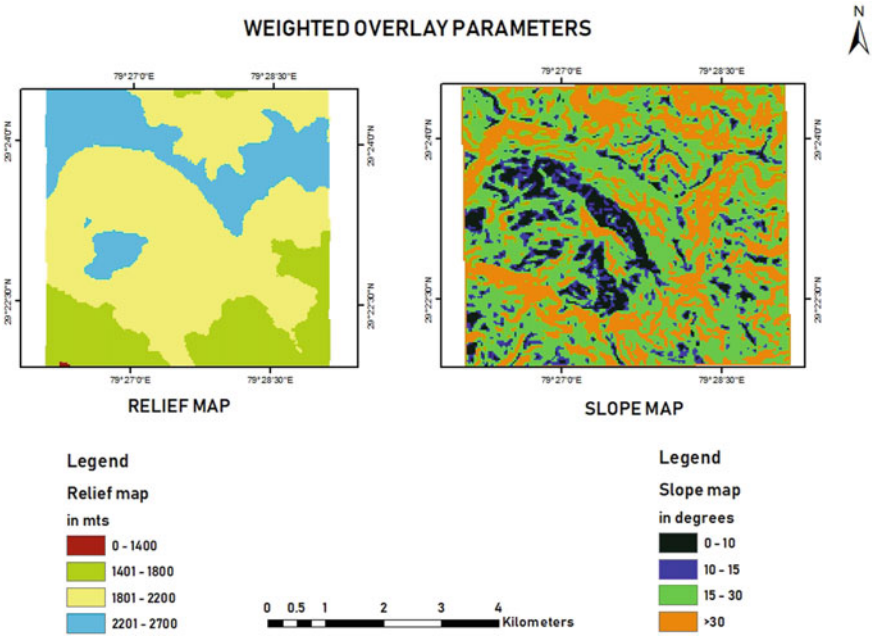

Fig. 23.16 Relief map and slope map of Nainital

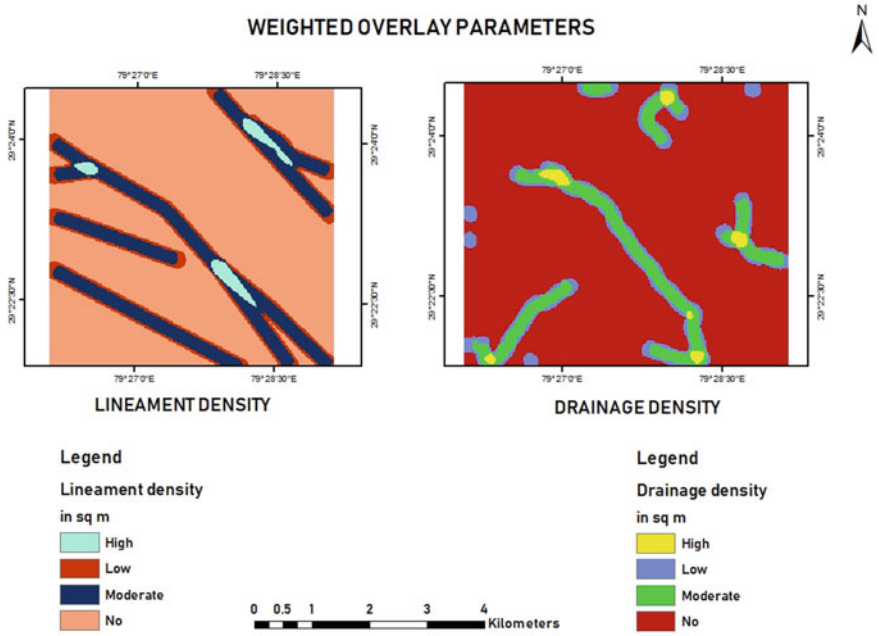

Fig. 23.17 Drainage density map and lineament density map of Nainital

23.4.4 Weighted Overlay Analysis for Groundwater Potential Zone Mapping

Each of these factors was classified into 4 classes. Slope map was classified as 0°–7°, 7°–15°, 15°–30° and more than 30°. The greater is the slope, the greater the runoff or lesser recharge of groundwater. Land Use map was classified into Forest area (major class in hilly regions), Built-up area, Agriculture or Water body (if any) and Barren Land. Drainage density and lineament density were classified into four zones of High, Moderate, Low, No density zones. Relief map was classified into 4 classes on the basis of the elevation ranges. Weightage assigned to each class, accordingly its importance in groundwater potential. Potential zone map area calculation has shown in Figs. 23.18, 23.19, 23.20, 23.21, 23.22 and 23.23.

23.4.5 Area Calculation and Correlation Graph

See Figs. 23.21, 23.22 and 23.23.

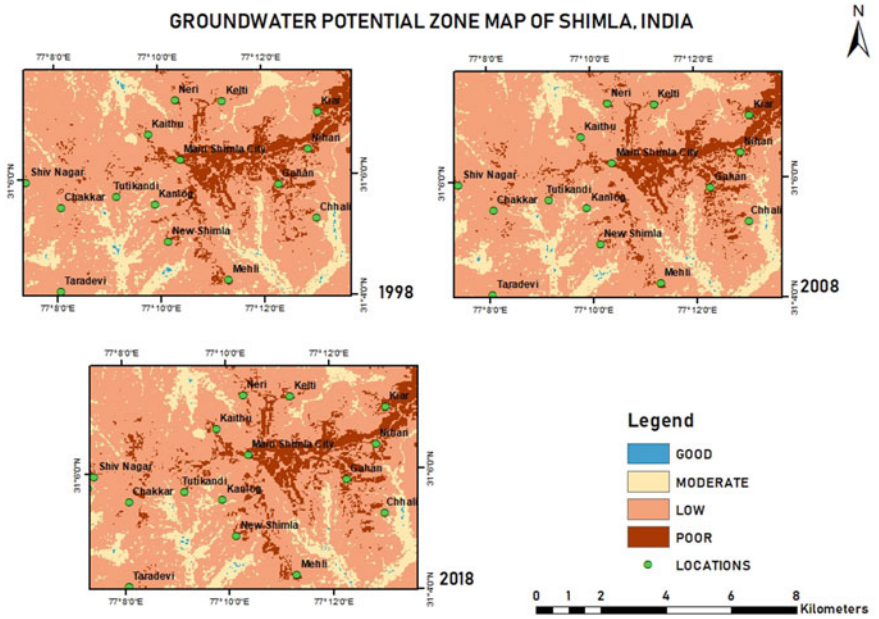

Fig. 23.18 Groundwater potential zone map of Shimla

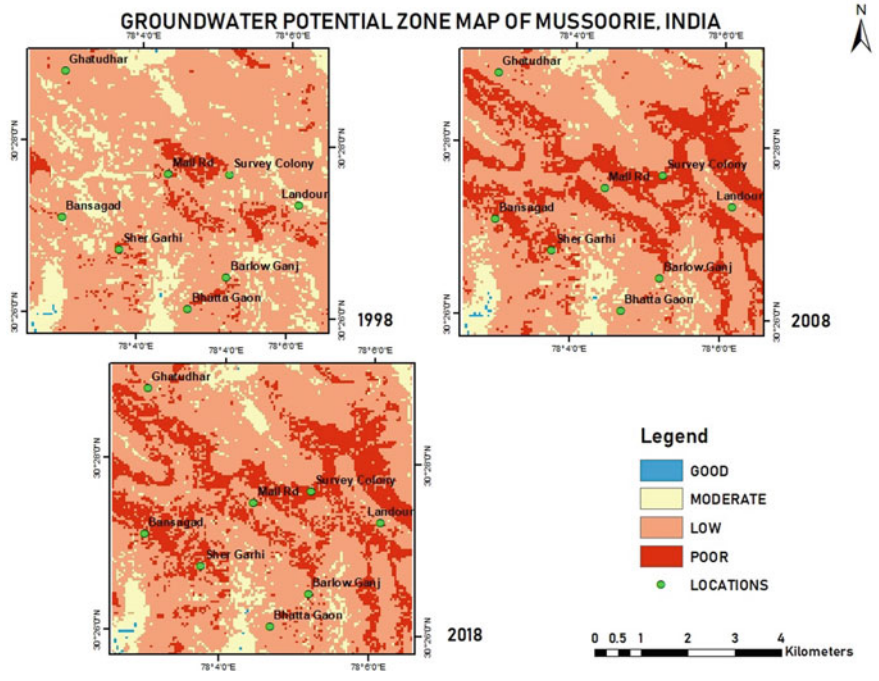

Fig. 23.19 Groundwater potential zone map of Mussoorie

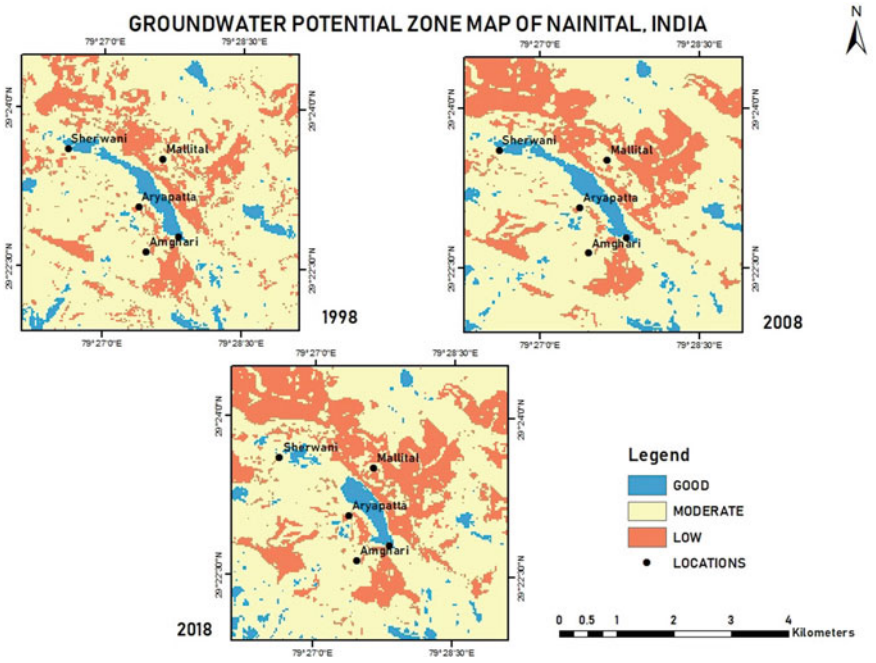

Fig. 23.20 Groundwater potential zone map of Nainital

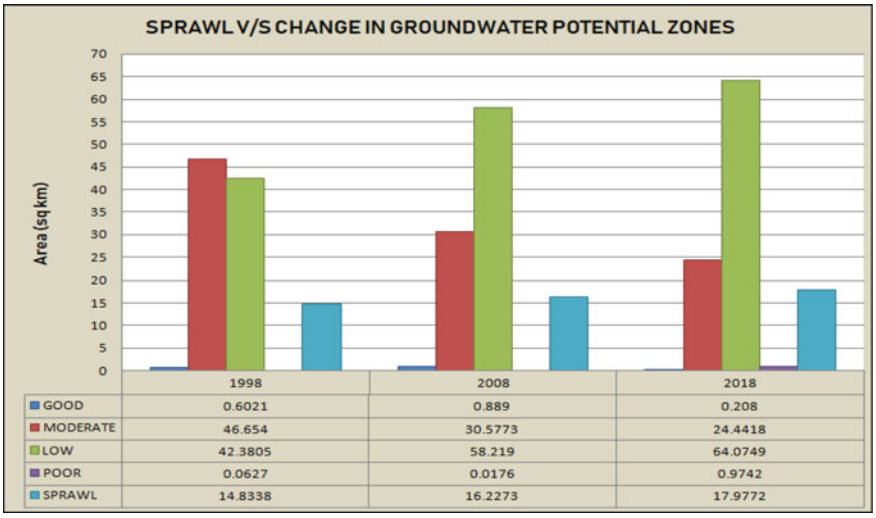

	1998	2008	2018
GOOD	0.6021	0.889	0.208
MODERATE	46.654	30.5773	24.4418
LOW	42.3805	58.219	64.0749
POOR	0.0627	0.0176	0.9742
SPRAWL	14.8338	16.2273	17.9772

Fig. 23.21 Change in groundwater potential zones as an effect of sprawl in Shimla

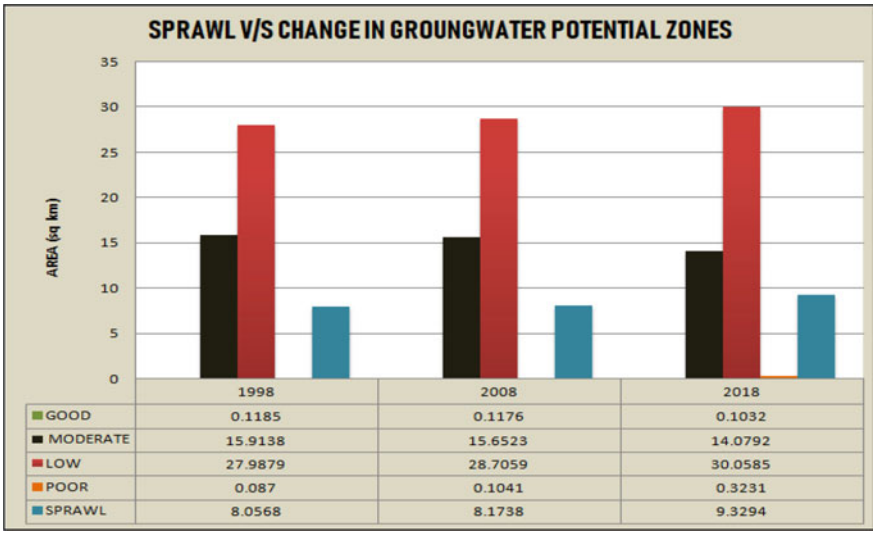

	1998	2008	2018
GOOD	0.1185	0.1176	0.1032
MODERATE	15.9138	15.6523	14.0792
LOW	27.9879	28.7059	30.0585
POOR	0.087	0.1041	0.3231
SPRAWL	8.0568	8.1738	9.3294

Fig. 23.22 Change in groundwater potential zones as an effect of sprawl in Mussoorie

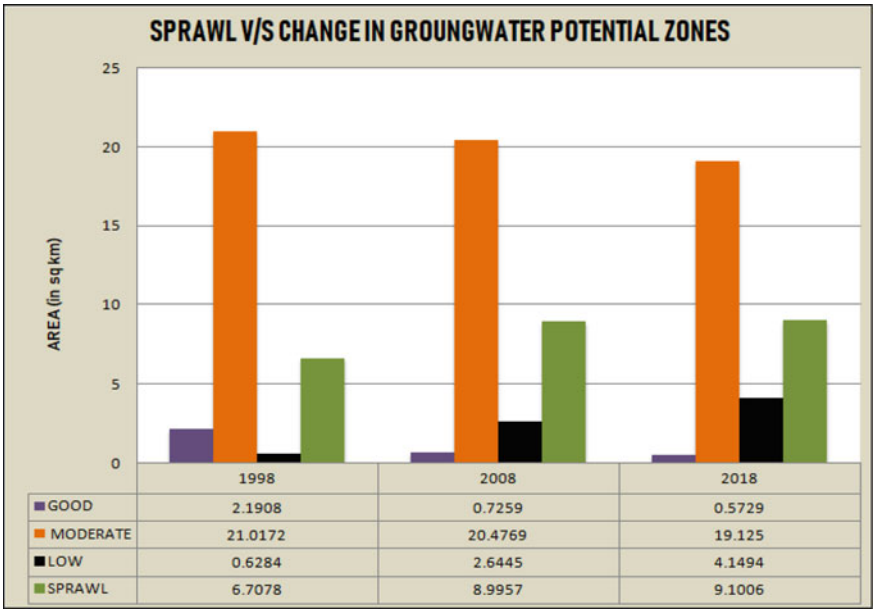

	1998	2008	2018
GOOD	2.1908	0.7259	0.5729
MODERATE	21.0172	20.4769	19.125
LOW	0.6284	2.6445	4.1494
SPRAWL	6.7078	8.9957	9.1006

Fig. 23.23 Change in groundwater potential zones as an effect of sprawl in Nainital

23.4.6 Comparative Assessment

In all the cases we see that the effect of sprawl directly effects all the zones. The area under Good is inversely related to Sprawl, which means that with increase in sprawl area under Good Groundwater Potential Zone decreases and Moderate and Low Groundwater Potential Zone increases. (Fig. 23.24).

In Shimla, there is a large area under Low Groundwater Potential Zone seen in 1998 and which has been tremendously increasing. The Good Groundwater Potential Zone remains negligible over the years and the Moderate zones too have been diminishing for worse.

In Mussoorie, the changes are mainly seen with the drastic increase in Poor Groundwater Zones while a large area under Low zones is changing to Poor zones. Due to its high relief, there are almost no Good Groundwater Potential Zones to be seen in Mussoorie since 2008.

In Nainital, there is no poor zone due to the presence of Naini Lake. There was very little area under Low Groundwater Potential Zone in 1998 but it has been majorly increasing since making it 5.0494 km^2 in 2018 from 1.6284 km^2 in 1998. The Good zones and Moderate zones are simultaneously decreasing.

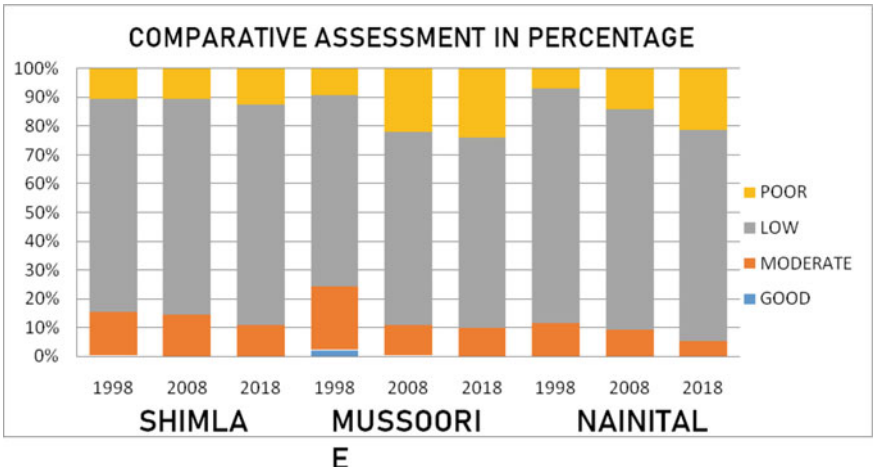

Fig. 23.24 Graph showing comparative assessment of Shimla, Nainital and Mussoorie cities of their groundwater potential zones

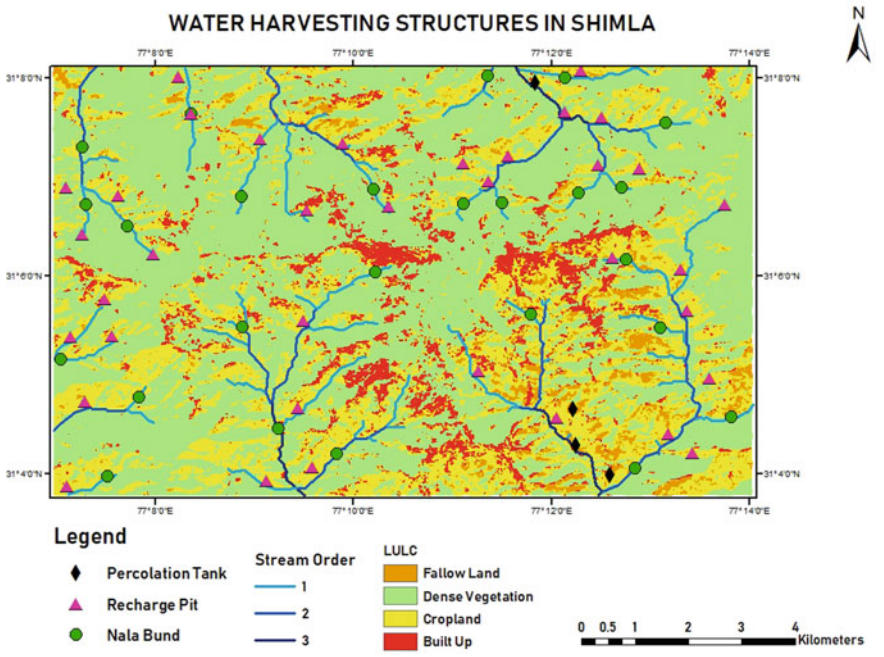

Fig. 23.25 Possible water harvesting structures in Shimla

23.4.7 Basin and Watershed Delineation for Water Harvesting Structures

As the change in Groundwater potential zones are seen to be only getting worse, the zones are changing from moderate low-poor zones, their respective watershed and basins were delineated, streams were assigned orders to suggest Water Harvesting structures. The mapping of Water harvesting structures requires a few factors to be considered, namely Stream order, Slope map and Land Use map. Percolation tanks, Recharge Pits, Nala Bunds and Farm ponds were suggested in order to hold the water from runoff and use it in household and agricultural purposes. (Figs. 23.25, 23.26 and 23.27).

23.5 Conclusions

In Shimla, the Built-up area was 10.83 km^2 in 1998, 16.95 km^2 in 2008 and 17.70 km^2 in 2018. Thus the major change was seen between 1998 and 2008. In Mussoorie, the Built-up area was 8.02 km^2 in 1998, 8.17 km^2 in 2008 and 9.32 km^2 in 2018. The major change is between 2008 and 2018. In Nainital, the Built-up area was

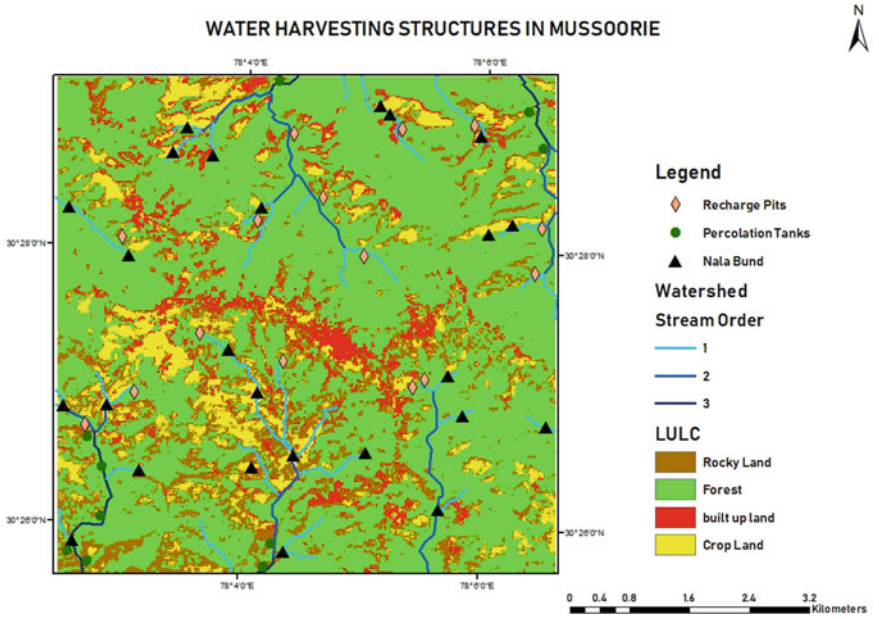

Fig. 23.26 Possible water harvesting structures in Mussoorie

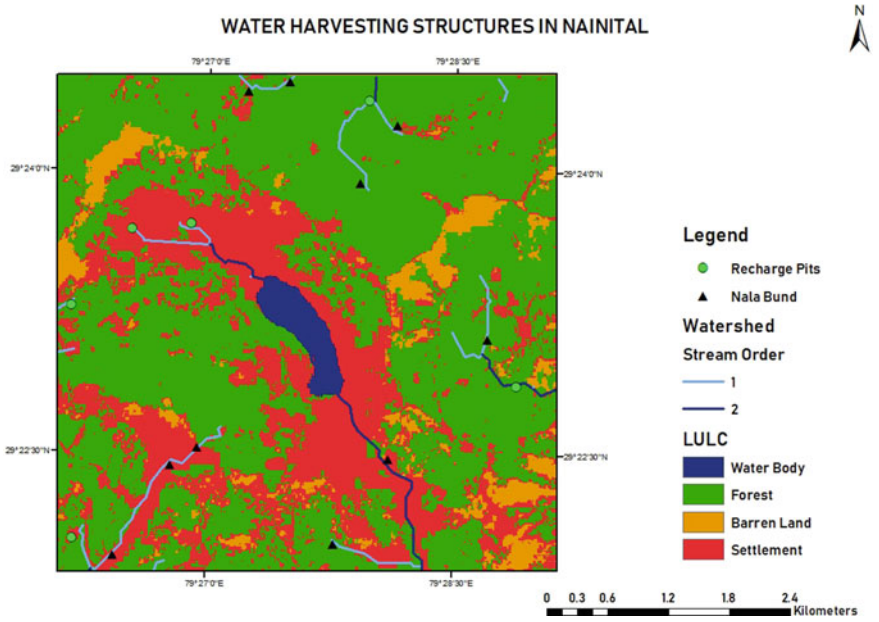

Fig. 23.27 Possible water harvesting structures in Nainital

6.70 km^2 in 1998, 8.15 km^2 in 2008 and 8.51 km^2 in 2018. So like Shimla, in this case, major change in area was seen between 1998 and 2008.In Shimla, there is a large area under Low Groundwater Potential Zone seen in 1998 and which has been tremendously increasing. The Good Groundwater Potential Zone remains negligible over the years and the Moderate zones too have been diminishing for worse. In Mussoorie, a drastic increase is observed in Poor Groundwater Zones while a large area under Low zones is changing to Poor zones. Due to its high relief, there are almost no Good Groundwater Potential Zones to be seen in Mussoorie since 2008. In Nainital, there is no poor zone due to the presence of Naini Lake. There was very little area under Low Groundwater Potential Zone in 1998 but it has been majorly increasing since, making it 5.04 km^2 in 2018 from 1.62 km^2 in 1998. The Good zones and Moderate zones are simultaneously decreasing. Area under Moderate Groundwater Potential zone in Shimla was 10.97 km^2 in 1998 and 8.64 km^2 by 2018, in Mussoorie, it was 9.34 km^2 in 1998 and 4.11 km^2 by 2018, in Nainital, it was 19.51 km^2 in 1998 and 17.52 km^2 by 2018 showing declination with increase in sprawl. Several small-scale methods can be applied to store and use water and for recharge of groundwater, which through the comparative assessment of the study areas is very essential in the case of Shimla, Mussoorie and Nainital.

References

Anbalagan R (1993) Environmental hazards of unplanned urbanization of mountainous terrains: a case study of a Himalayan town. Q J Eng GeolHydrogeol 28(3):179–184. https://doi.org/10.1144/GSL.QJEGH.1993.028.003.03

Azzam R, Strohschön R, Baier K, Lu L, Wiethoff K, Bercht AL, Wehrhahn R (2014) Water quality and socio-ecological vulnerability regarding urban development in selected case studies of Megacity Guangzhou, China. In: Kraas F, Aggarwal S, Coy M, Mertins G (Eds) Megacities, pp 33–58. https://doi.org/10.1007/978-90-481-3417-5_4

Ghosh P (2007) Urbanization—a potential threat to the fragile Himalayan environment. Curr Sci 93(2):128–127

Kamila R, Chandra Pal S (2015) Department of Geography, The University of Burdwan, Burdwan, West Bengal, India. Urban growth monitoring and analysis of environmental impacts on Bankura-I and II block using Landsat data. International Journal of Advanced Remote Sensing and GIS 4(1):965–975. https://doi.org/10.23953/cloud.ijarsg.91

Karthiyayini S, Vaardini US, Ragavi S (2016) Impact of urbanisation on groundwater—a review. Int J Appl Eng Res 11(3):378–383

Raviraj A, Kuruppath N, Kannan B (2017) Identification of potential groundwater recharge zones using remote sensing and geographical information system in Amaravathy Basin. J Remote Sens GIS 06(04). https://doi.org/10.4172/2469-4134.1000213

Tiwari PC, Tiwari A, Joshi B (2018) Urban growth in Himalaya: understanding the process and options for sustainable development. J Urban Reg Stud Contem India 4(2):15–27

Walker B (2011) Urban peaks in the Himalayas. China Dialogue. Retrieved from https://www.chinadialogue.net/article/show/single/en/4306-Urban-peaks-in-the-Himalayas

Chapter 24
Land Use/Land Cover Changes in Coastal Districts of Karnataka

Ashok Kumar and Anju Singh

Abstract Coastal environment has an instrumental bearing over the economy of the nation. By virtue of its diverse and precious resources productive habitats, rich biodiversity and its locational advantage to many of the human activities. It contains diverse and productive habitats for human settlements, resource development and local subsistence coastal zones have been among the most heavily utilized area because of their resources. The process of land acquisition for beach resort, hotels and industries has changed entirely the land use pattern of the coastal areas, leading to adverse effects on the environment, as well as on the local people. The increasing population and number of tourism in Karnataka coast, especially in the coastal strips, are the factor which leads to land use and land cover changes in the coastal zone. The area under irrigation, forest cover are increased, whereas the area under unirrigated and culturable waste land is decreased from 1995 to 2015. The coastal backwaters, estuaries, river mouths are well known for their productivity. Some of them are the Aghanashini, Kali, Sharavati, Mulki and Netrani river backwaters, are even today so. With passage of time, Land use and Land cover of coastal area undergoes significant change due to varying natural and anthropogenic causes. So it is essential to monitor the changes in land use and land cover at regular intervals for proper management of natural resources existing in an area. In the present study deals with the land use and land cover mapping and monitoring of the area around the river mouth, urban and village settlements and infrastructural activities Karnataka coast. The satellite data were interpreted based on visual interpretation keys to prepare land use and land cover map of year 1995 and 2015.

Keywords Coastal environment · River estuaries · Coastal features · Harvest food · River backwaters · Land uses land cover · Change detection · Satellite data

A. Kumar (✉)
Government First Grade College for Women Koppal, Karnataka 583231, India

A. Singh
Department of Geography, University of Delhi, AditiMahavidyalaya, Delhi 110039, India

R. B. Singh et al. (eds.), *Remote Sensing and Geographic Information Systems for Policy Decision Support*, Advances in Geographical and Environmental Sciences,
https://doi.org/10.1007/978-981-16-7731-1_24

24.1 Introduction

Kanara coast is a land of scenic beauty, located on the western coast of Karnataka state. The coastal area is known for sea, sand and sun. The small emerald on the western coast of Karnataka has natural aesthetic beauty, abundant greenery, beautiful and attractive sandy beaches, temples, churches, colourful and lively feasts and festivals, people with a rich cultural milieu. All these have made the Kanara coast, a prime tourist attraction not only among Indian states but also among the foreign tourists. The coastal region has a wide range of physical and social-cultural variations. The Western Ghats, Plateaus and sandy beaches reflect the geomorphic variations; on the other hand, environment of Kanara coast supports a variety of ecosystems and possesses rich biodiversity. As far as social-cultural identity is concerned, the Kanara coast is known for its prosperity and socio-economic well-being. A striking feature of Kanara coast is that it has varied geographical features with long coastal line, thick forest, perennial rivers and abundant flora and fauna (Dakshin Kannada District Gazetteer 1973).

24.2 Location and Extent

The Kanara coast is located in between 12º27′ and 15º32′ North latitude and 74º05′–75º45′ East longitudes, the total geographic area is 18,732 square kilometre, the coast line is 320 km long and 30–55 km wide in three districts of South Kanara, Udupi and North Kanara. The North Kanara district has 160 km long coastline while 98 km in Udupi district and the rest 62 km in South Kanara. There are three distinct agro-climatic zones ranging from plain coast lands, undulating hills in western part. The Arabian Sea in west and western scarps from east and coastal plain located in between with average width of 22 km. The average height of the region is 70–75 m, but in some places it can be as high as 150 m. There are ten major rivers draining their waters into the shore waters of Kanara coast (Singh 1997) (Fig. 24.1).

There are three districts consisting of total nineteen talukas of which eight are coastal talukas. In which five talukas are in North Kanara, two talukas are in Udupi and only one taluk is in South Kanara district. Kannada, Konkani and Tulu, Marathi is the major regional language spoken in this region. As per 2011 Census, the total population consists about 43, 63,617 with average density of 278 per square kilometre. The sand bars originated in important river estuaries include Netravati-Gurpur, Mulki, Hangarkatta, Gangolli, Sharavathi, Aghanashini, Gangavali and Kalinadi. There are number of sand dune physical features like barrier spits at Tannirbavi, Sasihitlu, Udyavara, Hoode, Hangarkatta and Kirimanjeshwara formed due to change in river course and deposition at mouth region, also causing river migration. Kanara coast has about 95 beautiful beaches that attract many national and international tourists and are suitable for beach tourism (Deshpande 1992).

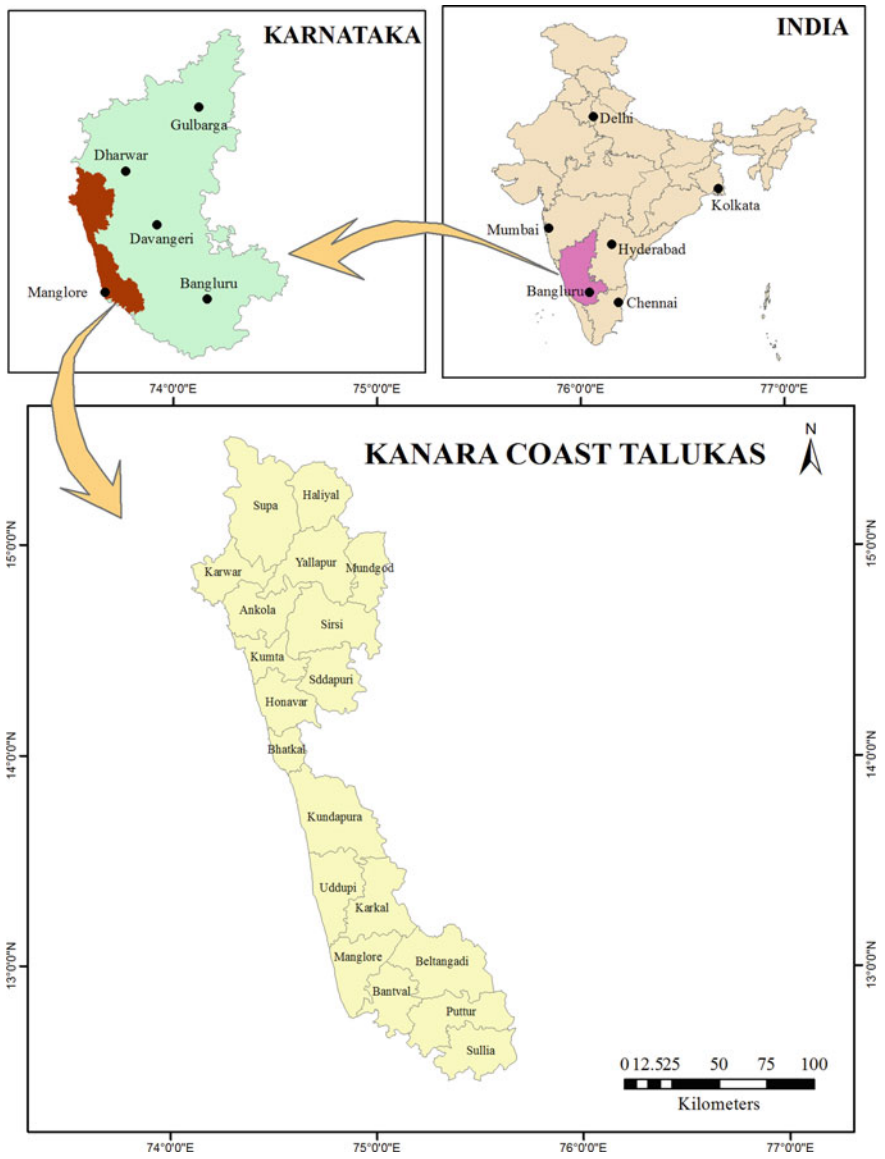

Fig. 24.1 Location and extent of the study area

24.3 Relief Features

The Mysore plateau is located over southeastern part of south Kanara district; it originated with Dharwar system and consists of volcanic rocks, crystalline schist and granites. Several rugged topography covered from western side and the Western

Ghats surrounded from east with 500 to 750 m. The Western Ghats also known as Sahyadri hills with elevation of 600–900 m height, it crosses parallel in all three districts of Kanara coast with unique natural beauty, having more than 10 biodiversity hotspots. The undulating plateau and coast line show the average relief about 1812 m in talukas of Yallapur, Mundgod and Sirsi in eastern part of study area due to sharp-edged Sahyadri hills. Its relief decreases towards western part of Kanara coast with less than 5 m near coast (Fig. 24.2).

The hilly chains of the Western Ghats which run north–south direction, parallel to the coast, act as the backbone of the district. These hills, unlike the rest of the Western Ghats, seldom exceed 600 m. At several places in the district, the hills directly run right into the sea, interrupting the continuity of the sea beaches in Karwar, Ankola, Honavar and Kumta talukas and providing ample rocky inter-tidal and sub-tidal habitats with their unique flora and fauna (Daniels 1989).

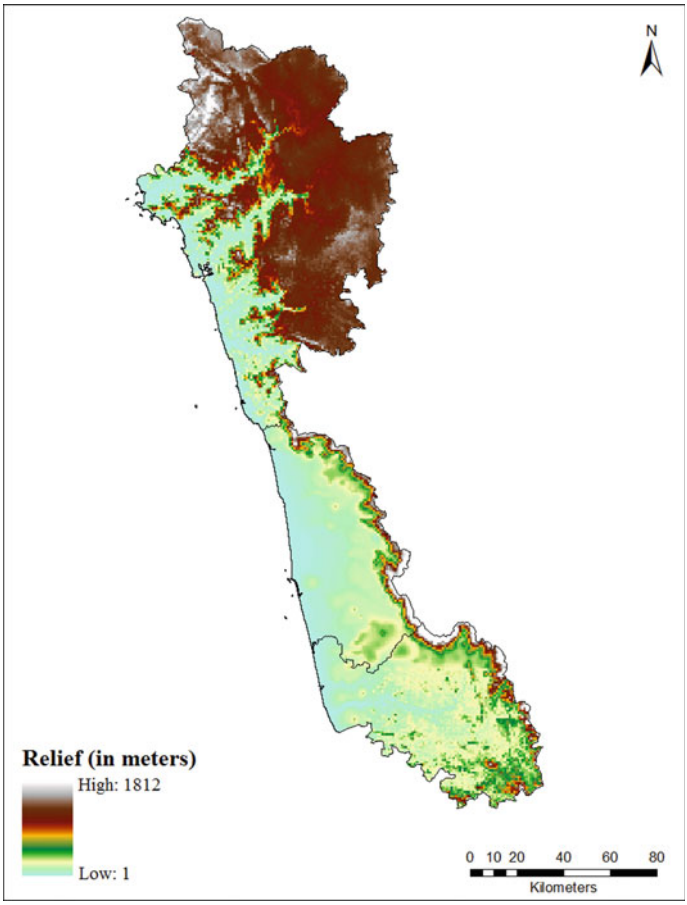

Fig. 24.2 Relief features of Kanara coast

On the river banks, the alluvial plains are found, fluvial basins of alluvial formation are found in the rivers of Kali, Gangavali, Aghanashini, Sharavati, Bedti, Venkatapur, Varada, Varahi, Mulki, Netravathy and Chakra. The *Gazani or Khar* lands are another important part of the plains. These *Gazani* lands are basically alluvial formations, which are favourable for the growth of mangroves. The bays form a part of the inner shelf zone, with depths varying from 3 to 16 m. These aspects represent the evidences for both an emergent and submergent coast, suggesting a compound nature of coast (Bannur 1994).

The coastal plains of Kanara coast are largely wave-cut platform, thus it is an erosional rather than depositional except some beaches. It has varying width of 25 km over Karwar taluka and about 45 km width in Mangalore. The average height is less than 200 m from the mean sea levels. The coastal track is steep-like terraces due to oscillations in the sea levels during the geological past. Features indicating the submergence such as drowned river valleys, lagoons, bars and wave-cut cliffs are common. There are no large river deltas along the coast owing to most active south west monsoon which produces waves with greater height. These washed the coast and carried down the riverine loads into the deep sea (Hegde 1999).

24.4 Drainage

Since history all the coastal rivers are the most important for economic, social and political development and fresh water resource for human beings. It is largely related to the availability and distribution of freshwater riverine systems. Kanara coast is the land of ten major rivers and many small tributaries, with their sources water are from Western Ghats (Chapman 1996). Coastal Kanara region receives heavy rainfall during monsoon period, the depth of flow of these rivers ranges from 9 to 10 m, and the riverbank height is about 12–15 m. Rivers created many magnificent physical features like waterfalls, caves and steep riverine valleys, in the region such as the Jog falls, the Lushington (Unchalli) falls and Magod falls across Sharavati, Aghanashini and Gangavali (Fig. 24.3 and Table 24.1).

24.5 Land Use/Land Cover Change in Kanara Coast

The land use refers to the several uses of land which are primarily the results of human activities on land while land cover refers to the cover of land surface as natural and biological phenomena such as vegetation, water bodies and others resulting due to land transformation. Land use gives an over view of how different patches of lands are being utilized under various anthropogenic activities. Land cover is a basic parameter which evaluates the content of earth surface as an important factor that affects the condition and functioning of the ecosystem. Land cover is a biophysical state of the

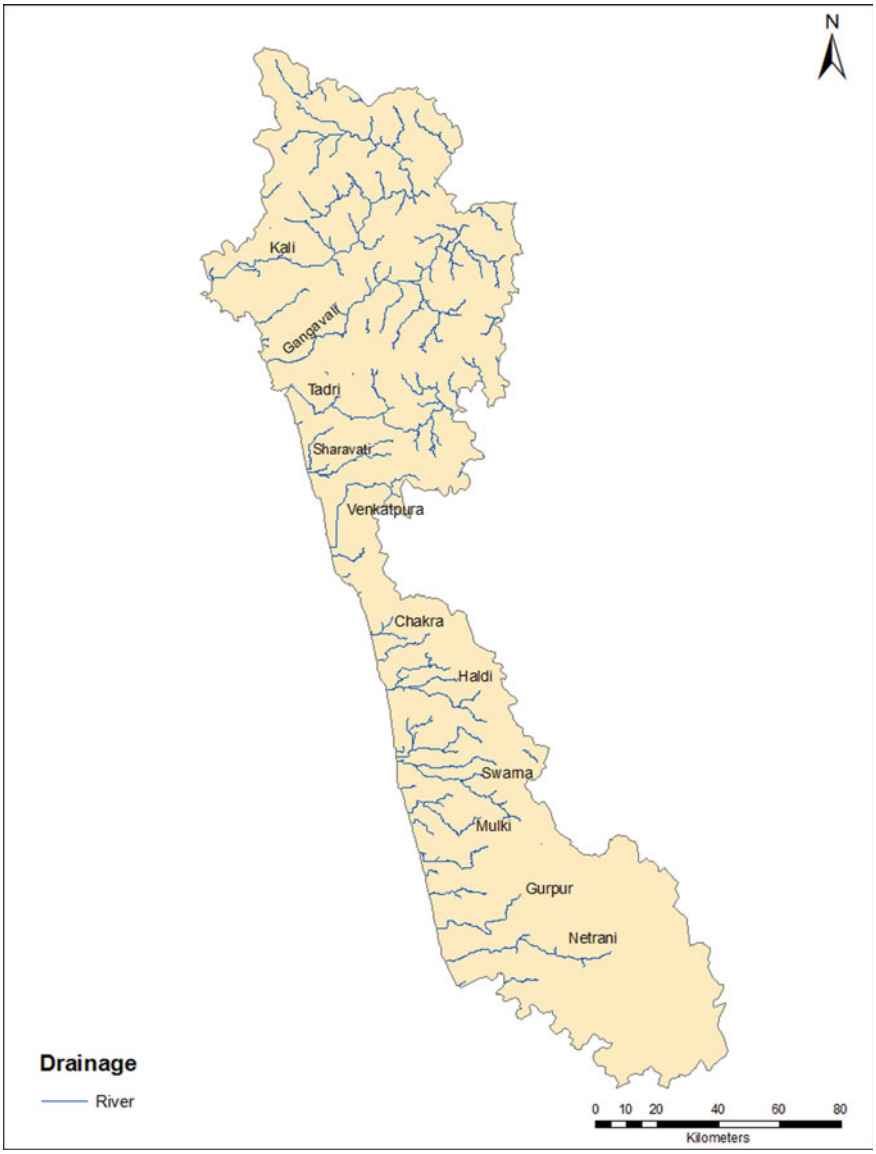

Fig. 24.3 Drainage system of Kanara coast

earth surface, which can be used to estimate the interaction of biodiversity with the surrounding environment.

In recent years, land use land cover analysis plays an important role in the fields of resource management and development studies. Land use and land cover in developmental studies has become increasingly important because the region plans to

Table 24.1 Major river system of Kanara coast

Major river basin	Average-annual flow (mm^3)	Length within the state (km)	Basin area (Sq. kms)
Kali river	6631	184	844
Gangavali/Bedti	4736	161	925
Aghanashini	2556	121	547
Sharavati river	7399	128	755
Venkatapur river	3066	45	335
Varada river	3505	96	244
Varahi	2263	66	756
Mulki	7575	106	3067
Netravathy	12,813	103	3222
Chakra	892	75	336
Total	**51,436**	**1195**	**12,898**

Source Ranganath (2010)

overcome the problems of haphazard, uncontrolled development, deteriorating environmental quality, loss of fertile agricultural lands, destruction of water bodies and loss of wildlife habitat (Arveti et al. 2016). Land use changes mostly result from individual and social responses to changing economic conditions, which are mediated by institutional factors. Opportunities and constraints for new land uses are created by markets and policies and are increasingly influenced by global factors. Globalization as such is not a driver of land use change but is a process that underlies the other driving forces land use change as the immediate and principal (Lambin et al. 2003). Change detection is the process of identifying difference in the state of an object or phenomenon by observing it at different time. Change detection in land use land cover can be performed on temporal scale such as decades to assess landscape changes caused due to anthropogenic activities on the land (Yadav et al. 2012). These anthropogenic activities are due to rapid growth of human population and demands of food resources.

24.6 Recent Developmental Activities in Kanara Coast

The last two decades from 1995 to 2015 there is drastically changed the physical landscape of Karnataka coastal districts, owing to rapid growth of settlements and increase in overall population of the rural villages contributing expansion of conversion of valuable forest land into built-up area. The expansion of New Mangalore harbour and other small ports into large ports for fishing and other commercial activities. The project Sky bird is the one of the big harbour of Indian Defence Ministry, which occupied large area and grabbed several islands for experimental purposes.

The improving infrastructure activities like expansion of National Highway no 17 from two lanes to six lanes highway also attracted the rural population to migrate near the highway. Increase in number of tourists from national and international causing upcoming of hotels and recreational centres in Karwar, Ankola, Bhatkal and Honavar. The increase in rural population caused expansion of agricultural landholdings and decrease in per head cultivable land. Conversion of forest land for cultivation, coastal mangroves and river backwater into fishing ponds and paddy cultivation and other aquaculture activities mainly over the low lying areas of river mouth. The traditional agricultural system has been changed into modern sophisticated profit motive cultivation of cash crops, which leading to mono-crop system and loss of fertility, over leaching of soil from high altitudinal areas. The natural water bodies converted into manmade lakes, and river flow has been stopped with construction of Dams and bands in interior parts of coastal talukas. The southern part of Kanara coastal talukas has increased with settlement construction and much change occurred in cultivable lands. But in North Kanara talukas, the land use and land cover mainly caused owing to construction of hotels and expansion of infrastructural activities.

24.7 Land Use Land Cover Change

In the Kanara coastal area, the utilization of land depends upon physical factors like topography, soil and climate as well as upon social factors such as population density, land tenure and infrastructure development. There are spatial and temporal variations in land utilization due to above factors.

The process of land acquisition for beach resort, hotels and industries has changed entirely the land use pattern of the coastal areas, leading to adverse effects on the environment, as well as on the local people. The increasing population and number of tourism in Kanara coast, especially in the coastal strips, are the factor which leads to land use and land cover changes in the coastal zone. The area under irrigation, forest cover are increased, whereas the area under unirrigated and culturable waste land is decreased from 1995 to 2015 (Figs. 24.4 and 24.5).

But maximum changes in irrigated land and forest area have increasing trend but lesser intensity as compared to 1995, there is a decreasing trend in unirrigated, culturable waste land and area not available for cultivation. In the processes of land use and land cover changes, the unirrigated area and change in the vegetation have been affected worst, especially sand dune vegetation and mangroves. However, the plantation constantly been done in the state but the area under plantation is decreasing with the developmental activities, while the area under deforestation is increasing every year. In 1995, the southern talukas of Kanara coast experiences intensive cultivation especially in South Kanara district as compared to northern talukas. Most of urban built-up are located over the coastal zone, and small villages are located over eastern region of study area. Forest cover is maximum in North Kanara talukas but in South Kanara and Udupi, forest cover is located over easten talukas of the district. The fallow/sediment land is maximum in northern Kanara coast, and many lakes, ponds

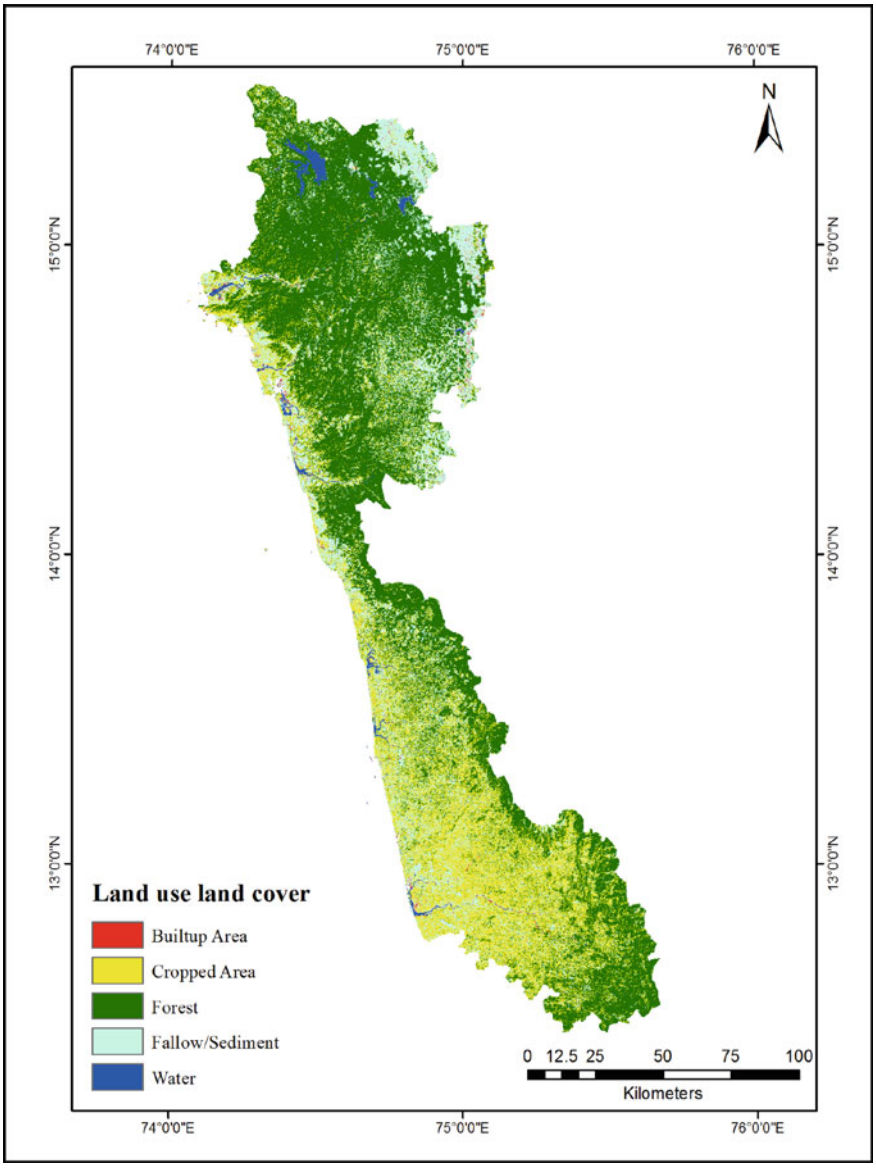

Fig. 24.4 Land use/land cover in 1995

and other water bodies are mainly sharp and swift flowing rivers, covers broad area near estuary region.

In the year 2015, land use land cover changed at faster rate as compared to 1995. The land for agricultural utilization has been increased in southern parts of the study area as well as it spreading towards northern talukas of North Kanara district, the

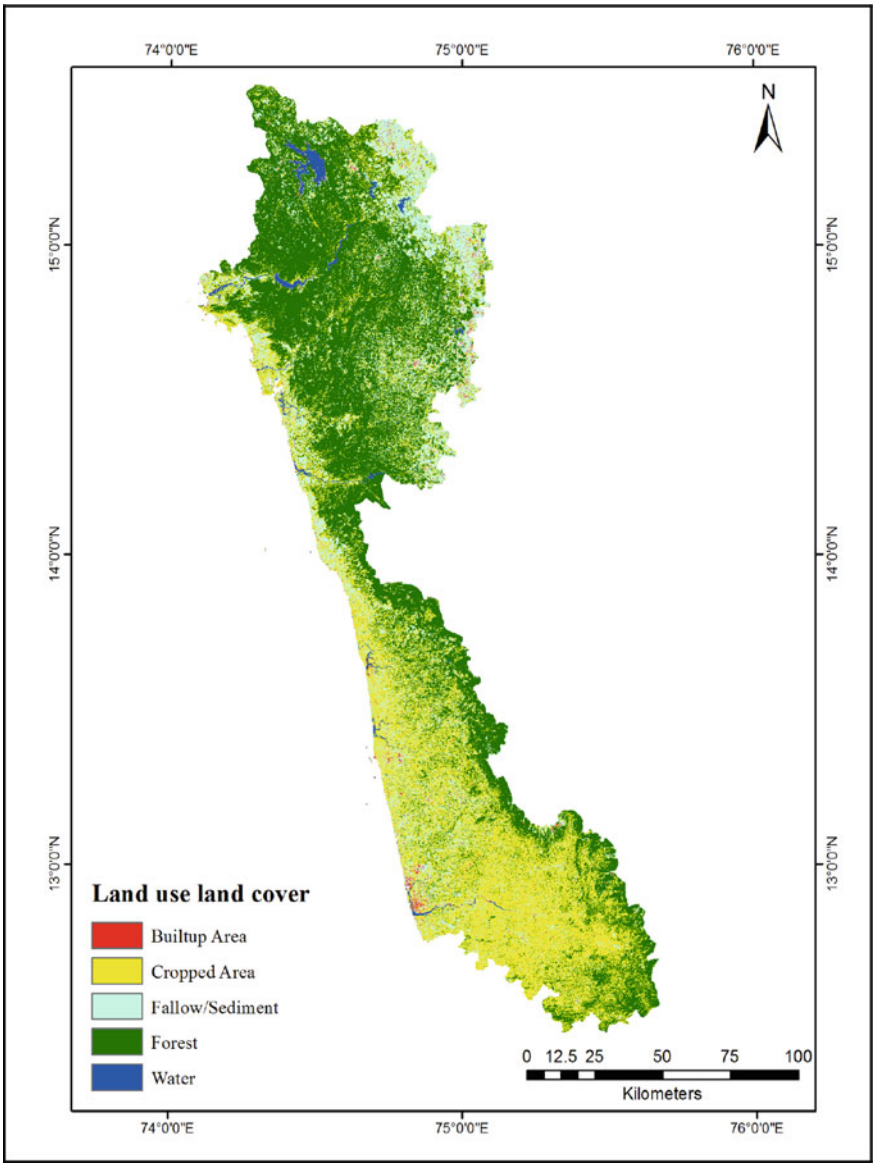

Fig. 24.5 Land use/land cover in 2015

earlier forest land of eastern talukas of Kanara coast was covered with thick forest but recently it has been cut in patches and converted for agricultural and plantation purposes. Forest area is also decreasing due to increase in population and spreading of villages in forest areas and cutting forest for settlement purposes. The built-up area increased especially in coastal area owing to overgrowth of town and cities.

The built-up area is mainly expanding to near sea due to increased tourism and other recreational activities. Therefore, in 2015, forest area is decreased and thick forest remained only in eastern portion of southern talukas and the central hilly regions of North Kanara district. The fallow land increased in northeastern talukas and few patches another talukas. The water river water bodies expanded their water cover area due to building of many dams and reservoirs, river mouth expanded due to increase in backwater cover.

24.8 Vegetation

The strong seasonal climate is found in rain-forested regions of Western Ghats, the Ghats has substantial tracts of the tropical lowland evergreen rain forest formation in areas where there is a dry season of up to seven months. In low land areas, the Sorab Ghat region *Kan* evergreen forest found, in the Karnataka state where annual rainfall is 1500–1800 mm combined with dry season (Whitmore 1984). The Ghat forests have floristically tropical vegetation, yet in the winter dry season, they are exposed to very low temperatures and tree falls to protect from winter cold. Owing to high altitude, ranges stop the clouds and cause the heavy rainfall during the monsoon season for about four months (Pascal 1986).

According to district handbook 2013–14, the forest cover is approximately 10,42,173 hectares with taluk-wise average forest cover is 54,851 hectares and total geographical area is 18,58,506 hectares, making Kanara coast as one of the most forested region in peninsular India. The most of forest cover is under the jurisdiction of the forest department and the revenue department (Fig. 24.6). The coastal taluk-wise distribution of forest area varies each other, the highest of forested land area 1,65,873 hectors in Supa taluk followed by Yallapur with 1,16,986 hectors and lowest is 2902 hectors in Mangalore owing to largest metropolitan city of Kanara coast maximum area is occupied for urban built-up and industrial and harbour developmental purposes. The tropical wet evergreen type forest is found in the eastern part and the tropical moist deciduous type forest facing the western side (Puri 1960). Champion and Seth (1968) have classified the forests of the eastern zone in the category of moist deciduous type and forests on the western slope covered with tropical evergreen type and have included. According to Arora (1961) the evergreen forests, deciduous forests and scrub forests are located in the region (Fig. 24.7).

The total forested area is highest in North Kanara district, but in recent years encouraged social forestry and plantation of trees over waste lands, barren lands, besides roads and plantation of coconut and other fruit-bearing trees surrounding the houses are contributing much for green forest (Fig. 24.8).

The vast forest ecosystems in river estuaries contain great mosaic of various habitats and sub-habitats that support tremendous biological diversity. While coastal sand dune also supports various types of flowering plants and also acts as habitation for small animals and bacteria. Most charismatic species, including flowering plants, mammals, birds and especially many marine fishes migrate twice in year to coastal

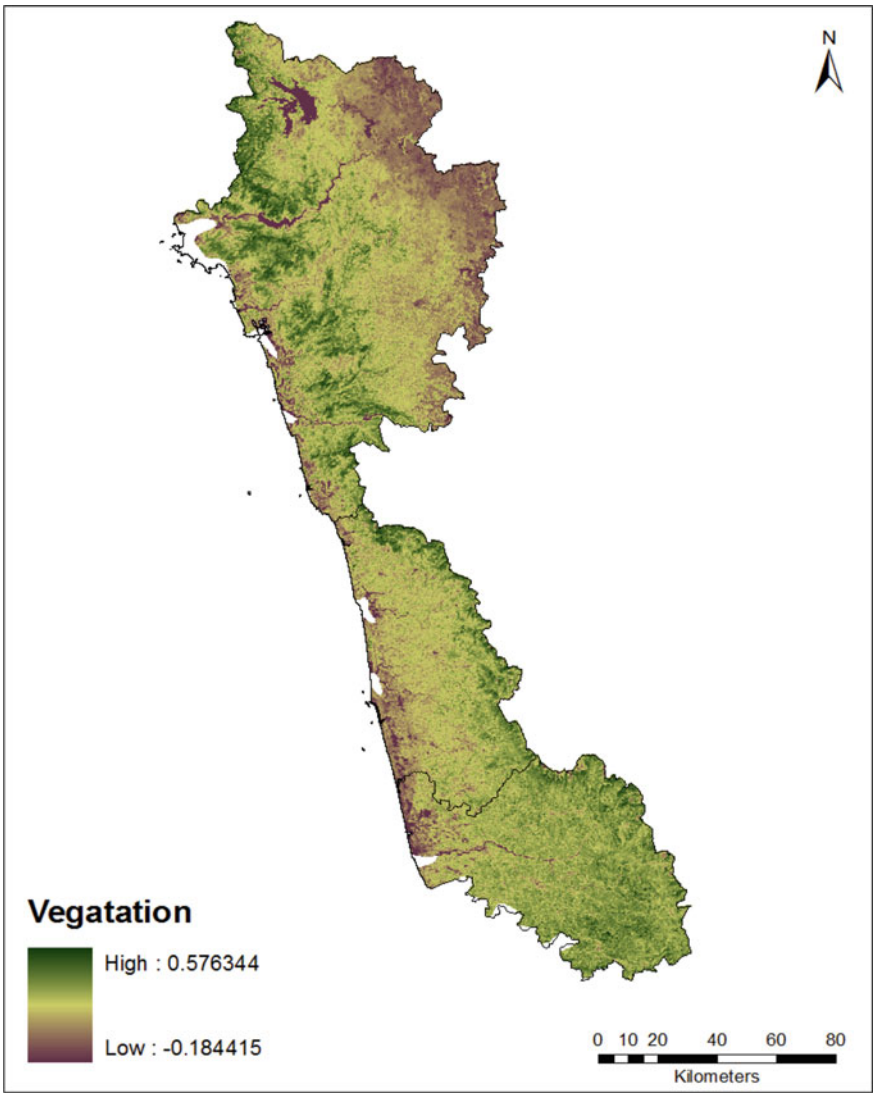

Fig. 24.6 Vegetation cover shown through NDVI in Kanara coast

mangroves areas for hatching the eggs. Therefore, mangrove forests at all major river mouths are very important for coastal biodiversity (Plates 24.1 and 24.2).

These forests of the Western Ghats perform several critical ecological functions that support agro-forestry, agriculture and other forest-based livelihoods in the district. The forests are also the catchments of important rivers such as the Aghnashini, Sharavathi, Kali and Gangavalli.

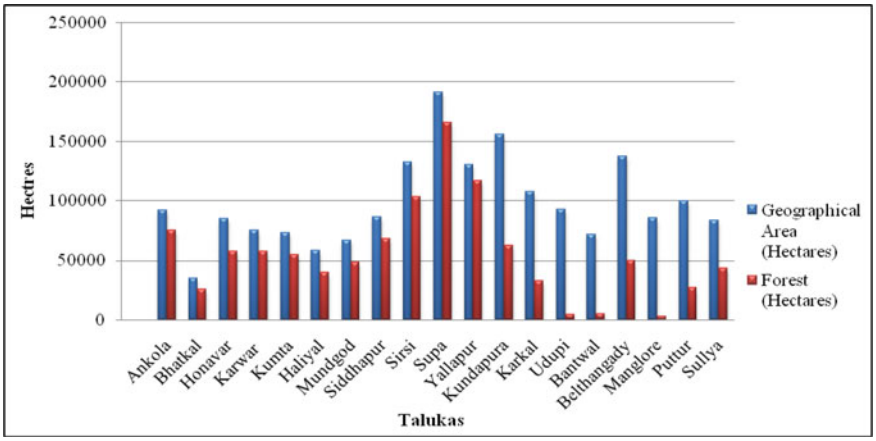

Fig. 24.7 Taluk-wise geographical area and forest cover in 2014 in hectares. *Source* Kanara Districts At Glance Mangalore, Udupi and Karwar, 2014–15

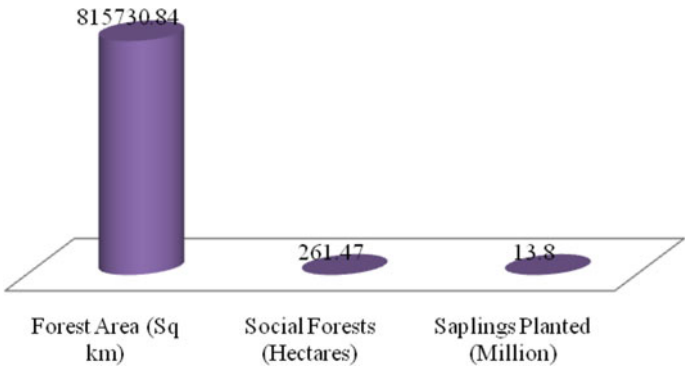

Fig. 24.8 Total forest area, social forestry and planted trees in 2012. *Source* Forest Department Government of Karnataka (2012)

24.9 Conclusion

However, it can be inferred that the Kanara coastal region has an advantageous location in terms of its human and natural resources. The geological formation left many old relic mountains and mineral resources. The region has been under the colonial influence and which has immensely affected the economy, literacy, culture and lifestyle of the people. The economy and the lifestyle are also highly influenced by the geographical features, therefore, the land use and land cover changes show the root of the problems of continuous increasing in population, settlements and decreasing in forest cover causing changes in long-term climate of the region.

Plate 24.1 Mangrove forest in river Haladi Estuary in Udupi taluk

Plate 24.2 Coastal sand dune vegetation in Tagore Beach in Karwar

References

Arora RK (1961) The forests of North Canara District scrubs. J Ind Bot Soc 40(2)

Arveti N, Etikala B, Dash P (2016) land use/land cover analysis based on various comprehensive geospatial data sets: a case study from Tirupati area, South India. Advances in Remote Sensing 5:73–82

Bannur CR (1994) Studies on Coastal Environs Using Remote Sensing Techniques and Morphology of the Beaches of North Kanara District. Karnataka University Dharwad, Karnataka India, p 136

Census of India (2011) Karnataka series-30: final population totals (state, district, taluk and town). Government of India, New Delhi

Champion HG, Seth SK (1968) A revised surveys of the forest types of India. Government of India Press, Nasik

Chapman D (ed) (1996) Water quality assessment: a guide to the use of biota sediments and water in environmental monitoring. Cambridge University Press, London
Dakshin Kannada District Gazetteer (1973) Karnataka Gazetteer Department. BWSSB Building Cauvery Bhavan, Bangalore
Daniels RJR (1989) A conservation strategy for the birds of uttara kannada district. PhD thesis, Centre for Ecological Sciences, Indian Institute of Science
Deshpande CD (1992) India: a regional interpretation. Northern Book Centre, New Delhi
Director of Planning, Statistics and Evaluation (2010) North Kanara District at a Glance, 2009–10. Government of Karnataka, Bangalore
Gomes OJF (2004) West coast. National Book Trust, New Delhi
Government of Karnataka (2012) A handbook of Karnataka 2012. Karnataka Gazetteer Department, Bangalore
Government of Karnataka. North Kanara District Statistics at a Glance, 2014–15. Zilla Panchayat, Karwar
Government of Karnataka, South Kanara District Statistics at a Glance, 2014–15. Published by District Statistical Office, Mangalore
Government of Karnataka. Udupi District Statistics at a Glance, 2014–15. District Statistical Office, Udupi
Hegde N (1999) Uttara Kannada District: a profile of development: planning, conservation and sustainable alternatives, Yellapur
Lambin EF, Geist HF, Lepers E (2003) Dynamics of land-use and land-cover change in tropical regions. Department of Geography, University of Louvain, Belgium LUCC, International Project Office
Pascal JP (1986) Explanatory booklet on the forest map of South India, French Institute, Pondicherry, pp 19–30
Puri GS (1960) Indian forest ecology, vol 1. Oxford Book Company, New Delhi
Ranganath (2010) Regional geography of Karnataka. Mysore Book House Publications. Mysore, pp 14–29
Singh RL (1997) India: a regional geography. UBS Publications, New Delhi
Udupi District Gazetteer (2012) Karnataka Gazetteer Department. Eighth Floor, BWSSB Building Cauvery Bhavan, Bengaluru.
Uttara Kannada District Gazetteer (1985) Karnataka Gazetteer Department. Eighth Floor, BWSSB Building Cauvery Bhavan, Bengaluru
Whitmore TC (1984) Tropical rain forest of the far east, 2nd edn. Oxford University Press, Oxford
Yadav P, Kapoor M, Sarma K (2012) Land use land cover mapping, change detection and conflict analysis of Nagzira-Navegaon Corridor, Central India using geospatial technology. Int J Remote Sens GIS 1:90–98

Chapter 25
Spatial Modelling for Municipal Solid Waste Management Using Remote Sensing and Geographic Information System

Dinesh Kumar Tripathi, Manish Kumar, and Vivekananda Biswas

Abstract Municipal solid waste management (MSWM) is a greatest challenge before environment scientists, urban planners and decision makers of the world. With the rapid urbanization, India is also facing massive waste management challenge. In the present study, an attempt was made to study the solid waste disposal problem and their proper management through spatial modelling using remote sensing and Geographic Information System techniques selecting a sample area of Almora town, Uttarakhand (India). Cartosat-1 data of the year 2016 was processed in Erdas Imagine 9.1 and ArcGIS 9.3 GIS packages to find out existing waste dumping ground/landfill sites and waste bins in the study area. The spatial modelling was carried out to determine the suitable sites for proper disposal of municipal solid waste (MSW) generated from Almora Town using GIS-based multi-criteria evaluation technique. In the study area, five sites were identified in which one has been proposed and recommended as the best suitable site.

Keyword Municipal solid waste management**.** Spatial modelling · remote sensing · geographic information system · multi-criteria evaluation technique

25.1 Introduction

In last few decades, there has been a significant increase in municipal solid waste (MSW) generation particularly in developing countries like India. This is largely

D. K. Tripathi (✉)
Rana Pratap Post Graduate College, Sultanpur 228001, UP, India

M. Kumar
Department of Geography, School of Basic Science, Central University of Haryana, Mahendragarh, Haryana, India
e-mail: manish.ks@cuh.ac.in

V. Biswas
Department of Urban Land Development and Management, Ethiopian Civil Service University (ECSU), Addis Ababa, Ethiopia

R. B. Singh et al. (eds.), *Remote Sensing and Geographic Information Systems for Policy Decision Support*, Advances in Geographical and Environmental Sciences,
https://doi.org/10.1007/978-981-16-7731-1_25

because of rapid population growth and industrialization. The per capita of MSW generated daily, in India ranges from 100 g in small towns as witnesses to 500 g in large towns (Singhal et al. 2000). At present in India, about 125 million tonnes of MSW is being generated annually, and it is estimated to increase at a rate of 1% to 1.33% per annum. (CPCB Report 2004). Over 377 million urban people live in 7,935 towns and cities and generate 62 million tonnes of MSW per annum. Due to increasing industrialization in the country, there is a strong possibility of increasing significantly the amount of MSW in the near future. (Shekdar et al. 1992, CPCB 2004; Sharma and Shah 2005). The proper management of MSW has emerged as a greatest challenge before environment scientists, urban planners and decision makers of the country. Presently, most of the MSW in India is being disposed unscientifically (Akolkar 2005). In various studies, it has been found that about 90% of MSW is disposed of unscientifically in open dumps and landfills, causing not only the health problem, but it has adverse impact on all the components of environment. (Kansal et al. 1998; Singh and Singh 1998; Gupta et al. 1998; Kansal 2002; Jha et al. 2003; Sharholy et al. 2005; Ray et al. 2005; Rathi 2006). Such type of improper disposal attracts birds, rodents and fleas to the waste dumping site which creates unhygienic conditions (Suchitra 2007).

The degradation of solid waste emits carbon dioxide (CO_2), methane (CH_4) and other trace gases. An unscientific landfill also becomes a cause to reduce the quality of drinking water in the area, which also increases the risk of diseases like jaundice, nausea and asthma (MeBean et al.1995; Dhere et al. 2008). Hence, it is a sensitive issue which concerns about serious environmental problems. The direct dumping of MSW in various cities of the country without inspection and segregation is giving rise to a serious problem like environmental pollution, due to which a variety of health-related problems are also increasing. Therefore, studying solid waste conditions in any area for proper waste management and planning is very crucial. Similarly, integrated systems of waste management focusing on the reduction of waste, reuse, recycle and finally the disposal of the remaining solid waste into the landfill is very much needed in sustainable city development (Simone et al. 2004). As sanitary land filling is an inevitable part of MSW management system (Tchobanoglous et al. 1993). Selection of a landfill for disposal of solid wastes requires processing and evaluation of a significant amount of spatial data with respect to various parameters governing the suitability of a site (Ojha et al. 2007). Selecting the optimum site for landfill can play an important role in reducing environmental pollution. However, it has become very difficult to fix landfill due to environmental pollution and opposition from residents. Wise usage of valuable and fixed land resources is a great challenge also. It is very important to keep in mind the various spatial, economic and social parameters in the process of selecting the suitable sites for solid waste disposal. Therefore, an optimal technique for compiling and analysing huge amount of data is also required. In this context, satellite remote sensing data and geographic information system (GIS) is a vital tool for processing, analysing and handling large volume of spatial and non-spatial data in short duration. In complex decision-making processes involving multi-thematic layers and their pairwise comparison, analytic hierarchy process (AHP) has proved to be a very useful decision-making tool. Several studies

related to the selection of suitable sites, therefore, are based on GIS and AHP (Akbari et al. 2008; Chang et al. 2008, Wang et al. 2009).

Over the past few decades, remote sensing has proved to be an extremely useful tool for monitoring and analysing the environment and its resources due to its ability to provide synaptic view of the earth's surface and its specific capability of repetitive coverage. Its multi-spectral capability helps in identifying diverse natural elements and due to its ability of the repetitive coverage, information related to the constant changes in the earth's surface and natural environment is available (Navalgund and Kasturirangan 1983). Technological development in computer science has introduced geographic information system (GIS) as an innovative tool in landfill process (Kontos et al. 2005). GIS has the capability of combining different types of spatial data with other quantitative, qualitative and descriptive databases. When it coupled with satellite data, provides an excellent framework of capturing, storing, synthesizing, measuring and analysing the information. Since, several socioeconomic and environmental factors should be considered in selecting suitable sites for landfill, utilization of GIS-aided methodology to find suitable MSW landfill site in Almora municipality might be useful. The objectives of the project were to find out the existing location of waste bins to provide some new suitable location for waste bins and to find out present location of the waste dumping ground/landfill site and to provide some suitable solid waste disposal sites using GIS techniques in study area.

25.2 Materials and Methods

25.2.1 Study Area

Municipal board and cantonment town Almora (administrative headquarters of Almora district, Uttarakhand) lies at 29.5971°N and 79.6591°E (area12.43 sq.km) in Kumaon Hills of the central Himalayan range (Fig. 25.1). Almora is located on a ridge at an average elevation of 1,861 m (6,106 ft.) above mean sea level and surrounded by thick forests of pine and fir trees. Rivers Koshi (Kaushiki) and Suyal (Salmale) flow alongside the town. The average annual temperature in Almora was recorded 23.5 °C (maximum 31.1 °C in June and minimum 13.3 °C in January). The average annual amount of precipitation in Almora was recorded. Almora has population of 35,513 (Census of India 2011). It is an important tourist place and records a large inflow of tourists both from both domestic and abroad. The improper disposal of solid wastes is a crucial problem in the Almora town. The spatial modelling using modern geospatial tools of remote sensing and GIS may contribute in proper management of MSW in Almora.

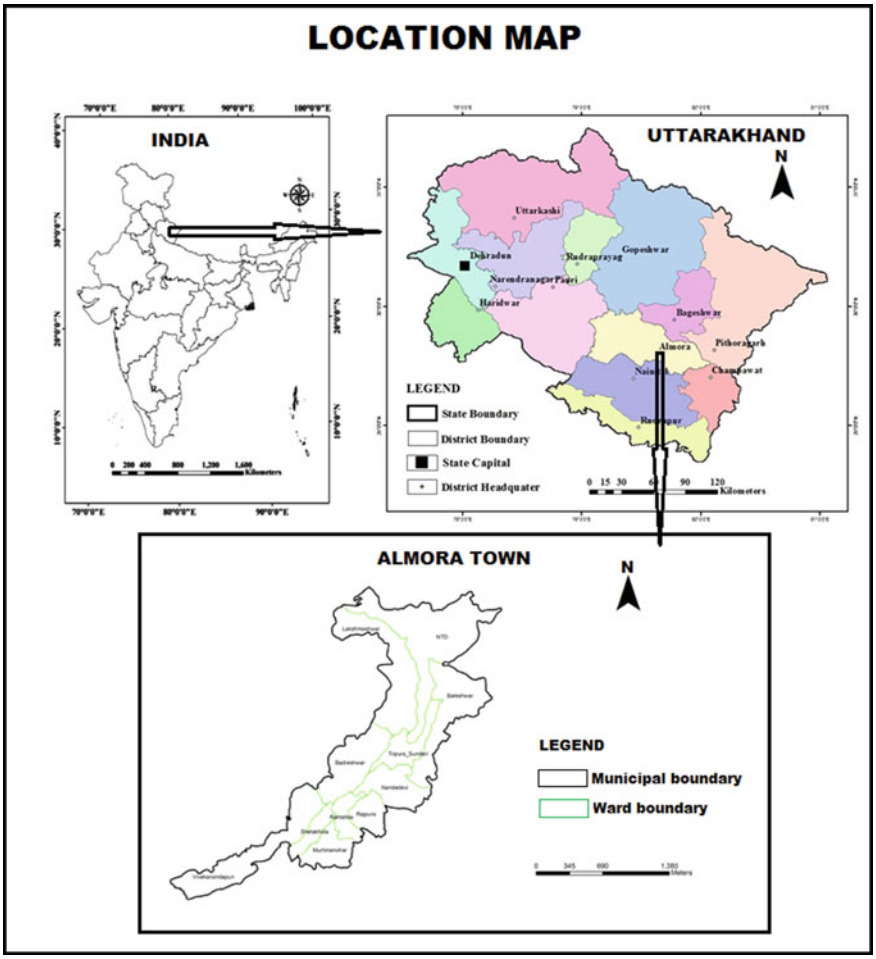

Fig. 25.1 Study area

25.2.2 Data and Software Used

To meet the set objectives of the study, high spatial resolution satellite data (2.5 m) of Cartosat-1(Panchromatic B/W, band- 0.52–0.85 μm) of the year 2017 was used. Cartosat-1 satellite (stereo pairs) is extremely useful in creating digital elevation models, ortho image products and value-added products for various GIS applications. Topographic map numbers 53 O/9 and 53O/10 (scale 1:50,000) of the Survey of India were used to prepare reference and base maps. ERDAS Imagine 9.1 and ArcGIS 9.3 packages were used for mapping and analysis. A GPS (Garmin-12) was used to know the exact coordinates of selected locations for waste bins.

25.2.3 Methodology

In the present study, a GIS-based multi-criteria decision-making (MCDM) system was developed to evaluate the suitable sites for MSWM in Almora municipal area, Almora district, Uttarakhand (India). For this purpose, four criteria, namely slope, road proximity, land use/land cover (LU/LC) and waste bins proximity were selected, and the maps were prepared to generate thematic information. All these thematic layers were analysed and integrated in ArcGIS 9.3. As per the suitability and importance for MSWM, each layer of the criterion was assigned internal weight score using Saaty's nine-point weighing scale ranging from 1 to 9 (Table 25.1). The pairwise comparison matrix was applied to create a ratio matrix. The pairwise comparisons were taken as input to produce output of relative weights.

Further, the criterion weights were computed through the some mathematical operations, i.e. sum of each column values of the pairwise comparison matrix, division of matrix elements by its column total to find out normalized pairwise comparison matrix and average of elements in each row of the normalized matrix to provide an estimate of the relative weights of the criteria being compared (Malczewski 1999). In order to prevent bias thought criteria weighting, the consistency ratio (CR) was used which measures how consistent the judgments have been relative to large samples of purely random judgments. The analytic hierarchy process (AHP), a method for multi-criteria decision-making (MCDM) which evolves qualitative data, was also considered in this study (Saaty 1994).The estimation of consistency was carried out by determining weighted sum vector and consistency vector. Further, the average value of the consistency vector (λ) and the consistency index, a measure of departure from consistency (CI) was calculated. The calculation of CI is based on the observation that λ is always $\geq$ (greater than or equal to) the number of criteria

Table 25.1 Nine point weighting scale for pairwise comparison (Saaty 1980; ESRI 1996)

Intensity of importance	Description	Suitability class
1	Equal importance	Lowest suitability
2	Equal to moderate importance	Very low suitability
3	Moderate importance	Low suitability
4	Moderate to strong importance	Moderately low suitability
5	Strong importance	Moderate suitability
6	Strong to very strong importance	Moderate high suitability
7	Very strong importance	High suitability
8	Very to extremely strong importance	Very high suitability
9	Extremely importance	Highest suitability

Table 25.2 Random index

Order Matrix	1	2	3	4	5	6	7	8	9	10
RI	0.00	0.00	0.58	0.9	1.12	1.24	1.32	1.41	1.45	1.49

under consideration (n) for positive, reciprocal matrices and λ=n, if the pairwise comparison matrix is consistent matrix. Accordingly, λ–n may denote the degree of inconsistency. This measure can be normalized as follows:

$CI = (\lambda\text{-}n) / (n\text{ -}1)$

Further, the consistency ratio (CR) was calculated to know goodness of CI. In the AHP, CI is compared with Random Index (RI) which can be expressed as-

$CR = CI/RI$

The RI is the consistency index of a randomly generated pairwise comparison matrix of order 1–10 obtained by approximating random indices using a sample size of 500 (Saaty 2000). As per the order of matrix, RI values were shorted and shown in Table 25.2. The CR < 0.10 denotes a reasonable level of consistency in the pairwise comparisons while the condition of CR > 0.10 indicates the inconsistent judgments and requires reconsideration and revision of original values in the pairwise comparison matrix.

Further, all vector layers were converted into raster data because in raster data format, computation is less complicated than vector data format (Chang 2006). The classified raster maps were integrated in raster calculator of ArcGIS 9.3 and multiplied with weightage to prepare final suitability map. It can be expressed as

Suitability map = Σ [criteria map * weight]

25.3 Results and Discussions

25.3.1 Criteria Mapping

To propose suitable waste dumping ground/landfill sites and waste bins in the study area, four criteria namely slope, settlement proximity, road proximity and existing bins were selected and map out and analysis.

25.3.1.1 Slope

Terrain slope is an important criterion in mountainous areas for evaluating land suitability for waste dumping ground/landfill sites and waste bins. Steeper slopes are disadvantageous which increase construction costs and prone to land slide and erosion during construction and subsequent use. Generally, slope greater than 10° has been classified as unsuitable for any type of construction. The higher slopes would also increase runoff of pollutants from the landfill, and thereby contaminate areas

further away from the landfill site (Lin and Kao 1999). It is suggested by Lin and Kao's study (1999) that a slope less than 12% would be suitable for the prevention of contaminant runoff. The slope map of study area was generated using digital elevation model (DEM) Fig. 25.2, and Table 25.3 illustrates the distribution of slope values in the study area ranges between 0° and 45°.

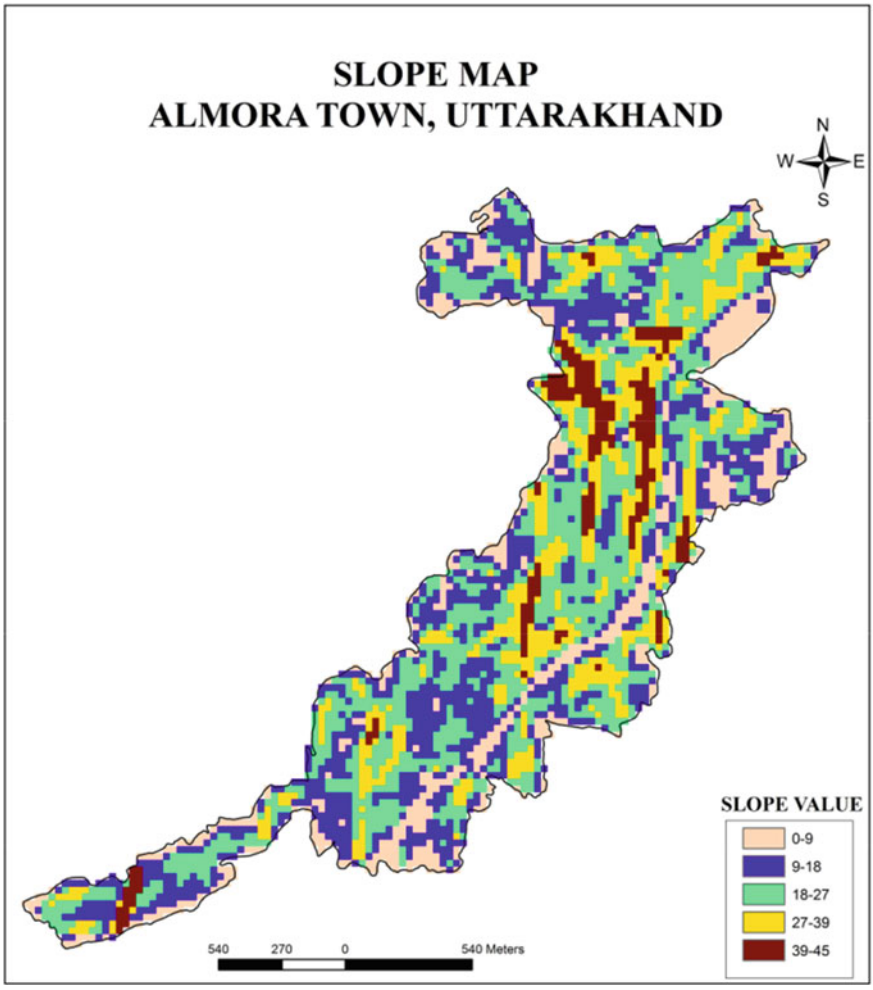

Fig. 25.2 Slope map of Almora Town, Uttarakhand

Table 25.3 Suitability scoring/ranking

Intensity of importance	Slope	Built-up area	Existing bins	Road proximity
9 (highest)	–	–	2000	5
8 (very high)	0–10	30	–	–
7 (high)	–	–	500	10
6 (moderate high)	10–15	50	-	–
5 (moderate)	–	–	100	–
4 (moderate low)	–	–	–	–
3 (low)	15–21	–	–	20
2 (very low)	21–29	–	30	50
1 (lowest)	29–45	160	10	1700

25.3.1.2 Road Proximity

Transportation services are extremely essential for reducing travel expenses to the suitable landfill sites and increasing the efficiency in transferring the waste to disposal sites (Ogra 2003). Construction of new road is expensive in hilly regions, thus being nearer to an existing road would be advantageous. The site suitability analysis involves the delineating the best route connecting to different points or identifying the best location for a specific use (McHarg 1969). In this study, road proximity map was created in GIS environment using high spatial resolution Cartosat 1 data. The distance map shows the distance of each and every pixel in metres from the nearest road. In the buffer map areas, distance up to 1700 m was considered in the analysis (Fig. 25.3).

25.3.1.3 Built-Up Area

The built-up area in Almora town was mapped using high-resolution satellite data and a built-up area proximity map was generated in ArcGIS (Fig. 25.4). According to Rahman (2011), the distance from urban built-up area should be at least 1 km and from isolated houses, it should be 500 m to locate a landfill site. Siddiqui et al. (1996) suggests that no new landfill site should be located closer than 0.4 km (0.25 m) from a collection of ten or more houses. On the other hand, the landfill site should be located within 10 km of an urban area due to the economic considerations.

25.3.1.4 Existing Bin Proximity

With the purpose of suitability analysis, existing MSW collection bins were identified and map out using Cartosat 1 satellite image and collateral thematic information.

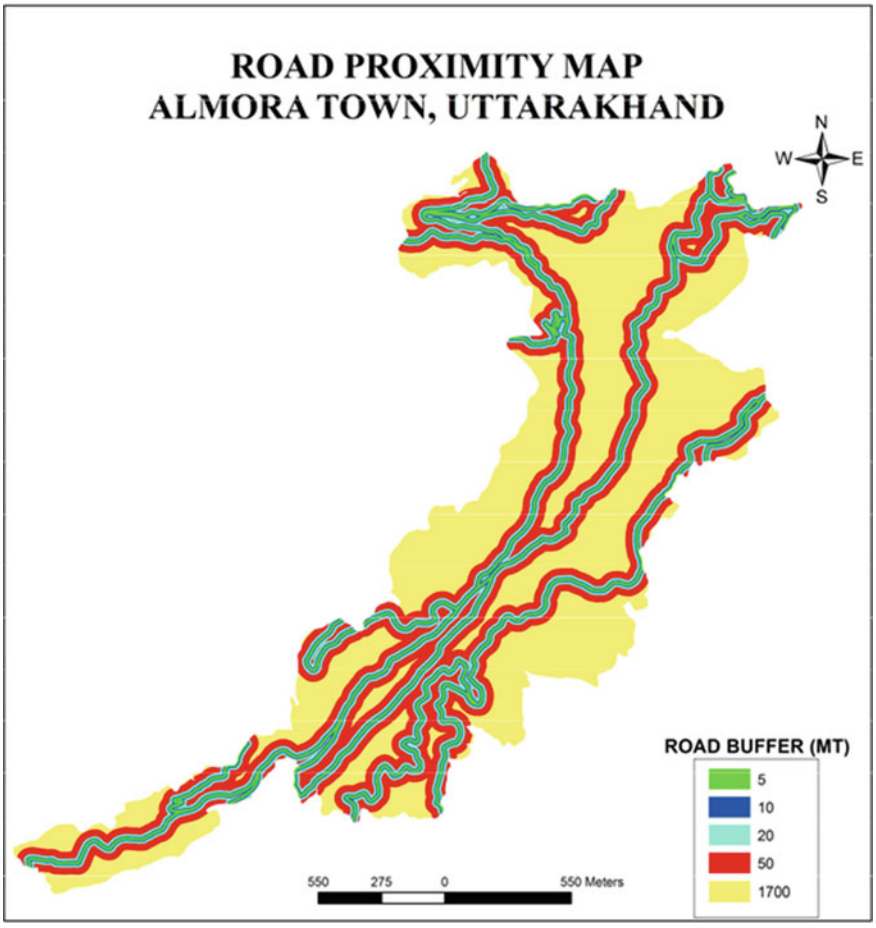

Fig. 25.3 Road proximity map of Almora Town, Uttarakhand

Further, the proximity zones were created around the bins with the distances of 10 m, 30 m, 100 m, 500 m and 2000 m (Fig. 25.5).

25.3.2 Scoring/Ranking of Criteria

In this study, scoring of each criteria map and their categories was carried out using nine-point weighting scale (Table 25.3). Using criteria weight, a pairwise comparison matrix was developed (Table 25.4). Further, all criteria were normalized and weights were computed for each criteria using ratio matrix and pairwise comparison method (Table 25.5).

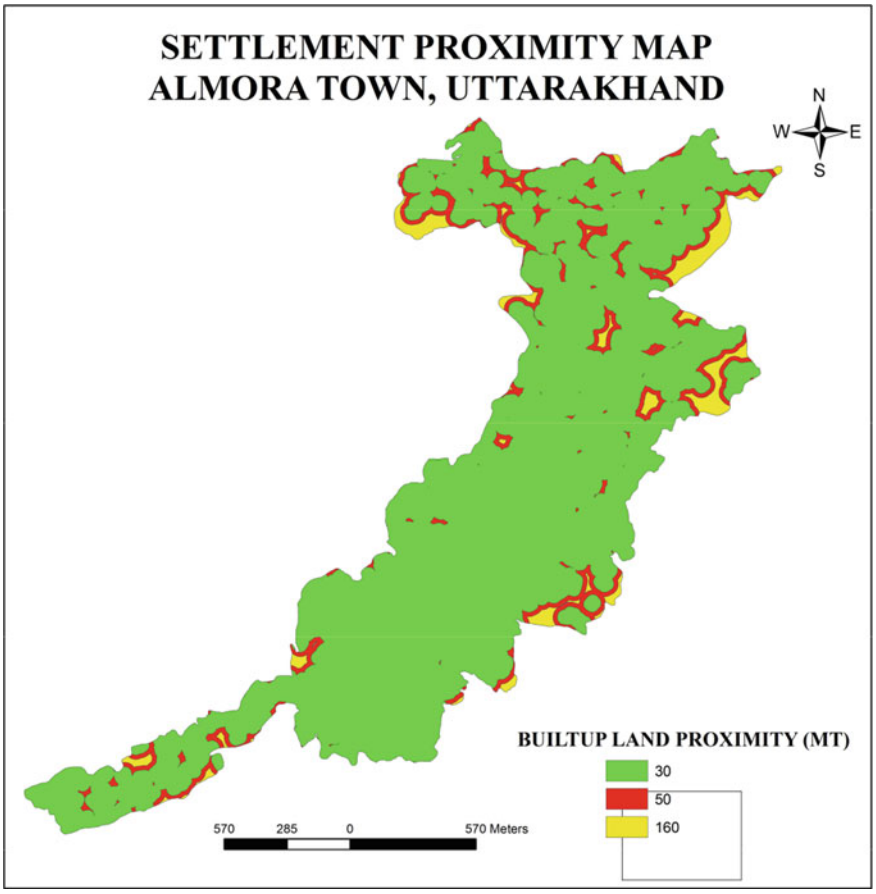

Fig. 25.4 Built-up area proximity map of Almora Town, Uttarakhand

25.3.3 Calculation of the Consistency Ratio

In order to verify the consistency of comparisons, the weighted sum vector and consistency vector were calculated (Table 25.6).

Condition 1 λ should be equal or greater than the number of criteria under consideration. The value calculated above satisfies this condition.

Calculation of consistency index (CI).

CI = (λ-n) / (n -1).

(4.01–4)/ (4–1) = 0.01/3 = 0.003.

Calculation of consistency ratio (CR).

CR = CI/RI.

0.003/0.9 (Since RI = 0.9 for n = 4) = 0.0033.

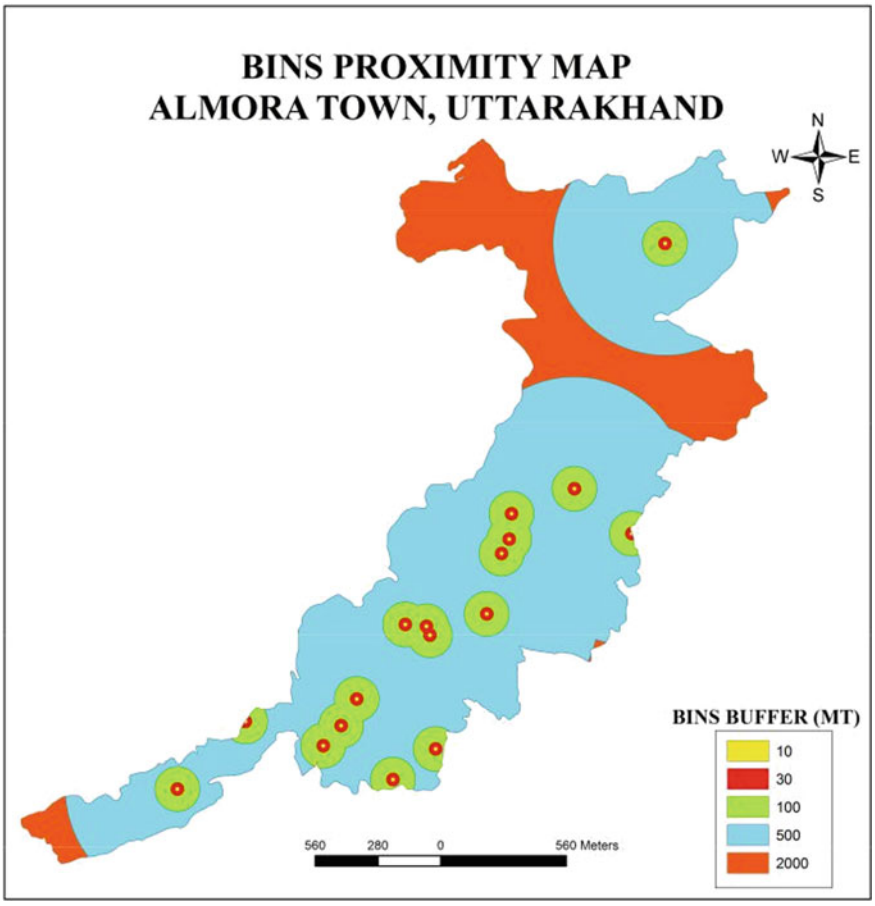

Fig. 25.5 Existing bin proximity map of Almora Town, Uttarakhand

Table 25.4 Pairwise comparison matrix

Criteria	Slope	Built-up area	Existing bins	Road proximity	Weight
Slope	1	4	6	9	0.59
Built-up area	0.25	1	4	6	0.25
Existing bins	0.17	0.25	1	24	0.11
Road proximity	0.11	017	0.25	1	0.04
Sum	1.53	5.42	11.25	20	1.000

Table 25.5 Normalized pairwise comparison matrix

Criteria	Slope	Built-up area	Existing bins	Road proximity	Weight
Slope	0.65	0.74	0.53	0.45	0.59
Built-up area	0.16	0.18	0.36	0.30	0.25
Existing bins	0.11	0.05	0.09	0.20	0.11
Road proximity	0.07	0.03	0.02	0.05	0.04
Sum	Sum	1.000	1.000	1.000	1.000

Table 25.6 Computation of consistency vector

Criterion	Weighted sum vector	Consistency vector
Slope	[(1)(0.59) + (4)(0.25) + (5)(0.11) + (6)(0.4)] / 0.59	4.42
Built-up area	[(0.25)(0.59) + (1)(0.25) + (4)(0.11) + (5)(0.04)] / 0.25	4.32
Existing bins	[(0.17)(0.59) + (0.25)(0.25) + (1)(0.11) + (1)(0.04)] / 0.11	3.91
Road proximity	[(0.11)(0.59) + (0.17)(0.25) + (0.5)(0.11) + (0.25)(0.25)] / 0.04	3.40

$\lambda = (4.42+4.32+3.91+3.40)/4 = 16.05/4 = 4.01$, Lambda ($\lambda$) is the average of consistency vector

Condition 2- Consistency ratio CR (0.0033) < 0.10 indicated a reasonable level of consistency in the pairwise comparisons. Therefore, the values obtained satisfy the said conditions, which denote that the weights obtained are agreeable.

25.3.4 Preparation of Suitability Map

In order to determine the suitable sites for proper disposal of MSW, the all criteria maps were converted into raster format and a score of each pixel was determine (Jain and Subbaiah 2007). The final sites suitability map was prepared integrating and overlying all criteria maps in GIS environment using following formula-

Suitability map = Σ *[criteria map * weight].*

Suitability = ([Slope] * 0.59).

+ ([Built-up Area] * 0.25).

+ ([Existing Bins proximity]*0.11).

+ ([Road proximity] * 0.04).

The final map of site suitability for waste bins (Fig. 25.6) illustrates that the study area was divided into five different suitable classes, viz. very high suitable, high suitable, moderately suitable, low suitable and very low suitable. The area under very high suitable, high suitable, moderately suitable, low suitable and very low

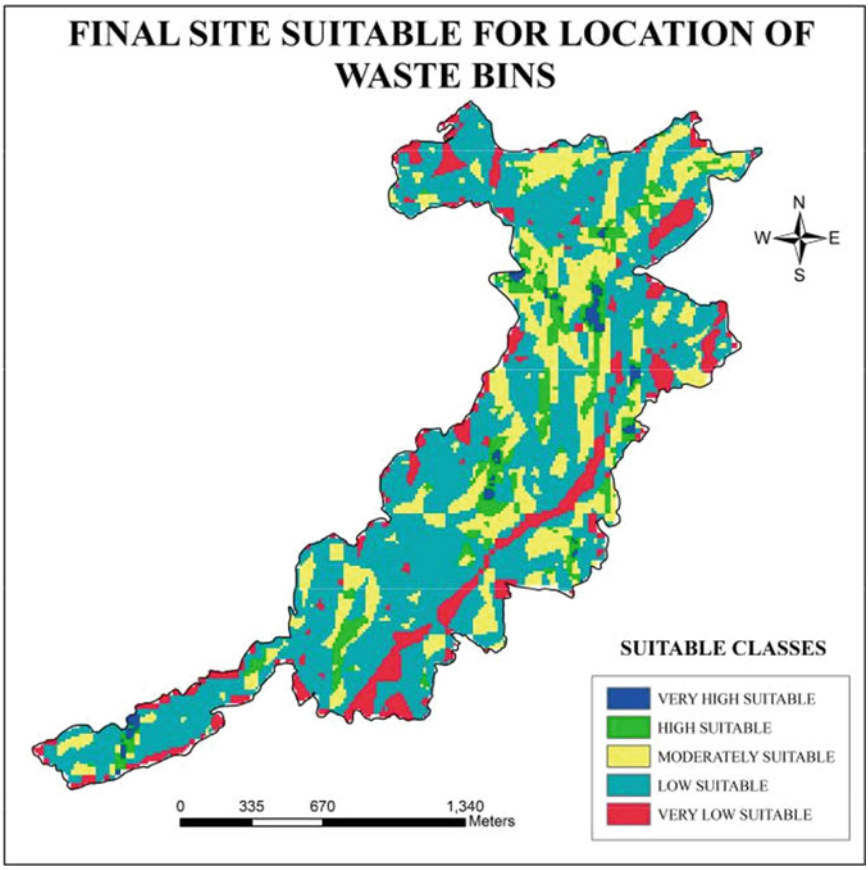

Fig. 25.6 Suitable sites for waste bin of Almora Town, Uttarakhand

suitable lands were observed 0.32km^2, 0.53km^2, 1.03 km^2, 9.48 km^2 and 1.0 5km^2, respectively (Table 25.7). About 85 per cent of the total area falls under low and very low suitability classes while only 6.9 per cent of land falls under high and very high suitable classes.

Table 25.7 Area under different suitability classes

Suitability classes	Area in km2	Area in %
Very high suitable	0.32	2.6
High suitable	0.53	4.3
Moderately suitable	1.03	8.3
Low suitable	9.48	76.3
Very low suitable	1.05	8.5

25.4 Conclusion

In the present study, suitable locations for solid waste disposal were suggested for Almora town. GIS coupled with remote sensing techniques is a most suitable tool to address spatial problems in finding suitable location for solid waste disposal. In this study, GIS-based multi-criteria evaluation technique proved a very useful technique for suitability analysis of Almora municipal area. This model can also helpful in urban decision-making process and may assist planners and authorities to formulate proper plan to clean and green cities of the region.

References

Akbari V, Rajabi MA, Chavoshi SH, Shams R (2008) Landfill site selection by combining GIS and fuzzy multi criteria decision analysis, Case study: Bandar Abbas. Iran. World Applied Sciences Journal 3:39–47

Akolkar AB (2005) Status of solid waste management in India, implementation status of municipal solid wastes, management and handling rules 2000. Central Pollution Control Board, New Delhi

Central Pollution Control Board (CPCB) (2004) Management of municipal solid waste. Ministry of Environment and Forests, New Delhi, India

Chang NB, Parvathinathan G, Breeden JB (2008) Combining GIS with fuzzy multicriteria decision-making for landfill sitting in a fast-growing urban region. J Environ Manage 87:139–153

Chang K T (2006) Raster data analysis. Introduction to geographic information system, New Delhi, Tata McGraw Hill

Dhere AM, Pawar CB, Pardeshi PB, Patil DA (2008) Municipal solid waste disposal in Pune city – an analysis of air and groundwater pollution. Curr Sci 95(6):773–777

Environmental Systems Research Institute Inc. ESRI (1996) Working with the ArcView spatial analyst. Redlands, California, USA

Gupta S, Krishna M, Prasad RK, Kansal A (1998) Solid waste management in India: options and opportunities. Resour Conserv Recycl 24:137–154

Jain K, Subbaiah YV (2007) Site suitability analysis for urban development using GIS. Journal of Applied Science 7(18):2576–2583

Jha MK, Sondhi OAK, Pansare M (2003) Solid waste management – a case study. Indian J Environ Prot 23(10):1153–1160

Kansal A (2002) Solid waste management strategies for India. Indian J Environ Prot 22(4):444–448

Kansal A, Prasad RK, Gupta S (1998) Delhi municipal solid waste and environment – an appraisal. Indian J Environ Prot 18(2):123–128

Kontos TD, Komilis DP, Halvadakis CP (2005) Siting MSW landfills with a spatial multiple criteria analysis methodology. Waste Manage 25:818–832

Lin H, Kao JJ (1999) Enhanced spatial model for landfill sitting analysis. J Environ Eng 125–9:845–851

Malczewski J (1999) Criterion weighting. GIS and multi-criteria decision analysis. New York, USA, Wiley: 182–187

McHarg IL (1969) Design with nature. The Natural History Press, Garden City, New York, USA

MeBean EA, Rovers F A and Farquhar G J (1995) Solid waste landfill engineering and design, Prentice Hall, NJ: 380

Navalgund RR and Kasturirangan K (1983) The remote sensing satellite – A programme overview. Proc. Indian Acad. Sci. Engg. Sci. –Remote Sensing 3 (6): 313–336

Ogra A (2003) Logistic management and spatial planning for solid waste management systems using geographical information system. In: Map Asia 2003 India
Ojha CSP, Goyal MK, Kumar S (2007) Applying fuzzy logic and the point count system to select landfill sites. Environ Monit Assess 135(1–3):99–106
Rahman S (2011) Application of GIS techniques in urban solid waste management in a part of Dhaka City: Mohammadpur Thana. Journal of Sustainable Development and Environment Protection 1(2):63–64
Rathi S (2006) Alternative approaches for better municipal solid waste management in Mumbai. India. Journal of Waste Management 26(10):1192–1200
Ray MR, Roychoudhury S, Mukherjee G, Roy S, Lahiri T (2005) Respiratory and general health impairments of workers employed in a municipal solid waste disposal at open landfill site in Delhi. Int J Hyg Environ Health 108(4):255–262
Saaty TL (1980) The analytic hierarchy process. McGraw-Hill, New York
Saaty TL (1994) Fundamentals of decision making and priority theory with the analytic hierarchy process. RWS Publications, Pittsburgh
Saaty TL (2000) Fundamentals of decision making and priority theory, 2nd edn. RWS Publications, Pittsburgh
Sharholy M, Ahmad K, Mahmood G, Trivedi RC (2005) Analysis of municipal solid waste management systems in Delhi – a review. Book of Proceedings for the second International Congress of Chemistry and Environment. Indore, India, pp 773–777
Sharma S, Shah KW (2005) Generation and disposal of solid waste in Hoshangabad. In: Book of Proceedings of the Second International Congress of Chemistry and Environment, Indore, India:749–751
Shekdar AV, Krshnawamy KN, Tikekar VG, Bhide AD (1992) Indian urban solid waste management systems – jaded systems in need of resource augmentation. Journal of Waste Management 12(4):379–387
Siddiqui MZ, Everett JW, Vieux BE (1996) Landfill siting using geographic information systems: A demonstration. J Environ Eng 122–6:515–523
Simone L, Bishop Ian D, David E (2004) Spatial-temporal model for demand allocation of waste landfills in growing urban regions. Comput Environ Urban Syst 28(4):353–385. https://doi.org/10.1016/S0198-9715(03)00043-7
Singh SK, Singh RS (1998) A study on municipal solid waste and its management practices in Dhanbad-Jharia coalifield. Indian J Environ Prot 18(11):850–852
Singhal S, Pandey S (2000) Solid waste management in India: Status and future directions. TERI Information Monitor on Environmental Sciences 6:1–4
Suchitra M (2007) Outside: Burnt or buried, garbage needs land, Down To Earth: 22–24
Tchobanoglous G, Theisen H, Vigil S (1993) Integrated Solid Waste Management. McGraw-Hill, New York
Wang G, Qin L, Li G, Chen L (2009) Landfill Site Selection Using Spatial Information Technologies and AHP: A Case Study in Beijing, China. J Environ Manage 90(8):2414–2421